21st Century COE Program

Final Report of

"Program for Arid Land Science"

Tottori University

2007

Contents

1. Outline

1) 21st Century COE Program

In response to a report by Japan's Ministry of Education, Culture, Sports, Science and Technology (MEXT), entitled "A Policy for the Structural Reform of Universities," this program was established in 2002 to cultivate a competitive academic environment among Japanese universities by giving targeted support to the creation of bases for world-class research and education (Centers of Excellence: COE). By raising the standards for both education and research at these centers, the program seeks to elevate Japanese universities to the ranks of the world's most prestigious institutions, while fostering the education of talented, creative people who will be qualified to assume future roles as world leaders.

In fiscal year (FY) 2002, 113 COEs (50 universities) were selected from among 464 applications (163 universities), including the Arid Land Research Center (ALRC).

2) Program for Arid Land Science

The objective of the Program for Arid Land Science is to develop a new arid land science, which is both innovative and multidisciplinary, that is without parallel in the world, with the goal of educating young researchers capable of fulfilling the abovementioned objectives of the program. The program will build upon knowledge and technologies from the field of agriculture that have been established by Tottori University and will aim to establish overseas research and educational bases in many of the world's arid regions.

(1) Operating period

FY2002 to FY2006

(2) Research field and keywords

Research field: environmental sciences

Keywords: combating desertification, environmental restoration technology, plant production, utilization of natural energy, socio-medical science

(3) Related faculties and centers

- Arid Land Research Center
- Bioresources Science, Bioenvironment Science, the United Graduate School of Agricultural Sciences
- Design and Information Engineering, Engineering of Social Development, Graduate School of Engineering
- Medicine, Graduate School of Medical Sciences

(4) Organization

Leader: Atsushi Tsunekawa

(Shinobu Inanaga from FY2002 to FY2004)

Research groups and researchers:

- **Environmental Monitoring**: Reiji Kimura, Mitsuhiro Inoue, Hiroshi Yasuda, Osamu Hinokidani, Hisao Anyouji, Hiroshi Nawata
- **Environmental Restoration Technology**: Norikazu Yamanaka, Tahei Yamamoto, Toshimasa Honna, Yoshinobu Kitamura, Atsushi Tsunekawa
- **Plant Production**: Kiyoshi Tanaka, Shinobu Inanaga, Yukihiro Sugimoto, Satoshi Yamada, Ping An
- **Utilization of Natural Energy**: Tsutomu Hayashi, Makio Kamichika
- **Socio-medical Science**: Youichi Kurozawa, Takayuki Nose

3) Objectives

Nearly half (41%) of the world's land surface is covered by arid lands that are increasingly being affected by desertification. Since ecosystems do not recognize political boundaries, scientific cooperation among nations is urgently needed if the problem of desertification is to be addressed. Japan has ratified the United Nations Convention to Combat Desertification (UNCCD), and under this agreement, provides both technical support and public financial support to meet its obligations. As a matter of fact, Japan has become the world's largest financial donor, but more technical support is required. Therefore, the promotion of research that will become the basis for combating desertification is an urgent priority.

The objectives of this program are to develop a new arid land science that is without parallel in the world, and to educate young researchers capable of fulfilling the abovementioned objectives. The program will build upon knowledge and technologies from the field of agriculture that have been established by Tottori University, and will establish overseas research and educational bases in many of the world's arid regions.

Further development of the program will be necessary to advance sciences that will further contribute to combating desertification around the world, educate young researchers in this field, and fulfill Japanese obligations under the UNCCD to provide financial, scientific, and technical support, and to recruit researchers. The relevant scientific knowledge that is available is insufficient to meet the UNCCD objectives, and development of the socio-medical field is especially primitive. As such, the program will enhance new development in sciences related to arid lands.

4) Outline of the research and education activities

As shown in Figure 1, the COE for arid land science has been developed with close ties between

research and education in collaboration with overseas research and educational bases. We have used this approach to establish the “new arid land science” defined in this project.

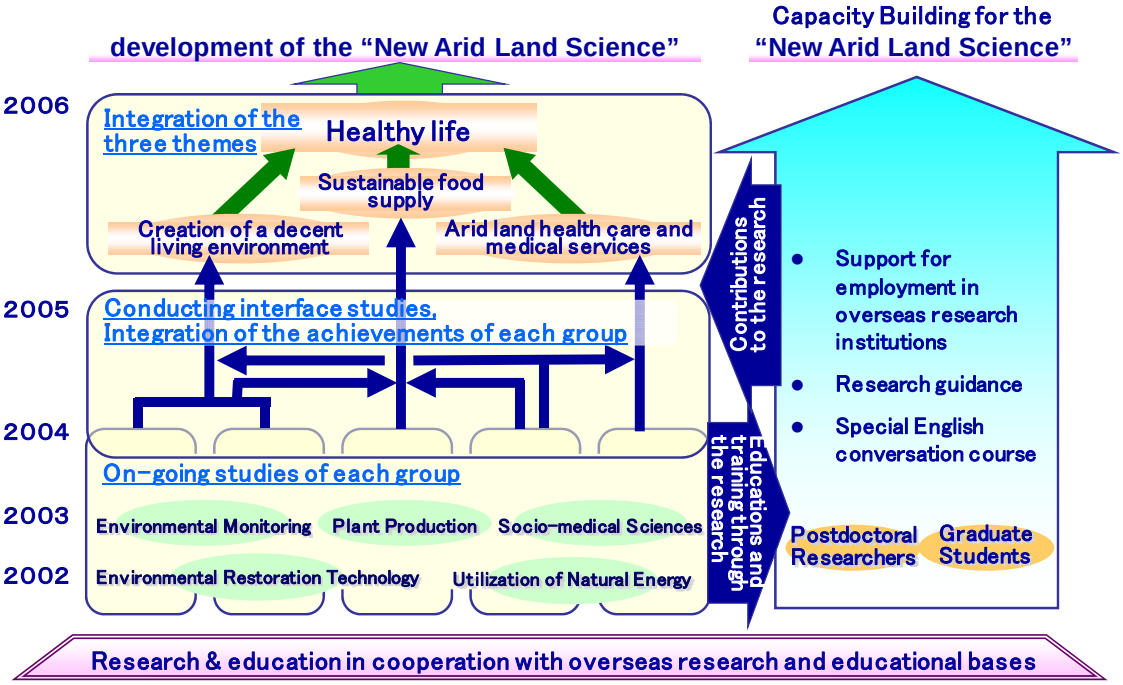

Fig. 1. Outline of the research and education activities of the center of excellence for arid land research.

Our research has systematized the achievements of this project and the related findings of previous research, leading to a unique framework for the new science. Previous research results and achievements have been summarized in two main categories: technologies for diagnosing desertification and technologies for combating desertification. Based on this knowledge, effective technical packages for combating desertification have been developed. These achievements have been published as “Dryland Science in the 21st Century: Sustainability of Nature and Society”.

The education component of the program has supported young researchers who will become key components of future networks by developing their research and English communication skills through visits of various durations to overseas research and educational bases and by providing lessons in conversational English. Information on international employment opportunities has been systematically collected and provided to young researchers to help them find rewarding positions at international research institutions that focus on desertification. As a result, the number of young researchers who have presented their research achievements at conferences and who have published journal articles are now 11 and 6 times previous levels respectively. English communication skills have also improved dramatically. Moreover, young researchers have conducted their studies from a multidisciplinary (holistic) perspective by engaging in joint research with colleagues from

other specialties.

5) Focal point

To establish the world's most advanced center of excellence for arid land science and to promote its future development, we have gone beyond developing the new arid land science to also focus on developing global research and educational networks. We are proud of the following major achievements:

To improve our international networks, we played a primary role in establishing the Global Network of Dryland Research Institutes (GNDRI, initiated by the call of the Desert Research Institute (DRI, http://www.dri.edu/), USA; the Jacob Blaustein Institute for Desert Research (BIDR, http://cmsprod.bgu.ac.il/Eng/Units/bidr), Israel; and ALRC, Japan), a network of the world's most advanced research institutions in arid land science. We have also decided to participate in Central and West Asia, in North Africa, and in neighboring dry areas in Western China, South Asia, and Saharan Africa as part of the international CWANA^{+} partnership that has been organized by ICARDA (http://www.icarda.org/) and the United Nations University (UNU). ALRC, a core institute in this program, provides National Joint-Use Facilities that are available to a network of joint-use researchers throughout Japan. ALRC has carried out an average of about 50 joint research projects every year. With this project, ALRC has come to play a role as a hub institute for domestic and international research networks. Overseas research and educational bases have been established, resulting in the promotion of research and education on arid land science in Japan even though there is no arid land in Japan. Furthermore, increasing publicity for the COE will attract excellent students from abroad and from Japanese universities who have a strong desire to build a career in arid land science, and highly motivated young researchers have already begun to gather at this COE and produce significant research results.

To establish a unique new arid land science that includes a range of disciplines outside the traditional "hard" sciences (including the arts and social sciences, socio-medical sciences, and natural energy), we have systematized the findings of previous research, of this project, and of research on appropriate technology. By focusing on sustainable development of the nature–society system in arid lands, we have developed a framework for a new arid land science that includes traditional knowledge and appropriate technologies. The result is a series of textbooks entitled "Dryland Science in the 21st Century: Sustainability of Nature and Society" (Kokon Shoin published Series 1 in March 2006; Series 3 and 5 were published in FY2007, and Series 2 and 4 will be published in FY2008.

2. Research achievements

Figure 2 illustrates and relationships among the five research groups and their research programs, which are together establishing a new and more holistic arid land science that will combat desertification and promote sustainable social and economic development in arid lands.

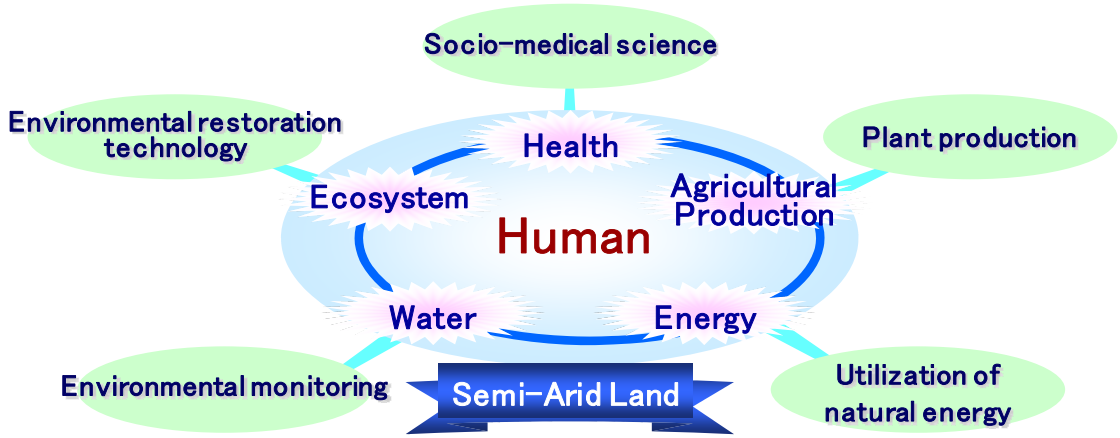

Fig. 2. Research programs and coordination among groups in developing the new arid land science.

The achievements of the five research groups are summarized in the following sections.

1) Environmental Monitoring group

This group conducted research designed to achieve three main objectives: “Elucidation of the process and effects of desertification” (the primary target), “Development of methods to evaluate desertification at a macro scale (Loess Plateau, China) and at the watershed scale (Liudaogou, Shenmu, Shaanxi, China)”, and “Development of measures of desertification”. Ecological assessments have been conducted and measurement techniques have been developed for soils, vegetation, meteorology, and water resources.

Development of evaluation methods for desertification

(1) Soils - Development of methods to monitor the movements of water and heat

(2) Water resources - Development of methods to monitor the hydrology and water balance in watersheds

(3) Vegetation and meteorology - Monitoring of desertification using biomass, soil moisture, and remote-sensing data

Development of measures of desertification

Proposal of appropriate land-use scenarios based on the water balance of an ecosystem and the water-use efficiency of its vegetation after evaluation of a watershed's current water balance (Fig. 3).

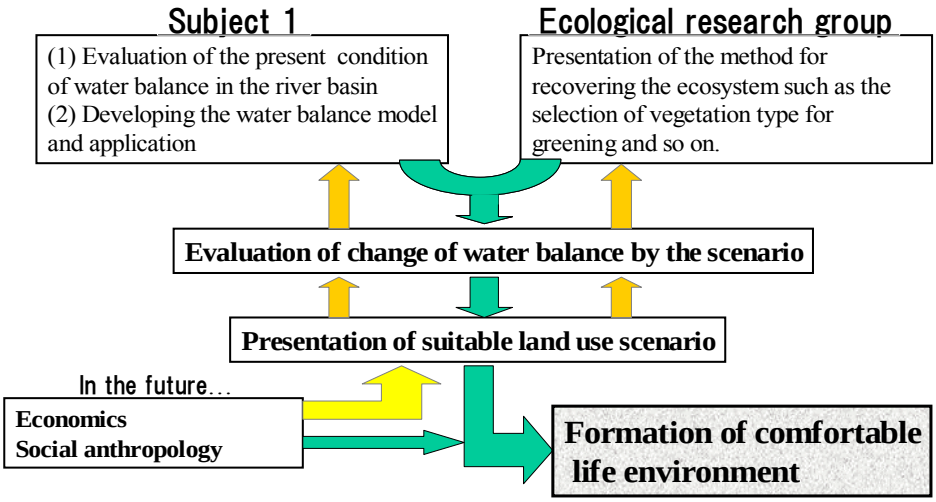

Fig. 3. Illustration of a process for developing restoration methods.

(1) A three-layer soil model was developed to quantify the movement of heat between bare soil surfaces and the atmosphere (Kimura et al. 2004a).

(2) A new sensor was developed to correctly measure moisture and salt contents in soils with a high salt concentration as a result of progressive salinization.

(3) The three-layer soil model and meteorological data from 43 observatories in the Loess Plateau of China were used to estimate the plateau's heat and water balances, to reveal the spatial distribution of soil moisture, and to provide a basis for discussing the plateau's physical features. Furthermore, the potential distribution of vegetation was determined by combining the data on the aridity of all areas in the Loess Plateau (estimated from seasonal changes in soil moisture), the distribution of soil moisture, and the present vegetation (identified by remote sensing). The results have revealed findings that were not documented in previous studies, and more correctly indicate the degree of desertification (Kimura et al. 2005).

(4) A model with a 1-km grid for estimating the distribution of monthly precipitation was developed using synoptic-scale analysis and topographic factorial analysis to permit statistical analysis of precipitation patterns. This study made it possible to show that

precipitation was the dominant factor responsible for desertification in the Loess Plateau at this grid scale (Takayama et al. 2004).

(5) In addition to the method for monitoring water balances in watersheds of the Loess Plateau, we developed an algorithm (using a numerical simulation model and remote-sensing technology) to estimate evapotranspiration from each land surface in a watershed. Land use in the watershed was evaluated using monitored data on water outflow and the new algorithm. In this study, water-use efficiency (WUE) was defined as protection from erosion achieved per water consumed. WUE of the vegetation in natural rangeland was better than that in other land-use systems. That is, natural rangeland provides the best protection against soil erosion, consumes less water, and retains relatively more water in the soil. Moreover, the usefulness of natural rangeland was recognized based on interviews with local users of the land and measurements of soil pH, nitrogen content, and hardness in the Loess Plateau (Kimura et al. 2007a; Kimura 2007b).

(6) The percolation characteristics of a check-dam farm and the responses of a huge watershed to rainfall were predicted from continuous measurements of soil water content and monitoring of ground and river water levels, thereby revealing the flow of water from the watershed to the check-dam farm. A management method for the water resources of a small watershed in the Loess Plateau was proposed using monitoring data and the water outflow model.

【Publication list】

- Anyoji H, Yasuda H, Procedure for Determining the Parameters in Linear and Non-linear Infiltration Equations. Sand Dune Research, 51: 131-144, 2005.
- Kato T, Kimura R, Kamichika M, Estimation of evapotranspiration, transpiration ratio and water-use efficiency from a sparse canopy using a compartment model. Agricultural Water Management, 65: 173–191, 2004.
- Kimura R, Kamichika M, Takayama N, Matsuoka N, Zhang X, Heat balance and soil moisture in the Loess Plateau, China. J. Agric. Meteorol, 60(2): 103-113, 2004a.
  <<ORIGINAL PAPER>>
- Kimura R, Okada S, Miura H, Kamichika M, Relationships among the leaf area index, moisture availability, and spectral reflectance in an upland rice field. Agric. Water. Management, 69: 83-100 , 2004b.
- Kimura R, Liu Y, Takayama N, Zhang X, Kamichika M, Matsuoka N, Heat and water balances of the bare soil surface and the potential distribution of vegetation in the Loess Plateau, China. Journal of Arid Environments, 63: 439-457, 2005. <<ORIGINAL PAPER>>

- Kimura R, Fan J, Zhang X, Takayama N, Kamichika M, Matsuoka N, Evapotranspiration over the grassland field in the Liudaogou basin of the Loess Plateau. Acta Oecologica, 29: 45-53, 2006.
- Kimura R, Bai L, Fan J, Takayama N, Hinokidani O, Evapo-transpiration estimation over the river basin of the Loess Plateau of China based on remote sensing. Journal of Arid Environments, 68: 53-65, 2007a. <<ORIGINAL PAPER>>
- Kimura R, Estimation of moisture availability over the Liudaogou river basin of the Loess Plateau using new indices with surface temperature. Journal of Arid Environments, 70: 237-252, 2007b. <<ORIGINAL PAPER>>
- Takayama N, Kimura R, Kamichika M, Matsuoka N, Zhang X, Climatic features of rainfall in the Loess Plateau in China. J. Agric. Meteorol, 60(3): 173-189, 2004. <<ORIGINAL PAPER>>
- Wang K, Zhang R, Yasuda H, Characterizing heterogeneity of soil water flow by dye infiltration experiments. Journal of Hydrology, 328: 559-571, 2006.
- Yasuda H, Wang K, Mohamed Abd Elbasit Mohamed Ahmed, Anyoji H, Zhang X, Analyses of Rainfall Time Series in the Loess Plateau of China. Periodical fluctuation and links with sea surface temperature. Journal of Agricultural Meteorology, 60: 617-620, 2005.
- Zeggaf TA, Anyoji H, Yasuda H, Performance comparison of transpiration models for maize crop under different crop canopies. Journal of Arid Land Studies, 15: 325-328, 2006a.
- Zeggaf TA, Anyoji H, Yasuda H, Fixed and variable light extinction coefficients for estimating plant transpiration and soil evaporation under irrigated maize. Agricultural Water Management, 84: 186-192, 2006b.

2) Environmental Restoration Technology group

This group conducted research on three main topics: "Establishment of water management technologies at a regional scale to prevent salinization", "Establishment of restoration technologies for degraded soils," and "Establishment of restoration technologies for biodiversity and forest ecosystems".

Establishment of water management technologies at a regional scale to prevent salinization

(1) Elucidation of saline movements in the soil in response to irrigation and the effects of groundwater level on soil salinization (study area: Luohuiqu irrigation area, Shaanxi, China)

In this study, salinization processes for a benchmark site were categorized, and the causal factors were elucidated. As remedial measures based on water management to prevent secondary salinization, researchers proposed the following ideas: (a) appropriate control of groundwater levels by improving the efficiency of drainage systems; (b) control of the saline

soil dumped by excavating new wells in fields; (c) management of the use of groundwater with high saline concentrations; (d) appropriate repair, maintenance, and management of the soil surface drainage system; (e) restoration of salinized farmland by means of “warp soil dressing (Soil dressing using flood flow)" technologies; and (f) application of biological drainage (i.e., using plant evapotranspiration to lower the water level) technologies along canals and around farm lots to prevent waterlogging.

(2) Effects of cultivating lowland rice on salinization in low-lying fields and in adjacent upland fields (study area: Central Asia)

This research investigated the fluctuation of salt concentrations in water in the upper soil layers during the irrigation period and the mechanisms responsible for upward movement of accumulated salts from lower soil layers. Accumulated salts in lower soil layers moved into upper soil layers by upward flux due to negative hydraulic gradients in the lower soil layers during the occasional interruption and resumption of irrigation water supply in the growing season Furthermore, the factors responsible for localized salinization under flooded conditions were also elucidated. By analyzing the causes of secondary salinization in irrigated farmlands, mitigation measures based on water management technologies were proposed to prevent salinization of lands (Kitamura et al. 2006).

Establishment of restoration technologies for degraded soils

(1) Basic research on the restoration of degraded soils was conducted using the facilities and equipment at ALRC. Elucidation of the mechanisms responsible for the creation of acidic and saline soils in drylands allowed researchers to investigate the reuse of recycled materials (i.e., the use of organic matter such as crop residues and animal manure) and the development of restoration methods based on this recycling of organic materials.

(2) The mechanisms responsible for the development of saline soils were investigated using Tottori sand dune soil, and a method for monitoring desertification was developed (Ould Ahmed et al. 2007).

(3) New aspects of the multiple effects of organic amendments in drylands, such as increasing Ca availability to plants were discovered.

(4) The mechanisms responsible for the development of acidic and saline soils and the effectiveness of amelioration using the application of artificial zeolites, were elucidated. (Andry et al. 2007; Yamada et al. 2007).

Establishment of restoration technologies for biodiversity and forest ecosystems

(1) Afforestation methods suitable for local environments in the Loess Plateau of China were studied by investigating differences in the water-use characteristics of indigenous and exotic

tree species, the structures of several forests, and the associated ecosystem functions.

(2) Comparative studies of the ecophysiological characteristics of exotic black locust (*Robinia pseudoacacia* L.) from North America and of an indigenous oak (*Quercus liaotungensis*) showed that the indigenous oak had higher drought tolerance than black locust.

(3) Studies of ecosystem functions showed that plantations of black locust developed more severe micro-environments and were less sustainable than natural forests in terms of their nutrient cycling. As a result, we proposed the necessity for ecosystem restoration using native plant species (Tateno et al. 2007).

【Publication list】

- Abou El-Hassan WH, Kitamura Y, Solomon H, Meleha M, Hasegawa K, Effect of subsurface drainage on rice cultivation and soil salinity in the Nile Delta. Transactions of The Japanese Society of Irrigation, Drainage and Reclamation Engineering, 73(2): 43-52, 2005.
- Abou El-Hassan WH, Zayed BA, Kitamura Y, Shehata SM, Zahor Ahmad and Faridullah, Effect of reuse drainage water management on rice growth, yield and water use efficiency under saline soils of Egypt. Asian Journal of Plant Sciences, 5(2): 287-296, 2006a.
- Abou El-Hassan WH, Kitamura Y, Gamal FS, Eneji AE, Assessment of surge irrigation technique under furrow irrigation system in the Nile Delt. International Journal of Agricultural Research, 1(5): 462-470, 2006b.
- Abou El-Hassan WH, Kitamura Y, Yang SL, Inosako K, Shimizu K, Nishiyama S, Effect of drainage water reuse on rice cultivation in the Nile Delta, Egypt. Journal of Sand Dune Research, 53(1): 19-32, 2006c.
- Abou El-Hassan WH, Kitamura Y, Inosako K, Shimizu K, Nishiyama S, Effect of water management and tillage practices on rice yield, water use efficiency and physical properties of paddy soil in the Nile Delta. Transactions of The Japanese Society of Irrigation, Drainage and Reclamation Engineering, 74(4): 39-47, 2006d.
- Al-Busaidi A, Yamamoto T, Inoue T, Irshad M, Mori Y, Tanaka T, Effects of seawater salinity on salt accumulation and barley (*Hordeum vulgare* L.) growth under different meteorological conditions. Journal of Food, Agriculture & Environment, 5 (2): 2007.
- Andry H, Yamamoto T, Rasiah V, Fukada M, Improving the Resistance of an Acid Soil to Water Erosion Using Artificial Zeolite and Hydrated Lime Amendments. Transactions of the Japanese Society of Irrigation, Drainage and Reclamation Engineering, 247: 53-64, 2007a.
- Andry H, Yamamoto T, Inoue M, Effectiveness of Hydrated Lime and Artificial Zeolite Amendments and Sedum Plant Cover in Controlling Soil Erosion from an Acid Soil. Australian Journal of Soil Research, 45: 266-279, 2007b. <<ORIGINAL PAPER>>
- Dehghanisanij H, Agass M, Anyoji H, Yamamoto T, Inoue M, Eneji AE, Improvement of saline

water use under drip irrigation system. Agricultural Water Management, 85(3): 233-242, 2006.

- Du S, Yamanaka N, Yamamoto F, Otsuki K, Wang S, Hou Q, The effect of climate on radial growth of Quercus liaotungensis forest trees in Loess Plateau, China. Dendrochronologia, 25: 29-36, 2007.
- Eneji AE, Honna T, Yamamoto S, Saitoh T, Masuda T, Nitrogen Transformation in Four Japanese Soils Following Manure + Urea Amendment. Communications in Soil Science and Plant Analysis, 33(1&2): 53-66, 2002.
- Eneji AE, Irshad M, Honna T, Yamamoto S, Endo T, Masuda T, Potassium, calcium, and magnesium mineralization in manure-treated soils. Communications in Soil Science and Plant Analysis, 34 (11-12): 1669-1679, 2003a.
- Eneji AE, Honna T, Yamamoto S, Masuda T, Endo T, Irshad M, Changes in humic substances and phosphorus fractions during composting. Communications in Soil Science and Plant Analysis, 34 (15-16): 2303-2314, 2003b.
- Eneji AE, Honna T, Yamamoto S, Masuda T, Influence of composting conditions on plant nutrient concentrations in manure compost. Journal of Plant Nutrition, 26(8): 1595-1604, 2003c.
- Eneji AE, Honna T, Yamamoto S, Irshad M, The Relationship Between Total and Available Heavy Metals in Composted Manure. Journal of Sustainable Agriculture, 23 (1): 125-134 , 2003d.
- Eneji AE, Yamamoto S, Wen G, Inanaga S, Honna T, A comparative evaluation of wet digestion and dry ashing methods for the determination of some major nutrients in composted manure. Toxicological & Environmental Chemistry, 87(2): 147- 158, 2005.
- Endo T, Yamamoto S, Honna T, Enej AE, Sodium-Calcium Exchange Selectivity as Influenced by Clay Minerals and Composition. Soil Science, 167(2): 117-125, 2002.
- Hennintsoa A., Yamamoto T, Rasiah V, Fukada M, Improving the resistance of an acid soil to water erosion using artificial zeolite and hydrated lime amendments. Transactions of the Japanese Society of Irrigation, Drainage and Reclamation Engineering, 247: 53-64, 2007.
- Irshad M, Enej AE, Honna T, Yamamoto S, Endo T, Nitrogen use and relationship between maize biomass and nutrient content in saline and non-saline soils. Sand Dune Research, 48(2): 49-56, 2002a.
- Irshad M, Yamamoto S, Eneji AE, Honna T, Endo T, Influence of Composted Manure and salinity on Growth and Nutrient Content of Maize Tissue. Sand Dune Research, 49(1): 1-9, 2002b.
- Irshad M, Yamamoto S, Eneji AE, Honna T, Endo T, Urea and Manure Effect on Growth and Mineral Contents of Maize under Saline Conditions. Journal of Plant Nutrition, 25(1): 189-200, 2002c.

- Irshad M, Honna T, Eneji AE, Yamamoto S, Wheat Response to Nitrogen Source under Saline Conditions. Journal of Plant Nutrition, 25(12): 2603-2612, 2002d.
- Irshad M, Honna T, Yamamoto S, Endo T, Eneji AE, Yamasaki N, The Effect of Salt Types on Nitrogen Release in Manured Soil. Sand Dune Research, 51(2): 67-74, 2004a.
- Irshad M, Honna T, Yamamoto S, Kato M, Endo T, Zahoor A, Interaction of Saline Water and Nitrogen on the Partitioning and Statistical Correlation of Mineral Elements in Maize Plant. Acta Agronomica Hungarica, 52 (2): 149 –156, 2004b.
- Irshad M, Yamamoto S, Honna T, Trace Elements Solubilization in Waste Amended Saline-Sodic Conditions. J. Food, Agriculture & Environment, 2 (3 & 4): 255-259, 2004c.
- Irshad M, Honna T, Yamamoto S, Eneji AE, Yamasaki N, Nitrogen Mineralization under Saline Conditions.Commun. Soil Sci. Plant Anal., 36(11 &12): 1681-1689 ,2005.
- Ishii Y, Sakamoto K, Yamanaka N, Wang L, Yoshikawa K, Light acclimation of needle pigment composition in Sabina vulgaris seedlings under nurse plant canopy. Journal of Arid Environments, 67: 403-415, 2006.
- Kitamura Y, Yano T, Honna T, Yamamoto S, Inosako K, Causes of farmland salinization and remedial measures in the Aral Sea basin - Research on water management to prevent secondary salinization in rice-based cropping system in arid land. Agricultural Water Management, 85(1-2): 1-14, 2006. <<ORIGINAL PAPER>>
- Otsuki K, Yamanaka N, Du S, Yamamoto F, Xue Z, Wang S, Hou Q, Seasonal Changes of Forest Ecosystems in an Artificial Forest of Robinia pseudoacacia in the Loess Plateau in China. Journal of Agricultural Meteorology, 60(5): 613-616, 2005.
- Ould Ahmed BA, Yamamoto T, Inoue M, Anyoji H, Drip irrigation schedules with saline water for sorghum under greenhouse condition. Transactions of the Japanese Society of Irrigation, Drainage and Reclamation Engineering, 244: 133-141, 2006.
- Ould Ahmed BA, Yamamoto T, Rasiah V, Inoue M, Anyoji H, The impact of saline water irrigation management options in a dune sand on available soil water and its salinity. Agricultural Water Management, 88: 63-72, 2007a. <<ORIGINAL PAPER>>
- Ould Ahmed BA, Yamamoto T, Inoue M, Interaction of temperature and solar radiation effect sorghum growth under drip irrigated saline water. Asian Journal of Plant Sciences, 6(2): 359-363, 2007b.
- Ravolonantenaina, AH, Rakotondrainibe JH, Yamamoto T, Eneji AE, Yasuda H, Technical evaluation of the borehole project in Mahajanga region of Madagascar and its effect on rural development. Transactions of the Japanese Society of Irrigation, Drainage and Reclamation Engineering, 244: 215-225, 2006.
- Solomon H, Kitamura Y, Li Z, Yamamoto S, Yang SL, Li P, Waleed A, Otagaki K, Classification of salinization processes in Luohui Irrigation Scheme, China -Part of water

management research to prevent salinization in semiarid land-. Journal of Arid Land Studies, 15(2): 89-105, 2005.

- Solomon H, Kitamura Y, Traditional irrigation management in Betmera-Hiwane, Ethiopia: the main peculiarities for the persistence of irrigation practices. Journal of Mountain Science, 3(2): 139-146, 2006.
- Tateno R, Tokuchi N, Yamanaka N, Du S, Otsuki K, Shimamura T, Xue Z, Wang S, Hou, Q, Comparison of litterfall production and leaf litter decomposition between an exotic black locust plantation and an indigenous oak forest near Yan'an on the Loess Plateau, China. Forest ecology and Management, 241: 84-90, 2007. <<ORIGINAL PAPER>>
- Yamada M, Fujiyama H, Endo T, Rikimaru UM, Sasaki Y, Yamamoto S, Honna T, Yamamoto T, Effect of K-type and Ca-type artificial zeoliotes applied to high sodic soil on the growth of plants different in salt tolerance. Soil Science and Plant Nutrition, 53: 471-479, 2007. <<ORIGINAL PAPER>>
- Yamamoto T, DehghaniSanij H, Agassi M, Rehabilitation techniques for degraded, irrigated soil in arid lands. Journal of International Society for Southeast Asian Agricultural Sciences, 10(1): 41-50, 2004.
- Yang SL, Takeuchi S, Yano T, Kitamura Y, Evapotranspiration from citrus trees growing in sandy soil under drip irrigation with saline water. Science in China (Series D), 45(0): 41-46, 2002a.
- Yang SL, Yano T, Aydin M, Kitamura Y, Takeuchi S, Short term effects of saline irrigation on evapotranspiration from lysimeter-grown citrus trees. Agricultural Water Management, 56(2): 131-141, 2002b.

3) Plant Production group

The plant production group focused its research in three main areas: "Mechanisms for the improvement of crop drought tolerance", "Cloning of genes related to drought tolerance and their use to generate drought-tolerant plants", and "Increased crop production by controlling root-parasitic weeds". They accomplished the following achievements:

Mechanisms for the improvement of crop drought tolerance

(1) Silicon application improved the drought tolerance of sorghum in dry soils by enhancing the water uptake ability of the plants (hydraulic conductivity) and by promoting root elongation (Hattori et al. 2005).

(2) The drought tolerance of a Sudanese sorghum cultivar was associated with its high ability to develop its root system (by branching and the growth of lateral roots, and the emergence

of nodal roots from higher internodes) in dry soils (Tsuji et al. 2005).

(3) Porous glass material (PGM) was able to absorb phosphates in wastewater, and the release of phytoavailable phosphates from PGM incorporated in the soil improved the growth of tomato plants (Nakazawa et al. 2006).

(4) Patterns of uptake and distribution of $^{22}Na^{+}$ in the leaves of several glycophtyes were investigated. Pumpkin plants accumulated and concentrated $^{22}Na^{+}$ in the proximal part of the petiole and transported very few $^{22}Na^{+}$ to leaf blade. Introduction of this mechanism for the regulation of sodium mobility in other species would generate new lines with higher salinity tolerance (Yamada et al. 2002).

Cloning of genes related to drought tolerance and their use to generate drought-tolerant plants

Three new genes whose expression was induced by drought or salinity stress were isolated from rice using the cDNA subtraction method (Qi et al. 2004, 2005a, 2005b). The expression of these genes was increased not only by drought or salinity but also by submergence, exposure to ethylene and abscisic acid, and other factors. One of the genes resembles the *E. coli* antiporter-regulating protein, and was named *OsARP*. We generated transgenic tobacco plants that overexpressed *OsARP* and confirmed that the transgenic plants showed higher salinity and drought tolerance.

Because evidence suggests that reactive oxygen species are prominent causes of plant damage under salinity and drought stress, we generated four kinds of transgenic tobacco, with enhanced production of superoxide dismutase (Badawi et al. 2004a), ascorbate peroxidase (Badawi et al. 2004b), dehydroascorbate reductase (Eltayeb et al. 2006), or monodehydroascorbate reductase (Eltayeb et al. 2007) and confirmed that all the transgenic plants showed more tolerance to salinity and drought stress.

Increased crop production by controlling root-parasitic weeds

Witchweed (*Striga* spp.) is a group of obligate root-parasitic weeds that are a scourge of agriculture and food security in many semiarid areas. One important aspect of the biology of these parasites that may permit the development of control methods is their requirement for signaling molecules that indicate the presence of suitable hosts. These molecules including (including germination stimulants) can induce germination of the seeds of these parasites in the absence of host roots or at great distances from these roots ("suicidal germination"). We have isolated two compounds (strigol and its deoxy derivative) from *Menispermum dauricum* and *Lotus japonicus* root cultures, respectively, demonstrating that these germination stimulants are of plant origin. We confirmed the involvement of endogenous ethylene in the germination of *Striga hermonthica*. The expression of ACC synthase and ACC oxidase genes in the seeds was

found to respond to a germination stimulant and to pretreatment in a moist warm environment, respectively.

【Publication list】

- An P, Inanaga S, Li XJ, Eneji AE, Zhu NW, Interactive effects of salinity and air humidity on two tomato cultivars differing in salt tolerance. Journal of Plant Nutrition, 28: 459-475, 2005.
- An P, Inanaga S, Zhu NW, Li XJ, Fadul HM, Mars M, Plant species as indicators of the extent of desertification in four sandy rangelands. African Journal of Ecology, 45: 94-102, 2007.
- Badawi GH, Yamauchi Y, Shimada E, Sasaki R, Kawano N, Tanana K, Tanaka, K, Enhanced tolerance to salt stress and water deficits by overexpressing superoxide dismutase in tobacco (*Nicotiana tabacum*) chloroplasts. Plant Science, 166(4): 919-928, 2004a.
- Badawi GH, Yamauchi Y, Shimada E, Sasaki R, Kawano N, Kubo A, Tanaka, K, Enhanced tolerance to salt stress and water deficits by overexpressig ascorbate peroxidase in tobacco (*Nicotiana tabacum*) chloroplasts. Physiolgia Plantarum, 121: 1-8, 2004b.
- Eltayeb AE, Kawano N, Badawi GH, Kaminaka H, Sanekata T, Morishima I, Shibahara T, Inanaga S, Tanaka K, Enhanced tolerance to ozone and drought stresses in transgenic tobacco overexpressing dehydroascorbate reductase in cytosol. Physiologia Plantarum, 127: 57-65, 2006.
- Eltayeb AE, Kawano N, Badawi GH, Kaminaka H, Sanekata T, Morishima, Shibahara T, Inanaga S , Tanaka K, Overexpression of monodehydroascorbate reductase in transgenic tobacco confers enhanced tolerance to ozone, salt and polyethylene glycol stresses. Planta, 225(5): 1255-1264, 2007. <<ORIGINAL PAPER>>
- Hattori T, Inanaga S, Araki H, An P, Morita S, Luxov M, Lux A, Application of silicon enhanced drought tolerance in Sorghum bicolor. Physiologia Plantarum, 23(4): 459-466, 2005. <<ORIGINAL PAPER>>
- Inoue T, Inanaga S, Sugimoto Y, El-Siddig K, Contribution of pre-anthesis assimilates and current photosynthesis to grain yield, and their relationships to drought resistance in wheat cultivars grown under different soil moisture. Photosynthetica, 42 (1): 99-104, 2004.
- Nakazawa R, Tomemori H, Hirano A, Mochizuki H, An P, Inanaga S, Effects of application of porous glass materials treated with phosphate on the growth of tomato plants and phyto-available phosphate in soil. Soil Science and Plant Nutrition, 52(4): 540-544, 2006. <<ORIGINAL PAPER>>
- Qi Y, Yamauchi Y, Ling J, Kawano N, Li D, Tanaka K, Cloning of a putative monogalactosyldiacylglycerol synthase gene from rice plants (*Oryza sativa* L.) and its expression in response to submergence and other stresses. Planta, 219: 450-458, 2004. <<ORIGINAL PAPER>>

- Qi Y, Yamauchi Y, Ling J, Kawano N, Li D, Tanaka K, The submergence –induced gene OsCTP in rice (*Oryza sativa* L.) is similar to *Escherichia coli* cation transport protein ChaC. Plant Science, 168(1): 15-22, 2005a.
- Qi Y, Yamauchi Y, Ling J, Kawano N, Li D, Tanaka K, Identification and cloning of a submergence induced gene OsGGT (glycogenin glucosyltransferase) from rice (*Oryza sativa* L.) by suppression subtractive hybridization. Planta, 221: 437-445, 2005b.
- Tsuji W, Inanaga S, Araki H, Morita S, An P, Sonobe K, Development and distribution of root system in two grain sorghum cultivars originated from Sudan under drought stress. Plant Production Science, 8(5): 553-562, 2005. <<ORIGINAL PAPER>>
- Yamada S, Takeoka A, Yamauchi M, 22Na+ and 36Cl- mobility in salinized excised leaves of several crop plants. Soil Sciecne and Plant Nutrition, 48(1): 23-29, 2002.
  <<ORIGINAL PAPER>>

4) Utilization of Natural Energy group

The Utilization of Natural Energy group has focused on the development of systems for generating electric power and producing water based on natural energy sources such as wind and solar power. As in the other research groups, the goal is to find ways to combat desertification and support greening of the desert. This work focused on two main areas: research on wind turbines suitable for use in desert environments, and the development of a device for extracting fresh water from moist air.

Development of a wind turbine suitable for desert environments

To develop a wind turbine suitable for desert environments, we developed three wind turbines for use in wind tunnel and field experiments: a multi-stage Savonius wind turbine, a straight-bladed vertical-axis wind turbine (VAWT), and a horizontal-axis wind turbine (HAWT). The three designs were compared in terms of their performance characteristics (e.g., torque).

The torque variation of a three-stage out-phase Savonius rotor decreases to about 1/6 of one-stage rotor. This small torque variation prevents the vibration that causes problems for one-stage rotors. Also, the three-stage out-phase Savonius rotor begins to rotate at lower wind velocities (the starting performance improved). Increasing the number of guide vanes of a Savonius rotor improves its starting performance; however, it also decreases the torque at high rotation speeds (Hayashi et al. 2004a, 2005b; Li et al. 2006).

Experimental analysis of the torque variation during one rotation of a straight-bladed VAWT, whose performance does not depend on wind direction (unlike a Savonius rotor), demonstrated its effectiveness. To improve the aerodynamic efficiency of this VAWT, we developed

equipment for measuring the aerodynamic characteristics of straight blades (i.e., two-dimensional wings) based on the use of two force sensors. Under the conditions of a moderate Reynolds number (Re = 150 000) that a small wind turbine blade sees, the aerodynamic characteristics (lift, drag, and moment efficiencies) of a two-dimensional wing moving at pitch frequencies of 0.16, 0.22, and 0.33 Hz, with an angle of attack between 4° and 20°, showed hysteresis. The hysteresis characteristics became unacceptably large as the pitch frequency increased (Hara et al. 2005b, 2005c).

Wind speed was varied like a sine wave by a special wind tunnel, and the performance of a straight-bladed VAWT was monitored under these conditions. Increasing the number of rotor blades improved the ability of the VAWT to respond rapidly to variations in wind speed. As a result of the transient-response characteristics of the VAWT in response to increasing wind speed, the rotor torque first increased, then the rotational speed increased (Kang et al. 2005).

For a wind turbine installed in hilly terrain, as in China's Loess Plateau, the wind is expected to flow uphill so that it blows upwards against the wind turbine rather than horizontally. To adapt a VAWT to such conditions, we developed an advanced VAWT with inclined straight-blades around a vertical axis for use in field tests. The possibility of torque increase by inclined blades for wind blowing upward or downward was demonstrated in the wind tunnel test. (Hara et al. 2005a)

Development of a device for extracting fresh water from moist air

To develop a device capable of extracting fresh water from moist air, we used a thermoelectric module equipped with Peltier devices to cool the air below its dew point.

Experiments were conducted in a controlled-environment chamber under several combinations of constant temperature and relative humidity so that we could investigate the effects of these parameters, as well as of the air flow rate, on the rate of water production. Water production increased at high relative humidity and with increasing air flow rate. However, water production began to decrease when the temperature of the cooled air in the device approached the dew point as a result of high air flow rates. As the air flow increased, the water production of heat exchanger with widths of 120 mm became bigger than that of heat exchanger with widths of 80 mm. The maximum water production was achieved when the temperature of the cooled air in the device fell to 2.5 to 4.8 °C below the dew point (Hayashi et al. 2004a, b, c).

Results of field experiments

As the first step in field experiments to test the ability to produce electric power and fresh water utilizing natural energy sources, we used experimental results and observed

meteorological data to simulate the energy and water production rates for the Tottori Sand Dune area. In this simulation, we assumed that operation of the water extraction device was controlled by both the dew point and the battery level. The water production rates were then calculated using a range of dew points and wind turbine performance levels (Hayashi et al. 2005d).

To validate these results, a field test of the system was carried out in the Tottori Sand Dune area in August 2005, and photovoltaic modules were used as the power source. This test demonstrated the system's ability to produce water using Peltier devices. The system produced a total of 12.7 kg of water in August 2005. The water production during the summer depended strongly on the operation efficiency of the system, which it was defined as the ratio of total hours during which it was able to operate to total hours of a month. The values of relative humidity and dew point in August were sufficiently high to satisfy the system's operational requirements. Since the relative humidity and dew point change gradually, the operation of the system depends primarily on the battery's voltage. The results also showed that the optimal period for producing water was from night to early morning. These results suggested that it will be necessary to increase the system's battery capacity or to change the system's controller so that it operates only during the optimal period. Nonetheless, the system developed during this study proved to be highly durable and reliable, without any equipment failures during the 2-year field experiment.

Moreover, the novel water-extraction device provided high performance (water production) and a compact design. (A patent for the device has been filed with the Patent Office of Japan.)

【Publication list】

- Hara Y, Kang I, Hayashi T, Paraschivoiu I, Measurements of Torque Characteristics of a Vertical Axis Wind Turbine with Inclined Straight Blades. The EXPO World Conference on Wind Energy, Renewable Energy, Fuel Cell (WCWRF 2005), Hamamatsu, Japan, CD-ROM, 2005a.
- Hara Y, Kang I, Moriya T, Ariyasu K, Hayashi T, Development of a Measuring System with Two Force Sensors of Aerodynamic Forces Acting on a Two-Dimensional Wing. The 6th KSME-JSME Thermal and Fluids Engineering Conference, Jeju, KOREA, CD-ROM, JE.08, 2005b.
- Hara Y, Kang I, Moriya T, Hayashi T, Aerodynamic Forces on an Airfoil in Pitching and/or in a Periodically Varying Wind. Proc. the 30th Annual Congress of the American Romanian Academy of Arts and Sciences (ARA), Chisinau, Moldova: 559-562, 2005c.

  <<ORIGINAL PAPER>>
- Hayashi T, Liu W, Sassa K, Hara Y, Possibility of Using a Mini Doppler Sodar for Wind

Characteristics Investigation. Proc. 1st World Wind Energy Conference and Exhibition, Berline, Germany, CD-ROM, VD1.21, 2002.

- Hayashi T, Li Y, Hara Y, Suzuki K, Wind Tunnel Tests on a Three-stage Out-phase Savonius Rotor. Proc. 2004 European Wind Energy Conference & Exhibition, London, UK, CD-ROM, 2004a.
- Hayashi T, Liu W, Nozima K, Hara Y, Tagawa K, A Study on a Water Maker System Using Peltier Devices Supplied With Electricity by Wind Power For The Purpose of Use in Arid Regions. Proceedings The 3rd World Wind Energy Conference & Renewable Energy Exhibition The 2nd Wind Power Asia, Beijing China, 2004b.
- Hayashi T, Hara Y, Tagawa K, Liu Y, Tanaka K, Nojima K, Development of Fresh Water Making Systems Using of Peltier Devices or Moisture Absorbent. The 30th Annual Congress of the American Romanian Academy of Art and Sciences (ARA), Chisinau, Moldova: 593-596, 2005a.
- Hayashi T, Li Y, Hara Y, Wind Tunnel Tests on a Different Phase Three-Stage Savonius Rotor. JSME International Journal, Series B, 48(1): 9-16, 2005b. <<ORIGINAL PAPER>>
- Hayashi T, Liu W, Nojima K, Hara Y, Tagawa K, A Study on a Water Maker System using Peltier Devices, The 6th KSME-JSME Thermal and Fluids Engineering Conference, Jeju, KOREA, CD-ROM,JE.08, 2005c. <<ORIGINAL PAPER>>
- Hayashi T, Tanaka K, Hara Y, Liu Y, Nojima K, Tagawa K, A Study on Water Making System Using Renewable Energy in Tottori Sand Dune. Proc. of the EXPO World Conference on Wind Energy, Renewable Energy, Fuel Cell (WCWRF 2005), Hamamatsu, Japan, CD-ROM, 2005d. <<ORIGINAL PAPER>>
- Kang I, Ariyasu K, Hara Y, Hayashi T, Paraschivoiu I, Characteristics of a Straight-Bladed Vertical Axis Wind Turbine in Periodically Varying Wind. The EXPO World Conference on Wind Energy, Renewable Energy, Fuel Cell (WCWRF 2005), Hamamatsu, Japan, CD-ROM, 2005. <<ORIGINAL PAPER>>
- Kang I, Hayashi T, Hara Y, Ariyasu K, A Measurement Method by Wind Tunnel Experiment of the Moment of Inertia of a Vertical Axis Wind Turbine. Renewable Energy 2006, Makuhari Messe, Chiba, Japan, CD-ROM, P-W-23: 889-892, 2006.
- Li Y, Hayashi T, Hara Y, Kawamura T, Performance of Different Phase Three-Stage Savonius Rotor. Renewable Energy 2006, Makuhari Messe, Chiba, Japan, CD-ROM, O-W-4-3: 787-790, 2006.

5) Socio-medical Science group

There have been many studies of common tropical infectious diseases such as malaria,

schistosomiasis, and dengue fever. Such studies have formed the basis for the field of tropical medicine. However, desertification and drought present a serious threat to the well-being and health of the populations in arid and semi-arid areas, yet despite the size and global extent of these populations, there have been few studies of dryland health and medicine. Thus, no specialized area of health science has been established for these regions. The Socio-medical Science group has thus set out to develop the field of dryland health and medicine in an attempt to improve the health of people living in these areas. The group's research has focused on two primary areas: "Simple and acceptable methods for assessing the health of people in arid or semi-arid areas", and "Prevention of diseases specific to arid and semi-arid areas".

Simple and acceptable methods for assessing the health of people in arid or semi-arid areas

Few studies have examined the health or the health-related quality of life (HR-QOL) of populations in arid and semi-arid areas, and no study has identified the factors that influence HR-QOL in these areas. To provide a preliminary basis for assessing health in these areas, we investigated the HR-QOL of inhabitants of China's Loess Plateau by using a 36-item short-form health survey instrument (SF-36) to explore the relationships among social factors, lifestyles, and health conditions and their impacts on HR-QOL (Mu et al. 2007, 2008). This survey was carried out by means of a questionnaire directed at the heads of households or their representatives. HR-QOL was assessed using a three-dimensional survey (SF-36) of general health perceptions, vitality, and general mental health: the potential risk factors capable of influencing HR-QOL were social factors (education, income, medical insurance, and access to medical care), lifestyles (regular physical exercise, cigarette smoking and alcohol intake), and health conditions (chronic diseases and respiratory symptoms). We used partial correlation coefficients and multiple-regression analysis to explore the factors capable of influencing HR-QOL. The HR-QOL scores for women were lower than those for men. The partial correlation coefficients between HR-QOL and chronic diseases, respiratory symptoms, access to medical care, medical insurance, age, and income were statistically significant.

Prevention of diseases specific to arid and semi-arid areas

Table 1 summarizes the most important diseases specific to arid and semi-arid areas.

Table 1. Specific diseases in arid and semiarid areas

- Heat illness
- Respiratory diseases due to dust and sandstorm
- Infectious diseases
  Zoonosis, Malaria
- Nutritional disorders
  Malnutrition, Deficiency of iodine
- Water pollution related diseases
- Disorders due to dryness

Heat-related illnesses include heat cramps, heat exhaustion, and heat stroke. Heat stroke can be particularly severe; it is often fatal when core temperatures rise to more than 40.5 °C. In Saudi Arabia, which has a very hot and dry climate, the number of deaths from heat stroke was more than 1000 during the 1985 Haj season. Most deaths were among pilgrims from outside Saudi Arabia. Our study indicated that rates of sweating were similar under low or high humidity at the same temperature, even though subjects felt less hot at low humidity. This difference between the perception of heat and the actual state of the victim's body may explain why many pilgrims from outside Saudi Arabia suffered heat stoke under the region's hot, dry conditions.

Dust and sandstorms have caused considerable damage to transportation systems, but their impact on public health is less well known. Floating dust can cause pneumoconiosis and is a potential allergen. Diagnosis or assessment of occupational pneumoconiosis is based on exposure to dust, symptoms, lung function tests (spirometry), chest X-rays, and (rarely) biopsies. However, a simple non-invasive method is needed for monitoring non-occupational pneumoconiosis in large populations. Urinary protein 1 (uP1) has been found to be a useful new lung-specific biomarker of several lung diseases. uP1 is a low-molecular-weight protein (16 kDa) synthesized by the non-ciliated bronchiolar Clara cells and secreted in large amounts into the lumen of the lungs. We investigated the relationship between uP1 values and changes in lung function as a result of pneumoconiosis (Kotani et al. 2007). The results suggest that measurement of uP1 may become a useful non-invasive index of the fibrotic changes that occur in pneumoconiosis.

【Publication list】

- Kotani K, Kawabata I, Mu H, Kurozawa Y, Itoh Y, Urinary protein 1/Clara cell 16 concentrations and lung functions in male subjects with pneumoconiosis. Ann Clin Biochem, 44: 560-562, 2007. <<ORIGINAL PAPER>>
- Mu H, Kurozawa Y, Kotani K, Liu G, Liu P, Nishino S, Ito TY, Tsunekawa A, Factors associated with health related quality of life in inhabitants of the Loess Plateau region. CAS-JSPS China-Japan Joint Open Seminar on Combating Desertification and Development in Inland China: 68-69, 2007. <<ORIGINAL PAPER>>
- Mu H, Kurozawa Y, Kotani K, Liu G, Liu P, Tsunekawa A, Nishino S, Ito TY, Health-related quality of life and recognition of desertification among inhabitants of the Loess Plateau region of China: findings for city and village communities. Journal of Environmental Health, 70: 38-43, 2008. <<ORIGINAL PAPER>>

3. Original papers

Full Paper

J. Agric. Meteorol. (農業気象) 60 (2): 103-113, 2004

Heat Balance and Soil Moisture in the Loess Plateau, China

Reiji KIMURA*,†, Makio KAMICHIKA*, Naru TAKAYAMA*,
Nobuhiro MATSUOKA** and Xingchang ZHANG***

* Arid Land Research Center, Tottori University, Tottori, 680-0001 Japan
** Faculty of Horticulture, Chiba University, Matsudo, 271-8510 Japan
*** Institute of Soil and Water Conservation, CAS, Yangling, Shaanxi, 712100 China

Abstract

A three-layer soil model was used for clarifying the heat balance and soil water content in the Loess Plateau, China, and applied to actual bare soil fields (Tottori Sand Dune and Shenmu District, Shaanxi Province, China). The difference between the observed and calculated evaporation per day was approximately 0.18 mm (5 W m^{-2}) to 0.21 mm (6 W m^{-2}). Because of its moderate mixture of sand, silt and clay, yellow loessial soil in Shenmu affects water retentivity and restriction of evaporation from the soil surface. The seasonal change of heat balance and soil water content was examined using meteorological data in Yulin near Shenmu. The annual means of sensible heat and latent heat flux were 23 W m^{-2} and 19 W m^{-2} (239 mm per year), respectively. The soil water content of the second and third layers remained comparatively high in winter.

Key words: Heat balance, Loess Plateau, Soil water content.

1. Introduction

The Loess Plateau in China is located in Long. 100-115°E and Lat. 34-40°N, and its range corresponds almost exactly to the middle reaches of the Hwang Ho (Yellow River). Annual precipitation is approximately 400 mm (minimum 150 mm, maximum 750 mm) with variability in time and space (Yang and Shao, 2000). According to the water deficit index *WDI* by Wang and Takahashi (1999) and aridity index by UNEP (1997), the Loess Plateau belongs to the semi-arid region. Compounding the problem is improper land use such as the over-cultivation, over-pasturing, and the over-deforestation, which resulted in the serious problem of desertification after the 17th century (Tamura, 1990). Yellow loessial soil is transported into rivers, and carried by winds to other countries, such as Japan. Additionally, for the people who inhabit the Loess Plateau, securing enough water for their daily needs is difficult. About 60 million people including farmers live here in spite of such an unstable condition. For several years, however, the reduction of farmland and promotion of greening have been recommended by the Chinese government. The need for an increase in vegetation is surely admitted in such a place. It is thought that important findings for dealing with desertification can be obtained by continuously monitoring such a greening region.

The amount of existing vegetation realistically shows the progressive degree of desertification, and the most important factor that supports plant production is soil moisture, which is the result of the heat and water balances. Consequently, the monitoring of desertification is possible by considering the relationship among the kind of existing vegetation, amount of existing vegetation, and the soil water content (Shinoda, 2002). That is, the seasonal change of the heat and water balances can become an important factor in searching for the current state of desertification. However, no detailed study on the seasonal change of the heat and water balances for bare soil surfaces in the whole area of the Loess Plateau has been carried out.

The following study was conducted to clarify the quantitative formulation of heat balance and soil water content for bare soil surface on the Loess Plateau. First, the soil model developed by Kondo and Xu (1997) was employed to calculate heat bal-

† Corresponding author: E-mail rkimura@alrc.tottori-u.ac.jp
Received on June 30, 2003.
Accepted on January 29, 2004.

ance and soil water content. The soil model by Kondo and Xu (1997) delimited the soil depth of 70 cm into ten layers in detail. In this study, a simple three-layer soil model in which the 70 cm soil depth was delimited to three layers (0–2, 2–22 and 22–70 cm) was applied in consideration of the depth of the root zone. Because the depth of the root zone is deep in a semi-arid region like the Loess Plateau, the number of such thick layers can be added to this model in considering the vegetation in the future. If the soil layers are delimited in detail, the model calculation is very complicated because of the complexity of weighting for the distribution of the root. The model was verified by comparing the observed results in the Tottori Sand Dune and the Loess Plateau (Shenmu District, Shaanxi Province, China). Next, the features of yellow loessial soil in Shenmu were defined by considering soil physics characteristics obtained by indoor experiments and model calculation. Finally, the seasonal variation of heat balance and soil water content was examined using meteorological data in Yulin near Shenmu.

2. Three-Layer Soil Model

The model divided the soil into three layers: 0–2, 2–22 and 22–70 cm. The time series of the vertical water movement by liquid and vapor phases, the volumetric soil water content in respective soil layers, and heat balance were calculated using the initial value and boundary conditions (Fig. 1). The initial and boundary conditions for water and thermal regimes were the same as those of Kondo and Xu (1997). The boundary conditions of the ground surface and the bottom, that is, $(Q_{liq})_{z=0}$, $(Q_{vap})_{z=0}$, $(Q_{liq})_{bottom}$, $(Q_{vap})_{bottom}$, are represented in Fig. 1. At the bottom, the heat exchange was assumed not to take place. The initial conditions of the volumetric soil water content θ and the soil temperature T_G will described in Chapters 3 and 5.

2.1 Heat balance on soil surface

The heat balance of the soil surface can be expressed by (Kondo, 2000)

$$(1-ref)S^{\downarrow}+\varepsilon L^{\downarrow}=\varepsilon\sigma T_s^4+H+lE+G. \quad (1)$$

Here, *ref* is the albedo of soil surface, $S^{\downarrow}$ the global solar radiation ($W\,m^{-2}$), ε the emissivity of the soil surface (assumed as unity in this study), $L^{\downarrow}$ the downward longwave radiation ($W\,m^{-2}$), σ the Stefan-Boltzman constant ($5.67\times10^{-8}\,W\,m^{-2}\,K^{-4}$), T_s the soil surface temperature (K), H the sensible heat flux ($W\,m^{-2}$), lE the latent heat flux ($W\,m^{-2}$), and G the soil heat flux ($W\,m^{-2}$).

The values of H and lE are given by (Kondo, 2000)

$$H=c_p\rho C_H U(T_s-T), \quad (2)$$

$$lE=l\rho C_H U\beta\{hq_{sat}(T_s)-q\}, \quad (3)$$

where

$$\beta=\frac{1}{1+C_H U(F/D)}, \quad (4)$$

$$h=\exp\left(\frac{g\psi(\theta)}{R_w T_G}\right), \quad (5)$$

$$F=f_A\exp(-f_B\theta^3)+f_C\left[\cos\left(\frac{\pi}{2}\frac{\theta}{\theta_{sat}}\right)\right]^{f_D},$$

$$0\leqq\theta<\theta_{sat}. \quad (6)$$

In the above, c_p is the specific heat of air ($J\,kg^{-1}\,K^{-1}$); ρ, the density of air ($kg\,m^{-3}$); C_H, the bulk transfer coefficient for sensible heat; U, T, and q the wind speed ($m\,s^{-1}$), temperature (℃) and specific humidity ($kg\,kg^{-1}$), respectively, at the observation height z (m); q_{sat} (T_s), the specific humidity at saturation at temperature T_s (K); l, the latent heat ($J\,kg^{-1}$) of evaporation of water; β, the evaporation efficiency by Kondo and Xu (1997); h, the relative humidity when the water vapor and liquid water are in equilib-

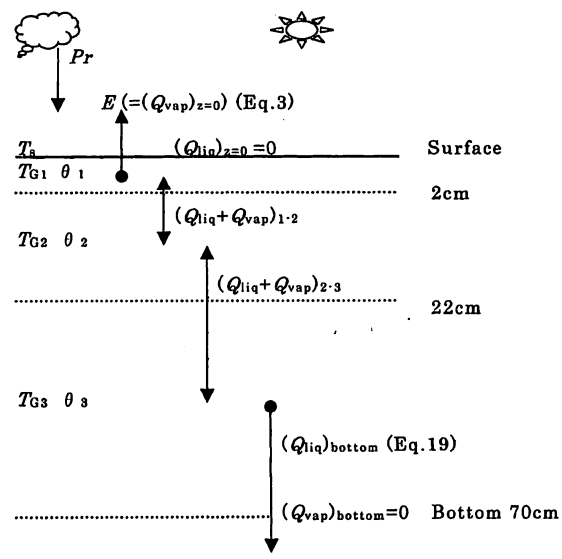

Fig. 1. Schematic representation of the three-layer soil model in this study. *Pr* is the precipitation; *E*, the evaporation; T_s, the surface temperature; T_{G1}, T_{G2} and T_{G3}, the soil temperature in respective layers; θ_1, θ_2 and θ_3, the volumetric soil water content in respective layers, Q_{liq}, the liquid phase of the water flux; Q_{vap}, the vapor phase water flux.

rium in small soil pores by Kondo and Xu (1997); F, the diffusion distance of water vapor (m) by Kondo and Xu (1997); D, the coefficient of molecular diffusion of water vapor in the air ($=2.54\times10^{-5}\,m^2\,s^{-1}$); g, the acceleration of gravity ($m\,s^{-2}$); $\psi(\theta)$, the soil water potential for the volumetric soil water content θ ($m^3\,m^{-3}$) (m); R_w, the gas constant of water vapor ($=461.5\,m^2\,K^{-1}\,s^{-2}$); T_G, the soil temperature (℃); f_A, f_B, f_C, and f_D the soil parameters defined in Eq. (6) (Table 1); and θ_{sat}, the θ at saturation.

In this study, G is expressed as (Kondo, 1994)

$$G=-\int_0^{0.7}\frac{d(c_G\rho_G T_G)}{dt}dz. \tag{7}$$

Here, c_G is the specific heat of soil ($J\,kg^{-1}\,K^{-1}$), ρ_G the bulk density of soil ($kg\,m^{-3}$), t the time (s), and z the depth (m).

Fukumoto and Hirota (1994) noted that the bulk transfer coefficient C_H can be expressed as

$$C_HU=0.0027+0.0031\times0.74U. \tag{8}$$

The coefficient is 0.74 when the wind speed at 2 m high is converted to that at 0.5 m high (roughness length $z_0=0.01$ m), by assuming the logarithmic wind profile.

T_s can be found through successive approximations of Eq. (1), with the fluxes H, lE and G evaluated from Eqs. (2) to (8).

2.2 Water and heat transfer within the soil

The temporal variation of soil water content and soil temperature in individual layers can be expressed by (Kondo and Xu, 1997)

$$\frac{\partial\theta}{\partial t}=-\frac{1}{\rho_w}\frac{\partial}{\partial z}(Q_{liq}+Q_{vap}), \tag{9}$$

$$\frac{\partial T_G}{\partial t}=-\frac{1}{c_G\rho_G}\frac{\partial Q_h}{\partial z}-\frac{lE_{soil}}{c_G\rho_G}, \tag{10}$$

where

$$Q_h=-\lambda_G\frac{\partial T_G}{\partial z}. \tag{11}$$

Here, ρ_w is the density of water ($=1{,}000\,kg\,m^{-3}$), Q_{liq} is the liquid water flux ($kg\,s^{-1}\,m^{-2}$), Q_{vap} is the water vapor flux ($kg\,m^{-2}\,s^{-1}$), lE_{soil} ($W\,m^{-2}$) is the latent heat flux within the soil, λ_G the thermal conductivity ($W\,m^{-1}\,K^{-1}$), and Q_h is the heat flux in soil ($W\,m^{-2}$). When $z\geqq0.02$ m, lE_{soil} is very small compared with $\partial Q_h/\partial z$, and negligible in the calculation at depths greater than 0.02 m (Kondo and Xu, 1997). The definition of depth between the respective layers, in which heat and water are transferred, is based on a study by Abramopoulos *et al.* (1988). That is, it was defined as the distance between the centers of the each layer. λ_G and $c_G\rho_G$ are given by (Kondo, 1994)

$$\lambda_G=0.251+0.5\theta^{1/3}, \tag{12}$$

$$c_G\rho_G=(1-\theta_{sat})c_s\rho_s+\theta c_w\rho_w, \tag{13}$$

where $c_s\rho_s$ is the thermal capacity of soil ($J\,m^{-3}\,K^{-1}$) and $c_w\rho_w$ is the thermal capacity of water ($=4.2\times10^6\,J\,m^{-3}\,K^{-1}$). The weighting for λ_G and $c_G\rho_G$ between the respective layers is set at 50%.

The liquid water flux Q_{liq} can be expressed by (Kondo and Xu, 1997)

$$Q_{liq}=-\rho_wK\left(\frac{\partial\psi}{\partial z}\right)-\rho_wK, \tag{14}$$

where

$$K=K_{sat}\left(\frac{\theta}{\theta_{sat}}\right)^c, \tag{15}$$

$$\psi=-4\times10^4\cdot\exp(-a\theta)-\frac{10^2}{1+(-10^2/X)},\quad \theta<\theta_{sat}, \tag{16}$$

where

$$X=\psi_{sat}\left(\frac{\theta}{\theta_{sat}}\right)^{-b}, \tag{17}$$

and

$$\psi=0,\quad \theta\geqq\theta_{sat}. \tag{18}$$

Here, K is the hydraulic conductivity ($m\,s^{-1}$); K_{sat}, the K at saturation; a, b and c, the soil parameters; and ψ_{sat}, the soil water potential at saturation. Assuming that the water flux at the bottom (z_{bottom}) occurs only in gravitational potential conditions, it is

Table 1. Soil parameters used in this study. Parameters for Tottori sand and clay loam in Lanzhou are the result from Kondo and Xu (1997).

Soil Place	Sand Tottori	Clay loam Lanzhou	Loess Shenmu
θ_{sat} ($m^3\,m^{-3}$)	0.43	0.53	0.434
θ_r ($m^3\,m^{-3}$)	0.086	0.34	0.19
$-\psi_{sat}$ (m)	0.1	0.04	0.04
K_{sat} ($10^{-5}\,m\,s^{-1}$)	48	0.5	2.4
a	330	80	110
b	0.9	4	4.0
c	6	11.2	10
f_A (m)	0.05	0.02	0.008
f_B (10^3)	9	0.4	7
f_C (10^{-4} m)	4	2	3.2
f_D	0.5	0.5	1.0
$c_s\rho_s$ ($10^6\,J\,m^{-3}\,K^{-1}$)	2.4	2.4	2.4
Soil texture			
Sand (%)	96	19	48
Silt (%)	1	55	39
Clay (%)	3	26	13

given as

$$Q_{liq}(z_{bottom}) = -\rho_w K. \quad (19)$$

In this study, the hydraulic conductivities between the first layer and the second layer K_{1-2} and between the second layer and the third layer K_{2-3} are defined as

$$K_{1-2}=0.9 \cdot K_1+0.1 \cdot K_2, \quad \theta_1<\theta_2, \quad (20)$$

$$K_{1-2}=0.1 \cdot K_1+0.9 \cdot K_2, \quad \theta_1 \geqq \theta_2, \quad (21)$$

and

$$K_{2-3}=0.5 \cdot K_2+0.5 \cdot K_3. \quad (22)$$

Here, K_1, K_2 and K_3 are the hydraulic conductivities for the respective layers. Equations (20) to (22) were determined by comparing the calculated results of liquid water flux with various weightings for the hydraulic conductivity, with that from a 10-layer model having a detailed range from 0 to 2 cm, 2 to 6 cm, 6 to 14 cm, 14 to 22 cm, 22 to 30 cm,··· up to a depth of 70 cm, so as to minimize the difference between them. In considering the liquid water flux between the first and the second layer, the weighting for the hydraulic conductivity is set at 90% for K_1 in Eq. (20) because the thickness and soil water content of the first layer are less than those of the second layer. If a weighting of 50% is given to K_1, water movement from the second layer becomes very large when $\theta_1<\theta_2$. When the soil water content in the first layer is equal to or larger than that in the second layer, the weighting for the hydraulic conductivity is set at 90% for K_2 in Eq. (21). The average of K_2 and K_3 is used for K_{2-3} in Eq. (22). The weighting for K_{2-3} has little effect on the calculated results of the heat balance. The water vapor flux Q_{vap} can be expressed by (Kondo and Xu, 1997)

$$Q_{vap}=\frac{\rho D}{F_n}\left(\frac{d[hq_{sat}(T_G)]}{dz}\right), \quad (23)$$

where

$$F_n=\frac{1.5dz}{\theta_{sat}-\theta}, \quad \theta<\theta_{sat}. \quad (24)$$

Here, F_n is the transport route of water vapor in the soil (m) (Kondo and Xu, 1997), and $q_{sat}(T_G)$ is the saturated specific humidity at the temperature T_G.

As seen in Fig. 1, the liquid water movement between the first layer and the atmosphere, and the water vapor movement at the bottom, are not considered (Kondo and Xu, 1997). The data used in this model are solar radiation, reflected solar radiation, downward longwave radiation, air temperature, wind speed, vapor pressure, and precipitation. Initial conditions are the volumetric soil water content and soil temperature in individual layers.

3. Verification of Three-Layer Soil Model

3.1 Tottori sand

The calculated result was verified using the observed data from the Tottori Sand Dune at the Arid Land Research Center, Tottori University, from 31 May to 7 June, 2002. The soil texture is sand (sand 96%, silt 1% and clay 3%) (Table 1). There was no rainfall during this period. The observation elements were the solar radiation (EKO; MS801), reflected solar radiation (EKO; MS62), downward longwave radiation (EKO; MS202), wind speed (YOUNG; YG3102) at a height of 2 m, precipitation, temperature, and relative humidity (VAISALA; HMP45A). These data were sampled every 10 s, then averaged over 1-h periods. Soil temperature was measured at depths of 1, 4, 10, 18, 26, 34, 42 and 50 cm using

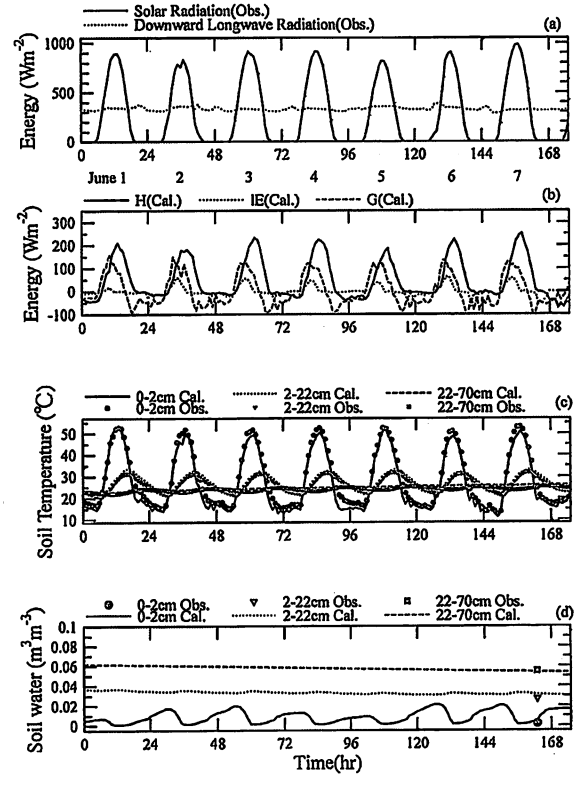

Fig. 2. Diurnal distributions of the (a) observed solar radiation, downward longwave radiation, (b) the calculated sensible heat flux, latent heat flux and soil heat flux, and (c) and (d) the calculated and observed soil temperature and soil water content in respective layers (0–2, 2–22 and 22–70 cm) for the Tottori sand, from 1 June to 7 June 2002 (7 days).

thermocouples. Soil water content was observed by gravimetric sampling at depths of 1, 4, 10, 18, 26, 34, 42, 50, 58 and 66 cm at 1800 JST.

Figure 2 illustrates the diurnal distributions of the observed solar radiation, downward longwave radiation, soil temperature, and soil water content in individual layers (0–2, 2–22 and 22–70 cm), as well as the calculated sensible heat flux, latent heat flux, soil heat flux, soil temperature and soil water content from 1–7 June, 2002 (7 days total). An initial value of the soil water content for the calculation was measured at 1800 JST on 31 May (Fig. 3). As there was no rainfall in this period, a dry soil surface layer (characteristic of sandy soil) developed. On 31 May, the volumetric soil water content in the first layer was 0.004 $m^3 m^{-3}$, with minimal water retentivity.

Figure 2c compares the observed values (filled marks) with the calculated values (lines) of soil temperature in the respective layers. The value for the first layer was observed at a depth of 1 cm; for the second layer, the mean value of observations at 4, 10 and 18 cm were used; and for the third layer, the mean value of observations at 26, 34, 42 and 50 cm were used. At night on 4 to 5 June, the calculated values of the first layer were lower than the observed values. The reason why the difference between them at night is large could not be clarified at the present time. When viewed overall, however, this calculated result was consistent with the actual situation.

Figure 2b presents the calculated results of heat balance, and Fig. 2d compares the observed (filled marks) and calculated (lines) soil water content. In this study, the accuracy of calculated heat energy, especially evaporation, was examined by comparing the observed and calculated soil water content, and accumulated evaporation, for the observation period.

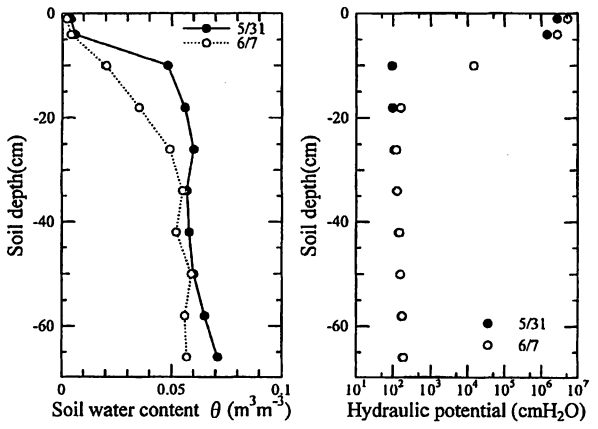

Fig. 3. Vertical distribution of soil water content and hydraulic potential on 31 May (dots) and 7 June (circles).

Accumulated evaporation for the observation period was calculated from the change of soil water content above the zero-flux plane (ZFP). Figure 3 depicts the vertical distribution of volumetric soil water content and hydraulic potential on 31 May and 7 June. The ZFP during this period existed between depths of 10 and 20 cm. The ZFP became deeper with drying by evaporation. Accumulated evaporation during this period was 0.84 mm when ZFP was 10 cm, and 3.2 mm when ZFP was 20 cm. Conversely, accumulated evaporation predicted by the simulation model was 2.1 mm. The difference between the observed and calculated evaporation per day was 0.18 mm (5 $W m^{-2}$). Additionally, the calculated values of the soil water content on the last day (7 June) were consistent with the observed values (Fig. 2d). Daily evaporation for this period ranged from 0.1 to 0.3 mm. The dry soil surface layer restricted evaporation remarkably well.

3.2 Yellow loessial soil in the Loess Plateau

The observation was performed in the experimental station (Liudaogou Basin) located in Shenmu District, Shaanxi Province, China (Fig. 4). In Shenmu, erosion by both wind and water are severe, and the amount of earth and sand deposited into the Yellow River was considered serious (Academia Sinica and Ministry of Water Resources, 1993). The station is located at 38°47′N latitude and 110°21′E longitude. The basin area is 7 km^2, and the altitude is 1,224 m. Most of the land surface is bare soil and short grass. According to statistics from 1957 to 1989 (33 years), the average annual temperature was 8.4℃ (the coldest −9.7℃ in January, the warmest 23.7℃ in July), with an average annual rainfall of 437 mm (minimum 109 mm, maximum 891 mm). These statistics, the water deficit index *WDI* by Wang and Takahashi (1999), and the radiative dryness index by Budyco (1956) indicate that this observatory is in a semi-arid region.

The soil texture in the experimental station is sandy loam (48% sand, 39% silt and 13% clay). The soil parameters used in this study are shown in Table 1. The parameters in Eqs. (15) to (18), which represent the water retention curve and the hydraulic conductivity, were determined using the results ob-

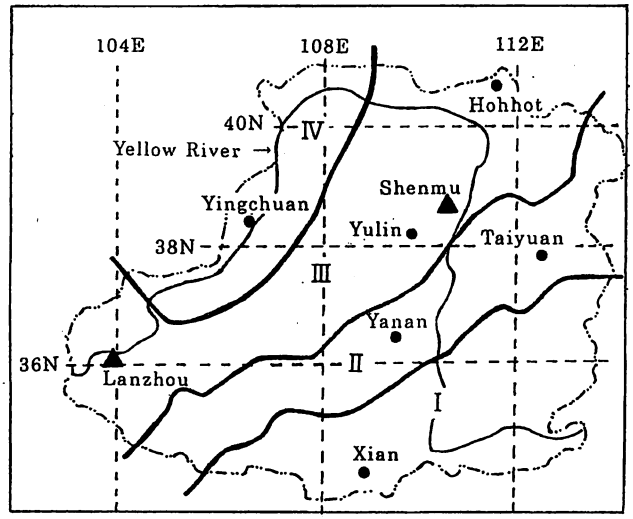

Fig. 4. Location and vegetative classification of the Loess Plateau and experimental site in Shenmu, Shaanxi Province, China. I: Forest. II: Forest and typical grass. III: Short grass. IV: Desert and short grass. This classification was quoted from Yang and Shao (2000). The chain line is the borderline of the Loess Plateau.

served by Yang and Shao (2000). Other parameters were determined by indoor experiments as described in Chapter 4.

Meteorological data were measured from 15 to 18 August 2002 (4 days). Solar radiation, reflected solar radiation, upward longwave radiation, and downward longwave radiation were measured with a four-component radiometer (EKO model MR40). A cup anemometer (YOUNG; YG3102) and ventilated psychrometer (Vaisala model HMP45A) were established at 2 m above the ground. Soil temperatures at 1, 4, 10, 18, 26, 34, 42 and 50 cm were measured by using thermocouples. These data were sampled every 10 s, then averaged over 1-h periods. Soil water content was measured at depths of 1, 4, 10, 18, 26, 34, 42, 50, 58 and 66 cm by gravimetric sampling at 1500 BST.

Figure 5 depicts the diurnal distributions of the observed solar radiation, downward longwave radiation, upward longwave radiation, soil temperature and soil water content in each layer (0–2, 2–22 and 22–70 cm), and the calculated upward longwave radiation ($=\sigma T_s^4$), sensible heat flux, latent heat flux, soil heat flux, soil temperature and soil water content from 15 to 18 August 2002 (4 days). Rainfall measured at 6.4 mm occurred in the evening of 14 August. An initial value of the soil water content for the calculation was measured at 1500 BST on 14 August ($\theta_1=0.0085$, $\theta_2=0.045$, $\theta_3=0.09$).

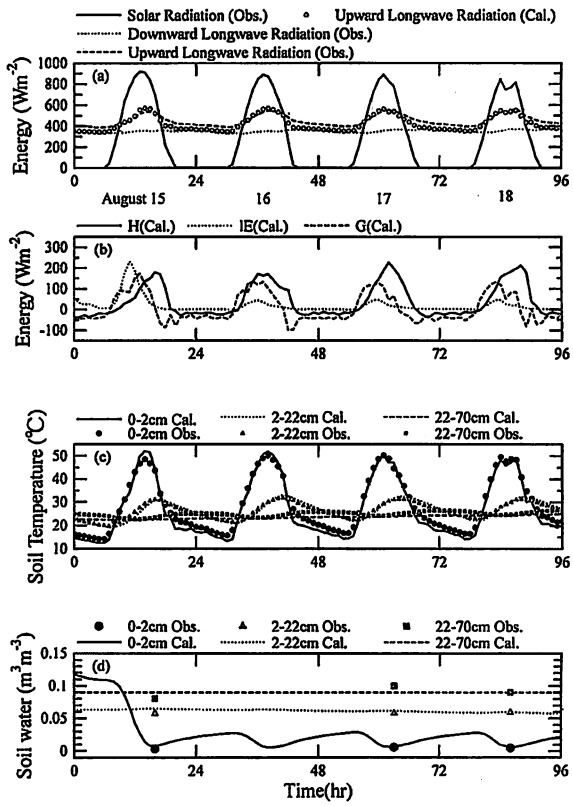

Fig. 5. Diurnal distributions of the (a) observed solar radiation, and downward and upward longwave radiation, and calculated upward longwave radiation, (b) the calculated sensible heat flux, latent heat flux and soil heat flux, and (c) and (d) the calculated and observed soil temperature and soil water content in individual layers (0–2, 2–22 and 22–70 cm) for the yellow loessial soil, from 15 to 18 August 2002.

Figures 5c and 5d compare the observed and calculated values of the soil temperature and soil water content. Calculated values correspond well with observed ones, as in Tottori Sand Dune. However, the calculated values of soil temperature for the first layer and the upward longwave radiation were lower than the observation values at night, as in Tottori Sand Dune.

Accumulated evaporation during the observation period (15 to 18 August) was calculated from the change of soil water content above the ZFP, as described in Section 3. 1. The ZFP during this period existed between depths of 4 and 8 cm. Accumulated evaporation during this period was 0.26 mm when ZFP was 4 cm, and 0.98 mm when ZFP was 8 cm. Conversely, the accumulated evaporation predicted by the simulation model was 1.09 mm. The difference between the observed and calculated evaporation per day was 0.21 mm ($6\,W\,m^{-2}$). This calculation accuracy was almost equal to that (0.173 mm $day^{-1}=5\,W\,m^{-2}$) evaluated by the soil model of Kondo *et al.* (1994) and Kondo and Xu (1997).

4. Features of Yellow Loessial Soil

Figure 6 illustrates the relationship between the volumetric soil water content and soil water potential. The circles represent observed values, and the solid line represents the result from Eq. (16). The dotted line represents Tottori Sand Dune, and the dashed line represents the clay loam in Lanzhou (19% sand, 55% silt, and 26% clay) (Table 1) by Kondo and Xu (1997). Lanzhou is located in the southwestern part of the Loess Plateau (Fig. 4). The soil water characteristics curve of yellow loessial soil is similar to that in Lanzhou. Assuming that the soil water potential at the wilting point is defined as −158.5 m (pF=4.2 was the assumed wilting point in this study) (Kawaguchi, 1991), the volumetric soil water content at the wilting point is 0.06 (Fig. 6). Hence, the soil water content θ_1 and θ_2 during this period did not support plant growth (Fig. 5). Here, θ_1 and θ_2 is the volumetric soil water content for the first and second layers, respectively (Fig. 1).

Figure 7 shows the relationship between the volumetric soil water content and the diffusion distance of water vapor F. The circles represent values observed in indoor experiments, and the solid line the result from Eq. (6). The dotted line represents the Tottori sand, and the dashed line represents the clay loam in Lanzhou, as determined by Kondo and Xu (1997). The value of F determined by indoor experiments can be estimated from Eqs. (3) and (4), that is

$$F=\frac{\rho D[hq_{sat}(T_s)-q]}{E}-\frac{D}{C_H U}. \tag{25}$$

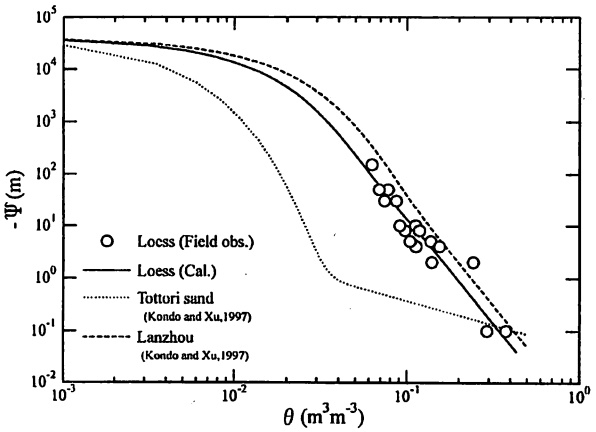

Fig. 6. Relationship between the volumetric soil water content and soil water potential. The circles represent observed values, and the solid line represents the result from Eq. (16) for yellow loessial soil. The dotted line represents the Tottori sand values, and the dashed line represents the values for clay loam in Lanzhou by Kondo and Xu (1997).

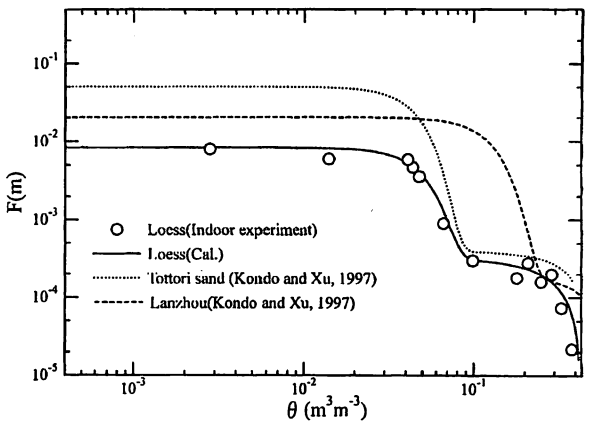

Fig. 7. Relationship between the volumetric soil water content and the diffusion distance of water vapor F. The circles represent values observed in indoor experiments, and the solid line represents the result from Eq. (6) for yellow loessial soil. The dotted line represents the Tottori sand results, and the dashed line represents the results for clay loam in Lanzhou by Kondo and Xu (1997).

F can be estimated by substituting the observed T_s, q, E, and C_HU into Eq. (25) (Kondo and Xu, 1997). As seen in Fig. 7, the relationship between θ and F for yellow loessial soil closely resembles that of Tottori sand, except for the maximum value of F. Resistance to evaporation drastically increases for $\theta \leqq 0.1$ ($m^3 m^{-3}$). Figure 8 depicts the relationship between the volumetric soil water content and the evaporation efficiency β derived using Eq. (4). β for yellow loessial soil drastically decreases for $\theta \leqq 0.1$ ($m^3 m^{-3}$). Assuming that the soil water potential at the field capacity is defined as -1 m (pF=2 was assumed to be the field capacity in this study) (Kawaguchi, 1991), θ at the field capacity (θ_f) of yellow loessial soil was 0.19 ($m^3 m^{-3}$) (Fig. 6). These results indicate that comparatively high evaporation continues up to the field capacity, but evaporation drastically decreases when $\theta \leqq 0.1$ ($m^3 m^{-3}$), because the upward water movement produced by capillary action is restricted due to the soil texture. Water permeability of this soil was comparatively high when compared with the clay loam in Lanzhou (see the value of K_{sat} in Table 1). These properties were reflected in the simulated result of latent heat flux lE in Fig. 5 b. The latent heat flux became large the day after the 14 August rainfall. However, evaporation was again restrained 2 days later (16 August), as in the result for Tottori Sand Dune.

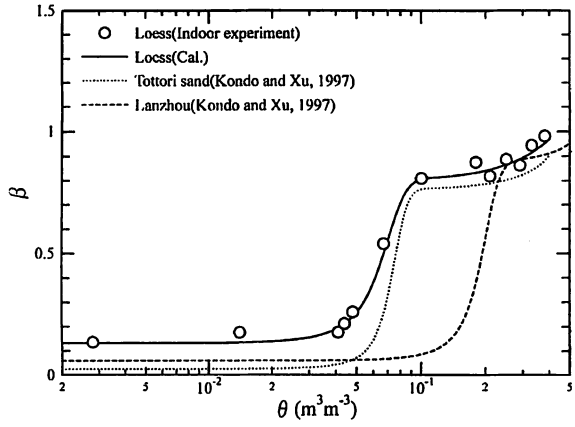

Fig. 8. Relationship between the volumetric soil water content and the evaporation efficiency β (A value of $C_HU=0.02$ m s^{-1} was adopted for the calculation). The circles represent values observed in indoor experiments, and the solid line represents the result from Eq. (4) for yellow loessial soil. The dotted line represents the Tottori sand values, and the dashed line represents the values for clay loam in Lanzhou by Kondo and Xu (1997).

As mentioned above, the following features of yellow loessial soil can be compared to those of Tottori sand and clay loam in Lanzhou:

(1) The water retentivity is superior to that of Tottori sand, and almost the same as that of clay loam in Lanzhou.

(2) The comparatively high evaporation rate continues up to the field capacity θ_f. However, evaporation efficiency drastically decreases when $\theta < \theta_f$ because of restricted upward water movement, as in Tottori sand. Conversely, evaporation from the clay loam continues steadily for a long time due to the capillary action. Figure 9 presents the simulated daily evaporation using the soil parameters for clay loam in Lanzhou. The evaporation rate is higher than that of yellow loessial soil. Although Lanzhou and Shenmu are located on the Loess Plateau, they exhibit quite different heat balances because of differences in soil physics.

(3) Yellow loessial soil affects both water retentivity and restriction of evaporation from the soil surface because of the moderate mixture of sand, silt and clay. This soil can be considered superior from the viewpoint of water retentivity under the top soil layer.

5. Seasonal Change of Heat Balance and Soil Water Content

In this portion of the study, the seasonal change of the heat balance and soil water content was considered using the soil parameters estimated in Chapter 4

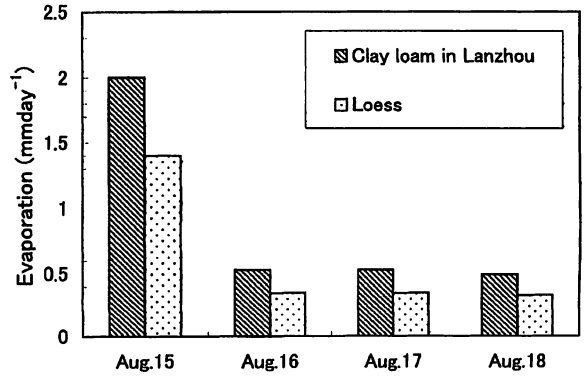

Fig. 9. Calculated daily evaporation using the soil parameters for clay loam in Lanzhou. Meteorological conditions used for the calculation were the same as in Fig. 5.

and meteorological data in Yulin near Shenmu (refer to Fig. 4). Because there was no meteorological observatory in Shenmu, the meteorological data of Yulin, which was the nearest Shenmu, was used. One of the advantages of the model used in this study is that the heat balance can be calculated by using the routine data of the meteorological observatory. Soil properties in Yulin are almost the same as those in Shenmu (Yang and Shao, 2000). The data used in the calculation are sunshine duration, the daily-mean air temperature, the daily maximum and minimum air temperatures, the daily-mean wind speed, the daily-mean specific humidity, and the daily amount of precipitation. Diurnal variations of meteorological data were required for the calculation. For this study, these variations were estimated by using a method of Kondo and Xu (1997). As for the initial conditions of θ and T_G, assumed values of θ and T_G are first substituted. The model calculations are repeated for a timescale of several years or more under the same pattern of weather conditions until θ and T_G in each layer approaches a steady-state. These results are then assumed as the initial conditions of θ and T_G.

When the seasonal variation of the heat balance, soil temperature, and soil water content is calculated, an accurate estimation value cannot be derived by using the boundary condition defined in Chapter 2. However, the boundary condition based on the observation can not be set because there is no observation data. Therefore, in this chapter, the ground soil is divided into 22 layers, the thickness of each layer is 0.02, 0.20, 0.48, 0.48, 0.48 m, $\cdots$, until a depth of 9.82 m is reached. The amplitude of the seasonal change of soil temperature was 0.2℃ in lower boundary (9.82 m). Moreover, the soil water content of the seventh layer was almost constant throughout the year. However, the calculation result of heat balance and soil water content by using the boundary condition defined in this chapter was not so different from the one defined by the boundary condition in Chapter 2 because the heat balance on the ground surface is mainly affected by the layer from surface to 1 m (Xu and Haginoya, 2001). When $T_G \leqq -3$℃, the liquid phase of the water flux Q_{liq} was assumed as zero (Xu and Haginoya, 2001). In Shenmu, it is thought that the air temperature falls to below 0℃, and the soil freezes during winter period. Therefore, it is necessary to consider a latent heat of freezing or melting in the calculation of soil temperature. However, because the soil water content in this region is comparatively small, the effect of latent heat on the change of soil temperature is smaller than the effect of heat conductivity. Consequently, the influence of latent heat was neglected in this study. Figure 10 shows the observed precipitation, calculated daily mean sensible, latent and soil heat fluxes, daily mean soil temperature, and the soil water content of respective layers at 1200 BST for 1999.

The peak of sensible heat flux appeared in summer (70 $W m^{-2}$). The annual mean of sensible heat flux was 23 $W m^{-2}$. The values of latent heat flux closely corresponded to the rainfall events, and the peak value was 110 $W m^{-2}$ (3.9 $mm day^{-1}$). The annual mean of latent heat flux was 19 $W m^{-2}$, and annual evaporation was 239 mm. Therefore, in 1999, 85% of the annual rainfall (283 mm) evaporated. The value of soil heat flux was within ± 20 $W m^{-2}$.

The seasonal change of soil temperature in the first layer T_{G1} and second layer T_{G2} showed the similar tendency. From December to February, the T_{G1} and T_{G2} fell to below 0℃, and the peak reached about −10℃. Takahashi *et al.* (2002) observed the daily mean soil temperature (depth; 10, 30, 60, and 100 cm) in Ansai (Shaanxi Province, China) about 100 km away from Yulin from 1998 to 1999. According to statistics from 1970 to 1997, the average annual temperature was 8.8℃ in Ansai (the coldest −6.8℃ in January, the warmest 22.4℃ in July), with an average annual rainfall of 423 mm (Takahashi *et al.*, 2002). Although the meteorological conditions were a little different, the seasonal change of T_{G2} and the vertical profile of soil temperature was a good likeness of the observation result by Takahashi *et al.* (2002). In the future, however, it will be necessary to do a long-term observation in the actual field, and to verify the calculation result. According to the observation result, it is necessary to consider the effect of thermal conductivity and thermal capacity for the frozen soil on the soil temperature.

The soil water content of the first layer was sensitively reactive to the rainfall event. A decrease in the soil water content of the second layer was remarkable for the period of summer when it rained little. However, the soil water content of the second and third layers remained comparatively high in winter. In the Loess Plateau, a "farmer's wisdom" is applied to cultivation practices in order to effectively

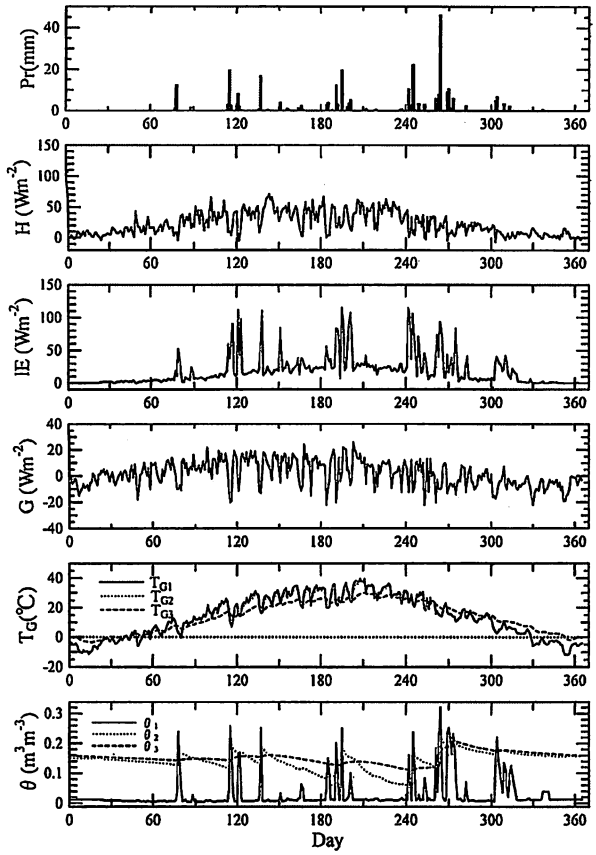

Fig. 10. The calculated results of seasonal change for Yulin in 1999. First panel is the daily amount of precipitation, second panel the result of daily mean sensible heat flux, third panel the latent heat flux, fourth panel the soil heat flux, fifth panel the soil temperature, and bottom panel the volumetric soil water content for respective layers at 1200 BST.

utilize the features inherent to yellow loessial soil: the soil water maintained in the previous year is utilized for cultivation the following year. However, considering that the field capacity in this region is 0.19 ($m^3 m^{-3}$), the soil water condition is very severe for crop production. Most of the rainfall is concentrated in the summer and autumn months (June to September) (Academia Sinica and Ministry of Water Resources, 1993). Therefore, rainfall can hardly be expected in the winter and spring. The wind speed is high in spring (Academia Sinica and Ministry of Water Resources, 1993), so it is during this time, when the soil surface dries out remarkably, that wind erosion is profuse.

This study examined the seasonal variation of the heat balance and soil water content in Shenmu. The soil types in the Loess Plateau were divided by the particle size distribution (Yang and Shao, 2000). In the future, the soil parameters of each soil used by the model calculation will be decided, and the heat balance and soil water content in the whole area of the Loess Plateau will be examined.

6. Conclusion

This study presented a three-layer soil model based on the soil model by Kondo and Xu (1997) and verified the model by comparing the observed results in the Tottori Sand Dune and the Loess Plateau (Shenmu District, Shaanxi Province, China). The model divided the soil into three layers, with thicknesses of 0–2, 2–22 and 22–70 cm. The time series of the vertical water movement by liquid and vapor phases, the volumetric soil water content in respective soil layers, and the heat balance were calculated by considering the initial value and boundary conditions.

There was good agreement between observed and calculated results of evaporation and soil water content. The difference between the observed and calculated evaporation per day was 0.18 mm (5 $W m^{-2}$) to 0.21 mm (6 $W m^{-2}$).

The yellow loessial soil affects both water retentivity and restriction of evaporation from the soil surface. Although they are both located on the Loess Plateau, Lanzhou and Shenmu presented quite different heat balances. That is, a large difference is caused in the climate depending on the soil particle size distribution.

The seasonal change of the heat balance and soil water content was considered using the meteorological data in Yulin near Shenmu. The annual means of sensible heat and latent heat flux were 23 $W m^{-2}$ and 19 $W m^{-2}$ (239 mm per year), respectively. Eighty-five percent of the annual rainfall (283 mm) evaporated. The soil water content of the first layer was sensitively reactive to rainfall events. The soil water content of the second and third layers remained comparatively high in winter.

Acknowledgements

The authors would like to express their gratitude to Dr. Kobayasi of the Faculty of Horticulture, Chiba University; Dr. Arai and students of the Arid Land Research Center, Tottori University; and Dr. Shao and the many researchers of Institute of Soil

and Water Conservation, CAS, China, for considerable advice and discussions on the present research. Thanks are also extended to Mr. Yao and Mr. Ma of Institute of Soil and Water Conservation, CAS, China, who kindly assisted with field experiments.

References

Abramopoulos, F., Rosenzweig, C. and Choudhury, B., 1988: Improved ground hydrology calculations for global climate models (GCMs): Soil water movement and evapotranspiration. *J. Climate,* **1**, 921–941.

Academia Sinica and Ministry of Water Resources, 1993: *Memoir of Northwestern Institute of Soil and Water Conservation 18.* Shaanxi Scientific and Technological Press, Xian, 144 pp. (in Chinese with English summary).

Budyco, M.I., 1956: *Heat balance of the Earth's surface.* Gidrometeozidat, Leningrad, 255 pp.

Fukumoto, M. and Hirota, K., 1994: The effect of surface soil moisture on heat balance at a bare soil surface. *J. Jpn. Soc. Hydrol. Water Resour.,* **7**, 393–401 (in Japanese with English summary).

Kawaguchi, K., 1991: *An introduction to pedology.* Yokendo, Tokyo, 279 pp. (in Japanese).

Kondo, J., 1994: *Meteorology of the water environment: Water and heat balance of the Earth's surface.* Asakura Shoten, Tokyo, 348 pp. (in Japanese).

Kondo, J., 2000: *Atmospheric science near the ground surface.* University of Tokyo Press, Tokyo, 324 pp. (in Japanese).

Kondo, J. and Xu, J., 1997: Seasonal variations in the heat and water balances for nonvegetated surfaces. *J. Appl. Meteorol.,* **36**, 1676–1695.

Kondo, J., Ooka, H., Matsushima, D. and Saigusa, N., 1994: A prediction model for the seasonal variation of evaporation from non-vegetated ground surfaces: (2) Experimental verification. *J. Jpn. Soc. Hydrol. Water Resour.,* **7**, 386–392 (in Japanese with English summary).

Shinoda, M., 2002: *Desert and climate.* Seizando, Tokyo, 169 pp. (in Japanese).

Takahashi, H., Araki, K., Nagasawa, T., Hongo, A., Zhang, J. and Li, S., 2002: The evapotranspiration on the slopes during spring in the Loess Plateau, China: A case of south faced and north faced slopes in Ansai county, Shaanxi Province. *J. Agric. Meteorol. Hokkaido,* **54**, 37–44 (in Japanese).

Tamura, S., 1990: *Basic studies on greening in the Loess Plateau in China.* Report of Monbusho Grant-in-Aid for Scientific Research (01102023) (in Japanese).

UNEP, 1997: *World atlas of desertification.* Arnold, London, 182 pp.

Wang, Q. and Takahashi, H., 1999: A land surface water deficit model for an arid and semiarid region: Impact of desertification on the water deficit status in the Loess Plateau, China. *J. Climate,* **12**, 244–257.

Xu, J. and Haginoya, S., 2001: An estimation of heat and water balances in the Tibetan Plateau. *J. Meteorol. Soc. Jpn.,* **79**, 485–504.

Yang, W. and Shao, M., 2000: *Study on the soil water in the Loess Plateau.* Science Publisher Press, Beijing, 305 pp. (in Chinese).

中国黄土高原における熱収支と土壌水分

木村玲二*・神近牧男*・高山　成*・松岡延浩**・張　興昌***

(* 鳥取大学乾燥地研究センター
** 千葉大学園芸学部
*** 中国科学院西北水土保持研究所)

要　　約

中国黄土高原での熱収支と土壌水分特性を明らかにするために，土壌3層モデルを用い，実際の裸地圃場に適用した（鳥取砂丘および中国陝西省神木県）。日蒸発量の観測値と計算値の差は0.18 mm（5 W m^{-2}）から0.21 mm（6 W m^{-2}）程度であった。神木地区の黄土は砂，シルト，粘土が適度に混ざり合っていることにより，保水性の効果と蒸発抑制効果の両面を併せ持っていた。神木に近い楡林の1999年の気象データを用い，熱収支と土壌水分の季節変化について考察した。年平均顕熱フラックスは23 W m^{-2}，年平均潜熱フラックスは19 W m^{-2}（239 mm per year）であった。冬季の第2層と3層の土壌水分は比較的高く維持されていた。

キーワード：黄土高原，土壌水分，熱収支

Return

ELSEVIER

Journal of Arid Environments 63 (2005) 439–457

Journal of Arid Environments

www.elsevier.com/locate/jnlabr/yjare

Heat and water balances of the bare soil surface and the potential distribution of vegetation in the Loess Plateau, China

R. Kimura[a,*], Y. Liu[b], N. Takayama[a], X. Zhang[c], M. Kamichika[a], N. Matsuoka[d]

[a]*Arid Land Research Center, Tottori University, Hamasaka 1390, Tottori 680-0001, Japan*
[b]*Graduate School of Environmental Studies, Nagoya University, Furo-cho, Chikusa-ku, Nagoya 464-8601, Japan*
[c]*Institute of Soil and Water Conservation, CAS, Yangling, Shaanxi 712100, China*
[d]*Faculty of Horticulture, Chiba University, Matsudo 271-8510, Japan*

Received 13 July 2004; accepted 2 March 2005
Available online 5 May 2005

Abstract

Spatial and temporal changes of heat and water balances are crucial to planting to combat desertification in the Loess Plateau of China. A three-layer soil model and meteorological data from 43 observatories were used to estimate the heat and water balances of the bare soil surface. Results indicate that the annual mean of sensible heat flux ranged from 13 to 36 $W m^{-2}$ and the latent heat flux from 14 $W m^{-2}$ (179 $mm yr^{-1}$) to 40 $W m^{-2}$ (521 $mm yr^{-1}$). Water retention and restriction of evaporation from the soil surface are affected by the yellow loessial soil including medium loam, light loam and sandy loam, but not heavy loam. The distribution of fractional extractable water and the existing vegetation have been compared to reveal the potential vegetation distribution leading to the aridity distribution in the plateau.

Keywords: Aridity; Evaporation; Heat flux; Soil water content; Three-layer soil model

*Corresponding author. Tel.: +81 857 21 7031; fax: +81 857 29 6199.
E-mail address: rkimura@alrc.tottori-u.ac.jp (R. Kimura).

0140-1963/$ - see front matter © 2005 Elsevier Ltd. All rights reserved.
doi:10.1016/j.jaridenv.2005.03.030

1. Introduction

The Loess Plateau of China (area: $62.68 \times 10^4\,km^2$; latitude: 34–40°N and longitude: 100–115°E) is located at an elevation ranging from 1000 to 1500 m above mean sea level (Yang and Shao, 2000). The annual precipitation varies from 400 to 500 mm; most of which occurs during June–September months. The water deficit index (WDI) and the aridity index indicate that the plateau is located in a semi-arid region (UNEP, 1997; Wang and Takahashi, 1999).

Since the 17th century, serious desertification has occurred in the Loess Plateau due to improper land use (like over-cultivation, over-grazing, over-deforestation, etc.) which caused critical soil erosion and water shortages in the lower reaches of the Yellow River (He et al., 2003). It became a source area of Asian dust in the spring when the soil surface is significantly dry (In and Park, 2002).

It has been suggested that desertification can be monitored using the relationships among the types and amount of existing vegetation and the soil water content (Shinoda, 2002). Soil moisture is the most important factor that supports plant production. It is necessary to understand the heat and water balances that generate the soil water dynamics of the local area in order to obtain the benefits from planting to combat desertification. For example, it can help in selecting appropriate drought resistant vegetation. However, there are presently no comprehensive studies of the heat and water balances in the Loess Plateau area.

We developed a three-layer soil model to study the heat and water balances of the bare soil surface in the Loess Plateau (Kimura et al., 2004a, b). This model can simulate temporal variations of water movement in liquid and vapor phases, the soil water content in the respective soil layers, and the heat balance. In this paper, we extend the study on heat and water balances of the bare soil surface by incorporating the seasonal changes of the sensible and latent heat fluxes and of the soil water content and the physical features of five typical soils of the plateau. We illustrate the potential distribution of vegetation by overlapping the existing vegetation distribution with that of the index (fractional extractable water remaining in the root zone θ_e by Black, 1979) derived from the soil water content. Finally, we describe the aridity distribution in the plateau.

2. The three-layer soil model

The soil model we developed divides the soil into three layers: 0–2, 2–22, and 22–70 cm (refer to Kimura et al., 2004a for details). The soil type was assumed to be the same from the ground surface to the bottom. Given the initial value and boundary conditions, the model can estimate the time-series changes of water movement in the liquid and vapor phases, the volumetric soil water content in the respective soil layers, and the heat balance.

The energy balance of the soil surface is expressed by (Kondo and Xu, 1997)

$$(1 - ref)S^{\downarrow} + \varepsilon L^{\downarrow} = \varepsilon\sigma T_s^4 + H + lE + G, \tag{1}$$

$$H = c_p \rho C_H U(T_s - T), \tag{2}$$

and

$$lE = l\rho C_H U\beta\{hq_{sat}(T_s) - q\}. \tag{3}$$

Here, *ref* is the albedo of the soil surface, $S^{\downarrow}$ is the global solar radiation ($W\,m^{-2}$), and ε is the emissivity of the soil surface (assumed as unity in this study). $L^{\downarrow}$ represents the downward longwave radiation ($W\,m^{-2}$), σ is the Stefan–Boltzman constant ($5.67 \times 10^{-8}\,W\,m^{-2}\,K^{-4}$), and T_s is the soil surface temperature (K). H designates the sensible heat flux ($W\,m^{-2}$), lE is the latent heat flux ($W\,m^{-2}$), and G is the soil heat flux ($W\,m^{-2}$). c_p corresponds to the specific heat of the air ($J\,kg^{-1}\,K^{-1}$); ρ is the density of the air ($kg\,m^{-3}$); C_H is the bulk transfer coefficient for sensible heat; and U, T, and q denote the wind speed ($m\,s^{-1}$), temperature (K) and specific humidity ($kg\,kg^{-1}$) at a given height z (m). $q_{sat}(T_s)$ represents the specific humidity at saturation at temperature T_s (K), l is the latent heat ($J\,kg^{-1}$) of the evaporation of water, β corresponds to the evaporation efficiency by Kondo and Xu (1997), and h is the relative humidity when the water vapor and liquid water are in equilibrium in the small soil pores (Philip, 1957).

The soil heat flux is given by

$$G = -\int_0^{0.7} \frac{d(c_G \rho_G T_G)}{dt}\, dz. \tag{4}$$

Here, c_G is the specific heat of the soil ($J\,kg^{-1}\,K^{-1}$), ρ_G is the bulk density of the soil ($kg\,m^{-3}$), T_G is the soil temperature (°C), t is the time (s), and z is the depth (m).

The water and heat transfer within the soil can be expressed as follows (Kondo and Xu, 1997):

$$\frac{\partial\theta}{\partial t} = -\frac{1}{\rho_w}\frac{\partial}{\partial z}(Q_{liq} + Q_{vap}), \tag{5}$$

$$Q_{liq} = -\rho_w K\left(\frac{\partial\psi}{\partial z}\right) - \rho_w K, \tag{6}$$

where

$$K = K_{sat}\left(\frac{\theta}{\theta_{sat}}\right)^c, \tag{7}$$

$$Q_{liq}(z_{bottom}) = -\rho_w K, \tag{8}$$

$$Q_{vap} = \frac{\rho D}{F_n}\left(\frac{d[hq_{sat}(T_G)]}{dz}\right), \tag{9}$$

and

$$\frac{\partial T_G}{\partial t} = -\frac{1}{c_G\rho_G}\frac{\partial Q_h}{\partial z} - \frac{lE_{soil}}{c_G\rho_G}, \tag{10}$$

where

$$Q_{\mathrm{h}} = -\lambda_G \frac{\partial T_G}{\partial z}. \tag{11}$$

Here, θ is the volumetric soil water content ($\mathrm{m^3\,m^{-3}}$), ρ_{w} is the water density ($=1000\,\mathrm{kg\,m^{-3}}$), Q_{liq} signifies the liquid water flux ($\mathrm{kg\,s^{-1}\,m^{-2}}$), and Q_{vap} represents the water vapor flux ($\mathrm{kg\,m^{-2}\,s^{-1}}$). K corresponds to the hydraulic conductivity ($\mathrm{m\,s^{-1}}$), ψ is the soil water potential (m), K_{sat} indicates K at saturation, and c represents the constant which changes with soil type. θ_{sat} denotes θ at saturation, $Q_{\mathrm{liq}}(Z_{\mathrm{bottom}})$ is the water flux at the bottom (z_{bottom}), and D corresponds to the coefficient of the molecular diffusion of water vapor in the air ($=2.54\times10^{-5}\,\mathrm{m^2\,s^{-1}}$). F_n is the transport route of water vapor in the soil (m), Q_{h} represents the heat flux in the soil ($\mathrm{W\,m^{-2}}$), lE_{soil} is the latent heat flux within the soil ($\mathrm{W\,m^{-2}}$), and λ_G is the thermal conductivity of the soil ($\mathrm{W\,m^{-1}\,K^{-1}}$).

The data used in the calculation included sunshine duration, the daily mean air temperature, the daily maximum and minimum air temperatures, the daily mean wind speed, the daily mean specific humidity, and the daily amount of precipitation. Diurnal variations of the meteorological data were required for the calculation. We used the method of Kondo and Xu (1997) to estimate these variations. From the daily mean air temperature, the daily maximum and minimum air temperatures, the daily variation of air temperature can be expressed as a trigonometric function having two temporal harmonics. The daily mean solar radiation flux is obtained from sunshine duration, and the daily variation of that can be described as the sum of trigonometric functions having four harmonics. The downward longwave radiation is obtained from solar radiation and vapor pressure. The downward longwave radiation, wind speed and specific humidity were assumed as constant during the day. Rainfall data from the observatories are given as total daily amounts and the temporal variation of precipitation intensity can be expressed as a function of precipitation and time.

T_{s} can be found through successive approximations of Eq. (1) with the fluxes H, lE and G evaluated from Eqs. (2)–(4). The time step for the model running is 1 h.

The initial and boundary conditions for the water and thermal regimes were the same as those of Kondo and Xu (1997). The liquid water movement between the first layer and the atmosphere and the water vapor movement at the bottom were not considered. No heat exchange was assumed at the bottom. The assumed values for the initial conditions of θ and T_G were used at the start. The model ran for several years under the same pattern of weather conditions until θ and T_G in each layer approached a steady state. These results were then used as the initial conditions of θ and T_G.

It was observed that the model results of the soil water content and evaporation agreed well with those obtained by gravimetric sampling and lysimeter. Also the observed results of the column experiments revealed that the model simulation represented the qualitative differences in evaporation due to soil texture in the Loess Plateau (Yang and Shao, 2000; Kimura et al., 2004a, b).

3. Model parameterization

3.1. Soil types in the Loess Plateau

The typical soil types in the Loess Plateau include heavy loam, medium loam, light loam, and sandy loam (Yang and Shao, 2000). Sand was also included in this study since some parts of the Mu-Us desert cover the northwest portion of the plateau. Table 1 indicates the particle size distribution of each soil type. The soil characteristics differ depending on the distribution rate of the sand and clay.

Fig. 1a and b depict respectively, the distribution of soil and vegetation types and the 43 weather stations (Table 2) involved in the plateau (He, 1989; Wang and Takahashi, 1999; Yang and Shao, 2000).

3.2. Parameterization

This section provides a simple description of the parameterization of soil water potential Ψ, surface albedo *ref*, and evaporation efficiency β. Refer to Kimura et al. (2004b) for a more detailed description.

3.2.1. Soil water potential

The soil water potential is given by Kondo and Xu (1997) as

$$\psi = -4 \times 10^4 \exp(-a\theta) - \frac{10^2}{1 + (-10^2/X)} \quad \theta < \theta_{\text{sat}}, \tag{12}$$

where

$$X = \psi_{\text{sat}} \left(\frac{\theta}{\theta_{\text{sat}}} \right)^{-b}, \tag{13}$$

and

$$\psi = 0, \quad \theta \geqslant \theta_{\text{sat}}. \tag{14}$$

Here, a and b are constants which are specific to soil type and Ψ_{sat} is the soil water potential at saturation. Table 3 lists the soil parameters and constants for each soil.

Table 1
Particle size distribution in the Loess Plateau

Soil texture	Content (%)		
	>0.05 mm	0.01–0.05 mm	<0.01 mm
Heavy loam	9	42	49
Medium loam	11	50	39
Light loam	21	54	25
Sandy loam	48	39	13
Sand (Mu US)	98	1	1

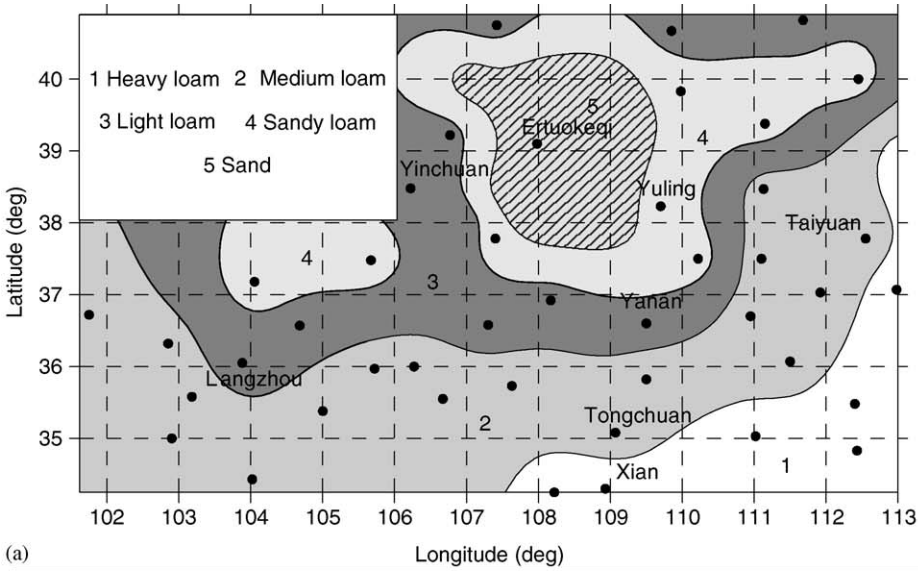

(a)

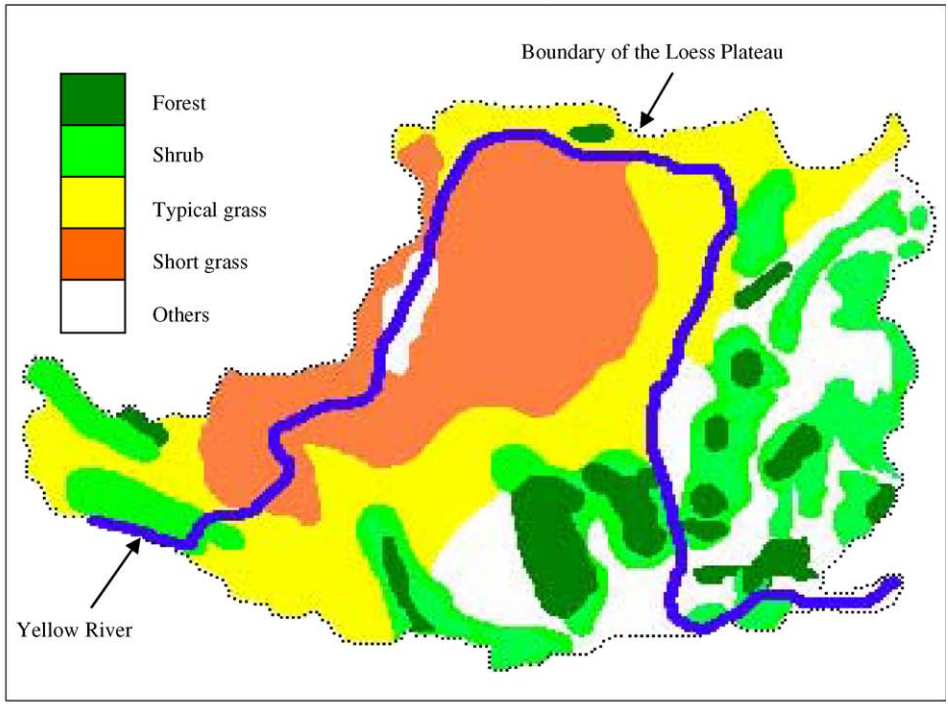

(b)

Fig. 1. Distribution of (a) soil and (b) vegetation in the Loess Plateau.

Table 2
Observatories used in this study

Station number	Place name	Lat. (degree)	Long. (degree)	Altitude (m)	Rn (W m^{-2})	E (mm)	θ_e
52797	Jingtai	37.18	104.05	1631	42	217	0.48
52866	Xining	36.72	101.75	2295	45	341	1.02
52876	Minghe	36.32	102.85	1814	43	298	0.88
52889	Langzhou	36.05	103.88	1517	41	278	0.81
52895	Jingyuan	36.57	104.68	1398	41	250	0.7
52984	Lingxia	35.58	103.18	1917	46	334	1.02
52996	Huajialing	35.38	105	2451	59	300	1.01
53446	Baotou	40.67	109.85	1067	41	229	0.84
53463	Huhehaote	40.82	111.68	1063	42	313	1.08
53478	Youyu	40	112.45	1346	43	250	0.99
53513	Linghe	40.75	107.42	1039	38	200	0.42
53519	Huinong	39.22	106.77	1091	43	179	0.04
53529	Ertuokeqi	39.1	107.98	1380	45	202	0.68
53543	Tongshen	39.83	109.98	1460	49	296	1.04
53564	Hequ	39.38	111.15	862	40	278	1.01
53614	Yinchuan	38.48	106.22	1111	42	198	0.49
53646	Yuling	38.23	109.7	1058	41	255	0.91
53664	Xinxian	38.47	111.13	1013	45	287	0.99
53705	Zhongning	37.48	105.67	1183	47	219	0.72
53723	Yanchi	37.78	107.4	1348	47	257	0.93
53738	Wuqi	36.92	108.17	1331	43	292	1.06
53754	Shuide	37.5	110.22	930	45	268	0.96
53764	Lishi	37.5	111.1	951	43	296	0.88
53772	Taiyuan	37.78	112.55	778	42	259	0.9
53787	Yushe	37.07	112.98	1041	49	406	0.74
53817	Guyuan	36	106.27	1753	50	287	1.02
53821	Huanxian	36.58	107.3	1256	44	303	1.06
53845	Yanan	36.6	109.5	959	45	315	1.12
53853	Xixian	36.7	110.95	1053	43	272	1
53863	Jiexiu	37.03	111.92	744	41	291	0.92
53868	Lingfen	36.07	111.5	450	38	274	1.07
53903	Xiji	35.97	105.72	1917	49	265	0.96
53915	Pingliang	35.55	106.67	1347	44	277	1.03
53923	Xifenzhen	35.73	107.63	1421	48	277	1.05
53942	Luochuan	35.82	109.5	1160	46	275	1.05
53947	Tongchuan	35.08	109.07	979	45	288	1.06
53959	Yuncheng	35.03	111.02	376	55	464	0.89
53975	Yangcheng	35.48	112.4	660	55	473	0.94
56080	Hezhuo	35	102.9	2910	54	393	1.03
56093	Minxian	34.43	104.02	2315	52	356	1.02
57034	Wugong	34.25	108.22	448	50	478	0.81
57036	Xian	34.3	108.93	398	49	459	0.82
57071	Menjing	34.83	112.43	323	59	521	0.94

R_n is the annual means of the net radiation, E the annual total evaporation, and θ_e the mean value of the fractional extractable water in the rainy season (June to September) in 1998

Table 3
Soil parameters and constants of the respective soil

	θ_{sat}	θ_f	θ_w	θ_M	Ψ_{sat}	a	b	$K_{sat} \times 10^{-5}$	c	f_{Max}
Heavy loam	0.476	0.31	0.16	0.24	0.04	35	4	0.1	10	0.02
Medium loam	0.451	0.25	0.10	0.18	0.04	60	5.5	0.5	11.2	0.008
Light loam	0.435	0.21	0.09	0.15	0.04	65	4.5	0.9	10	0.008
Sandy loam	0.434	0.19	0.05	0.12	0.04	110	4	2.4	10	0.008
Sand	0.36	0.12	0.035	0.08	0.2	160	1.5	9	8	0.01

Table 4
Constants for the albedo

	θ_{min}	θ_{max}	ref_{min}	ref_{max}
Heavy loam	0.05	0.2	0.09	0.27
Medium loam	0.11	0.25	0.16	0.27
Light loam	0.11	0.25	0.16	0.27
Sandy loam	0.07	0.21	0.17	0.27
Sand	0.03	0.1	0.16	0.22

The values of θ_f and θ_w in Table 3 are the field capacity and wilting point where the pF value ($pF = \log_{10}|\Psi \times 100|$(cm)) is 2 ($\Psi = -1$ m) and 4.2 ($\Psi = -158$ m). The experimental results by Naruoka and Yamamoto (1992) and Yang and Shao (2000) were used to determine constants a and b.

3.2.2. Albedo

The relationship between volumetric soil water content θ and albedo ref for five soil types were observed and reported (Kondo and Xu, 1997; Kimura et al., 2004b). The albedo of each soil was defined by the following equation in this study.

$$ref = \xi\theta + \chi, \quad \theta_{min} \leqslant \theta \leqslant \theta_{max}, \tag{15}$$

where

$$\xi = \frac{ref_{min} - ref_{max}}{\theta_{max} - \theta_{min}}, \tag{16}$$

$$\chi = ref_{max} - \xi\theta_{min}, \tag{17}$$

and

$$ref = ref_{max}, \quad \theta < \theta_{min}, \tag{18}$$

$$ref = ref_{min}, \quad \theta > \theta_{max}. \tag{19}$$

Here, θ_{min} and θ_{max} are the volumetric soil water content at an inflection point of ref. ref_{min} and ref_{max} are the minimum and the maximum values of the albedo. These constants are included in Table 4.

3.2.3. Evaporation efficiency

Evaporation efficiency β is the ratio of bulk transfer coefficient for latent heat to that for sensible heat, and ranges from 0 to 1.0. β is determined using the diffusion distance of water vapor F and the coefficient of the molecular diffusion of water vapor D ($=2.54\times10^{-5}\,m^2\,s^{-1}$) (Kondo and Xu, 1997).

$$\beta=\frac{1}{1+C_H U(F/D)}. \tag{20}$$

F indicates the diffusion distance of water vapor from the liquid surface in the soil where evaporation into the atmosphere occurs (Kondo and Xu, 1997).

Based on the observed data and the experimental results (Kondo and Xu, 1997; Kimura et al., 2004b), the relationship between the volumetric soil water content θ and F were determined from the following equation.

$$F=f_A\exp(-f_B\theta^3)+f_C\left[\cos\left(\frac{\pi}{2}\frac{\theta}{\theta_{sat}}\right)\right]^{f_D},\quad 0\leqslant\theta<\theta_{sat}. \tag{21}$$

Here, f_A, f_B, f_C, and f_D are the constants which are specific to soil type.

Kimura et al. (2004b) parameterized the value of F, which varies with soil type, as

$$F=0.00032\left[\cos\left\{\frac{\pi}{2}\left(\frac{0.833\theta}{\theta_{sat}}\right)\right\}\right]^{1.5},\quad \theta/\theta_M\geqslant1, \tag{22}$$

$$F=f_{Max}\times\exp\left[-9000\left(\frac{0.1\,\theta}{\theta_M}\right)^3\right],\quad \theta/\theta M<1, \tag{23}$$

with

$$\theta_M=\frac{\theta_f+\theta_w}{2}. \tag{24}$$

Here, f_{Max} is the maximum value of F, θ_f is the field capacity, and θ_w is the wilting point. The values of θ_M and f_{Max} of each soil are provided in Table 3.

4. Results and discussion

4.1. Heat and water balances

The seasonal variations of the daily amount of precipitation and the daily means of the sensible and latent heat fluxes for all soil types are presented (Fig. 2). The sensible and latent heat fluxes were computed using Eqs. (2) and (3). As precipitation at the Loess Plateau was statistically normal, we used the meteorological data from 1998 for the calculation (Takayama et al., 2004).

The sensible heat flux peak appeared in summer (June–July) in all locations. H generally exhibited a sinusoidal pattern throughout the year in Yuling and Ertuokeqi, where rainfall is less than in other locations. The latent heat flux

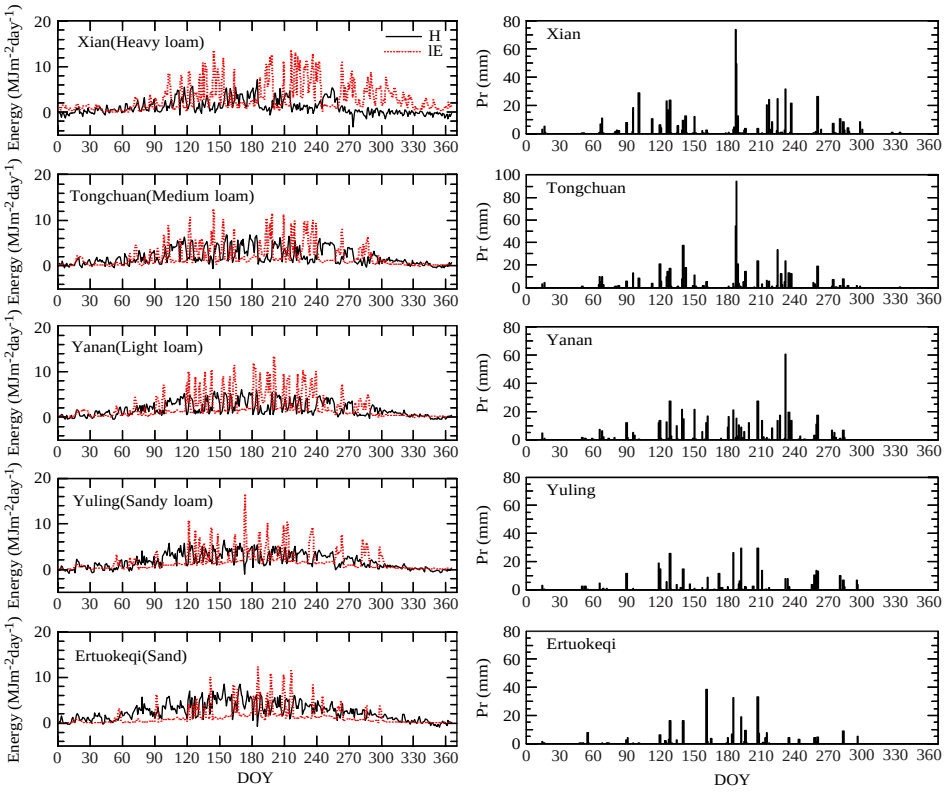

Fig. 2. Seasonal changes of the daily amount of precipitation (mm) and the daily means of the sensible and latent heat fluxes ($MJ\,m^{-2}\,day^{-1}$) in 1998.

approximately corresponded to the rainfall events. Especially in Xian, Tongchuan and Yanan, there were many days when *lE* was greater than *H* because of a lot of precipitation events. Steady evaporation after rainfall continued for a period in the heavy loam of Xian. In contrast, evaporation was restrained several days later in the sandy loam and sand.

The spatial distributions of sensible and latent heat flux annual means in the Loess Plateau in 1998 are illustrated (Fig. 3). The contour lines were determined from calculated results of 43 observatories using the nearest neighbor method. The annual means of the sensible heat flux ranged from 13 to 36 $W\,m^{-2}$. The sensible heat flux became significant (36 $W\,m^{-2}$) around 35°N and 105°E because of the relatively high altitude (2451 m), which restrains evaporation due to the relatively lower temperature. The sensible heat flux was greater in the desert area near Yinchuan, while the latent heat flux annual mean ranged from 14 $W\,m^{-2}$ (179 $mm\,yr^{-1}$) to 40 $W\,m^{-2}$ (521 $mm\,yr^{-1}$). It increased from Xian to Taiyuan in the northeast in particular. In contrast, the annual mean of the latent heat flux gradually decreased from Xian to Yinchuan in the northwest.

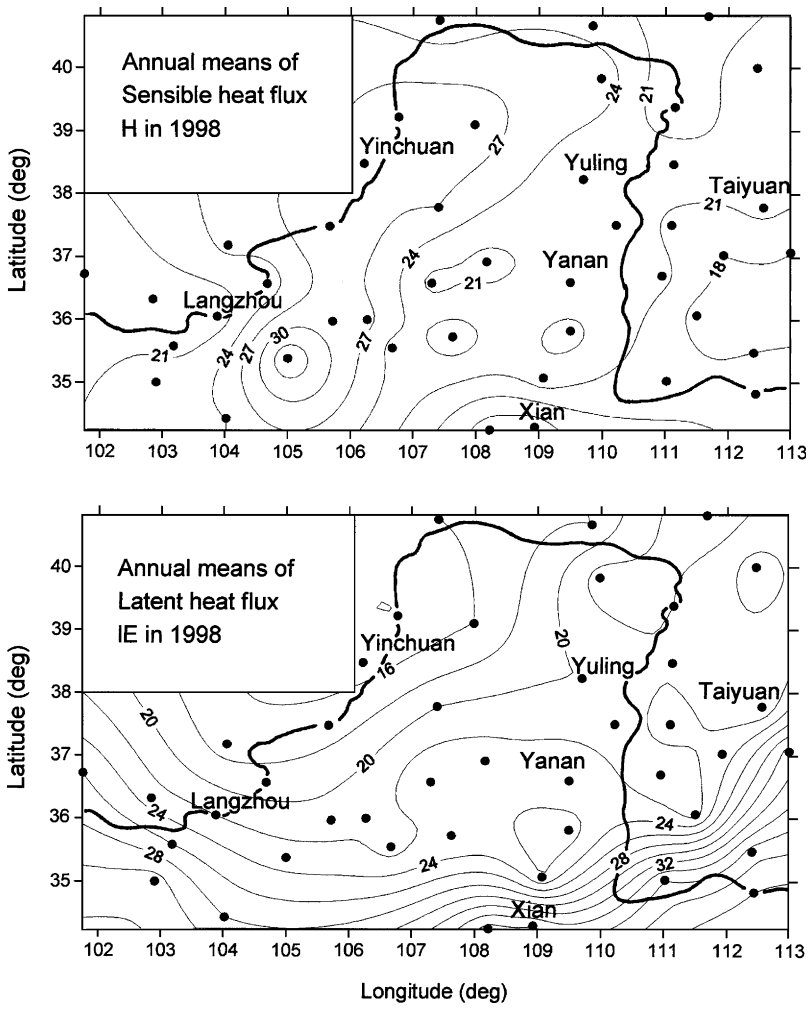

Fig. 3. Spatial distribution of the annual means of the sensible and latent heat fluxes ($W\,m^{-2}$) in the Loess Plateau in 1998.

Fig. 4 depicts the spatial distribution of annual precipitation Pr and the drainage $Pr-E$ in the Loess Plateau in 1998. Pr ranged from 174 to 784 $mm\,yr^{-1}$, and $Pr-E$ from 0 to 346 $mm\,yr^{-1}$.

4.2. Soil water dynamics

Fig. 5 presents the seasonal variations of soil water in the respective layers. There were some days when θ_1 in Xian and Tongchuan was close to the saturated soil water content θ_{sat}, due to the low infiltration rate (refer to saturated hydraulic conductivity

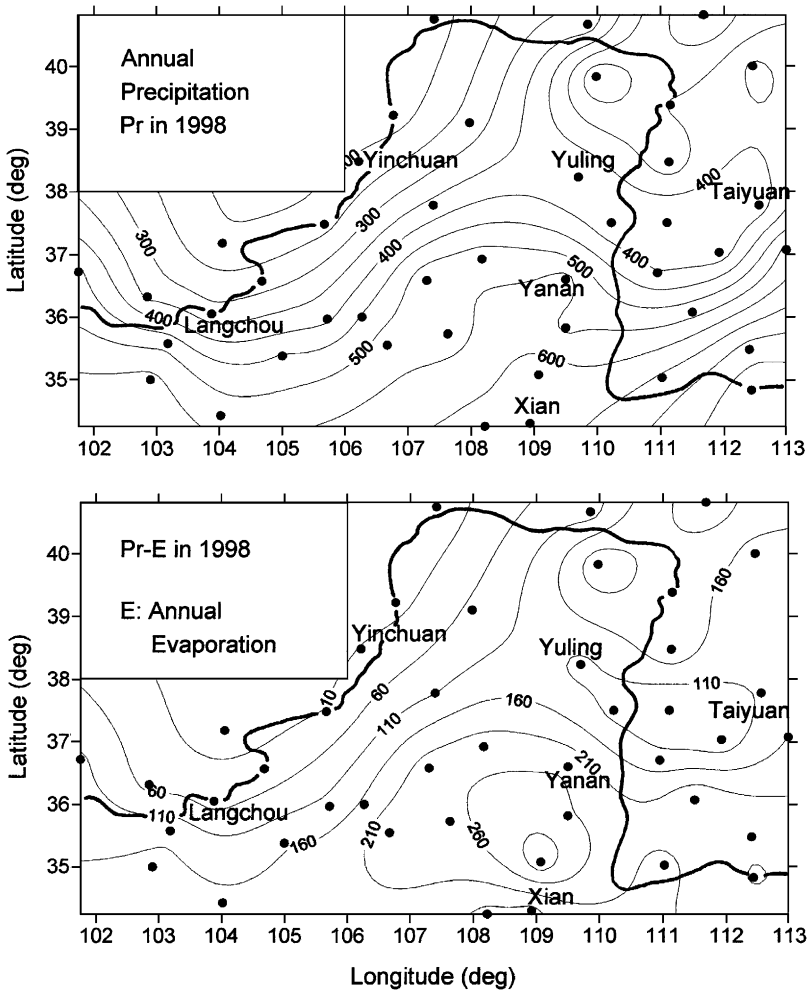

Fig. 4. Spatial distribution of annual rainfall Pr (mm) and the drainage $Pr–E$ (mm) in the Loess Plateau in 1998.

K_{sat} in Table 3). The decrease of soil water content in the first layer after a rainfall was slower in Xian, Tongchuan, and Yanan than at Yuling and Ertuokeqi since water supplied to the first layer lasted longer. However, the soil water content in the first layer after a rainfall in Yuling and Ertuokeqi decreased remarkably due to the rupture of capillary continuity (Kimura et al., 2004a).

We next examined the soil water content in the second and third layers (θ_2 and θ_3). The relatively steady evaporation in the heavy loam of Xian continued due to capillary action, so the decrease in soil water content of the second and third layers was greater than that at the other four locations. The soil water content of the medium loam, light loam, sandy loam, and sand remained relatively high in the

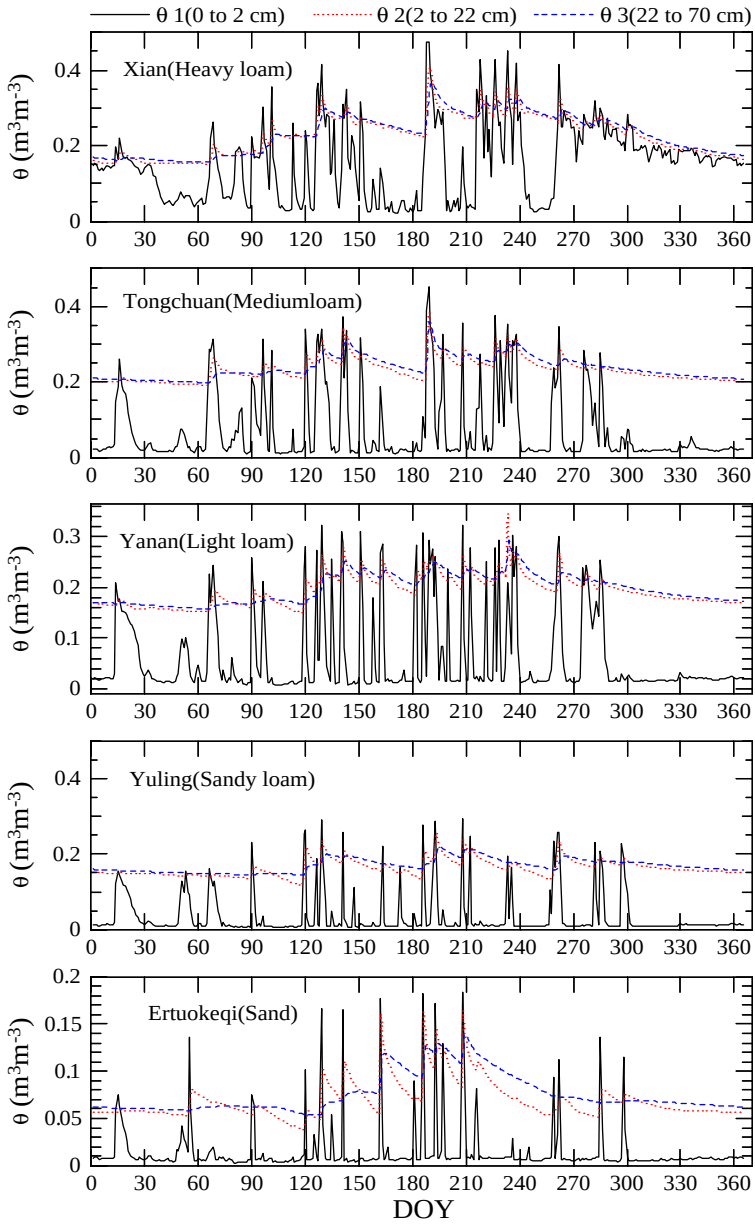

Fig. 5. Seasonal variations of the soil water content in the respective soil layers.

winter, when it rained little. The results of Kimura et al. (2004b) indicate that yellow loessial soil, except for the heavy loam, affects both water retentivity and restriction of evaporation from the soil surface due to the moderate mixture of sand, silt, and

clay. These soil types are superior to heavy loam from the standpoint of water retention in the lower layer. "Farmer's wisdom" is applied to cultivation practices in the Loess Plateau to effectively utilize the features inherent in yellow loessial soil; soil water maintained from the previous year is utilized for cultivation in the following year.

4.3. Fractional extractable water

The extractable water in soil is ecologically significant for the vegetation. Black (1979) expressed this critical aspect using the fractional extractable water remaining in the root zone θ_e, as given by

$$\theta_e = \frac{\theta - \theta_w}{\theta_f - \theta_w}. \tag{25}$$

Kimura and Kondo (1999) examined the relationship between θ_e and the leaf transfer coefficient in five soil types and two vegetation types (grass and sorghum). Their result indicated that the leaf transfer coefficient drastically decreases when $\theta_e < 0.3$. Black (1979) also suggested that the ratio of actual evapo-transpiration to equilibrium evapo-transpiration in Douglas fir trees begins to decrease when $\theta_e < 0.4$. Fig. 6 illustrates the seasonal change of θ_e in the respective areas. θ_e in Eq. (25) is the

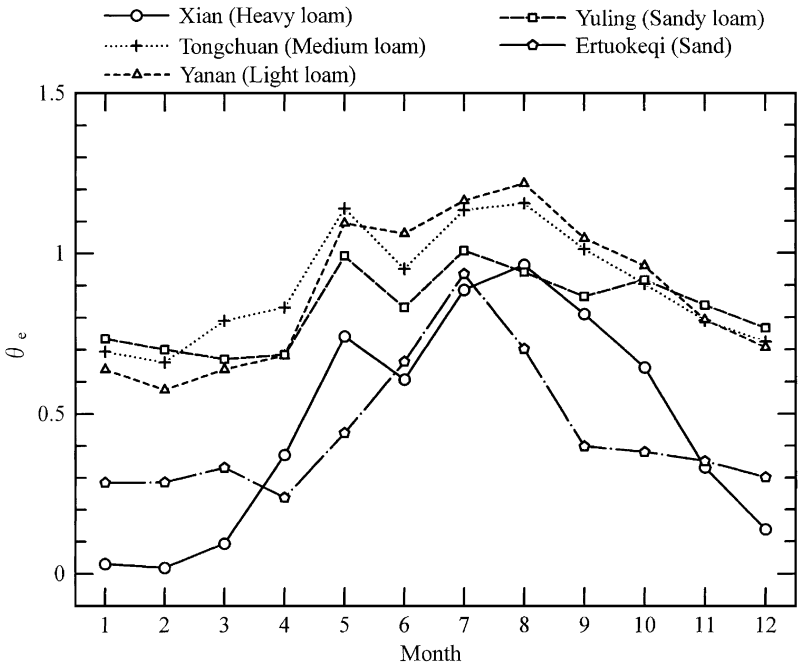

Fig. 6. Seasonal changes of the fractional extractable water θ_e in Xian, Tongchuan, Yanan, Yuling, and Ertuokeqi.

mean value of the second and third layers. It must be noted that soil water changes due to root water uptake were not considered. The rainy season in the plateau is from June to September, and the peak of θ_e appeared in this season. The annual rainfall in Ertuokeqi is comparatively small (272 mm yr^{-1}), so θ_e is less than 0.5 except in the rainy season. θ_e was smaller in Xian than at the other locations (Tongchuan, Yanan, and Yuling) throughout the year despite the significant amount of rainfall (601 mm yr^{-1}) since water loss by evaporation for heavy loam is greater than for other soils. In contrast, θ_e remained substantial in Tongchuan ($Pr = 634$ mm yr^{-1}), Yanan (568 mm yr^{-1}), and Yuling (353 mm yr^{-1}), even in winter, when it rains little. θ_e has occasionally exceeded 1.0 in the rainy season, and the forest has been found around Tongchuan and Yanan. The annual precipitation in Yuling is less than that in Xian; however, the water retention of sandy loam is superior to that of heavy loam due to its physical characteristics.

Variations between the annual rainfall and the mean value of θ_e (June–September) are presented (Fig. 7). The result in the drought year of 1999 is also provided for Xian, Tongchuan, Yanan, Yuling, and Ertuokeqi. The dispersion between θ_e and the annual precipitation became small when $Pr > 300$ mm, except for heavy loam. The soil water content was close to the field capacity when $Pr > 400$ mm. However, the precipitation intensity controls θ_e when $Pr < 300$ mm. θ_e will differ, even with the same amount of precipitation. These tendencies can be observed from symbols a and b for light loam and c and d for sandy loam in Fig. 7. Concentrated rainfall tends to keep the θ_e high; 70 mm of rainfall per day occurred (symbol a). Most rainfall evaporates and the soil water retentivity becomes low after a uniform rain (symbol b).

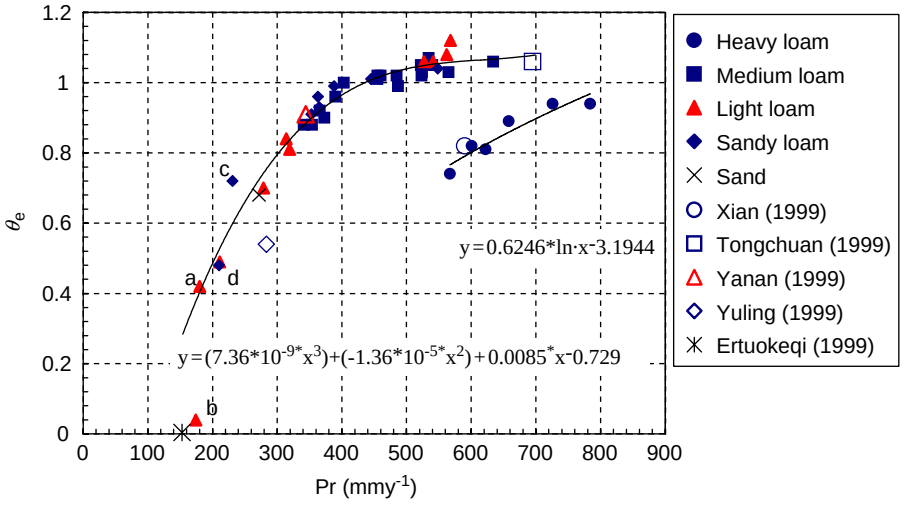

Fig. 7. Relationship between θ_e and the annual rainfall.

4.4. Classification of aridity

The degree of aridity is important in arid land studies. The representative arid indices include the radiative dryness index (Budyco, 1956) and E_p/Pr (e.g., Penman, 1948; UNEP, 1997), where E_p is the potential evaporation and Pr is the precipitation. They are based on the concept of heat and water balances and are limited in classifying the degree of aridity. It is more realistic to monitor the seasonal variation of the soil water content to determine the aridity. We used θ_e as the aridity index. The dispersion between θ_e and the annual precipitation became small when $Pr > 300$ mm, except for the heavy loam, as seen in Fig. 7. However, the precipitation intensity strongly influenced θ_e when $Pr < 300$ mm. A linear relation was found for the heavy loam. While θ_e changes substantially with the precipitation intensity when $Pr < 300$ mm, the relationship between the annual rainfall and θ_e can be represented as below (solid line in Fig. 7).

$$\theta_e = 0.6246 \ln(Pr) - 3.1944, \text{ Heavy loam, } 567 < Pr < 784, \tag{26}$$

$$\theta_e = (7.36 \times 10^{-9}\, Pr^3) + (-1.36 \times 10^{-5}\, Pr^2) + 0.0085 Pr - 0.729, \quad \text{Except for heavy loam,} \quad 180 < Pr < 634, \tag{27}$$

These relationships were gleaned from data from 1998. However, there are large inter-annual variations in the annual precipitation in semi-arid regions, such as the Loess Plateau. The mean value of the annual precipitation from 1980 to 2000 was thus applied to the above equations to calculate θ_e. Fig. 8 depicts the spatial distribution of θ_e estimated from the above equations. The classification of the arid

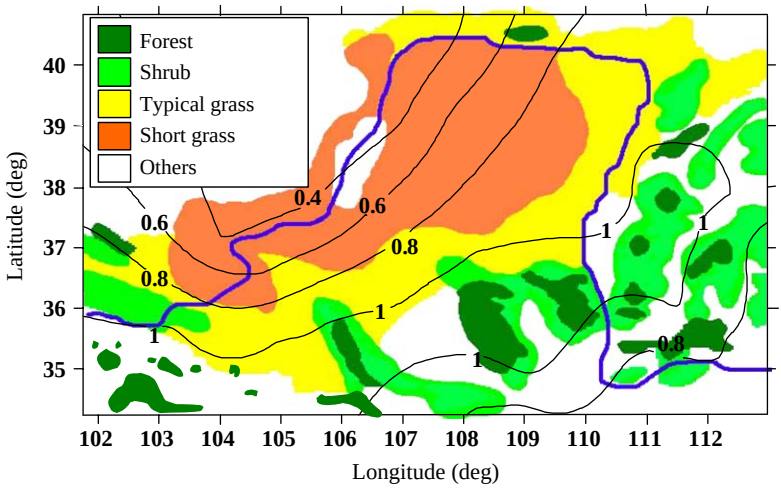

Fig. 8. Spatial distribution of θ_e using the mean value of the annual rainfall from 1980 to 2000 and Eqs. (26) and (27), and comparison between the distribution of θ_e and the existing vegetation.

Table 5
Ratio for respective vegetation with different distribution patterns of θ_e

Vegetation type	Forest (%)	Shrub (%)	Typical grass (%)	Short grass (%)
$\theta_e < 0.4$	0	0	3	17
0.4–0.6	0	0	2	31
0.6–0.8	3	5	12	32
0.8–1.0	22	51	68	20
$\theta_e > 1.0$	75	44	15	0

zones by UNEP (1997) could not detect these tendencies since the evaporation intensity is related to the soil's physical properties as well as climatic conditions.

A steady value of θ_e should not appear where $Pr < 300$ mm, i.e., when $\theta_e < 0.8$, as described in Section 4.3. The growth of vegetation is unstable in such places. Table 5 includes the ratio for each vegetation with different distribution patterns of θ_e. These were detected by overlapping the distribution of the existing vegetation (Fig. 1b) with the distribution of θ_e (see Fig. 8). A large fraction of forest (97%) exists where $\theta_e > 0.8$. In particular, 75% of the forest is present where $\theta_e > 1.0$. The remaining 3% is present where the effect of orographic precipitation is strong.

Ninety-five percent of the shrub growth was found where $\theta_e > 0.8$. The remaining 5% could be found where the effect of orographic precipitation is strong, as with the forest.

Eighty-three percent of typical grass is present where $\theta_e > 0.8$. Forest and shrubs would certainly have originally existed in such a place. The land use in this area includes plant fields on terraces, a gully erosion field, and a pasture field.

Eighty percent of the short grass can be found where $\theta_e < 0.8$. The remaining 20% ($0.8 < \theta_e < 1.0$) is in the Mu-Us desert, which lies to the west of Yuling. This area is the typical grassland where Mongolians engaged in stock-farming in ancient times. Desertification has progressed rapidly since the 1950s due to human activities (Inner Mongolian Research Group, 1992; Xue, 1996; Bo and Long, 2002). While shrub and typical grass could potentially grow in this region, desertification continues due to improper land use, such as over-grazing (Bo and Long, 2002). Wang and Takahashi (1999) analysed the impact of desertification and suggested that this region should be carefully conserved or protected. Numerical experiments indicate that desertification in the Inner Mongolian grassland influences the regional climate, leading to reduced evaporation, reduced rainfall, and increased surface temperature (Xue, 1996).

Based on these results, the aridity was classified as

$\theta_e \geqslant 1.0$, Forest area,
$0.8 \leqslant \theta_e < 1.0$, Shrub and typical grass area,
$\theta_e < 0.8$, Short grass area.

The biomass is affected by the precipitation intensity in areas where $\theta_e < 0.8$. Miyazaki et al. (2003) while reporting the heat balance, leaf area index, and biomass in central Mongolia (annual precipitation: 200 mm) observed that rainfall intensity

at the beginning of summer (June to July) greatly influences vegetation activity. Thus, maintaining sufficient soil water content in the growth period (June to July) will greatly affect subsequent vegetation activity.

It is very difficult to classify the aridity in the Loess Plateau, where $\theta_e < 0.8$, since θ_e varies greatly with the rainfall intensity. Classification based on the annual precipitation is also difficult for areas where $\theta_e < 0.8$. An evaluation method that combines the seasonal changes of θ_e with the biomass change monitored by remote sensing would be more effective for examining the aridity in such areas.

5. Conclusions

We studied the heat and water balances of bare soil and examined the physical features of five soil types in the Loess Plateau. We also explored the potential distribution of vegetation and determined the aridity in the plateau.

We estimated the seasonal changes of the sensible and latent heat fluxes using meteorological data from 1998. The annual means of the sensible heat flux ranged from 13 to 36 $W m^{-2}$, while the latent heat flux was from 14 $W m^{-2}$ (179 $mm yr^{-1}$) to 40 $W m^{-2}$ (521 $mm yr^{-1}$).

The relationship between the annual precipitation and annual evaporation indicated that evaporation depended greatly both on the rainfall amount and on the soil type and precipitation intensity. The results also indicated that both water retention and restriction of evaporation from the soil surface were affected by yellow loessial soil that included medium loam, light loam, and sandy loam, but not heavy loam.

The dispersion between the fractional extractable water θ_e and the annual precipitation became small when $Pr > 300$ mm, except for the heavy loam. The soil water content was close to the field capacity when $Pr > 400$ mm. However, precipitation intensity influences θ_e when $Pr < 300$ mm, even with the same amount of precipitation. A linear relation was found between θ_e and Pr for the heavy loam.

We also explored the potential distribution of vegetation in the Loess Plateau by comparing the distribution of θ_e and the present vegetation. A large fraction of forest (97%) existed where $\theta_e > 0.8$. Ninety-five percent of the shrub growth was found where $\theta_e > 0.8$. Eighty-three percent of the typical grass was growing where $\theta_e > 0.8$. Forest and shrubs are expected to grow in such areas. Vegetation growth is expected to be unstable due to the dependence of θ_e on rainfall intensity in areas where $\theta_e < 0.8$, where 80% of the short grass could be found.

Acknowledgements

The authors would like to express their gratitude to Dr. Shao and many researchers of the Institute of Soil and Water Conservation, CAS, China, and students of the Arid Land Research Center, Tottori University, for their advice and discussions regarding the present research. Thanks are also extended to Mr. Yao

and Mr. Ma of the Institute of Soil and Water Conservation, CAS, China, who kindly assisted with the field experiments. This research was supported by the 21st Century COE Program of the Ministry of Education, Culture, Sports, Science and Technology.

References

Black, T.A., 1979. Evapotranspiration from Douglas fir stands exposed to soil water deficits. Water Resources Research 15, 164–170.

Bo, W., Long, J., 2002. Landscape change and desertification development in the Mu-Us Sand land, Northern China. Journal of Arid Environments 50, 429–444.

Budyco, M.I., 1956. Heat Balance of the Earth's surface. Gidrometeozidat, Leningrad 255pp.

He, M., 1989. Vegetation map of China. Atlas of China Natural Conservation. Science Press, Beijing, pp. 50–51.

He, X., Li, Z., Hao, M., Tang, K., Zheng, F., 2003. Down-scale analysis for water scarcity in response to soil-water conservation on Loess Plateau of China. Agriculture Ecosystems and Environment 94, 355–361.

In, H.J., Park, S.U., 2002. A simulation of long-range transport of yellow sand observed in April 1998 in Korea. Atmospheric Environment 36, 4173–4187.

Inner Mongolian Research Group, 1992. Studies on control of desertification and development of agriculture at arid land areas in China; Construction of pilot farm at the Mu Us Shamo desert in the Inner Mongolia autonomous region. 212pp (in Japanese).

Kimura, R., Kondo, J., 1999. Studies on the relationships among the leaf transfer coefficient for water vapor, soil water content and spectral reflectance. Journal of the Meteorological Society of Japan 77, 873–886.

Kimura, R., Kamichika, M., Takayama, N., Matsuoka, N., Zhang, X., 2004a. Heat balance and soil moisture in the Loess Plateau, China. Journal of Agricultural Meteorology 60, 103–113.

Kimura, R., Takayama, N., Kamichika, M., Matsuoka, N., 2004b. Soil water content and heat balance in the Loess Plateau; Determination of parameters in the three-layer soil model and experimental result of model calculation. Journal of Agricultural Meteorology 60, 55–65 (in Japanese with English summary).

Kondo, J., Xu, J., 1997. Seasonal variations in the heat and water balances for nonvegetated surfaces. Journal of Applied Meteorology 36, 1676–1695.

Miyazaki, S., Miyamoto, T., Kaihotsu, I., Yasunari, T., Davaa, G., Oymbattar, D., Natsagdorj, L., 2003. Proceedings of the Fifth International GAME conference. 1, 107.

Naruoka, M., Yamamoto, T., 1992. Soil moisture distribution of drip irrigation method in pilot farm of the Mu Us Shamo desert. Studies on control of desertification and development of agriculture at arid land areas in China, pp. 129–133.

Penman, H.L., 1948. Natural evaporation from open water, bare soil, and grass. Proceedings of the Royal Society of London 193A, 120–145.

Philip, J.R., 1957. Evaporation, and moisture and heat fields in the soil. Journal of Meteorology 14, 354–366.

Shinoda, M., 2002. Desert and Climate. Seizando, Tokyo 169pp (in Japanese).

Takayama, N., Kimura, R., Kamichika, M., Matsuoka, N., Zhang, X., 2004. Climatic feature of rainfall in the Loess Plateau in China. Journal of Agricultural Meteorology 60, 173–189.

UNEP, 1997. World Atlas of Desertification. Arnold, London, pp. 1–182.

Wang, Q., Takahashi, H., 1999. A land surface water deficit model for an arid and semiarid region: Impact of desertification on the water deficit status in the Loess Plateau, China. Journal of Climate 12, 244–257.

Xue, Y., 1996. The impact of desertification in the Mongolian and the Inner Mongolian grassland on the regional climate. Journal of Climate 9, 2173–2189.

Yang, W., Shao, M., 2000. Study on the soil water in the Loess Plateau. Science Publisher Press, Beijing 305pp (in Chinese).

ELSEVIER

Journal of Arid Environments 68 (2007) 53–65

Journal of Arid Environments

www.elsevier.com/locate/jnlabr/yjare

Evapo-transpiration estimation over the river basin of the Loess Plateau of China based on remote sensing

R. Kimura[a,*], L. Bai[b], J. Fan[c], N. Takayama[a], O. Hinokidani[d]

[a]*Arid Land Research Center, Tottori University, Hamasaka 1390, Tottori 680-0001, Japan*
[b]*Faculty of Horticulture, Chiba University, Matsudo 271-8510, Japan*
[c]*Institute of Soil and Water Conservation, CAS, Yangling, Shaanxi 712100, China*
[d]*Faculty of Engineering, Tottori University, Koyama, Tottori 680-8552, Japan*

Received 12 October 2005; received in revised form 22 March 2006; accepted 23 March 2006
Available online 11 May 2006

Abstract

In northeastern Loess Plateau of China, wind and/or water erosion are severe, and the amount of earth and sand pouring into the Yellow River is large. It is necessary to establish a land-use system that guarantees the water cycle in the river basin to prevent soil erosion and utilize land resources continuously. We targeted the water balance, especially regarding evapo-transpiration (ET), over the river basin in the northeastern Loess Plateau. For ET estimation, an algorithm referring to the SEBAL method (a remote sensing surface energy balance algorithm for land) based on remote sensing was outlined and validated with the observation result over natural grassland. ET by land-use difference and the spatial distribution of ET over the river basin were examined using the algorithm.

Keywords: Evapo-transpiration; Grassland; Landsat 5; Remote-sensing; SEBAL

1. Introduction

Two-fifths of the land area in China is threatened by wind or water soil erosion. Five billion tons of sediment are transported into the sea annually (Coen, 2003). In particular, the earth and sand flowing out from the Loess Plateau to the Yellow River has reached 1.6

*Corresponding author. Tel.: +81 857 21 7031; fax: +81 857 29 6199.
E-mail address: rkimura@alrc.tottori-u.ac.jp (R. Kimura).

0140-1963/$ - see front matter
doi:10.1016/j.jaridenv.2006.03.029

billion tons year^{-1} in the downstream areas. The riverbed has increased by 10 cm every year; in 1972, for the first time in Chinese history, the Yellow River ran dry before reaching the sea (He et al., 2003). Increased sediment loads have led to flooding risks and threatened the lives of many people. Asian dust caused by wind erosion in the spring, when the soil surface is very dry, is also a serious environmental problem in China and in the neighboring areas of Mongolia, Korea, and Japan (In and Park, 2002).

In the northeastern Loess Plateau, erosion by both wind and water are severe, and the amount of sediment flowing into the Yellow River is particularly large. To prevent soil erosion and utilize land resources continuously, it is necessary to establish a land-use system that guarantees the water cycle in the river basin. Recently, positive results were obtained in the EROCHINA project entitled "A participatory approach for soil and water conservation planning, integrating soil erosion modeling and land evaluation, to improve the sustainability of land use on the Loess Plateau in Northern China" from the viewpoint of the soil's physical and chemical properties, runoff discharge, and soil erosion (e.g. Chen et al., 2003; Coen, 2003; Elsen et al., 2003; Messing et al., 2003; Stolte et al., 2003a b;). However, no comprehensive studies of water balance have been conducted, especially regarding evapo-transpiration (ET) over the river basin of the Loess Plateau.

This study was conducted to clarify the quantitative formulation of ET over the river basin using remote-sensing techniques. First, we outlined the algorithm for ET estimation referring to the concept of Bastiaanssen et al. (1998a) and Tasumi (2003), and validated the estimation result with the observation ET over the grassland (Kimura et al., 2005a). Next, ET was estimated by land-use differences using the algorithm, and the spatial distribution of ET over the river basin was examined.

2. Observation site and experimental method

The observation data was taken at an experimental station of the Liudaogou Basin located in Shenmu District, Shaanxi Province, China (38°47′latitude and 110°21′longitude; Fig. 1) from 5 June to 31 August 2004 (Kimura et al., 2005a). The basin area is 7 km^2, and the altitude is 1224 m. According to statistics from 1957 to 1989, the average annual temperature was 8.4 °C (the coldest −9.7 °C in January and the warmest 23.7 °C in July), with an average annual rainfall of 437 mm (minimum 109 mm, maximum 891 mm) (Academia Sinica and Ministry of Water Resources, 1993).

The soil texture at the experimental station was sandy loam (48% sand, 39% silt, and 13% clay). The station was covered by the dominant grass species, *Stipa bungeana. Trin*. Plant height was 10–15 cm, and the leaf area index (LAI) was 0.7–1.0 during this period. The root zone was within 34 cm. Fig. 1 depicts the land-use type in the Liudaogou Basin. On the hillside, rain-fed cultivation (e.g. millet, soybean, mugwort, and potato) has been conducted. Irrigated farmlands lie in the lowland areas (e.g. maize). On steep slopes with an inclination over 25°, the planting of grass and/or shrub has been recommended by the Chinese government since 1999. In 1993, most of the area was farmland, while grassland and shrub sharply increased in 2004. Compared to 1993, shrub increased by 6% and grassland increased by 22% in 2004. The percentage of farmland decreased from 73% to 43% (Kimura et al., 2005a).

Meteorological data included air temperature (Valsala; HMP45A; instrumental height 150 cm), humidity (Vaisala; HMP45A; 150 cm), wind speed (Young; 03001; 220 cm), precipitation (Davis Inst. Corp.; Rain Collector II), solar radiation, reflected solar

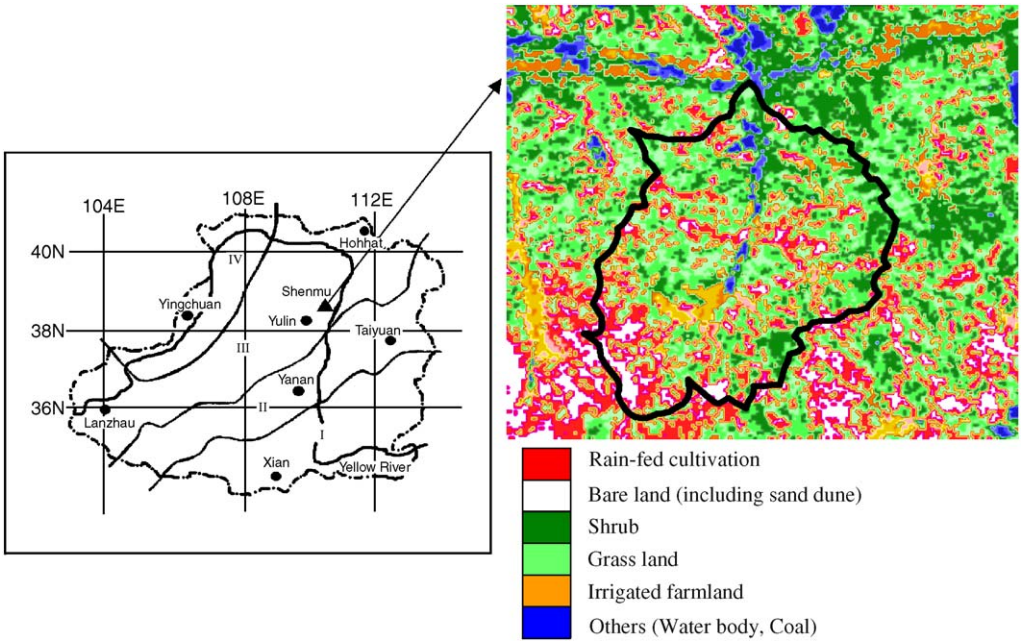

Fig. 1. Location and vegetative classification of the Loess Plateau and land-use classification in the Liudaogou Basin: I. Forest. II. Forest and typical grass. III. Short grass. IV. Desert and short grass. The dashed and dotted line is the borderline of the Loess Plateau. The bold line is the watershed divide of the Liudaogou Basin.

radiation, upward long-wave radiation, downward long-wave radiation (Kipp & Zonen; CNR-1; 175 cm), soil water content at ten depths (Delta-T; ML2X; 6, 10, 18, 26, 34, 42, 50, 58, 66 and 100 cm), and soil temperatures at eight depths (Thermocouple; 1, 4, 10, 18, 26, 34, 42 and 50 cm). Meteorological data were sampled every minute with a datalogger (Cambell Scientific; CR10X), and averages were computed every hour. The soil water content was sampled at 1200 and 2400 BST.

We used the zero flux plane (ZFP) method for observing ET over the grassland (Arya et al., 1975; Scott, 1993). The ZFP separates the region of the soil where the water flow (hydraulic gradient) is upward from that where the water flow is downward. Accumulated ET for the observation period can be calculated from the change of soil water content above the ZFP (Kimura et al., 2005a). ET could not be observed during and following the rainfall events, since the ZFP was near the surface. Accordingly, we interpolated for the data deficit period by using the Penman–Monteith equation and surface resistance, which were represented as a function of soil water content. The root mean squared error between the observed and the calculated values of ET was 0.55 mm day^{-1}. This error was close to the observational error, and the total simulated ET agreed with the observation during the growing period (Kimura et al., 2005a).

When applying ET estimation for the small river basin, a higher spatial resolution satellite image (e.g. LANDSAT TM/ETM + and ASTER) is preferred. In this study, LANDSAT5 TM images were used. Only three images could be obtained during the observation period (on 16 June, 2 July, and 3 August 2004).

3. Algorithm for ET estimation

The heat balance of the surface can be expressed by the following equations:

$$R_n = H + \lambda E + G, \tag{1}$$

$$R_n = (1 - ref)S^{\downarrow} + L^{\downarrow} - L^{\uparrow}. \tag{2}$$

Here, R_n is the net radiation ($W\,m^{-2}$), H the sensible heat flux ($W\,m^{-2}$), λE the latent heat flux ($W\,m^{-2}$), G the soil heat flux ($W\,m^{-2}$), *ref* the surface albedo, $S^{\downarrow}$ the global solar radiation ($W\,m^{-2}$), $L^{\downarrow}$ the downward long-wave radiation ($W\,m^{-2}$), and $L^{\uparrow}$ the upward long-wave radiation ($W\,m^{-2}$).

The values of H are given using the bulk equation by

$$H = c_p \rho C_H U(T_s - T). \tag{3}$$

Here, c_p is the specific heat of air ($J\,kg^{-1}\,K^{-1}$), ρ the density of air ($kg\,m^{-3}$), C_H the bulk transfer coefficient for sensible heat, U the wind speed ($m\,s^{-1}$), T_s the surface temperature (°C or K), and T the temperature (°C or K).

We referred to the SEBAL algorithm for estimating the sensible heat flux H (Bastiaanssen et al., 1998a; Tasumi, 2003). SEBAL assumes that temperature difference T_s–T (dT in the following) in Eq. (3) is linearly proportional to the surface temperature T_s. dT can be developed using two extreme pixels, termed cold pixel and hot pixel. The cold pixel was selected from the deep water surface, and it was assumed that $H = 0$ (i.e. $dT = 0$). In the hot pixel, ET from a very dry bare soil surface was assumed to be zero. Accordingly, sensible heat flux was calculated as follows:

$$H = R_n - G, \tag{4}$$

$$G = \left[\frac{T_s}{ref}(0.0038ref + 0.0074ref^2)(1 - 0.98\mathrm{NDVI}^4)\right] R_n. \tag{5}$$

Here, NDVI is the normalized differential vegetation index. Eq. (5) was cited from Bastiaanssen (2000). Surface albedo *ref* and NDVI could be estimated from the reflectance of each band (Bands 1, 2, 3, 4, 5, and 7 of LANDSAT5 TM), and the upward long-wave radiation and T_s could be calculated from Band 6 (Bastiaanssen, 2000; Tasumi, 2003). Thermal correction was not applied to T_s. Tasumi (2003) suggested that the error in T_s estimation is absorbed at dT estimation when uncorrected T_s is used, and therefore a bias does not appear in the final ET estimation. For $S^{\downarrow}$ and $L^{\downarrow}$, we used the observation data of the meteorological station. dT in the hot pixel was calculated by substituting $C_H U$ and H into Eq. (3). $C_H U$ can be expressed using the atmospheric stability function (Dyer and Hicks, 1970; Kondo et al., 1978) as shown below:

$$C_H U = \frac{k u_*}{\left(\ln(z - d/z_T) + \psi_H\right)}, \tag{6}$$

$$u_* = \frac{kU}{\left(\ln(z - d/z_0) + \psi_M\right)}, \tag{7}$$

$$\psi_M = \ln\frac{(x_0^2 + 1)(x_0 + 1)^2}{(x^2 + 1)(x + 1)^2} + 2(\tan^{-1} x - \tan^{-1} x_0) : \text{unstable}, \tag{8}$$

$$\psi_M = 2.333 \ln \frac{1 + 3\zeta + 10\zeta^3}{1 + 3\zeta_0 + 10\zeta_0^3} : \text{stable}, \tag{9}$$

$$\psi_H = 2 \ln \frac{y_T + 1}{y + 1} : \text{unstable}, \tag{10}$$

$$\psi_H = 400 \ln \frac{1 + 0.0175\zeta + 0.005\zeta^2}{1 + 0.0175\zeta_T + 0.005\zeta_T^2} : \text{stable}, \tag{11}$$

$$x = (1 - 16\zeta)^{1/4}, \tag{12}$$

$$x_0 = (1 - 16\zeta_0)^{1/4}, \tag{13}$$

$$\zeta = \frac{-0.4g(z - d)H}{c_p \rho T u_*^3}, \tag{14}$$

$$\zeta_0 = \frac{-0.4g z_0 H}{c_p \rho T u_*^3}, \tag{15}$$

$$y_T = (1 - 16\zeta_T)^{1/2}, \tag{16}$$

$$y = (1 - 16\zeta)^{1/2}, \tag{17}$$

$$\zeta_T = \frac{-0.4g z_T H}{c_p \rho T u_*^3}. \tag{18}$$

Here, k is the von Karman's constant ($= 0.4$), u_* the friction velocity ($\mathrm{m\,s^{-1}}$), z the observational height of wind speed (m), d the zero plane displacement (m), z_T the roughness length for sensible heat (m), Ψ_H the stability correction factor for sensible heat, z_0 the roughness length for momentum (m), Ψ_M the stability correction factor for momentum, and g the acceleration ($= 9.8\,\mathrm{m\,s^{-2}}$). The value of U at the weather station was converted into the wind speed at 100 m considering the atmospheric stability (Eq. (7)), assuming that friction velocity u_* was constant with height over the weather station. In SEBAL, wind speed at 100 m above the land surface is assumed to be uniform over the satellite image (Bastiaanssen, 2000).

d, z_0, and z_T were determined by the following equations (Allen et al., 1998):

$$d = \frac{2}{3} H_c, \tag{19}$$

$$z_0 = 0.123 H_c, \tag{20}$$

$$z_T = 0.1 z_0, \tag{21}$$

where H_c is the plant height (m), calculated as

$$H_c = 0.601\mathrm{LAI}, \tag{22}$$

$$\mathrm{LAI} = -\ln[(0.66 - \mathrm{SAVI})/1.08]/2.02, \tag{23}$$

where SAVI is the soil-adjusted vegetation index (Huete, 1988). These two equations were derived from field observation using the spectral irradiance instrument (Analytical Spectral Device Inc., FieldSpec FR). Fig. 2 indicates the relationship among LAI, SAVI, and H_c. The dotted line is the result of an equation by Bastiaanssen (1998). While the relationship was slightly different from the observation, the sensitivity of ET estimation to these differences was small. To find the dT of the hot pixel, the loop of Eqs. (6)–(18) was repeated until convergence in $C_H U$ was met. The sand dune area, located in the south-western part of the basin, was selected as the hot pixel. The value of d and z_0 were then assumed as zero and 0.01 m (Oke, 1978).

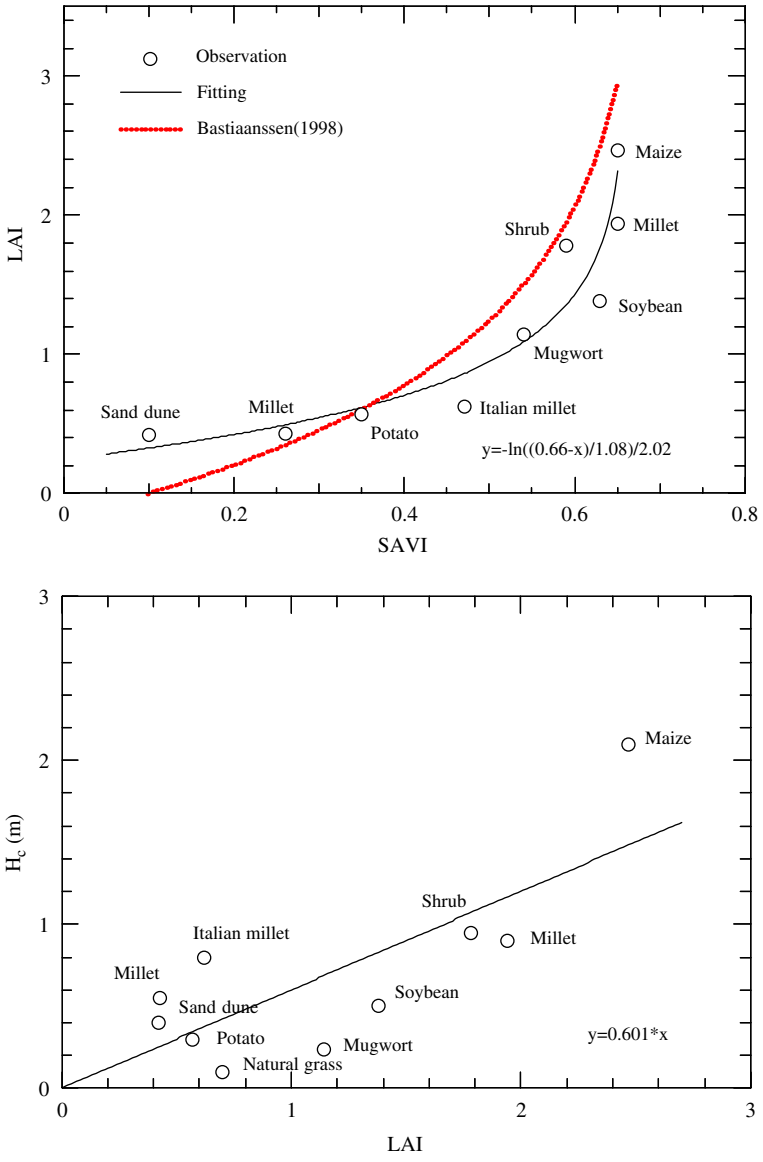

Fig. 2. Relationships among leaf area index (LAI), soil-adjusted vegetation index (SAVI), and plant height (H_c).

The sensible heat flux H and $C_H U$ for the target pixel can also be calculated using the above procedure and dT function. Latent heat flux λE for the target pixel can be calculated as the residual of Eq. (1). In the SEBAL, 24-h ET was estimated assuming a constant evaporative fraction during a day (Bastiaanssen, 2000), while Tasumi (2003) adopted another fraction using the alfalfa reference ET. In this study, we used the fraction using a reference crop ET (ET_0) by Allen et al. (1998) as

$$\mathrm{ETF} = \frac{\mathrm{ET_{inst}}}{\mathrm{ET_{0inst}}}, \tag{24}$$

$$\mathrm{ET_{0inst}} = \frac{0.408\Delta(R_n - G) + \gamma(37/T)U\{e_s - e_a\}}{\Delta + \gamma(1 + 0.34U)}, \tag{25}$$

where ETF is the fraction at the satellite image time, ET_{inst} is estimated ET for the target pixel at the satellite image time (mm h^{-1}), ET_{0inst} is reference crop ET at the selected weather station at the satellite image time (mm h^{-1}), Δ is the slope of the saturation vapor pressure curve at air temperature T (K), γ is the psychrometric constant (kPa °C^{-1}), e_s is the saturation vapor pressure at air temperature (kPa), and e_a is the actual vapor pressure (kPa). Assuming that the ETF was equal to the 24-h ETF, the 24-h ET was estimated with the equation below:

$$\mathrm{ET_{(24)}} = \mathrm{ETF}\,\mathrm{ET_{0(24)}}, \tag{26}$$

$$\mathrm{ET_{0(24)}} = \frac{0.408\Delta(R_n - G) + \gamma(900/T)U\{e_s - e_a\}}{\Delta + \gamma(1 + 0.34U)}. \tag{27}$$

Here, $ET_{(24)}$ is the 24-h ET, and $ET_{0(24)}$ is the 24-h ET_0 at the selected weather station.

4. Results and discussion

4.1. Validation of ET estimation

Fig. 3 depicts the seasonal variations of daily precipitation, 24-h ET, 24-h ET_0, and ETF over the grassland. Total precipitation was 338 mm during this period. ET_0 was at its maximum at 7 mm day^{-1} in July, gradually decreasing thereafter. ET was approximately 1 mm day^{-1}, except for a comparatively large value after the rainfall events. This value was somewhat small compared to that with crops. On many days, ETF was under 0.5. Zhao et al. (2004) estimated the seasonal change of ET from an alfalfa field in Dingxi County of Gansu province on the Loess Plateau. Daily ET ranged from 2 to 3 mm day^{-1} in the summer season. The ET from the grassland was small compared with that from alfalfa. Chikaarashi et al. (1979) reported that ET over grassland (mixed planting of *Digitaria adscendes* $H_{ENR.}$, *Setaria vividis* P. $B_{EAUR.}$ var. *minor* O_{HWI}, *Cuperus microiria* $S_{TEUD.}$, and *Justica procumbens* L. var. *leucantha* H_{ONDA}) growing in Japan was 1.6 times greater than evaporation from the soil surface during the growing period (1.24 times for a decade). Kimura et al. (2005a) confirmed that ET from grassland was about 1.5 times greater than evaporation from the soil surface during the growing period, and annual ET was 1.24 times that of annual evaporation. These results coincided with the findings of Chikaarashi et al. (1979).

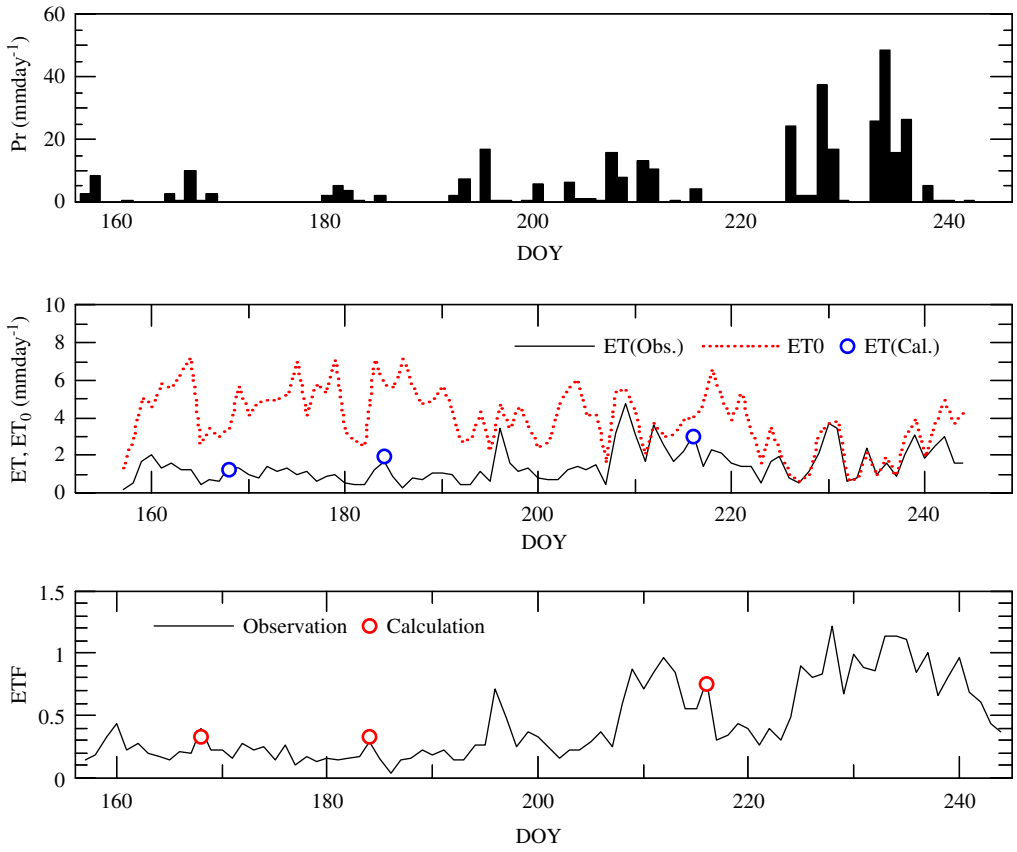

Fig. 3. Seasonal distributions of daily precipitation (*Pr*), daily evapo-transpiration (ET), daily reference evapo-transpiration (ET_0), and the fraction using a reference crop evapo-transpiration (ETF). The symbols represent the calculated results using the algorithm. DOY refers to day of year.

Table 1
Estimated soil-adjusted vegetation index (SAVI), leaf area index (LAI), plant height (H_c), surface albedo (*ref*), normalized differential vegetation index (NDVI), and observed surface albedo over the grassland

	SAVI	LAI	H_c	*ref*	NDVI	*ref* (obs.)
16 June (DOY = 168)	0.13	0.35	0.20	0.19	0.14	0.16
2 July (DOY = 184)	0.11	0.33	0.20	0.20	0.16	0.20
3 August (DOY = 216)	0.18	0.40	0.24	0.19	0.25	0.17

DOY refers to day of year.

Table 1 presents the estimated result of SAVI, LAI, H_c, *ref*, NDVI, and observed *ref* of grassland. During this period, observed LAI ranged from 0.7 to 1.0. While the estimation was slightly smaller than that of the observation, the effect of this difference on the ET estimation was small in the algorithm. The estimated *ref* almost coincided with the observation.

Table 2
Comparison of the observed and calculated values of the evapo-transpiration (mm day^{-1})

	ET (obs.)	ET (ETF)	ET (EF)
16 June (DOY = 168)	1.4	1.2	1.2
2 July (DOY = 184)	1.7	1.9	1.9
3 August (DOY = 216)	3.1	3.0	3.3

ET (ETF) denotes the result using the reference crop evapo-transpiration (Eq. (24)), and ET (EF) the result using the evaporative fraction by Bastiaanssen (2000) (Eq. (28)).

Fig. 3 illustrates the estimation result of 24-h ET and ETF over grassland. Table 2 also reveals the estimation result for three days. Here, ET estimation using the evaporative fraction by Bastiaanssen (2000) is also presented. The evaporative fraction is

$$\mathrm{EF} = \frac{\mathrm{ET}_{\mathrm{inst}}}{(R_{\mathrm{n}} - G)_{\mathrm{inst}}}, \tag{28}$$

where $(R_{\mathrm{n}}-G)_{\mathrm{inst}}$ is the observed value at the selected weather station at the satellite image time. The root mean squared error between the observed ET and the estimated ET was 0.17 mm day^{-1} using Eq. (24), whereas it was 0.20 mm day^{-1} using Eq. (28). The result using Eq. (24) was a little better than that of Eq. (28). According to the sensitivity analysis, an error of 0.41 mm day^{-1} existed in estimating ET with an observational error of $\pm 10\%$ in net radiation, 0.2 °C in air temperature, 0.5 m s^{-1} in wind speed, and $\pm 2\%$ in humidity. The estimated error was within the meteorological observation error.

4.2. Estimating evapotranspiration over the Liudaogou Basin

Fig. 4 presents the spatial distribution of ET over the Liudaogou Basin on 2 July 2004 using the algorithm. ET was distributed from 0 to 5.5 mm day^{-1}. ET from lowland areas beside the river channel was large, while that from the rain-fed farmland and the bare land was small. Table 3 compares ET by land-use types for 3 days. ET from the farmland with irrigation was the largest, compared with that from other land cover. ET from rain-fed farmland almost coincided with that of grassland. The farm production in this area is low, owing to the shortage of soil water, carbon, and nitrogen content in the soil (Bai et al., 2004). ET from shrubs was large, compared with that from grassland. Chikaarashi et al. (1979) reported that ET over shrub (*Amorpha fruticosa* L.) growing in Japan was 1.8 times greater than that from the grassland during the growing period. As Tables 3 and 4 demonstrate, ET from the shrub-land was 1.4 times that of grassland; thus, this result was comparatively close to the findings of Chikaarashi et al. (1979). In this basin, *Caragana korshinskii* (shrub type) has been artificially seeded to prevent soil erosion. However, it was considered that the grassland was more appropriate from the point of water-use efficiency (WUE). Here, WUE was defined as protection from erosion achieved per water consumed (Kimura et al., 2005a). According to field experiment results in the river basin on the Loess Plateau, 6750 kg ha^{-1} soil was lost from the bare soil surface by soil erosion, and 3750 kg ha^{-1} soil was lost from farmland; in contrast, 93 kg ha^{-1} was lost from natural grassland and 60 kg ha^{-1} from the forest (Smil, 1996). Comparing the amount of loss from the grassland with that from the forest does not reveal much difference between them: so

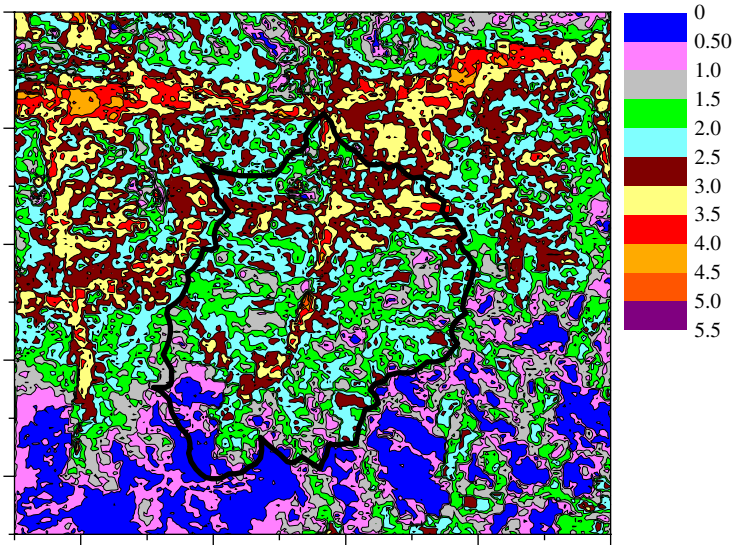

Fig. 4. Spatial distribution of daily evapotranspiration over the Liudaogou Basin on 2 July 2004. The bold line is the watershed divide of the basin.

Table 3
Comparison of the evapo-transpiration by land-use difference for 3 days (mm day^{-1})

	16 June (DOY = 168)	2 July (DOY = 184)	3 August (DOY = 216)	Average
Farmland (irrigation)	2.3	2.9	4.0	3.1
Farmland (rain-fed)	1.2	1.3	3.0	1.8
Shrub	1.2	2.9	4.0	2.7
Grassland	1.2	1.9	3.0	2.0

Table 4
Comparison of evapo-transpiration by land-use difference during the observation period (mm)

Total Pr	ET_0	ET (grassland)	ET (shrub)	ET (farmland with irrigation)	ET (rain-fed farmland)
338	346	127	171	197	114

WUE is comparatively high in the grassland. According to Kimura et al. (2005b), the aridity index in this area has potential for supporting grassland. To prevent further soil erosion, it is very important to cover the bare land surface with such natural grassland. Since 1984, alfalfa has been artificially seeded, but *Stipa bungeana* is the dominant species in this basin (Bai et al., 2004).

Table 4 depicts ET by land-use difference during the observation period. ET of grassland is presented in Fig. 3. As for other land-use ET, we first calculated from Table 3 how many times as large as the ET from grassland are the ET from farmland with

irrigation, the ET from rain-fed farmland, and the ET from shrub. Next, we estimated the land-use ET by multiplying those values by ET from grassland in Table 4. We investigated the surface runoff in the small basin of the Liudaogou (1 km^2). When considering the land use in this small basin, the amount of ET was 132 mm during the observation period in Table 4. The residual 206 mm corresponded to runoff and infiltration. According to the observation, the amount of surface runoff was 88 mm, so 26% of the rainfall was distributed in the surface runoff. The sum of rain-fed farmland and shrub area accounted for 66% of this small basin (shrub was 23%, and rain-fed farmland was 43%). It was considered that turning these land covers into grassland was important for preventing soil erosion and for water storage in the ground, considering the high WUE of grassland. Hereafter, we will observe the other water balance components and evaluate water balance in detail.

In SEBAL, seasonal ET estimation employs an assumption similar to that made for 24-h ET estimation; namely, 24-h ETF for an image date can be applied to ETF for a certain time period. Such an assumption was used in Table 4. However, this assumption does not apply in the case of a long period between satellite images. If we can estimate seasonal ET using the most recent satellite images possible, the accuracy of the amount of ET over the river basin will improve during the target period.

5. Conclusions

An algorithm for estimating the ET referring to the SEBAL method was introduced and validated with observation over grassland. In this algorithm, the following calculation was adopted:

(1) d, z_0, and z_T were estimated using the simple equations by Allen et al. (1998). The equations for LAI and H_c were derived from field observation. LAI estimation using the empirical equations by Bastiaanssen (1998) was slightly different from the observation, but the effect of this difference on the ET estimation was small.
(2) For estimating the 24-h ET, we utilized the fraction using the ET_0 by Allen et al. (1998). The result was slightly better than that of the evaporative fraction (Eq. (28)).
(3) Thermal correction was not applied to the surface-temperature estimation. While some error may occur in the R_n calculation due to the error in $L^{\uparrow}$, much of this error impact is calibrated into the dT function at the cold and hot pixels. For general operational purposes, uncorrected surface temperature is recommended (Tasumi, 2003).

The SEBAL method has been verified in many places, such as Turkey, China, and Egypt (e.g. Bastiaanssen et al., 1998b; Bastiaanssen, 2000; Chemin et al., 2004). However, few references have been made to the natural grassland in semi-arid regions. Applicability to such natural vegetation was confirmed in this study.

Acknowledgments

The authors would like to express their gratitude to Dr. Mingan Shao and their many colleagues in China. This research was supported by the JSPS Core University Program and the 21st Century COE Program of the Ministry of Education, Culture, Sports, Science and Technology.

References

Academia Sinica and Ministry of Water Resources, 1993. Memoir of Northwestern Institute of Soil and Water Conservation, vol. 18. Shaanxi Scientific and Technological Press, Xian (144pp.) (in Chinese).

Allen, R.G., Pereira, L.S., Raes, D., Smith, M., 1998. Crop Evapotranspiration: Guidelines for Computing Crop Water Requirements. FAO, Rome (300pp.).

Arya, L.M., Farrell, D.A., Blake, G.R., 1975. A field study of soil water depletion patterns in presence of growing soybean roots: I. Determination of hydraulic properties of the soil. Soil Science Society of America Proceedings 39, 424–430.

Bai, L., Kobayashi, T., Li, Y., Zhang, X., Shao, M., Kamichika, M., 2004. A study on the suppress of vegetation and their factors in Liudogou test site in northern Loess Plateau, China. Journal of Japanese Society of Revegetation Technology 30, 187–192 (in Japanese with English summary).

Bastiaanssen, W.G.M., 1998. Remote Sensing in Water Resources Management: The State of the Art. International Water Management Institute, Colombo, SriLanka.

Bastiaanssen, W.G.M., 2000. SEBAL-based sensible and latent heat fluxes in the irrigated Gediz Basin, Turkey. Journal of Hydrology 229, 87–100.

Bastiaanssen, W.G.M., Menenti, M., Feddes, R.A., Holtslag, A.A.M., 1998a. A remote sensing surface energy balance algorithm for land (SEBAL) 1. Formulation. Journal of Hydrology 212–213, 198–212.

Bastiaanssen, W.G.M., Pelgrum, H., Wang, J., Ma, Y., Moreno, J.F., Roerink, G.J., van der Wal, 1998b. A remote sensing surface energy balance algorithm for land (SEBAL) 2. Validation. Journal of Hydrology 212–213, 213–229.

Chemin, Y., Platonov, A., UI-Hassan, M., Abdullaev, I., 2004. Using remote sensing data for water depletion assessment at administrative and irrigation-system levels: case study of the Ferghana Province of Uzbekistan. Agricultural Water Management 64, 183–196.

Chen, L., Messing, I., Zhang, S., Fu, B., Ledin, S., 2003. Land use evaluation and scenario analysis towards sustainable planning on the Loess Plateau in China-case study in a small catchment. CATENA 54, 303–316.

Chikaarashi, H., Hattori, S., Takeuchi, N., 1979. A study of the water balance by the different vegetation cover in the sloping lysimeter. Bull. For. & For. Res. Inst. 303, 1–46.

Coen, J.R., 2003. Introduction: soil erosion and participatory land use planning on the Loess Plateau in China. CATENA 54, 1–5.

Dyer, A.J., Hicks, B.B., 1970. Flux–gradient relationships in the constant flux layer. Quarterly Journal of Royal Meteorological Society 96, 715–721.

Elsen, E., Hessel, R., Liu, B., Trouwborst, K.O., Stolte, J., Ritsema, C.J., Blijenberg, H., 2003. Discharge and sediment measurements at the outlet of a watershed on the Loess Plateau of China. CATENA 54, 147–160.

He, X., Li, Z., Hao, M., Tang, K., Zheng, F., 2003. Down-scale analysis for water scarcity in response to soil-water conservation on Loess Plateau of China. Agricultural Ecosystems and Environments 94, 355–361.

Huete, A.R., 1988. A soil-adjusted vegetation index (SAVI). Remote Sensing of Environment 25, 295–309.

In, H.J., Park, S.U., 2002. A simulation of long-range transport of yellow sand observed in April 1998 in Korea. Atmospheric Environment 36, 4173–4187.

Kimura, R., Fan, J., Zhang, X., Takayama, N., Kamichika, M., Matsuoka, N., 2005a. Evapotranspiration over the grassland field in the Liudaogou basin of the Loess Plateau, China. Acta Oecologica, in press.

Kimura, R., Liu, Y., Takayama, N., Zhang, X., Kamichika, M., Matsuoka, N., 2005b. Heat and water balances of the bare soil surface and the potential distribution of vegetation in the Loess Plateau, China. Journal of Arid Environments 63, 439–457.

Kondo, J., Kanechika, O., Yasuda, N., 1978. Heat and momentum transfers under strong stability in the atmospheric surface layer. Journal of Atmospheric Science 35, 1012–1021.

Messing, I., Chen, L., Hessel, R., 2003. Soil conditions in a small catchment on the Loess Plateau in China. CATENA 54, 45–58.

Oke, T.R., 1978. Boundary Layer Climates. Methuen & Co., New York (272pp.).

Scott, W.K., 1993. A field test of a soil-based measure of evapotranspiration. Soil Science 156 (6), 396–404.

Smil, V., 1996. The Bad Earth: Environmental Degradation in China (Japanese translation by Fukao, Y. and Koosaki, S.). Japan UNI Agency, Inc., Tokyo, 289pp. (in Japanese).

Stolte, J., Venrooij, B., Zhang, G., Trouwborst, K.O., Liu, G., Ritsema, C.J., Hessel, R., 2003a. Land-use induced spatial heterogeneity of soil hydraulic properties on the Loess Plateau in China. CATENA 54, 59–75.

Stolte, J., Liu, B., Ritsema, C.J., Elsen, H.G.M., Hessel, R., 2003b. Modelling water flow and sediment processes in a small gully system on the Loess Plateau in China. CATENA 54, 117–130.

Tasumi, M., 2003. Progress in operational estimation of regional evapotranspiration using satellite imagery. Ph.D. Thesis, University of Idaho, USA, 357pp.

Zhao, C., Feng, Z., Chen, G., 2004. Soil water balance simulation of alfalfa (*Medicago sativa* L.) in the semiarid Chinese Loess Plateau. Agricultural Water Management 69, 101–114.

ELSEVIER

Journal of Arid Environments 70 (2007) 237–252

Journal of Arid Environments

www.elsevier.com/locate/jaridenv

Estimation of moisture availability over the Liudaogou river basin of the Loess Plateau using new indices with surface temperature

R. Kimura*

Arid Land Research Center, Tottori University, Hamasaka 1390, Tottori 680-0001, Japan

Received 6 June 2006; received in revised form 1 November 2006; accepted 15 December 2006
Available online 20 February 2007

Abstract

This study presents developments of indices for surface moisture condition estimations aiming at a more mechanistic approach compared to previous indices. Moisture availability (m_a), calculated as the ratio of actual evapotranspiration (ET) to reference evapotranspiration (ET_0), and soil water content were estimated over a river basin on the Loess Plateau of China using two newly developed indices. A modified temperature–vegetation dryness index (MTVDI) was calculated from satellite-derived surface temperature, and aerodynamic minimum and maximum surface temperatures estimated from meteorological data. MTVDI corresponded well to seasonal variations of m_a over an area of varied land use, and especially well in areas of grassland. A wet-edge index was derived from the relationship between MTVDI and the normalized differential vegetation index (NDVI), the MTVDI–NDVI triangle space, which is achieved by plotting MTVDI as a function of NDVI. The wet-edge index showed the relationship to m_a of various land surfaces and soil water contents in the river basin. However, we concluded that a wider range of vegetation cover and soil moisture content were needed to calculate a meaningful wet-edge index. These two indices have advantages that can estimate surface moisture condition qualitatively. They can be used as aridity and/or drought indices.

Keywords: Evapotranspiration; Reference evapotranspiration; Remote sensing; Surface temperature; Vegetation index

*Tel.: +81 857 21 7031; fax: +81 857 29 6199.
E-mail address: rkimura@alrc.tottori-u.ac.jp.

0140-1963/$ - see front matter © 2007 Elsevier Ltd. All rights reserved.
doi:10.1016/j.jaridenv.2006.12.021

1. Introduction

Many studies of the degree of aridity in arid or semi-arid regions are based on climatic data. Aridity indices used include the radiative dryness index defined by Budyco (1956) and the E_p/Pr ratio (e.g., Penman, 1948; Thornthwaite and Wilm, 1944; UNEP, 1997), where E_p is potential evaporation and Pr is precipitation. Wang and Takahashi (1999) pointed out that these indices were developed from semi-empirical relationships between observed evapotranspiration (ET) and climatic factors, and do not capture physical processes in the soil–vegetation–atmosphere continuum (SVAC). However, these convenient indices are still used in the classification of aridity (Millennium Ecosystem Assessment, 2005; UNEP, 1997).

Many studies of land-surface aridity have used satellite data. The most often used indices are the normalized differential vegetation index (NDVI; Rouse et al., 1974), the soil-adjusted vegetation index (SAVI; Huete, 1988), and the modified SAVI (MSAVI; Qi et al., 1994), all of which use remotely sensed data of visible and near-infrared wavelengths. These methods have been used to estimate changes in vegetation, surface soil moisture, and ET. Recently, the potential for the combined use of microwave and optical data as an aid for crop management has been explored (Moran et al., 1997), and an algorithm combining satellite data with meteorological data (e.g., SEBAL, a remote-sensing surface energy balance algorithm for land; Bastiaanssen et al., 1998) was developed and used to estimate water balance at river-basin scale (Bastiaanssen, 2000; Kimura et al., 2007).

Of the many indices that use remotely sensed data, the relationship between surface temperature (T_s) and vegetation indices (e.g., NDVI) has, in particular, been used to investigate the vegetation and moisture conditions of land surfaces (e.g., Luquet et al., 2004; Moran et al., 1994; Nemani et al., 1993; Sandholt et al., 2002; Vidal and Devaux-Ros, 1995). These approaches can be grouped into three broad categories:

(1) The T_s–NDVI relationship (e.g., Goward et al., 1985; Nemani and Running, 1989) typically shows a strong negative relationship between surface temperature and the spectral vegetation index. The slope of the T_s–NDVI curve provides information on moisture conditions, such as stomatal resistance and ET at the intrinsic surface (e.g., deciduous forest).
(2) The T_s–NDVI method was later extended to develop a soil-canopy water deficit index (WDI) using information in the T_s–NDVI space (Moran et al., 1994); the WDI was originally derived from the concept of crop water stress index (CWSI) introduced by Jackson et al. (1981). This approach uses a "vegetation index–temperature (VIT) trapezoid", and is based on the hypothesis that a trapezoidal shape will result from a plot of the difference between observed surface temperature and air temperature ($T_s - T_a$) vs. vegetation index at the intrinsic surface (e.g., an alfalfa crop) if there is sufficient variation of fractional vegetation cover and surface water conditions. For this approach, a range of vegetation cover and soil water content investigated is a critical factor in determining the shape of the trapezoid, and thus demonstrating the relationship.
(3) Following Moran et al. (1994), Sandholt et al. (2002) developed a simplified land surface dryness index (TVDI). In this approach, a scatterplot of remotely sensed surface temperature and NDVI was assumed to take a triangular shape, and the TVDI could be estimated from the dry and wet edges of the triangle (Fig. 1). The TVDI

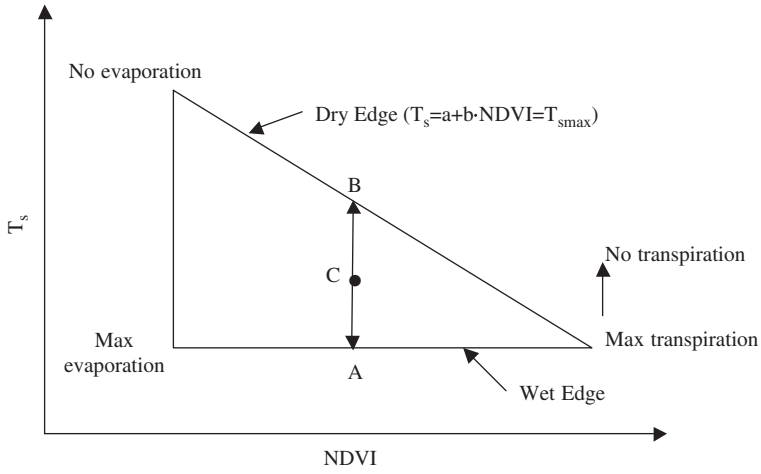

Fig. 1. T_s–NDVI triangle space (after Sandholt et al., 2002). TVDI of point C can be estimated as AC/AB.

approach was applied by Sandholt et al. (2002) in northern Senegal to a 140 × 140 km area of mixed land cover (which included dry grasslands, areas of shrubs, and cultivated areas) and related to soil moisture status.

The TVDI approach has an advantage over other indices (such as the T_s–NDVI curve and the VIT trapezoid) in that it can be applied to mixed land surfaces, and derives surface moisture status from satellite information only. However, since the determination of the maximum and minimum surface temperature in the TVDI equation is comparatively empirical, the TVDI approach has some limitations when applied on a small scale.

We developed a MTVDI and wet-edge index, a conceptually new index incorporating the general principles of Jackson et al. (1981), Moran et al. (1994) and Sandholt et al. (2002), and which combines the use of meteorological data and remotely sensed satellite data. We applied MTVDI and wet-edge index to the Liudaogou River basin on the Loess Plateau of China, and validated our results using moisture availability ($m_a = ET/ET_0$, where ET_0 is the reference ET defined by Allen et al., 1998) for different land surfaces and soil water contents.

2. Indices

2.1. Temperature–vegetation dryness index

Fig. 1 illustrates the T_s–NDVI triangle space (Sandholt et al. 2002). A negative relationship between T_s and NDVI is shown by the dry edge (the hypotenuse of the triangle), which represents the upper limit of T_s. The left side of the triangle represents the bare soil relationship in the range from dry to wet. The wet edge was assumed to be a horizontal line, as opposed to a sloping wet edge as in the trapezoid approach (Moran et al., 1994).

TVDI is defined as

$$\mathrm{TVDI} = \frac{T_s - T_{s\min}}{a + b \times \mathrm{NDVI} - T_{s\min}}, \tag{1}$$

where T_s is the observed surface temperature (°C or K), $T_{s\,min}$ (the wet edge) is the minimum surface temperature within the triangle, and a and b are coefficients defining the dry edge, calculated as a linear fit to data. The value of $a + b \times$ NDVI (the dry edge) can be represented by $T_{s\,max}$, where $T_{s\,max}$ is the maximum surface temperature for a particular value of NDVI. $T_{s\,min}$ and $T_{s\,max}$ are estimated as the mean minimum and maximum surface temperatures over small intervals of NDVI. TVDI at point C (Fig. 1) can be estimated as AC/AB.

Sandholt et al. (2002) suggested that the spatial variation of TVDI reflected variations of surface moisture on a fine scale. Although this method offers useful information about surface moisture, it has some limitations.

- In order to define the dry and wet edges, a large study area is needed so that surface moisture status can be obtained for a wide range of vegetated surfaces. This is difficult to achieve in the small river basins typical of arid or semi-arid regions.
- Calculation of the dry and wet edges is comparatively empirical, because the size of the area studied determines the shape of the triangle.

2.2. A new MTVDI

We defined the MTVDI as follows (Fig. 2):

$$\mathrm{MTVDI} = \frac{T_s - T_{s\,min}}{T_{s\,max} - T_{s\,min}}, \tag{2}$$

where T_s is the observed surface temperature at a given pixel of remotely sensed data (°C or K), and $T_{s\,min}$ and $T_{s\,max}$ are minimum and maximum surface temperatures for the reference crop (Allen et al., 1998) simulated using energy balance equations and meteorological data. The effects of varieties of physiological activities on T_s can be separated from the effects of meteorological varieties by normalization.

The basic equation for the heat balance of a land surface is

$$R^{\downarrow} - G = \sigma T_s^4 + H + \lambda E, \tag{3}$$

where

$$R^{\downarrow} = (1 - \mathrm{ref})S^{\downarrow} + L^{\downarrow}, \tag{4}$$

and $R^{\downarrow}$ is the total incident radiation ($\mathrm{W\,m^{-2}}$), G is the soil heat flux ($\mathrm{W\,m^{-2}}$), σ is the Stefan–Boltzmann constant ($5.67 \times 10^{-8}\,\mathrm{W\,m^{-2}\,K^{-4}}$), H is the sensible heat flux ($\mathrm{W\,m^{-2}}$),

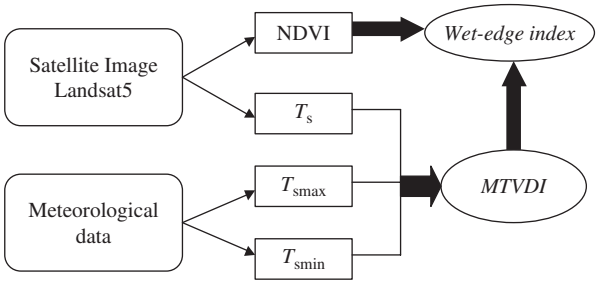

Fig. 2. Flowchart of the method for estimating the MTVDI and the wet-edge index.

λE is the latent heat flux ($W\,m^{-2}$), ref is the surface albedo, $S^{\downarrow}$ is the global solar radiation ($W\,m^{-2}$), and $L^{\downarrow}$ is the downward long-wave radiation ($W\,m^{-2}$).

The fluxes H and λE can be expressed by the bulk transfer equations:

$$H = c_p \rho C_H U(T_s - T) \tag{5}$$

and

$$\lambda E = \lambda \rho C_H U \beta \{q_{sat}(T_s) - q\}, \tag{6}$$

where c_p and ρ are the specific heat ($J\,kg^{-1}\,K^{-1}$) and density ($kg\,m^{-3}$) of the air, C_H is the bulk transfer coefficient, U is the wind speed ($m\,s^{-1}$), T is the air temperature (°C), λ is the latent heat of vaporization ($J\,kg^{-1}$), β is the evapotranspiration efficiency (which has a value of one at sufficient wet condition and a value of zero at the sufficient dry condition ($ET \approx 0$)), $q_{sat}(T_s)$ is the specific humidity at saturation at T_s ($kg\,kg^{-1}$), and q is the specific humidity ($kg\,kg^{-1}$). Substitution of Eqs. (5) and (6) into Eq. (3) yields the following equation for T_s:

$$R^{\downarrow} - G - \sigma T_s^4 - c_p \rho C_H U(T_s - T) - \lambda \rho C_H U \beta \{q_{sat}(T_s) - q\} = 0. \tag{7}$$

In Eq. (7), it is assumed that the canopy and ground can be regarded as a single plane surface.

Allen et al. (1998) recommended the use of a reference ET (ET_0) value to estimate actual ET. ET_0 can be derived from the original Penman–Monteith equation and a hypothetical reference crop with an assumed crop height of 0.12 m, a fixed surface resistance of $70\,s\,m^{-1}$, and a surface albedo of 0.23. The aerodynamic resistance (r_a) of a reference crop surface can be defined (Allen et al., 1998) and converted into $C_H U$ as follows:

$$r_a = \frac{208}{U} = \frac{1}{C_H U}. \tag{8}$$

The soil heat flux (G) as expressed by Allen et al. (1998), is:

$$G = 0.1 \times R_n, \tag{9}$$

$$R_n = (1 - \mathrm{ref})S^{\downarrow} + L^{\downarrow} - \sigma T_s^4, \tag{10}$$

where R_n is the net radiation ($W\,m^{-2}$). In this study, $T_{s\,max}$ and $T_{s\,min}$ in Eq. (2) are defined as T_s for a reference crop when $\beta = 0$ and 1, respectively.

According to Jackson et al. (1981) and Moran et al. (1994), both the CWSI and the WDI are related to the actual and potential ET rates of a surface, that is,

$$\frac{\lambda E}{\lambda E_p} = 1 - \mathrm{CWSI} = \frac{T_s - T_{s\,max}}{T_{s\,min} - T_{s\,max}}, \tag{11}$$

$$\frac{\lambda E}{\lambda E_p} = 1 - \mathrm{WDI} = \frac{(T_s - T_a) - (T_s - T_a)_{dry}}{(T_s - T_a)_{wet} - (T_s - T_a)_{dry}}, \tag{12}$$

where λE is the actual ET, λE_p is the potential ET, T_a is the air temperature (°C or K), and the wet and dry indices correspond to the left and right limits of the trapezoid. The MTVDI concept is similar to those for CWSI and WDI (Eqs. (11) and (12)).

The wet edge index is derived from the MTVDI–NDVI triangle space (Fig. 2). The wet edge is estimated as the mean minimum MTVDI value over small intervals of NDVI.

3. Errors and assumptions in the estimation of MTVDI

There may be some errors in the estimation of MTVDI from satellite data and meteorological data:

- No atmospheric correction or surface emissivity correction was applied in the T_s estimation. However, surface emissivity was given as 0.98 for respective land surfaces in the estimation. It should be noted that surface emissivity is different from each land surface. Generally, it is difficult to get a meteorological data for atmospheric corrections in arid or semi-arid regions. Atmospheric corrections and uncertainties in surface emissivity associated with satellite-borne surface radiometric temperatures lead to uncertainties of 1–3 °C in T_s (Campbell and Norman, 1998).
- It is assumed that the radiometric surface temperature (T_s of Eq. (2)) and aerodynamic surface temperature ($T_{s\,min}$ and $T_{s\,max}$ of Eq. (2)) are the same in this study. However, they are not exactly the same according to Campbell and Norman (1998).
- According to the sensitivity analysis, there was an error of 0.41 mm d^{-1}in the estimation of ET. The error of 0.41 mm d^{-1} corresponds to the energy level of 12 W m^{-2} and an aerodynamic surface temperature of 2 °C.
- The estimated error for radiometric surface temperature is almost the same as that for aerodynamic surface temperature. It is assumed that these errors will be negated by normalization in the calculation of MTVDI.
- The value of T_s can be affected by shade arising from orographic effects. Estimates of $T_{s\,min}$ and $T_{s\,max}$ in Eq. (2) must take the effect of shade into account. Because most of the slopes in our study area face either east or west, with an inclination of less than 25°, we assumed that shade had no effect on our MTVDI estimation. (In such a condition, solar radiation in the slopes is almost same as that in the flat surface (Tsuboi, 1990)).

4. Test site and analysis methods

4.1. Site description and experimental method

The study area was the Liudaogou River Basin located in Shenmu District, Shaanxi Province, China (38°47′N 110°21′E) (Fig. 3). The basin size is approximately 3 × 4 km. According to statistics from 1957 to 1989, the average annual temperature is 8.4 °C (the coldest −9.7 °C in January, the warmest 23.7 °C in July), with an average annual rainfall of 437 mm (minimum 109 mm, maximum 891 mm) (Academia Sinica and Ministry of Water Resources, 1993). In this basin, both wind erosion and water erosion are severe, and the amount of earth and sand deposited in the Yellow River is considered to be a serious problem (Academia Sinica and Ministry of Water Resources, 1993). Heavy rainfall in the summer is the main cause of soil erosion in Shenmu. The aridity index used by UNEP (1997) indicates that this district lies in a semi-arid region. According to the potential distribution of vegetation determined by Kimura et al. (2005), the original vegetation type in this district would have been grassland.

Fig. 3 shows land use in the Liudaogou Basin. Production levels from rain-fed cultivation on hillsides (e.g., millet, soybean, mugwort, and potato) are very low, owing to a shortage of soil water and the low carbon and nitrogen content in the soil. Soil water

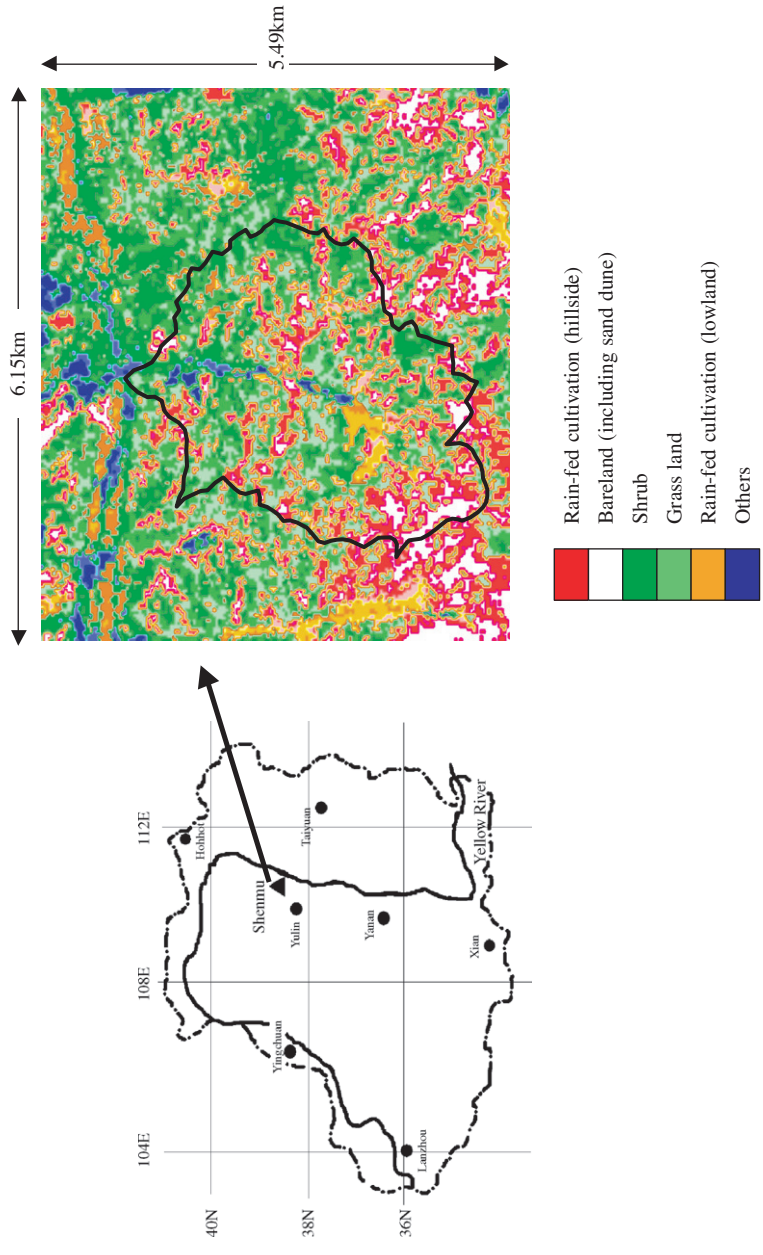

Fig. 3. Location of the Loess Plateau and land-use classification in the Liudaogou Basin. The bold line shows the boundary of the watershed.

content is comparatively high in lowland areas, where maize is cultivated. Natural and introduced grasses and shrubs grow on the steep slopes. The soil texture at the experimental site is sandy loam (48% sand, 39% silt, and 13% clay). The site is covered by the locally dominant grass species, *Stipa bungeana* Trin. Grass height at the time of our study was 10–15 cm, and the leaf area index (LAI) was 0.7–1.0 during the growing season. The root zone extended to a depth of 34 cm. Some seasonal variations of ET and surface resistance are described by Kimura et al. (2006).

Meteorological data was recorded from June 2004 to September 2005 and included air temperature (Vaisala; HMP45A; instrument height 150 cm); humidity (Vaisala; HMP45A; 150 cm); wind speed (Young; 03001; 220 cm); precipitation (Davis Inst. Corporation; Rain Collector II); solar radiation, comprising reflected solar radiation, upward long-wave radiation, and downward long-wave radiation (Kipp and Zonen; CNR-1; 175 cm); soil water content at 10 depths (Delta-T; ML2X; 6, 10, 18, 26, 34, 42, 50, 58, 66 and 100 cm); and soil temperatures at eight depths (Thermocouple; 1, 4, 10, 18, 26, 34, 42 and 50 cm). The meteorological sensors were sampled with a datalogger and multiplexor (Campbell Scientific; CR10X and AM16/32) at 1-min intervals, and averages were computed hourly. The soil water content was sampled daily at 1200 and 2400 BST. Soil-moisture sensors were set horizontally, except for one that was installed vertically from the soil surface to a depth of 6 cm to provide an average soil moisture to that depth.

LANDSAT5 TM images were used to determine NDVI and T_s. The resolutions of bands 1–5, and 7 are 30 m, and that of band 6 is 120 m. Seven images were obtained within the meteorological observation period. Acquisition dates of the images are shown in Fig. 5.

4.2. Observed ET and estimation of ET and ET_0

Observed ET and estimation of ET and ET_0 were used in the calculation of m_a that was a validation data for indices (Eqs. (13) and (15)).

The zero flux plane (ZFP) method was used to determine ET over the grassland (Arya et al., 1975; Scott, 1993). The ZFP method separates the region of the soil where water flow (hydraulic gradient) is upward from that where water flow is downward. Cumulative ET for the observation period can be calculated from the change of soil water content above the ZFP. We could not observe ET during and following rainfall events, because the ZFP was then too near the surface. We, therefore, used the Penman–Monteith equation and surface resistance (which is a function of soil water content) to interpolate and fill these gaps in the data. The root mean square error between the observed and the calculated values of ET was 0.55 mm d^{-1}. This error was close to the observational error, and the total simulated ET agreed with that observed during the growing period (Kimura et al., 2006).

ET was not observed in cultivated areas (hillside and lowland) or shrub land. We used the SEBAL algorithm (Bastiaanssen et al., 1998) to estimate ET in these areas. SEBAL uses spectral radiances recorded by satellite sensors and meteorological data to determine the heat balance components at land surfaces. Instantaneous ET is estimated as a residual of the heat balance. Daily ET can be computed from the evaporative fraction. SEBAL has been verified in many places, including Turkey, China, and Egypt. Kimura et al. (2007) applied SEBAL in natural grasslands in the Liudaogou Basin and found that the root mean square error between the observed and estimated ET was 0.17 mm d^{-1}. The estimated error was within the meteorological observational error.

This study used a reference crop ET (ET_0) defined by Allen et al. (1998) to examine the moisture availability (m_a) over the several types of land surface. For areas other than grassland, the following equations were used to estimate m_a:

$$m_a = \frac{ET_{inst}}{ET_{0\,inst}}, \tag{13}$$

$$ET_{0\,inst} = \frac{0.408\Delta(R_n - G) + \gamma(37/T)U(e_s - e_a)}{\Delta + \gamma(1 + 0.34U)}, \tag{14}$$

where ET_{inst} is estimated ET using SEBAL for the target pixel at the time of capture of the satellite image (mm h^{-1}), $ET_{0\,inst}$ is reference crop ET at the selected weather station at the time of capture of the satellite image (mm h^{-1}), Δ is the slope of the saturation vapor pressure curve at air temperature (kPa $°C^{-1}$), γ represents the psychrometric constant (kPa $°C^{-1}$), T and U are the air temperature (K) and wind speed (m s^{-1}) at 2 m height, e_s is the saturation vapor pressure at air temperature (kPa), and e_a is the actual vapor pressure (kPa).

In grassland areas, the following equations were used to estimate m_a:

$$m_a = \frac{ET_{(24)}}{ET_{0\,(24)}}, \tag{15}$$

$$ET_{0\,(24)} = \frac{0.408\Delta(R_n - G) + \gamma(900/T)U(e_s - e_a)}{\Delta + \gamma(1 + 0.34U)}, \tag{16}$$

where $ET_{(24)}$ is the 24-h observed ET using the ZFP method, and $ET_{0\,(24)}$ is the 24-h ET_0 at the selected weather station. According to Allen (2000), m_a in Eq. (13) can be assumed to be the same as that in Eq. (15); that is, m_a is presumed to be constant during a single day.

5. Results and discussion

5.1. Application of MTVDI

The relationship of TVDI and MTVDI to m_a (ET/ET_0) over the Liudaogou Basin on 2 July 2004 was shown in Fig. 4. Although both indices show a good correspondence to moisture availability, the coefficient of determination (R^2) for MTVDI and m_a was higher than that for TVDI. Same tendencies were recognized in all acquisition dates of the images.

A plot of MTVDI as a function of NDVI, also showing the wet edge, for each LANDSAT TM image is shown in Fig. 5. The wet edge differs for each image; the significance of this is discussed in Section 5.2.

When there are varied land uses and conditions of variable surface moisture are introduced, the triangle shapes in the MTVDI–NDVI space of Fig. 5 can be regarded as equivalent to those of Sandholt et al. (2002), except for the dry winter season (23 November 2004 in Fig. 5). However, the triangle may not be determined correctly from satellite data if the area of interest does not include a full range of land-surface conditions. Therefore, calculation of the dry and wet edges in the TVDI equation was empirical. However, the MTVDI equation was not affected by the triangle shape.

Fig. 6 presents the relationship between m_a and MTVDI for all the land surfaces in the study area together, and for grassland alone, using the seven LANDSAT TM images. With

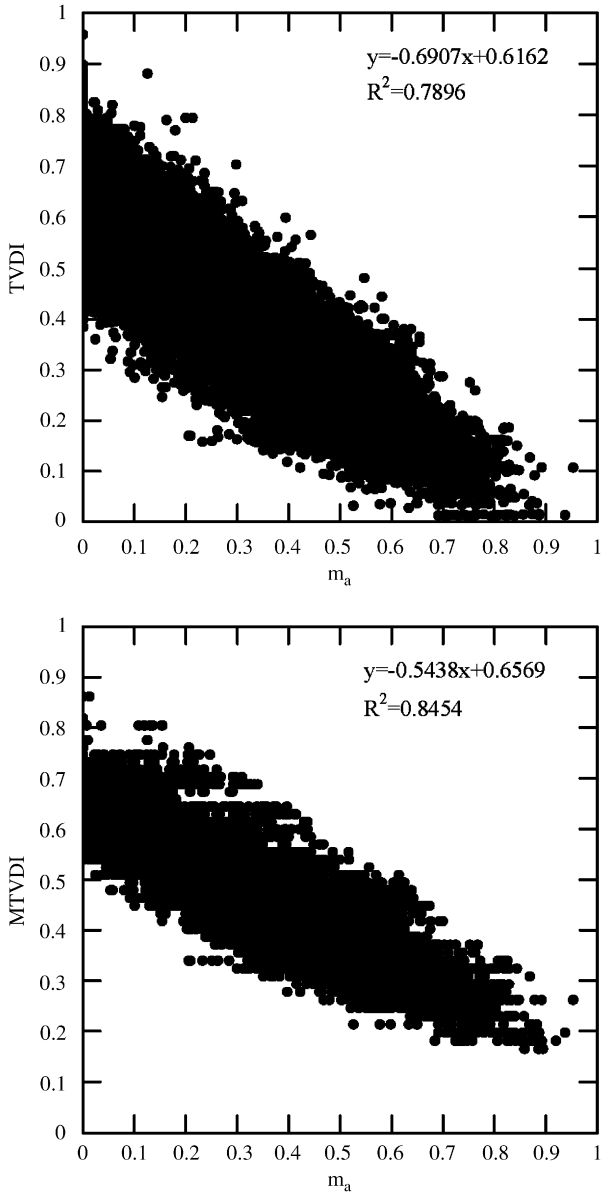

Fig. 4. Relationship of TVDI and MTVDI to moisture availability (m_a).

the exception of grassland areas, ET was estimated using the SEBAL algorithm, which has some limitations:

- In the dry winter season, most of the vegetation in the basin died, so transpiration would have been minimal. The algorithm does not allow for this.
- Two pixels within the area of interest are used to fix boundary conditions for the energy balance in the SEBAL calculation. These are known as the ''hot pixel'' and the ''cold

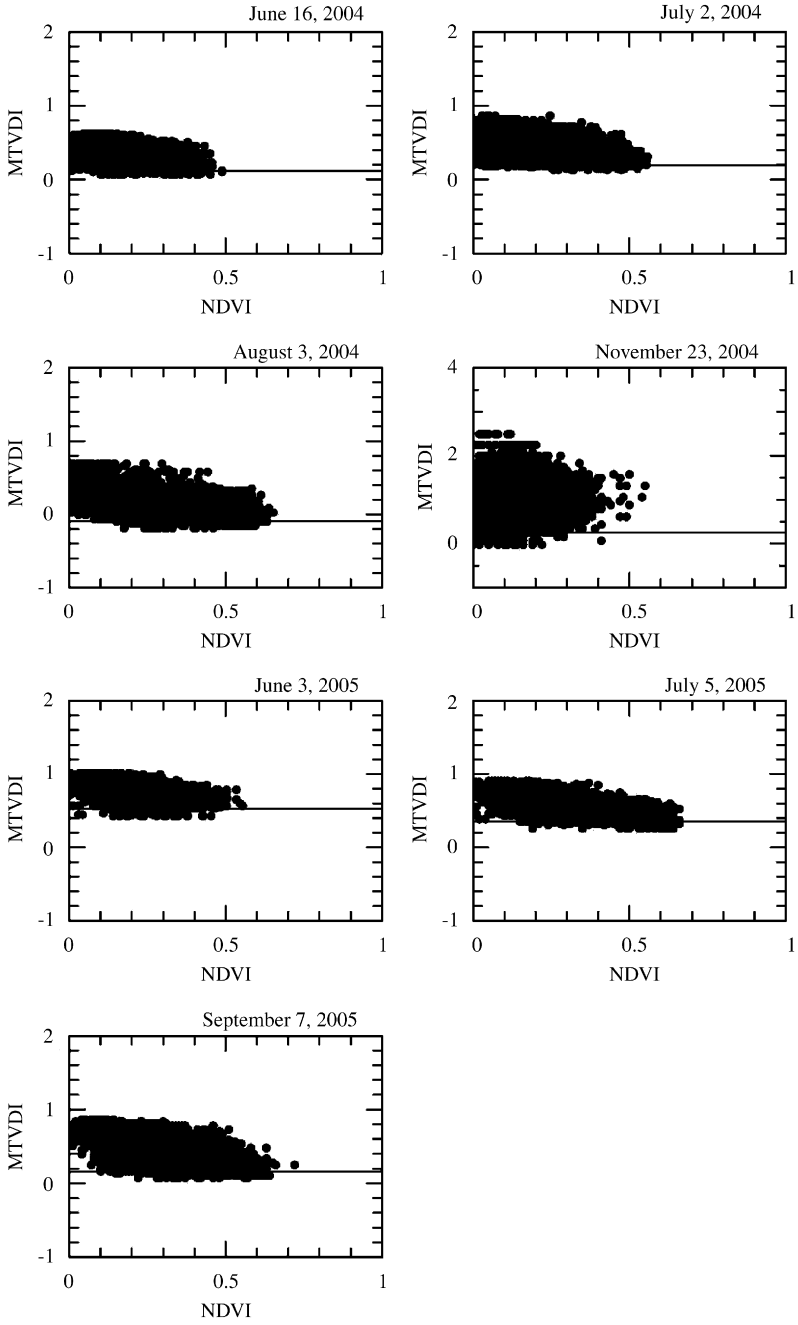

Fig. 5. MTVDI–NDVI space for the 7 LANDSAT TM images used in this study. The wet edge is shown as a straight line, and was calculated as the mean minimum MTVDI over the NDVI intervals (Sandholt et al. 2002).

pixel''. The hot pixel is selected as a dry, bare area where ET is assumed to be zero. In this study, an area of sand dunes near the basin boundary was used as the hot pixel. This approach cannot be applied immediately after rainfall, because of the resulting evaporation in the ''hot pixel''.

For this latter reason, fewer estimations of ET were possible in the cultivated areas and shrub lands (Fig. 6a). The MTVDI corresponded well to the seasonal variation of m_a for the various land surfaces, especially for the grassland, and the coefficient of determination (R^2) for MTVDI and m_a ($R^2 = 0.8746$; Fig. 6b) was higher than that for mixed land uses.

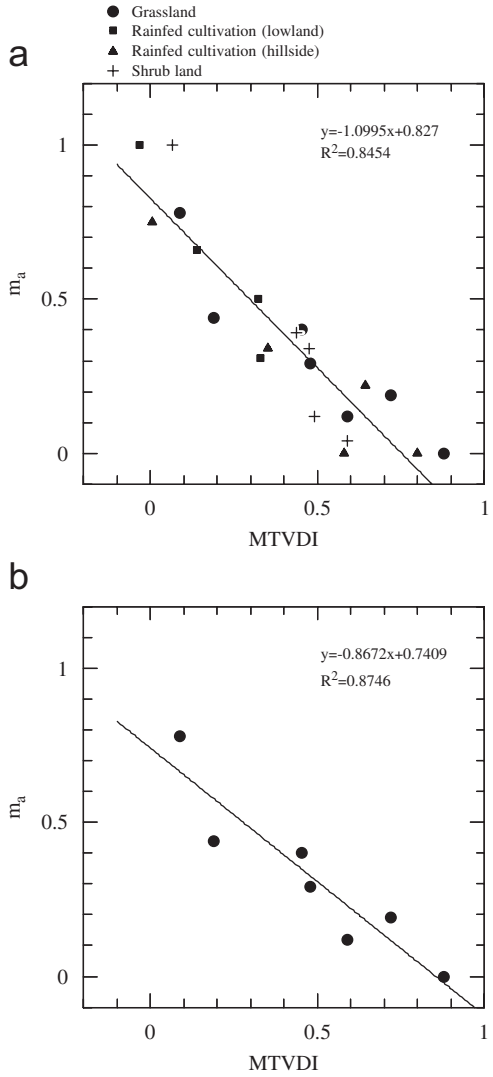

Fig. 6. Relationship between moisture availability (m_a) and MTVDI: (a) for different land surfaces and (b) for grassland alone.

5.2. Wet-edge index

The relationship between the wet edge and m_a for the different land surfaces is shown in Fig. 7. We found that m_a tended to decrease with increases in the wet edge. Fig. 8 shows the relationships between m_a and the fractional extractable water remaining in the root zone (θ_e), which can be represented by the equation:

$$\theta_e = \frac{\theta - \theta_w}{\theta_f - \theta_w}, \tag{17}$$

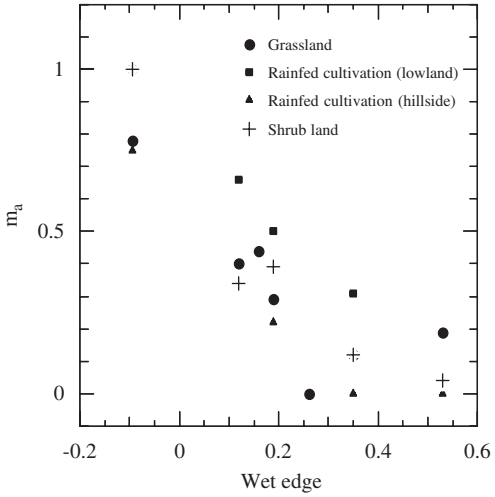

Fig. 7. Relationship between moisture availability (m_a) and the wet-edge value for different land surfaces.

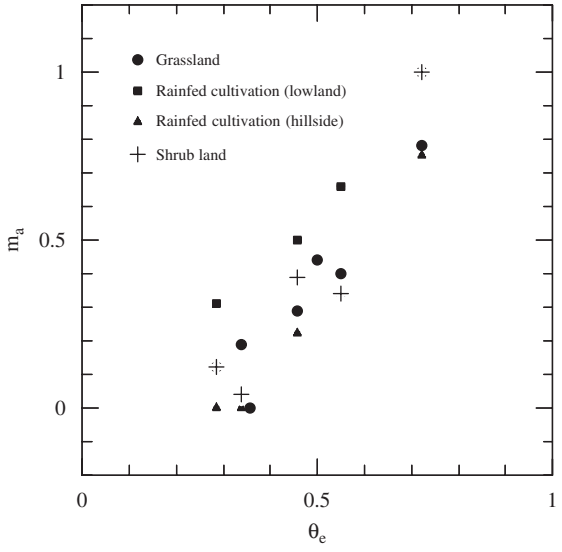

Fig. 8. Relationship between moisture availability (m_a) and the fractional extractable water remaining in the root zone (θ_e) for different land surfaces.

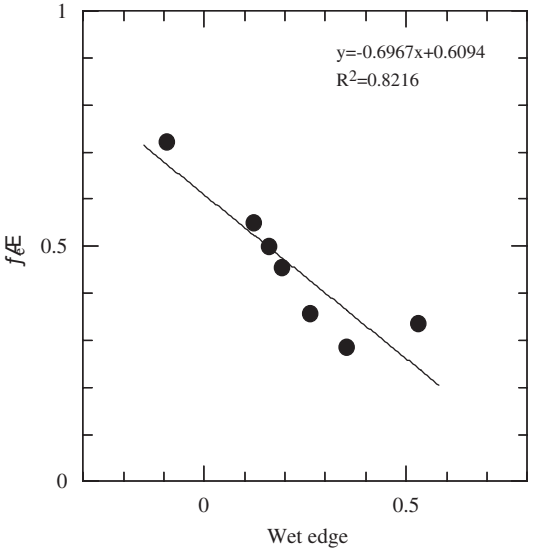

Fig. 9. Relationship between the fractional extractable water remaining in the root zone (θ_e) and the wet-edge value.

where θ is the average volumetric soil water content in the root zone ($m^3\,m^{-3}$) (to a depth of 34 cm), θ_f is the field capacity ($0.19\,m^3\,m^{-3}$), and θ_w is the wilting point ($0.05\,m^3\,m^{-3}$) of volumetric soil water content. Although the value of θ_e was observed in the grassland, m_a tended to increase with increases in θ_e. We assumed that θ_e in the grassland was representative of the soil water content throughout the basin. However, θ_e should actually be observed for each of the land surfaces.

Fig. 9 shows the relationship between the wet edge and θ_e. A good correspondence is evident ($R^2 = 0.8216$). These results suggest it might be possible to use the wet edge as an index to approximate the surface moisture status over the entire river basin. However, the wet edge is greatly affected by variability in land-surface conditions; that is, the types and distribution of vegetation cover and variability of soil moisture content. The size of the study area will be important when using the wet-edge index.

6. Conclusions

Two new indices (MTVDI and the wet-edge index) for estimating m_a and soil water content were introduced and compared with observations over the Liudaogou Basin of the Loess Plateau of China. MTVDI was determined from satellite-derived surface temperature and aerodynamic minimum and maximum surface temperatures from meteorological data. MTVDI was demonstrated to have a relationship to the seasonal change of m_a for mixed land surfaces, and especially for grassland areas ($R^2 = 0.8746$). The wet-edge index was estimated from the MTVDI–NDVI triangle space. Wet-edge values reflected the seasonal variation of m_a in land surfaces of variable cover and for variations in soil water content in grassland areas ($R^2 = 0.8216$). These indices have advantages that can estimate surface moisture condition such as m_a qualitatively. They should be used as the aridity and/or drought indices. It should be noted that such indices do not adequate to

the quantitative estimation for m_a and/or ET. Additional work in other river basins is required to further test these indices.

There are some limitations to the use of MTVDI and the wet-edge index.

(1) These indices were significantly affected by meteorological conditions when calculating the aerodynamic surface temperature, so they are limited to small-scale uses. For applying to large-scale uses, a detailed grid of meteorological data is needed.
(2) For estimating the wet edge, a range of vegetation cover and soil water content is needed. The use of this index will be difficult in areas where vegetation cover does not greatly vary, and where there is limited water. Consequently, the wet-edge index is comparatively empirical, as were past indices such as TVDI.

If in the future a detailed grid of meteorological data can be applied, these indices will be useful tools for water management and for the detection of water stress of vegetation at river-basin scale. However, any stress factors such as nutrient limitations, disease, insect predation could reduce m_a. Additional work is required to separate such stresses from water limitations.

Acknowledgements

The author expresses his gratitude to Dr. J. Fan and his many colleagues in China. This research was supported by the JSPS Core University Program and the 21st Century COE Program of the Ministry of Education, Culture, Sports, Science and Technology.

References

Academia Sinica and Ministry of Water Resources, 1993. Memoir of Northwestern Institute of Soil and Water Conservation 18. Shaanxi scientific and technological press, Xian, 144pp. (in Chinese).

Allen, R.G., 2000. Using the FAO-56 dual crop coefficient method over an irrigated region as part of an evapotranspiration intercomparison study. Journal of Hydrology 229, 27–41.

Allen, R.G., Pereira, L.S., Raes, D., Smith, M., 1998. Crop Evapotranspiration: Guidelines for Computing Crop Water Requirements. FAO, Rome, 300pp.

Arya, L.M., Farrell, D.A., Blake, G.R., 1975. A field study of soil water depletion patterns in presence of growing soybean roots: I. Determination of hydraulic properties of the soil. Soil Science Society Of America Proceedings 39, 424–430.

Bastiaanssen, W.G.M., 2000. SEBAL-based sensible and latent heat fluxes in the irrigated Gediz Basin, Turkey. Journal of Hydrology 229, 87–100.

Bastiaanssen, W.G.M., Menenti, M., Feddes, R.A., Holtslag, A.A.M., 1998. A remote sensing surface energy balance algorithm for land (SEBAL) 1. Formulation. Journal of Hydrology 212–213, 198–212.

Budyco, M.I., 1956. Heat Balance of the Earth's Surface. Gidrometeoizdat, Leningrad, 255pp.

Campbell, G.S., Norman, J.M., 1998. An Introduction to Environmental Biophysics. Springer, New York, 286pp.

Goward, S.N., Cruickhanks, G.D., Hope, A.S., 1985. Observed relation between thermal emission and reflected spectral radiance of a complex vegetated landscape. Remote Sensing of Environment 18, 137–146.

Huete, A.R., 1988. A soil adjusted vegetation index (SAVI). Remote Sensing of Environment 25, 295–309.

Jackson, R.D., Idso, S.B., Reginato, R.J., Pinter, P.J., 1981. Canopy temperature as a crop water stress indicator. Water Resource Research 17, 1133–1138.

Kimura, R., Bai, L., Fan, J., Takayama, N., Hinokidani, O., 2007. Evapotranspiration estimation over the river basin of the Loess Plateau of China based on remote sensing. Journal of Arid Environments 68, 53–65.

Kimura, R., Fan, J., Zhang, X., Takayama, N., Kamichika, M., Matsuoka, N., 2006. Evapotranspiration over the grassland field in the Liudaogou basin of the Loess Plateau. Acta Oecologica 29, 45–53.

Kimura, R., Liu, Y., Takayama, N., Zhang, X., Kamichika, M., Matsuoka, N., 2005. Heat and water balances of the bare soil surface and the potential distribution of vegetation in the Loess Plateau, China. Journal of Arid Environments 63, 439–457.

Luquet, D., Vidal, A., Dauzat, J., Begue, A., Olioso, A., Clouvel, P., 2004. Using directional TIR measurements and 3D simulations to assess the limitations and opportunities of water stress indices. Remote Sensing of Environment 90, 53–62.

Millennium Ecosystem Assessment, 2005. Ecosystems and Human Well-being. World Resources Institute, Washington, DC, 25pp.

Moran, M.S., Clarke, T.R., Inoue, Y., Vidal, A., 1994. Estimating crop water deficit using the relation between surface-air temperature and spectral vegetation index. Remote Sensing of Environment 49, 246–263.

Moran, M.S., Vidal, A., Troufleau, D., Qi, J., Clarke, T.R., Pinter, P.J., Mitchell, T.A., Inoue, Y., Neale, C.M.U., 1997. Combining multifrequency microwave and optical data for crop management. Remote Sensing of Environment 61, 96–109.

Nemani, R., Pierce, L., Running, S., Goward, S., 1993. Developing satellite-derived estimates of surface moisture status. Journal of Applied Meteorology 32, 548–557.

Nemani, R.R., Running, S.W., 1989. Estimation of regional surface resistance to evapotranspiration from NDVI and thermal IR AVHRR data. Journal of Applied Meteorology 28, 276–284.

Penman, H.L., 1948. Natural evaporation from open water, bare soil, and grass. Proceedings of the Royal Society of London 193A, 120–145.

Qi, J., Chehbouni, A., Huete, A.R., Kerr, Y.H., Sorooshian, S., 1994. A modified soil adjusted vegetation index. Remote Sensing of Environment 48, 119–126.

Rouse, J.W., Haas, R.H., Scell, J.A., Deering, D.W., Harlan, J.C., 1974. Monitoring the vernal advancement of retrogradation of natural vegetation. NASA/GSFC, Type III, Final Report. Greenbelt, MD, 371pp.

Sandholt, I., Rasmussen, K., Andersen, J., 2002. A simple interpretation of the surface temperature/vegetation index space for assessment of surface moisture status. Remote Sensing of Environment 79, 213–224.

Scott, W.K., 1993. A field test of a soil-based measure of evapotranspiration. Soil Science 156 (6), 396–404.

Thornthwaite, C.W., Wilm, H.G., 1944. Report of the committee on transpiration and evaporation, 1943–44. Transactions of the American Geophysical Union 25, 683–693.

Tsuboi, Y., 1990. Agricultural Meteorology. Yokendo, Tokyo, pp. 283.

UNEP, 1997. World Atlas of Desertification. Arnold, London, pp. 1–182.

Vidal, A., Devaux-Ros, C., 1995. Evaluating forest fire hazard with a Landsat TM derived water stress index. Agricultural and Forest Meteorology 77, 207–224.

Wang, Q., Takahashi, H., 1999. A land surface water deficit model for an arid and semiarid region: impact of desertification on the water deficit status in the Loess Plateau, China. Journal of Climate 12, 244–257.

Full Paper

J. Agric. Meteorol. (農業気象) 60 (3): 173-189, 2004

Climatic Features of Rainfall in the Loess Plateau in China

Naru TAKAYAMA*, Reiji KIMURA*, Makio KAMICHIKA*,
Nobuhiro MATSUOKA** and Xingchang ZHANG***

* Arid Land Research Center, Tottori University, Tottori, 680-0001 Japan
** Faculty of Horticulture, Chiba University, Matsudo, 271-8510 Japan
*** Institute of Soil and Water Conservation, Chinese Academy of Science, Yangling, Shaanxi, 712100 China

We have researched environmental monitoring to support anti-desertification activities in the Loess Plateau. In this thesis, the spatial distribution, the variance (stability) and the trend of annual precipitation were studied. In addition, the stability of precipitation in the summer rainy season was estimated from the viewpoint of seasonal features of precipitation. The sampling distribution of the mean of the annual precipitation was resampled by the Bootstrap method at each observation point, and the mean of the annual precipitation was estimated by interval estimation. The time series trend of the annual precipitation was analyzed by using the interval estimation mean of the annual precipitation. The stability of precipitation in the summer rainy season was analyzed from the relationship between the precipitation ratio and the precipitation stability index for the period of five days. It seems that the mean of annual precipitation was the lowest in the Tengeri Desert and the Wulanbu Desert. But the region on the Quilian mountain range at the west side of those deserts near Menyuan had much precipitation. The rainfall increased in low-latitude regions. The variation of annual precipitation was the largest in the northern Maowusu Desert, the northeastern Wulanbu Desert, and around Wugong. In contrast, the variations of annual precipitation were small around Menyuan. We could not see a trend for annual precipitation in the whole of the Loess Plateau from 1980 to 2000. However, it seems that there were significant trends at a few observation points. We proposed the rainy season stability index $\{RSS_{(j)}\}$ based on the relationship between the precipitation ratio $PRP_{(i,j)}$ and the precipitation stability index $PSI_{(i,j)}$. The analysis of the feature of precipitation by using $RSS_{(j)}$ clarified that the rainy season is not equally stable between the east side and the west side of the Loess Plateau, even if the annual precipitation is at the same level.

Key words: The features of precipitation, Precipitation ratio, Precipitation stability index, The Loess Plateau, Rainy season stability index.

1. Introduction

The Loess Plateau in China is a semi-arid area located E100° to 115° and N34° to 40°. The landscape of the Loess Plateau is represented by stair-type field in which even mountaintops are cultivated, and erosion valleys (gullies). This region is the front line of desertification in China. About 70% of the annual precipitation is concentrated in the summer (China Meteorological Administration, 1994) and loess soil is very highly erodible, so steep gullies are formed in the Loess Plateau. About 1.6 billion tons of soil per year flow out from the Yellow River (Niu and Liu, 1989) and about 90% of that originates from the Loess Plateau (Nagasawa *et al.*, 1993).

The current desertification of China, as represented by the Loess Plateau, is the result of the form of agriculture in each era, the scale of economic activity, and the natural recoverability determined by precipitation and the ecosystem. Desertification has thus repeatedly advanced and retreated following a complex pattern (Zhu *et al.*, 1989; Zhu, 1990; Yoshino, 1997). However, the Chinese government is trying to prevent soil erosion by restoring vegeta-

Presented at the Annual Meeting of Chugoku-Shikoku Branch on November 12, 2003.
Received on October 20, 2003.
Accepted on April 30, 2004.

tion. Therefore, cultivation on steep hills and pasturing have been forbidden or restricted.

It is extremely important to study the climatic features, especially rainfall, in order to prevent desertification by suitable afforestation. We have done research on environmental monitoring necessary to support anti-desertification activities in the Loess Plateau from 2001 in cooperation with Institute of Soil and Water Conservation, the Chinese Academy of Science. In this thesis, the spatial distribution, the variability (stability) and the trend of annual precipitation were studied. The stability of precipitation in the summer rainy season at each point was estimated from the viewpoint of seasonal feature of precipitation.

The Mann-Kendall test (Kendall, 1938), a kind of non-parametric test method, is often used for trend analysis of precipitation (Molnar and Ramirez, 2001; Lazaro *et al.*, 2001) because of the difficulty of collecting long-term data to define the probability density function of precipitation. However, according to distribution of precipitation over approximately 100 years at six of points in Japan (Liu *et al.*, 1999), the distribution of annual precipitation became asymmetrical when the data was totaled over short terms. In this study, the Loess Plateau is located in the summer rain zone in which cloudbursts happen suddenly, so the probability distribution of precipitation may be asymmetric. Moreover, it is difficult to examine the probability distribution of precipitation based on many observation points and long periods of data collection.

In this study, the interval estimation of the population mean of annual precipitation was performed. The Bootstrap method (Efron, 1982) was used to resample the sample distribution of the mean of annual precipitation for the interval estimation. The spatial distribution and time series trend of annual precipitation were analyzed using the estimated interval mean of annual precipitation as the standard value. In addition, the precipitation ratio in the period $\{PRP_{(i,j)}\}$ and the precipitation stability index $\{PSI_{(i,j)}\}$ were defined to analyze feature of seasonal rainfall. The variability (stability) of precipitation in the summer rainy season was analyzed from the relationship between $PRP_{(i,j)}$ and $PSI_{(i,j)}$ at each point.

2. Methods

2.1 Study area

The study area extends from N33°35′ to N41°34′ and from E98°13′ to E118°9′. This area is inland and includes the Loess Plateau. The location of the observation points and geographical features are shown in Fig. 1. The name of each observation point is shown in Fig. 2 and the coordinates of each point

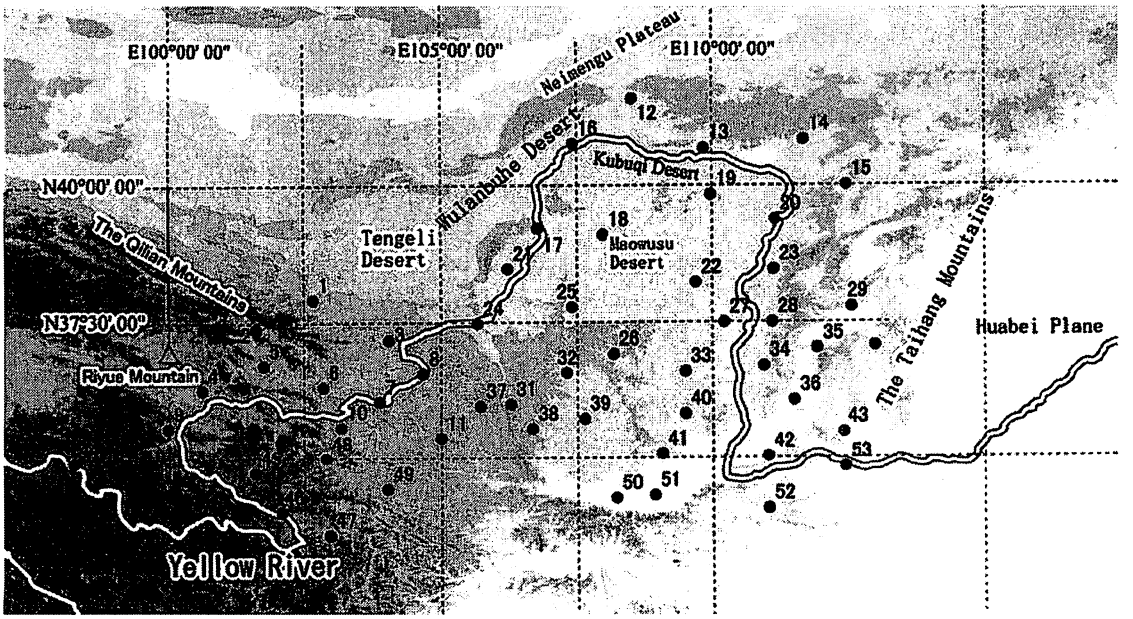

Fig. 1. Topographic features in the Loess Plateau, and location of each observation point.

Table 1. Observation point's names, point code, latitude, longitude and the interval mean of annual precipitation with 95% of confidence level.

Observation points	Code	Position (degree)		95% interval estimation of the annual precipitation	
		Latitude	Longitude	$P_{d(j)}$ (mm)	$P_{u(j)}$ (mm)
Wuwei	1	37.92	102.67	153.1	186.8
Menyuan	2	37.38	101.62	495.7	561.6
Jingtai	3	37.18	104.05	159.4	195.3
Qiapuqia	4	36.27	100.62	291.6	342.0
Xining	5	36.72	101.75	347.3	400.5
Minghe	6	36.32	102.85	308.6	364.2
Langzhou	7	36.05	103.88	279.1	323.5
Jingyuan	8	36.57	104.68	207.3	259.2
Xinghai	9	35.58	99.98	332.0	379.1
Lingxia	10	35.58	103.18	458.6	513.8
Huajialing	11	35.38	105.00	417.9	494.4
Wulatehouqi	12	41.57	108.52	173.1	211.4
Baotou	13	40.67	109.85	265.5	335.2
Huhehaote	14	40.82	111.68	353.7	431.8
Youyu	15	40.00	112.45	365.3	427.5
Linghe	16	40.75	107.42	125.8	171.8
Huinong	17	39.22	106.77	138.0	186.4
Ertuokeqi	18	39.10	107.98	221.1	291.7
Tongshen	19	39.83	109.98	325.6	410.7
Hequ	20	39.38	111.15	333.9	410.2
Yinchuan	21	38.48	106.22	157.0	197.4
Yuling	22	38.23	109.70	330.4	392.1
Xinxian	23	38.47	111.13	431.3	502.2
Zhongning	24	37.48	105.67	165.5	219.0
Yanchi	25	37.78	107.40	245.9	305.5
Wuqi	26	36.92	108.17	401.1	474.5
Shuide	27	37.50	110.22	382.9	451.2
Lishi	28	37.50	111.10	407.1	497.7
Taiyuan	29	37.78	112.55	379.9	461.5
Yushe	30	37.07	112.98	461.9	552.3
Guyuan	31	36.00	106.27	393.0	467.1
Huanxian	32	36.58	107.30	358.3	462.2
Yanan	33	36.60	109.50	463.7	564.1
Xixian	34	36.70	110.95	436.0	516.1
Jiexiu	35	37.03	111.92	386.5	472.1
Lingfen	36	36.07	111.50	418.6	483.5
Xiji	37	35.97	105.72	369.3	435.0
Pingliang	38	35.55	106.67	430.1	527.2
Xifenzhen	39	35.73	107.63	469.6	568.1
Luochuan	40	35.82	109.50	532.8	625.0
Tongchuan	41	35.08	109.07	537.9	658.3
Yuncheng	42	35.03	111.02	476.8	572.4
Yangcheng	43	35.48	112.40	535.3	642.6
Maduo	44	34.92	98.22	303.1	347.3
Henan	45	34.73	101.60	520.4	586.5
Maqu	46	34.00	102.08	550.1	621.1
Ruoergai	47	33.58	102.97	619.3	690.6
Hezhuo	48	35.00	102.90	495.4	549.6
Minxian	49	34.43	104.02	517.5	594.6
Wugong	50	34.25	108.22	505.1	645.7
Xian	51	34.30	108.93	506.4	619.8
Lushi	52	34.05	111.03	587.3	703.2
Menjing	53	34.83	112.43	538.4	657.9

are shown in Table 1. There are various descriptions of the extent of the Loess Plateau. In this thesis, the eastern border of the Loess Plateau is the Taihang Mountains, the western border is Riyue Mountain, the southern border is the Guanzhang Basin including Xian (51), and the northern border is the desert area. The Loess Plateau was formed by particles transported and accumulated by wind from the desert zone (Naruse and Ono, 1997). These particles are carried by the northwest wind from Siberian high (Liu *et al.*, 1992). The Tibetan Plateau and the glacier of the Konlun Mountains also supply loess (Smalley and Krinsley, 1978; Fang, 1995).

Xian (51), located in the southeast part of the study area, is at the southern end of the Loess Plateau. The southern side of the Loess Plateau is a plain where wheat is more actively cultivated (Shaanxi Measurement Committee, 1999). Because Xian (51) is in the plain zone, the observation points located in the southern portion of the loess zone in the study area are Tongcheng (19) and Yangcheng (43). Vegetation becomes sparser and sparser as we go north from Xian (51) in the province of Shaanxi. A dune appears in the Maowusu Desert near Yuiling (22), and Wulatehouqi (12) in northernmost part of the study area is located in the desert area called the Inner Mongolian Plateau (Liu, 1998). A mountainous region of 4,000 to 5,000 m altitude is found in the southwest of Wuwei (1), located on the western edge of the Tengeri Desert. The Taihang Mountains (2,000 to 3,000 m class) are found along the eastern edge in the study area. Its east side is the North China Plain that includes Beijing, and its west side is the Loess Plateau.

2.2 Rainfall data and test of homogeneity

The precipitation data used in this study is daily precipitation acquired at the meteorological observation stations (53 points) located around the Yellow River from 1961 to 2000. It is necessary to note the homogeneity of measurements when we treat long-term meteorological data. Buildings around the observation point and a change in the measuring method will have degraded the homogeneity of the data (Jones, 1995). The Thom test was used to check the homogeneity of precipitation data. The Thom test is used to check the homogeneity of long-term meteorological data as recommended by WMO, although it is a non-parametric test (Peinado-Serna, 1985).

The quotient of annual precipitation and observation days was calculated as the mean of precipitation of a day for every year from 1961 to 2000 because the data includes failed observations. The mean of precipitation of a day at observation point j for each year y is designated as $X_{(y,j)}$. The median of distribution of $X_{(y,j)}$ is designated as X_{med}. When the number of data for which $X_{(y,j)} > X_{\mathrm{med}}$ is R, R can be approximated by the normal distribution with a mean $E(R)$ and variance $Var(R)$ if the number of data N exceeds 25 and the population of $X_{(y,j)}$ is homogeneous.

$$E(R)=\frac{N+2}{2} \tag{1}$$

$$Var(R)=\frac{N(N-2)}{4(N-1)} \tag{2}$$

The test statistic is

$$Z=\frac{R-E(R)}{\sqrt{Var(R)}} \tag{3}$$

The null hypothesis is rejected if $|Z| \leqq 2.58$, when the level of significance is defined as $\alpha=0.01$. The Thom test confirmed the homogeneity of the precipitation data for all the observation points.

2.3 Interval estimation of mean value of annual precipitation

First, "the average annual precipitation" is defined at each observation point. The trend of annual precipitation was examined by comparing "the average annual precipitation" and "the annual precipitation of each year." However, there were many failed observations during 1961 to 1979, so the annual precipitation could not be calculated at most observation points. The failed observations are not interpolated from presumed values. Only measurements from 1980 to 2000 with few failed observations are used.

The arithmetic mean of annual precipitation of 21 years may be considered as "the average annual precipitation." However, influences caused by periodic or abrupt climate changes, a distribution of atmospheric pressure each year, and the weather are included in annual precipitation. When the distribution of annual precipitation of 21 years is asymmetric, the point prediction of the arithmetic mean will be not able to represent "the average annual precipitation." In this study, the interval estimation of the population mean of annual precipitation was calculated with a confidence coefficient of 95%. It is thought that the population mean of annual precipi-

tation is in the estimated section at the probability of 95%. The lower and upper bounds of this estimated section were defined as $P_{d(j)}$ and $P_{u(j)}$ (mm), respectively. Details of the population type and variance are not known, so the parametric estimation method cannot be applied. The interval estimation of the population mean was estimated using the Bootstrap resample method (Efron, 1982). The interval estimation of the population mean can be estimated without assuming the normality of the population by using this method. The following were thus employed.

1) The annual precipitation in year "y" at observation point "j" ($P_{(y,j)}$: mm) was numbered as $P_{(1980,j)}\rightarrow 0$, $P_{(1981,j)}\rightarrow 1$, .., $P_{(2000,j)}\rightarrow 20$.
2) Twenty-one random numbers from 0 to 20 were made, and the value of $P_{(y,j)}$ corresponding to each random number was chosen as the sample distribution.
3) The arithmetic mean of annual precipitation (M_1) was calculated from the sample distribution chosen in step 2).
4) The arithmetic means of M_2, .., M_{10000} were calculated by repeating procedures 2) and 3).
5) The resampled distribution of M_1, .., M_{10000} is a nearly normal distribution, so $P_{d(j)}$ and $P_{u(j)}$ of M_n were obtained from the 2.5 and 97.5 percentiles of this distribution, respectively.
6) $P_{d(j)}$ and $P_{u(j)}$ of each observation point was estimated by the same procedures.

Because there were no data for 2001 at Tongcheng (19), the interval estimation was done by using the precipitation data for the 20 years from 1980 to 1999. Tongcheng (19) was an important observation point located in the south end of the loess zone, so the data for Tongcheng was used in the analysis. To examine the influences of failed observation in 2000, the difference was examined between the sample distribution of 1980–2000 and 1980–1999 for the population mean of annual precipitation at all other observation points. Each sample distribution was resampled by using the Bootstrap method to test the significance of difference of the population mean. As a result, only two observation points, at Xinghai (9) and Jingtai (3), had a difference of population mean with a 95% level of confidence. However, the differences in annual precipitation were only 3 to 5 mm, so we judged that there is little problem with the Tongcheng data.

2.4 Analysis of change of annual precipitation

The 95% confidence interval of the mean of annual precipitation ($P_{d(j)} \leqq P_{(y,j)} \leqq P_{u(j)}$) at each observation point is defined as the average annual precipitation. Years with less precipitation than the confidence interval ($P_{(y,j)} < P_{d(j)}$) are defined as years with only a little precipitation. Years with more precipitation than the confidence interval ($P_{(y,j)} > P_{u(j)}$) are defined as years with much precipitation. Years with much precipitation and years with only a little precipitation were examined to determine the differences compared with the average annual precipitation. The annual precipitation deviation index and the annual precipitation variation index are defined in the following equations.

(Years with only a little precipitation)

$$PDI_{(y,j)} = P_{(y,j)} - P_{d(j)} \quad (4)$$

(Years with much precipitation)

$$PDI_{(y,j)} = P_{(y,j)} - P_{u(j)} \quad (5)$$

(Other years)

$$PDI_{(y,j)} = 0 \quad (6)$$

$$PCV_{(y,j)} = \frac{2 \times PDI_{(y,j)}}{P_{u(j)} + P_{d(j)}} \quad (7)$$

where, $PDI_{(y,j)}$ (mm) is the annual precipitation deviation index, $PCV_{(y,j)}$ is the annual precipitation variation index, and the subscripts y and j refer to year and each observation point's code, respectively. $PDI_{(y,j)}$ represents the difference between annual precipitation and the average annual precipitation. The normalized $PDI_{(y,j)}$ divided by the mean of $P_{d(j)}$ and $P_{u(j)}$ is $PCV_{(y,j)}$. $PCV_{(y,j)}$ is used to examine the time series trend of annual precipitation between the points. The normalized index $PCV_{(y,j)}$ is similar to that used by Liu and Yin (2001) for spatial examination of the time change of rain in summer in the East Tibet Plateau.

2.5 Analysis of pattern of seasonal rainfall

The seasonal rainfall pattern is more important when considering the water problem in the Loess Plateau, although precipitation is also important. In this study, we researched the expectation of seasonal precipitation at each observation point and considered the pattern of seasonal rainfall.

One year is divided into 73 five-day period. The mean precipitation $P_{(y,t,j)}$ in the period of t at point j from 1980 to 2000 was calculated as $P_{m(t,j)}$, and the standard deviation was calculated as $P_{sd(t,j)}$. The coefficient of variation $PSI_{(t,j)}$ was calculated from

$P_{m(t,j)}$ and $P_{sd(t,j)}$.

$$PSI_{(t,j)}=\frac{P_{sd(t,j)}}{P_{m(t,j)}} \quad (8)$$

$PSI_{(t,j)}$ is defined as the precipitation stability index. The precipitation stability index is a coefficient of variation of $P_{(y,t,j)}$ for 20 or 21 years at each observation point. $PSI_{(t,j)}$ means that there was stable rainfall if $PSI_{(t,j)}$ was smaller.

Next, the precipitation ratio in the period was defined as in the next equation.

$$PRP_{(t,j)}=\frac{P_{m(t,j)}}{P_{m(j)}}\times 100 \quad (9)$$

$PRP_{(t,j)}$ is the precipitation ratio in the period of t (%). $P_{m(j)}$ is the mean of the annual precipitation during 1980 to 2000 at point j (mm). The expectation and stability of seasonal rainfall at each observation point were estimated from the relation between $PRP_{(t,j)}$ and $PSI_{(t,j)}$.

3. Results and Discussion

3.1 Spatial distribution of annual precipitation

The mean of the sample distribution of annual precipitation calculated by the Bootstrap resample method is shown in Fig. 2. This value is almost equal to the mean of 21-year annual precipitation at each observation point. Table 1 presents the estimated interval mean of annual precipitation $\{P_{d(j)}$ and $P_{u(j)}\}$ at each observation point.

The regions where the means of annual precipitation were the least were the Tengeri desert area that extends from N37°30′ to N40°0′ and E103°0′ to E105°30′, and the Wulanbu desert that extends from N39°30′ to N40°0′ and E106°0′ to E107°0′. There was more precipitation in the southern area than in the northern area. But, the region on the Quilian mountain range at the west side of those deserts near Menyuan (2) (N37°30′, E101°20′) had much precipitation. This spatial distribution of annual precipitation was similar to that of the Chinese climate resource map (China Meteorological Administration, 1994). Moreover, Liu and Yin (2001) showed there is 300 mm to 350 mm of precipitation around Menyuan (2) from June to August, by using detailed surface observation data over the Eastern Tibetan Plateau. Menyuan (2) is located in the Quilian mountain range on the east edge of the Tibetan Plateau. Wuwei (1) is one of the least precipitation regions in this study area; though located on the east side of Menyuan (2), it is located on the west edge of the Tengeri Desert. There is a mountainous district of 4,000–5,000-meter height between two observation points, and it is suggested that the influence of topographic features for the prevailing wind dominates the precipitation of the two observation points.

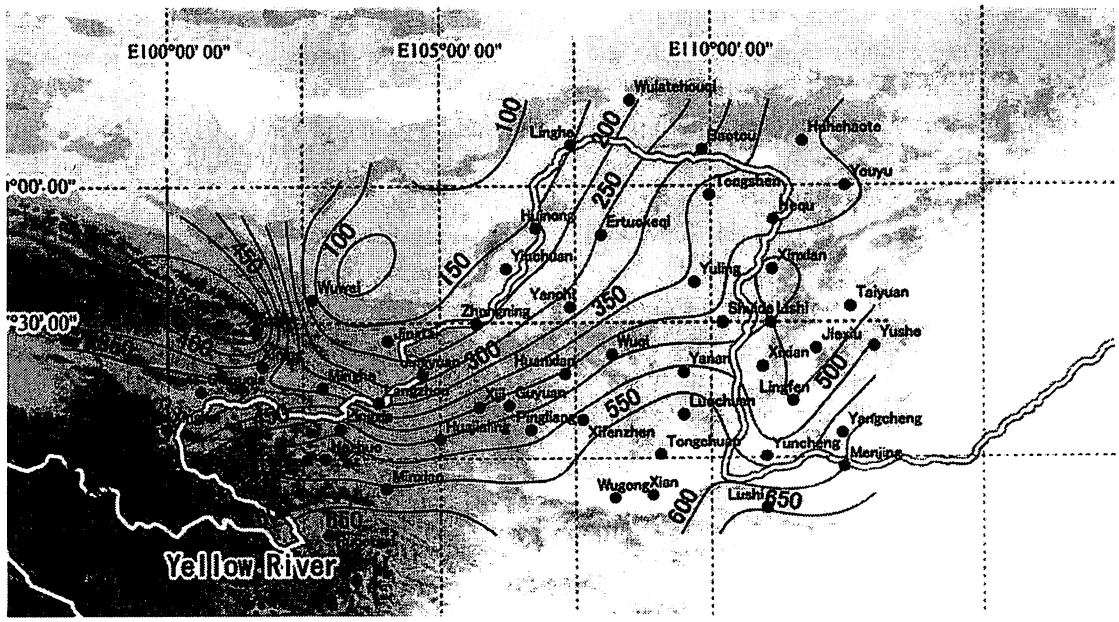

Fig. 2. Spatial distribution of the mean of annual precipitation in the Loess Plateau (mm).

Actually, we can see that the west prevailing wind dominates from the North Atlantic to East Asia along 35°N, by using the mean 1961–1990 summer 600-hPa wind fields (Liu and Yin, 2001). Menyuan (2) is under the influence of this west prevailing wind. However, around Menyuan (2), the east prevailing wind dominated when the summer precipitation was less than in a normal year. That is, the orographic precipitation of the Quilian mountain range might be an important factor of the feature of spatial distribution of precipitation around Menyuan (2).

3.2 Trend of annual precipitation

Each observation point for each year was classified as a year with only a little precipitation, a year with much precipitation, or the average annual precipitation by the method detailed in paragraph 2.4 based on $P_{d(j)}$ and $P_{u(j)}$. $PDI_{(y,j)}$ for each year at each observation point from 1980 to 2000 are shown in Table 2. In Table 2, the positive values indicate years with much precipitation, negative values indicate years with only a little precipitation, — indicate the average annual precipitation, and an "×" indicates no data.

First, we analyzed the tendency of annual precipitation in the whole study area. Each year from 1980 to 2000 was classified based on three indexes, the number of observation points classified as years with much precipitation, years with only a little precipitation, and the mean of $PDI_{(y,j)}$. The mean of $PDI_{(y,j)}$ represents the tendency of annual precipitation over the whole of the study area. The other two indexes represent whether tendency of precipitation for each year is over a large area or over a local area. The mean of $PDI_{(y,j)}$ at each observation point, the number of points with much precipitation (positive points), the number of points with only a little precipitation (negative points), and the difference between them are shown in Table 3. However, the fiscal year was permuted in ascending order based on the mean of $PDI_{(y,j)}$. We see from Table 3 that in eight years when precipitation was the least (1997, 1986, 1991, 1999, 1980, 2000, 1982, 1987), the mean of $PDI_{(y,j)}$ and the difference between negative and positive values were much lower than in other years. We therefore considered that the precipitation was less than standard amounts in these eight years (low precipitation years). Moreover, we assumed that the precipitation was of standard amounts in 7 years (1995, 1993, 1981, 1994, 1996, 1989, 1998), and was more than standard amounts (heavy precipitation years) in six years (1984, 1992, 1990, 1988, 1985, 1983).

We see from Table 3 that there have been no years with much precipitation since 1992. This means that the rainfall in the whole study area may be decreasing. To examine this, we investigated the annual variation in the mean of $PCV_{(y,j)}$ at all observation points $\{PCV_{(y)}\}$. Figure 3(a) depicts the annual variation of $PCV_{(y)}$. The time series trend of $PCV_{(y)}$ was examined by linear regression, although most observation points did not have decreasing or increasing trends of $PCV_{(y,j)}$ within a 95% confidence level. However, $PCV_{(y,j)}$ included a time series trends with a 95% confidence level at Langzhou (7), Henan (45) and Wugong (50), and with a 99% confidence level at Yanan (33). The annual variations of $PCV_{(y,j)}$ at Yanan, Wugong and Langzhou are shown in Figs. 3(b), (c) and (d). It seems that there were a decreasing trends of rainfall at Yanan (33), Wugong (50) and Henan (45). On the other hand, it seems that there was an increasing trend of rainfall at Langzhou (7). Significance of trend was judged by analysis of variance at these four points. However, the correlation is low and the inclination is also small in Langzhou (7) and Henan (45).

3.3 Relationship between trend of annual precipitation and spatial distribution of rainfall

In this chapter, we discuss whether the tendency of annual precipitation influences the spatial distribution of precipitation.

First, the spatial distributions of $PCV_{(y,j)}$ in 1997 and 1986 are shown in Figs. 4(a) and (b). The spatial distribution of $PCV_{(y,j)}$ differed greatly though both 1997 and 1986 were years with only a little precipitation. $PCV_{(y,j)}$ had a negative deviation throughout the entire study area, and it was especially large around Linghe (16), located in the northern Maowusu Desert and in the northeastern Wulanbu Desert in 1986. In contrast, the distribution of $PCV_{(y,j)}$ in 1997 had a positive deviation around Linghe, Wulanbu Desert and Baotou (13), although the negative deviation was larger than in 1986 in the southern part of the study area. The spatial distributions of $PCV_{(y,j)}$ were also examined for 2000, 1999, 1991, 1987, 1982, and 1980, which were considered low precipitation years. However, we could not find a typical type of rainfall spatial distribution in low

Table 2. The annual precipitation deviation index $\{PDI_{(y,j)}\}$

Observation points	Code	Annual precipitation deviation								
		1980(−)	1981	1982(−)	1983(+)	1984(+)	1985(+)	1986(−)	1987(−)	1988(+)
Wuwei	1	−24.0	−36.5	−36.1	16.5	−15.0	57.8	—	—	—
Menyuan	2	−50.7	72.0	−4.8	—	−20.9	43.3	−26.4	−8.7	69.9
Jingtai	3	−19.7	−20.7	−64.6	7.7	—	46.0	—	−22.3	29.7
Qiapuqia	4	−18.2	14.5	−10.4	68.5	−42.7	42.7	—	—	56.0
Xining	5	−72.5	7.2	−88.6	—	−25.6	47.5	−4.2	−8.7	—
Minghe	6	−90.1	−38.9	−51.3	—	−16.3	23.9	−9.6	−39.4	37.2
Langzhou	7	−89.9	−78.5	−45.6	—	26.5	56.8	—	−2.4	—
Jingyuan	8	−71.9	−51.8	−70.4	—	2.8	157.6	—	−21.8	6.4
Xinghai	9	−76.0	21.0	—	51.8	—	23.2	4.1	—	—
Lingxia	10	−93.7	77.9	−29.8	—	71.5	—	−32.1	−46.7	—
Huajialing	11	46.1	—	−124.9	85.6	144.0	30.0	—	−28.5	—
Wulatehouqi	12	−8.5	60.0	−45.0	−29.8	15.1	—	—	0.5	−21.4
Baotou	13	−70.0	—	−68.2	—	—	20.0	−53.9	−72.9	45.3
Huhehaote	14	−50.5	23.3	−18.4	—	53.4	1.4	−91.4	−107.8	—
Youyu	15	−70.6	—	3.0	68.6	—	−9.7	−72.1	−34.2	46.5
Linghe	16	−33.0	—	−27.3	—	36.1	−4.7	−69.9	—	96.1
Huinong	17	−45.9	−74.9	−33.4	—	66.8	10.1	−42.8	—	83.5
Ertuokeqi	18	−7.5	−29.8	−58.1	—	106.8	32.7	−45.2	−17.1	3.9
Tongshen	19	−77.6	—	—	−11.4	—	—	−45.5	−37.4	103.5
Hequ	20	−86.9	20.6	—	—	—	—	—	—	97.4
Yinchuan	21	−58.8	−57.4	−32.2	—	25.6	—	−0.2	—	3.5
Yuling	22	−70.1	24.1	—	−34.4	14.5	70.4	−4.5	1.6	148.7
Xinxian	23	−18.2	—	−50.6	−16.8	−76.6	38.8	−6.0	—	128.4
Zhongning	24	−64.5	—	−83.5	89.0	−13.5	116.5	−33.3	−13.5	−6.7
Yanchi	25	−100.6	—	−74.2	−18.3	11.1	93.5	−9.1	−48.7	—
Wuqi	26	—	4.5	−123.0	8.0	6.6	156.9	−57.4	−131.1	12.1
Shuide	27	4.4	1.2	—	20.6	−13.3	65.0	−29.6	—	94.5
Lishi	28	—	—	—	—	—	247.1	−79.8	11.4	97.1
Taiyuan	29	−46.8	−38.2	—	37.5	−34.3	81.0	−122.2	—	119.2
Yushe	30	−29.4	35.5	10.1	—	—	68.6	−143.4	−17.8	29.0
Guyuan	31	—	38.9	−110.9	41.5	56.8	51.8	−72.9	−53.0	11.4
Huanxian	32	−54.1	—	−57.8	—	—	75.7	−55.5	−74.3	157.0
Yanan	33	—	209.9	−1.2	116.6	—	44.4	−14.5	—	179.4
Xixian	34	—	65.3	−86.4	23.1	—	93.9	−60.2	—	45.5
Jiexiu	35	—	—	0.2	19.8	29.2	151.1	−109.9	18.9	189.1
Lingfen	36	—	−5.6	—	32.0	30.3	24.7	−88.4	−38.8	69.9
Xiji	37	−15.7	—	−106.9	7.9	24.0	100.2	−21.1	−16.8	5.9
Pingliang	38	—	91.1	−112.0	104.8	16.2	—	−114.7	—	−2.4
Xifenzhen	39	—	66.0	−44.4	104.0	9.7	—	−108.3	−37.7	160.1
Luochuan	40	—	9.0	−3.0	167.2	53.6	8.7	−136.0	—	80.2
Tongchuan	41	−5.5	1.8	18.0	231.1	115.3	—	−132.1	−32.7	82.7
Yuncheng	42	—	−2.1	89.3	167.0	24.1	25.8	−172.9	—	—
Yangcheng	43	27.1	−81.6	120.2	63.8	133.8	—	−113.1	—	—
Maduo	44	−19.9	21.6	—	—	−17.6	—	−11.4	—	−98.4
Henan	45	—	103.1	11.3	114.2	47.7	20.1	—	−24.2	−49.3
Maqu	46	−12.8	188.6	−20.0	—	14.2	—	14.0	−26.7	—
Ruoergai	47	—	69.2	—	37.6	172.3	3.0	−34.1	−124.9	−11.1
Hezhuo	48	−121.4	17.7	−2.2	—	105.5	17.4	−32.5	—	—
Minxian	49	—	41.4	−36.1	67.7	114.7	113.1	—	−75.8	51.5
Wugong	50	—	54.6	—	312.5	298.0	—	−103.1	—	120.9
Xian	51	—	106.3	−7.8	283.4	45.2	−15.2	−103.6	—	38.5
Lushi	52	8.7	—	9.5	208.7	177.4	—	−154.3	14.8	−34.6
Menjing	53	33.1	−120.6	—	121.0	88.0	—	−74.9	—	7.9
Number of negative points		32	13	33	5	10	3	41	27	7
Number of positive points		5	27	8	29	32	36	2	5	34
Mean of $PDI_{(y,j)}$		−42.0	20.2	−35.8	75.5	44.3	57.2	−62.2	−34.9	55.7

for each year at each observation point from 1980 to 2000.

index ($PDI_{(y,j)}$: mm)

1989	1990(+)	1991(−)	1992(+)	1993	1994	1995	1996	1997(−)	1998	1999(−)	2000(−)
—	—	−51.5	—	64.5	—	23.2	40.3	—	—	—	—
169.1	—	−64.2	37.8	—	—	—	−32.2	−16.1	—	−91.7	—
—	—	−50.5	6.2	8.5	58.3	0.5	—	8.7	14.8	−9.9	−42.8
98.3	−36.7	−13.6	8.3	55.5	−1.6	−47.0	−24.4	—	—	—	−47.6
79.9	−14.2	−104.1	24.7	2.2	17.6	—	1.6	9.4	59.8	11.4	−4.3
—	—	−100.2	94.5	90.4	—	7.3	—	18.0	—	12.5	—
−0.2	—	—	—	—	—	44.7	45.3	−43.7	—	5.1	36.4
−3.6	—	—	—	—	—	36.4	—	−17.1	20.0	17.4	—
104.0	−4.2	−78.9	—	—	18.5	—	−6.0	—	—	—	−84.7
—	—	−3.6	95.0	41.7	—	—	—	−96.2	—	—	—
—	105.8	−83.5	—	4.9	−28.4	−35.9	−44.5	−62.7	—	40.1	—
−15.0	43.6	−7.0	51.2	—	45.7	52.5	−1.9	−31.0	−19.6	—	—
—	50.6	−31.7	75.2	−30.2	18.5	—	117.9	76.6	—	—	−104.3
—	42.2	—	97.9	−58.4	71.8	31.7	0.0	—	130.4	−97.4	−36.9
56.7	79.2	21.5	70.2	−107.3	—	19.3	—	−53.5	—	−41.1	—
—	—	−8.0	18.3	−36.1	4.6	71.3	—	41.7	8.6	−11.4	−29.8
—	—	—	—	—	42.8	69.9	−7.1	−17.1	—	−18.0	−46.7
153.2	12.7	—	64.8	−20.7	—	68.5	—	−76.4	—	−67.8	−55.0
39.2	61.7	−11.6	111.5	−46.2	77.7	—	—	—	136.8	−51.0	−144.6
19.3	—	—	110.2	−94.6	—	88.3	22.7	−76.1	34.3	−106.4	−108.9
15.9	55.9	—	89.7	−33.6	—	35.7	−3.8	−0.6	13.6	—	−23.2
−51.2	—	—	37.0	−28.7	64.0	—	—	−13.9	—	−47.6	−75.1
—	—	—	128.0	−57.9	—	—	111.0	−83.8	—	−60.2	41.5
—	70.4	−20.3	—	—	—	15.4	10.8	−30.2	12.1	—	−3.6
—	27.7	—	—	−15.8	86.9	—	43.0	—	59.6	—	−85.1
—	101.8	−43.5	—	—	33.4	—	—	−18.1	52.2	—	−2.5
−11.4	62.2	—	−3.7	−17.9	133.0	—	4.1	−68.1	−20.2	−89.2	−105.3
—	102.4	−14.4	—	—	15.4	−25.1	—	−93.4	−53.6	−161.6	—
—	7.7	—	—	—	—	27.7	190.5	−132.1	−7.0	−31.6	—
124.5	166.0	−17.5	−57.0	—	6.7	—	17.2	−144.7	14.4	−89.9	−3.9
—	85.3	−79.1	123.9	−8.6	36.8	—	—	−47.7	—	−65.1	—
−10.7	268.0	−66.5	—	−16.1	—	—	33.7	−81.1	78.9	−78.8	−26.1
−16.3	—	−12.0	−1.2	3.3	42.8	−103.0	—	−91.6	3.7	−119.4	−96.4
−63.0	—	−34.8	—	172.4	1.5	—	36.1	−123.6	−33.0	−81.9	−20.7
—	9.9	—	—	21.2	—	−48.7	—	−123.0	−20.5	−97.8	−65.9
6.8	3.9	−66.8	—	2.2	36.9	−46.3	75.8	−116.9	50.9	−74.9	—
—	166.8	−14.6	30.4	—	—	12.8	−14.8	−101.5	—	−12.3	—
—	137.1	−157.7	30.7	—	0.7	−20.5	135.2	−101.6	—	—	−66.5
—	191.0	−25.0	66.7	—	—	−135.8	—	−131.3	—	−33.3	−3.9
−53.7	8.1	—	—	—	60.2	−190.9	—	−129.7	—	−10.0	66.3
—	—	—	—	−36.1	—	−202.3	110.3	−141.5	—	36.7	×
60.0	—	−95.5	—	—	—	−13.9	30.3	−191.5	85.4	−20.4	−49.2
—	—	−121.3	—	—	—	−41.1	181.6	−196.3	83.5	−48.7	—
138.3	−9.6	—	36.0	15.2	—	−18.0	—	—	—	0.3	−5.6
—	−37.1	−68.3	37.2	−77.9	—	64.8	−20.4	−9.3	—	—	−96.5
77.6	−87.3	—	17.2	−83.6	—	—	−101.7	−2.9	42.1	17.9	−28.0
−2.7	—	−55.1	—	—	—	—	—	−77.0	110.9	−11.5	−26.9
—	22.1	−73.9	61.6	−29.8	19.8	—	11.9	—	15.6	—	−56.5
—	35.9	−26.3	58.1	—	−53.5	—	−41.1	−155.8	—	−15.8	—
—	—	—	—	−98.7	−56.3	−156.6	—	−174.0	—	—	−86.0
6.7	−47.9	—	—	−65.7	—	−194.2	93.6	−144.4	—	—	—
84.7	−64.6	−119.7	12.0	—	—	−78.2	—	−107.9	120.6	−147.3	—
—	96.5	−148.0	−6.7	—	−48.1	—	80.1	−270.5	126.3	−10.7	136.1
10	8	33	4	20	5	16	12	40	6	30	31
16	26	1	27	12	22	17	21	5	22	8	4
38.7	50.4	−54.3	49.2	−15.1	26.1	−20.8	33.2	−76.4	40.0	−43.7	−38.6

Table 3. The mean of $PDI_{(y,j)}$ at each observation point, the number of points with much precipitation (Positive points), the number of points with only a little precipitation (Negative points) and the value of Negative subtracted from Positive.

Tendency of rainfall	Year	Negative points	Positive points	Positive−Negative	Mean of $PDI_{(y,j)}$
Low precipitation years	1997	40	5	−35	−76.4
	1986	41	2	−39	−62.2
	1991	33	1	−32	−54.3
	1999	30	8	−22	−43.7
	1980	32	5	−27	−42.0
	2000	31	4	−27	−38.6
	1982	33	8	−25	−35.8
	1987	27	5	−22	−34.9
Average precipitation years	1995	16	17	1	−20.8
	1993	20	12	−8	−15.1
	1981	13	27	14	20.2
	1994	5	22	17	26.1
	1996	12	21	9	33.2
	1989	10	16	6	38.7
	1998	6	22	16	40.0
Heavy precipitation years	1984	10	32	22	44.3
	1992	4	27	23	49.2
	1990	8	26	18	50.4
	1988	7	34	27	55.7
	1985	3	36	33	57.2
	1983	5	29	24	75.5

precipitation years.

Figures 5(a) and (b) present the spatial distribution of $PCV_{(y,j)}$ in 1985 and 1983. For heavy precipitation years, regions of both positive deviations of $PCV_{(y,j)}$ and negative deviations existed, and the difference was larger and more regional than in low precipitation years. Moreover, areas with positive deviation of $PCV_{(y,j)}$ were distributed regionally and were remarkable, so we considered that there were some areas with regional intensive rainfall in the case of heavy precipitation years.

Figure 6 illustrates the spatial distribution of the standard deviation of $PCV_{(y,j)}$ and depicts the degree of variation of annual precipitation from 1980 to 2000. The variation of annual precipitation was the largest from the northern Maowusu Desert, the northeastern Wulanbu Desert, and around Wugong (50). Annual precipitation exhibited both a decreasing trend and remarkable variation at Wugong. In contrast, the vicinity of N37°30′ E101°20′ that centers on Menyuan (2) and their south mountains area exhibited small variations in annual precipitation.

3.4 Seasonal rainfall pattern in the Loess Plateau

Figure 7 presents the relationship between $PRP_{(t,j)}$ and $PSI_{(t,j)}$ at Menyuan (2) and Linghe (16). $PRP_{(t,j)}$ indicates the ratio of precipitation to annual precipitation in the period of t. $PSI_{(t,j)}$ indicates the degree of variation of precipitation from the annual precipitation in the period of t. Explanatory notes in Fig. 7 showed changes for five periods. In winter, there was only a little rainfall and the rainfall was unstable. However, stable rainfall occurred from spring to summer. Rainfall decreased and was becoming unstable from autumn to winter again. We can recognize from Fig. 7 that there is little precipitation and the form of rainfall is unstable, from late autumn to early spring. $PRP_{(t,j)}$ increased and $PSI_{(t,j)}$ decreased from spring to summer, so it indicates the transition to the stable rainfall season. That is, the relationship between $PRP_{(t,j)}$ and $PSI_{(t,j)}$ shows typical features of rainfall in the Loess Plateau. So, the variability (stability) of precipitation in the summer rainy season was analyzed from the relationship between $PRP_{(t,j)}$ and $PSI_{(t,j)}$ at each observation point. To perform this analysis, the relationship between $PRP_{(t,j)}$ and $PSI_{(t,j)}$ was

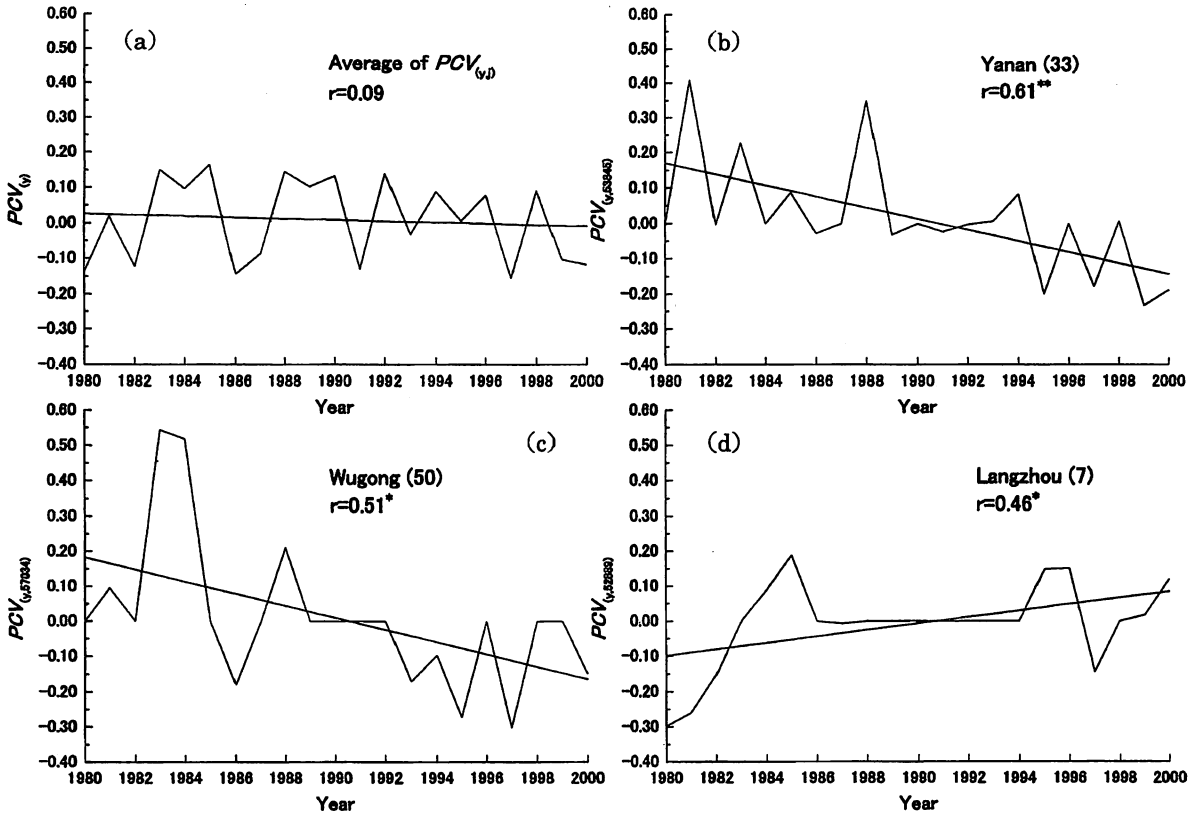

Fig. 3. (a) Time series of the mean of coefficient of variation of annual precipitation $\{PCV_{(y)}\}$. (b), (c), (d) Time series of the coefficient of variation of the annual precipitation $\{PCV_{(y,j)}\}$ at observation stations. (b) Yanan (33), (c) Wugong (50) and (d) Langzhou (7). Subscripts y and j refer to year and each observation point's code, respectively.

approximated by Eq. (10) at each observation point. These approximated lines were defined as the line of rainfall feature.

$$PSI_{(i,j)}=a_{(j)}\ln^{PRP(i,j)}+RSS_{(j)} \qquad (10)$$

The constant of the equation was defined as the rainy season stability index at observation point j $\{RSS_{(j)}\}$. Figure 8 illustrates the lines of rainfall features at Huinong (17), Ruoergai (47) and Yanan (33). $RSS_{(j)}$ becomes smaller if the summer rainy season is stable, so it clarifies the features of rainfall at each station. We could obtain lines of rainfall features with 95% confidence level approximation at all 53 observation points.

Figure 9 shows the spatial distribution of $RSS_{(j)}$ in the Loess Plateau, and Fig. 10 shows the relationship between the mean of annual precipitation ($P_{m(j)}$) and $RSS_{(j)}$. $RSS_{(j)}$ was the largest around the Tengeri Desert and the Wulanbu Desert. In contrast, $RSS_{(j)}$ was small over the Quilian mountain range located on the west side of two deserts, and was small in its southern mountain range, too. This tendency was similar to the spatial distribution of the variation of annual precipitation indicated in Fig. 6.

$P_{m(j)}$ and $RSS_{(j)}$ are negatively correlated in Fig. 10. It follows from Fig. 10 that the rainy season of the region where annual precipitation is a little is also unstable. We could classify all observation points to 8 groups, based on their geographical position and the feature of rainfall; the results are shown in Figs. 9 and 10. Following this classification, it became clear that the rainy season is not equally stable in the east and in the west sides of the Loess Plateau even if annual precipitation is at the same level.

4. Conclusion

In this thesis, we researched the features of rainfall, to perform the environmental monitoring necessary to support anti-desertification activities in the

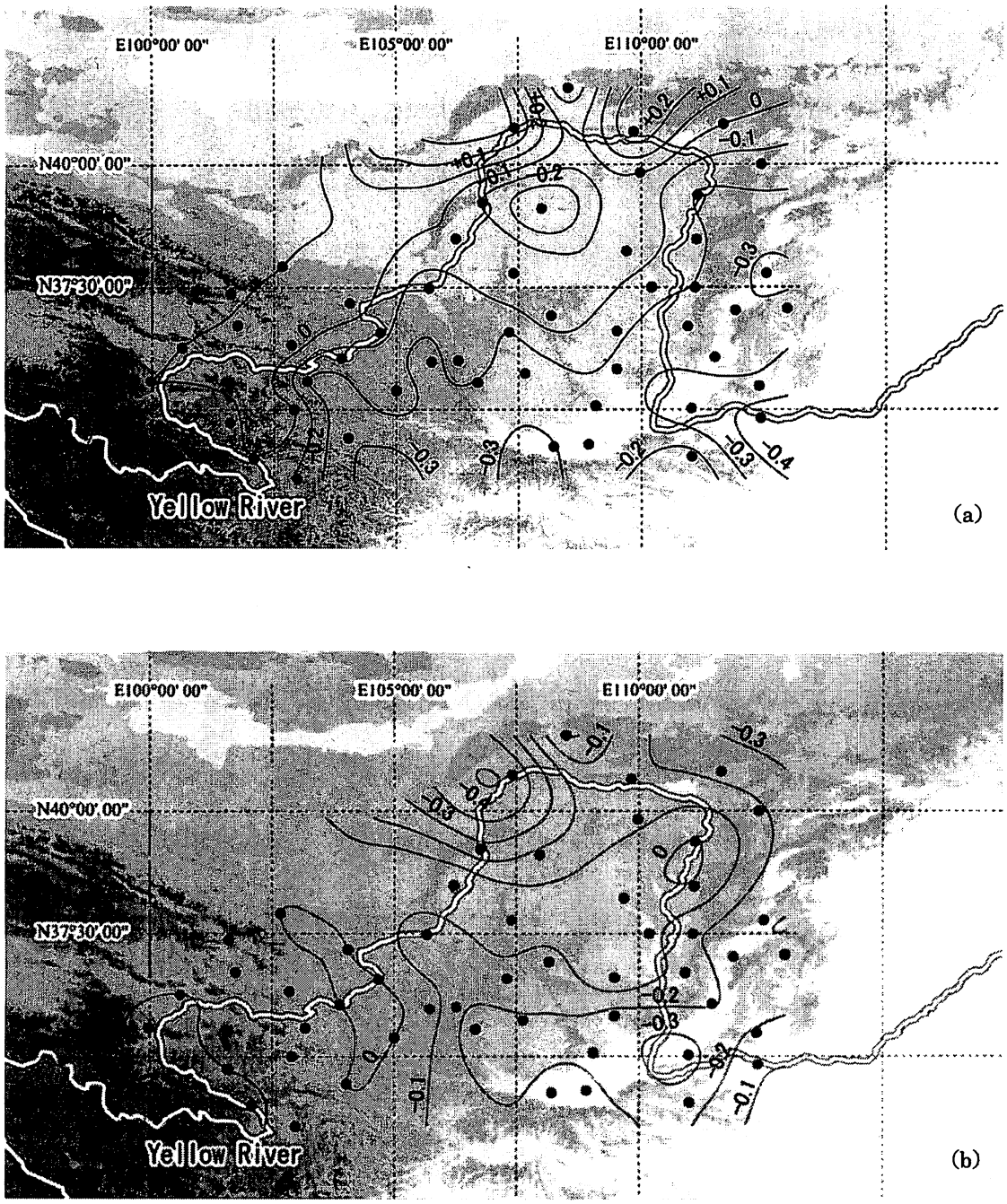

Fig. 4. Spatial distribution of $PCV_{(y,j)}$ in the case of low precipitation years. (a) 1997, (b) 1986.

Loess Plateau. First, the spatial distribution, stability and trend of the annual precipitation were studied. Next, the seasonal pattern of rainfall and the stability of rainfall in the summer rainy season were studied. As a result, the following conclusions were obtained.

- It seems that the mean annual precipitation is the lowest in the Tengeri Desert and the Wulanbu Desert (N38° to 41°, E104° to 107°). The mean annual precipitation increased in low-latitude regions. But, the Quilian mountain range, located on the west side of two deserts (around N37°30′ and E101°20′), had much precipitation.
- We could not see increasing or decreasing trends in annual precipitation in the whole of the Loess Plateau from 1980 to 2000 in this analysis. How-

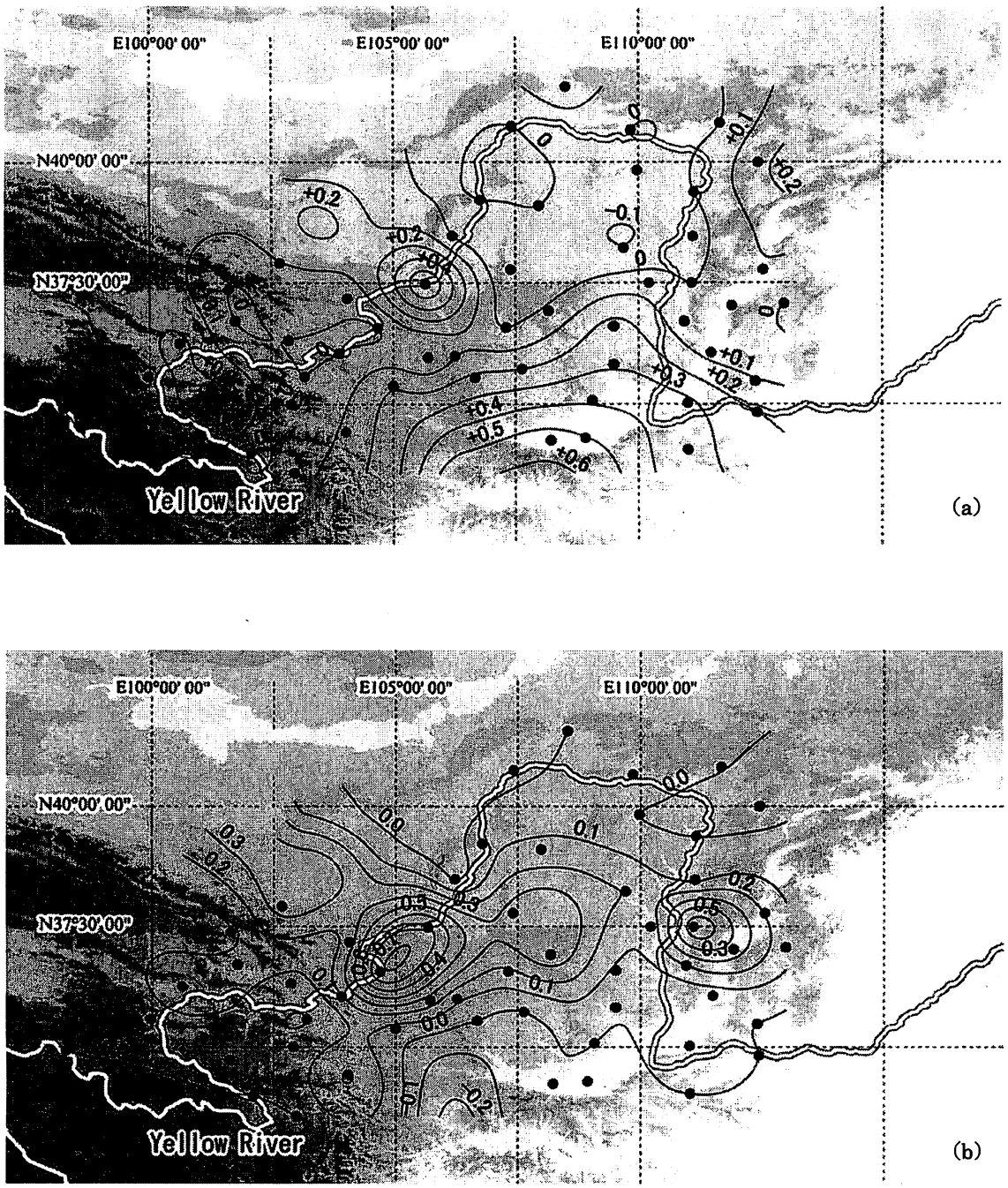

Fig. 5. Spatial distribution of $PCV_{(y,j)}$ in the case of heavy precipitation years. (a) 1983, (b) 1985.

ever, it seems that there was a significant trend in annual precipitation at a few observation points.

- The variation of annual precipitation was the largest from the northern Maowusu Desert, northeastern Wulanbu Desert, and around Wugong (50). In contrast, the variations of annual precipitation were small around Menyuan located on the Quilian mountain range at west of the Tengeri Desert (N37°30′, E101°20′).
- We proposed the rainy season stability index $\{RSS_{(j)}\}$ based on the relationship between the precipitation ratio in the period $PRP_{(i,j)}$ and the precipitation stability index $PSI_{(i,j)}$. It clarified that the rainy season is not equally stable for the

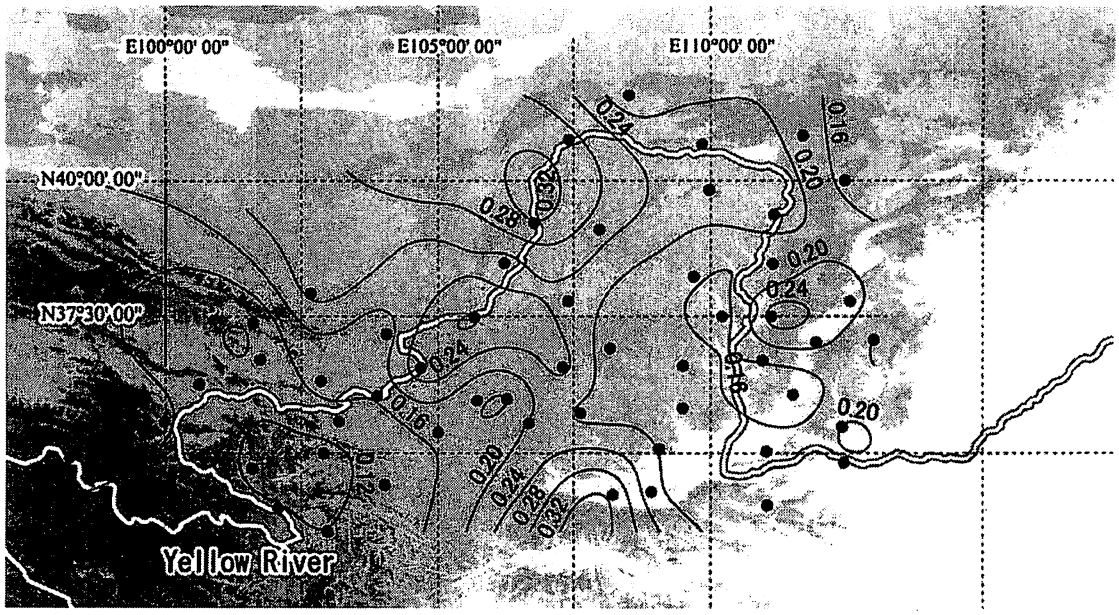

Fig. 6. Spatial distribution of the standard deviation of $PCV_{(y,j)}$ from 1980 to 2000.

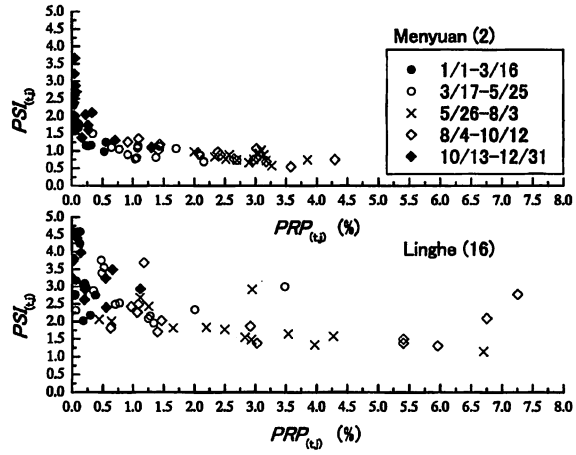

Fig. 7. Relationship between the precipitation ratio in the period of t $\{PRP_{(t,j)}\}$ and the precipitation stability index $\{PSI_{(t,j)}\}$ at Menyuan (2) and Linghe (16).

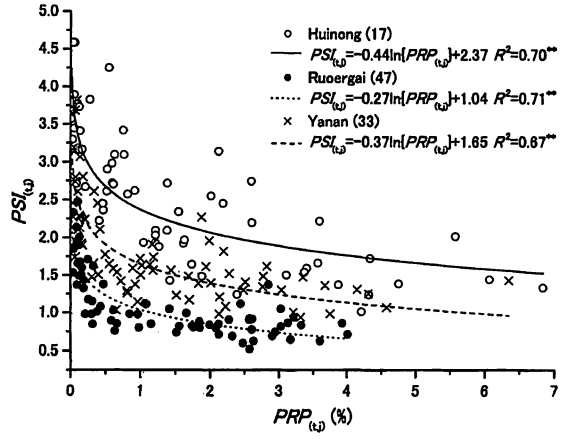

Fig. 8. Lines of rainfall features at Huinong (17), Ruoergai (47) and Yanan (33).

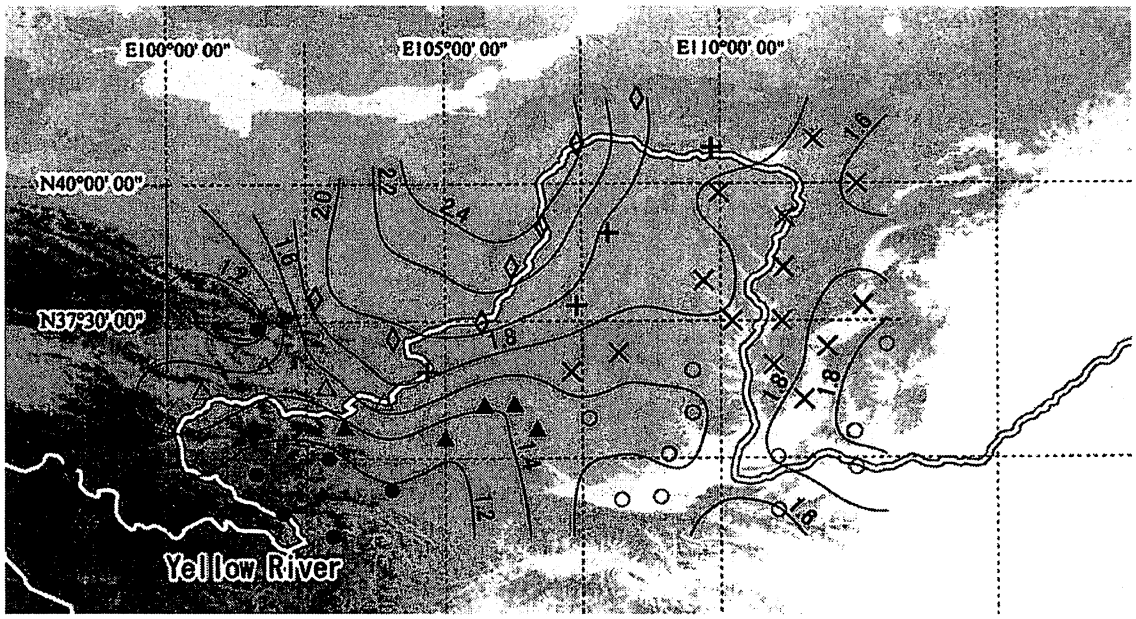

Fig. 9. Spatial distribution of the rainy season stability index $\{RSS_{(j)}\}$ in the Loess Plateau.

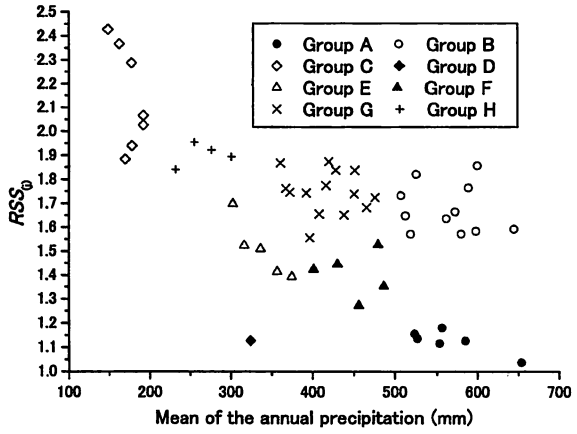

Fig. 10. Relationship between the mean of annual precipitation $(P_{m(j)})$ and the rainy season stability index $\{RSS_{(j)}\}$. The explanatory notes for the group correspond to the explanatory notes in Fig. 9.

east side and the west side of the Loess Plateau even if the annual precipitation is at the same level.

References

China Meteorological Administration, 1994: *The Collection of Chinese climate resource maps.* China Maps Publishing Company, Beijing, pp. 105–202 (中国気象局, 1994: 中国気候資源地図集. 中国地図出版社, 北京, pp. 105–202).

Efron, B., 1982: *The jackknife, the bootstrap and other resampling plans.* Society for Industrial and Applied Mathematics, Philadelphia, 92 pp.

Fang, X. M., 1995: The origin and provenance of the Malan loess along the eastern margin of the Qinghai-Xizang (Tibetan) Plateau and its adjacent area. *Sci. China (B),* **25**, 426–432.

Jones, P., 1995: The instrumental record: its accuracy and use in attempts to identify the 'CO_2 signal.' In *Analysis of climate variability. Application of statistical techniques* (eds. by Von Storch, H. and Navarra, A.). Springer, Berlin, pp. 54–75.

Kendall, M. G., 1938: A new measure of rank correlation. *Biometrika,* **30**, 81–93.

Lazaro, R., Rodrigo, F. S., Gutierrez, L., Domingo, F. and Puigdefabregas, J., 2001: Analysis of a 30-year rainfall record (1967–1997) in semi-arid SE Spain for implications on vegetation. *J. Arid Environ.,* **48**, 373–395.

Liu, G., Ishikawa, S., Nagasawa, S. and Maruyama, T., 1999: Study on probability density function for maximum amount of rainfall in a year. *J. Jpn.*

Soc. Hydrol. Water Resour., **12**, 502–510.

Liu, M.(ed.), 1998: *Natural geography in China.* China Atlas Publishing Company, Beijing, 252 pp.（刘　明光主編，1998：中国自然地理図集．中国地図出版社，北京，252 pp.）.

Liu, X. and Yin, Z., 2001: Spatial and temporal variation of summer precipitation over the Eastern Tibetan Plateau and the North Atlantic Oscillation. *J. Climate,* **14**, 2896–2909.

Liu, X., Shaw, J., Liu, T., Heller, F. and Yuan, B., 1992: Magnetic mineralogy of Chinese loess and its significance. *Geophys. J. Intern.,* **108**, 308–310.

Molnar, P. and Ramirez, J. A., 2001: Recent trends in precipitation and streamflow in the Rio Puerco Basin. *J. Climate,* **14**, 2317–2328.

Nagasawa, T., Takahashi, H., Guoliang, C. and Xinming, M., 1993: Characteristics of soil erosion in the Loess Plateau, China—Survey in Guyuan Prefecture, Ningxia Huizu Autonomous Region—. *J. Soc. Environ. Sci. Jpn.,* **6**, 277–285.

Naruse, T. and Ono, Y., 1997: Paleoenvironments of monsoon Asia during the last glacial age and role of Himalaya-Tibetan Highland, viewed from loess and eolian dust. *J. Geography,* **106**, 205–217.

Niu, L. and Liu, H.(eds.), 1989: *Result of 30 years in irrigation from the Yellow River. Land improvement in China.* The Japanese Institute of Irrigation and Drainage, Tokyo, **7**, 111 pp.（牛　立峰・劉　好智（編），1989：人民勝利渠引黄灌漑三十年．中国の土地改良．日本農業土木総合研究所，東京，**7**，111 pp.）.

Peinado-Serna, A., 1985: *Lecciones de climatologa.* Instituto Nacional de Meteorologa, Madrid, 111 pp.

Shaanxi Measurement Committee, 1999: *Shaanxi, China resources atlas.* Xian Atlas Publishing Company, Xian, 157 pp.（陝西省計測委員会，1999：陝西省資源地図集．西安地図出版社，西安，157 pp.）.

Smalley, I. J. and Krinsley, D. H., 1978: Loess deposits associated deserts. *Catena,* **5**, 53–66.

Yoshino, M., 1997: *Desertification in China.* Daimeido Ltd., Tokyo, 300 pp.

Zhu, Z., 1990: Desertification in the northern territory of China. *J. Chin. Geography,* **1** (1), 61–70.

Zhu, Z., Lin, S. and Di, X., 1989: *Theory of desertification in China.* Science Press, Beijing, 126 pp.（朱　震達・劉　恕・邸　醒民，1989：中国的沙漠化及其治理．科学出版社，北京，126 pp.）.

中国黄土高原における降水の気候学的特徴

高山　成*・木村玲二*・神近牧男*・松岡延浩**・張　興昌***

(* 鳥取大学乾燥地研究センター
** 千葉大学園芸学部
*** 中国科学院西北水土保持研究所)

要　約

黄土高原における砂漠化対処に必要な環境モニタリングを目的として，降水の特性について検討した。まず黄土高原における年降水量について，空間分布，安定性（ばらつき），トレンドを調べた。次に降水の季節パターンに着目し，夏季を中心とした雨季において，降水がどの程度安定して出現するかについて検討した。

はじめに 1980 年から 2000 年までの 53 地点の日降水量データを基に，Bootstrap 法より年平均降水量の区間推定を行った。さらにこの区間推定値を基準として年降水の時系列トレンドを調べた。次に 1 年を 5 日間単位の期間に分け，各期間の期間降水比 $\{PRP_{(i,j)}\}$ と降水安定度 $\{PSI_{(i,j)}\}$ との関係より，各地点における降水の季節パターンについて検討した。

年降水量の平均は Tengeri（騰格里）沙漠，Wulanbu（ウランブ）砂漠の周辺（N38～41°, E104～107°）で最も少なく，低緯度になるほど降水量は増加した。しかし，2 つの砂漠の西側に位置する Quilian（チーリエン）山脈周辺の地域（N37°30′，E101°20′）は多降水な地域であった。また，Maowusu（毛烏素）砂漠北部と Wulanbu 砂漠北東の地域，Wugong（武功）周辺の地域は，年降水量の変動が最も大きいが，Quilian 山脈周辺の多降水地域やその南方の山岳地域などは年降水の変動が小さかった。年降水量のトレンドについては黄土高原全域を平均した場合，有意なトレンドは見出せなかった。しかし，個別の観測点について見た場合には，数箇所の観測点で増加または減少のトレンドを有する可能性が示唆された。

本研究では期間降水比 $\{PRP_{(i,j)}\}$ と降水安定度 $\{PSI_{(i,j)}\}$ との関係から雨季安定度 $\{RSS_{(j)}\}$ を提示し，夏季を中心とした雨季における降水の安定度（変動度）を評価した。その結果，黄土高原においては同程度の年降水量の地域であっても，東側地域が西側地域よりも雨季に出現する降水が不安定であることが明らかとなった。

キーワード: 雨季安定度，降水安定度，期間降水比，黄土高原，降水特性

CSIRO PUBLISHING
www.publish.csiro.au/journals/ajsr
Australian Journal of Soil Research, 2007, 45, 266–279

Effectiveness of hydrated lime and artificial zeolite amendments and sedum (*Sedum sediforme*) plant cover in controlling soil erosion from an acid soil

Henintsoa Andry[A,B], *Tahei Yamamoto*[A], *and Mitsuhiro Inoue*[A]

[A]Arid Land Research Center, Tottori University, 1390 Hamasaka, Tottori 680-0001, Japan.
[B]Corresponding author. Email: andry@alrc.tottori-u.ac.jp

Abstract. There are over 350 different species of sedum (*Sedum* spp.) and most of them can tolerate harsh conditions including very cold to hot temperatures, drought, and poor and stony soil. Sedum plants are used in rock gardens and edging flower beds, and for greening the tops of buildings, cottages, and thatched roofs. However, little is known about the effectiveness of sedum as vegetation cover in protecting soil erosion from a road embankment made of acid soil. Acid soil is believed to be vulnerable to soil erosion and is not suitable for plant growth. Liming treatment is required first before revegetation to alleviate the soil acidity; however, lime incorporation may affect the soil physical properties and, consequently, runoff and sediment generation. A rainfall simulation study was conducted to test the effectiveness of hydrated lime and artificial zeolite as amendments and *Sedum sediforme* (*Rupestria* group) as vegetation cover in controlling soil erosion from an acid soil taken from mountain cuts in Yamaguchi prefecture, Japan, where it is used for road embankment. The soil was treated with 0.5% lime and 10% zeolite. Two rainfall intensities of 30 and 60 mm/h were tested for 2 and 1 h, respectively, on sedum-growing soil plots measuring 0.50 by 0.30 by 0.05 m. Three levels of vegetation cover (bare soil, 25%, 75%) of sedum plant of 5-month growth under 2-day irrigation intervals were tested.

The incorporation of hydrated lime and artificial zeolite amendments improved wet aggregate stability, which contributed to significant decrease in surface runoff, sediment concentration, and total soil loss by rain splash from the bare soil. Zeolite was more effective in promoting plant growth than the lime treatment; as a result the decrease in sediment generation and soil loss by rain splash, compared with the control, was larger with zeolite than with lime. Under both intensities of simulated rain, the sediment concentration and total soil loss by rain splash decreased significantly ($P < 0.05$) with increasing surface cover. The correlation between cumulative soil loss (CSL) and cumulative surface runoff was linear and significant ($P < 0.001$) and the slope coefficient decreased with increasing surface cover. This suggests that the sediment carrying capacity or the erosivity of the surface runoff was constant and it decreased with increasing surface cover. The sedum cover reduced the CSL up to 72 and 79% under 30 and 60 mm/h rainfall intensities, respectively. The mean weight diameter of the soil sediment transported by runoff and soil loss by rain splash were significantly increased, and therefore, the silt and clay proportion of the crust material formed on the soil surface decreased up to 6 and 16% under 25 and 75% vegetation cover, respectively. These results demonstrate that hydrated lime and artificial zeolite could be used as amendments and sedum plant as vegetation covers in controlling soil erosion from an acid soil.

Additional keywords: acid soil, sedum plant, amendment, soil erosion, aggregate size distribution.

Introduction

Land disturbance from construction activities has resulted in many-fold increases in soil erosion over pre-construction periods (Goldman *et al.* 1986), and sediment has become the principal transport medium for a range of pollutants entering the watercourses. On the other hand, the soil material used for construction engineering generally comes from marginal soils, such as saline or acidic soils, because of increasing need of land of good quality for agriculture. In Japan, acid soils are found in many areas of the islands as a result of geological characteristics such as deep weathering of granitic rocks, sulfuric acid leaching due to oxidation of pyrite, and volcanic ash generated by Holocene volcanic activity. In Yamaguchi prefecture situated in the western edge of the Japanese island of Honshu, acid sulfate soil taken from mountainside is used for highway road embankments in the local areas (Maeda Cooperation and Asanuma Gumi 1999). However, a construction made from this acid soil is believed to be vulnerable to soil erosion due to weak physical structure and extremely acidic properties of the material (Menzies 2003; Huygens *et al.* 2005). The off-site impacts of acid soil erosion, such as siltation of reservoirs, the breaking of waterways and channels, pollution of water bodies, and effects on aquatic habitats, are of equal concern (Midmore *et al.* 1996). The consequences of acid soil erosion on the environment are exacerbated on road embankments, where the potential for surface runoff and soil erosion is largely due to the unique topography (El-Swaify 1997). In fact, the implementation of soil management practices such as

10.1071/SR07012 0004-9573/07/040266

remediation of soil acidity following revegetation needs to be taken into account in building road embankments from acidic soils, in order to address the soil erosion issue and to maintain ecological conditions in the area.

The extremely acidic conditions encountered in the acid soils represent a soil constraint for plant growth (Menzies 2003). Acid neutralisation is therefore required to decrease soil acidity and Al toxicity, and increase the availability of phosphorus. Edmeades and Ridley (2003) suggested that the best management practice for soils showing Al toxicity was to treat the acidity first, because this would promote adequate root growth and function and allow nutrients and water to be taken up more effectively. They also reported that the most direct way to decrease Al toxicity was to increase the soil pH. Alkaline materials such as limes are often used for this purpose (Edmeades and Ridley 2003; Wong and Swift 2003); however, there are conflicting results about the impact of liming on physical properties of acid soils with regard to soil erosion. Several workers have reported lime-induced decrease in surface cracking and increase in water-holding capacity (Hoyt 1981), and increase in aggregate stability and infiltration (Roth and Pavan 1991). Others have reported increase in clay dispersion and decreased aggregate stability (Roth and Pavan 1991; Tarchitzky *et al.* 1993). Also, soil hydraulic characteristics such as infiltration, water retention, and hydraulic conductivity were found to be decreased by lime application (Roth and Pavan 1991). These negative impacts imply potential for high runoff and sediment generation after liming, especially when the soil surface is covered with insufficient vegetation or on a soil surface where the plants are in the early stage of their growth.

In most field soils the detrimental effects of liming at low rates on soil physical properties were observed during the first 1–3 months of application, and after 6 months, soil aggregation and infiltration were found to increase substantially (Roth and Pavan 1991). High application rates have been found to be more effective in overcoming the initial detrimental effects (Roth and Pavan 1991), suggesting that application rates affect the benefits of lime on soil physical properties. Most of the aforementioned studies were performed using commercial lime, which is less soluble than hydrated lime, but the latter is more expensive (Kirchhof *et al.* 1995). It is thus conceivable that for research purposes the use of hydrated lime may provide quick information on beneficial effects of lime on runoff and sediment generation.

Another soil amendment that has recently received increasing attention with regard to the improvement in soil physical and chemical properties is fly-ash (recycling material) and its industrially modified form, artificial zeolite (Yamada *et al.* 2002). Zeolite has been found to be effective in rectifying soil sodicity (Yamada *et al.* 2002) and acidity (Lin *et al.* 2003), and in improving the acid soil structure (Andry *et al.* 2007). Though zeolite is more expensive than lime or hydrated lime, its longevity in the field may compensate for annual repeated application costs of lime. Furthermore, utilisation of fly-ash is an increasingly important waste disposal issue, in both developing and developed countries. The global production of coal fly-ash in thermal power plants exceeds 550 Mt/year, while the recycling rate is only about 15–20%. Thus, the disposal of the remaining 80–85% is a major environmental issue (Claus 1994). However, before zeolite can be recommended for wider use there is a need for comparative information on hydrated lime *v.* zeolite, particularly with regard to their effect on runoff and sediment generation and also plant growth on acid soils.

The use of vegetation as a bio-engineering tool for erosion control and road embankment stabilisation has occurred for centuries, but its popularity has increased in the recent decades. This is because it is a low cost technique and is a 'soft' approach, instead of using 'hard' conventional engineering structures that are considered a visual degradation of the environment. Its use has been facilitated in recent years because more knowledge on vegetation is now available for application in engineering designs (Rey 2005). Moreover, the implementation of vegetation cover is a sustainable solution to control soil erosion from a construction such as road embankment. Vegetation cover can control erosion efficiently (Cerdà 1999; Rey *et al.* 2004). In fact, the influence of vegetation cover on soil erosion takes place by both reducing the kinetic energy of falling rain drops and the hydrodynamic power of flowing water. Vegetation barrier interception of rainfall not only reduces the runoff volume, but also protects surface soil from being detached and the detached soil particles being transported (Beuselinck *et al.* 2000; Lee *et al.* 2000; Rey 2004, 2005; Pan *et al.* 2006). Thus, vegetation barriers have the ability to reduce flow velocity, which in turn reduces the erosivity forces (Pan and Shangguan 2005). In addition, the soil structure under vegetation cover is improved, with higher infiltration capability, and plant roots reinforcing the soil aggregate to resist high erosive forces (Barthès and Roose 2002). However, the effectiveness of vegetation cover in controlling soil erosion is generally related to vegetation morphology and site topographic conditions. Selecting an appropriate plant that requires minimal management is a key to success for long-term soil erosion conservation.

Sedum species (Crassulaceae), often called stonecrop, have succulent leaves and a waxy cuticle. The morphology of this plant permits it to be categorised among the plants serving as vegetation barriers (such as grasses, woody species, etc.) in preventing soil erosion (Beuselinck *et al.* 2000; Lee *et al.* 2000; Rey 2004, 2005; Pan *et al.* 2006). There are >350 different species, most of which can survive in very cold to hot temperatures and dry conditions, and they tend to grow in poor and stony soil as well as in slightly acidic and alkaline soils (Stephenson 1994). Sedums are used in rock gardens and as edges in flower beds, and for greening the tops of buildings, cottages, and thatched roof, because of low water requirement and management needs. However, little is known about the characteristics of the sedum plant in controlling soil erosion induced by water.

It is known that runoff and sediment generation following a rainfall event are controlled by many factors such as rainfall intensity and duration (e.g. Hanke *et al.* 2004), soil characteristics (Barthès and Roose 2002; Shainberg *et al.* 2003), soil management (Haynes and Naidu 1998; Andry *et al.* 2007), surface cover (Agassi and Levy 1991; Mandal *et al.* 2005), and site topography (El-Swaify 1997). However, the integrated impact of the soil and non-soil factors on runoff and sediment

generation and the link between them is poorly understood for acidic soils. Thus, the objectives of this study were to investigate (*i*) the comparative effect of hydrated lime and artificial zeolite as amendments, and (*ii*) the effectiveness of *Sedum sediforme* (*Rupestria* group) as vegetation cover on an acid soil taken from Yamaguchi prefecture in Japan, in controlling runoff and sediment generation characteristics, at different rain intensities.

Materials and methods

Soil used in this study

The soil used in this study is classified as an acid clay loam, based on the textural triangle (Gee and Bauder 1986). The soil was taken from the B horizon of a profile developed an orange-yellowish sedimentary rock in a non-agricultural field in Yamaguchi prefecture, Japan. The soil is strongly acidic with a pH of 3.0–3.5. The cation exchange capacity (CEC) is relatively high, whereas the content of soil organic carbon is low. The dominant exchangeable cation is Ca^{2+} followed by Al^{3+}, Mg^{2+}, Na^{+}, and K^{+}. The dominant exchangeable anion is SO_4^{2-} followed by Cl^{-}. The clay, silt and sand contents are 365, 345, and 290 g/kg, respectively.

The soil was air-dried, ground to aggregate size <5 mm, and then sieved through a 2-mm screen, and the material passed through the sieve was used in this study.

Soil amendments

A Ca-type artificial zeolite and hydrated lime of 70% alkalinity were used as amendments to alleviate the soil acidity and Al toxicity for plant growth, and to rectify acidity-induced impact on soil physical factors that control sediment generation.

The amendments were mixed with dry soil at 10% for zeolite and 0.5% for lime. These 2 rates were selected based on the research undertaken by Yamamoto *et al.* (2002) and Haynes and Naidu (1998), respectively. The ratio of the amended soil is defined as a mass of the amendment divided by the total mass (mass of soil + mass of amendment). The amended dry soil was left in the mixing box for 2 weeks before use for the investigation. Some physicochemical properties of the amended soils are shown in Table 1.

Vegetation cover

Sedum sediforme (*Rupestria* group) was used as live surface (Fig. 1). Air-dried soil material (≤2 mm) was packed in small tray of size 0.30 by 0.50 by 0.05 m. The tray was uniformly filled with a 15.0-mm filter layer of gravel (3–4 mm), on which a 30-mm-thick soil layer was packed to an average dry bulk density of 1.30 Mg/m^3. The plants (stem with root and leaf) were spread on the soil surface of the prepared soil tray during root initiation. Three levels of live-surface mulching were used: bare soil, and 0.15 and 0.45 kg plants/m^2. During a preliminary experiment, the mulching of 0.60 kg plant material/m^2 achieved almost 100% soil coverage. These 3 live surface mulching ratios corresponded to a vegetation cover index of 0, 25, and 75%, respectively.

The 3 aforementioned vegetation covers were allowed to grow on the untreated and treated acid soils for 5 months under irrigation at 2-day intervals and at an air temperature of 25°C. Prior to the soil erosion experiment, vegetation cover was measured by taking vertical photographs of the surface for each plot with a digital camera, and the leaf area index (LAI) was determined by using LAI32 soft (Yamamoto 2000). The average LAI computed from the 25 and 75% cover treatments were, respectively, 0.20 and 0.62 cm^2/cm^2 for the control, 0.30 and 0.83 cm^2/cm^2 for zeolite, and 0.28 and 0.79 cm^2/cm^2 for lime treatments. Although there was this small discrepancy of actual vegetation cover between different treatments, the cover has been defined as 0, 25 and 75% in this study for comparison of its effectiveness under different amendments.

Soil physical and chemical characterisation

Soil was sampled before starting the erosion experiment, air-dried, and analysed for different physicochemical characteristics. The amended and unamended air-dried soil aggregates were used for the determination of electrical conductivity at 1 : 5 ratio, soil pH at 1 : 2.5 ratio, and soil organic carbon with C/N coder apparatus. The CEC was determined after leaching successively with 0.1 M $BaCl_2$ and 0.005 M $MgSO_4$ solutions (Rhoades 1982), and exchangeable aluminum was determined after extraction with potassium chlorite at 1 : 2.5 ratio using atomic absorption spectroscopy (Thomas 1982).

Table 1. Some properties of the acid soil amended with hydrated lime and artificial zeolite after 5 months of irrigation at 2-day intervals

Values in parentheses are standard deviations

Properties	Unit	Control	0.5% Lime	10% Zeolite
Electrical conductivity 1 : 5	dS/m	2.09 (±0.14)	2.27 (±0.25)	2.05 (±0.17)
pH_{H_2O} 1 : 2.5		3.43 (±0.09)	7.15 (±0.11)	7.23 (±0.31)
Cation exchange capacity	$cmol_c/kg$	15.53 (±2.26)	23.12 (±1.23)	37.43 (±0.67)
Exchangeable aluminum	$cmol_c/kg$	3.20 (±0.16)	0.15 (±0.04)	0.000
Soil organic carbon	g/kg	16.5 (±2.31)	18.56 (±0.67)	19.67 (±2.13)
Saturated hydraulic conductivity (Ks)	10^{-5} cm/s	3.07 (±0.26)	4.98 (±0.43)	7.45 (±0.54)
Saturated water content (at soil pF 0)	cm^3/cm^3	0.36 (±0.02)	0.40 (±0.01)	0.47 (±0.02)
Water content at soil pF2 (θ_{pF2})	cm^3/cm^3	0.30 (±0.004)	0.37 (±0.003)	0.43 (±0.005)
Water retentivity ($\theta_{pF2} - \theta_{pF3}$)	cm^3/cm^3	0.07 (±0.001)	0.10 (±0.002)	0.03 (±0.001)
Available water content ($\theta_{pF2} - \theta_{pF4.2}$)	cm^3/cm^3	0.10 (±0.02)	0.19 (±0.01)	0.23 (±0.005)

Fig. 1. Morphology of *Sedum sediforme* used in this study and its effect on soil surface.

A modified fast-wetting in water method, based on Le Bissonnais (1996), was used to measure the aggregate stability on average clod of 6 mm diameter taken from bare soil surface. Horizontal movement of 4 cm amplitude for a sieve of 106 μm diameter immersed in a container of tap water was applied for 5 min. The material left after wet-shaking was carefully removed, and the sand-size fractions were determined after dispersion with sodium hexametaphosphate.

The saturated hydraulic conductivity (Ks) was measured using 100-cm^3 soil columns taken from undisturbed soil surface of bare soil. The soil column was saturated from the bottom for 2 days and the Ks measurements commenced when the water flux throughout the soil layer was constant. The Ks was computed using the Klute and Dirksen (1986) falling-head method.

The water content (θ) at soil pF of 0, 2, 3, and 4.2 was determined by suction after 48 h of saturation of a 100-cm^3 soil column taken from undisturbed surface of bare soil.

Rainfall simulation experiment

A drip-type rainfall simulator facility at the Arid Land Research Center, Tottori University, Japan, with raindrop fall-height of 12 m was used in this study. From this height, the raindrops were expected to reach the terminal velocity of natural rainfall at the soil surface (Epema and Riezebos 1983). Two rainfall intensities of 30 and 60 mm/h were used separately for 2 and 1 h, respectively. The rainfall distribution uniformity was set at 95%, and about 85% of the drops were >2 mm in diameter. The kinetic energy of the simulated rainfall was computed using the formula proposed by van Dijk *et al.* (2002), $e_k = 28.3\,[1 - 0.52\exp(-0.042\,I)]$ (where e_k is the kinetic energy and I is the rainfall intensity). The kinetic energy of the simulated rainfall was 24.13 and 27.12 J/m^2.mm for the 30 and 60 mm/h rainfall intensities, respectively. The experimental setup is shown in Fig. 2.

The soil trays under different vegetation covers were placed at a 10° slope, which is believed to be the average slope used in the road embankment construction and were subjected to simulated rainfall using tap water (EC, 0.13 dS/m). The runoff samples at 10-min intervals were collected and quantified. The particle size distribution of the sediment in the runoff subsamples was determined with a nest of sieves (2000–1000 μm, 1000–500 μm, 500–250 μm, 250–106 μm, and ≤106 μm, which could, respectively, be considered as average opening size of 1500, 750, 350, 175, and 53 μm). The sediment in the runoff subsamples was also determined gravimetrically after oven drying at 105°C for 48 h.

Splash losses were collected with 2 collecting panels (30 by 50 cm) attached to the soil plot on each one of the 50-cm sides but not from the 30-cm sides due to practical difficulties. The splash sediments were collected throughout the experiment. Since splash was not collected from the 30-cm sides of the soil plot, the total soil splash loss refers to the total amount collected rather than the total amount that actually occurred (Abu-Hamdeh *et al.* 2006). The particle size distribution of soil splash sediment was determined with a nest of sieves with average aperture of 1500, 750, 350, 175, and 53 μm.

After rainfall simulation exercise, the surface of the soil plot was left to air-dry for 48 h. Three samples were then taken along the slope length of the soil surface. The particle size distribution of the fine material formed from the soil surface was determined with a nest of sieves with average aperture of 1500, 750, 350, 175, and 53 μm.

Three replications were used for each treatment. The triplicate data were subjected to mean separation analysis using 1-way ANOVA test at significance of $P = 0.05$.

Results and discussion

Effect of amendments on the soil physicochemical characteristics of the acid soil

Selected characteristics for the air-dried soil before the start of rainfall treatments are summarised in Table 1. There was no significance difference ($P > 0.05$) in the soil EC between the

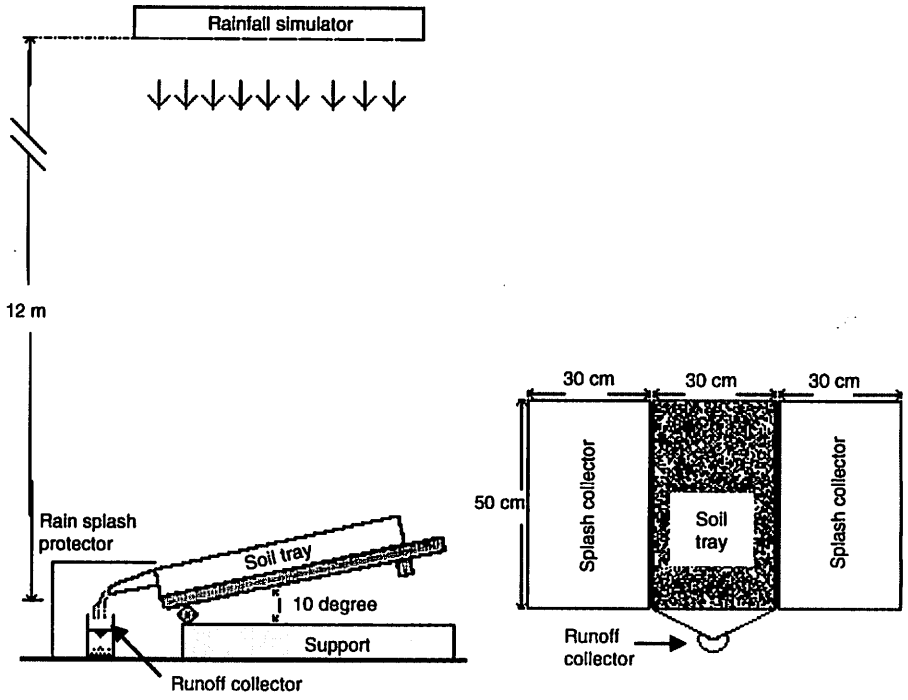

Fig. 2. Rainfall simulation experimental setup.

3 amendment treatments. The soil pH increased by application of amendments. The exchangeable Al^{3+} decreased significantly ($P < 0.05$) with the application of amendments, and the decrease was higher with zeolite than lime.

The aggregate size fraction obtained after fast-wetting in tap water of aggregate size >106 μm as affected by the amendment treatments is shown in Fig. 3. This aggregate size fraction is usually considered as appropriate to assess ability of soils to withstand rain impact energy-induced sediment generation and also responsible for decreasing water infiltration (Mandal *et al.* 2005). There were significant differences ($P < 0.01$) among the treatments. The percentage increase in the stability of the aforementioned fraction after amendment was 8% for lime and 13 for zeolite. Thus, zeolite was more effective in stabilising larger size fractions than lime, suggesting that sediment generation after zeolite amendment would be less than that after amendment with lime (Barthès and Roose 2002). On the other hand, the decrease in the silt and clay proportion (≤106 μm or an average opening size of 53 μm) with amendment incorporation may contribute to a decrease in the crust formation on the soil surface after being impacted by rainfall energy.

The saturated hydraulic conductivity (Ks) of the soils increased significantly ($P < 0.05$) with amendment, but the magnitude varied according to the type of the amendment (Table 1). A positive correlation was found between Ks and the aggregate size fraction >160 μm ($r = 0.89$, $P < 0.001$). It was also found that the water content (θ) at different soil pF values and available water content ($\theta_{pF2} - \theta_{pF4.2}$) increased significantly ($P < 0.05$) with amendment (Table 1). Thus, increase in wet aggregate stability, hydraulic conductivity of soil, and its ability to hold water with amendment would result in reduction in runoff and the associated sediment generation (Barthès and Roose 2002).

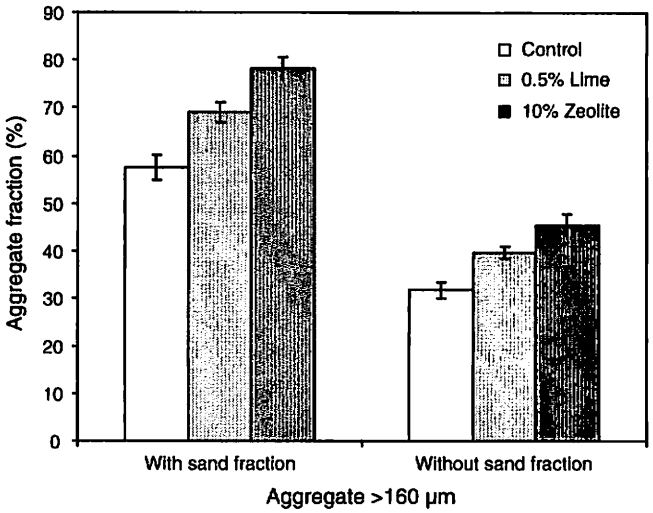

Fig. 3. Soil aggregate stability as affected by amendments.

Effects of amendments and sedum cover on surface runoff

The time-incremented surface runoff (SR) data for different intensities of rainfall (Fig. 4) indicate qualitatively similar temporal dynamics regardless of the treatments. In general there were 3 phases; the first phase was characterised by near zero SR; the second phase by a rapidly increasing linear mode reaching a maximum; and the third phase by a relatively slower

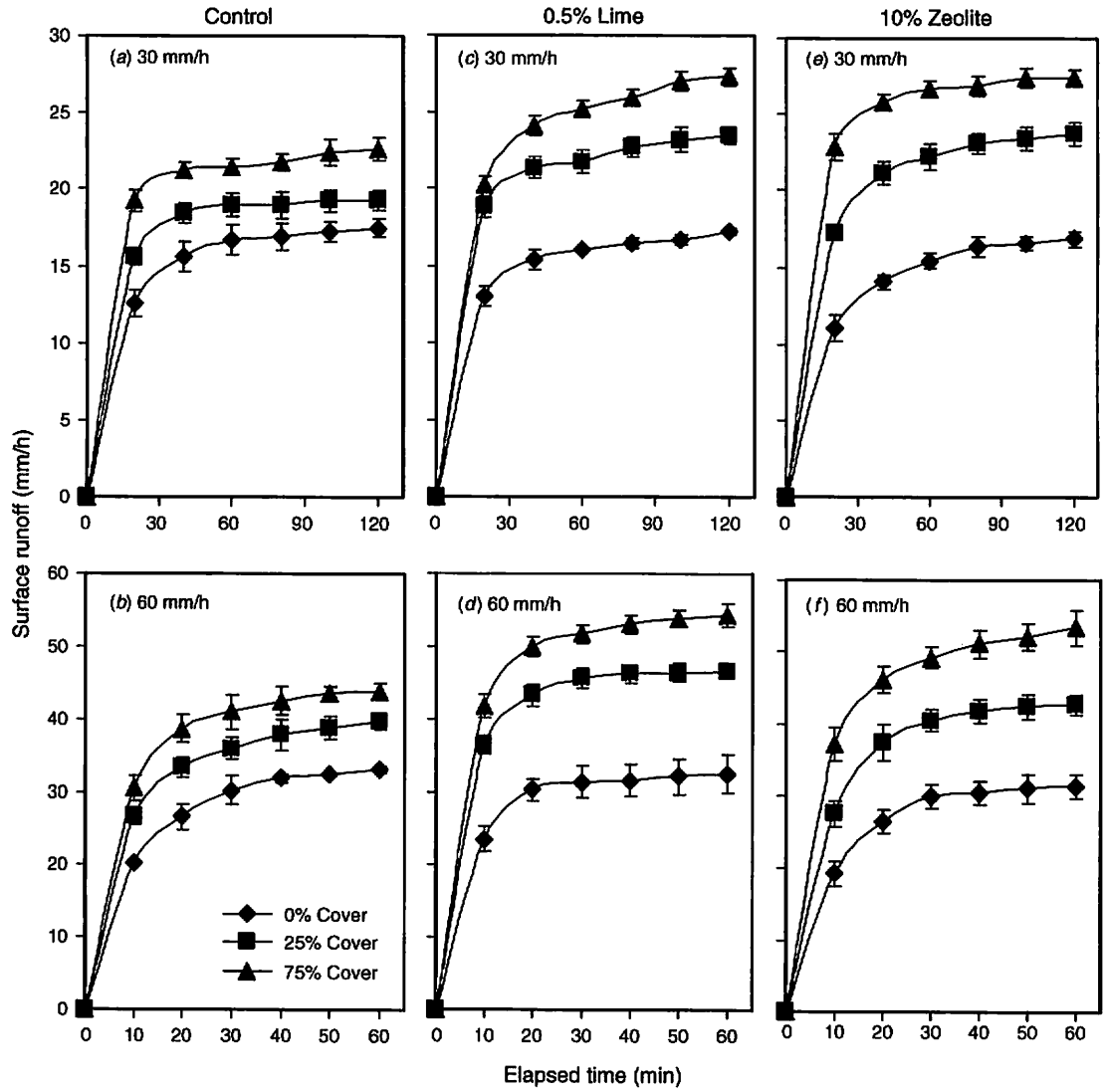

Fig. 4. Effect of sedum cover on surface runoff from soils subjected to 30 and 60 mm/h rainfall intensity.

but linear rate of increase to reach a final maximum. The SR in the first phase, which is determined by the ponding time or surface runoff initiation, was zero in all of the treatments due to the effect of soil moisture as a result of irrigation given during the establishment of sedum cover. Focusing on the bare soil, the linear phase decreased with application of the amendment, and in this regard, soil treated with zeolite was more effective. This decrease could be the result of water infiltration improvement because of the amendment application. The third phase in SR, showing a near horizontal mode with time, is a reflection of hydraulic steady-state that was established between the surface ponded water and subsoil hydraulic properties (Andry *et al.* 2007) such as saturated Ks and surface water retention (Table 1).

On the other hand, it was found that the SR increased significantly ($P < 0.05$) with increasing sedum cover under the 2 rainfall intensities regardless of the amendment application. This increase in SR with vegetation cover is contrary to the results reported in the literature (e.g. Mandal *et al.* 2005). Cerdà (1999) reported that the vegetation cover enhanced infiltration and reduced surface runoff and erosion, and the variability in runoff and erosion decreased as vegetation cover increased. This inconsistency of the SR result with other reports could be attributed to the difference in soil plot size (slope length and soil width) and the raindrop energy dissipation. It is known that slope length can affect the SR features for water erosion (Chaplot and Le Bissonnais 2003). Also, all the aforementioned studies were field experiments where the slope length was generally >1 m. There is a report of a significant relationship between rainfall energy dissipation and the soil plot size (Loch and Foley 1992). Agassi and Levy (1991) reported that up to 15% of the rain was lost as a rain splash, which decreased significantly with an increase in stone covers from 0 to 25 and 50%. In fact, in a laboratory study of Pan *et al.* (2006), conducted under a ryegrass cover, an increase of SR with increasing vegetation cover was obtained, which is similar to our result. One possible

reason for the increase in SR is that although sedum cover could dissipate the rainfall energy and slow down the water flow, due to short slope length (only 0.50 m), the increase in ponding time would have not happened; as a result there was no water infiltration improvement as was also observed by Mandal *et al.* (2005).

The overall observation was that lime amendment generated more SR than zeolite treatment, and this result is consistent with the soil aggregate stability test (Fig. 3), saturated hydraulic conductivity, and the surface water retention results shown in Table 1. On the other hand, the computed average LAI of the 25 and 75% vegetation cover, which affected SR, was higher with zeolite (0.30 and 0.83 cm^2/cm^2, respectively) than with lime (0.28 and 0.79 cm^2/cm^2, respectively) treatment. It was found that SR increased significantly with increasing vegetation cover; however, the lesser SR from the soil treated with zeolite compared with lime treatment, despite of the increase in the actual coverage as indicated before, implies the substantial effect of soil physicochemical properties in controlling soil erosion between the 2 treatments.

Effects of amendments and sedum cover on sediment generation

The time-incremented sediment concentration (SC) data for different intensities of rainfall (Fig. 5) indicate qualitatively similar temporal dynamics regardless of the treatments. The SC decreased significantly ($P < 0.05$) with amendment under both rainfall intensities, in particular with zeolite treatment. The cumulative soil loss of the 0% cover soil decreased significantly ($P < 0.05$) with amendment and the decrease was more with zeolite (Fig. 6). This decrease was consistent with the fast wetting aggregate stability results in Fig. 3.

The SC decreased significantly ($P < 0.05$) with increasing sedum cover under both rainfall intensities and the magnitude

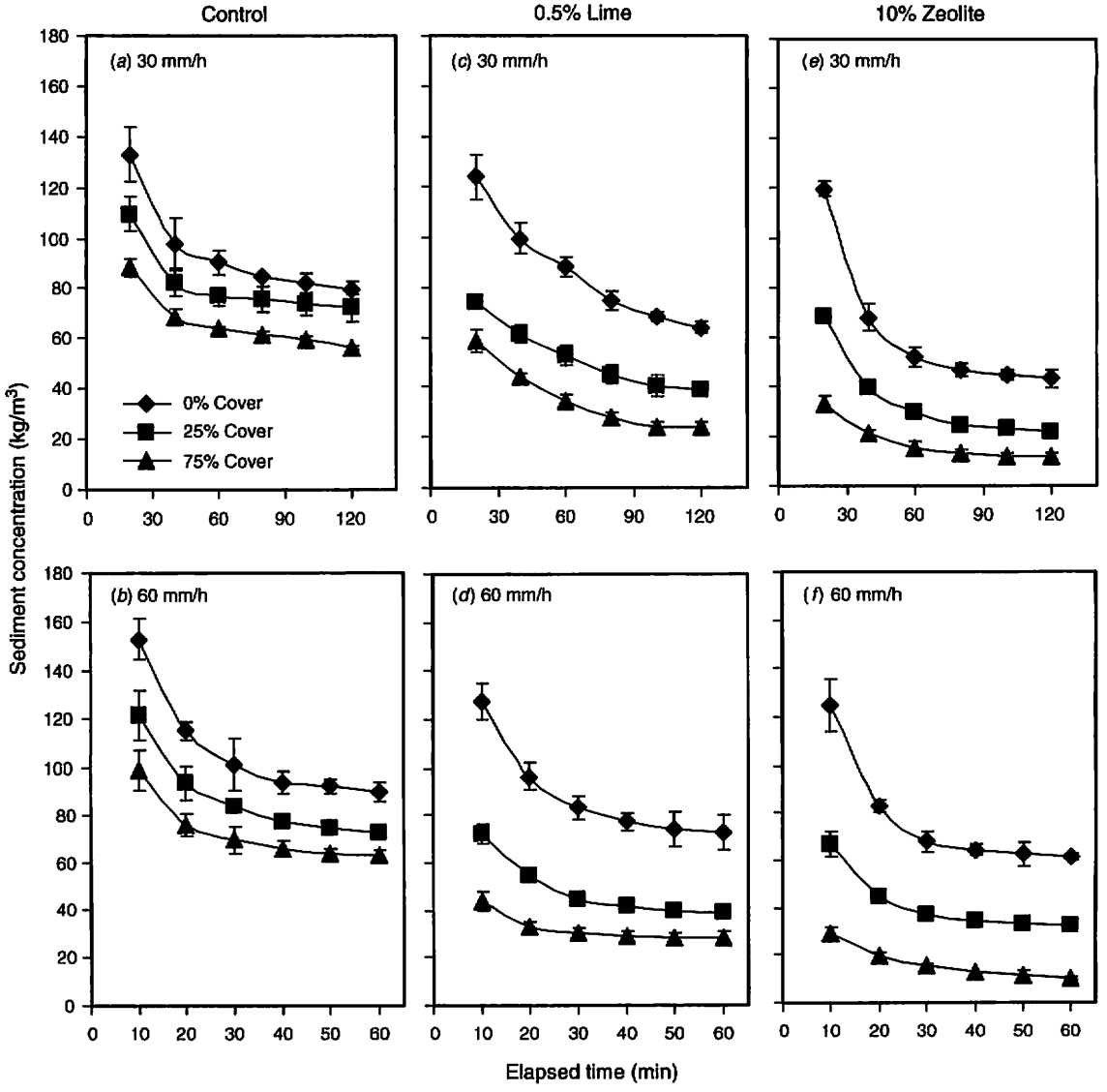

Fig. 5. Effect of sedum cover on sediment concentration from soils subjected to 30 and 60 mm/h rainfall intensity.

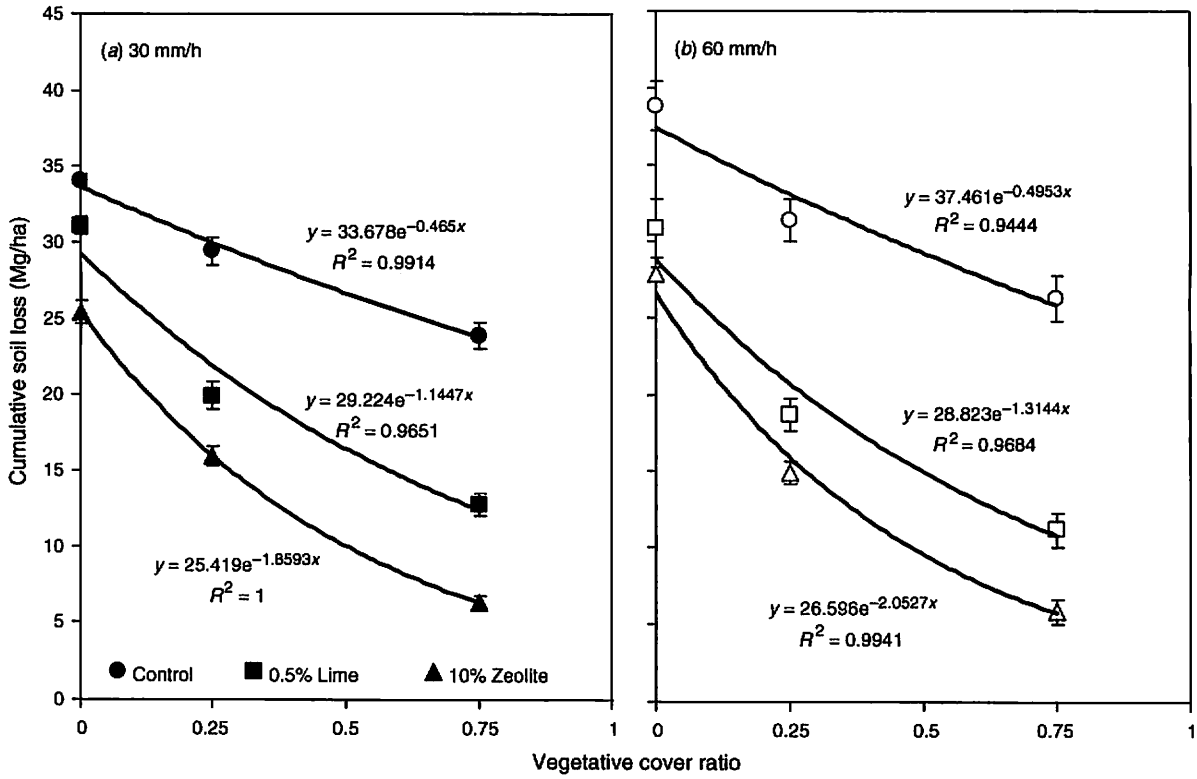

Fig. 6. Cumulative soil loss carried through runoff from soils as affected by vegetative cover ratio subjected to 30 and 60 mm/h rainfall intensity.

differed in accordance with the type of the amendment used (Fig. 5). It was found that the sedum plant cover with zeolite treatment was more effective than with lime. The actual average LAI of the 25 and 75% vegetation cover treatments, as indicated before, was higher with zeolite than with lime treatment; probably, this difference in the actual coverage affected the SC. This result suggests that the sedum cover determines the amount of sediment detached by protecting the soil surface against the raindrop energy as suggested by Mandal *et al.* (2005) and also the overflow entrainment as suggested by Pan and Shangguan (2005). Based on the Fig. 5, a non-linear regression analysis of the effect of rain depth (p, rain intensity × elapsed time) on SC could be made, described by the equation $SC = a \times \exp(-b \times p)$, $R^2 = 0.89$ and $P < 0.001$, where p is rain depth, and a and b are empirical coefficients. Similar trends have also been reported by Cerdà (2001) showing that the SC was greater at the time of runoff initiation and diminished gradually until the end of a 60-min application of rain.

It was found that the cumulative soil loss (CSL) decreased exponentially and significantly ($P < 0.05$) with increasing vegetation cover ratio, and the slope of the function increased significantly with the amendment treatment at both rainfall intensity treatments (Fig. 6). The percentage decrease of CSL due to 25 and 75% cover subjected to 30 mm/h rainfall intensity was respectively 15 and 30% for control, 40 and 60% for lime, and 40 and 75% for zeolite. With 60 mm/h rainfall intensity, the percentage decrease due to 25 and 75% vegetation cover was, respectively, 20 and 35% for control, 40 and 65% for lime, and 45 and 80% for zeolite. These results imply that the reduction in soil loss caused by the vegetation cover seems to be higher under high rainfall intensity.

It was also found that the relationship between CSL and cumulative surface runoff (CSR) is linear ($CSL = A \times CSR$, $R^2 = 0.9$ and $P < 0.001$), in which the coefficient (A) decreased with increasing vegetation cover. This linear correlation suggests that the capacity of the surface runoff to carry sediment remained constant and decreased with soil cover.

The particle size distribution of sediment carried through the runoff (Fig. 7) indicates that the aggregates of average size 175 and 375 μm increased significantly ($P < 0.05$) with increasing vegetation cover, and this increase was more conspicuous under low rain intensity treatment. However, some significant increases ($P < 0.05$) were also found in the aggregates of average size 750 and 1500 μm under the high intensity rainfall treatment regardless of soil amendment. The significant increase in large aggregate fractions, which are the most susceptible aggregates on the soil surface to be broken down by the rainfall energy (Barthès and Roose 2002), suggests that the sedum cover interception could dissipate the rainfall energy. The proportion of silt and clay (≤53 μm) dominated in all the sediments and accounted for >55% of total weight. These particles, which are mostly responsible for the crusting, decreased significantly ($P < 0.05$) with vegetation cover. In spite of these positive effects of vegetation cover, there was still some soil loss, which decreased significantly ($P < 0.05$)

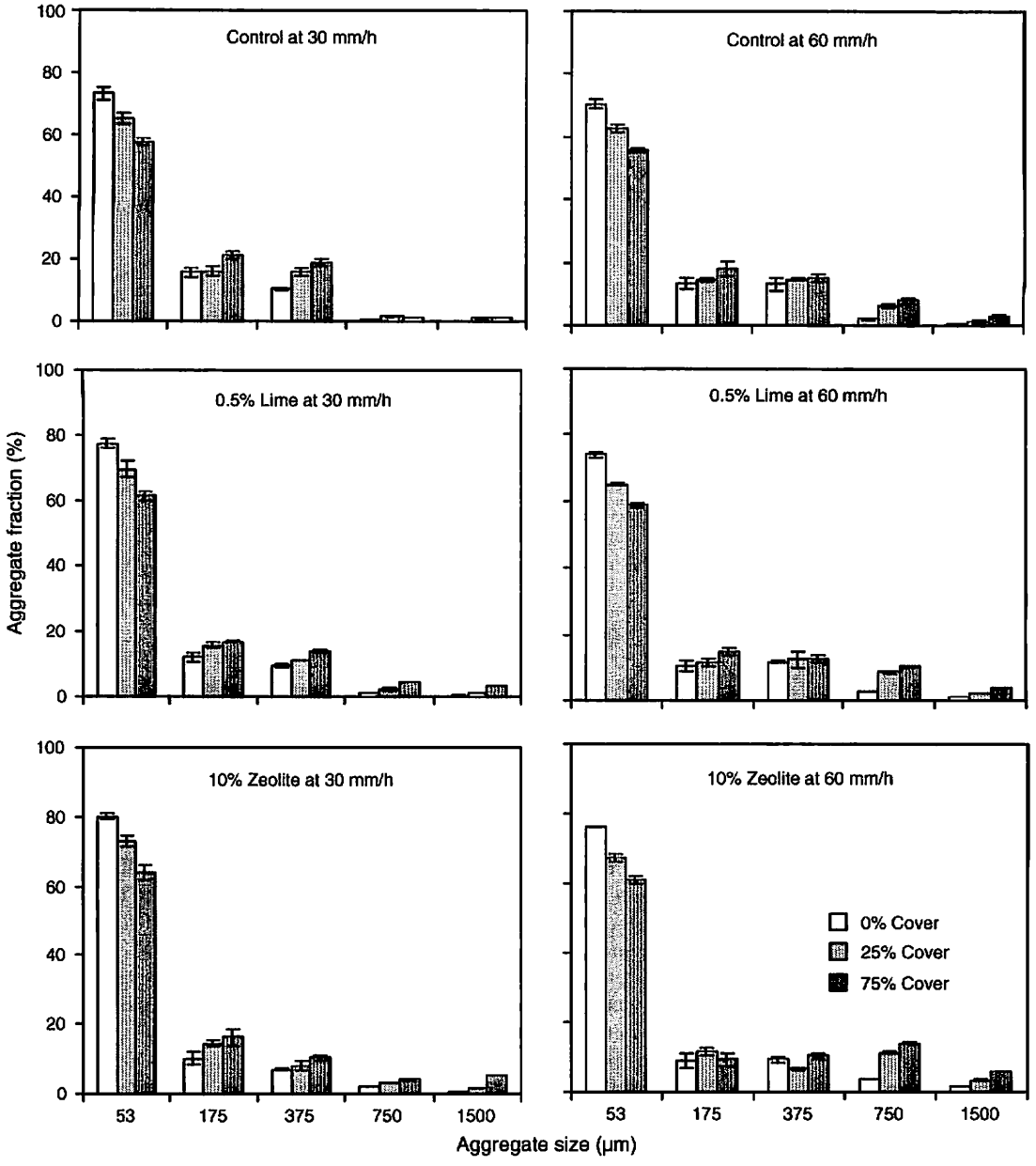

Fig. 7. Effect of sedum cover on particle size distribution of the soil loss carried through runoff from soils subjected to 30 and 60 mm/h rainfall intensity.

with increasing surface runoff, and suggests that the overflow entrainment was among the main forces driving erosion under vegetation cover.

The best fitting equation for the mean weight diameter (MWD) of sediment was a non-linear growth function given by the equation $MWD\ (c) = a + (b - a)\ e^{-kc}$, RMSE < 0.002, where MWD is mean weight diameter of soil sediment under c vegetation cover ratio, and a, b, and k are empirical coefficients, which is derived from the results of non-linear regression analysis for the effect of vegetation cover on MWD of the soil sediment carried through runoff. The equations for different soil treatments are presented in Fig. 8. The improvement of soil aggregate stability (Fig. 3) on one hand and the amelioration of sedum plant growth on the other hand because of the amendment are among the main factors which contributed to the increase in the MWD of the sediment. The soil treated with zeolite had the most effective surface protection among the 3 treatments, regardless of the rainfall intensity, and this effectiveness was consistent with both soil aggregate stability test and the increase in the vegetation cover.

Effects of amendments and sedum cover on soil splash

The total soil losses by rain splashing are given in Fig. 9. Rainfall intensity did not have any significant effect ($P > 0.05$) on total soil splash collected. Agassi and Levy (1991) also reported that rain intensity had no significant effect on the water splash. On the

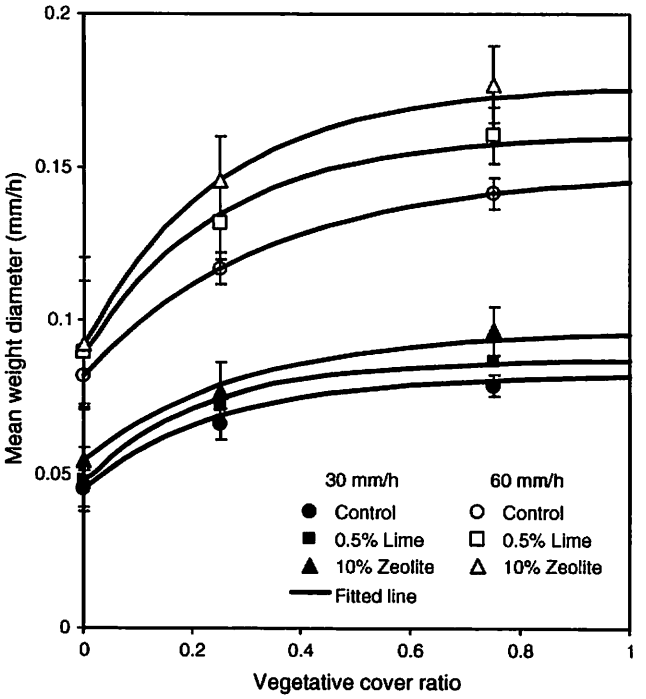

Fig. 8. Characteristic of soil aggregate size of the soil loss through runoff as a function of vegetative cover ratio under 30 and 60 mm/h rainfall intensity.

bare soil, soil splash decreased significantly ($P < 0.05$) with amendment, and treatment with zeolite was more effective than lime. The effectiveness of zeolite and lime amendments on soil splash may depend on the soil pretreatments such as incubation and irrigation, because we found in a separate study (Andry *et al.* 2007) that the aforementioned amendment treatments did not have a significant effect ($P > 0.05$) under 2-week incubation without adding water (Andry *et al.* 2007). Therefore, these changes could be explained on the basis of the effect of aging and prewetting on soil aggregate stability (Shainberg *et al.* 2003) and also the microbial activity (Chan and Heenan 1999). The reduction was 10% for soil treated with lime and 25% with zeolite amendment.

An increase in the vegetation cover decreased the soil splash exponentially and significantly ($P < 0.05$) and this decrease was affected by the amendments, more so with zeolite than with lime (Fig. 9). This result was not surprising, because it was found that the sedum plant adapted better to zeolite amendment than to lime application (actual cover, as indicated before, 30 and 83% for zeolite *v.* 28 and 79% for lime in the 25 and 75% vegetation cover treatments, respectively), even though the EC and pH of soil were not significantly different between the 2 amendment treatments (Table 1). Compared with bare soil, the reduction as a result of 25 and 75% vegetation cover, respectively, was 16 and 30% under control, 40 and 60% under lime, and 40 and 75% under zeolite.

The particle size distribution of the total soil loss by splashing as affected by vegetation cover is shown in Fig. 10. It was noticed that the proportion of the silt and clay and also particle sizes of 750 and 1500 μm in the soil loss by splashing was higher in the soil treated with zeolite than that treated with lime and the soil under control treatment. The average particle size of 175, 375, 750, and 1500 μm each contributed to about 10–25% of

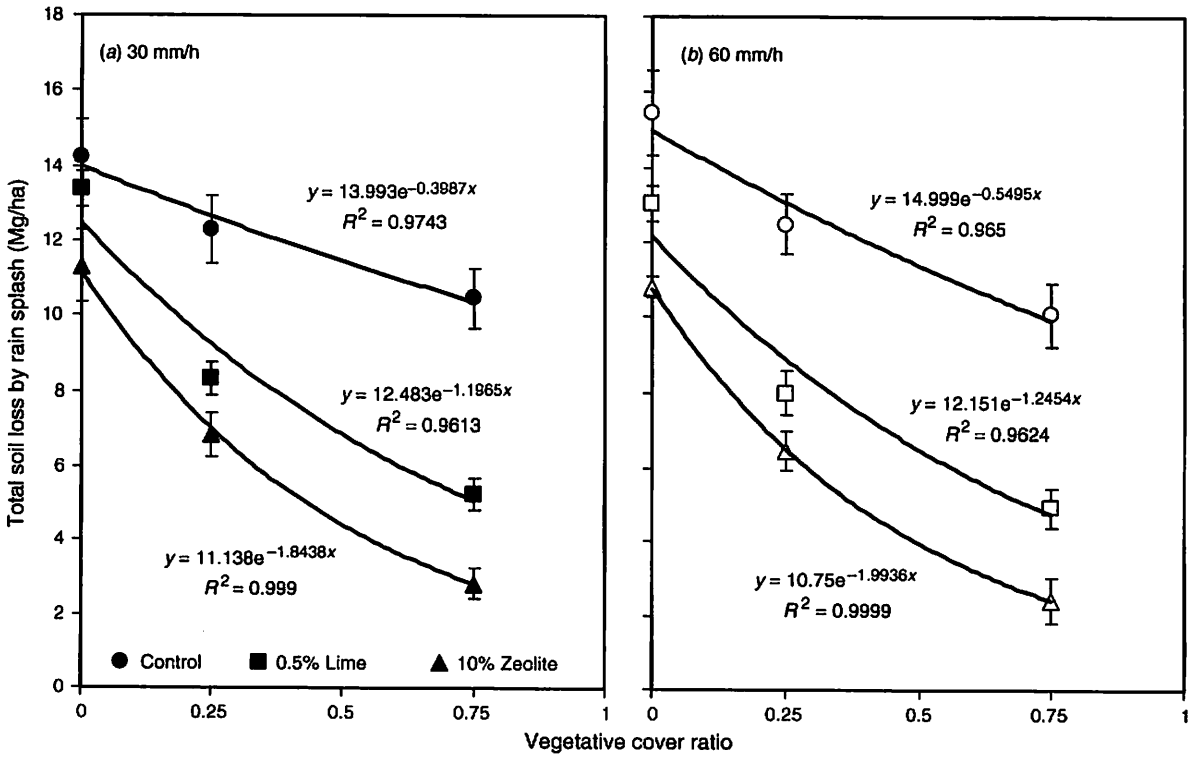

Fig. 9. Total soil loss by rain splashing from soils as affected by vegetative cover ratio subjected to 30 and 60 mm/h rainfall intensity.

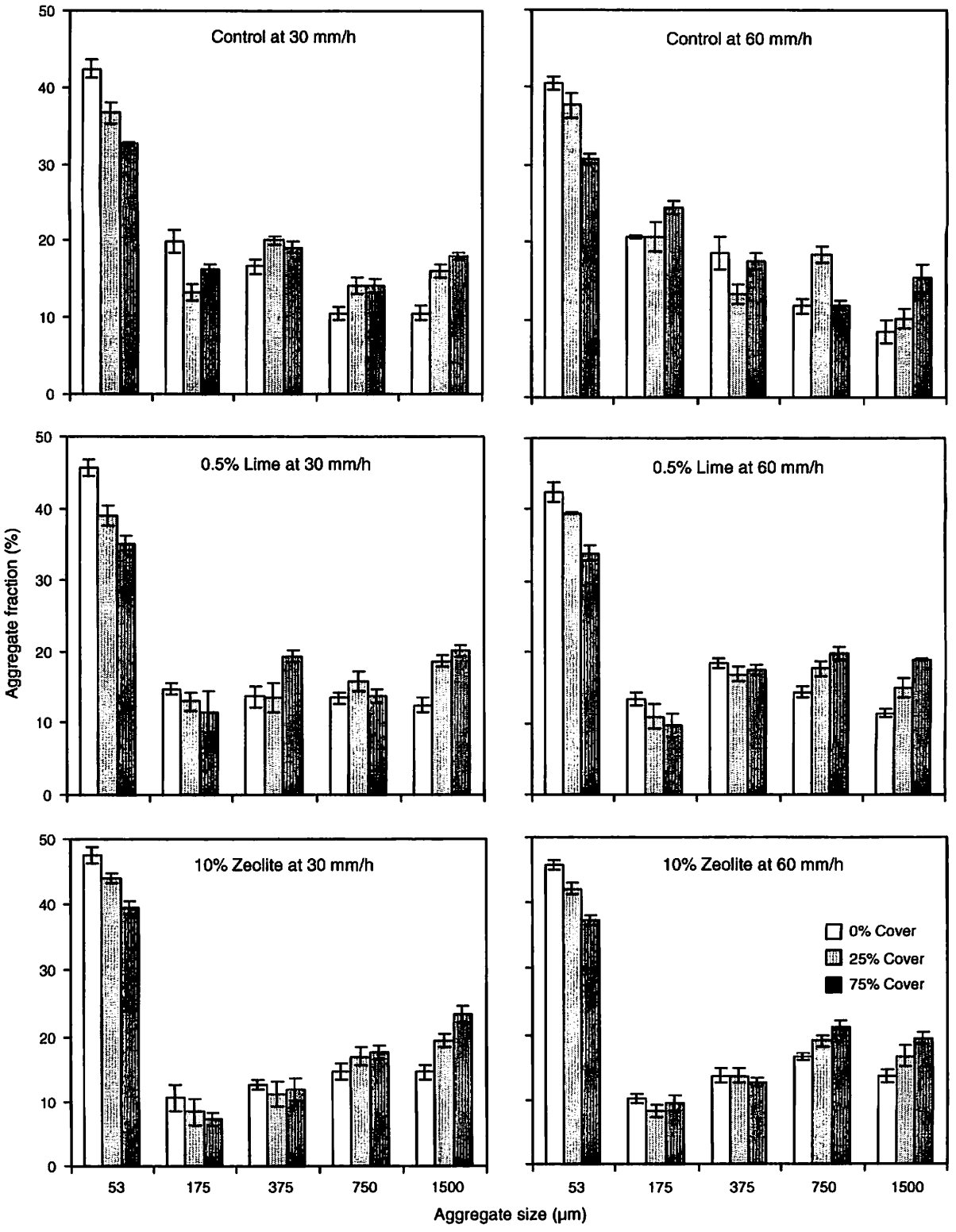

Fig. 10. Effect of sedum cover on particle size distribution of soil loss by rain splashing collected at 30 and 60 mm/h rainfall intensity.

total soil loss, and the proportion of silt and clay (≤53 μm), which dominated in the total soil splash, contributed about 35–45%. The average particle sizes of 750 and 1500 μm increased significantly ($P < 0.05$) with increasing vegetation cover, and the proportion of silt and clay decreased significantly ($P < 0.05$) with increasing vegetation cover. As shown in Fig. 11,

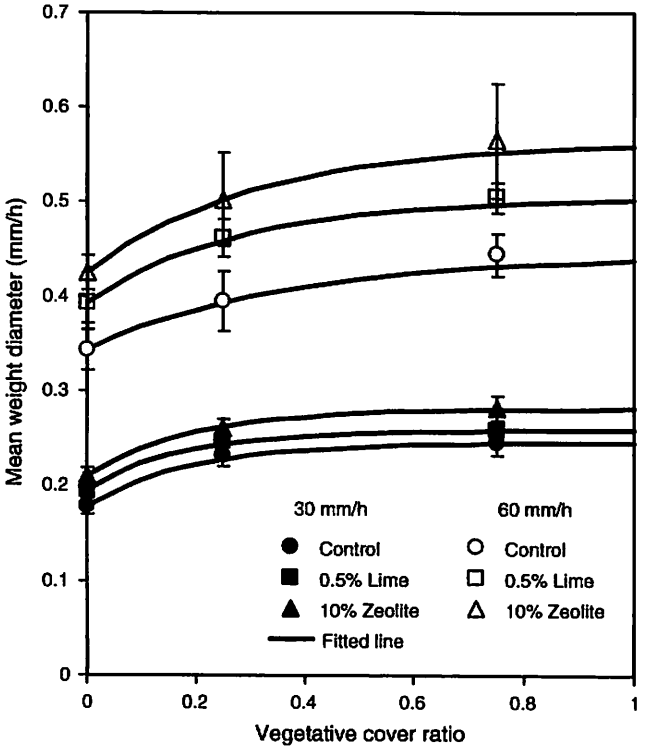

Fig. 11. Characteristic of soil aggregate size of the soil loss by rain splashing as a function of vegetative cover ratio under 30 and 60 mm/h rainfall intensity.

it was found that the vegetation cover was more effective under high rainfall intensity than low. The best fitting regression equation relating the MWD of the soil loss by rain splash with the vegetation cover ratio (c) was a non-linear function given by the equation $MWD\ (c) = a + (b - a)\ e^{-kc}$, RMSE < 0.005. Based on this regression analysis, the soil treated with zeolite had the most effective surface protection among the 3 treatments, in spite of the fact that under this amendment there was a significantly larger proportion of silt and clay in the soil loss by splashing compared with the other treatments.

Based on the comparison of particle size distribution in the sediment and total soil loss by splashing, it appears that soil sediment was more affected by rainfall energy and entrainment of overflow than soil loss by rain splash, as also reported by Abu-Hamdeh *et al.* (2006). Since the surface runoff increased significantly with increasing vegetation cover, the dependence of vegetation cover effectiveness on rainfall intensity may support our assumption that overflow entrainment could be among the major forces driving erosion under vegetation cover.

Effects of amendments and sedum cover on the particle size of soil surface

The fine materials formed on the surface under the 3 vegetation cover treatments were sampled and their particle size distribution was determined (Fig. 12). It was found that rainfall intensity did not have a significant effect ($P > 0.05$) on the particle size distribution on the surface of the bare soil or on the surface under vegetation cover. In fact, the particle size distribution shown in Fig. 12 was of the fine material formed after the rainfall simulation exercise, which is completely different from the method used for sediment concentration. The particle size distribution of sediment concentration shown in Fig. 7 was determined from computation of the average of the data taken at every 10-min interval, which showed a significance difference ($P < 0.05$) as a result of variation in rainfall intensity.

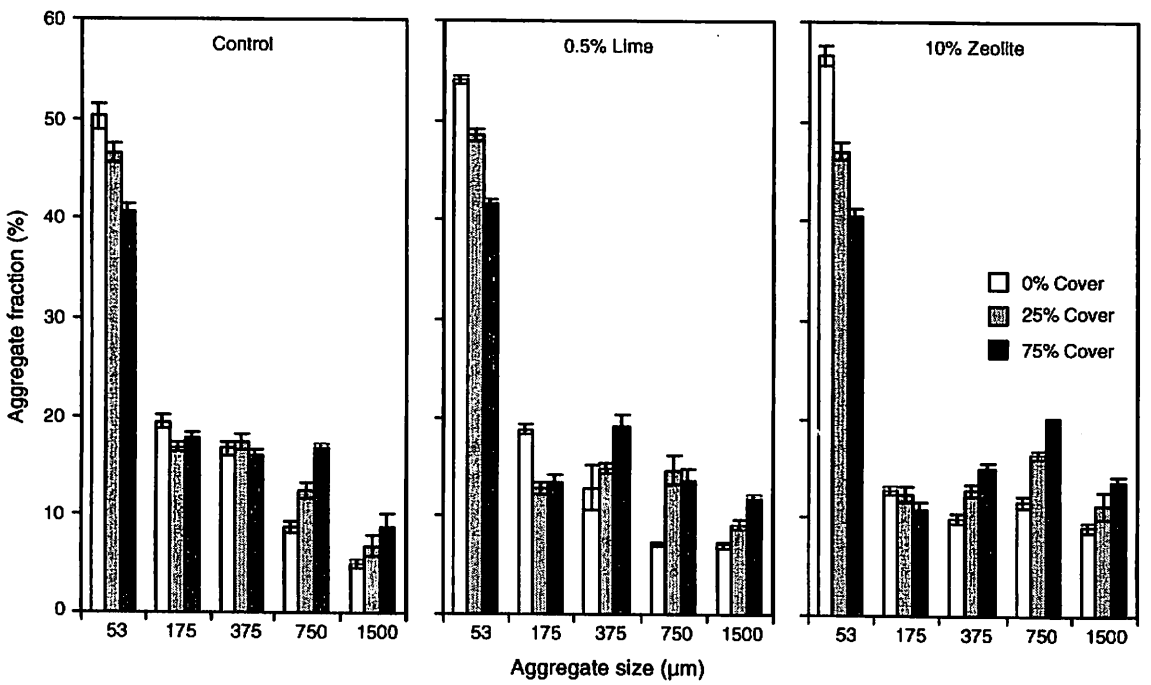

Fig. 12. Particle size distribution of the fine material formed on soil surface under the three levels of vegetation cover.

On the bare soil, the particle size distribution changed significantly ($P < 0.05$) with amendment. The application of amendment significantly increased ($P < 0.05$) the proportion of silt and clay (≤53 μm) particles, which are mostly responsible for the crusting, by 6% with zeolite and 4% with lime compared with the control. However, the aggregate size of 750 and 1500 μm increased significantly ($P < 0.05$) by 3 and 4% with zeolite and 0 and 2% with lime, respectively, compared with the control. Thus, the large aggregate size of soil treated with zeolite was more resistant to breakdown than that of the soil treated with lime, and this result is consistent with the results on soil aggregate stability, SR and SC described above.

The significant difference ($P < 0.05$) in the particle size distribution between the surface of the bare soil and the soil surface under vegetation cover would imply that the vegetation cover could intercept the rainfall and dissipate its energy. With a vegetation cover of 25 and 75%, the proportion of silt and clay (≤53 μm) decreased significantly ($P < 0.05$), respectively, by 4 and 10% on control, 6 and 12% with lime, and 9 and 16% with zeolite. The aggregate sizes of 750 and 1500 μm, which are usually considered as appropriate to assess the ability of soils to withstand rainfall energy-induced sediment generation and water infiltration inhibition (Barthès and Roose 2002; Abu-Hamdeh *et al.* 2006), increased significantly ($P < 0.05$) with increasing vegetation cover. The percentage increase of the 750 μm fraction with 25 and 75% vegetation cover, respectively, was 4 and 8% on control soil, 8 and 7% with lime, and 5 and 8% with zeolite. The percentage increase of the 1500 μm fraction with 25 and 75% vegetation cover, respectively, was 2 and 4% on control soil, 2 and 5% with lime, and 2 and 5% with zeolite. The significant improvement in particle size distribution of the fine material formed on the soil surface under vegetation cover would imply that the effect of rainfall energy dissipation by vegetation cover interception could partly be the cause of the significant increases in SR with vegetation cover.

Conclusion

This acid soil is used for road embankment in Yamaguchi prefecture but is susceptible to water erosion. Because of being extremely acidic, this soil is not suitable for plant growth. The incorporation of artificial zeolite and hydrated lime amendments significantly decreased surface runoff (SR), sediment concentration (SC), and total soil loss by rain splash. The reduction in SR, SC, and total soil losses by splash are linked to the increase in aggregate stability, particularly of the fractions > 106 μm. The reduction in SR from the amended soil is due to the increase in saturated hydraulic conductivity. Thus, we conclude that an increase in wet aggregate stability increased the resistance to sediment generation through improvement in soil water properties, and in this regard, zeolite was more effective than lime.

Sedum cover increased significantly surface runoff; however, it decreased significantly the sediment concentration, soil loss, and total soil loss by rain splash. The particle size distribution of the soil sediment and soil splash was changed significantly, which led to a decrease in the proportion of silt and clay, which is mostly responsible for crusting the soil surface. Based on the comparison of particle size distribution between the sediment concentration and the total soil loss by splashing, the soil sediment was more affected by strength, such as the effect of rainfall energy and the entrainment of overflow, than soil loss by rain splash. The reduction in sediment concentration, soil loss, and total soil loss by rain splash was greater on soils subjected to high rainfall intensity than low rainfall intensity. The increase in surface runoff with vegetation cover could be associated with the slope length of soil plot and the dissipation of rainfall energy. The improvement in mean weight diameter of sediment carried through runoff with vegetation cover subjected to 2 rainfall intensities could be expressed by a mathematical relationship with high degree of reliability.

Plant growth was better with zeolite than the lime treatment. This contributed to an increase in mean weight diameter of sediment and of soil loss by rain splashing and a decrease in crust formation on the soil surface. Being a processed waste material from fly-ash, the beneficial utilisation of zeolite is encouraged not only by the power industry but by the society at large for waste recycling. On the other hand, sedum is known as a plant highly tolerant of water stress and it requires minimal management, and its plantation is encouraged not only at the bio-engineering level but also because of the concern about global warming. These findings may have implication for water erosion modelling and conservation of acid soils. Further research is, however, needed to clarify the longevity of the effectiveness of sedum plant in controlling soil erosion from acid soil treated with zeolite or lime.

Acknowledgments

The authors gratefully acknowledge the technical assistance provided by T. Shimizu and S. Moritani during the rainfall simulation. H. Andry gratefully acknowledges the Japanese Ministry of Education, Culture, Sports, Science and Technology to undertake this study at ALRC, Tottori University, Japan. Acknowledgment is also extended to Dr Mohan Saxena, visiting professor at ALRC, for his editorial comments.

References

Abu-Hamdeh NH, Abo-Qudais SA, Othman AM (2006) Effect of soil aggregate size on infiltration and erosion characteristics. *European Journal of Soil Science* **57**, 609–616.

Agassi M, Levy GJ (1991) Stone-cover and rain intensity: effects on infiltration, erosion and water wash. *Australian Journal of Soil Research* **29**, 565–575. doi: 10.1071/SR9910565

Andry H, Yamamoto T, Rasiah V, Fukada M (2007) Improving the resistance of an acid soil to water erosion using artificial zeolite and hydrated lime amendments. *Transactions of The Japanese Society of Irrigation, Drainage and Reclamation Engineering* **247**, 53–64.

Barthès B, Roose E (2002) Aggregate stability as an indicator of soil susceptibility to runoff and erosion; validation at several levels. *CATENA* **47**, 133–149. doi: 10.1016/S0341-8162(01)00180-1

Beuselinck L, Steegen A, Govers G, Nachtergaele J, Takken I, Poesen J (2000) Characteristics of sediment deposits formed by intense rainfall events in small catchments in the Belgian Loam Belt. *Geomorphology* **32**, 69–82. doi: 10.1016/S0169-555X(99)00068-9

Cerdà A (1999) Parent material and vegetation affect soil erosion in Eastern Spain. *Soil Science Society of America Journal* **63**, 362–368.

Cerdà A (2001) Effects of rock fragment cover on soil infiltration, interill runoff and erosion. *European Journal of Soil Science* **52**, 59–68. doi: 10.1046/j.1365-2389.2001.00354.x

Chan KY, Heenan DP (1999) Lime-induced loss of soil organic carbon and effect on aggregate stability. *Soil Science Society of America Journal* **63**, 1841–1844.

Chaplot VAM, Le Bissonnais Y (2003) Runoff features for interrill erosion at different rainfall intensities, slope lengths, and gradients in an agricultural loessial hillslope. *Soil Science Society of America Journal* **67**, 844–851.

Claus LB (1994) Coal-use residues. In 'Legislation for the management of coal-use residues'. Technical Report No. IEACR/68, pp. 15–22. (IEA Coal Research: London)

van Dijk AIJM, Bruijnzeel LA, Rosewell CJ (2002) Rainfall intensity–kinetic energy relationship: a critical literature appraisal. *Journal of Hydrology* **261**, 1–23. doi: 10.1016/S0022-1694(02)00020-3

Edmeades DC, Ridley AM (2003) Using lime to ameliorate topsoil and subsoil acidity. In 'Handbook of soil acidity'. (Ed. Z Rengel) pp. 297–336. (Marcel Dekker, Inc.: New York)

El-Swaify SA (1997) Factors affecting soil erosion hazards and conservation needs for tropical steeplands. *Soil Technology* **11**, 3–16. doi: 10.1016/S0933-3630(96)00111-0

Epema GF, Riezebos HTh (1983) Fall velocity of water drops at different heights as a factor influencing erosivity of simulated rain. *CATENA Supplement* **4**, 1–17.

Gee GW, Bauder JW (1986) Particle-size analysis. In 'Methods of soil analysis, Part I. Physical and mineralogy methods'. SSSA Book series No. 5, 2nd edn. (Ed. A Klute) pp. 383–411. (Soil Science Society of America and American Society of Agronomy: Madison, WI)

Goldman SJ, Jackson K, Bursztynsky TA (1986) 'Erosion and sediment control handbook.' (McGraw Hill: New York)

Hanke M, Perry D, Kung K-JS, Bubenzer G (2004) A low-intensity, high-uniformity water application system. *Soil Science Society of America Journal* **68**, 1833–1837.

Haynes RJ, Naidu R (1998) Influence of lime, fertilizer and manure applications on soil organic matter content and soil physical conditions. A review. *Nutrient Cycling in Agroecosystems* **51**, 123–137. doi: 10.1023/A:1009738307837

Hoyt PB (1981) Improvement in soil tilth and rape seed emergence by lime application on acid soils in the Peace River region. *Canadian Journal of Soil Science* **61**, 91–98.

Huygens D, Boeckx P, Van Cleemput O, Oyarzún C, Codoy R (2005) Aggregate and soil organic carbon dynamics in South Chilean Andisols. *Biogeosciences* **2**, 159–174.

Kirchhof G, Layawardane NS, Blackwell J, Murray E (1995) Lime-slotting technique to ameliorate subsoil acidity in a clay soil. I. Effects on soil pH and physical characteristics. *Australian Journal of Soil Research* **33**, 425–441. doi: 10.1071/SR9950425

Klute A, Dirksen C (1986) Hydraulic conductivity and diffusivity: laboratory methods. In 'Methods of Soil analysis, Part I. Physical and mineralogy methods'. SSSA Book series No. 5, 2nd edn. (Ed. A Klute) pp. 687–734. (Soil Science Society of America and American Society of Agronomy: Madison, WI)

Le Bissonnais Y (1996) Aggregate stability and assessment of soil crustability and erodibility: I. Theory and methodology. *European Journal of Soil Science* **47**, 425–437. doi: 10.1111/j.1365-2389.1996.tb01843.x

Lee KH, Isenhart TM, Schultz RC, Mickelson SK (2000) Multi-species riparian buffers trap sediment and nutrients during rainfall simulations. *Journal of Environmental Quality* **29**, 1200–1205.

Lin C, Long X, Xu S (2003) Amendment of minesite acid sulfate soils and the use of vetiver grass for re-vegetation in Dabaoshan Mine, Northern Guangdong, China. In 'Conference on Vetiver and Exhibition: Proceedings of the Third International Vetiver Conference'. 6–9 October 2003, Guangzhou, China. pp. 427–431.

Loch RJ, Foley JL (1992) Effects of plot size on size distributions of water-stable material at the soil surface under simulated rain. *Australian Journal of Soil Research* **30**, 113–118. doi: 10.1071/SR9920113

Maeda Cooperation and Asanuma Gumi (1999) Reformed investigation for retaining wall and road in the construction areas of the Sanyo automobile highway (in Japanese).

Mandal UK, Rao KV, Mishra PK, Vittal KPR, Sharma KL, Narsimlu B, Venkanna K (2005) Soil infiltration, runoff and sediment yield from a shallow soil with varied stone cover and intensity of rain. *European Journal of Soil Science* **56**, 435–443. doi: 10.1111/j.1365-2389.2004.00687.x

Menzies NW (2003) Toxic elements in acid soils: chemistry and measurement. In 'Handbook of soil acidity'. (Ed. Z Rengel) pp. 267–298. (Marcel Dekker, Inc.: New York)

Midmore DJ, Jansen HGP, Dumsday RG (1996) Soil erosion and environmental impact of vegetable production in the Cameron Highlands, Malaysia. *Agriculture, Ecosystems & Environment* **60**, 29–46. doi: 10.1016/S0167-8809(96)01065-1

Pan C, Shangguan Z (2005) Influence of forage grass on hydrodynamic characteristics of slope erosion. *Journal of Hydraulic Engineering* **36**, 271–277.

Pan C, Shangguan Z, Lei T (2006) Influence of grass and moss on runoff and sediment yield on sloped loess surfaces under simulated rainfall. *Hydrological Processes* **20**, 3815–3824. doi: 10.1002/hyp.6158

Rey F (2004) Effectiveness of vegetation barriers for marly sediment trapping. *Earth Surface Processes and Landforms* **29**, 1161–1169. doi: 10.1002/esp.1108

Rey F (2005) Efficacité des ouvrages de génie biologique pour le piégeage des sédiments dans des ravines incisées dans des marnes (Alpes du Sud, France). *Géomorphologie: relief, processus, environnement* **1**, 21–30.

Rey F, Ballais JL, Marre A, Rovéra G (2004) Rôle de la végétation dans la protection contre l'érosion hydrique de surface. *Comptes rendus. Géoscience* **336**, 991–998.

Rhoades JD (1982) Cation exchange capacity. In 'Methods of soil analysis, Part II. Chemical and microbiological properties'. SSSA Book series No. 5, 2nd edn. (Eds AL Page, RH Miller, DR Keeney) pp. 149–157. (Soil Science Society of America and American Society of Agronomy: Madison, WI)

Roth CH, Pavan MA (1991) Effects of lime and gypsum on clay dispersion and infiltration in samples of a Brazilian oxisoil. *Geoderma* **48**, 351–361. doi: 10.1016/0016-7061(91)90053-V

Shainberg I, Mamedov AI, Levy GJ (2003) Role of wetting rate and rain energy in seal formation and erosion. *Soil Science* **168**, 54–62. doi: 10.1097/00010694-200301000-00007

Stephenson R (1994) 'Sedum: cultivated stonecrops.' (Timber Press, Inc.: Hong Kong)

Tarchitzky J, Chen Y, Banin A (1993) Humic substances and pH effects on sodium-and calcium-montmorillonite flocculation and dispersion. *Soil Science Society of America Journal* **57**, 367–372.

Thomas GW (1982) Exchangeable cations. In 'Methods of soil analysis, Part II. Chemical and microbiological properties'. SSSA Book series No. 5, 2nd edn. (Eds AL Page, RH Miller, DR Keeney) pp. 159–165. (Soil Science Society of America and American Society of Agronomy: Madison, WI)

Wong MTF, Swift RS (2003) Role of organic matter in alleviating soil acidity. In 'Handbook of soil acidity'. (Ed. Z Rengel) pp. 337–358. (Marcel Dekker, Inc.: New York)

Yamada M, Uehira M, Hun LS, Asahara K, Endo T, Eneji AE, Yamamoto S, Honna T, Yamamoto T, Fujiyama H (2002) Ameliorative effect of K-type and Ca-type artificial zeolite on the growth of beets in saline and sodic soils. *Soil Science and Plant Nutrition* **45**, 651–658.

Yamamoto K (2000) Estimation of the canopy gap size using two photographs at different heights. *Ecological Research* **15**, 203–208. doi: 10.1046/j.1440-1703.2000.00341.x

Yamamoto T, Yamada M, Guang W, Yuya A (2002) Application of recycling materials for soil degradation in arid land. *Journal of Japanese Society of Irrigation, Drainage and Reclamation Engineering* **70**, 579–600 [in Japanese].

Manuscript received 22 January 2007, accepted 16 May 2007

available at www.sciencedirect.com

ScienceDirect

journal homepage: www.elsevier.com/locate/agwat

Causes of farmland salinization and remedial measures in the Aral Sea basin—Research on water management to prevent secondary salinization in rice-based cropping system in arid land

Yoshinobu Kitamura [a,b,*], *Tomohisa Yano* [c], *Toshimasa Honna* [a], *Sadahiro Yamamoto* [a,b], *Koji Inosako* [a,b]

[a] *Faculty of Agriculture, Tottori University, Koyamacho-Minami 4-101, Tottori 680-8553, Japan*
[b] *Japan Science and Technology Agency (JST), 4-1-8, Honcho, Kawaguchi-shi, Saitama 332-0012, Japan*
[c] *Tottori University, Hamasaka 1390, Tottori 680-0001, Japan*

ARTICLE INFO

Article history:
Accepted 11 March 2006
Published on line 21 April 2006

Keywords:
Secondary salinization
Water management
Water and salt balance
Central Asia
Arid land
Rice-based crop rotation system

ABSTRACT

In the Lower Syr Darya region of the Aral Sea basin, secondary salinization of irrigated lands has been a crucial problem. To clarify the mechanism of secondary salinization, studies on water and salt behavior were conducted in an irrigation block where a rice-based cropping system has been practiced. Results of on-site studies are summarized as follows: (1) since the performance of land-leveling for rice cultivation was extremely poor, the water level was maintained high enough to submerge the highest portion of each plot, and this causes wastage of irrigation water and salt accumulation. (2) A large portion of water introduced to rice plots tends to be released into field drains. (3) Due to excessive irrigation of rice plots with slightly saline river water, dissolved salts were mainly deposited in upland plots in the block and its periphery. Changes in salt accumulation rates were dependent upon the scale of annual changes in the farmland areas that were converted from the upland condition to submerged condition in a process of crop rotation. (4) A remarkable finding was obtained on salt behavior in saturated shallow soil layers of rice plots. An initial decrease in soil water salinity in the shallow layer is due to the leaching effects of infiltration during the initial stage, and the subsequent gradual increase is more likely a consequence of mixing with the saline water that remains in the finer soil pores combined with the concentration effects of crop water uptake, and the upward flow from the lower layers due to occasional interruption and resumption of irrigation water supply. (5) Because seepage water from rice plots flows underneath the field drain, the rise of the groundwater table and salt accumulation were accelerated in the adjacent upland plots. Thus, mixed cropping with rice and upland crops based on a crop rotation system in an irrigation block accelerates waterlogging and salt accumulation in upland plots. Based on these results, several remedial measures were recommended to overcome problems on secondary salinization as follows: (1) avoid mixed cropping with rice and upland crops, and unify either upland crops or rice in an irrigation block to control groundwater table; (2) decrease conveyance and field application losses through improved canal construction and management performance, introduction of canal lining, and improved land-leveling performance; (3) maintain and operate drainage canals

* *Corresponding author*. Tel.: +81 857 31 5394; fax: +81 857 31 5394.
E-mail address: ykita@muses.tottori-u.ac.jp (Y. Kitamura).
0378-3774/$ – see front matter
doi:10.1016/j.agwat.2006.03.007

to enhance function, particularly installation of subsurface tile drainage for enhancing subsurface drainage function and management of drainage outfall for minimizing environmental degradation caused by saline drainage water in the downstream area; (4) develop a design and management technique of evaporation pond for better effluent management and reuse of drainage water at the outfall of each irrigation block; (5) reduce the water supplied for rice and its use for other crops, or returning the saved water to the river for downstream users including returning to the environment; (6) conclude international water and/or drainage rights agreements among riparian countries and enactment of a basin-wide management regulation to control water withdrawal and drainage.

1. Introduction

The lower river basin of the Syr Darya, which rises in the Tien Shan Range, meanders mainly in lowland deserts that receive a low precipitation of 100–200 mm year^{-1} and finally flows into the Aral Sea. Water withdrawals for irrigated lands along the river have been conducted since the 1960s. Irrigated agriculture of rice-based cropping system in the Kzyl-Orda region of the Lower Syr Darya is important to both the national and regional economy. Since rice is a high water-consuming crop, water withdrawals have sharply increased with an increase in the area planted with rice. The sizable discharge of drainage from irrigated lands has also sharply increased the river water salinity level. Under these conditions, the salinity of the lower reaches of the Syr Darya has increased from 0.4–0.6 g L^{-1} to 1.3–2.0 g L^{-1} in the last three decades (Dmitriev, 1995).

Also, due to excessive and inefficient water use, secondary salinization (irrigation-induced salinization) of lands exists in irrigated areas in the region. The estimated average water distribution and delivery efficiency for the Lower Syr Darya basin is 0.64, and the estimated irrigation application efficiency is 0.60 (EC, 1995). Thus, the overall irrigation efficiency is extremely low (0.38); approximately 62% of the withdrawn water is estimated to be lost before it reaches the field and becomes available for use in crop production. These water losses raise the level of the groundwater table and cause waterlogging and land salinization. Salt accumulation in farmlands results in an increase in abandoned lands and environmental degradation in the region.

A large part of these problems is attributable to the poor water management of canals and fields under large-scale canal irrigation systems. Thus, proper water management is essential for preventing secondary salinization and sustainable agriculture in the region. In this study, based on the analysis on water and salt behavior in an irrigation block located in the Kzyl-Orda region of the Lower Syr Darya, we attempted to identify the causes of secondary salinization and suggest remedial measures to overcome the problems from the viewpoint of water management.

2. Materials and methods

2.1. Outline of study area

Shamenov kolkhoz (originally a collective farm during the ex-USSR era, was privatized after independence, and hereinafter called kolkhoz) located in the Kzyl-Orda state of Kazakhstan, which is a rice bowl in the Lower Syr Darya basin, was selected as the study area (Fig. 1). Although the kolkhoz has a gross area of 19,000 ha, only 1900 ha or 10% of the area was sporadically reclaimed for agricultural purposes. Land reclamation was conducted mainly in water-accessible areas with comparatively low and flat topography. The areas with poor water accessibility due to undulating topography were left as wastelands. Of the 1900 ha of reclaimed and later cultivated areas in the kolkhoz, an area of 600 ha has been abandoned due to severe salt accumulation. The phenomenon of salt accumulation showed a tendency to concentrate in small localized spots within irrigated blocks. When the soil salinity reached a certain level in some of the areas of limited crop production, they were abandoned. This situation is commonly observed in many kolkhozes in the state.

The study area has a continental climate. Average annual precipitation is 120 mm, which is partial to spring and fall. Average annual potential evapotranspiration is 2000 mm. Despite the high latitude (45°N), the summer is extremely hot with an average temperature of 27 °C and a maximum temperature in excess of 40 °C. Winter is extremely cold with an average temperature of −5 °C and a minimum temperature below −25 °C. For the normal growth of rice, the cropping season must be set from late April to early September. Since there is no effective rainfall during the rice cropping season, irrigation is a prerequisite for growing rice.

For the study on water and salt balance, Yeltai block (Fig. 2) was selected as the study area. Irrigation water for the block is transported through the Yeltai Canal, which is diverted from the main canal (Communism Canal) in the kolkhoz. The Yeltai Canal separates into two branch canals—the Northern Branch Canal for the Northern Sub-block and Southern Branch Canal for the Southern Sub-block. Surface and subsurface drainage water from farmlands is collected by the main drain (Yeltai drain) and drained off to the tributary of the Syr Darya river. Out of the block area of 827 ha, an area of 716 ha was cultivated. The remaining 111 ha, including roads, canals, and drains, was not allotted for cultivation either because it was designated inappropriate for the purpose at the time of development (101 ha) or because it was abandoned later (10 ha). This block is characterized as well-consolidated, i.e., irrigation canal and drainage systems are set independently, and every individual plot has access to a field canal and a field drain,

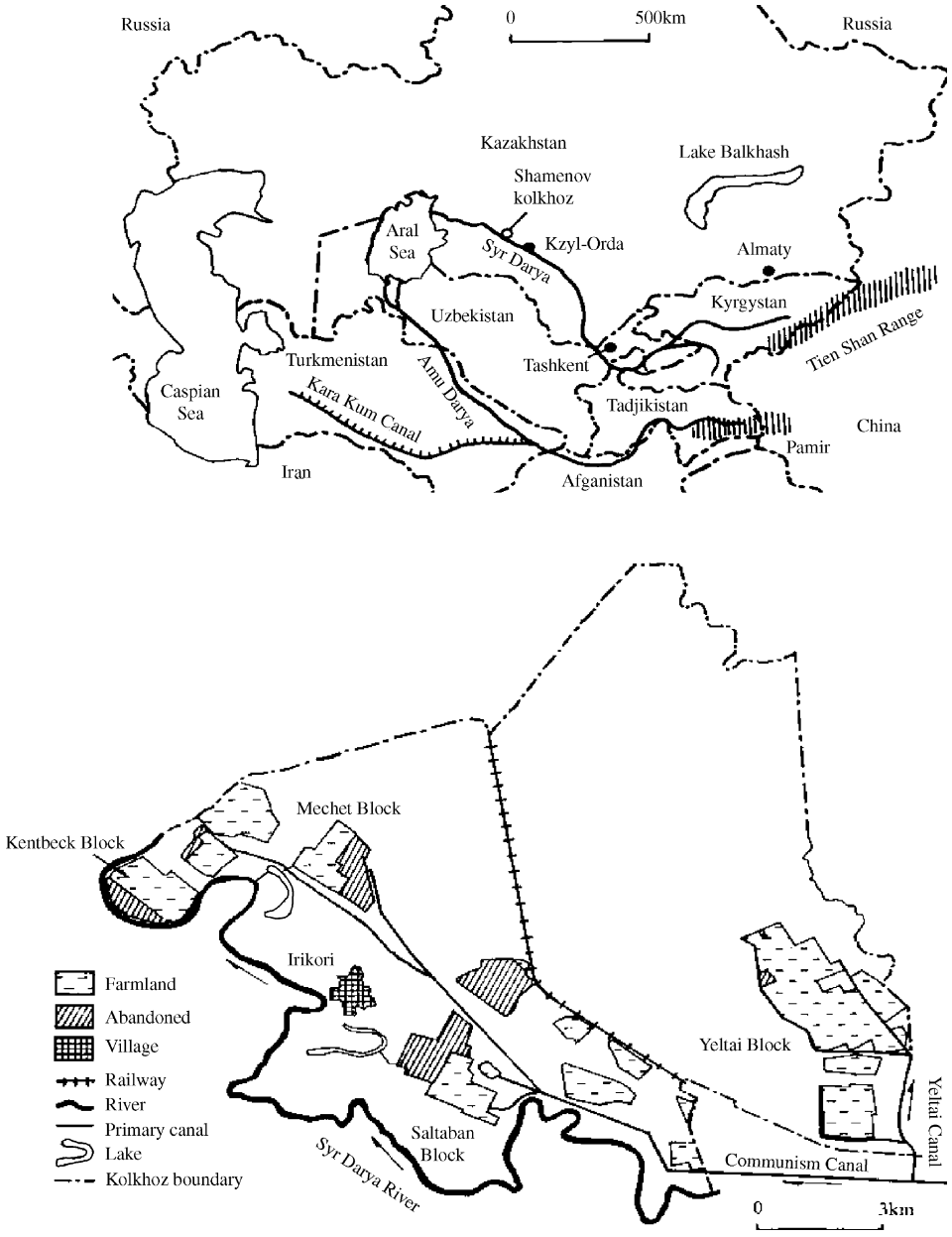

Fig. 1 – Location and plan of the studied kolkhoz in the Lower Syr Darya basin.

through its inlet and outlet, respectively. The size of these plots varied from 1.5 to 3.5 ha with approximately 2.5 ha on average. The spacing of field canals is approximately 400 m. Field drains run in between field canals at intervals of approximately 400 m. The soil texture of the drain-bed was classified as clay.

Based on the soil analysis performed in a rice plot of the Yeltai block in the 1997 crop season, the soil texture of the plot was classified as clay loam at depths of less than 70 cm, loam at depths from 70 to 140 cm, and again clay loam from 140 to 200 cm (Hillel, 1998). The soil of the plot was classified as saline soil, because the electric conductivity (EC) of the saturated soil extract (ECe) was approximately 10 dS m^{-1}, and the pH was between 7 and 8. The groundwater depth was approximately 250 cm in the plot during the non-irrigation period.

2.1.1. *Water quality in the study area*

Characteristics of water quality for surface water and groundwater in the Lower Syr Darya basin in and around the Shamenov kolkhoz are summarized in Table 1 (Kitamura et al., 2000b). EC was measured using an EC meter; pH was measured using a pH meter, cations and anions were measured by atomic absorption spectrophotometry and ion chromatography, respectively.

2.1.1.1. Surface water. Judging from the EC and total dissolved solids (TDS), the irrigation water appeared suitable for direct

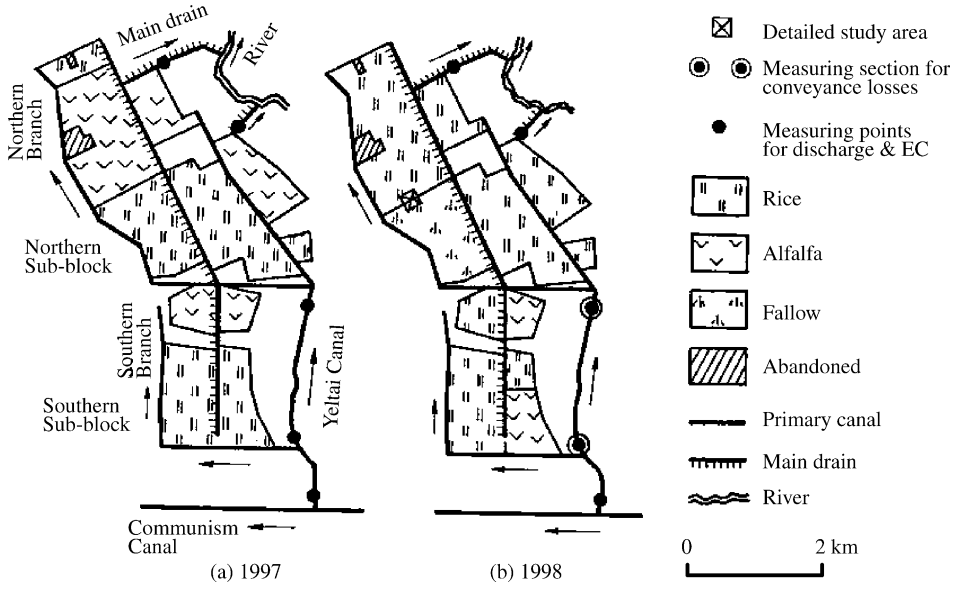

Fig. 2 – Cropping pattern in Yeltai irrigation block.

use. Only magnesium (Mg^{2+}) and the ratio of Mg^{2+} to calcium (Ca^{2+}), i.e., Mg^{2+}/Ca^{2+}, exceeded the usual range for irrigation water. Therefore, the water has a tendency to affect crop growth mainly by reducing calcium uptake and causing calcium deficiency (Gupta, 1990). Drainage water falls in the range designated for severe restriction for irrigation purposes (Ayers and Westcot, 1985). In fact, considerable drainage water is finally drained off to the river, and it causes adverse effects on water quality in the lower reaches, including the Aral Sea. However, a series of recent researches (Maas and Grattan, 1999; Kaffka, 2001; Kaffka et al., 2002; Oster and Grattan, 2002) suggests the possibility of effective reuse of saline drainage water for salt-tolerant crops and reducing salt loads in return flows (Oster and Wichelns, 2003).

Based on the water quality data for surface water in and around the kolkhoz, distinct linear relationships with and without a constant term were obtained between EC (dS m^{-1}) and TDS (mg L^{-1}) as follows:

$$\mathrm{TDS} = 753.5\mathrm{EC} \quad (r^2 = 0.981) \tag{1a}$$

$$\mathrm{TDS} = 816.0\mathrm{EC} - 169.97 \quad (r^2 = 0.987), \tag{1b}$$

where r^2 is the square of correlation coefficient.

2.1.1.2. Groundwater. As compared with the surface water, the quality of groundwater was more saline. Groundwater in abandoned farmlands was extremely unusable. As indicated

Table 1 – Characteristics of water quality related to salinity in the Lower Syr Darya basin (Kitamura et al., 2000b)

Parameter (units)	Water quality in and around Shamenov kolkhoz				Usual range for irrigation (FAO[a])
	Surface water			Groundwater	
	River and irrigation canal water	Ponded water in rice fields	Drainage water	Cultivated and abandoned fields	
EC (dS m^{-1})	1.31–2.88	1.84–3.06	2.63–4.40	4.13–73.00	0–3
TDS (mg L^{-1})	955–2151	1384–2337	2053–4143	2765–86360	0–2000
Ca^{2+} (meq L^{-1})	4.6–9.3	6.2–9.1	8.4–19.2	20.3–29.1	0–20
Mg^{2+} (meq L^{-1})	5.6–11.3	7.3–12.7	11.6–18.3	20.8–437.0	0–5
Na^{+} (meq L^{-1})	5.9–17.0	7.7–15.1	13.1–20.9	17.3–982.6	0–40
CO_3^{2-} (meq L^{-1})	–	–	–	–	0–0.1
HCO_3^{-} (meq L^{-1})	–	–	–	–	0–10
Cl^{-} (meq L^{-1})	4.5–12.2	6.0–13.1	12.6–25.1	26.0–795.9	0–30
SO_4^{2-} (meq L^{-1})	11.2–22.4	14.0–24.9	23.7–43.7	13.6–633.5	0–20
K^{+} (meq L^{-1})	0.1–0.3	0.2–0.3	0.2–0.5	0.6–3.2	0–2
pH	7.6–8.14	7.75–7.94	7.62–8.10	7.42–8.14	6.0–8.5
SAR	2.46–6.08	2.70–5.36	4.13–5.04	3.68–129.36	0–15
Mg^{2+}/Ca^{2+}	1.05–1.44	1.10–1.72	0.95–1.63	0.90–15.90	0–1

[a] Ayers and Westcot (1985).

in Table 1, the groundwater in this area is almost within the range designated for severe restriction, and thus, it cannot potentially be used for irrigation purposes without creating significant problems. Recent achievements, however, clearly indicate that saline-sodic waters ($4 < EC\ [dS\ m^{-1}] < 20$ or 30; $10 < SAR < 40$) can be used to irrigate appropriately tolerant crops to salinity provided that the root zone salinity is controlled and adequate soil permeability to both water and air can be maintained (Kaffka et al., 2002; Oster and Grattan, 2002).

2.1.2. *Cropping schedule*

In the Kzyl-Orda region, an eight-year crop rotation system has been popularly practiced for some decades (Konokhova, 1985). The rice-based eight-year rotation system has been practiced in the study area (Yeltai block). Under this system, two cropping methods are applicable: one is practiced by introducing only one scheduled cropping pattern in a whole block every year (mono cropping), and the other is practiced by intentionally introducing eight patterns (mixed cropping). In the Yeltai block, the latter method was practiced, i.e., the block is divided into eight rotation blocks and a scheduled cropping pattern is allotted in each rotation block. The order and frequency of crops is: first and second years, rice; third year, cultivated fallow; fourth and fifth years, rice; sixth year, wheat cover cropped with alfalfa; and seventh and eighth years, alfalfa. Under this rotation program, approximately half the irrigated area is allotted for rice cropping and the remainder is maintained under upland conditions for fodder crops or fallow. In most rice producing areas in Kazakhstan, this cropping pattern has been the basis for the design and construction of new rice land development.

2.2. *Water balance in the study block*

In order to clarify the water balance in the Yeltai block, measurement of flow discharge was conducted using a current meter (Model CM-1BN, produced by Toho Dentan Co., Ltd., Japan) both at the head of the Yeltai Canal and the ends of the main drain in two irrigation seasons (Fig. 2).

The water balance in an irrigated area for a certain period is expressed by the following equation:

$$\begin{aligned}\Delta &= W_r + W_i - W_c + W_{g_1} - W_{g_2} - W_d - W_{et} \\ &= W_r + W_i - W_c - W_p - W_d - W_{et},\end{aligned} \quad (2)$$

where Δ is the changes in total existing water in the area, W amount of water (in terms of depth of water spread uniformly over the soil surface), and W_p is the amount of water outflow from the area by percolated water originating from irrigation water, i.e., deep percolation ($W_p = W_{g_2} - W_{g_1}$). Subscript r represents the rain water, i irrigation water, c canal loss, d surface drainage water, g_1 groundwater inflow, g_2 groundwater outflow, p percolated water, and et is the evapotranspiration (ET).

Since there is no effective rainfall during the irrigation season in the study area, W_r in a normal year can be disregarded.

When considering the entire cropping season, Δ can be regarded as zero and Eq. (2) can be simplified as follows:

$$W_i - W_d = W_c + W_{et} + W_p. \quad (3)$$

Thus, by measuring W_i at the head of the Yeltai Canal and W_d at the end of the main drain and a drain outfall, $W_c + W_{et} + W_p$ is calculated and is regarded as the total amount of water consumed in the area.

2.3. *Salt balance in the study block*

The salt balance in an irrigated area for a certain period is expressed by the following equation:

$$\Delta S_a = W_r S_r + W_i S_i + W_{g_1} S_{g_1} - W_d S_d - W_{g_2} S_{g_2} - P_s, \quad (4)$$

where ΔS_a is the changes in salt amount in the area, W amount of water (in terms of depth of water spread uniformly over the soil surface), S salt concentration, P_s amount of salt removed by harvesting plant, and $W_p S_p$ is the amount of salt outflow from the area by percolated water originating from irrigation water

$$W_p S_p = W_{g_2} S_{g_2} - W_{g_1} S_{g_1},$$

by regarding W_r and P_s as zero, ΔS_a can be simplified as follows:

$$\Delta S_a = W_i S_i - W_d S_d - W_p S_p. \quad (5)$$

Thus, using observed W_i, S_i, W_d, and S_d, the sum of ΔS_a and $W_p S_p$ can be calculated as $\Delta S_a + W_p S_p = W_i S_i - W_d S_d$, which is the change in the amount of salt in the area, including changes in groundwater salt in and around the area caused by irrigation and drainage practice. Using the relationship between TDS and EC for surface water, i.e., Eq. (1a) or (1b), S_i and S_d can be estimated from the observed EC values by using an EC meter (Model CM-21P, supplied by DKK-TOA Corporation, Japan) at the head of the Yeltai Canal and ends of the main drain, respectively (Kitamura et al., 2000b).

2.4. *Conveyance losses in a distribution canal*

For the measurement of conveyance losses from the existing canal, a 2-km section with no surface lateral inflow and outflow was selected in the Northern Branch Canal of the block (Fig. 2). The study was performed using an inflow–outflow method, which is based on the direct measurement of discharge by using the current meter alternately at the upstream and downstream ends of the section when canal flow was in a steady state (Kraatz, 1977). Prior to and after the discharge measurement, the height of the water at both the ends was repeatedly checked by reading the graduated gauges installed to identify the flow condition of the canal section. The following equation (Kitamura, 1990) was applied for calculating conveyance losses per unit length:

$$L_n = \left\{1.0 - \left(\frac{Q_{out}}{Q_{in}}\right)^{1/L}\right\} \times 100, \quad (6)$$

where L_n represents conveyance loss rate (% km^{-1}), Q_{in} inflow into the canal section ($m^3\ s^{-1}$), Q_{out} outflow from the canal section ($m^3\ s^{-1}$), and L represents length of the canal section (km).

2.5. *Land leveling and water management in rice plots*

In order to assess the land leveling performance for rice cultivation, a grid survey of leveling was performed in two plots prior to the commencement of irrigation. These plots, with respective areas of 2.4 and 1.8 ha enclosed by solid levees (with a sufficiently high freeboard that could hold water up to a depth of 30 cm), are typical of the block. Ponding depth was manually monitored with a graduated gauge installed during the irrigation period in order to obtain a correlation with land leveling performance.

2.6. *Impact of crop rotation system and drainage system on water and salt behavior in an irrigation block*

The aim was to determine the impact of a rotation that combined rice and upland crop farming on water and salt behavior in and around an irrigation block. During 1998, we measured the groundwater table, hydraulic head of soil water under submerged condition, and EC in a selected detailed-study area that consisted of a rice plot (2.4 ha, 136 m × 177 m) and its adjacent fallow plot (2.1 ha, 119 m × 177 m) along with a field drain between them (Fig. 3). Based on the crop rotation system, alfalfa was grown on the rice plot and rice was grown on the fallow plot during the previous year.

Water was released from the main canal to the Yeltai canal starting on May 3, 1998, and irrigation of the rice plot started on May 9, 1998. Subsequently, the occasional interruption and resumption of water application was repeated three times during the first 51 days. The plot was then continuously irrigated during the last 53 days. On August 16, the amount of water application was reduced, because the rice was beginning to ripen. Water application was stopped on August 20. On August 23, the only surface water present in the rice plot was located in depressions. Rice was harvested with a combine harvester on September 13.

Hydraulic head was measured at the ponded water surface and at depths of 0.6, 1.15, 1.8, and 3.0 m in the rice plot. EC of ponded water and soil water was also measured at each point and depth in the rice plot. The water table and EC in the field drain and the adjacent fallow plot were also recorded. Measurement of the groundwater table was performed through 50-mm diameter PVC pipe installed in the fallow plot. The bottom 1-m section of the pipe was perforated. The perforated portion was covered with a non-cotton cloth and enveloped in a gravel filter. The bottom of the pipe was set at depth of 1.95 m below soil surface in the fallow plot. Measurement of the hydraulic head and soil water EC was performed through piezometers installed at depths of 0.6, 1.15, 1.8, and 3.0 m. A piezometer was installed using a non-perforated pipe at each depth. The holes were bored manually by 100-mm auger to respective depths, and 50-mm diameter PVC pipes were inserted. Sand was placed around the bottom ends, and clayey soil was tamped in above the sand filters. The spaces surrounding the pipes were then filled with clayey soil, tamped down firmly with a metal rod, and sealed at the soil surface with clayey soil. The EC meter was equipped with a probe that was either lowered into each piezometer or it was used to test water samples pumped from each piezometer. A staff gauge was installed in the field drain for measuring the water level.

3. Results and discussion

3.1. *Causes of secondary salinization related to water management*

Based on the on-site studies in the study area, causes of secondary salinization were linked to the soil and water management and have been summarized as follows:

3.1.1. Seepage and operational losses from the canal system

3.1.1.1. Heavy seepage losses from the canal system. Based on the field measurement of inflow and outflow in a 2-km section in the Northern Branch Canal of the Yeltai block (Fig. 2), the

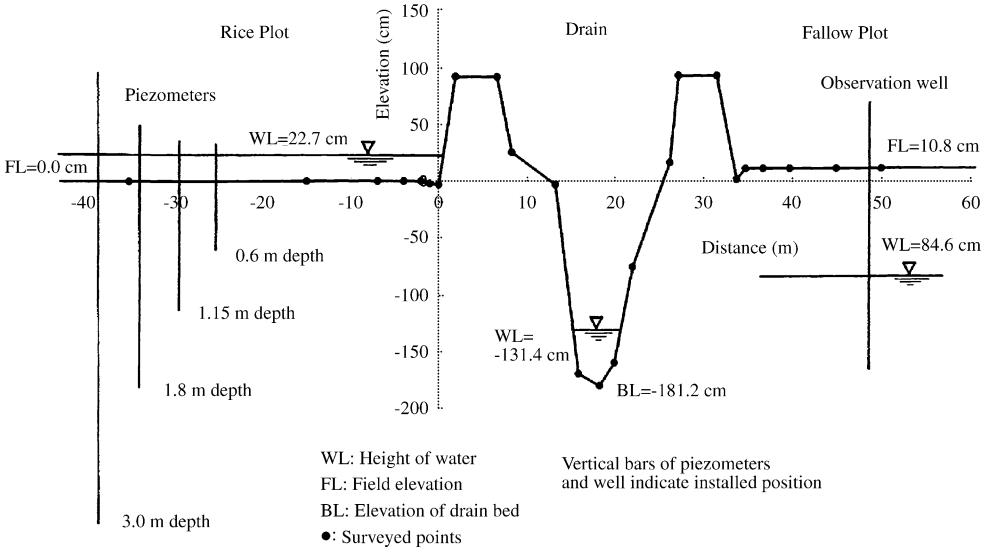

Fig. 3 – Cross-section of the detailed study area and the position of piezometers and an observation well with hydraulic profile as on July 24, 1998 (Kitamura et al., 2000b).

Table 2 – Components of water consumption for rice in the study block

Year	Rice plots irrigated (ha)	Period of water balance (days)	Withdrawal at canal head (1) (mm (m^3 s^{-1}))	Canal losses (2) = (1) × 0.277 (mm)	Field intake (3) = (1) − (2) (mm (mm d^{-1}))	Field consumption (4) (mm (mm d^{-1}))	Drained (5) (mm (mm d^{-1}))
1997	384	128	6136 (2.32)	1700	4436 (34.7)	1259 (9.8)	3177 (24.8)
1998	537	123	3990 (2.23)	1105	2885 (23.5)	1123 (9.1)	1762 (14.3)

Note: (4) = (3) − (5).

equation $Q_{out} = 0.8875Q_{in}$ ($r^2 = 0.7739$) was obtained. Substituting $Q_{out}/Q_{in} = 0.8875$ and $L = 2$ in Eq. (6), the conveyance losses in a distribution canal (L_n) were estimated to be approximately 5.8% km^{-1} (Kitamura et al., 2000a). Such heavy conveyance losses from earth-made canals cause waterlogging and salt accumulation in the adjacent area.

3.1.1.2. Heavy operational losses due to insufficient function and poor management of canal system. The result of the water balance study carried out in the Yeltai block (716 ha) is summarized in Table 2 (Kitamura et al., 2000a). In Table 2, the total losses of the distribution system, i.e., the conveyance losses from the head of the Yeltai Canal to the turnouts of the field canals (length: 17.6 km), were estimated at 27.7% based on the observed conveyance losses of 5.8% km^{-1}. During the irrigation season each year, the observed water profile in the irrigation canal of the Yeltai block was almost the upper critical level whenever water was distributed to the rice plots. Therefore, it is most probable that the amount supplied at the head of the canal was equal to the conveyance capacity regardless of crop water requirement in the command area as shown in Table 2. This is due to several reasons: (1) to secure a hydraulic head required for gravity irrigation under inefficient function and poor management of the canal system in the extremely flat topography; (2) to maintain deep water in rice plots; (3) to supplement canal losses; (4) insufficient efforts by farmers for saving water attributed to extremely low water charge, i.e., approximately US$ 0.704 per 1000 m^3 (Kitamura et al., 2000a). Thus, the smaller the rice-cropped area in the block, the larger the water delivered to the block (in mm) per unit area of rice-cropped. The total water discharged at the canal head was 3990 mm in 1998, whereas it was estimated to be as high as 6136 mm in 1997. Generally, due to the abovementioned causes, the water delivered to rice plots is exceedingly high.

This situation exacerbated unnecessary water supply and unexpected water behavior causing waterlogging and salt accumulation in and around the area.

3.1.2. *Insufficiency of drainage system*

Field drains failed not only to sever the hydraulic continuity between rice plots and upland plots, such as fallow and alfalfa plots, but are not effective in removing salts from rice plots to drains due to a lack of subsurface drainage. Because of the seepage flow beneath the field drain from the rice plot, the rise in the groundwater table and salt accumulation are accelerated in the adjacent fallow plot (Kitamura et al., 2000b).

This is suggested based on the observed fluctuations of hydraulic conditions among the rice plot, fallow plot, and field drain as shown in Fig. 3. Depending on the fluctuations of hydraulic conditions, the groundwater level in a fallow plot always maintained a higher head than the water level of the field drain and showed a sensitive reaction to the ponding water level and hydraulic head in the shallow soil layer in the rice plot (Figs. 3 and 4). In Fig. 4, the groundwater table data at the observation well was available only after May 16, 1998, because of the limited depth of the well (1.95 m in depth), namely the groundwater table at the observation well was deeper than 1.95 m below the soil surface before May 16, 1998. The significant drops of hydraulic head of soil in the rice plot and water table of the fallow plot after August 16, 1998 were due to the termination of water deliveries to the rice plot in preparation for harvesting. Based on the much deeper groundwater tables (more than 2.0 m below soil surface) observed at several points nearer to the irrigation canals in the fallow plot during the irrigation period, we deny the possibility of the existence of hydraulic linkage between the observation well and irrigation canals. We infer that seepage water from the rice plot flows through the permeable soil strata that is hydraulically linked to the fallow plot underneath the field drain bed, which raises the groundwater table, and leads to salt accumulation in the fallow plot. The limited subsurface water flow from the paddy plot to the field drain is probably due to a combination of low hydraulic gradients along the water flow path from the field to the drain, made lower because of the thick sediment located along the bottom of the drain, and to the well–compacted soil of banks used as farm roads for vehicles and heavy machinery which reduces the saturated hydraulic conductivity of the soil along the lower portions of the drain banks. Consequently, rice cultivation does not result in adequate salt removal by leaching.

3.1.3. *Imbalance of water and salts in an irrigation block*

3.1.3.1. Imbalance between inflow of salts into irrigated area and outflow of salts from the area. Based on our salt balance study carried out in the Yeltai block, a considerable amount of

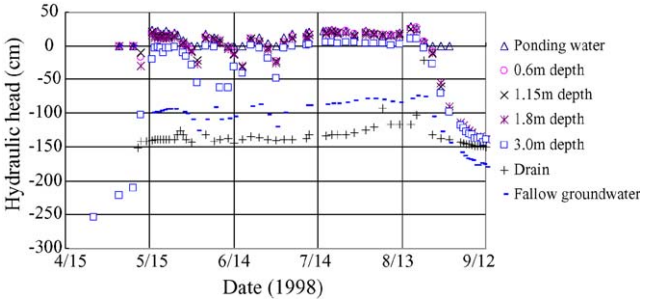

Fig. 4 – Change in hydraulic head in a rice plot and its adjacent fallow plot (Kitamura et al., 2000b).

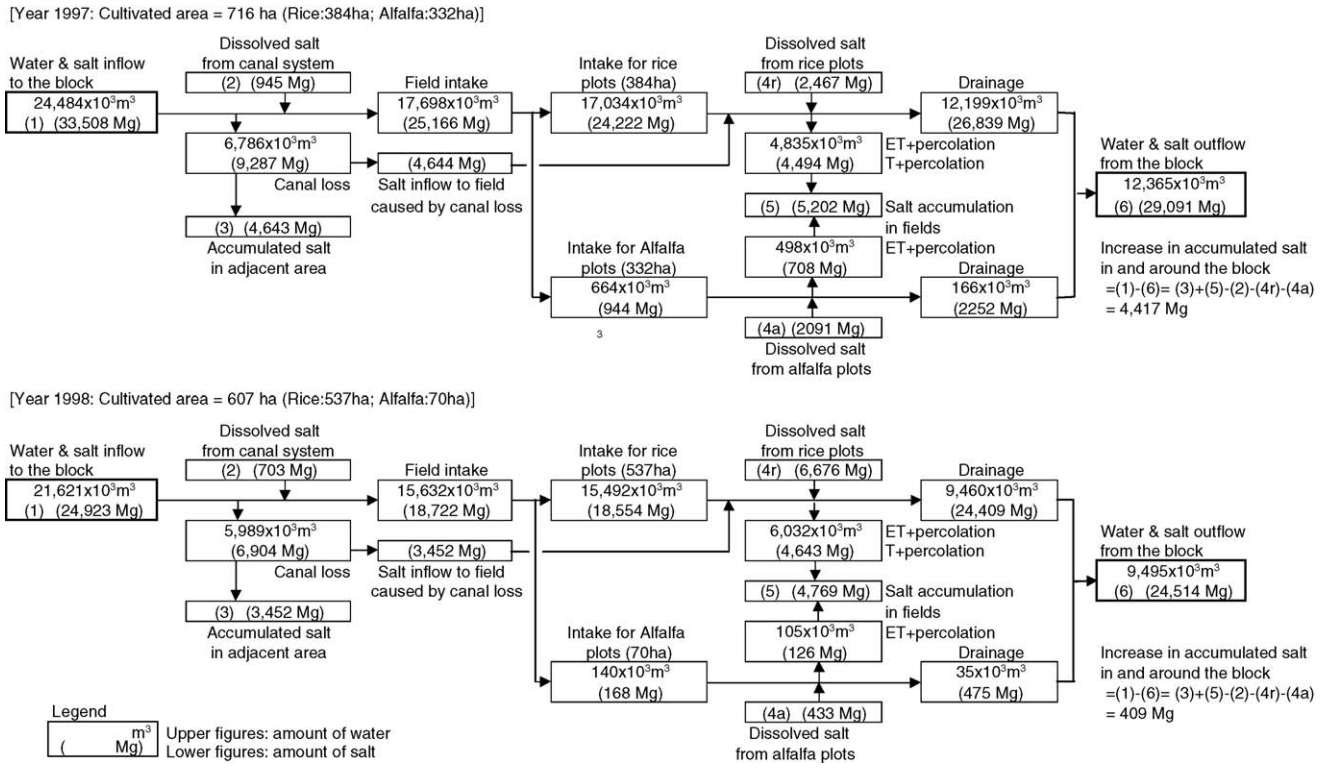

Fig. 5 – Water and salt balance diagram in the study block.

dissolved salts remained in and around the block (Kitamura et al., 2000b). This situation brings about a steady increase in accumulated salts in and around the block every irrigation season. The result of water and salt balance in the Yeltai block is roughly summarized in Fig. 5. Only salt inflow and outflow was obtained by direct measurements, and the other elements of salt movement were calculated based on the respective elements of water movements, taking into account their respective EC values. As almost all the branch canals run along the periphery of the block, we assumed that the amount of salt transports attributable to canal seepage can be divided into two equal halves, i.e., one half of the amount was moved and deposited in an area outside the boundary of the block, and the other half was deposited into fields along the canal. We estimated the amount of dissolved salt from the canal based on the average increase rate of EC along the canal as described later. Percolation and transpiration were considered to be the only contributors to the salt accumulation in and around rice plots; evaporation from the water surface was not regarded as a contributor. To calculate the amount of salt accumulated in the root zone due to water uptake by rice plants, we used the roughly estimated value of 460 mm for transpiration during the growing season (Rockström, 2003). The amount of water drained from alfalfa plots was estimated based on the assumption that about 25% of the applied water seeps in field drains after each irrigation event. The salinity of the drainage water from alfalfa plots was regarded to be of the same level as that of the soil water of shallow layer (at a depth of 0.6 m) observed at the beginning of the irrigation season (approximately 18.00 dS m^{-1}, as shown in Fig. 6). The salt outflow from alfalfa plots was estimated by multiplying the assumed amount of drainage water from the plots with the assumed salinity content of the drainage water. The EC values of respective elements of water movements are applied as shown in Table 3. Based on the values of the respective elements of salt and water movements estimated, we calculated salt accumulation in alfalfa plots, salt outflow from rice plots, and finally obtained the amount of dissolved salt from rice plots that is required for maintaining a salt balance in rice plots. The salt balance was also simplified as shown in Table 4. The increase in accumulated salt in and around the block during each irrigation season, i.e., ($\Delta S_a + W_p S_p$) in Eq. (5) that is equal to column (7) of Table 4 or (1) – (6) = (3) + (5) – (2) – (4) in Fig. 5 (salt-inflow to the block–salt-outflow from the block), was 4417 Mg (6.2 Mg ha^{-1},

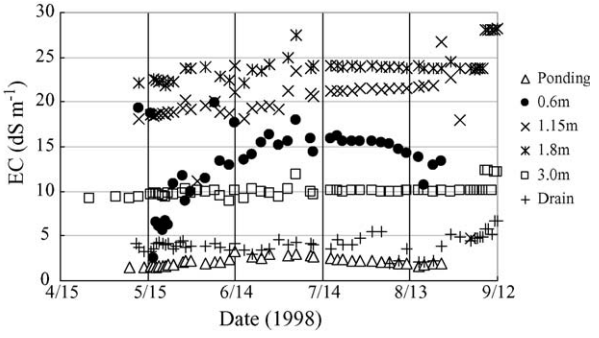

Fig. 6 – Change in EC of groundwater in rice plot (Kitamura et al., 2000b).

Table 3 – Applied EC values of respective elements of water movements

Elements of water movement	Applied EC values (dS m^{-1})		Remarks
	1997	1998	
Inflow to the block	1.82	1.53	Average of observed EC at the head of the Yeltai Canal
Canal loss	1.82	1.53	Average of observed EC at the head of the Yeltai Canal
Field intake	1.89	1.59	Calculated EC (EC_x) using $EC_x = EC_U(1 + 0.0046x)$
Intake for rice plots	1.89	1.59	Calculated EC (EC_x) using $EC_x = EC_U(1 + 0.0046x)$
Intake for alfalfa plots	1.89	1.59	Calculated EC (EC_x) using $EC_x = EC_U(1 + 0.0046x)$
Accumulated salt in rice plots	1.89	1.59	Calculated EC (EC_x) using $EC_x = EC_U(1 + 0.0046x)$
Accumulated salt in alfalfa plots	1.89	1.59	Calculated EC (EC_x) using $EC_x = EC_U(1 + 0.0046x)$
Drainage water from the block	3.12	3.43	Average of observed EC at the end of the main drain
Drainage water from alfalfa plots	18.00	18.00	Applied the EC value of the soil water of shallow layer observed at the beginning of the irrigation season

Table 4 – Salt balance in the study block (716 ha)

Year	Salt inflow to the block (1) (Mg)	Dissolved salt from canal (2) (Mg)	Accumulated salt in adjacent area (3) (Mg)	Dissolved salt from fields (4) (Mg)	Accumulated salt in fields (5) (Mg)	Drained salt from the block (6) (Mg)	Increase in accumulated salt in the block (7) (Mg)
1997	33508	945	4643	4483	5202	29091	4417
1998	24923	703	3452	7109	4769	24514	409

Note: (7) = (1) − (6) = (3) + (5) − (2) − (4).

48.2 kg ha^{-1} d^{-1}) in 1997 and 409 Mg (0.6 Mg ha^{-1}, 4.6 kg ha^{-1} d^{-1}) in 1998, respectively. The reasons for the large difference in the salt accumulation rate between two seasons are: (1) the water quality of the source was slightly better in 1998 than that in 1997 (Fig. 7), (2) less irrigation water was applied in 1998 than in 1997 (Table 2), and (3) higher salinity of drainage water, i.e., a higher amount of dissolved salt from the block, was observed in 1998 than that in 1997 (Fig. 7). The first two reasons are of minor significance, whereas the third reason is the main contributing factor. The third reason was due to the significant increase in the area of farmlands converted from upland condition to submerged condition in 1998 as compared with that in 1997. Due to the annual crop rotation in the study block, the area of farmlands under rice cultivation that was newly converted from those under upland condition in the previous year was 297 ha in 1998, whereas in 1997, only 31 ha were converted from upland condition.

3.1.3.2. *Over irrigation of rice-planted plots*. A large amount of water is irrigated to rice-planted plots during the irrigation season. In the Yeltai block, the water delivered to field canals for rice plots was 4436 mm in 1997 and 2885 mm in 1998 as shown in Table 2 (Kitamura et al., 2000a). These excessive amounts result from several reasons, including the prevention of an increase in salinity of ponded water in rice plots. This situation brings about waterlogging and salt accumulation in the adjacent upland areas.

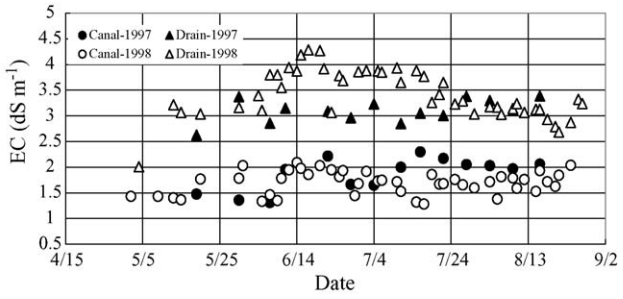

Fig. 7 – Variation in EC value of canal water (Yeltai block).

Field consumption, i.e., (4) = (3)−(5) in Table 2, is the sum of ET and deep percolation in rice plots. Thus, the daily field consumption is estimated to be approximately 9.5 (9.1–9.8) mm d^{-1}. ET in rice plots was not observed throughout the season, however, assuming that ET is approximately 6–7 mm d^{-1}, the downward percolation flow is obtained at around 2.5–3.5 mm d^{-1}.

The amount of drained water from the block widely differed each year. The difference in the amounts of water intake by rice plots between two different years is almost equivalent to the drained amount. In other words, the remainder after subtracting the amount of water used in a rice plot (9.5 mm d^{-1}) from the amount of water supplied through an inlet to each plot consists of surface and subsurface drainage. Based on the on-site situation, it can be understood that surface drainage occupies an overwhelmingly large portion of the total drained amount. This is the major reason behind the drainage water salinity being far lower than the soil water salinity in the adjacent rice plot (Fig. 6).

3.1.3.3. *Introduction of saline river water with TDS more than 1000 mg L^{-1} for irrigation*. The salinity of river water varies from 1.31 to 2.88 dS m^{-1} (average 1.78 dS m^{-1}) in EC and from 955 to 2151 mg L^{-1} (average: 1285 mg L^{-1}) in TDS during irrigation periods as shown in Table 1 (Kitamura et al., 2000b). The application of saline water to irrigation aggravates salt accumulation in and around the irrigated area.

3.1.3.4. *Dissolution of accumulated salts from canal systems*. The salts accumulated along canal systems dissolve in irrigation water resulting in an increase in salinity. Based on the observation of the canal water salinity (EC) in the Aitek Canal, which is the headrace canal used to convey river water to the kolkhoz, the relationship between EC at the head (EC_U) and that at the end located 50 km downstream of the head (EC_D) can be expressed as $EC_D = 1.23EC_U$ ($r^2 = 0.675$). Thus, the EC of canal water increases 1.23 times while it flows a distance of 50 km, or the relationship can be expressed as $EC_x = EC_U(1 + 0.0046x)$, where EC_x is the EC at a point located x km downstream of the head. As mentioned above, this relationship was applied to obtain a rough estimate of the amount of dissolved salt from canal system as shown in Fig. 5. Thus, the dissolution of accumulated salts from canal systems is also one of the causes for secondary salinization in irrigated areas.

3.1.4. *Causes attributed to water and land management in an irrigation block*

3.1.4.1. *Compounded factors to increase soil salinity in the shallow soil layers in rice plots*. The observed results of the EC of soil water and hydraulic head in the rice plot are shown in Figs. 6 and 4, respectively. Fig. 8 shows the change in hydraulic gradient at each layer between the observed depths. Figs. 4 and 8 suggest that water moved from the soil surface to the deeper layers under submerged condition. However, water moved upward in some layers, particularly the 0.6–1.15 m layer, under the non-submerged condition before irrigation was restarted after an interruption. The high EC value of soil water at 1.80 m is attributed to the existence of a heavily salt-accumulated layer at a depth of approximately 1.80 m (Fig. 6). The salinity of soil water at a depth of 3 m was a constant value of 9–10 dS m^{-1} without any significant variation throughout the period. This suggests that the soil layer at a depth of approximately 3 m was in a primary groundwater flow pathway throughout a year.

In the experimental rice plot in the Yeltai block, soil water salinity at a depth of 0.6 m in the rice plot displayed a very interesting variation throughout the irrigated period as shown in Fig. 6. At the beginning of the irrigation period, the soil water salinity at 0.6 m had high EC (approximately 18 dS m^{-1}), which then decreased sharply to the same level as that of the ponded water (approximately 2.5 dS m^{-1}). However, the EC increased gradually and leveled off after it reached a certain salinity level (15–16 dS m^{-1}). The behavior of soil water salinity at shallow depths can be explained as follows.

The initial high EC resulted from the upward flow of saline water from the lower layer of 0.6–1.15 m due to large negative hydraulic gradients (-13.8×10^{-2}) at the beginning of the irrigation season (Fig. 8). The next sudden decrease in soil water salinity in the shallow layer is due to leaching effects of downward infiltration during the initial stage. The subsequent gradual increase in soil water salinity in the shallow layer is more likely a consequence of mixing of the downward flowing water with the saline water that remains in the finer soil pores combined with the concentrating effects of crop water uptake and occasional upward flow from the lower layer of 0.6–1.15 m due to negative hydraulic gradients (Fig. 8). The mixing process is accelerated by the occurrence of large negative hydraulic gradients by the fluctuation of the water table due to the occasional interruption and resumption of irrigation water supply during the season. The incidence of high EC values in the shallow layer rises with the occurrence of large negative hydraulic gradients as shown in Fig. 8.

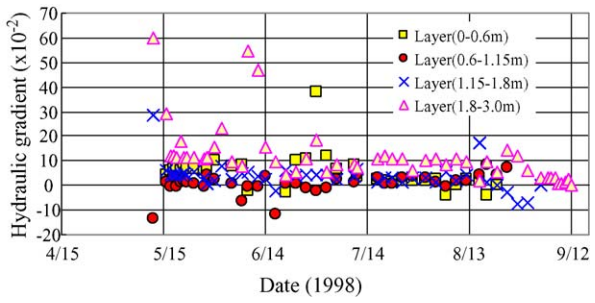

Fig. 8 – Change in hydraulic gradient at each soil layer.

Salt-accumulated spots were often seen in rice plots after ponded water had been drained off for harvesting. Such spots are often formed above permeable layers. In those spots, the magnitude of occasional upward water flow is much stronger than that in the other area. This accelerates the convection of salt from deeper layers, and thus, the soil water salinity remains high in shallow layers. The spots above permeable layers obstruct the normal growth of rice and cause a marked decrease in yield because of the high content of dissolved salts in shallow layers.

3.1.4.2. *Application of an eight-year crop rotation system in an irrigation block*. The operation of a crop rotation system involves mixed cropping with rice and upland crops within an irrigation block and promotes seepage flow along with salt transport from rice plots to adjacent upland plots (Kitamura et al., 2000b). As mentioned in Section 3.1.2, there is a possibility that this system has induced waterlogging and salt accumulation in upland areas adjacent to rice plots in and around the irrigation block. In this kolkhoz, some blocks in which this system had been practiced for several decades consist of abandoned farmlands in almost half the original gross area due to salt accumulation. Even in the newly developed blocks having limited abandoned farmlands, it is anticipated that the salt accumulation will be accelerated, and concurrently, abandoned farmlands will increase if the eight-year rotation system continues to be practiced.

3.1.4.3. *Poor land leveling and careless field water management*. It was revealed that the performance of land leveling was extremely low in rice plots. For example, the undulation varied from −15.4 to +14.9 cm with a standard deviation (S.D.) of 6.5 cm in a 2.4 ha plot and from −17.9 to +16.6 cm with a S.D. of 6.85 cm in another 1.8 ha plot (Kitamura et al., 2000a). Under such field conditions, it is very likely that a high ponding depth is maintained so as to ensure that the highest portion in each plot remains wet. This deep-water management accelerates waterlogging and salt accumulation in the adjacent upland areas.

Fig. 9 shows the pattern of ponding depth in a 2.4 ha plot during the irrigation period. As shown in Fig. 9, the plot was supplied with water until the highest portion was saturated, and subsequently, water intake was discontinued to allow the complete absorption of the irrigated water by the soil. This intermittent process was repeated three times during the first

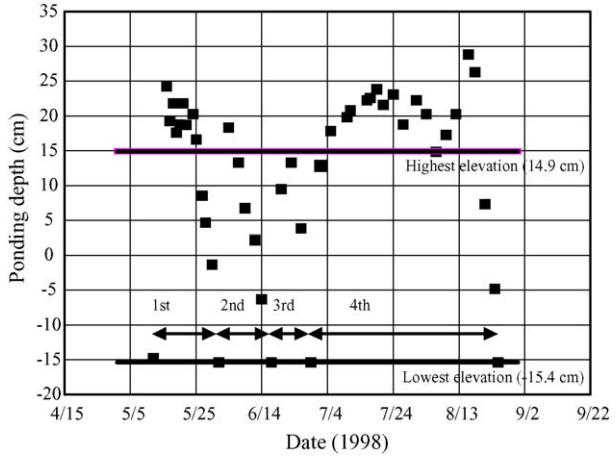

Fig. 9 – Change in ponding depth in a rice plot (Yeltai block).

two months. The plot was then continuously irrigated during the latter two months.

The first irrigation was performed after sowing in saturated soil and maintaining a ponding depth at approximately 20 cm for 10 days. This is required to meet the greatest water demand rate among several irrigation events. Based on the analysis of the volumetric composition of vapor phases in the soil layers above the groundwater table conducted immediately before the first irrigation, the water requirement for saturating soil was estimated to be approximately 100 mm. When ponded water was absorbed into the soil, the seed started to germinate. The second irrigation was started when ponded water disappeared from the lowest portion and was suspended when the highest portion was submerged. The third irrigation was also performed in the same manner. During the fourth irrigation, the ponding depth was maintained at approximately 20–25 cm, i.e., 5–10 cm at the highest portion and 35–40 cm at the lowest portion, from early July to late August. The commencement of the fourth continuous irrigation coincided with the end of the tillering stage and the beginning of the panicle formation stage. This irrigation was continued until the crop was ready or nearly ripe for harvest.

Based on the existing field water management, we confirmed that a large quantity of water was introduced to a rice plot despite the region's water scarcity. Maintenance of a high ponded water level was mainly attributed to the poor performance in land leveling rather than reasons such as prevention of rice plants from lodging and regulation of soil temperatures.

3.2. *Remedial measures to prevent secondary salinization*

Solving the abovementioned causes directly becomes remedial measures to prevent secondary salinization. Since, in many cases, these causes interact with each other and are attributable to the restriction of the natural environment, comprehensive measures should be undertaken.

3.2.1. *Measures for alleviation of canal losses and waterlogging*

The problem of heavy seepage from canals is attributable to not only the leaky characteristic of non-lined canals but also their long conveyance distance. In general, irrigation systems have long canals due to the flat topography in the region. It is inevitable to increase the canal length in order to introduce and convey water from a river to an irrigated area by gravity. Moreover, the marked characteristic of the Syr Darya river is that it is liable to meander on account of a remarkably gentle bed slope and a high coefficient of river regime (the ratio of maximum to minimum stream flow) in the lower reaches. The distribution of oxbow (crescent-shaped) lakes along the river is also an evidence of this characteristic. Therefore, the points of diversion (withdrawal) should be decided as the place where the river has a steady flow and solid banks, although the conveyance distance becomes longer. Alternative measures require investment, and economical evaluation is needed based on investment efficiency; these measures include an improvement in structures and are as follows.

(1) Introduce pumping irrigation instead of gravity irrigation, and select a site for withdrawal at a point closer to the area to be irrigated to shorten the conveyance distance as far as possible.
(2) In case gravity irrigation is applied, head works should be constructed to secure sustainable diversion at a point closer to the command area.
(3) Provide lining to earth-made canals or introduce pipeline system for pumping irrigation.
(4) In case lining is economically difficult, it is recommended to introduce special methods in canal construction to control canal seepage such as a crushing and compaction method.
(5) Conduct the operation and maintenance of the canal system in a conscientious manner so as to preserve its original conveyance capacity; if this is not done, the water level would exceed the permissible water level for conveying required discharge, and this would cause waterlogging in the adjacent area. Thus, special attention should be paid to keep the canal free from silting, weeds, aquatic weeds, and trash. In the Yeltai block, canal system was always affected by clogging due to floating debris, mainly twigs of thorny shrubs that were used for fences; concurrently, this increased the roughness coefficient and reduced the conveyance capacity of the canal.
(6) Bio-drainage is listed as a possible measure to be introduced along canals and around farm lots for preventing waterlogging and salinization. This method involves growing certain types of plants that habitually draw their main water supply directly from the canal seepage water or the capillary fringe immediately above it (Heuperman, 1999; Bhutta and Chaudhry, 2000) and maintaining the groundwater table at a safe level that prevents waterlogging, which depends on the soil texture at least 2 m from the soil surface (Vlek et al., 2002). This method is also effective for the improvement of the environment in the region. The growing of poplars (*Populus* spp.) and tamarisks (*Tamarix gallica*) is applicable to the method (Bhutta and Chaudhry, 2000; IPTRID, 2002). However, salt-tolerant trees such as tamarix could concentrate the salt in the root zone to high levels because trees usually exclude sodium and chloride ions from the transpiration stream. The salt accumulation processes in

the root zone and the water table underlying the trees will have to be managed to achieve long-term sustainability. This often involves some form of physical drainage input to remove salts from the root zone (IPTRID, 2002).

3.2.2. *Improvement in hydraulic structures of the canal system*

Since the problem of operational losses caused by inefficient hydraulic function of canal system is closely related to the measures mentioned in Section 3.2.1, remedial measures should be planned comprehensively in consideration of the hydraulic function. One difficulty is that gates are either aged and damaged or not installed at points where hydraulic control and regulation are vital. In fact, the stoppage of canal flow is very difficult in the kolkhoz. When it is necessary to stop the canal flow, a bulldozer has to be used to dump earth and sand into the canal to bank up the flow. This operation accelerates siltation in the canal system and causes canal losses.

Due to the absence of proper gate structures to control water level in the canal system, an extra water supply besides the field irrigation requirement is needed to maintain the required hydraulic gradient for irrigating fields by gravity. This is one of the main causes of the lowered irrigation efficiency in the area. This problem can be greatly improved by installation of sturdy gates for water level regulation and their correct operation. Thorough understanding and strengthening of systematized organization of the farmers are prerequisites for the appropriate operation and maintenance of the system.

3.2.3. *Improvement in drainage management*

Poor physical function and deteriorated management of drainage system lead to destruction of the water and salt balance, and thus, these accelerate salt accumulation in an irrigated area. The basic concept to prevent secondary salinization is to maintain the overall salt balance in an irrigated area by draining off the excessive salt, which is equivalent to the amount of salt inflow introduced to the area with irrigation water. For this purpose, proper management is required for the improvement and maintenance of the function of a drainage system. Judging from the low salinity level of drainage water (EC: 2.6–4.4 dS m^{-1}) as compared with that of soil water (EC: 10–25 dS m^{-1}) in the adjacent rice plot in the Yeltai block (Kitamura et al., 2000b), it is obvious that subsurface drainage is not correctly functioning in the system. Since the drainage and salinity control of an irrigated area by only an open drain system poses limitations, installation of subsurface tile drainage is recommended for supplementing the open drain system to enhance the drainage efficiency (IPTRID, 2001). A tile drain system can effectively remove accumulated salts from the root zone; however, its introduction appears quite difficult from the viewpoint of the region's economical situation. In case tile drainage system is installed in an area with high salt accumulation, the danger of deterioration of the water quality of the downstream reaches is a possibility due to the outflow of huge amount of accumulated salts from the area; hence, adequate attention should be paid in this regard. Drainage measures should be decided after due consideration of the effects on the environment of the downstream area. The management of drainage outfall of each irrigated area, in particular, appears to be a key issue for minimization of environmental degradation caused by saline drainage water in the downstream area (Rhoades, 1989; Oster and Wichelns, 2003).

In the future, each irrigated area should be well equipped with a special pond at the end of the drainage system to control the quantity and quality of drainage water to be drained off to the downstream. It is desirable to develop a design and management technique of evaporation pond for better effluent management at the outfall of each irrigation block. Existing oxbow lakes are available for the ponds, and the plan should be based on thoughtful consideration of the natural ecosystem. Prior to this, a certain agreement on allowable water quality of drainage from each irrigated area should be concluded among riparian countries. If the management of drainage outfall is combined with the reuse of drainage water for irrigation of salt tolerant crops (forages), the salinity of the drainage water would increase further and its volume would decrease, which can facilitate its final disposal in evaporation ponds (Kaffka, 2001; Kaffka et al., 2002; Oster and Grattan, 2002).

3.2.4. *Improvement in field management including soil and water management*

Since several of the abovementioned causes of secondary salinization are related to each other, the measures against them should be conjunctively investigated. To improve these issues, the following measures are proposed:

(1) The eight-year crop rotation system, which has been practiced popularly in the region, should be modified to a new system in which wet rice plots and dry upland plots within the same irrigation block are not combined. In other words, the new system is still a rotational system, but it should unify each irrigation block either an upland condition or a rice plot condition.
(2) The land leveling should be performed as precisely as possible. Generally, the ponding depth of a rice plot is maintained deep in the region, and this results in an increase in irrigation water losses. The deep ponding management may be necessitated in case of rice cultivation not only to protect rice plants from lodging and cold temperature damage but also to submerge the higher portion created by the poor land leveling. Thus, precise land leveling will increase the possibility of decreasing the ponding depth and improving the efficiency of water use. Furthermore, this allows canal water level to be relatively low so that canal losses can also be reduced.
(3) In order to prevent a gradual increase in salinity of ponded water and soil water in shallow layers caused by the occasional convection of salt from deeper layers, a continuous supply of fresh water, which allows the ponded water to spill over from the outlet to the field drain, was carried out by the farmers. Thus, this inevitably results in excessive water supply. Therefore, it is fundamentally undesirable to carry out rice cultivation in such areas with saline soils. However, rice cultivation has played an important role in the regional economy, and farmers have been cultivating rice for a long period of time; hence, it is unrealistic to deny and stop its cultivation. It is essential to

strengthen water saving management based on a full cognizance of the dependence of the regional economy on rice cultivation. Since only limited references are available on the speed of salt movement in saturated soils at the field scale (Grünberger et al., 2003; Kirk et al., 2003), further experiments are required to clarify the impact of upward transport of salts on the salinization in submerged rice plots. For example, percolation control methods, such as puddling and subsoil compaction (Yamazaki, 1976; Sharma and Bhagat, 1993), can be considered as measures to prevent the upward flux of dissolved salts. Some advanced study is required to quantitatively clarify the effects of such methods on the salt flux by convection, dispersion, and diffusion in each soil texture.

(4) In salt-accumulated spots consisting of permeable soil layers in rice plots, some measures such as replacing or mixing the existing soils with impermeable soils are required to reduce the upward movement of salts, which result in occasional interruption and resumption of irrigation water supply.

(5) It is necessary to correct farmers' attitude on the value of water. The present water charge is considerably cheap and does not encourage water conservation by farmers (Anderson, 1997). Therefore, the water charge should be revised to an appropriate level to encourage water conservation by farmers.

3.2.5. *Conclusion of international treaty on water withdrawal and drainage*

Among the proposed measures, this issue is the most important and urgent matter. The introduction of a large amount of saline river water with TDS greater than 1000 mg L^{-1} into an irrigated area is equivalent to the massive input of salts in an agricultural land, and it directly causes salt accumulation in the area. The salinity of river water increases toward the downstream area of the Syr Darya river. This is due to the repeated use of river water from the upstream reaches to the downstream reaches. Introduction of greater amounts of river water into irrigated lands and draining off saline water in the upper reaches of the river results in increased water salinity in the downstream reaches. Therefore, it is necessary for riparian countries and irrigation communities to consult and conclude agreements, including detailed regulations on water withdrawal from the river, and removal of drainage water and salt loads to the river with each other. Based on the agreement, proper basin-wide water resources management should be carried out.

4. Conclusions

The results of a series of on-site experiments conducted on water and salt behavior in an irrigated kolkhoz where a rice-based cropping system has been practiced in the Lower Syr Darya river basin of Kazakhstan are as follows. The causes of secondary salinization in irrigated areas are: (1) heavy seepage losses from canal systems, (2) heavy operational losses due to insufficient function and poor management of canal systems, (3) insufficient function and poor management of drainage systems, (4) imbalance between inflow of water and salt into irrigated area and outflow of those from the area, (5) over-irrigation of rice-planted plots, (6) application of an eight-year crop rotation system in an irrigation block, (7) poor land-leveling and careless field water management, (8) introduction of saline river-water with TDS greater than 1000 mg L^{-1} for irrigation, and (9) dissolution of accumulated salts from canal systems.

In order to overcome the above problems, the following remedial measures are recommended: (1) avoid mixed cropping with rice and upland crops and unify either upland crops or rice in an irrigation block to control groundwater table; (2) decrease conveyance and field application losses through improved canal construction and management performance, introduction of canal lining, and improved land-leveling performance; (3) maintain and operate drainage canals to enhance function, in particular, install subsurface tile drainage for enhancing subsurface drainage function and management of drainage outfall for minimizing environmental degradation caused by saline drainage water in the downstream area; (4) develop a design and management technique of evaporation pond for better effluent management and reuse of drainage water at the outfall of each irrigation block; (5) reduce the applied water to rice and use it for other crops, or return the saved water to the river for downstream users including returning to the environment; (6) conclude international water and/or drainage rights agreements among riparian countries and enact a basin-wide management regulation to control water withdrawal and drainage.

Acknowledgments

This research was partly conducted under the 21st Century COE Program (Program for Arid Land Science) funded by the Japanese Ministry of Education, Culture, Sports, Science and Technology, and the Core Research for Evolutional Science and Technology (CREST) (Research on Sustainable Water Policy Scenarios for River Basin with Rapidly Increasing Population) sponsored by the Japan Science and Technology Agency (JST). Thanks to referees and colleagues whose comments and questions helped us improve the paper.

REFERENCES

Anderson, R.C., 1997. Environmental damage assessment of the Aral Sea disaster, Environmental Policy and Technology Project, Issue Paper No.1, U.S. Agency for International Development, p. 25.

Ayers, R.S., Westcot, D.W., 1985. Water Quality for Agriculture. FAO Irrigation and Drainage Paper No. 29. Rome, Italy, p. 176.

Bhutta, M.N., Chaudhry, M.R., 2000. Biological control of waterlogging. In: Proceedings of Eighth ICID International Drainage Workshop. New Delhi, India, (Bio-Drainage), pp. 33–45.

Dmitriev, L.N., 1995. The problem of agricultural crop diversity in the lower part of the Syr Darya Basin. In: Symposium on the Aral Sea and the Surrounding Region-Irrigated Agriculture and the Environment, Lake Biwa Research Institute, Otsu, Shiga, Japan, , March 29, p. 6.

European Commission, 1995. Water resources management and agricultural production in the Central Asian Republics, WARMAP Project Report, vol. 1–6.

Grünberger, O., Hartmann, C., Bourdon, E., Lesturgez, G., Yuvaniyama, A., Sukchan, S., Ruaysoongnern, S., 2003. Detailed characterization of a spreading saline patch inside a paddy field of Northeast Thailand. In: The Second International Conference on Soil Quality Evolution Mechanism and Sustainable Use of Soil Resources, Yingtan, PR China (from Gregory Lesturgez's Homepage).

Gupta, I.C., 1990. Use of Saline Water in Agriculture—A Study of Arid and Semi-Arid Zones of India. Oxford & IBH Publishing Co. Pvt. Ltd., India, p. 308.

Heuperman, A., 1999. Hydraulic gradient reversal by trees in shallow water table areas and repercussions for the sustainability of tree-growing systems. Agric. Water Manage. 39, 53–167.

Hillel, D., 1998. Environmental Soil Physics. Elsevier Academic Press, New York, pp. 43–44.

International Programme for Technology and Research in Irrigation and Drainage (IPTRID), 2001. Drainage and Sustainability, IPTRID Issues Paper 3, FAO, Rome, p. 28.

International Programme for Technology and Research in Irrigation and Drainage (IPTRID), 2002. Biodrainage—Principles, Experiences and Applications, Knowledge Synthesis Report No. 6, FAO, Rome.

Kaffka, S., 2001. Salt tolerant forages for the reuse of saline drainage water. In: Proceedings of 31st California Alfalfa and Forage Symposium, Modesto, CA, pp. 197–206.

Kaffka, S.R., Oster, J.D., Corwin, D.L., 2002. Using forages and livestock to manage drainage water in the San Joaquin Valley. In: Proceedings of 17th WCSS, Thailand, pp. 2059-1–2059-12.

Kirk, G.J.D., Solivas, J.L., Alberto, M.C., 2003. Effects of flooding and redox conditions on solute diffusion in soil. Eur. J. Soil Sci. 54, 617–624.

Kitamura, Y., 1990. Management of irrigation systems for rice double cropping culture in the tropical monsoon area, Technical Bulletin of the Tropical Agriculture Research Center No. 27, pp. 1–28.

Kitamura, Y., Yano, T., Yasuda, S., Oba, T., 2000a. Water balance in an irrigation block under rice-based cropping system in Central Asia—research on water management to prevent secondary salinization in Arid Land (I). Trans. Jpn. Soc. Irri. Drain. Reclam. Eng. 205, 55–64.

Kitamura, Y., Yano, T., Yasuda, S., Oba, T., 2000b. Water and salt behavior in an irrigation block under rice-based cropping system in Central Asia—Research on water management to prevent secondary salinization in Arid Land (II). Trans. Jpn. Soc. Irri. Drain. Reclam. Eng. 206, 47–56.

Konokhova, V., 1985. Rice growing. Mir Publishers, Moscow, USSR, p. 180 (English translation of "ИЗДАТЕЛЬСТВО [КОЛОС] published in 1982).

Kraatz, D.B., 1977. Irrigation Canal Lining, FAO land and water development series No. 1, FAO Land and Water Development Division, Food and Agricultural Organization of the United Nations, Rome, pp. 38–39.

Maas, E.V., Grattan, S.R., 1999. Crop yield as affected by salinity. In: Skaggs, R.W., van Schilfgaarde, J. (Eds.), Agricultural Drainage. Agronomy Monograph 38. ASA, CSSA, SSSA, Madison, WI, pp. 55–108.

Oster, J.D., Grattan, S.R., 2002. Drainage water reuse. Irrig. Drain. Syst. 16, 297–310.

Oster, J.D., Wichelns, D., 2003. Economic and agronomic strategies to achieve sustainable irrigation. Irrig. Sci. 22 (3–4), 107–120.

Rhoades, J.D., 1989. Intercepting, isolating, and reusing drainage waters for irrigation. Agric. Water Manage. 16 (1–2), 37–52.

Rockstöm, J., 2003. Water for food and nature in drought-prone tropics: vapour shift in rain-fed agriculture. Philos. Trans. R. Soc. Lond. B 358, 1997–2009.

Sharma, P.K., Bhagat, R.M., 1993. Puddling and compaction effects on water permeability of texturally different soils. J. Indian Soc. Soil Sci. 41, 1–6.

Vlek, P.L.G., Martius, C., Schoeller-Schletter, A., Wehrheim, P., 2002. Economic and ecological restructuring of land- and water use in the Region Khorezm (Uzbekistan): a pilot project in development research, Project Proposal, ZEF/UNESCO Khorezm Project, ZEF, Bonn, Germanay, p. 90.

Yamazaki, F., 1976. Farmland Engineering, vol. 1. Tokyo University Publication, Tokyo, 100–130 (in Japanese).

available at www.sciencedirect.com

ScienceDirect

journal homepage: www.elsevier.com/locate/agwat

The impact of saline water irrigation management options in a dune sand on available soil water and its salinity

B.A. Ould Ahmed [a,*], T. Yamamoto [a], V. Rasiah [a,b], M. Inoue [a], H. Anyoji [a]

[a] Tottori University, Arid Land Research Center, 1390 Hamasaka, Tottori 680-0001, Japan
[b] Department of Natural Resources & Mines, 28 Peters Street, Mareeba, Qld 4880, Australia

ARTICLE INFO

Article history:
Accepted 2 October 2006
Published on line 9 November 2006

Keywords:
Saline water irrigation
Available soil water
Soil water salinity
Sorghum
Sustainability

ABSTRACT

In this study the effect of two levels of irrigation input, each at two frequencies, were assessed on sorghum (*Sorghum bicolor* (L.) Moench) grain yield as impacted by available soil water after irrigation and the electrical conductivity of soil water (EC_{sw}) in a dune sand, in a greenhouse experiment. Saline water (7.32 dS m^{-1}) at input amounts equivalent to 50% or 100% of pan evaporation was applied daily or every second day. Using time domain reflectometry technique, soil water content and EC_{sw} were monitored simultaneously just before and 1–2 h after irrigation. The cumulative recharge by irrigation in the top 25 cm of the profile ranged from 309 to 662 mm and it depended on irrigation input amounts, which ranged from 382 to 765 mm, and frequency. The potential cumulative evapotranspiration (ET_c) was 578 mm. The daily recharge matched against the corresponding ET_c indicated that grain yield might have been impacted by water stress in the 50% irrigation input, regardless of the frequency, but not in the 100% input treatment. The daily EC_{sw} in the root-zone matched against the FAO threshold (13.6 dS m^{-1}) indicated the possibility of salinity stress during the late maturity stage in the 50% input treatment, regardless of the irrigation frequency, but no stress in the 100% input treatment. Though there was no water or salinity stress in the every second day irrigated 100% input treatment, the significant relative yield reduction, compared with the daily 100% input, is attributed to inherent limited available soil water capacity and rapid percolation losses between irrigations in this sand. The results indicate daily irrigation at 100% input is the most appropriate saline water irrigation management option for this dune sand.

1. Introduction

Dwindling supplies of quality water for irrigation and increasing demand from other users are forcing farmers to use saline irrigation waters (Rhoades, 1987; Rhoades et al., 1992; Shani and Dudley, 2001). Several workers (Shani and Dudley, 2001; Gideon et al., 2002; Katerji et al., 2003) have indicated that when saline waters are used for irrigation due attention should be given to minimize root-zone salinity. Others have indicated the need for selection and use of appropriate irrigation systems and practices that will supply just sufficient quantity of water to the root-zone to meet the evaporative demand and minimize salt accumulation in the root-zone (Fisher, 1980; Munns, 2002). The third approach is to select crops/varieties that can tolerate water and salinity stress to a given degree (DeMalach and Pasternak, 1993; Mastrorilli et al., 1995; Claudivan et al., 2005).

In the Mauritanian semi-arid regions, irrigated rice production, even using quality water (0.10–0.25 dS m^{-1}), has led to rising groundwater levels and increases in soil water

* *Corresponding author*. Tel.: +81 857 21 7213; fax: +81 857 29 6199.
E-mail addresses: ahmed@alrc.tottori-u.ac.jp, a_bouya@yahoo.com (B.A. Ould Ahmed).
0378-3774/$ – see front matter
doi:10.1016/j.agwat.2006.10.001

salinity (2.20 dS m^{-1}) in the root-zone (Josserand and Silva, 2002; van Asten et al., 2003). In this country sorghum, which occupies 60% of the total area under grain production, is a dryland crop grown mostly in the arid to semi-arid regions. Sorghum is widely used for human consumption and as feed and fodder (Ministère du développement rural, 1998). Josserand and Silva (2002) reported that sorghum in Mauritania accounts for 25% of the total grain production. Farmers frequently face crop failure due to drought, but supplementary or full irrigation for this crop has never been tried out. This may be partially due to insufficient water resources other than groundwater, which is primarily used for human and livestock consumption. The wells are usually 5–20 m deep and the dry-out during consecutive dry years. The groundwater tends to become saline after years of water extraction. Under such circumstances, people abandon saline wells and move to new wells. This suggests that even if supplementary irrigation is introduced for sorghum, the potential for irrigation induced salinity risk is high and the sustainability of the already fragile soil resources may be at risk.

Data from vegetable producing semi-arid regions of Mauritania indicate that salinity is already an issue in the groundwater irrigated projects (SONADER, 1998; Josserand and Silva, 2002). Irrigation is usually gravity fed and the water application efficiency is very low. The needs for introduction of new irrigation systems and improvements in existing practices, at least in the intensive vegetable producing regions, have been identified. The drip irrigation is the most efficient system in delivering just the required amount of water directly in the crop root-zone (Shalhevet, 1991). The use of such system is particularly important where limited water resources, including saline groundwater, are used for irrigation. However, the coast of installation and maintenance and the technical skills required for its operation are high for a country like Mauritania. Nevertheless, for future planning purposes at least some limited background information about appropriate management practices is required for saline water irrigation in drip systems (Ayers and Westcot, 1985; Pasternak and DeMalach, 1987; Gideon et al., 1995) to sustain productivity and soil resource utilization in this country. Thus, a greenhouse experiment was conducted, mimicking Mauritanian conditions, to assess the effect of two water input amounts, each at two frequencies, on sorghum grain yield as impacted by available soil water and its EC_{sw} in a dune using saline irrigation water in drip irrigation system (DIS).

2. Materials and methods

2.1. Experiment

The experiment was conducted in a greenhouse located at the Arid Land Research Center, Tottori University in Tottori, Japan. The textural composition of the soil is 95% sand, 1.3% silt, and 3.7% clay and is usually referred to as dune sand. The water holding capacity of this soil sand is 0.05 $cm^3\,cm^{-3}$ (0.027 $cm^3\,cm^{-3}$ is wilting point and 0.08 $cm^3\,cm^{-3}$ is field capacity, and these correspond to matric potentials of −1.6 and −0.0055 MPa), respectively.

A randomized complete block design with three replicates was used in this study. The treatments consisted of two irrigation input amounts, 50% (EP0.5) and 100% (EP1.0) of open-pan evaporation, which was measured in the greenhouse. These amounts were applied at two frequencies (daily and every second day). In the every second irrigated treatment, the input on a particular day is equal to the amount applied on the previous day plus the amount due on that particular day of the daily irrigated treatment. This implies the total irrigation input during the growing season in the daily and every second day irrigated treatment are approximately equal for a given input treatment. Sorghum was sown, along lateral lines just by the emitters, on 1 April 2004 at 12 plants per block and harvested on 15 July 2004. Fertilizer was applied, at 180 kg h^{-1} N, 45 kg h^{-1} P, 80 kg h^{-1} K, just before seeding and incorporated into the soil.

The experimental area was irrigated using DIS and each treatment plot (1.2 m × 1.2 m) was fed by three laterals that branched off from the sub-main pipe. There were 4 emitters, spaced 30 cm apart, on each one of the 120 cm long laterals. The discharge rate from the emitters was 2 L h^{-1}, which was maintained by an operating pressure of 0.1 MPa. Saline water (EC = 7.32 dS m^{-1}) irrigation commenced 2 weeks after sowing and continued until 15 July 2004. However, crop establishment was achieved using 65 mm of quality water (EC = 0.11 dS m^{-1}), i.e. during the first 2 weeks. The total saline water irrigation input in the EP1.0 was around 765 mm for daily and every second day frequency and that for EP0.5 it was around 380 mm. A water-tank was used to prepare saline water, covered to minimize evaporation and cleaned once in every 5 days. The salinity of the irrigation water used in this study was based on invoking two assumptions. First, the average salinity of groundwater in Mauritania is 8.0 dS m^{-1} and secondly the FAO has determined that when saline waters of 6.8 dS m^{-1} were used for irrigating sorghum this could lead to 50% yield reduction. Therefore we decided to use an average between 8.0 and 6.8 dS m^{-1}. At harvest the grain yield was measured after oven drying at 70 °C for 48 h.

A control using quality irrigation water and the associated irrigation option treatments were not included in this experiment due to inadequate greenhouse space. However, during the subsequent year a control using quality irrigation water (EC = 0.11 dS m^{-1}) at EP1.0 on daily basis was included in an experiment in the same greenhouse and the grain yield from this control is included as the background in this paper.

2.2. Weather condition

Humidity and temperature were measured every 15 min using (HOBO H8 PRO SERIES LOGGER). The air temperature (maximum, minimum and daily mean) during the growing season increased from April until July and decreased thereafter. The mean monthly temperatures were 20 °C for April, 24 °C for May, 25 °C for June, and 30.1 °C for July. During the growing season the lowest daily mean temperature was 11 °C in April and the highest was 48 °C in July. The mean monthly humidity ranged from 56% to 69%. The lowest diurnal variation in humidity was 33% in June and the highest was 97% in April. The weather data were used to compute daily crop evapotranspiration (ET_c).

2.3. Crop evapotranspiration computation

Evaporation from open-pans were measured from three small pans (E_{sp}), 0.2 m internal diameter, located in the greenhouse and was converted to class A evaporation (EP) using Agodzo et al.'s (1997) equation:

$$EP = aE_{sp}^{b} \quad (1)$$

where a and b are fitting parameters and $a = 0.58$ and $b = 1.3$.

The EP in Eq. (1) was converted to potential evapotranspiration (ETo) using Doorenbos and Pruitt (1977) equation,

$$ETo = K_{pan}\,EP \quad (2)$$

The K_{pan} in Eq. (2) is 0.8 and this value was obtained following Agodzo et al. (1997) rationale for greenhouse condition using Doorenbos and Pruitt (1977) procedure.

The ETo from Eq. (2) was converted to crop evapotranspiration (ET_c) using Doorenbos and Pruitt (1977) equation,

$$ET_c = K_c\,ETo \quad (3)$$

where K_c is crop factor and we used the Allen et al. (1998) published K_c values for the early (ES), mid (MS) and late (LS) growth stages of sorghum and they are 0.7, 1.1 and 0.55, respectively. For simulating the semi-arid Mauritania growing condition, we assumed that the ES is approximately the first 35 days after seeding, MS from day 35 to 75, and LS from day 75 to 106.

2.4. Soil water content, bulk electrical conductivity and irrigation

Simultaneous volumetric soil water content (θ_v) and soil water electrical conductivity (EC_{sw}) distributions in the root-zone were monitored using time domain reflectometry (TDR) method (Topp et al., 1980; Dehghanisanij et al., 2004; Inoue, 2006). The TDR sensors were installed vertically at two depths (10 and 25 cm) along the dripper lines and near to the emitters. The TDR sensor installation depths were based on Yamamoto and Cho (1978) findings who reported the most effective root-water uptake zone in this dune sand under drip irrigation is the top 25 cm. Depending on the irrigation frequency, the TDR readings were taken just before and 1–2 h after every irrigation. The difference ($\Delta\theta_v$) between θ_v before and after irrigation, at a given depth for a treatment, is considered as the net recharge. Thus, the $\Delta\theta_v$ from a given depth segment multiplied by that depth is equal to the amount of water replenished after irrigation. We consider that most of the recharge was used by the crop between two consecutive irrigations.

2.5. TDR calibration for the determination of soil water salinity, EC_{sw}

There are few published reports on how TDR can be used to monitor EC_{sw}. Dehghanisanij et al. (2004) and Inoue (2006) developed functional relationships involving TDR dielectric constant (K_d), θ_v, and the TDR conductivity reading (ECa) to compute soil solution EC_{sw}. The general form of the equation is

$$EC_{sw} = \frac{EC\,a - B(\theta_v)}{A(\theta_v)} \quad (4)$$

The θ_v in Eq. (4) was computed using K_d of TDR readings. The equation proposed by Inoue (2006) for EC_{sw} computation is

$$EC_{sw} = \frac{EC\,a - 0.00425\theta - 0.00631}{7.05\theta^4 - 2.17\theta^3 + 0.56\theta^2 + 0.0727\theta - 0.0004} \quad (5)$$

The estimates obtained using Eq. (5) were compared with experimentally determined electrical conductivity (EC_{exp}) of soil solution (Inoue, 2006; Dehghanisanij et al., 2004). In this calibration, irrigation waters of different salinity in different amounts were added to known soil mass in beakers and the TDR was used to record θ_v and ECa. These values were used in Eq. (5) to compute EC_{sw}. When EC_{sw} obtained using Eq. (5) was compared with EC_{exp} and this indicated there was a relative error of 16%, which we considered as unsatisfactory. Therefore, we developed our own predictive equation for EC_{sw},

$$EC_{sw} = \frac{EC\,a - 0.016\theta v - 0.009}{4.286\theta v^2 - 0.6491\theta v + 0.0416} \quad (6)$$

The estimates for A and B, in Eq. (4), were obtained from regression analysis of experimental data collected in this study using Inoue (2006) procedure. The estimates obtained using Eq. (6) produced a relative error of 2.7%, thus the EC_{sw} values reported in this manuscript are all computed using Eq. (6).

2.6. Statistical analysis

The mean, simple correlation, and stepwise multiple regression analyses were performed on the data using the SAS/Statg (1991) software package.

3. Results and discussion

3.1. Soil water content (θ_v)

The volumetric soil water content (θ_v) data shown in Fig. 1 indicate that θ_v varied temporally depending on the time of measurement (before and after irrigation on a given day), the crop age, irrigation input and frequency and the profile segment. The mean values indicate the average θ_v after irrigation > before irrigation (obvious), EP1.0 > EP0.5, and daily irrigation > every second day, and 10–25 cm segment > 0–10 cm segment (Table 1). The data indicate the temporal dynamics in θ_v depended primarily on irrigation input and frequency. The data also indicate the profile was recharged by irrigation to 25 cm depth, and the recharge in general was higher in 10–25 cm segment than in 0–10 cm (not shown). Previous studies (Yamamoto and Cho, 1978) from the same greenhouse for sorghum indicated that the major root-water uptake took place from the top 25 cm of soil profile, therefore hereafter we will place our emphasis on changes in θ_v and profile recharge that occurred in the in top 25 cm depth.

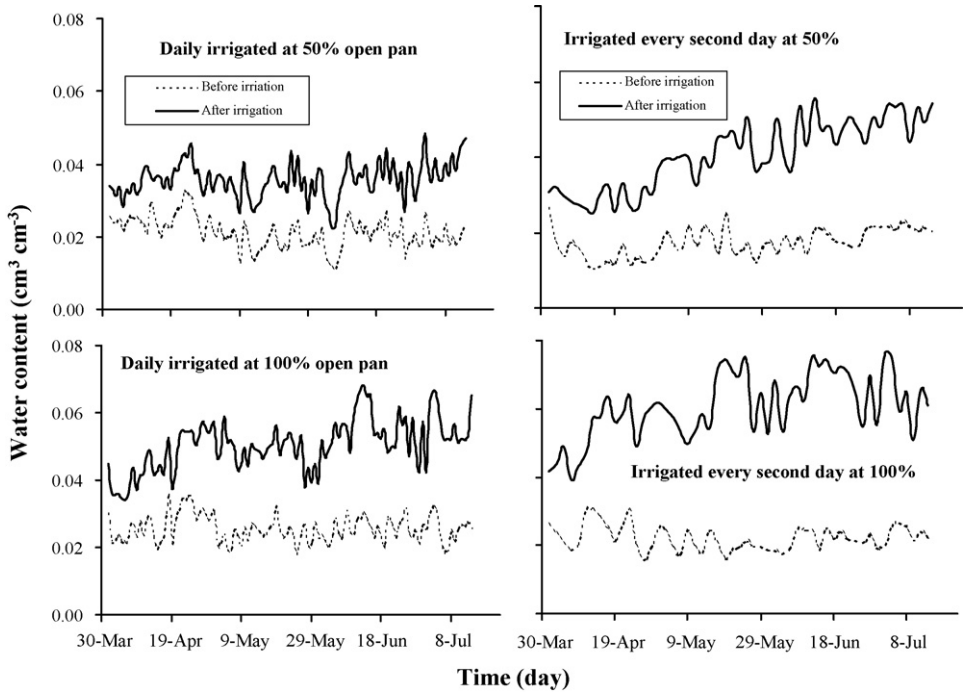

Fig. 1 – The temporal dynamics of soil water content just before and 1–2 h after irrigation, in the different irrigation treatments.

3.2. *Available soil water and productivity*

In this section we converted the changes ($\Delta\theta_v$) in θ_v that occurred between before and after irrigation in the top 25 cm of the profile to millimetre of water and compare it with irrigation input and sorghum potential crop evapotranspiration, ET_c (Fig. 2). The recharge in the 0–25 cm segment of the daily irrigated EP0.5 was approximately equal to the irrigation input, indicating the applied water was in the top 25 cm of the profile after 1–2 h of irrigation. The ET_c throughout the growing season was usually higher than the recharge in the 0–25 cm, suggesting the irrigation input was not sufficient to meet the ET_c, and consequently a sustainable productivity issue (Agodzo et al., 1997). In the daily

Table 1 – The ranges (minimum and maximum) and average water content during the growing season under different irrigation input and schedules

Time	Irrigated daily					
	At 50% of pan evaporation			At 100% of pan evaporation		
	Range	Mean	Recharge	Range	Mean	Recharge
Soil water ($cm^3\ cm^{-3}$)						
In 0–10 cm soil layer						
Before irrigation	0.016–0.037	0.024 ± 0.003		0.020–0.040	0.028 ± 0.007	
After irrigation	0.021–0.055	0.034 ± 0.005	0.010	0.022–0.061	0.041 ± 0.004	0.013
In 10–25 cm soil layer						
Before irrigation	0.015–0.052	0.032 ± 0.007		0.017–0.057	0.033 ± 0.007	
After irrigation	0.036–0.074	0.052 ± 0.009	0.020	0.032–0.078	0.059 ± 0.008	0.025
Irrigated every second day						
In 0–10 cm soil layer						
Before irrigation	0.016–0.033	0.020 ± 0.004		0.005–0.047	0.024 ± 0.003	
After irrigation	0.020–0.047	0.030 ± 0.003	0.010	0.018–0.076	0.038 ± 0.007	0.014
In 10–25 cm soil layer						
Before irrigation	0.017–0.036	0.029 ± 0.008		0.020–0.044	0.030 ± 0.005	
After irrigation	0.022–0.065	0.041 ± 0.005	0.012	0.026–0.063	0.047 ± 0.007	0.017

Recharge is the difference between the mean of after and before irrigation soil water content.

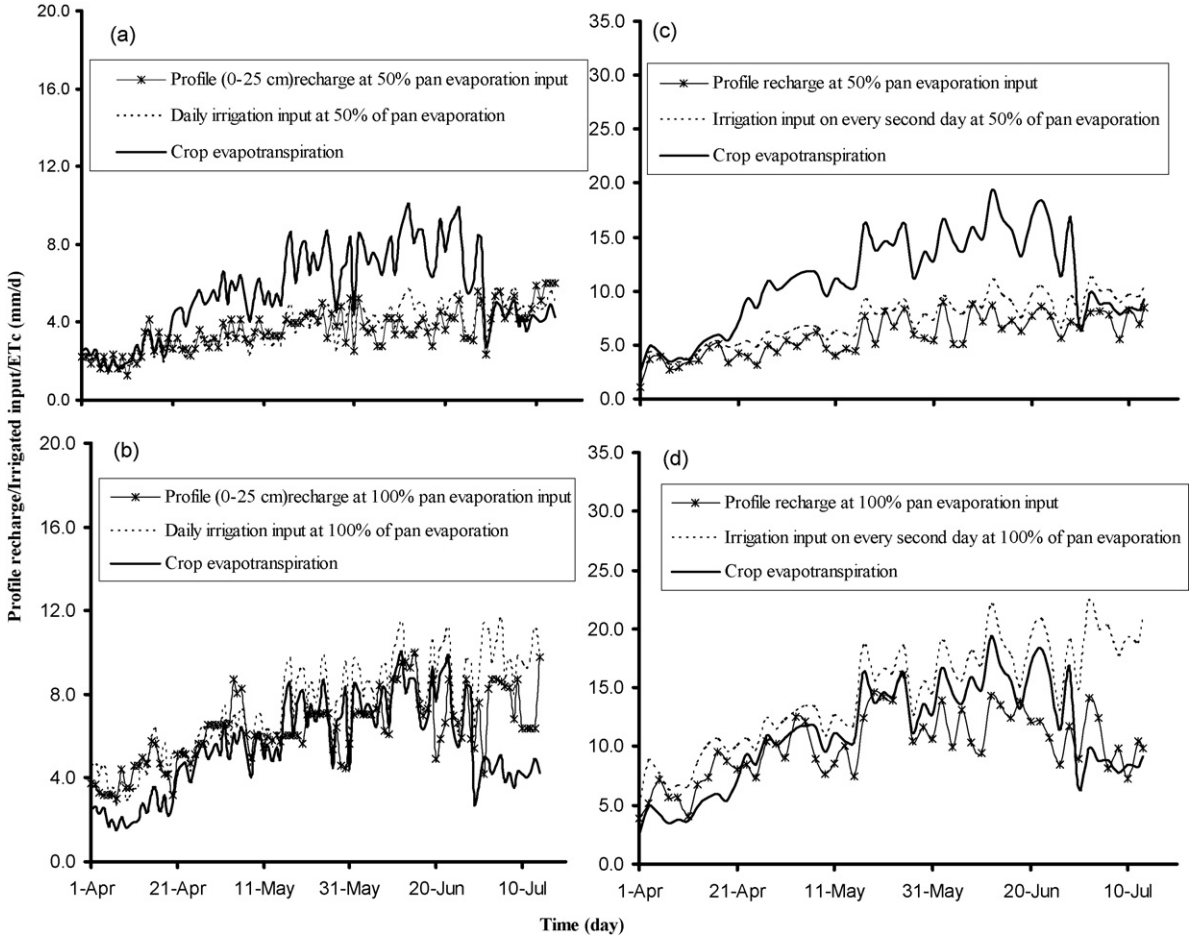

Fig. 2 – The profile recharge (the difference between after and before irrigation soil water content multiplied by 250 mm), the irrigation input, and potential evapotranspiration (ET_c).

irrigated EP1.0, the recharge through irrigation input and the ET_c were approximately equal to or overlapped with each other, indicating that irrigation input recharged the depleted profile and it was sufficient to meet ET_c, provided the recharge was not lost through percolation to depth > 25 cm.

In the every second day irrigated treatment, the trends observed for ET_c at EP0.5 and EP1.0 input are qualitatively similar to that observed in the daily irrigated treatments (Fig. 2c and d). The irrigation recharge in 0–25 cm of the every second day irrigated practice was less than the irrigation input, regardless of the irrigation input. The difference between irrigation input and recharge (Table 2) is larger in the EP1.0 input treatment (229 mm) than EP0.5 input (73 mm). A comparison of the difference between irrigation input and recharge in the EP1.0 of daily and every second day irrigated schedule indicates the difference is larger (299 mm) in the

Table 2 – The cumulative profile recharge and percolation losses under different irrigation input and frequency treatments

Irrigation and soil water	Irrigated daily		Irrigated every second day	
	50% of pan evaporation (EP0.5) (mm of water during the growing season)	100% of pan evaporation (EP1.0) (mm of water during the growing season)	50% of pan evaporation (EP0.5) (mm of water during the growing season)	100% of pan evaporation (EP1.0) (mm of water during the growing season)
Irrigation input	383	765	382	765
Profile (25 cm) recharge	379	662	309	536
Percolation to depth > 25 cm	4 (1%)	103 (14%)	73 (19%)	229 (30%)

Functional relationship between cumulative recharge (CR) or percolation below (PR) 25 cm depth and total irrigation input (II), irrigation frequency (IF) and the interaction involving (II and IF). $CR = 88.91 + 0.92II - 0.17II \times IF$ ($R^2 = 0.99$; $P < 0.01$), $PR = -88.91 + 0.08II + 0.17II \times IF$ ($R^2 = 0.99$, $P < 0.02$). The numbers within parenthesis in the percolation losses row are percolation losses in percent to depths > 25 cm.

latter than the former (103 mm). The aforementioned recharge versus input differences suggests that percolation losses to depths > 25 cm, during 1–2 h after irrigation, and it increased with increasing irrigation input and with increasing intervals. Assuming that soil evaporation losses during 1–2 h after irrigation are similar in different input treatments, it seems that approximately 41% of the total growing season input in the every second day irrigated EP1.0 percolated to depths > 25 cm compared with 16% in the daily irrigated EP1.0, 24% in every second day irrigated EP0.5, and <1% in daily irrigated EP0.5. It seems relatively drier profile conditions in the every second day irrigated treatment favored more rapid percolation losses than the daily irrigated treatment. This suggests frequent irrigation is preferable over less frequent to reduce percolation losses below the active root-zone in this dune sand.

Thus, it seems the daily irrigated EP1.0 is the optimum irrigation management practice for this dune sand in relation to profile recharge and leaching of salts below the active root-zone.

The cumulative potential ET_c (578 mm) during the growing season was met satisfactorily by the cumulative profile recharge (662 mm) in the daily irrigated EP1.0 treatment. In the every second day irrigated EP1.0 treatment there was a deficit of 42 mm compared with approximately 200 mm deficit in the daily irrigated EP0.5 and 270 mm in the every second irrigated EP0.5 treatments. Thus, it seems the available soil water deficit induced stress was probably highest in the every second day irrigated EP0.5 treatment, followed by daily irrigated EP0.5 and every second day irrigated EP1.0 treatments. The results indicate that for meeting the seasonal potential ET_c, form irrigation profile recharge, and for optimum drainage below the crop root-zone in this dune sand, the daily irrigated EP1.0 management practice is the best irrigation management option.

The cumulative profile recharge (PR), computed for each treatment, matched against the corresponding irrigation input indicates percolation losses of approximately 1% in the daily irrigated EP0.5 and 14% in EP1.0 to depths > 25 cm and 19% in EP0.5 and 30% in EP1.0 of the every second day irrigated treatments. The PR increased with increasing irrigation input (II) but at a given II it decreased with decreasing frequency (Table 2). This suggests that more percolation to depths > 25 cm in the every second day irrigated treatment than the daily irrigated.

Though leaching fractions were not intentionally included in the irrigation input treatments, substantial percolation losses (PL) occurred, particularly in the every second day irrigated treatment including the EP0.5 input treatment, which we believe was the most stringent input treatment. There are at least two aspects that need attention with regard to the PL. First, the PL seems to increase with increasing input (II) and with decreasing irrigation frequency (IF) and this is supported by the multiple regression equation provided in Table 2. The interaction involving II and IF indicates that when the IF increased to every second day the PL also increased. We however, intuitively, anticipated the PL to be smaller in the every second day irrigated (less

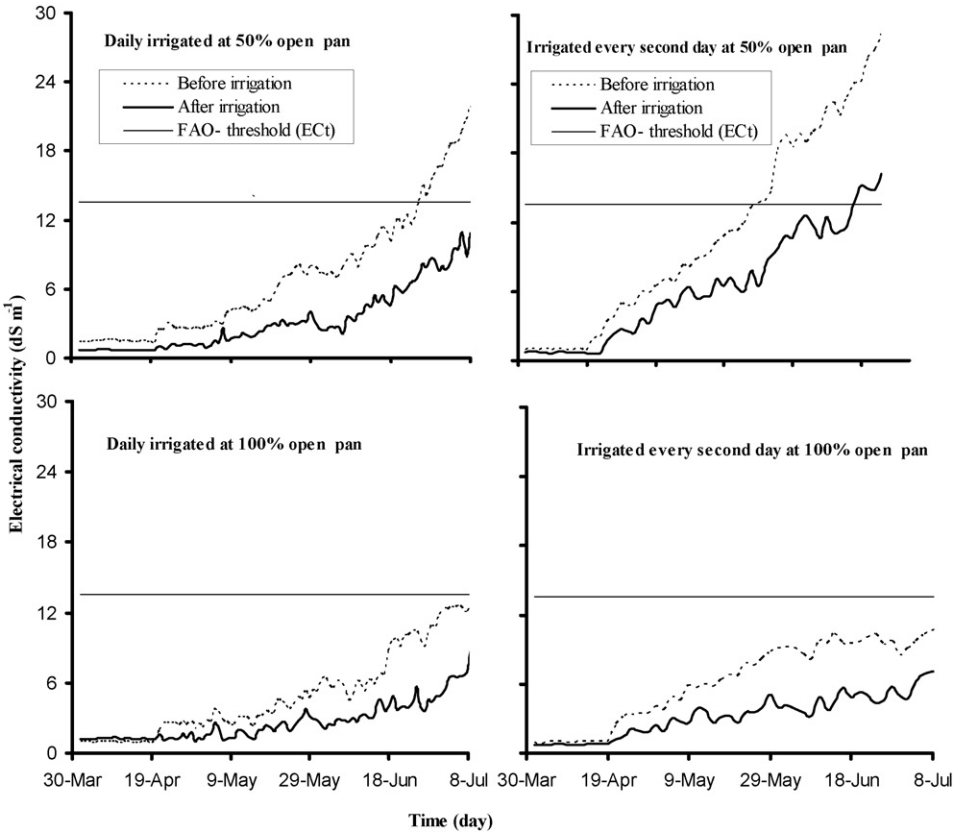

Fig. 3 – The temporal dynamics in electrical conductivity of soil water, monitored just before and 1–2 h after irrigation compared with FAO threshold value of 13.6 dS m^{-1} for sorghum.

Table 3 – The average electrical conductivity of the soil water (EC_{sw}) under different irrigation treatments in different segments of the dune sand profile and the yield

Irrigation treatment	Average EC_{sw} (dS m^{-1})				Slope 'B' in Eq. (7)		
	Relative yield (%)	0–10 cm	10–25 cm	0–25 cm	0–10 cm	10–25 cm	0–25 cm
50% input daily	39	15.88 ± 1.78	14.13 ± 0.28	14.94 ± 1.16	26.52	115.12	45.52
50% input every second day	29	18.12 ± 3.41	15.97 ± 1.13	17.34 ± 2.28	15.43	29.96	18.98
100% input daily	75	8.72 ± 1.02	8.04 ± 0.47	8.44 ± 0.68	–	–	–
100% input every second day	55	9.39 ± 1.82	8.58 ± 0.43	9.38 ± 0.60	–	–	–

frequent) treatment than the daily treatment. Contrary to this expectation an opposite trend was observed and we speculate this was due to increases in percolation in this sandy soil with increasing in soil dryness. Secondly, the water retention ability of this soil is so poor that irrigation input in the every second day irrigated treatment equivalent to twice as that in the daily irrigated led to increased percolation, and consequently it might have resulted in higher crop water stress in the former than the latter treatment.

3.3. *Electrical conductivity of soil water (EC_{sw}) and irrigation*

3.3.1. *Temporal dynamics of EC_{sw}*

The data for the electrical conductivity of soil water (EC_{sw}) shown in Fig. 3 indicates that regardless of the irrigation input or frequency the mean EC_{sw} in the top 25 cm soil layer increased with time. The differences between the before and after irrigation curves indicate the EC_{sw} decreased rapidly after irrigation, increased until the next cycle of irrigation and the trend was consistent throughout the growing season. The trends were qualitatively similar across treatments, but the magnitudes varied with irrigation input and frequency. Approximately 60 days after seeding, the EC_{sw} increased rapidly between irrigation events particularly in the EP0.5 input practice and more specifically during late maturity stage, regardless of irrigation frequency. The EC_{sw} dynamics, particularly the values before irrigation, indicate the crop was subjected to salinity stress as the EC_{sw} values during certain growth stage exceeded the threshold level (Tanji and Kielen, 2002).

3.3.2. *Seasonal mean EC_{sw} and threshold salinity (EC_t)*

Shalhevet (1994) proposed the use of growing season average EC_{sw} to assess salinity stress on crop yield against the Tanji and Kielen (2002) proposed threshold (EC_t) values. The FAO proposed threshold EC_t are based on soil saturation paste extract procedure and these values can be converted to EC_{sw} by multiplying the extract values by 2 (Maas and Hoffman, 1977; Letey et al., 1985; Letey and Dinar, 1986; Oster, 1994; Shalhevet, 1994). The proposed paste extracted threshold EC_t for 0% sorghum yield reduction due to salinity is 6.8 dS m^{-1}. We therefore selected the EC_t as 13.6 dS m^{-1} (i.e. $EC_t \times 2 = EC_{sw}$) to assess the possibility of salinity stress in the temporal data (Fig. 3). The data indicate that there should have been no salinity stress in the EP1.0 input treatment regardless of the irrigation frequency. On the other hand under EP0.5 treatment the EC_{sw} exceeded the threshold value at late stage of crop growth under both frequencies of irrigation, implying that the crop might have faced some salinity stress. However, as this occurred during the late maturity stage its impact on grain yield may be questionable.

Another approach is to assess growing season mean EC_{sw} in the root-zone against the EC_t (Letey et al., 1985; Oster, 1994; Shalhevet, 1994). The growing season mean EC_{sw} in the top 25 cm of the daily irrigated EP1.0 treatment was 3.4 dS m^{-1} compared with 7.1 dS m^{-1} for EP0.5. The EC_{sw} in the every second day irrigated EP1.0 was 5.1 and 5.9 dS m^{-1} in EP0.5. The average EC_{sw} values suggest the crop was not subjected to salinity stress, regardless of the irrigation management practices. According to other workers (Shalhevet, 1994) the mean EC_{sw} for a given growth stage can also be used as a guide to assess salinity impact during that growth stage or during a given period. Thus, we computed the mean EC_{sw} during the period when EC_{sw} exceeded EC_t (Table 3). The mean EC_{sw} during late maturity stage in the EP0.5 irrigation input was higher than the threshold EC_t value, regardless of irrigation frequency, suggesting potential salinity stress-induced grain yield reductions in these treatments. The mean EC_{sw} in EP1.0 during the period when EC_{sw} for EP0.5 exceeded EC_t is higher than the corresponding seasonal mean (see above) but less than EC_t, indicating no possibility for any salinity induced yield reduction in EP1.0 even during the late maturity stage (Table 4).

Table 4 – Sorghum grain yield as affected by different irrigation input and frequencies

Grain yield	Irrigation treatment			
	Irrigated daily at		Irrigated every second day at	
	50% of pan evaporation (EP0.5)	100% of pan evaporation (EP1.0)	50% of pan evaporation (EP0.5)	100% of pan evaporation (EP1.0)
Yield (kg m^{-2})	0.128 ± 0.011	0.226 ± 0.035	0.090 ± 0.012	0.170 ± 0.026
Control yield in 2005	–	0.315 ± 0.031	–	–

Table 5 – Simple linear correlation between sorghum relative grain yield (%) and cumulative recharge (mm) in the top 25 cm during the growing season or the mean electrical conductivity (EC_{sw}) of soil water or mean electrical conductivity during the period when it was greater than threshold salinity, or total irrigation input (mm), or irrigation frequency (where daily irrigation = 1 and every second day irrigation = 2)

Independent variable	Intercept	Slope	R^2	P
Cumulative recharge	−9.99	0.13	0.99	0.004
Growing season mean EC_{sw}	94.39	−7.07	0.97	0.03
Late season mean EC_{sw}	104.8	−4.42	0.95	0.05
Irrigation frequency (IF)	ns			
Total irrigation input (II)	2.98	0.081	0.79	0.10

R^2 = coefficient of determination, p = probability at which the relationship is significant.

3.4. *Sorghum grain yield, profile recharge, the mean EC_{sw}, as affected by irrigation input and frequency*

3.4.1. *Discriminating the impact of soil moisture stress versus salinity stress on grain yield*

The cumulative profile recharge (PR) that occurred during the growing season, the growing season mean electrical conductivity (EC_{sw}-gm), the late season mean conductivity (EC_{sw}-ls), total irrigation input (II), and irrigation frequency (IF) were each individually correlated with relative grain yield (Table 5). The PR, EC_{sw}-gm and EC_{sw}-ls were each significantly correlated with grain yield (Table 5). The stronger significant relationship between relative yield (RY) and PR as compared to RY and II indicates that the available soil water, through irrigation recharge, played a major role rather than II per se in determining grain yield. This is basic to all the grain yield models available in literature, particularly those developed by Letey et al. (1985) for irrigated conditions and more specifically when saline water was used for irrigation. We mentioned elsewhere in the text the low water holding capacity of the soil contributed to high percolation losses. Thus, the yield reduction under less frequent irrigation, but under similar total irrigation input as in more frequent irrigation, is attributed to accelerated percolation losses and low water holding capacity in this soil. Though percolation losses below root-zone, based on the amount of irrigation input, cannot be predicted our results indicate that in sandy soils less frequent irrigation at high input may lead to larger losses and this aspect needs to be considered in deciding irrigation management options with regard to input and frequency of application. For sandy soils similar to the one tested in this study frequent irrigations in small amounts, may be even twice in a day, seem to be more appropriate than once everyday.

We mentioned elsewhere in the text the impact of salinity on grain yield is questionable. To resolve this contradiction we conducted a stepwise multiple regression analysis with relative grain yield (Y_r) as a function of PR, EC_{sw}-gm, and EC_{sw}-ls, the analysis indicated that Y_r was mainly affected by PR. However, when we included in EC_{sw}-ls, which was marginally significant in the stepwise procedure the analysis produced a non-significant positive coefficient for EC_{sw}-ls, which is physically impossible. Thus the stepwise analysis conclusively indicated that grain yield depended only on PR, which depended both irrigation input (II) and irrigation frequency (IF) and described by the equation provided in Table 2.

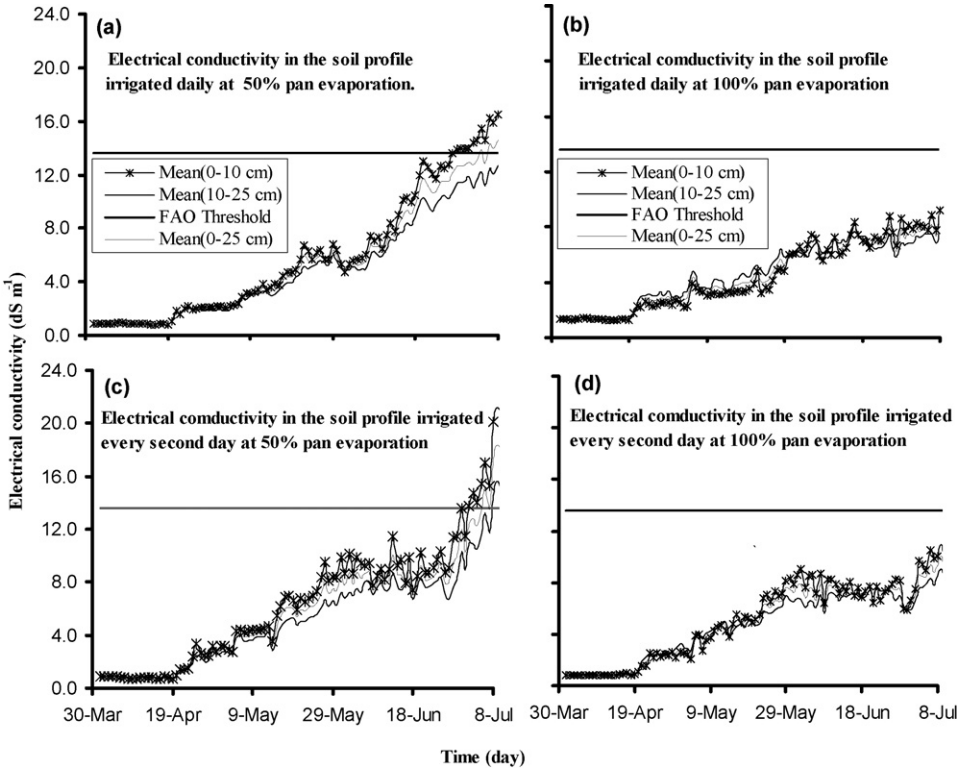

Fig. 4 – The mean electrical conductivity in different segments of the profile under different irrigation treatments compared with FAO threshold value of 13.6 dS m^{-1} for sorghum.

The simple linear correlation indicated that grain yield was impacted by the growing season mean EC_{sw} (Table 5). Earlier, based on the threshold salinity (EC_t) concept we indicated the impact of salinity stress on grain yield was marginal (Figs. 3 and 4). Thus, further clarification is needed in the impact of salinity stress on grain yield.

3.4.2. *Production functions for assessing salinity stress on yield*

Letey et al. (1985) proposed a model to predict salinity associated grain yield reductions. The model was based on three functional relationships, of which only one, yield versus growing season average EC_{sw}, can be directly applied in this study and this relationship is significant (Table 5). The other two functional relationships, yield versus cumulative ET_c, and average EC_{sw} versus leaching fraction (LF), cannot be tested due to unavailability of data. Therefore, we cannot use the yield model of Letey et al. (1985) in this study. Other secondary functional relationship proposed by these workers, yield versus total irrigation input, though proposed for non-saline water irrigation, was tested and produced a relationship significant only at $P < 0.10$ (Table 5), suggesting insufficient data and/or application frequency masking irrigation input impact. As mentioned elsewhere because the percolation losses in the dune sand was high, we tested the significance of yield versus the cumulative profile recharge (PR), a surrogate for irrigation input, and found the relationship produced the highest R^2 value compared with the other functional relations tested (Table 5).

To further explore salinity-induced grain yield reduction we adapted Maas and Hoffman (1977), M–H (1977) relationship between relative yield (Y_r) and average root-zone salinity. The average root-zone salinity in the original M–H formulation is based on the electrical conductivites of extracts obtained from saturated-soil pastes, which we replaced with the TDR monitored average electrical conductivity of soil water (EC_{sw}) and adapted equation is

$$Y_r = 100 - B(EC_{sw} - EC_t) \quad \text{for} \quad EC_{sw} > EC_t \tag{7}$$

By definition, Eq. (7) is applicable only when $EC_{sw} > EC_t$, therefore it can be applied only to late maturity stages of EP0.5 input treatments. The B in Eq. (7) is slope of the yield salinity curve and other terms have already been defined. By rearranging the terms in Eq. (7) for B, we computed B for EP0.5 treatment (Table 3). The computed B values may not be directly comparable to those reported in the literature, because EC_{sw} in Eq. (7) is soil water salinity value whereas in the original M–H formulation it is paste extract values.

The higher B values are indicative of more salinity stress and less Y_r and vice versa (Shalhevet, 1994). The B values (Table 3) indicate the impact of salinity on grain yield was higher in the daily irrigated EP0.5 than every second day irrigated EP0.5, but mean EC_{sw} for late maturity stage (Table 5) indicates the stress should have been larger in the every second day irrigated EP0.5 than the daily irrigated EP0.5. We are unable to provide any reason for this contradiction. However, in general, the production functions reported in literature were developed and tested using data from repeated application of saline water for several seasons or years (Letey et al., 1985).

The data sets gathered and tested to explore production functional relationships in our study appear to be rather small, as this greenhouse experiment was conducted for only one season.

It should be noted the salinity stress (Figs. 3 and 4) that was observed during the late maturity stage, in both the daily and every second day irrigated EP0.5, corresponded with decreases in ET_c (Fig. 2), which probably was met by profile recharge and therefore no water stress should have occurred during this period. This suggests the late maturity stage salinity stress might have contributed towards the reduction in Y_r in the EP0.5 treatments.

The data for every second day irrigated EP1.0 (Fig. 2d) suggest there was no water stress, because irrigation in general exceeded ET_c. The average EC_{sw} indicate there was no salinity stress in this treatment, the question now arises as to what caused the reduction in Y_r in every second day irrigated EP1.0. We propose at least two reasons. First, we have already shown the profile recharge was less than the input and substantial percolation losses (Table 2) occurred within 1–2 h after irrigation, thereby reducing the available soil water to cover the 2 consecutive days, particularly during the second day after irrigation. To resolve this issue one should have the water content data on the second day after irrigation and that at depths >25 cm unfortunately, we did not collect this data. Second, the water holding capacity of this dune sand is very low (0.05 $cm^3\ cm^{-3}$) and the water content in the 0–25 cm segment during the second day was probably insufficient to meet crop ET_c.

Because the experiment was conducted only for one growing season, it is not known whether repeated irrigation for several years may lead to gradual build up of salinity in this dune sand. Further studies are required and are in progress. In this regard leaching studies involving quality water, if available, or with saline water to leach out major proportion of the accumulated salt is suggested. The leaching may be carried out before seeding or after crop harvest. Either of the leaching practice may help to keep the soil resource sustainable even under saline water irrigation.

The marginal to no significant impact of salinity on grain yield is attributed to few unresolved issues. These are based on the observation that in general the average EC_{sw} in the soil profile is less than the salinity of irrigated water (EC_i). The discrepancy could be attributed to several reasons (i) underestimation by TDR; (ii) the rapid percolation carrying the salt below the monitored depth, through high conductivity of sand; (iii) salt accumulation on the surface (visual observation). Though, we suspect there was general under prediction of EC_{sw} by TDR, nevertheless the technology is sound for routine monitoring, but needs further fine tuning with regard to calibration, particularly for sandy soils with very low water holding capacity.

4. Conclusions

The grain yield of sorghum, grown on dune sand and irrigated with 7.32 dS m^{-1} saline water, indicated no water or salinity stress when the crop was irrigated daily at 100% of open-pan evaporation. On the other hand the crop was subjected to both

water and salinity stresses in the 50% open-pan input, regardless of whether the crop was irrigated daily or every second day. The unintended percolation below the root-zone was very high, particularly when dune sand was irrigated less frequently and at high input levels. The salinity stress in the 50% irrigation input appeared only during late maturity stage. The substantial yield reduction in the 100% open-pan input irrigated every second day, compared with the corresponding daily irrigation, is attributed to low water holding capacity and rapid percolation losses in this dune sand. Irrigation schedules based on open-pan measurement is relatively low-tech compared with that based on sophisticated profile water depletion or crop evapotranspiration (ET_c) computations. Therefore, we recommend the use of this approach for irrigation scheduling in situations where sophistication is limited. In general, we conclude that saline waters of salinity similar to that used in this study can be used for irrigating sorghum grown in sandy soils of semi-arid regions, e.g. Mauritania, at input levels at least equal to the open-pan evaporation and irrigated daily to reduce or minimize water and salinity stresses. For such an irrigation management option in sandy soils we recommend the use of drip irrigation system.

REFERENCES

Agodzo, S.K., Nishio, T., Yamamoto, T., 1997. Trickle irrigation of okra based on small pan evaporation schedule under glasshouse condition. Rural Environ. Eng. J. 33, 19–36.

Allen, R.G., Pereira, L.S., Raes, D., Smith, M., 1998. Crop evapotranspiration. FAO Irrigation and Drainage Paper 56. FAO, Rome.

Ayers, R.S., Westcot, D.W., 1985. Water quality for agriculture. FAO Irrigation and Drainage Paper 29. FAO, Rome.

Claudivan, F.L., José, C., Marco, A.O., Hugo, A.R., 2005. Changes in growth and in solute concentration in sorghum leaves and roots during salt stress recovery. Environ. Exp. Bot. 54, 69–76.

Dehghanisanij, H., Yamamoto, T., Inoue, M., 2004. I. Practical aspects of TDR for simultaneous measurements of water and solute in a dune sand field. J. Jpn. Soc. Soil Phys. 98, 21–30.

DeMalach, Y., Pasternak, D., 1993. Agriculture in a desert saline environment—a case study. In: Marani-Bettolo, G.B. (Ed). Agriculture and the Quality of Life—New Global Trends. In: Proceeding of an International Conference held at The Ponitificia Academia Scientiarum, Ex Aedibvs acadimicis in Civitate Vaticana, Rome, Italy, pp. 97–126.

Doorenbos, J., Pruitt, W.O., 1977. Crop water requirements. FAO Irrigation and Drainage Paper 24, Rome.

Fisher, R.A., 1980. Influence of water stress on crop yield in semiarid regions. In: Turner, N.C., Kramer, P.J. (Eds.), Crop Water Requirements. Conf., September 11–14 1984, Paris, INRA, Paris, pp. 221–234.

Gideon, O., DeMalach, Y., Gillerman, L., David, I., 1995. Pear response to saline water application under subsurface drip irrigation. In: Proceedings of the Fifth International Microirrgation Congress, Orlando, FL, April 2–6, pp. 97–103.

Gideon, O., DeMalach, Y., Gillerman, L., David, I., Lurie, S., 2002. Effect of water salinity and irrigation technology on yield and quality of pears. Biosyst. Eng. 81, 237–247.

Inoue, M., 2006. In: Proceedings of International Workshop on Research Progress and Current Issue of Unsaturation Processes in Vadose Zone, 16 December 2005. University of Tsukuba, Japan, p. 59.

Josserand, H., Silva, A., 2002. Special report FAO/WFP crop and food supply assessment mission to Mauritania, December 3 2002. Homepage http://www.fao.org/documents/show_cdr.asp?url_file=/docrep/005/y8163e/y8163e00.htm.

Katerji, N., van Hoorn, J.W., Hamdy, A., Mastrorilli, M., 2003. Salinity effect on crop development and yield analysis of salt tolerance according to several classification methods. Agric. Water Manage. 62, 37–66.

Letey, J., Dinar, A., 1986. Simulated crop-water production functions for several crops when irrigated with saline waters. HILGARDIA 54 (1), 1–31.

Letey, J., Dinar, A., Knapp, K.C., 1985. Crop-water production functions model for saline irrigation waters. Soil. Sci. Soc. Am. J. 49, 1005–1009.

Maas, E.V., Hoffman, G.J., 1977. Crop salt tolerance—current assessment. J. Irrig. Drain. Div. ASCE 103, 115–134.

Mastrorilli, M., Katerji, N., Rana, G., 1995. Water efficiency and stress on grain sorghum at different reproductive stage. Agric. Water Manage. 28, 23–34.

Ministère du développement rural, 1998. Raport de situation d'agrigulture. Nouakchott, Mauritania, pp. 4, unpublished.

Munns, R., 2002. Comparative physiology of salt and water stress. Plant Cell Environ. 25, 239–250.

Oster, J.D., 1994. Irrigation with poor quality water—review article. Agric. Water Manage. 25, 271–297.

Pasternak, D., DeMalach, Y., 1987.In: Saline water irrigation in the Negev Desert Paper presented at the Regional conference on Agriculture Food Production in the Middle-East, January 21-26, Athens, Greece, p. 24.

Rhoades, J.D., 1987. Use of saline water for irrigation. Water Qual. Bull. 12, 14–20.

Rhoades, J.D., Kandiah, A., Mashali, A.M., 1992. The use of saline waters for crop production. FAO Irrigation and Drainage Paper No. 48, Rome, Italy.

SAS, 1991. SAS/STAT Procedure Guide for Personnel Computers. Version 5. Statistical Analysis Systems Institute Inc., Cary, NC.

Shalhevet, J., 1991. Using water of marginal quality for crop production: major issues, water use efficiency in agriculture. In: Shalhevet, J., Cangmimg, L., Yuexian, X. (Eds.), Proceedings of the Binational China–Israel Workshop, Beijing, China. Peril publ. Rehovot, Israel, pp. 17–53.

Shalhevet, J., 1994. Using water of marginal quality for crop production: major issues. Agric. Water Manage. 25, 233–269.

Shani, U., Dudley, L.M., 2001. Field studies of crop response to water and salt stress. Soil Sci. Soc. Am. J. 65, 1522–1528.

SONADER, 1998. Rapport sur l'alcalinité des sols du périméter de Foum Gleita. Présentation à l'atelier de sensibilisaion sur les problémes de dégradation des sols à Foum Gleita, Nouakchott, Mauritania, pp. 6, unpublished.

Tanji, K.K., Kielen, N.C., 2002. Agricultural drainage water management in arid and semi-arid areas. FAO Irrigation and drainage paper No. 61. FAO, Rome.

Topp, C.G., Davis, J.L., Annan, A.P., 1980. Electromagnetic determination of soil water content: measurement in coaxial transmission lines. Water Resour. Res. 16, 574–582.

van Asten, P.J.A., Barbiéro, L., Wopereis, M.C.S., Maeght, J.L., van der Zee, S.E.A.T.M., 2003. Actual and potential salt-related soil degradation in an irrigated rice scheme in the Sahelian. Agric. Water Manage. 60, 13–32.

Yamamoto, T., Cho, T., 1978. Soil moisture content distribution in main root-zone and water application efficiency of crops-studies on trickle irrigation method in sand field. Trans. Jpn. Soc. Irrig. Drain. Reclam. Eng. 75, 33–40.

Available online at www.sciencedirect.com
ScienceDirect
Forest Ecology and Management 241 (2007) 84–90
Forest Ecology and Management
www.elsevier.com/locate/foreco

Comparison of litterfall production and leaf litter decomposition between an exotic black locust plantation and an indigenous oak forest near Yan'an on the Loess Plateau, China

Ryunosuke Tateno [a,*], Naoko Tokuchi [b], Norikazu Yamanaka [c], Sheng Du [c], Kyoichi Otsuki [d], Tetsuya Shimamura [e], Zhide Xue [f], Shengqi Wang [f], Qingchun Hou [g]

[a] *Faculty of Agriculture, Kagoshima University, Kagoshima 890-0065, Japan*
[b] *Field Science Education and Research Center, Kyoto University, Kyoto 606-8502, Japan*
[c] *Arid Land Research Center, Tottori University, Tottori 680-0001, Japan*
[d] *Faculty of Agriculture, Kyushu University, Fukuoka 861-2415, Japan*
[e] *Water Resources Research Center, Disaster Prevention Research Institute, Kyoto University, Uji 611-0011, Japan*
[f] *Northwest A & F University, Yangling, Shaanxi 712100, China*
[g] *Institute of Soil and Water Conservation, Chinese Academy of Sciences and Ministry of Water Resources, Yangling, Shaanxi 712100, China*

Received 6 April 2006; received in revised form 28 December 2006; accepted 29 December 2006

Abstract

Litterfall production, the amount of organic matter on the forest floor, and litter decomposition rates were studied in an exotic nitrogen (N)-fixing black locust (*Robinia pseudoacacia*) plantation and an indigenous non-N-fixing oak (*Quercus liaotungensis*) forest near Yan'an, on the Loess Plateau, China. The chemical composition of litterfall and soil was also examined. Litterfall production was similar in the two forests; however, the amount of N in litterfall was greater in the black locust plantation than in the oak forest because of the high N concentration of black locust leaves. The decomposition rate of black locust leaves was higher than that of oak leaves, most likely because of the higher N content of black locust leaves. These results suggested that N cycling was greater and faster in the black locust plantation than in the oak forest. However, faster decomposition caused the disappearance of the organic layer from the forest floor in the black locust plantation. Furthermore, despite greater N cycling in the black locust plantation, the soil N content was lower than in the oak forest. Our results indicated that the black locust plantation might be more susceptible to soil erosion than the oak forest. In addition, our study suggested that the black locust plantation had advantages in short-term N uptake, growth, and N cycling; however, it had disadvantages in soil development and regeneration and sustainable land management.

Keywords: Organic matter cycling; Nitrogen fixation; Revegetation; Semi-arid

1. Introduction

Exotic species have been widely introduced for revegetation of arid and semi-arid areas. Functional differences in exotic species often alter the productivity, decomposition, and nutrient and hydrological cycling of local ecosystems (Usher, 1988; Vitousek, 1990; Ohte et al., 2003). Revegetation has often caused other problems, such as groundwater deficits resulting from higher water consumption by the planted tree species (e.g. Ohte et al., 2003). Ohte et al. (2003) reported that the water use efficiency of an introduced *Salix* sp. was lower than that of indigenous species. As a result of the extravagant water use and deep rooting depth of *Salix* sp., areas dominated by this introduced tree tend to show groundwater deficits. Thus, it is important to investigate differences between exotic and indigenous species, not only in vegetation recovery ability, but also in terms of functional differences and their consequences.

On the Loess Plateau in the semi-arid region of central China, which is located in the middle reaches of the Yellow River and covers most parts of Shanxi, Gansu, Ninxia, Shaanxi, Henan, Inner Mongolia and Qinhai Provinces, the nitrogen (N)-fixing exotic black locust (*Robinia pseudoacacia*) has been widely used for revegetation (Zheng, 1985; Shan et al., 2003).

* Corresponding author. Tel.: +81 99 285 8572; fax: +81 99 285 8572.
E-mail address: tateno@agri.kagoshima-u.ac.jp (R. Tateno).

0378-1127/$ – see front matter © 2007 Elsevier B.V. All rights reserved.
doi:10.1016/j.foreco.2006.12.026

This species is native to North America and shows remarkable growth in semi-arid environments (Zheng, 1985; Shan et al., 2003). The water use efficiency and drought tolerance of this species are lower than that of indigenous species such as *Quercus liaotungensis* and *Acer stenolobum* (Yamanaka et al., 2006; Du et al., 2007a). Recently, it was reported that a ''dry soil horizon'' near the forest limit for dryness develops in black locust plantations, which results in wilting of the top of the crown and causes the deaths of individual trees (Hou et al., 1999; Wang et al., 2001). It is therefore necessary to reconsider the use of non-indigenous trees for revegetation. Although previous studies have reported on propagation, plantation techniques and the physiological behavior in relation to nutrient and water conditions (Li et al., 1996; Liu et al., 2003; Shan et al., 2003; Wang et al., 2003; Cao et al., 2005), N accumulation and cycling have not been examined for *R. pseudoacacia* in semi-arid areas. Production in semi-arid ecosystems is thought to be co-limited by N and water availability (Hooper and Johnson, 1999). Therefore, investigating the differences in organic matter and N cycling between indigenous forests and exotic plantations may be useful in determining alternate revegetation methods in this region.

In semi-arid ecosystems, soil organic matter and N pools tend to be small compared to the flux of organic matter and N from litterfall (Crawford and Gosz, 1982). Understanding the decomposition of litterfall is critical for predicting plant growth and N supply and cycling. Decomposition dynamics are strongly affected by biotic and abiotic factors (e.g., Swift et al., 1979). For example, decomposition and immobilization are closely related to leaf properties, such as the carbon (C) to N ratio and specific leaf area, which vary widely among species (Takeda et al., 1987; Hobbie, 1992; Berendse, 1994; Cornelissen, 1999; Osono and Takeda, 2001), and environmental conditions, such as soil moisture and temperature (e.g., Swift et al., 1979).

The balance between litter production and decomposition controls the development of the soil organic layer and the pattern of soil N accumulation. The soil organic layer plays a critical role in species regeneration in arid and semi-arid environments (Pugnaire et al., 1996; Barritt and Facelli, 2001). The presence of an organic layer has both negative and positive effects on understory development via plant regeneration processes, such as germination, growth, and mortality. Furthermore, the organic layer considerably increases the soil infiltration capacity and mitigates water and wind erosion (e.g., Pimentel and Kounang, 1998). Thus, organic matter and N-cycling dynamics are closely related to regeneration processes and soil development. Therefore, understanding organic matter and N-cycling dynamics within forests is important for both revegetation and sustainable land management in arid and semi-arid areas.

The objective of this study was to compare the organic matter turnover and N cycling between an indigenous oak forest and a black locust plantation. We investigated organic matter and N cycling, litter decomposition, and the accumulation of organic matter and N on the forest floor and in soil in both forest types. We discussed the merits and detriments of black locust plantations.

2. Materials and methods

2.1. Study sites

The study sites were located on Mt. Gonglushan, near Yan'an, Shaanxi Province, China (36°25.40′N, 109°31.53′E; 1353 m a.s.l.). On the Loess Plateau, the amount of precipitation and the occurrence of forest gradually decrease northwestward, and Yan'an is located in the forest–grassland zone (Cheng and Wan, 2002). The mean annual precipitation and air temperature during 1982–2003 were 514 mm and 10.2 °C, respectively, according to data from a local meteorological station. Details of the study site were given by Yamanaka et al. (2004) and Otsuki et al. (2005).

According to local farmers, this area was colonized 50–60 years ago and was cultivated after native oak forests were cleared. Cultivated lands in this area were not irrigated or fertilized and were cultivated for about 30 years. Black locust was planted on abandoned cultivated lands 20–30 years ago. Considerable numbers of trees from the remaining oak forests were cut for firewood and charcoal. According to tree-ring analyses, the oak forests comprised 55–60-year-old secondary forest and the black locust plantation was 29 years old at the time of this study (Table 1; Du et al., 2007b).

2.2. Vegetation census

Six study plots were placed in an artificial *R. pseudoacacia* plantation and an indigenous *Q. liaotungensis* forest in 2002. The species and diameter at breast height (DBH) were recorded for all trees >1 cm in DBH in each plot.

Table 1
Stand structure of study plots

Plot	Density (trees ha^{-1})	Mean DBH (cm)[a]	Max DBH (cm)	Mean height (m)[a]	Max height (m)	Total BA (m^2 ha^{-1})	Max age (yr)
Quercus liaotungensis							
Q0	2375	7.6 (5.5)	23.9	5.0 (2.0)	9.2	16.3	55
Q1	4188	4.3 (4.9)	29.4	5.2 (2.4)	11.1	14.1	59
Q2	2713	5.1 (5.1)	23.8	7.7 (2.3)	11.7	12.9	60
Robinia pseudoacacia							
R0	1713	8.6 (2.8)	15.3	8.2 (2.2)	12.8	22.1	27
R1	2736	10.0 (4.8)	20.7	9.0 (2.8)	13.6	24.0	–
R2	2736	10.6 (5.2)	24.6	8.3 (2.4)	11.6	26.1	–

[a] Mean (S.D.).

2.3. Litterfall collection

Ten 0.25 m^2 litter traps each were located in the black locust plantation and the oak forest. Litterfall was collected monthly from 2003 to 2004. All collections were sorted into leaves, twigs, and other organs, and dried at 70 °C for 72 h. Each fraction was weighed separately for each litter trap, ground into powder, and analyzed for total N and C content using an NC analyzer (NC-900; Shimadzu, Kyoto, Japan).

2.4. Analysis of organic and mineral soil layers

Five 1 m^2 subplots were established in each forest to estimate the extent of the soil organic layer. Organic matter was carefully collected by hand and weighed after drying at 70 °C for 72 h.

Mineral soil samples were collected from both forests. In each forest, one soil sample was collected from each of six depths (0–5, 5–10, 10–30, 30–50, 50–70, and 70–100 cm). The samples were divided into fine soil (grains < 2 mm in diameter), gravel (>2 mm), roots, and litter. Fine soil was ground into powder, and the total N and C contents were determined using an NC analyzer (NC-900; Shimadzu, Kyoto, Japan).

2.5. Litterbag method

The leaf litter decomposition rate was measured using a litterbag method. During the period of leaf fall, we collected newly fallen leaves from the forest floor and immediately dried them at 70 °C. We filled 2-mm mesh nylon litterbags (10 cm × 10 cm) with 2 g dry weight of leaf litter of *R. pseudoacacia* or *Q. liaotungensis*. Litterbags of each species were placed in both the black locust plantation and the oak forest on 20 November 2004. Litterbags were collected eight times: after 4, 5, 6, 7, 8, 9, 10, and 11 months. We collected 10 litterbags of each species from each forest at each sampling time. The samples were weighted after drying at 70 °C for 72 h, ground into powder, and stored in plastic bags until chemical analysis. Total N and C contents were determined using an NC analyzer (NC-900; Shimadzu, Kyoto, Japan).

The amounts of lignin contained in the leaf litter samples were estimated by gravimetry according to a standardized method using hot sulfuric acid digestion (King and Heath, 1967).

2.6. Statistical analysis

Decomposition constants (k) of leaf litter were calculated using the exponential decay model (Olson, 1963) as follows:

$$\frac{W_t}{W_0} = e^{-kt}$$

where W_0 is the original litter weight, and W_t is the litter weight after a given period of time t. The data used for the calculation of decomposition constants were the mean remaining weight of 10 replications at each collection date.

We compared the amount of litterfall and organic layer and the accumulation of N in the soil and the organic layer between the black locust plantation and the oak forest using t-tests. A two-way analysis of variance (ANOVA) was used to investigate the effect of species and soil depth on the soil N content. We used the software SPSS for Windows (SPSS Inc., Chicago, USA) for all statistical analyses.

3. Results

3.1. Stand structure

Stand structure of the study plots was summarized in Table 1. The mean DBH ranged from 8.6 to 10.6 cm in black locust plantations and from 4.3 to 7.6 cm in oak forests. The maximum DBH ranged from 15.3 to 24.6 cm in black locust plantations and from 23.8 to 29.4 cm in oak forests. The maximum height ranged from 11.6 to 13.6 m in black locust plantations and from 9.2 to 11.7 m in oak forests. The total basal area ranged from 22.1 to 26.1 $m^2\ ha^{-1}$ in black locust plantations and from 12.9 to 16.3 $m^2\ ha^{-1}$ in oak forests.

3.2. Litterfall production and N cycling

The amount of litterfall (mean ± S.D.) was 3.8 ± 0.6 t $ha^{-1}\ year^{-1}$ in the black locust plantation and 4.2 ± 1.1 t $ha^{-1}\ year^{-1}$ in the oak forest; however, this difference was not significant ($t = 1.1, p > 0.05$; Fig. 1a). The amount of leaf fall was 3.1 ± 0.5 t $ha^{-1}\ year^{-1}$ in the black locust plantation and 3.3 ± 0.5 t $ha^{-1}\ year^{-1}$ in the oak forest; again, this difference was not significant ($t = 0.83$, $p > 0.05$; Fig. 1a).

The amount of N in litterfall was significantly greater in the black locust plantation (56.5 ± 7.3 kg $ha^{-1}\ year^{-1}$) than in the oak forest (39.1 ± 15.5 kg $ha^{-1}\ year^{-1}$; $t = -3.20$, $p < 0.01$; Fig. 1b). Similarly, the amount of N in leaf fall was significantly greater in the black locust plantation (43.3 ± 4.9 kg $ha^{-1}\ year^{-1}$) than in the oak forest (25.5 ± 4.3 kg $ha^{-1}\ year^{-1}$; $t = -8.68$, $p < 0.001$; Fig. 1b).

The percentage of N in black locust and oak litterfall was 1.49 and 0.93%, respectively, and the percentage of N in black locust and oak leaf litter was 1.39 and 0.77%, respectively (Fig. 1c). The C:N ratio of black locust and oak litterfall was 31.9 and 58.4, respectively, and the C:N ratio of black locust and oak leaf litter was 29.7 and 48.3, respectively.

3.3. Decomposition rate

The decomposition rate, k, of *R. pseudoacacia* was 0.47 $year^{-1}$ in the black locust plantation and 0.48 $year^{-1}$ in the oak forest (Fig. 2). The k of *Q. liaotungensis* was 0.15 $year^{-1}$ in the black locust plantation and 0.21 $year^{-1}$ in the oak forest (Fig. 2). Thus, the k of *R. pseudoacacia* was greater than that of *Q. liaotungensis* in both forest types. However, the effect of forest type was less important than that of species.

Initial N contents of leaf litter used for litter bag experiment were 1.23 and 0.53% for *R. pseudoacacia* and *Q. liaotungensis*, respectively. Initial C:N ratio of leaf litter were 34.7 and 81.3

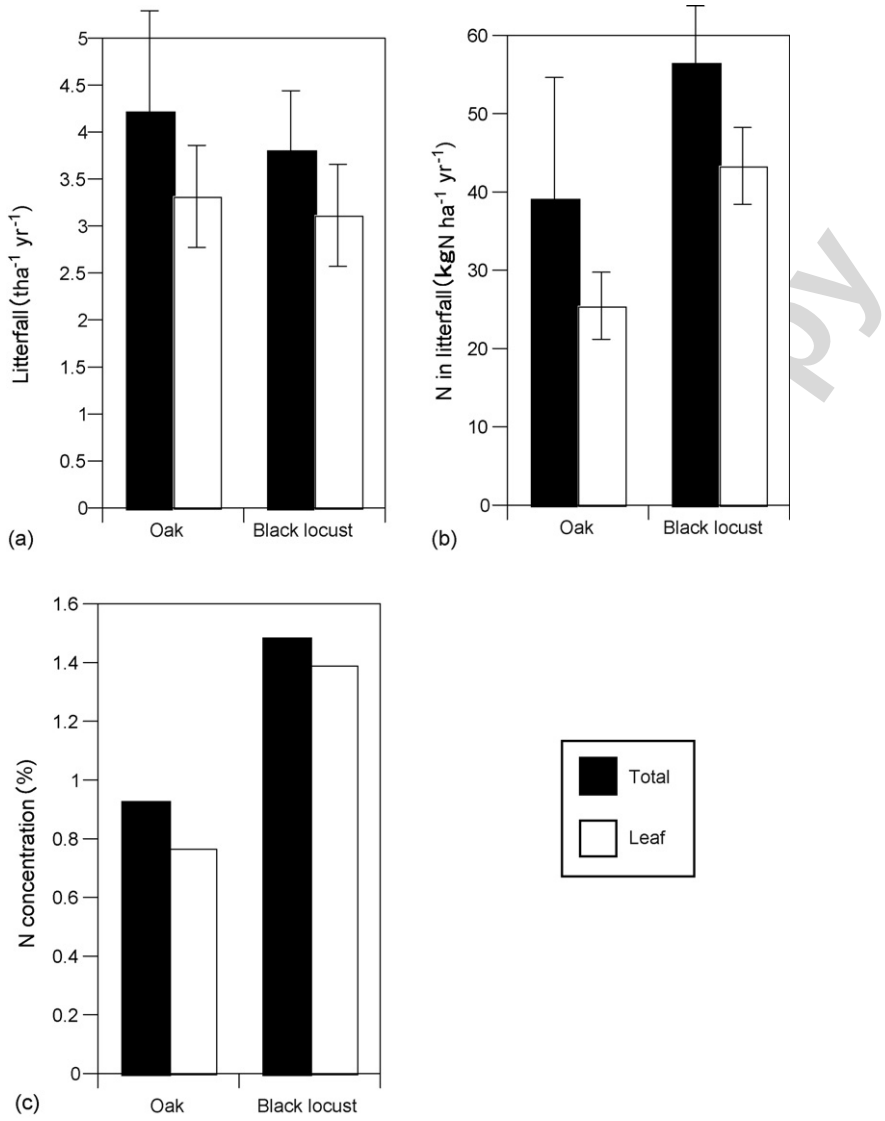

Fig. 1. (a) Amount of litterfall, (b) N in litterfall, and (c) the concentration of N in litterfall in an oak forest and a black locust plantation (mean ± S.D.). Black bars (■) indicate total litterfall; white bars (□) indicate leaf fall.

for *R. pseudoacacia* and *Q. liaotungensis*, respectively. Initial lignin content of leaf litter were 270.5 and 246.2 mg g^{-1} for *R. pseudoacacia* and *Q. liaotungensis*, respectively. Lignin to N ratio of leaf litter was 22.1 and 46.7 for *R. pseudoacacia* and *Q. liaotungensis*, respectively.

3.4. Amount of organic matter and N on the forest floor and in soil

Whereas both the semi-decomposed, fragmented organic matter layer (F horizon) and humus layer (H horizon) were developed in the oak forest, only the F horizon was observed in the black locust plantation. The total amount of organic matter on the forest floor was significantly lower in the black locust plantation (5.5 ± 1.1 t ha^{-1}) than in the oak forest (Fig. 3; 18.6 ± 4.0 t ha^{-1}; $t = 5.41$, $p < 0.05$). The estimated turnover rate (amount of organic matter on the forest floor/annual litter fall) of the forest floor was 1.4 years in the black locust plantation and 4.4 years in the oak forest.

N accumulation in the organic layer was 103 ± 13 kg N ha^{-1} in the black locust plantation and 199 ± 49 kg N ha^{-1} in the oak forest; however, this difference was not significant ($t = 2.675$, $p = 0.12$). The estimated turnover rate (annual litter fall/amount of organic matter on the forest floor) of the forest floor N was 1.8 years in the black locust plantation and 5.1 years in the oak forest. The C:N ratio of organic horizons in black locust plantations was 19.5. The C:N ratio of organic horizons in oak forests was 52.6 and 20.0 for F and H horizons, respectively.

The soil N and C contents decreased with soil depth in both forests (Fig. 4 a and b). The soil N contents were higher in the oak forest than in the black locust plantation. These differences were more obvious in the shallow soil layers than in the deep layers. The accumulation of N at a soil depth of 0–100 cm was 0.6627 ± 0.0876 kg N m^{-2} in the oak forest and 0.5619 ± 0.1676 kg N m^{-2} in the black locust plantation. The accumulation of C at a soil depth of 0–100 cm was 9.9663 ± 0.7464 kg C m^{-2} in the oak forest and 10.7560 ± 2.1576 kg C m^{-2} in the black locust plantation. For both the N and C

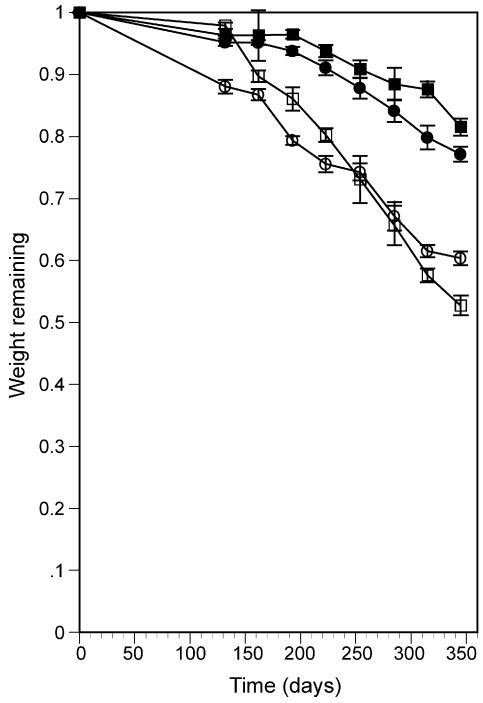

Fig. 2. Changes in the remaining weight of leaf litter during 12 months of decomposition in litter bags (mean ± S.E.). Open circles (OB) (○) and closed circles (OO) (●) indicate leaves of black locust and oak, respectively, placed in the oak forest; open squares (BB) (□) and closed squares (BO) (■) indicates leaves of black locust and oak, respectively, placed in the black locust plantation. The decomposition rate constants (k) were 0.21, 0.48, 0.15, and 0.47 for OO, OB, BO, and BB, respectively.

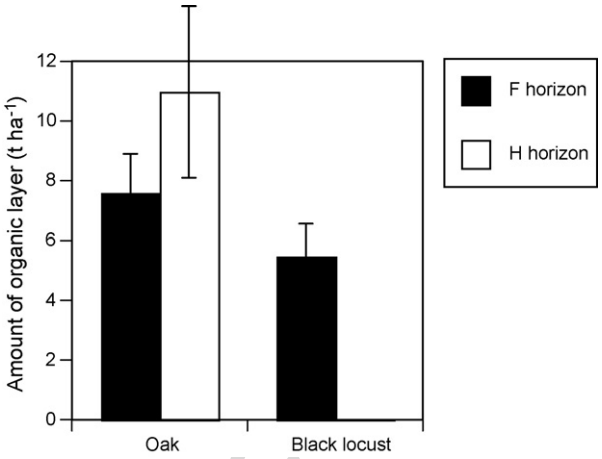

Fig. 3. Amount of the organic layer in the oak forest and black locust plantation (mean ± S.D.). Black bars (■) indicate the F horizon; white bars (□) indicate the H horizon.

accumulation at this depth, there were no significant differences between the black locust plantation and the oak forest ($t = 0.75$, $p = 0.49$ for N and $t - 0.49$, $p = 0.65$ for C). The soil C:N ratio increased with depth in both forests (Fig. 4c), and the soil C:N ratio was higher in the black locust forest than in the oak forest.

4. Discussion

The litterfall production rate was only slightly higher in the oak forest than in the black locust plantation. In general, the leaf

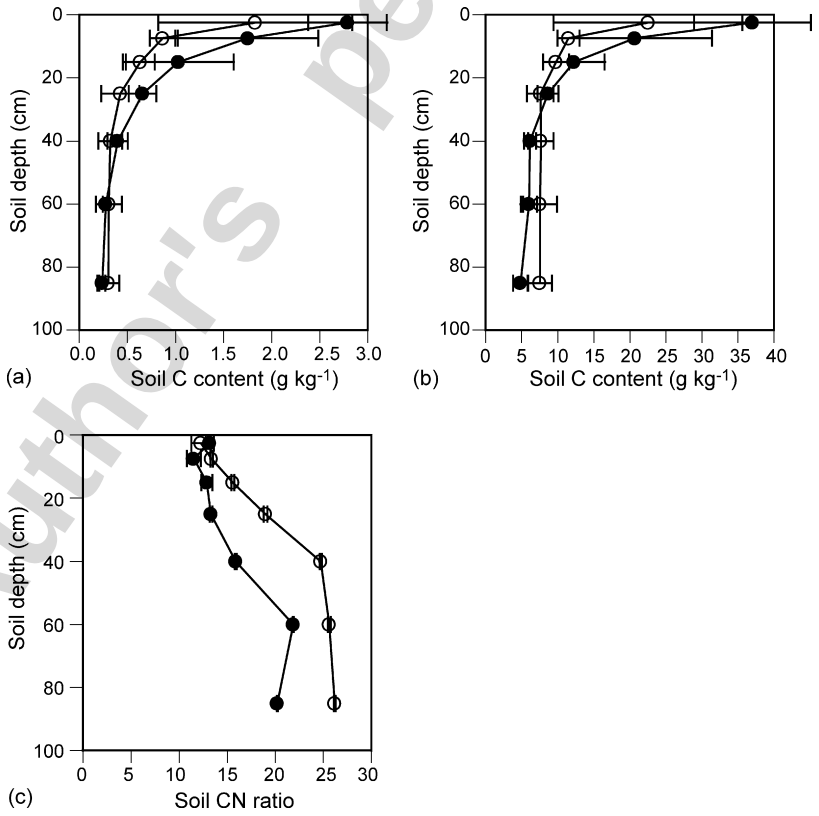

Fig. 4. (a) Soil N content, (b) soil C content, and (c) soil C:N ratio in the oak forest and black locust plantation. Closed circles (●) indicate oak forest; open circles (○) indicate black locust plantation (mean ± S.D.).

N concentration of N-fixing trees is higher than that of non-N-fixing trees (Killingbeck, 1996; Aerts and Chapin, 2000). We found a greater concentration of N in leaf litter of black locust than in that of oak. As a result, the annual N cycling via litterfall was higher in the black locust plantation than in the oak forest. The amount of N cycling in both sites was comparable to that of other ecosystems, such as wet temperate forests (Vitousek, 1982).

Decomposition is strongly affected by biotic and abiotic factors (Swift et al., 1979). Our results suggest that the quality of the leaf litter is more important than that of the site for litter decomposition. This may be primarily because the leaf C:N ratio and lignin/N ratio, which are good indicators of the decomposition rate (e.g., Swift et al., 1979), were lower in N-fixing species than in oak. These results are consistent with previous studies that have reported faster decomposition rates of N-fixing than non-N-fixing species (Aerts and Chapin, 2000). Recent studies reveals rapid initial decomposition does not always lead to low accumulation of organic matter. Forests with N-rich, rapidly decomposing litter often accumulate large amounts of organic matter, especially if the litter is rich in lignin (Berg et al., 1996). Differences in lignin contents between two species were far less than those of nitrogen contents, and it may suggest that differences in N content was major factor influences on decomposition rate in this study site. Furthermore, leaf anatomy also affects the decomposition rate (Cornelissen et al., 1999). Black locust leaves have a higher specific leaf area (SLA; unit leaf area per unit leaf mass) than oak leaves (Yamanaka et al., unpublished data), which may have contributed to the higher decomposition rate of black locust.

Site conditions, such as soil moisture, temperature and fertility, also affect decomposition (Swift et al., 1979; Schuur, 2001 but see Prescott, 1995). Otsuki et al. (2005) reported that the soil moisture content of this black locust plantation was significantly lower than that of the oak forest, which was caused by its sparser canopy. Furthermore, a higher soil temperature was recorded in the black locust plantation than in the oak forest (Otsuki et al., 2005). Despite differences in environmental conditions such as soil moisture and temperature, the forest type did not affect the decomposition rate in this study.

As reflected by differences in the decomposition rate between the species, there was a clear difference in soil organic matter accumulation between the forest types. Whereas both F and H horizons were observed in the oak forest, only an F horizon occurred in the black locust plantation. There were few seedlings and little understory vegetation in the black locust plantation, whereas many seedlings and abundant understory vegetation were evident in the oak forest (Yamanaka et al., 2004). In general, the accumulation of organic matter affects seedling recruitment and mortality (e.g., Barritt and Facelli, 2001). In the black locust forest, seedling mortality may be high because of the poorly developed organic layer. The differences in litterfall production, decomposition, and organic matter accumulation, which were mainly caused by functional differences in the N-use strategy of these two species, may be critical for the regeneration process in this area via the interrelationship between plant and soil systems.

Annual inputs of N to soil systems via litterfall were far greater in the black locust plantation than in the oak forest. Higher soil N accumulation by N-fixing trees has been reported in many forested ecosystems (Boring and Swank, 1984a,b; Sanginga, 1990; Danso et al., 1992). N-fixing trees often are planted as "fertilizers." For example, Boring and Swank (1984a) reported that 33–75 kg N ha^{-1} $year^{-1}$ N are fixed by symbiotic N-fixers and accumulated in the soil each year in the Appalachian Mountains, USA, where the annual precipitation is about 1800 mm. Because the forests studied here were about 30 years old, we expected that a substantial amount of N would have accumulated in the soil, even though a considerable amount had been removed by crop harvesting and erosion during the period of cultivation. However, we found no significant difference in soil N between the two forest types.

There are several possible explanations for this inconsistency. In arid and semi-arid environments, soil erosion caused by precipitation and/or wind tends to be more severe than in other ecosystems (Breshears et al., 2003). In particular, erosion tends to occur when there is no vegetation or humus cover (Pimentel and Kounang, 1998). Only an F layer was observed in the black locust plantation. The F horizon showed high temporal variation and was very small just before leaf fall. In contrast, the H horizon was quite stable. Thus, surface soil erosion may have caused low N and C accumulation in the surface soil of the black locust plantation. Furthermore, decomposed leaf litter may be blown away by wind. In this region, average of maximum daily wind strength from 19 March 2005 to 17 July 2005 were 1.9 ± 0.7 and 1.0 ± 0.5 m s^{-1} (mean $\pm$ S.D.) in the black locust plantation and in the oak forest, respectively (Otsuki et al. unpublished data). The decomposing black locust leaf litter was thinner and more fragmented than that of oak. Therefore, a considerable amount of leaves may be removed by wind especially in black locust plantations. Thus, the development of an organic soil layer via decomposition may have been prevented in the black locust plantation. In this area, where soil erosion caused by water and wind is severe, black locust plantations may not be effective as fertilizers.

In arid and semi-arid regions, revegetation is important for maintaining local environments and restraining the expansion of desert areas. Over the short term, the high growth rate and N-fixing ability of black locust under severe conditions may make this an advantageous species for revegetation (Zheng, 1985; Shan et al., 2003). If the N fixed by this species was effectively held in ecosystems via soil–plant systems, plantations of this species would be desirable. However, it appears that black locust plantations are disadvantageous, not only for soil development and regeneration, but also for sustainable land management. From the viewpoint of sustainability, black locust plantations should be gradually shifted to forests of indigenous tree species.

Acknowledgments

We received support from many institutes and individuals in the People's Republic of China. This work was supported in

part by the Japan Society for the Promotion of Science-Chinese Academy of Science (JSPS-CAS) Core-University Program "Researches on Combating Desertification and Developmental Utilization in Inland China."

References

Aerts, R., Chapin III, F.S., 2000. The mineral nutrition of wild plants revisited: a re-evaluation of processes and patterns. Adv. Ecol. Res. 30, 1–67.

Barritt, A.R., Facelli, J.H.M., 2001. Effects of *Casuarina pauper* litter and grove soil on emergence and growth of understorey species in arid lands of South Australia. J. Arid Environ. 49, 569–579.

Berendse, F., 1994. Litter decomposability—a neglected component of plant fitness. J. Ecol. 82, 187–190.

Berg, B., Ekbohm, G., Johansson, M.B., McClaugherty, C., Rutigliano, F., Virzo De Santo, A., 1996. Maximum decomposition limits of forest litter types. A synthesis. Can. J. Bot. 74, 659–672.

Boring, L.R., Swank, W.T., 1984a. The role of black locust (*Robinia pseudo-acacia*) in forest succession. J. Ecol. 72, 749–766.

Boring, L.R., Swank, W.T., 1984b. Symbiotic nitrogen fixation in regenerating black locust (*Robinia pseudoacacia* L.) stands. Forest Sci. 30, 528–537.

Breshears, D.D., Whicker, J.J., Johansen, M.P., Pinder, J.E., 2003. Wind and water erosion and transport in semi-arid shrubland, grassland and forest ecosystems: quantifying dominance of horizontal wind-driven transport. Earth Surf. Process. Landforms 28, 1189–1209.

Cao, S., Chen, L., Gao, W., 2005. Sylvicultural technique on three types of soil in hilly-gully regions of Loess Plateau. Chin. J. Ecol. 24, 1537–1542 1552 (in Chinese with English abstract).

Cheng, J.M., Wan, H.E., 2002. Vegetation Construction and Soil and Water Conservation in the Loess Plateau of China. China Forestry Publishing House, Beijing (in Chinese).

Cornelissen, J.H.C., Pérez-Harguindeguy, N., Díaz, S., Grime, J.P., Marzano, B., Cabido, M., Vendramini, F., Cerabolini, B., 1999. Leaf structure and defence control litter decomposition rate across species and life forms in regional floras on two continents. New Phytol. 143, 191–200.

Crawford, C.S., Gosz, J.R., 1982. Desert ecosystems: their resources in space and time. Environ. Conser. 9, 181–196.

Danso, S.K.A., Bowen, G.D., Sanginga, N., 1992. Biological nitrogen in trees in agroecosystems. Plant Soil 141, 177–196.

Du, S., Yamanaka, N., Yamamoto, F., Han, R., Liang, Z., Hou, Q., 2007a. Photosynthesis and water relations in two tree species from the Chinese Loess Plateau under moisture stress. In: El-Beltagy, A., Saxena, M.C., Wang, T. (Eds.), Human and Nature—Working Together for Sustainable Development in Drylands, Proceedings of Eighth International Conference on Development of Drylands, February 25–28, 2006, Beijin, China. ICARDA, Aleppo, Syria, in press.

Du, S., Yamanaka, N., Yamamoto, F., Otsuki, K., Wang, S., Hou, Q., 2007b. The effect of climate on radial growth of *Quercus liaotungensis* forest trees in Loess Plateau, China. Dendrochronologia, in press.

Hobbie, S.E., 1992. Effects of plant species on nutrient cycling. Trends Ecol. Evol. 7, 336–339.

Hooper, D.U., Johnson, L., 1999. Nitrogen limitation in dryland ecosystems: responses to geographical and temporal variation in precipitation. Biogeochemistry 46, 247–293.

Hou, Q.C., Han, R.L., Han, S.F., 1999. A preliminary study on dry soil layer of artificial forest land on the loess plateau. Soil Water Conser. China 5, 11–14 (in Chinese).

Killingbeck, K.T., 1996. Nutrients in senesced leaves: keys to the search for potential resorption and resorption proficiency. Ecology 77, 1716–1727.

King, H.G.C., Heath, G.W., 1967. The chemical analysis of small samples of leaf material and the relationship between the disappearance and composition of leaves. Pedobiologia 7, 192–197.

Li, H.J., Wang, M.B., Chen, L.F., Chai, B.F., 1996. Study on hydrologic ecology of *Robinia pseudoacacia* plantation in northwestern Shanxi. Acta Phytoecol. Sin. 20, 151–158 (in Chinese).

Liu, S.M., Chen, H.B., Sun, C.Z., Sun, B.Y., 2003. A study of the drought resistance of the main forestation trees in loess plateau. J. Northwest Sci.-Tech. Univ. Agric. Forest. 31, 149–153 (in Chinese).

Ohte, N., Koba, K., Yoshikawa, K., Sugimoto, A., Matsuo, N., Kabeya, N., Wang, L., 2003. Water utilization of natural and planted trees in the semiarid desert of inner Mongolia, China. Ecol. Appl. 13, 337–351.

Olson, 1963. Energy storage and the balance of producers and decomposers in ecological systems. Ecology 44, 322–331.

Osono, T., Takeda, H., 2001. Organic chemical and nutrient dynamics in decomposing beech leaf litter in relation to fungal ingrowth and succession during 3-year decomposition processes in a cool temperate deciduous forest in Japan. Ecol. Res. 16, 649–670.

Otsuki, K., Yamanaka, N., Du, S., Yamamoto, F., Xue, Z., Wang, S., Hou, Q., 2005. Seasonal changes of forest ecosystem in an artificial forest of *Robinia pseudoacacia* in the Loess Plateau in China. J. Agric. Meteorol. 60, 613–616.

Pimentel, D., Kounang, N., 1998. Ecology of soil erosion in ecosystems. Ecosystems 1, 416–426.

Prescott, C.E., 1995. Does nitrogen availability control rates of litter decomposition in forests? Plant Soil 168–169, 83–88.

Pugnaire, F.I., Haase, P., Puigdefabregas, J., 1996. Facilitation between higher plant species in a semiarid environment. Ecology 77, 1420–1426.

Sanginga, N., 1990. Influence of reference trees on N2 fixation estimates in *Leucaena lecocephala* and *Acacia albida* using 15N labeling techniques. Biol. Fertil. Soils 9, 341–346.

Schuur, E.A., 2001. The effect of water on decomposition dynamics in mesic to wet Hawaiian montane forests. Ecosystems 4, 259–273.

Shan, C.J., Liang, Z.S., Hao, W.F., 2003. Review on growth of locust and soil water in loess plateau. Acta Bot. Boreal-Occident Sin. 23, 1341–1346 (in Chinese).

Swift, M.J., Heal, O.W., Anderson, J.M., 1979. Decomposition in terrestrial ecosystems. Studies in Ecology, vol. 7. Blackwell, Oxford, pp. 372.

Takeda, H., Ishida, Y., Tsutsumi, T., 1987. Decomposition of leaf litter in relation to litter quality and site conditions. Memoirs College Agri. Kyoto Univ. 13, 17–38.

Usher, M.B., 1988. Biological invasions of nature reserves: a search for generalizations. Biol. Conser. 44, 119–135.

Vitousek, P.M., 1982. Nutrient cycling and nutrient use efficiency. Am. Nat. 4, 553–572.

Vitousek, P.M., 1990. Biological invasions and ecosystem processes: towards an integration of population biology and ecosystem studies. Oikos 57, 7–13.

Wang, L., Shao, M.A., Hou, Q.C., 2001. The analysis of dried soil layer of artificial *Robinia pseudoacacia* forestry land in the Yan'an experimental area. Acta Bot. Boreal-Occident Sin. 21, 101–106 (in Chinese).

Wang, H.Z., Han, R.L., Ran, L.G., Qi, W.J., Wang, P.Z., 2003. Effect of different soil water state contents on water status of *Quercus liaotungensis* and *Acer stenolobum* var. *megalophyllum*. J. Northwest Forest. Univ. 18, 1–5 (in Chinese).

Yamanaka, N., Du, S., Yamamoto, F., Otsuki, K., Xue, Z., Wang, S., Hou, Q., 2004. Differences in understory species diversity between artificial Robinia forests and natural Quercus forest in Loess Plateau near Yanan, China. In: Proceeding of Core University Program Japan-China Joint Open Seminar on Combating Desertification and Development in Inland China of Year 2004, ALRC, Tottri, Japan, pp. 55–56.

Yamanaka, N., Yamamoto, F., Du, S., Otsuki, K., Xue, Z., Han, R., Liang, Z., Hou, Q., 2006. Leaf water potential of 14 woody species in the Loess Plateau near Yan'an, China. J. Jpn. Soc. Reveg. Technol. 32, 143–148 (in Japanese with English abstract).

Zheng, W.J., 1985. Tree Flora of China, vol. 2. China Forestry Publishing House, Beijing (in Chinese).

Soil Science and Plant Nutrition (2007) 53, 471–479 doi: 10.1111/j.1747-0765.2007.00157.x

ORIGINAL ARTICLE

Effect of K-type and Ca-type artificial zeolites applied to high sodic soil on the growth of plants different in salt tolerance

Mina YAMADA[1], Hideyasu FUJIYAMA[2], Tsuneyoshi ENDO[2], Maki Uehira RIKIMARU[2], Yoko SASAKI[2], Sadahiro YAMAMOTO[2], Toshimasa HONNA[2] and Tahei YAMAMOTO[1]

[1]*Arid Land Research Center, Tottori University, Tottori 680-0001 and* [2]*Faculty of Agriculture, Tottori University, Tottori 680-8553, Japan*

Abstract

The present study aimed to investigate the effects of K-type and Ca-type artificial zeolites on the growth and water and element absorptions of kidney bean (*Phaseolus vulgaris* L.), tomato (*Lycopersicon esculentum* Mill), maize (*Zea mays* L.) and beet (*Beta vulgaris* L.) in high sodic soil. Tottori sand dune soil, which was used as a control, was converted to high sodic soil mixed with salts. Each type of zeolite was mixed into the high sodic soil at rates of 0, 1, 2 and 5%. The results showed that kidney bean, tomato and maize died in high sodic soil 25–27 days after transplanting (DAT), whereas beet survived, although its growth was extremely suppressed at 26 DAT. The addition of Ca-type zeolite improved growth in all of the tested plants. Even 4 DAT the growth of beet was improved by recovery of water absorption, and growth of tomato was improved by recovery of Ca and K absorptions and cation balance, and restriction of Na absorption. Growth of kidney bean and maize improved at 11 or 13 DAT by recovery of water absorption and Ca and K absorptions. After 4 DAT, water absorption and P and K absorptions of beet were highly recovered compared with those of the other plants; beet growth improved to a large degree. The ameliorative effect of 5% Ca-type zeolite was lower than that of 2% in tomato, maize and beet because the excessive uptake of Ca restricted P transport from root to shoot, and high electrical conductivity of the soil solution restricted water uptake. Even 1% K-type zeolite addition suppressed growth of beet at 4 DAT, and the addition of 2% or 5% of K-type zeolite suppressed the growth of tomato and maize 11 or 13 DAT. Higher concentrations of HCO_3^- and CO_3^{2-}, and pH of the soil solution of K-type zeolite treatments might inhibit water absorption by roots.

Key words: artificial zeolite, element absorption, pH, sodic soils, water absorption.

INTRODUCTION

Salinization and sodication of soils are major problems in farming in arid and semi-arid regions. The low osmotic potential in saline soil (electrical conductivity > 4 dS m^{-1}) inhibits water uptake by plants (Lea-Cox and Syvertsen 1993). Plant growth is extremely restricted in sodic soil (exchangeable sodium percentage > 15 and pH > 8.5) by the toxicity of Na and B (Maas 1984), by the decrease in K, Ca and Mg uptake (Bernstein *et al.* 1974, Perez-Alfocea *et al.* 1993), and by the low availability of Fe, Mn, Zn and Cu (Page *et al.* 1996).

The disposal of coal fly ash, which is generated in thermal power plants, is a serious environmental problem (Clarke 1994). As the artificial zeolite that is produced from coal ash is abundant in Ca and/or K, we expect that the addition of zeolite can ameliorate plant growth in sodic soils. The addition of K and Ca has been shown to ameliorate plant growth in high Na conditions (Grieve and Fujiyama 1987).

Most studies related to the hazards of NaCl (Grattan and Grieve, 1999) and the response of plants to Na have been investigated using solution cultures. However, solution culture cannot reproduce the soil condition. We reproduced sodic soils with high concentrations of Na^+, CO_3^{2-} and HCO_3^- from sandy soil. The addition of

Correspondence: H. FUJIYAMA, Faculty of Agriculture, Tottori University, 4-101 Koyama Minami, Tottori 680-8553, Japan. Email: fujiyama@muses.tottori-u.ac.jp

Received 25 December 2006.

Accepted for publication 7 April 2007.

5% (w/w) of both zeolites improved growth in beet, which is salt tolerant and grows in a wide range of sodicity levels (Yamada *et al.* 2002) and Ca-type zeolite saved maize (moderately salt sensitive) and can be grown in high sodic soils (M. Yamada *et al.*, unpubl. data, 2000). However, the ameliorative effect of zeolites at an early stage remains unclear because, in general, any effects were analyzed approximately 50 days after transplanting. In the present study, therefore, the effect of zeolites on plant growth was investigated from 4 days to 4 weeks after transplanting. Application of artificial zeolite is attractive if it can improve the growth of glycophytes, which are generally salt sensitive. In this study, we also examined tomato and kidney bean, which are moderately salt sensitive and salt sensitive, respectively (Maas 1984). As the addition of 5% K-type, and Ca-type zeolite in particular, was excessive for maize growth in a low sodic soil (M. Yamada *et al.*, unpubl. data, 2000), we included treatments of 1% and 2% of both types of zeolites in this study.

MATERIALS AND METHODS

Preparation and chemical analysis of soil

The experimental set up for the current study was similar to that described by Yamada *et al.* (2002). Tottori sand dune soil was used for this experiment. The soil was converted into saline high sodic soil (HSO) by adding 0.2, 0.2 and 1.5 cmol kg^{-1} $CaCl_2 \cdot 2H_2O$, $MgSO_4 \cdot 7H_2O$ and Na_2CO_3, respectively. A non-sodicated control soil (CO) was also included. Air-dried K-type or Ca-type zeolites (Kimura Chemical Plants, Amagasaki City, Japan) were uniformly applied to the HSO at rates of 1, 2 and 5% (equivalent to 10, 20 and 50 g kg^{-1}). These treatments were denoted as KZ1, KZ2 and KZ5 and CAZ1, CAZ2 and CAZ5, respectively. Four kilograms of soil was placed into each 4 L pot. Basal doses of NH_4NO_3, $NH_4H_2PO_4$ and K_2SO_4 were also applied at rates of 0.36, 0.18 and 0.13 cmol kg^{-1} soil. Potassium was not applied in the KZ treatments. The treatments were replicated four times. The pH, electrical conductivity (EC) and concentration of cations and anions in both zeolites and those for saturation extracts of soils before plant cultivation were measured and the exchangeable sodium percentage (ESP) was calculated as described previously (Yamada *et al.* 2002).

Cultivation and chemical analysis of plants

Kidney bean (*Phaseolus vulgaris* L. cv. Naaru), tomato (*Lycopersicon esculentum* Mill cv. Saturn), maize (*Zea mays* L. cv. Yellow dent) and beet (*Beta vulgaris* L. cv. Sugarmangold) were grown in the glass-dome of the Arid Land Research Center, Tottori University, Tottori, Japan, where the maximum temperature was kept below 30°C in 2000. Seeds were sown in 6 cm diameter vinyl pots filled with CO soils and then seedlings were transplanted to the 4 L pots. One to 15 shoots were harvested at 4 days after transplanting (DAT), 11 or 13 DAT (11–13 DAT) and 25, 26 or 27 DAT (25–27 DAT). At the last sampling, the roots were also harvested. The sowing, transplanting and sampling dates are shown in Table 1. Fresh and dry weights of plant species were measured and the water deficit (WD) of shoots was calculated as described previously (Yamada *et al.* 2002). The K, Na, Ca and Mg concentrations (cmol kg^{-1}, hereafter referred to by the element name with a subscript c) of shoots and roots were measured as described previously (Yamada *et al.* 2002) at 4 DAT and 25–27 DAT. The P concentration (P_c) of shoots and roots was determined by the vanado-molybdate yellow method. The concentration ratios of Na to K, Ca and Mg of shoots were calculated at 4 DAT and the ratio of Na to (K + Ca + Mg) was also calculated at 25–27 DAT. The relative dry weight and mineral uptakes of each treatment to CO were calculated at 25–27 DAT. Data were analyzed statistically and the means were compared using Duncan's new multiple range test ($P < 0.05$).

RESULTS

Chemical properties of soil

In HSO, the Na^+, CO_3^{2-} and HCO_3^- concentrations for saturation extracts were extremely high, whereas the Ca^{2+}, Mg^{2+} and K^+ concentrations were lower than those in CO (Table 2). The CAZ treatments increased cation concentrations and decreased CO_3^{2-} and HCO_3^- concentrations,

Table 1 Date of sowing, transplanting and sampling of each plant species in 2000

Plant	Sowing	Transplanting	Sampling		
			1st	2nd	3rd
Kidney bean	30-Aug	8-Sep	12-Sep (4)	19-Sep (11)	4-Oct (26)
Tomato	3-Aug	31-Aug	4-Sep (4)	11-Sep (11)	25-Sep (25)
Maize	5-Aug	11-Aug	15-Aug (4)	24-Aug (13)	7-Sep (27)
Beet	25-Aug	14-Sep	18-Sep (4)	27-Sep (13)	10-Oct (26)

Numbers in parentheses refer to the days after transplanting.

Table 2 Chemical properties of the soils before cultivation

	Concentration ($cmol_c\ kg^{-1}$) for saturation extracts								EC			
	K^+	Na^+	Ca^{2+}	Mg^{2+}	Cl^-	NO_2^-	NO_3^-	SO_4^{2-}	CO_3^{2-}	HCO_3^-	($dS\ m^{-1}$)	pH	ESP	Classification
CO	0.15 b	0.06 a	0.44 c	0.51 c	0.31 b	0.00 a	0.29 c	0.55 e	0.000 a	0.01 a	3.9 a	6.23 a	−5 a	nSa • nSo
HSO	0.04 a	1.43 b	0.00 a	0.00 a	0.36 b	0.00 a	0.28 c	0.60 f	0.015 c	0.26 d	5.2 c	9.93 d	78 g	Sa • So
HSO-KZ1	0.04 a	1.37 b	0.01 a	0.01 a	0.09 a	0.07 b	0.05 a	0.07 a	0.024 d	0.26 d	3.9 a	9.89 d	58 e	nSa • So
HSO-KZ2	0.08 ab	1.45 b	0.01 a	0.00 a	0.09 a	0.07 b	0.05 a	0.07 a	0.035 e	0.28 e	4.2 a	10.03 d	62 e	Sa • So
HSO-KZ5	2.36 b	1.20 b	0.00 a	0.00 a	0.34 b	0.00 a	0.29 c	0.41 c	0.062 f	0.34 f	5.0 b	10.43 e	69 f	Sa • So
HSO-CAZ1	0.07 ab	2.43 d	0.08 b	0.02 a	0.16 a	0.12 d	0.09 b	0.12 b	0.008 b	0.13 c	6.5 d	8.39 c	46 d	Sa • So
HSO-CAZ2	0.07 ab	1.93 c	0.08 b	0.02 a	0.13 a	0.10 c	0.07 ab	0.09 ab	0.008 b	0.13 c	5.6 c	8.52 c	39 c	Sa • So
HSO-CAZ5	0.10 ab	2.42 d	0.71 d	0.07 b	2.15 c	0.00 a	0.30 c	0.47 d	0.000 a	0.05 b	9.8 e	7.95 b	22 b	Sa • So

Different letters indicate significant differences at $P < 0.05$ using Duncan's new multiple range test. CO, control soil; HSO, high sodic soil; KZ1, KZ2, KZ5, CAZ1 CAZ2 and CAZ5, 1, 2 and 5% (w/w) K-type or Ca-type zeolite treatments, respectively; EC, electrical conductivity; ESP, exchangeable sodium percentage; nSa • nSo, non-saline • non-sodic soil (EC < 4.0 and ESP < 15); nSa • So, non-saline • sodic soil (EC<4.0 and ESP>15); Sa • So, saline • sodic soil (EC > 4.0 and ESP > 15) (US Salinity Laboratory Staff 1954).

ESP and pH. The CAZ5 doubled the EC level of the soil compared with HSO. The KZ treatments increased the CO_3^{2-} and HCO_3^- concentration and decreased the Cl^- and SO_4^{2-} concentration and EC for saturation extracts of soil. In HSO-KZ2 and HSO-KZ5, the pH was higher than 10.

Plant growth

Even by 4 DAT, the shoot dry weight of maize and beet in HSO was significantly smaller than in CO (Table 3). At 11–13 DAT, the relative dry weight of whole plants of beet, tomato, kidney bean and maize in HSO to CO was 0.36, 0.36, 0.20 and 0.18. After 11–13 DAT, the

Table 3 Dry weight (g $plant^{-1}$) of the shoots and roots of the plants

	Shoots	Shoots	Shoots	Roots
Kidney bean	4 DAT	11 DAT	26 DAT	26 DAT
CO	0.086 a	0.303 d	1.49 b	0.336 c
HSO	0.073 a	0.062 a	dead	dead
HSO-KZ1	0.076 a	0.081 ab	dead	dead
HSO-KZ2	0.078 a	0.084 ab	dead	dead
HSO-KZ5	0.074 a	0.069 a	dead	dead
HSO-CAZ1	0.079 a	0.115 bc	0.24 a	0.031 b
HSO-CAZ2	0.085 a	0.131 c	0.28 a	0.077 b
HSO-CAZ5	0.081 a	0.119 bc	0.28 a	0.068 a
Tomato	4 DAT	11 DAT	25 DAT	25 DAT
CO	0.032 ab	0.140 d	1.12 c	0.120 c
HSO	0.029 ab	0.051 a	dead	dead
HSO-KZ1	0.033 b	0.038 a	dead	dead
HSO-KZ2	0.027 a	0.031 a	dead	dead
HSO-KZ5	0.031 ab	0.025 a	dead	dead
HSO-CAZ1	0.034 b	0.089 b	0.28 a	0.059 b
HSO-CAZ2	0.040 c	0.100 c	0.36 b	0.051 b
HSO-CAZ5	0.031 ab	0.073 b	0.23 a	0.031 a
Maize	4 DAT	13 DAT	27 DAT	27 DAT
CO	0.075 d	0.499 d	3.47 c	1.90 b
HSO	0.059 bc	0.091 a	dead	dead
HSO-KZ1	0.055 b	0.082 a	dead	dead
HSO-KZ2	0.052 ab	0.077 a	dead	dead
HSO-KZ5	0.045 a	0.071 a	dead	dead
HSO-CAZ1	0.066 cd	0.242 c	0.83 a	0.54 a
HSO-CAZ2	0.066 cd	0.270 c	1.33 b	0.84 a
HSO-CAZ5	0.052 ab	0.181 b	0.69 a	0.49 a
Beet	4 DAT	13 DAT	26 DAT	26 DAT
CO	0.023 d	0.095 d	0.437 d	0.102 cd
HSO	0.014 b	0.034 b	0.066 b	0.012 a
HSO-KZ1	0.010 a	0.014 a	0.032 ab	0.005 a
HSO-KZ2	0.010 a	0.013 a	0.022 a	0.003 a
HSO-KZ5	0.009 a	0.012 a	0.013 a	0.002 a
HSO-CAZ1	0.019 c	0.072 c	0.304 c	0.095 c
HSO-CAZ2	0.017 c	0.075 c	0.337 c	0.121 d
HSO-CAZ5	0.017 bc	0.065 c	0.305 c	0.072 b

Different letters indicate significant differences at $P < 0.05$ using Duncan's new multiple range test. CO, control soil; HSO, high sodic soil; KZ1, KZ2, KZ5, CAZ1 CAZ2 and CAZ5, 1, 2 and 5% (w/w) K-type or Ca-type zeolite treatments, respectively; DAT, days after transplanting.

Table 4 Water deficit (%) of plant shoots

	4 DAT	11 DAT	26 DAT
Kidney bean			
CO	0.00 a	0.00 a	0.00 a
HSO	3.23 cd	24.5 bc	–
HSO-KZ1	3.17 bcd	13.1 d	–
HSO-KZ2	3.93 d	39.0 cd	–
HSO-KZ5	4.40 d	30.9 d	–
HSO-CAZ1	1.09 ab	−0.70 ab	4.48 a
HSO-CA72	1.48 abc	−0.85 ab	−0.52 a
HSO-CAZ5	1.71 abc	−0.74 ab	−1.38 a
Tomato			
CO	0.00 a	0.00 a	0.00 a
HSO	1.22 ab	2.30 b	–
HSO-KZ1	2.36 c	5.80 b	–
HSO-KZ2	3.32 d	3.76 b	–
HSO-KZ5	3.69 d	4.81 b	–
HSO-CAZ1	0.85 ab	1.15 a	0.26 a
HSO-CAZ2	0.96 ab	1.20 a	0.16 a
HSO-CAZ5	1.14 b	1.93 a	−1.87 a
Maize			
CO	0.00 a	0.00 a	0.00 a
HSO	2.87 c	7.90 b	–
HSO-KZ1	3.63 cd	7.77 b	–
HSO-KZ2	4.03 d	9.94 b	–
HSO-KZ5	5.50 e	8.20 b	–
HSO-CAZ1	3.29 cd	2.12 a	−0.67 a
HSO-CAZ2	1.86 b	1.64 a	1.02 a
HSO-CAZ5	3.80 cd	2.62 a	0.97 a
Beet			
CO	0.00 a	0.00 a	0.00 a
HSO	2.49 a	5.58 a	1.35 ab
HSO-KZ1	6.69 b	14.0 b	3.14 ab
HSO-KZ7	11.0 d	23.0 c	4.00 b
HSO-KZ5	15.8 e	28.0 c	9.82 c
HSO-CAZ1	0.26 a	0.09 a	−0.22 a
HSO-CAZ7	0.16 a	−0.18 a	−0.26 a
HSO-CAZ5	0.62 a	0.53 a	0.67 ab

Different letters indicate significant differences at $P < 0.05$ using Duncan's new multiple range test. CO, control soil; HSO, high sodic soil; KZ1, KZ2, KZ5, CAZ1 CAZ2 and CAZ5, 1, 2 and 5% (w/w) K-type or Ca-type zeolite treatments, respectively; DAT, days after transplanting.

Table 5 Concentration of elements (cmol kg^{-1}) in plant shoots 4 days after transplanting

	P	K	Na	Ca	Mg
Kidney bean					
CO	7.79 bc	99.4 b	1.08 a	26.9 d	32.1 d
HSO	8.01 c	68.8 a	72.0 cd	7.50 a	12.6 a
HSO-KZ1	7.10 ab	70.3 a	45.9 bc	7.50 a	11.7 a
HSO-KZ2	7.28 abc	76.4 a	90.1 d	8.98 a	14.7 b
HSO-KZ5	6.97 ab	75.1 a	68.0 cd	9.36 a	12.6 a
HSO-CAZ1	7.58 abc	94.7 b	14.0 a	17.0 b	19.8 c
HSO-CAZ2	7.05 ab	99.6 b	7.89 a	21.7 c	19.8 c
HSO-CAZ5	6.87 a	103 b	6.39 a	36.7 e	20.5 c
Tomato					
CO	8.37 b	106 c	13.2 a	46.2 c	62.5 d
HSO	8.69 b	49.5 a	162 c	28.6 a	36.4 ab
HSO-KZ1	8.32 b	53.5 a	156 c	24.5 a	34.5 a
HSO-KZ2	8.25 b	53.8 a	167 c	26.5 a	33.7 a
HSO-KZ5	8.00 b	66.1 b	166 c	26.0 a	33.8 a
HSO-CAZ1	7.81 b	64.0 b	123 b	34.7 b	38.1 bc
HSO-CAZ2	7.33 ab	67.5 b	108 b	36.6 b	37.7 bc
HSO-CAZ5	6.26 ab	65.9 b	104 b	53.2 d	39.9 c
Maize					
CO	22.3 c	92.7 d	0.06 a	14.1 d	30.6 e
HSO	17.4 b	32.2 a	21.9 b	3.86 a	21.0 b
HSO-KZ1	15.0 ab	30.2 a	29.6 c	3.08 a	17.2 a
HSO-KZ2	17.5 b	31.6 a	18.2 b	3.38 a	20.7 b
HSO-KZ5	16.2 b	33.0 a	6.73 a	3.09 a	17.2 a
HSO-CAZ1	13.7 a	46.5 b	51.2 d	5.54 b	23.3 c
HSO-CAZ2	16.8 b	60.3 c	53.1 d	8.20 c	26.0 d
HSO-CAZ5	15.3 ab	59.1 c	32.4 c	15.0 d	24.0 cd
Beet					
CO	20.9 a	155 b	124 a	17.7 b	58.7 b
HSO	24.7 ab	75.6 a	229 bc	10.6 a	37.3 a
HSO-KZ1	34.9 c	98.3 a	198 b	11.4 a	38.5 a
HSO-KZ2	32.0 bc	96.7 a	196 b	12.2 a	39.5 a
HSO-KZ5	35.8 c	98.8 a	194 b	13.1 a	42.6 a
HSO-CAZ1	25.4 ab	81.0 a	255 c	10.7 a	37.5 a
HSO-CAZ2	28.2 abc	90.2 a	321 d	13.3 a	45.4 a
HSO-CAZ5	21.2 a	85.9 a	276 cd	22.6 c	45.0 a

Different letters indicate significant differences at $P < 0.05$ using Duncan's new multiple range test. CO, control soil; HSO, high sodic soil; KZ1, KZ2, KZ5, CAZ1 CAZ2 and CAZ5, 1, 2 and 5% (w/w) K-type or Ca-type zeolite treatments, respectively.

maize, kidney bean and tomato plants were dead, and beet growth was considerably restricted in HSO.

The KZ treatments significantly decreased shoot dry weight of beet and KZ5 decreased the weight of maize already at 4 DAT (Table 3). After 11–13 DAT, the KZ treatments suppressed growth of beet continuously, and also tended to suppress growth in maize and tomato. The CAZ treatments significantly increased shoot dry weight of beet and CAZ2 also increased the weight of tomato at 4 DAT. After 11–13 DAT, the CAZ treatments significantly improved growth in all the examined plants. The ameliorative effect was significantly larger in CAZ2 than in CAZ5 and on roots than on shoots, except for kidney bean. The relative dry weight of whole plants of beet, maize, tomato and kidney bean in CAZ2 to that in the control was 0.85, 0.40, 0.33 and 0.20, at 25–27 DAT.

Water status

Among the treatments, the water deficit (WD) in kidney bean, tomato and beet was found to be: CAZ1 ≒ CAZ2 ≒ CAZ5 < HSO < KZ1 < KZ2 ≒ KZ5 at 4 DAT (Table 4). The WD of maize differed and was in the order: CAZ2 < HSO ≒ CAZ1 ≒ CAZ5 < KZ1 ≒ KZ2 < KZ5 at 4 DAT.

Table 6 Concentration of elements (cmol kg^{-1}) and ratio of Na to (K + Ca + Mg) in beet 26 days after transplanting

	P	K	Na	Ca	Mg	Na/(K + Ca + Mg)
Beet shoots						
CO	14.1 c	173 e	47 a	22.9 e	77.1 d	0.17 a
HSO	2.24 a	23.3 a	336 de	6.1 a	25.0 ab	6.23 d
HSO-KZ1	2.17 a	19.4 a	346 ef	11.2 bc	26.3 ab	6.40 d
HSO-KZ2	1.87 a	23.8 a	300 cd	11.6 bc	21.1 a	5.73 d
HSO-KZ5	4.19 b	44.5 b	259 c	21.7 e	31.9 b	2.65 b
HSO-CAZ1	17.0 d	139 d	99 b	42.5 f	56.7 c	0.41 a
HSO-CAZ2	17.7 d	47.6 b	384 f	9.65 b	32.8 b	4.27 c
HSO-CAZ5	13.3 c	67.9 c	292 c	24.8 e	34.1 b	2.30 b
Beet roots						
CO	7.48 b	31.0 c	3.0 a	21.3 a	12.4 ab	0.05 a
HSO	1.38 a	9.88 a	57.8 be	14.9 a	15.4 bc	1.72 bc
HSO-KZ1	1.75 a	5.40 a	66.3 cd	14.2 a	16.5 bcd	1.96 c
HSO-KZ2	1.88 a	3.76 a	69.6 de	13.9 a	14.2 abc	2.20 c
HSO-KZ5	1.35 a	2.93 a	32.4 b	15.9 a	9.95 a	1.19 abc
HSO-CAZ1	2.36 a	21.9 b	40.8 be	17.0 a	16.9 cd	0.74 ab
HSO-CAZ2	3.06 a	21.9 b	38.5 b	17.9 a	16.3 bcd	0.68 ab
HSO-CAZ5	2.94 a	33.9 c	39.1 b	35.9 b	20.1 d	0.44 a

Different letters indicate significant differences at $P < 0.05$ using Duncan's new multiple range test. CO, control soil; HSO, high sodic soil; KZ1, KZ2, KZ5, CAZ1 CAZ2 and CAZ5, 1, 2 and 5% (w/w) K-type or Ca-type zeolite treatments, respectively.

In all the tested plants, the water status in the CAZ treatments was found to be similar to that in CO at 11–13 DAT up to 25–27 DAT. The KZ treatments significantly increased the WD in beet until 26 DAT and tended to increase WD in tomato at 11 DAT.

Absorption of elements

At 4 days after treatment

The K_c, Ca_c and Mg_c of shoots in HSO were significantly lower than those of CO in all tested plants (Table 5). Under HSO, the Na_c of maize was tremendously increased and that of kidney bean increased 67-fold, tomato by 12-fold and beet by 1.8-fold compared to CO. The KZ1 and KZ2 did not differ for element concentrations, regardless of the plant species. The KZ5 decreased significantly the Na_c and Mg_c of shoots in maize. The K_c of shoot in KZ treatments was the same as HSO, although K-fertilizer was not supplied to all of the tested plants. The CAZ1, CAZ2, and especially CAZ5, increased Ca_c, K_c and Mg_c in all plant species except beet. The CAZ treatments decreased Na_c of shoots in kidney bean and tomato, but increased the concentration in maize. In beet, the Ca_c of shoots in CAZ5 was twice that in HSO.

At 25, 26 or 27 days after treatment

In beet, the P_c and K_c of shoots and roots and the Ca_c and Mg_c of shoots in the CAZ treatments was considerably higher than the concentrations in HSO (Table 6). The relative K uptake in the roots and P uptake in the shoots in the CAZ treatments compared with CO in beet were also considerably higher than the concentrations in the other plants (Fig. 1). The relative P uptake in the shoots in CAZ5 compared with CO of tomato and maize was markedly lower than in CAZ1 and CAZ2.

Cation balance

The cation balance was not affected by KZ2 in kidney bean, tomato or maize, but a slightly decreased Na/K, Na/Ca and Na/Mg was observed in beet (Fig. 2). The CAZ2 greatly reduced the Na/K, Na/Ca and Na/Mg of shoots in kidney bean and halved it in tomato. In beet, the CAZ2 did not affect the cation balance at 4 DAT (Fig. 2), but Na/(K + Ca + Mg) of shoot in CAZ treatments was lower than HSO at 26 DAT (Table 6). In maize, Na/K, Na/Ca and Na/Mg in HSO were the lowest of all the tested plants. The CAZ2 increased Na/Mg and Na/ K at 4 DAT, but its value was lower than that recorded for the other plants (Fig. 2).

DISCUSSION

As the ESP of HSO was very high (78), glycophytes might suffer from Na toxicity and reduced absorption of Ca, Mg and K. The high pH condition (> 9.9) of HSO may damage roots and have a bad influence on water and nutrition absorption. In this study, growth reducing factors and the effect of zeolite addition were discussed from early stages after transplanting in HSO treatments.

The addition of Ca-type zeolite improved growth in all of the tested plants, although the improving factors

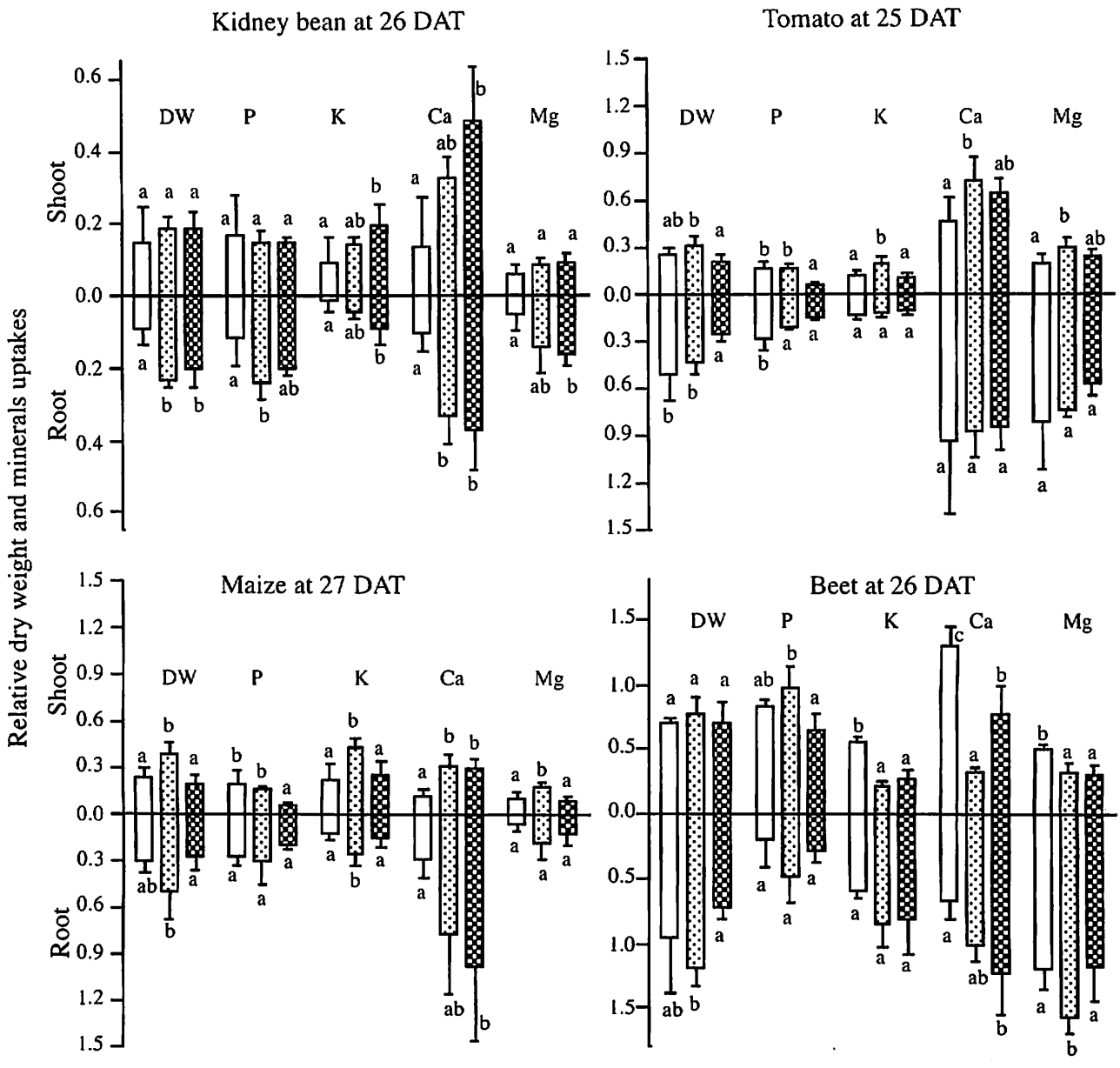

Figure 1 Relative dry weight (DW) and mineral uptake in the Ca-type zeolite (CAZ) treatment compared to the control. Different letters indicate differences at $P < 0.05$ using Duncan's new multiple test. (□) CAZ1, (▨) CAZ2 and (▩) CAZ5 refer to the 1, 2 and 5% (w/w) Ca-type zeolite treatments, respectively. Error bars are standard deviation. DAT, days after transplanting.

varied among plant species. In kidney bean, the HSO treatment resulted in the highest WD and lowest Mg_c among the four species. The Na_c increase and Ca_c decrease in the HSO treatment followed those recorded in maize, although growth inhibition was not observed at 4 DAT (Tables 3,4,5). The dry weight in HSO, however, decreased with markedly high WD at 13 DAT (Tables 3,4). Deteriorated nutritional status and water status just after transplanting, therefore, had a negative influence on growth afterwards. Although the CAZ treatments suppressed Na absorption and increased the absorption of K, Ca and Mg and improved cation balance, and improved water status at 4 DAT, the growth improvement was observed 13 DAT. The ameliorative effect of CAZ treatments on kidney bean was lower than that observed for the other plant species at 26 DAT. This might be because of the extremely lower relative uptake of K in root and Mg in shoot in CAZ compared with that in CO at 26 DAT in kidney beans compared with the other plant species (Fig. 1).

In tomato, growth did not decrease in HSO at 4 DAT, despite the deteriorated nutritional status (Tables 3,5). As the growth proceeded, however, the nutritional status became worse followed by deterioration of water

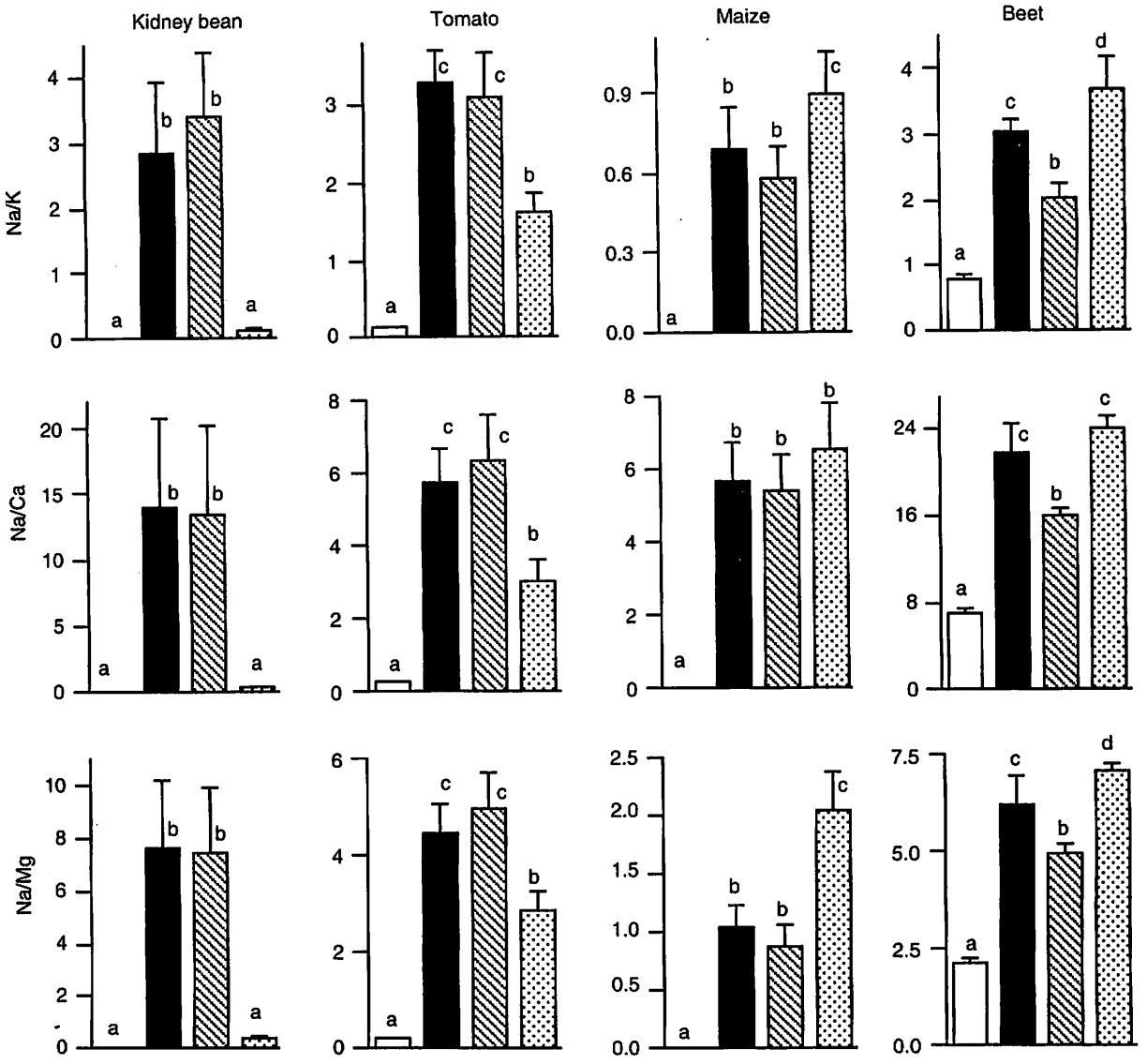

Figure 2 Concentration ratios of Na to K, Ca and Mg in shoots 4 days after transplanting (□) CO, (■) HSO, (▨) KZ2 and (⊡) CAZ2 refer to control soil, high sodic soil and 2% (w/w) K-type or Ca-type zeolite treatments, respectively. Different letters indicate differences at $P < 0.05$ using Duncan's new multiple test. Error bars are standard deviation.

absorption, and finally growth decreased at 11 DAT. Even at 4 DAT, dry weight in CAZ2 was significantly higher, and that in CAZ1 trended to be higher, than that in HSO. The CAZ treatments could not improve water status, but increased absorption of Ca and K and decreased absorption of Na and improved cation balance, which might result in improved growth (Tables 3,4,5). Tomato showed the lowest WD among the four species in HSO until 11 DAT, and decreases in WD in the CAZ treatments were smaller than those recorded in the other species, indicating that the effect of improved water absorption was lowest in tomato.

In maize, the increase in Na_c and decrease in Ca_c and K_c were markedly higher in HSO at 4 DAT, and water absorption was severely inhibited, and these were the main causes of growth reduction (Tables 3,4,5). The CAZ treatments did not improve water status at 4 DAT. They improved K and Ca status, but enhanced absorption of Na and growth did not change. At 13 DAT, the CAZ treatments improved water status and as a consequence growth was improved. Not only recovery of K and Ca absorptions but also that of water absorption are necessary for improvement of growth of maize in HSO.

The beet WD value was not higher than those of the other plant species in HSO, presumably assuming that increased Na_c and decreased K_c, Ca_c and Mg_c would cause severe growth inhibition (Tables 3,4,5). However, beet growth was improved by CAZ treatments, although the

increment of Ca_c and K_c was the smallest among the plant species and CAZ treatments increased Na_c (Tables 3,5). The larger decreases in WD as a result of the CAZ treatments might contribute to amelioration of the growth at 4 DAT (Table 4). Beet could quickly respond to the improved water status. At 26 DAT, the P_c of beet in HSO was much lower than that in CO, although there was no difference in available P concentration for saturation extracts of soil between CO and the other treatments (M. Yamada *et al.*, unpubl. data, collected in 2000). Root growth of beet was markedly improved by CAZ treatments compared to shoot growth, which might result in increased P absorption and contribute to improved growth (Tables 3,6). In addition, CAZ treatments improved K uptake of root and the cation balance of shoots (Fig. 1, Table 6). These, as well as a marked improvement in water absorption, brought the highest growth improvement among the plant species (Tables 3,4).

The ameliorative effect of CAZ5 was lower than that of CAZ2 in tomato, maize and beet (Table 3). The Ca_c in CAZ5 was 2–3-fold higher than that in CAZ2 at 4 DAT in all tested species (Table 5) and this tendency continued to 25–27 DAT (Table 6, data shown for beet). In contrast, shoot P_c in beet and tomato in CAZ5 was lower than that in CAZ2 even at 4 DAT. At 25–27 DAT CAZ5 reduced P_c in the shoots by 51% for tomato, 75% for maize and 75% for beet compared to CAZ2. A lower relative P absorption in CAZ5 than in CAZ2 (Fig. 1) could be associated with inhibited P transport from root to shoot in the presence of excessive Ca under CAZ5. These results were supported by our previous unpublished findings for maize in low sodic soil and by the findings of Ruiz and Romero (1998). The WD in CAZ5 was higher than that in CAZ2 in tomato and maize until 11–13 DAT and in beet until 26 DAT because of the higher EC in CAZ5 (Table 2). These results indicated that the addition of CAZ5 was in excess for plants at HSO.

The CAZ treatments improved growth of all the tested plant species. Conversely, KZ treatments had significantly suppressed beet growth by 4 DAT and KZ5 and KZ2 suppressed the growth of tomato and maize by 13 DAT (Table 3). The concentrations of Fe, Mn, Zn and Cu in the shoots in the HSO and KZ treatments were higher than the critical level (data not shown). However, water status was aggravated in tomato and maize by KZ treatments at 4 DAT, and damaged growth later (11 or 13 DAT). A markedly high WD, even in KZ1, seriously damaged growth in beet at 4 DAT. In contrast, the WD of all the other tested plant species was lowered by the CAZ treatments (Table 4). The absorption of the elements was less affected by KZ treatment (Table 5). Thus, the effect of K-type and Ca-type zeolite on water status was opposite and only Ca-type zeolite improved nutritional status. Thus, these zeolites had quite a different effect on plant growth.

Why was the effect of both zeolites on water status so different? In KZ5 and KZ2, the concentration of HCO_3^- and CO_3^{2-} and the pH of soil solution were higher than in the HSO and CAZ treatments (Table 2), which might injure root growth and cause inhibition of water absorption (Table 4). Peiter *et al.* (2001) showed that HCO_3^- inhibited root elongation. Bie *et al.* (2004) suggested that $NaHCO_3$ was more toxic to lettuce growth than Na_2SO_4. In contrast, the addition of CAZ decreased the CO_3^{2-} and HCO_3^- concentration of soil solution (Table 2). It was considered that improved water uptake in the CAZ treatments resulted from the absence of root damage by CO_3^{2-} and HCO_3^-. The higher sensitivity of the beet roots to the higher CO_3^{2-} and HCO_3^- concentrations in KZ treatments severely suppressed water absorption at 4 DAT, whereas the mitigated WD by the CAZ treatments was possibly accounted for by the morphologically fine absorption roots of beet (Osaki *et al.* 1995).

The addition of Ca-type zeolite could ameliorate the growth of glycophytes in high sodic soil from early stages by recovery of water status in beet, nutritional status in tomato, and both water and nutritional status in kidney been and maize. However, the addition of K-type zeolite suppressed the growth of beet, maize and tomato by inhibiting water absorption.

ACKNOWLEDGMENTS

The authors are grateful to Mr K. Ogawa and Mr Y. Kageyama (Kimura Chemical Plants), and Mr I. Ueyama, Mr T. Shimizu and Dr M. Irshad (Arid Land Research Center, Tottori University) for their assistance and English correction. This research was conducted as part of a research project entitled: "Research for the improvement of the saline soil by using artificial zeolites" sponsored by Kimura Chemical Plants, Japan.

REFERENCES

Bernstein L, Francois LE, Clark RA 1974: Interactive effects of salinity and fertility on yields of grains and vegetables. *Agron. J.*, 66, 412–421.

Bie Z, Ito T, Shinohara Y 2004: Effects of sodium sulfate and sodium bicarbonate on the growth, gas exchange and mineral composition of lettuce. *Scientia Horticulturae*, 99, 215–224.

Clarke L 1994: Legislation for the Management of Coal-use Residues, Technical Report No. IEACR/68, p. 75, IEA Coal Research, London.

Grattan SR, Grieve CM 1999: Salinity-mineral nutrient relations in horticultural crops. *Scientia Horticulturae*, 78, 127–157.

Grieve CM, Fujiyama H 1987: The response of two rice cultivars to external Na/Ca ratio. *Plant Soil*, 103, 245–250.

Lea-Cox JD, Syvertsen JP 1993: Salinity reduces water use and nitrate-N-use efficiency of citrus. *Ann. Bot.*, 72, 47–54.

Maas EV 1984: Salt tolerance of plants. In CRC Handbook of Plant Science in Agriculture. II. Ed BR Christie, pp. 57–75, CRC Press, Florida.

Osaki M, Shinano T, Matsumoto M *et al.* 1995: Productivity of high-yielding crops V. Root growth and specific absorption rate of nitrogen. *Soil Sci. Plant Nutr.*, 41, 635–647.

Page AL, Chang AC, Adriano DC 1996: Deficiencies and toxicities of trace elements. In Agricultural Salinity Assessment and Management. ASCE Manuals and Reports on Engineering Practice, No. 71. Ed KK Tanji, pp. 138–160, American Society of Civil Engineers, New York.

Peiter E, Yan F, Schubert S 2001: Lime-induced growth depression in Lupinus species: Are soil pH and bicarbonate involved? *J. Plant Nutr. Soil Sci.*, 164, 165–172.

Perez-Alfocea F, Esrañ MT, Caro M, Bolarín MC 1993: Response of tomato cultivars to salinity. *Plant Soil*, 150, 203–211.

Ruiz JM, Romero L 1998: Calcium impact on phosphorus and its main bioindicators: Response in the roots and leaves of tobacco. *J. Plant Nutr.*, 21, 2273–2285.

Yamada M, Uehira M, Hun LS *et al.* 2002: Ameliorative effect of K-type and Ca-type artificial zeolites on the growth of beets in saline and sodic soils. *Soil. Sci. Plant Nutr.*, 48, 651–658.

Planta (2007) 225:1255–1264
DOI 10.1007/s00425-006-0417-7

ORIGINAL ARTICLE

Overexpression of monodehydroascorbate reductase in transgenic tobacco confers enhanced tolerance to ozone, salt and polyethylene glycol stresses

Amin Elsadig Eltayeb · Naoyoshi Kawano · Ghazi Hamid Badawi · Hironori Kaminaka · Takeshi Sanekata · Toshiyuki Shibahara · Shinobu Inanaga · Kiyoshi Tanaka

Received: 1 May 2006 / Accepted: 20 September 2006 / Published online: 17 October 2006

Abstract Ascorbate (AsA) is a major antioxidant and free-radical scavenger in plants. Monodehydroascorbate reductase (MDAR; EC 1.6.5.4) is crucial for AsA regeneration and essential for maintaining a reduced pool of AsA. To examine whether an overexpressed level of MDAR could minimize the deleterious effects of environmental stresses, we developed transgenic tobacco plants overexpressing *Arabidopsis thaliana* MDAR gene (*AtMDAR1*) in the cytosol. Incorporation of the transgene in the genome of tobacco plants was confirmed by PCR and Southern-blot analysis and its expression was confirmed by Northern- and Western-blot analyses. These transgenic plants exhibited up to 2.1-fold higher MDAR activity and 2.2-fold higher level of reduced AsA compared to non-transformed control plants. The transgenic plants showed enhanced stress tolerance in term of significantly higher net photosynthesis rates under ozone, salt and polyethylene glycol (PEG) stresses and greater PSII effective quantum yield under ozone and salt stresses. Furthermore, these transgenic plants exhibited significantly lower hydrogen peroxide level when tested under salt stress. These results demonstrate that an overexpressed level of MDAR properly confers enhanced tolerance against ozone, salt and PEG stress.

Keywords Ascorbate · Monodehydroascorbate reductase · Oxidative stress · Reactive oxygen species · Vitamin C

List of abbreviations

APX	Ascorbate peroxidase
AsA	Ascorbate
DHA	Dehydroascorbate
DHAR	Dehydroascorbate reductase
GSH	Glutathione
MDAR	Monodehydroascorbate reductase
MDHA	Monodehydroascorbate
PEG	Polyethylene glycol
ROS	Reactive oxygen species

A. E. Eltayeb · H. Kaminaka · K. Tanaka (✉)
Laboratory of Plant Biotechnology, Faculty of Agriculture, Tottori University, Koyama, Tottori 680-8553, Japan
e-mail: jotanaka@muses.tottori-u.ac.jp

N. Kawano · S. Inanaga
Japan International Research Center for Agricultural Sciences, Ohwashi, Tsukuba, Ibaraki 305-8686, Japan

G. H. Badawi
Department of Agronomy, Faculty of Agriculture, University of Khartoum, Shambat 3114, Sudan

T. Sanekata
Laboratory of Veterinary Infectious Disease, Faculty of Agriculture, Tottori University, Koyama, Tottori 680-8553, Japan

T. Shibahara
Division of Laboratory Animal Science, Research Center for Bioscience and Technology, Tottori University, Yonago, Tottori 683-8503, Japan

A. E. Eltayeb
Agricultural Research and Technology Corporation, Wad Medani 126, Sudan

Introduction

Abiotic stresses including salt, drought and ozone are known to accelerate the accumulation of reactive

oxygen species (ROS) such as singlet oxygen (O_2^1), superoxide radical (O_2^-), hydrogen peroxide (H_2O_2) and hydroxyl radical (OH) in plant cells. Detoxification of ROS in plant cells is accomplished by enzymatic and non-enzymatic scavenging systems. Plants detoxify ROS by a combination of antioxidants such as ascorbate (AsA) and glutathione (GSH) and antioxidative enzymes such as superoxide dismutase (SOD), ascorbate peroxidase (APX) and catalase (CAT). Antioxidative enzymes involved in the ascorbate–glutathione (AsA–GSH) cycle, mainly monodehydroascorbate reductase (MDAR), dehydroascorbate reductase (DHAR) and glutathione reductase (GR) are crucial for plant defense against oxidative stress (Mittler 2002).

AsA is a major redox buffer in plants (Pignocchi and Foyer 2003a), a cofactor of many enzymes (Smirnoff and Wheeler 2000), a regulator of cell division and growth (Kerk and Feldman 1995) and a molecule for signal transduction in plants (Noctor et al. 2000). AsA is synthesized in the mitochondria and consequently transported to other compartments of plant cells (Horemans et al. 2000). Most of AsA is reported to be localized in the cytoplasm (Pignocchi et al. 2003b), up to 10% in the apoplast (Noctor and Foyer 1998) and 12–30% could accumulate in chloroplasts (Horemans et al. 2000).

As a major antioxidant, AsA can directly scavenge free radicals (Halliwell and Gutteridge 2000), and is considered to be of paramount importance as an electron donor for H_2O_2 detoxifications via APX in plant cells (Noctor and Foyer 1998). APX uses two molecules of AsA to reduce H_2O_2 to water with two molecules of monodehydroascorbate (MDHA) being generated in this reaction. In turn, MDAR uses NAD(P)H as electron donor to reduce MDHA enzymatically to AsA (Hossain et al. 1984). Being an unstable radical due to its short lifetime, MDHA spontaneously disproportionates to AsA and dehydroascorbate (DHA) if not rapidly reduced to AsA (Noctor and Foyer 1998). DHAR catalyzes the reduction of DHA to AsA using reduced glutathione (GSH). Since DHA is also an unstable molecule, if not rapidly reduced to AsA, it undergoes spontaneous and irreversible hydrolysis to 2,3-diketogulonic acid (Deutsch 2000).

With its ability to directly regenerate AsA, MDAR plays an important role in maintaining reduced pool of AsA. An activity of MDAR has been described in several plant cell compartments such as chloroplasts (Hossain et al. 1984), mitochondria and peroxisomes (Jiménez et al. 1997) and cytosol (Dalton et al. 1993). Cytosolic MDAR has been purified from cucumber (*Cucumis sativus*) fruits (Hossain and Asada 1985), soybean (*Glycine max*) root nodules (Dalton et al. 1992) and potato (*Solanum tuberosum*) tubers (Borraccino et al. 1986). A mitochondrial MDAR has been purified from potato (*S. tuberosum*) tubers (De Leonardis et al. 1995) and recently a chloroplastic MDAR from spinach (*Spinacia oleracea*) leaves (Sano et al. 2005). MDAR cDNAs have been cloned from several plant species such as pea (*Pisum sativum* L.) leaves (Murthy and Zilinskas 1994), tomato (*Lycopersicon esculentum* Mill.) fruit (Grantz et al. 1995). MDAR cDNA from *Brassica campestris* has been cloned and analyzed for its mRNA level in response to oxidative stress (Yoon et al. 2004). Leterrier et al. (2005) reported the functional analysis by activity and protein expression of the pea *MDAR1* gene under some environmental stresses.

Genes for MDAR have been localized to several subcellular compartments including the plastids, mitochondria, microbodies and cytoplasm (Conklin and Barth 2004). Among *Arabidopsis* MDAR genes, although *AtMDAR1* possesses C-terminal AKI tripeptide that resembles matrix peroxisomal targeting signal (PTS1), in vivo sorting of *AtMDAR1* to peroxisomes was incomplete due to a functionally inefficient peroxisomal targeting (Lisenbee et al. 2005). Organelle-specific markers were unable to detect epitope-tagged *AtMDAR1* in cell compartments other than cytosol or peroxisomes of *Arabidopsis* and tobacco BY-2 suspension cells (Lisenbee et al. 2005).

The use of transgenic plants with manipulated levels of antioxidative enzymes is an important demonstration tool to study the defense mechanisms against oxidative stress (Foyer et al. 1994). Among antioxidative enzymes involved in the GSH–AsA cycle, overexpressing GR, APX and DHAR in transgenic plants is extensively reported, whereas overexpressing MDAR has received the least attention. Several reports about transgenic plants that express gene constructs for either cytosolic or chloroplast-targeted expression of APX or GR are reviewed by Allen et al. (1997). Targeting DHAR overexpression to either cytosol or chloroplast of transgenic plants have been reported (Kwon et al. 2001; Chen et al. 2003; Ushimaru et al. 2005). In our laboratory, we previously reported the stress tolerance of transgenic tobacco plants with overexpressed levels of APX (Badawi et al. 2004a), SOD (Badawi et al. 2004b) and DHAR (Eltayeb et al. 2006).

The physiological importance of MDAR-overexpression in protecting transgenic plants against oxidative stress imposed by various environmental stresses is still not fully clarified. Therefore, in this study we

report the development of transgenic tobacco plants overexpressing MDAR and its physiological importance in protecting plants against various stresses such as ozone, salt and polyethylene glycol (PEG)-induced stress.

Materials and methods

Construction of plant expression vector and tobacco transformation

Arabidopsis thaliana (ecotype Columbia) seeds obtained from the Biological Resource Center of Ohio State University (Columbus, OH, USA) were grown in a growth chamber at 25°C and 12 h light cycle. The cDNA encoding *A. thaliana* MDAR (*AtMDAR1*; *At3g52880*) was amplified by reverse transcription polymerase chain reaction (RT-PCR) from *A. thaliana* total RNA using primers (5′-ATGGCGGAGAAGAG CTTTAAG-3′) and (5′-TCAGATCTTAGCTGCGA AG-3′). The ends of the amplified fragment were modified by PCR to introduce *Sma*I sites using SmMDSe primer (5′-CGCCCGGGCTCCACCATG GCTATGGCGGAGAAGAGCTTA-3′) and SmMDAn primer (5′-ACGGGCCCGTCAGATCTTAGC TGCGAA-3′). The end-modified fragment was digested with *Sma*I and cloned in the corresponding site of pBI121 plant expression vector down stream of CaMV35S (cauliflower mosaic virus promoter) and upstream of nopaline synthase (*nos*) terminator. This construct (pBI–MDAR) was introduced into *Agrobacterium tumefaciens* strain C58C1 by electroporation. Sterile leaf discs from *Nicotiana tabacum* (SR-1) were used for *Agrobacterium*-mediated gene transfer to generate transgenic tobacco plants as described previously (Eltayeb et al. 2006). To verify the presence of MDAR transgene in the genome of transgenic plants by PCR, genomic DNA was isolated from transgenic and non-transformed (SR-1) control plants leaves using ISOPLANT II kit (Nippon gene Co., Ltd., Toyama, Japan). PCR was conducted using the isolated DNA, and SmMDSe and SmMDAn primers.

Southern- and Northern- blot analyses

Southern-blot analysis using DNA isolated from MDAR transgenic and non-transformed control (SR-1) plants was performed to further confirm the incorporation of MDAR transgene in the genome of transgenic plants and to determine the independent transgenic lines. Northern-blot analysis using RNA isolated from MDAR transgenic and SR-1 control plants was conducted to determine transgenic plants that expressed MDAR transgene. Both Southern and Northern analyses were carried out as described previously (Eltayeb et al. 2006).

Western-blot analysis

The full length MDAR cDNA was cloned down stream of 6× His-tag sequence in *Sma*I site of the pQE-32 vector (Qiagen, Valencia, CA, USA). Expression and purification of the His-tagged recombinant MDAR protein was conducted using Ni-NTA agrose system (QIAexpress®, Qiagen) as instructed by manufacture. Antibodies against the purified recombinant MDAR protein were raised by injecting this protein into guinea pig. Protein samples isolated from MDAR transgenic and SR-1 control plants were used to conduct Western blot analysis as described previously (Eltayeb et al. 2006).

Monodehydroascorbate reductase activity and levels of reduced and oxidized AsA

Monodehydroascorbate reductase activity was assayed sepctrophotometrically according to the method of Hossain and Asada (1984) with slight modification. Leaf samples (0.2 g) from MDAR transgenic and SR-1 control plants were frozen in liquid nitrogen, grounded to powder in pre-cooled mortars and homogenized with 2 ml extraction buffer (1 mM ascorbate in 50 mM potassium phosphate buffer pH 7.8). The slurry was centrifuged (15,000*g*, 4°C) for 20 min and the supernatant (crude extract) was used immediately for the enzyme assay. The assay was performed at 25°C with a reaction mixture containing 0.1 M Tris–HCl pH 7.2, 0.2 mM NADH, 2 mM ascorbic acid, 1 unit ascorbate oxidase and crude extract. The decrease in absorbance at 340 nm due to ascorbate was monitored and the activity was calculated using absorbance coefficient of 6.2 mM^{-1} cm^{-1}. Total protein was determined according to Bradford (1976). The reduced and oxidized levels of AsA were determined according to Eltayeb et al. (2006).

Plant growth condition

The transgenic progeny (T_1) from the self-pollinated primary transformed lines (T_0) were germinated on kanamycin-containing MS medium (Murashige and Skoog 1962), whereas SR-1 seeds were germinated on antibiotic-free MS medium and maintained in a growth chamber for 6 weeks at 12 h light cycle, 25°C and 23% RH. Seedlings were transplanted in vermiculite,

maintained in controlled conditions (25°C, 45–55% RH and 14 h light cycle) and irrigated with water supplied with 1 ml l^{-1} nutrients solution (Hyponex 5–10–5, Hyponex, Osaka, Japan). Unless mentioned elsewhere, three replications of 8- to 10-week-old plants that were uniform in height and number of leaves were used in all stress evaluation experiments.

Determination of hydrogen peroxide

Hydrogen peroxide contents were determined by peroxidase-coupled assay using 4-aminoantipyrine and phenol as donor substrate (Frew et al. 1983) with slight modifications. Leaf samples (0.2 g) from MDAR transgenic and SR-1 control plants were frozen in liquid nitrogen, grounded to fine powder in pre-cooled mortars and then homogenized in 2 ml of 5% (w/v) trichloroacetic acid (TCA). The homogenate was centrifuged (15,000*g*, 4°C) for 20 min and the supernatant (50 µl) was added to 1 ml reaction mixture containing 2 mM phenol, 1.5 mM 4-aminoantipyrine, 0.1 M Tris–HCl buffer (pH 7.0) and 2 units peroxidase. Quinoneimine formation was measured at 505 nm. Absorbance resulted from any interfering substances was measured and subtracted in a separate 1 ml reaction containing 7 µl of 1 M tricine in 6 M KOH to neutralize the extract, 2 mM phenol, 1.5 mM 4-aminoantipyrine, 0.1 M Tris–HCl buffer (pH 7.0), 0.2 units catalase, incubated for 10 min at room temperature and finally 2 units peroxidase were added. Calibrations were carried using H_2O_2 standard curve.

Applying ozone, salt and PEG stresses

SR-1 control plants and MDAR transgenic lines (Mda1, Mda3 and Mda6) were selected for ozone and salt stress experiments and transferred to growth chamber (Koito Co. Ltd., Tokyo, Japan). Ozone stress was applied by fumigation with 0.2 ppm ozone generated using OES-10A ozone generator (Dylec Inc., Osaka, Japan), and the accurate fumigation level was continuously monitored by ozone monitor (Ozone Monitor, model 1200, Dylec). Salt stress was applied by irrigating plants with 0.3 M NaCl solution supplied with 1 ml l^{-1} Hyponex nutrient solution, renewed every day for eight days. Plants were allowed to recover from salt stress by irrigation with non-saline water supplied with 1 ml l^{-1} Hyponex nutrient solution for further eight days. SR-1 control plants and two MDAR transgenic lines (Mda3 and Mda6) were selected for PEG-induced stress experiment. PEG-induced stress was applied by irrigating plants with 10% (w/v) PEG solution supplied with 1 ml l^{-1} Hyponex nutrient solution.

Net photosynthesis and chlorophyll-fluorescence measurements

A portable photosynthesis system (LI-6400; Li-Cor Inc., Lincoln, NE, USA) was used to measure net photosynthesis (µmol CO_2 m^{-2} s^{-1}) starting from zero time immediately before applying stress and continued for a designated time. Chlorophyll-fluorescence measurements were performed with a portable PAM-2100 fluorometer (Heinz Walz, Effeltrich, Germany) as instructed by manufacture. Effective quantum yield of PSII (Y) was calculated as: $Y = \Delta F/F'_{\mathrm{m}} = (F'_{\mathrm{m}}F_t)/F'_{\mathrm{m}}$, where F_t is the fluorescence yield at any given time (steady state) and F'_{m} is the maximum fluorescence yield reached in a pulse saturating light during illumination.

Data analysis

Data points represent the mean of three replications. Data were analyzed using Student's *t* test at 95% confidence limit.

Results

Generation of MDAR-overexpressing transgenic tobacco

The cDNA encoding *AtMDAR1* under the control of the CaMV35S promoter and upstream of the *nos* terminator of the plant expression vector pBI121 was mobilized in *A. tumefaciens* strain C58C1 and used for *Agrobacterium*-mediated gene transfer of *N. tabacum* cv. SR-1. Analysis by PCR using genomic DNA isolated from transgenic and SR-1 control plants confirmed the presence of the transgene in five MDAR transgenic lines (Fig. 1a). Southern-blot analyses using genomic DNA isolated from transgenic and SR-1 control plants confirmed that MDAR transgenic plants had independently incorporated two to four copies of the introduced MDAR transgene (Fig. 1b). Northern-blot analysis using RNA isolated from MDAR transgenic and SR-1 control plants indicated that MDAR transgenic plants had expressed the MDAR transgene (Fig. 1c). Western-blot analysis using antibodies raised against MDAR detected high levels of MDAR protein (47 kDa) derived from MDAR transgene in the extracts prepared from transgenic plants but not from SR-1 control plants (Fig. 2).

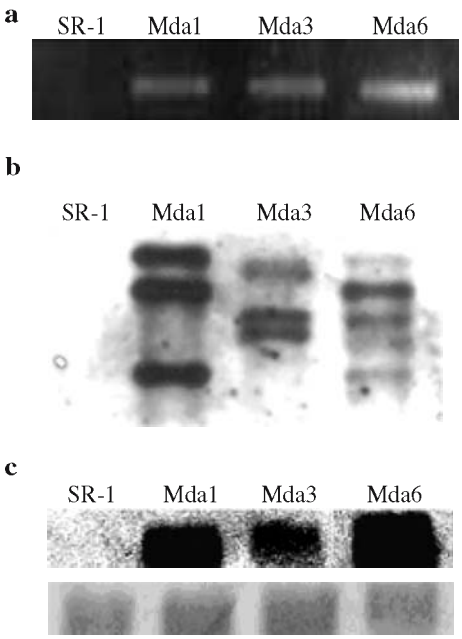

Fig. 1 a–c PCR, Southern- and Northern-blot analyses of MDAR transgenic plants. **a** Detection of MDAR transgene by PCR using genomic DNAs isolated from MDAR transgenic and SR-1 control plants. **b** Southern-blot analysis. DNAs (10 μg) from MDAR transgenic and SR-1 control plants were digested with *Eco*RI, loaded in agrose gel, denatured, neutralized, transferred to nylon membrane (Hybond™-N+, Amersham, UK) and hybridized with DIG-labeled MDAR cDNA probe. **c** Northern-blot analysis. Total RNA (20 μg) from MDAR transgenic and SR-1 control plants were denatured in formaldehyde gel, transferred to nylon membrane (Hybond™-N+) and hybridized with DIG-labelled MDAR cDNA probe. SR-1, control plant. MDAR transgenic lines are represented by Mda1, Mda3, Mda4, Mda6 and Mda9

Higher MDAR activity and increased AsA levels in MDAR transgenic plants

The MDAR-enzyme assay was carried out using leaf crude extracts from MDAR transgenic plants and SR-1 control plants grown under normal conditions. Compared to SR-1 control plants, Mda1, Mda3 and Mda6 transgenic lines exhibited increased MDAR activity to 1.5-, 2.1- and 1.6-fold, respectively (Fig. 3a). The level of AsA and DHA in leaves of control and transgenic plants were measured to determine the metabolic consequences of MDAR-overexpression. Compared to SR-1 control plants, the level of AsA in Mda1, Mda3 and Mda6 transgenic lines increased to 2.0-, 2.2- and 2.2-fold, respectively (Fig. 3b), and the level of DHA decreased by 24.1, 26.2 and 23.1%, respectively. The redox status of ascorbate (AsA:DHA) increased from a ratio of 1.7 in SR-1 control plants to 3.8, 5.1 and 3.9 in Mda1, Mda3 and Mda6 transgenic lines, respectively.

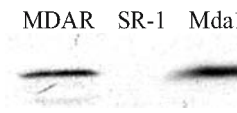

Fig. 2 Immunoblotting of proteins from MDAR transgenic and SR-1 control plants. Proteins samples (25 μg) were separated by SDS-PAGE, transferred to Hybond ECL nitrocellulose membrane and applied to immunoblotting. SR-1; control plant, MDAR; His-tagged recombinant protein. MDAR transgenic lines are represented by Mda1, Mda3 and Mda6

Enhanced tolerance to ozone stress in MDAR transgenic plants

Exposure to ozone can inhibit photosynthesis (Runeckles and Chevone 1992). Fumigation of MDAR transgenic and SR-1 control plants with 0.2 ppm ozone resulted in a steady decrease in their net photosynthetic rate. The net photosynthesis of MDAR transgenic lines was significantly ($P < 0.05$) higher than SR-1 control plants after exposure longer than 2 h

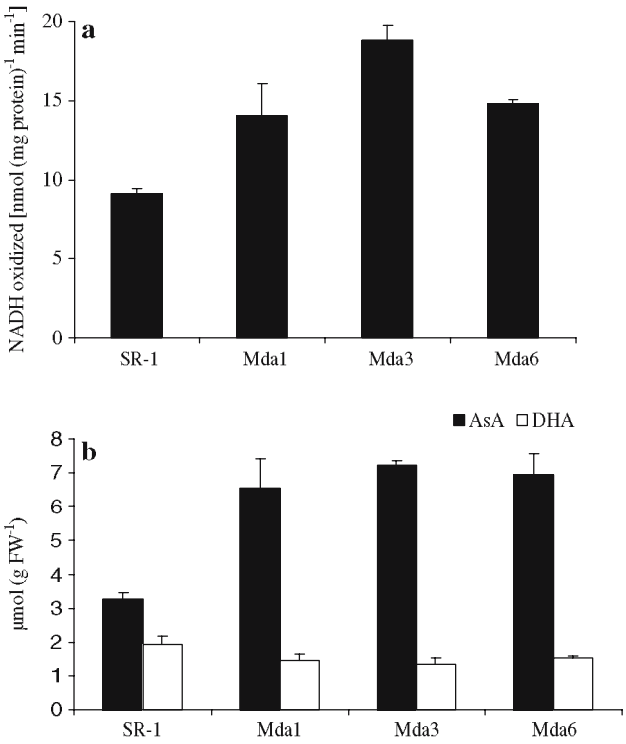

Fig. 3 a, b MDAR enzyme activity and levels of ascorbate. **a** MDAR activity measured in leaves of MDAR transgenic and SR-1 control plants. Mean values ± SE from triplicate determinations. **b** Levels of reduced ascorbate (AsA) and dehydroascorbate (DHA) in MDAR transgenic and SR-1 control plants. MDAR transgenic lines are represented by Mda1, Mda3 and Mda6. Mean values ± SE from triplicate determinations

(Fig. 4a). After 30 h of ozone stress, Mda1, Mda3 and Mda6 transgenic lines maintained 48.2, 47.2 and 42.3% of their original photosynthesis, respectively, compared to 31.3% for SR-1 control plants.

Ozone fumigation is reported to cause a depression of the quantum yield of photosynthesis (Barnes et al. 1990), and reduction on photosynthesis activity revealed by changes in chlorophyll-fluorescence characteristics (Agrawal et al. 1993). To determine the photochemical efficiency under ozone stress, two MDAR transgenic lines and SR-1 control plants were exposed to 0.2 ppm ozone for 6 h. As estimated by ($\Delta F/F'_m$), the effective PSII photon yield was substantially reduced in all plants, with greater reduction in SR-1 control plants. MDAR transgenic plants maintained significantly ($P < 0.05$) higher effective PSII yield during the entire period of stress (Fig. 4b).

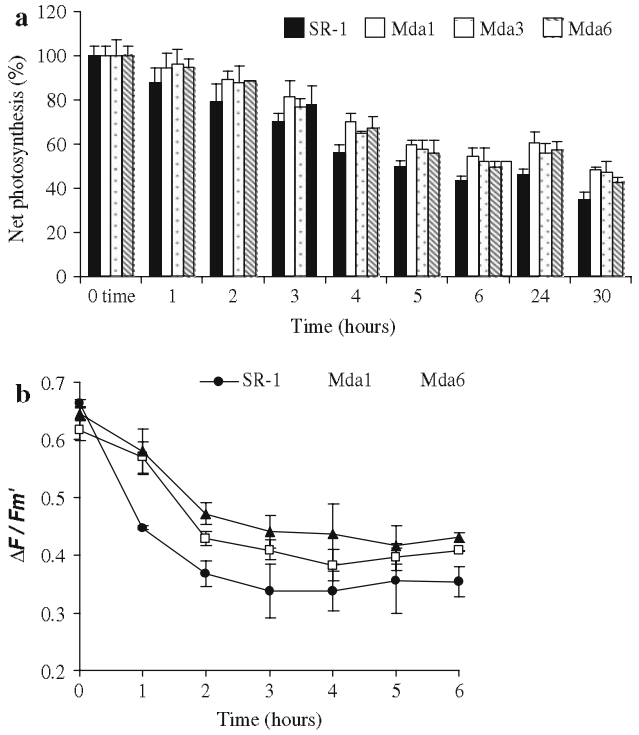

Fig. 4 **a**, **b** Net photosynthesis (%) and PSII effective quantum yield ($\Delta F/F'_m$) of MDAR transgenic and control plants (SR-1) during ozone stress. **a** The 100% net photosynthesis (μmol CO_2 m^{-2} s^{-1}) for SR-1, Mda1, Mda3 and Mda6 is 16.8, 16.2, 16.0 and 16.6, respectively. The 100% net photosynthesis measurement for each line was taken immediately before fumigation with 0.2 ppm ozone (0 time). Mean values ± SE from triplicate determinations. **b** Effective PSII photon-yield estimated by the fluorescence parameter $\Delta F/F'_m$ during ozone stress imposed on MDAR transgenic and SR-1control plants. Mean values ± SE from triplicate determinations

Enhanced tolerance to salt stress

We investigated the effect of salt stress on net photosynthesis of MDAR transgenic and SR-1control plants during 8 days. Although the net photosynthesis decreased in both transgenic and control plants, the net-photosynthetic rate of MDAR transgenic plants was significantly ($P < 0.05$) higher than that of SR-1 control plants during the entire period of the stress (Fig. 5a). After 8 days of salt stress, Mda1, Mda3 and Mda6 transgenic lines maintained 17.2, 23.1 and 19.0% of their original photosynthesis respectively, compared to only 9.8% for SR-1 control plants. Furthermore, after 8 days recovery period, Mda1, Mda3

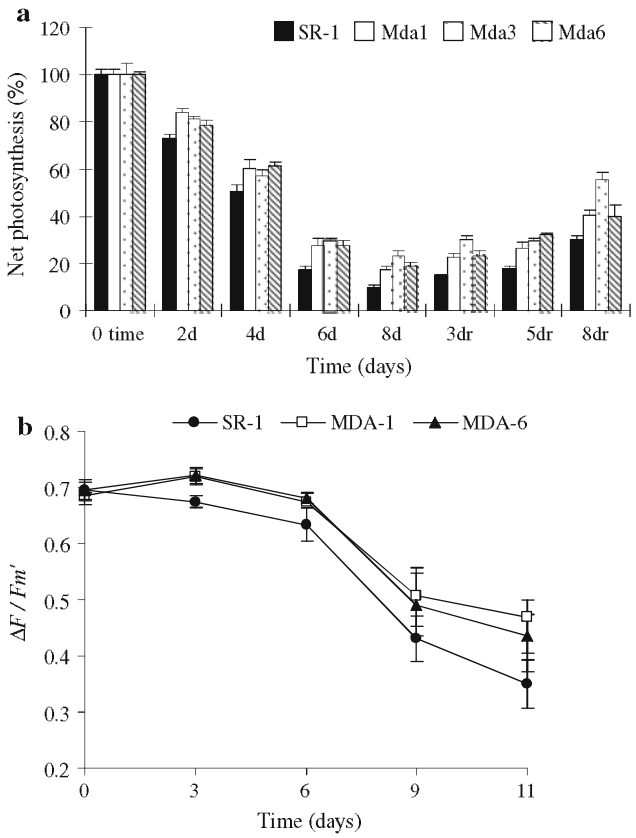

Fig. 5 **a**, **b** Net photosynthesis (%) and PSII effective quantum yield ($\Delta F/F'_m$) of MDAR-overexpressing transgenic and control plants (SR-1) during salt stress. **a** The 100% net photosynthesis (μmol CO_2 m^{-2} s^{-1}) for SR-1, Mda1, Mda3 and Mda6 is 17.8, 17.8, 17.5 and 17.4, respectively. The 100% net photosynthesis measurement for each line was taken immediately before applying stress (0 time); 2d, 4d, 6d and 8d are 2, 4, 6 and 8 days of salt stress, respectively; 3dr, 5dr and 8dr are 3, 5, and 8 days of recovery, respectively. Mean values ± SE from triplicate determinations. **b** Effective PSII photon yield estimated by the fluorescence parameter $\Delta F/F'_m$ during salt stress imposed on MDAR-overexpressing transgenic and SR-1control plants. Mean values ± SE from triplicate determinations

and Mda6 transgenic lines recovered 41.0, 55.6 and 40.0% of their original net photosynthesis, respectively, compared to only 30.2% for SR-1 control plants.

The photochemical efficiency under salt stress was determined using two MDAR transgenic lines and SR-1 control plants. As a result of salt stress, the effective PSII photon yield ($\Delta F/F'_m$) was reduced in all plants, with a greater reduction on SR-1 control plants compared to MDAR transgenic plants. During the entire period of the stress, MDAR transgenic plants maintained significantly ($P < 0.05$) higher effective PSII photon yield (Fig. 5b).

Hydrogen peroxide content under salt stress

Since high salinity is reported to induce oxidative stress (Hernández et al. 1993), the levels of H_2O_2 in both MDAR transgenic and SR-1 control plants were measured before and after salt stress treatments. Prior to the treatment, the level of H_2O_2 in all plants was low, with level of H_2O_2 significantly ($P < 0.05$) lower in MDAR transgenic plants than SR-1 control plants. After 4 days of salt stress, the level of H_2O_2 substantially increased to approximately fourfold in all plants, but remains significantly ($P < 0.05$) lower in all MDAR transgenic plants compared to SR-1 control plants (Fig. 6).

Enhanced tolerance to PEG-induced stress

Compared to salt stress, the decrease in net photosynthesis of plants caused by 10% (w/v) PEG-induced stress was relatively lower. MDAR transgenic plants showed significantly ($P < 0.05$) higher net photosynthesis rates (Fig. 7). After 8 days of PEG-induced stress, Mda3 and Mda6 transgenic lines maintained 68.5 and 67.1% of their original photosynthesis, respectively, compared to only 58.6% for SR-1 control.

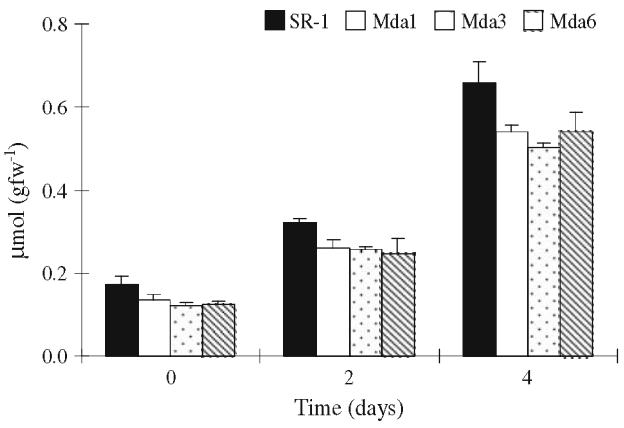

Fig. 6 The levels of H_2O_2 in leaves of MDAR-overexpressing transgenic and control plants (SR-1) before and during salt stress. MDAR transgenic lines are represented by Mda1, Mda3 and Mda6. Mean values ± SE from triplicate determinations

Discussion

To efficiently regenerate AsA from MDHA we developed transgenic tobacco plants overexpressing the *AtMDAR1* gene. MDAR transgenic plants showed a significant increase in MDAR activity compared to SR-1 control plants (Fig. 3a). These results indicate that the enhanced MDAR activity in transgenic plants has resulted from the introduced MDAR transgene. The level of AsA and its redox state were markedly increased in MDAR transgenic plants compared to SR-1 control plants (Fig. 3b). This increase could be attributed to that transgenic plants were more efficient in converting MDHA to AsA before being disproportionated into the fully oxidized DHA form, that may rapidly hydrolyzes into 2,3-diketogulonic acid. Efficient cycling between reduced and oxidized forms of AsA minimizes DHA degradation (Horemans et al. 2000). Therefore, the increase in AsA level and the decrease in DHA coupled with the improved redox state of AsA in MDAR transgenic plants could be understood through the enhanced recycling capacity resulted from the enhanced MDAR activity.

Upon exposure to high concentrations of ozone, plants respond by triggering various defense systems including the antioxidative mechanisms (Sharma and Davis 1997). Ozone sensitivity is generally correlated with AsA status of the leaf tissues (Conklin et al. 1996; Conklin and Barth 2004). The enhanced tolerance to ozone in our transgenic plants (Fig. 4a) could be due to the elevated levels of AsA (Fig. 3b), which mainly resulted from the enhanced activity of MDAR (Fig. 3a). Several reports have indicated that higher activities of scavenger antioxidant enzymes may protect from oxidative stress (Asada 1997; Pasqualini et al. 2001).

The higher redox state of ascorbate in MDAR transgenic tobacco plants could also explain the enhanced tolerance to ozone stress, which is consistent with the results reported by Sanmartin et al. (2003) that a decreased AsA/DHA ratio increased ozone sensitivity in transgenic tobacco plants overexpressing cucumber ascorbate oxidase gene. Furthermore, apoplastic AsA represents the first line of defense against potentially damaging external oxidants such as ozone, SO_2 and NO_2 (Plöchl et al. 2000; Barnes et al. 2002).

Overexpressing MDAR in cytosol might have maintained continuous flux of reduced AsA towards apoplast and consequently provided better protection against ozone. These results are in general agreement with several reports indicating the importance of AsA in providing resistance against oxidative stress imposed by ozone (Tanaka et al. 1985; Sharma and Davis 1997; Eltayeb et al. 2006). Although plants can limit ozone damage by avoiding ozone entry to the interior of the leaf through stomatal closure, Chen and Gallie (2005) have clearly shown that increasing the level of AsA confers greater protection against ozone than increasing avoidance.

AsA is important in photo-protection and the regulation of photosynthesis (Noctor and Foyer 1998), and probably plays an important role in providing resistance to oxidative stress imposed by ozone exposure (Sharma and Davis 1997). The effective PSII photon-yield decreased more rapidly in SR-1 control plants than in MDAR transgenic plants under ozone stress (Fig. 4b). Therefore, the greater protection of PSII photochemical activity in MDAR transgenic plants might be conferred by efficient supply of the regenerated AsA maintained by MDAR-overexpressed levels.

The enhanced tolerance to salt stress in term of higher net photosynthesis in MDAR transgenic plants (Fig. 5a) could be understood through the higher levels of AsA and its maintained redox status. These results are in good agreement with our previous report that transgenic tobacco plants overexpressing DHAR in cytosol and had higher AsA/DHA ratio showed enhanced tolerance to salt stress (Eltayeb et al. 2006), and with Yamamoto et al. (2005) who reported that transgenic tobacco plants expressing ascorbate oxidase gene in antisense orientation exhibited higher AsA/DHA ratio, higher photosynthetic activity and lower H_2O_2 contents.

Under salt stress, AsA is important in protecting and restoring the photochemical activity of PSII as demonstrated using the ascorbate-deficient *Arabidopsis* mutant (Huang et al. 2005). MDAR transgenic plants maintained greater PSII photon yield under salt stress compared to SR-1 control plants (Fig. 5b), which could be attributed to the increased level of AsA and the redox state.

Ascorbate regeneration is necessary for the reductive detoxification of H_2O_2 (Hossain et al. 1984), as well as its biosynthesis (Wheeler et al. 1998). Excess accumulation of H_2O_2 is one of the mechanisms by which plants are damaged under salt and drought stresses (Mittler 2002). H_2O_2 is able to pass through cell membranes and reach cell locations remote from its site of formation (Foyer et al. 1997). MDAR transgenic plants showed significantly lower levels of H_2O_2 (Fig. 6) and higher photosynthetic activity (Fig. 5a) under salt stress compared to SR-1 control plants which could be mainly due to a fast removal of H_2O_2 during stress resulting from the elevated levels of AsA. Moreover, under salinity conditions AsA is reported to be mainly regenerated from MDHA (Mittova et al. 2000). Therefore, the enhanced tolerance to salt stress in MDAR transgenic plants could also be attributed to the overexpressed levels of MDAR that efficiently regenerated protective levels of AsA. These are consistent with the results reported by Huang et al. (2005) that H_2O_2 increased more dramatically in an ascorbate-deficient *Arabidopsis* mutant than in wild type plant under salt stress.

The higher photosynthetic rates in MDAR transgenic plants under PEG-induced water stress (Fig. 7) could be attributed directly to the higher levels of AsA in these transgenic plants. Similarly, we have demonstrated that elevating AsA levels by overexpressing DHAR enhanced photosynthetic activity in transgenic tobacco plants under PEG-induced stress (Eltayeb et al. 2006). Moreover, Adriano et al. (2005) reported that the level of total AsA that could limit cellular damage caused by ROS is an important attribute linked to drought tolerance in four interspecific *Prunus* hybrids.

The reduction on net photosynthesis in both transgenic and controlled plants with the advancement of the stresses might be mainly due to the accumulation of ROS including H_2O_2, which exceeds ROS scavenging capacity of antioxidant enzymes functioning on its removal.

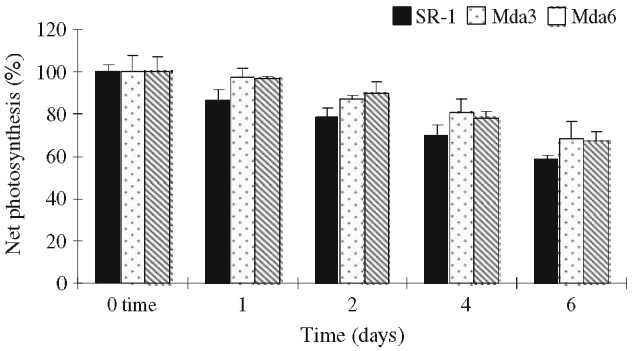

Fig. 7 Net photosynthesis (%) during PEG stress imposed on MDAR-overexpressing transgenic and control plants (SR-1). 100% net photosynthesis (μmol CO_2 m^{-2} s^{-1}) for SR-1, Mda1, Mda3 and Mda6 is 15.6, 15.7, 15.0 and 15.9, respectively. The 100% net photosynthesis measurement for each line was taken immediately before applying 10% (w/v) PEG solution (0 time). Mean values ± SE from triplicate determinations

In conclusion, our results suggest that elevating AsA levels through overexpression of MDAR would significantly contribute in enhancing plants tolerance to oxidative stress. Further studies in the consequences of MDAR-overexpression on the redox state of glutathione and on the activation status of other antioxidant enzymes are needed and will be very valuable in answering any questions that might remain.

Acknowledgments This work was supported by the Strategic International Cooperative Program from Japan Science and Technology Agency (JST), 21st Century COE Program for Arid Land Science from Japan ministry of Education, Culture, Sports, Science and Technology (MONBUSHO) and the Core University Program from Japan Society for the Promotion of Science (JSPS).

References

Adriano S, Angelo CT, Bartolomeo D, Cristos X (2005) Influence of water deficit and rewatering on the components of the ascorbate–glutathione cycle in four interspecific *Prunus* hybrids. Plant Sci 169:403–413

Agrawal M, Krizek DT, Argawal SB, Kramer GF, Lee EH, Mirecki RM, Rowland RA (1993) Influence of inverse day/night temperature on ozone sensitivity and selected morphological and physiological responses of cucumber. J Am Soc Hortic Sci 118:649–654

Allen RA, Webb RP, Schake SA (1997) Use of transgenic plants to study antioxidant defenses. Free Radic Biol Med 23:473–479

Asada K (1997) The role of ascorbate peroxidase and monodehydroascorbate reductase in H_2O_2 scavenging in plants. In: Scandalios JG (ed) Oxidative stress and the molecular biology of antioxidant defenses. Cold Spring Harbor Laboratory Press, New York, pp 715–735

Badawi GH, Kawano N, Yamauchi Y, Shimada E, Sasaki R, Kubo A, Tanaka K (2004a) Over-expression of ascorbate peroxidase in tobacco chloroplasts enhances the tolerance to salt stress and water deficit. Physiol Plant 121:131–238

Badawi GH, Yamauchi Y, Shimada E, Sasaki R, Kawano N, Tanaka K, Tanaka K (2004b) Enhanced tolerance to salt stress and water deficit by overexpressing superoxide dismutase in tobacco (*Nicotiana tabacum*) chloroplast. Plant Sci 166:919–928

Barnes JD, Velissariou D, Davison AW, Holevas CD (1990) Comparative ozone sensitivity of old and modern Greek cultivars of spring wheat. New Phytol 116:707–714

Barnes JD, Zheng Y, Lyons TM (2002) Plant resistance to ozone: the role of ascorbate. In: Omasa K, Saji H, Youssefian S, Kondo N (eds) Air pollution and plant biotechnology. Springer, Tokyo, pp 235–254

Borraccino G, Dipierro S, Arrigoni O (1986) Purification and properties of ascorbate free radical reductase from potato tubers. Planta 167:521–526

Bradford MM (1976) A rapid and sensitive method for the quantitation of microgram quantities of protein utilizing the principle of protein-dye binding. Anal Biochem 72: 248–254

Chen Z, Gallie DR (2005) Increasing tolerance to ozone by elevating foliar ascorbic acid confers greater protection against ozone than increasing avoidance. Plant Physiol 138:1673–1689

Chen Z, Young TE, Ling J, Chang SC, Gallie DR (2003) Increasing vitamin C content of plants through enhanced ascorbate recycling. Proc Natl Acad Sci USA 100:3525–3530

Conklin PL, Barth C (2004) Ascorbic acid, a familiar small molecule intertwined in the response of plants to ozone, pathogens and the onset of senescence. Plant Cell Environ 27:959–970

Conklin PL, Williams EH, Last RL (1996) Environmental stress sensitivity of an ascorbic acid-deficient *Arabidopsis* mutant. Proc Natl Acad Sci USA 93:9970–9974

Dalton DA, Langeberg L, Robbins M (1992) Purification and characterization of monodehydroascorbate reductase from soybean root nodules. Arch Biochem Biophys 292: 281–286

Dalton DA, Baird LM, Langeberg L, Taugher CY, Anyan WR, Vance CP, Sarath G (1993) Subcellular localization of oxygen defense enzymes in soybean (*Glycine max* [L.] Merr.) root nodules. Plant Physiol 102:481–489

De Leonardis S, De Lorenzo G, Borraccino G, Dipierro S (1995) A specific ascorbate free radical reductase isozyme participates in the regeneration of ascorbate for scavenging toxic oxygen species in potato tuber mitochondria. Plant Physiol 109:847–851

Deutsch JC (2000) Dehydroascorbic acid. J Chromatogr 88:301–309

Eltayeb AE, Kawano N, Badawi GH, Kaminaka H, Sanekata T, Morishima I, Shibahara T, Inanaga S, Tanaka K (2006) Enhanced tolerance to ozone and drought stresses in transgenic tobacco overexpressing dehydroascorbate reductase in cytosol. Physiol Plant 127:57–65

Foyer CH, Lelandais M, Kunert KJ (1994) Photooxidative stress in plants. Physiol Plant 92:696–717

Foyer CH, Lopez-Delgado H, Dat JE, Scott IM (1997) Hydrogen peroxide and Glutathione associated mechanisms of acclamatory stress tolerance and signaling. Physiol Plant 100:241–254

Frew J, Jones P, Scholes G (1983) Spectophotometric determination of hydrogen peroxide and organic hydroperoxides at low concentrations in aqueous solution. Anal Chim Acta 155:130–150

Grantz AA, Brummell DA, Bennett AB (1995) Ascorbate free radical reductase mRNA levels are induced by wounding. Plant Physiol 108:411–418

Halliwell B, Gutteridge JMC (2000) Free radicals in biology and medicine. Oxford University Press, New York

Hernández JA, Corpas FJ, Gomez M, Del Río LA, Sevilla F (1993) Salt induced oxidative stress mediated by activated oxygen species in pea leaf mitochondria. Physiol Plant 89:103–110

Horemans N, Foyer Ch, Potters G, Asard H (2000) Ascorbate function and associated transport systems in plants. Plant Physiol Biochem 38:531–540

Hossain MA, Asada K (1984) Inactivation of ascorbate peroxidase in spinach chloroplast on dark addition of hydrogen peroxide: Its protection by ascorbate. Plant Cell Physiol 25:1285–1295

Hossain MA, Asada K (1985) Monodehydroascorbate reductase from cucumber is a flavin adenine dinucleotide enzyme. J Biol Chem 260:12920–12926

Hossain MA, Nakano Y, Asada K (1984) Monodehydroascorbate reductase in spinach chloroplasts and its participation in regeneration of ascorbate for scavenging hydrogen peroxide. Plant Cell Physiol 25:385–395

Huang C, He W, Guo J, Chang X, Su P, Zhang L (2005) Increased sensitivity to salt stress in an ascorbate-deficient *Arabidopsis* mutant. J Exp Bot 56:3041–3049

Jiménez A, Hernández JA, del Río LA, Sevilla F (1997) Evidence for the presence of the ascorbate-glutathione cycle in mitochondria and peroxisomes of pea leaves. Plant Physiol 114:275–284

Kerk NM, Feldman LJ (1995) A biochemical model for the initiation and maintenance of the quiescent centre: implication for organization of root meristems. Development 121:2825–2833

Kwon SY, Ahn YO, Lee HS, Kwak SS (2001) Biochemical characterization of transgenic tobacco plants expressing a human dehydroascorbate reductase gene. J Biochem Mol Biol 34:316–321

Leterrier M, Corpas FJ, Barroso JB, Sandalio LM, del Río LA (2005) Peroxisomal monodehydroascorbate reductase. Clone characterization and functional analysis under environmental stress conditions. Plant Physiol 183:2111–2123

Lisenbee CS, Lingard MJ, Trelease RN (2005) *Arabidopsis* peroxisomes possess functionally redundant membrane and matrix isoforms of monodehydroascorbate reductase. Plant J 43:900–914

Mittler R (2002) Oxidative stress, antioxidants and stress tolerance. Trends Plant Sci 7:405–410

Mittova V, Volokita M, Guy M, Tal M (2000) Activities of SOD and the ascorbate–glutathione cycle enzymes in subcellular compartments in leaves and roots og the cultivated tomato and its wild salt-tolerant relative *Lycopersicon pennellii*. Physiol Plant 110:42–51

Murashige T, Skoog F (1962) A revised medium for rapid growth and bioassays with tobacco tissue cultures. Physiol Plant 15:473–497

Murthy SS, Zilinskas BA (1994) Molecular cloning and characterization of a cDNA encoding pea monodehydroascorbate reductase. J Biol Chem 269:31129–31133

Noctor G, Foyer CH (1998) Ascorbate and glutathione: keeping active oxygen under control. Annu Rev Plant Physiol Plant Mol Biol 49:249–279

Noctor G, Veljovic-Jovanivic S, Foyer CH (2000) Peroxide processing in photosynthesis: antioxidant coupling and redox signalling. Phil Trans R Soc Lond B 355:1465–1475

Pasqualini S, Batini P, Ederlina L, Porceddu A, Piccioni C, De Marchis F, Antonielli M (2001) Effects of short-term ozone fumigation on tobacco plants: response of the scavenging system and expression of the glutathione reductase. Plant Cell Environ 24:245–252

Pignocchi C, Foyer CH (2003a) Apoplastic ascorbate metabolism and its role in the regulation of cell signalling. Curr Opin Plant Biol 6:379–389

Pignocchi C, Fletcher JM, Wilkinson JE, Barnes JD, Foyer CH. (2003b) The function of ascorbate oxidase in tobacco. Plant Physiol 132:1631–1641

Plöchl M, Lyons T, Ollerenshaw J, Barnes J (2000) Simulating ozone detoxification in the leaf apoplast through the direct reaction with ascorbate. Planta 210:454–467

Runeckles VC, Chevone BI (1992) Crop responses to ozone. In: Lefohn AS (ed) Surface level ozone exposures and their effects on vegetation. Lewis, Chelsea, UK, pp 189–252

Sanmartin M, Drogoudi PA, Lyons T, Pateraki I, Barnes J, Kanellis AK (2003) Over-expression of ascorbate oxidase in the apoplast of transgenic tobacco results in altered ascorbate and glutathione redox states and increased sensitivity to ozone. Planta 216:918–928

Sano S, Tao S, Endo Y, Inaba T, Hossain MA, Miyake C, Matsuo M, Akoi H, Asada K, Saito K (2005) Purification and cDNA cloning of chloroplastic monodehydroascorbate reductase from spinach. Biosc Biotechnol Biochem 69:762–772

Sharma YK, Davis KR (1997) The effects of ozone on antioxidant responses in plants. Free Radic Biol Med 23:480–488

Smirnoff N, Wheeler GL (2000) Ascorbic acid in plants: biosynthesis and function. Crit Rev Plant Sci 19:267–290

Tanaka K, Suda Y, Kondo N, Sugahara K (1985) O_3 tolerance and the ascorbate-dependent H_2O_2 decomposing system in chloroplasts. Plant Cell Physiol 26:1425–1431

Ushimaru T, Nakagawa T, Fujioka Y, Daicho K, Naito M, Yamuchi Y, Nonaka H, Amako K, Yamawaki K, Murata N (2005) Transgenic *Arabidopsis* plants expressing the rice dehydroascorbate reductase gene are resistant to salt stress. J Plant Physiol. DOI 10.1016/j.jplph.2005.10.002

Wheeler GL, Jones MA, Smirnoff N (1998) The biosynthesis pathway of vitamin C in higher plants. Nature 393:365–369

Yamamoto A, Bhuiyan NH, Waditee R, Tanaka Y, Esaka M, Oba K, Jagendorf AT, Takabe T (2005) Suppressed expression of the apoplastic ascorbate oxidase gene increases salt tolerance in tobacco and *Arabidopsis* plants. J Exp Bot 56:1785–1796

Yoon H, Lee H, Lee I, Kim K, Jo J (2004) Molecular cloning of monodehydroascorbate reductase gene from *Brassica campestris* and analysis of its mRNA level in response to oxidative stress. Biochem Biphys Acta 1658:181–186

PHYSIOLOGIA PLANTARUM 123: 459–466. 2005
Printed in Denmark – all rights reserved

doi: 10.1111/j.1399-3054.2005.00481.x

Application of silicon enhanced drought tolerance in *Sorghum bicolor*

Taiichiro Hattori[a,*], Shinobu Inanaga[a], Hideki Araki[b], Ping An[a], Shigenori Morita[c], Miroslava Luxová[d] and Alexander Lux[e]

[a]*Arid Land Research Center, Tottori University, 1390 Hamasaka, Tottori, Tottori 680-0001, Japan*
[b]*Faculty of Agriculture, Yamaguchi University, 1677-1 Yoshida, Yamaguchi, Yamaguchi 753-8515, Japan*
[c]*Field Production Science Center, Graduate School of Agricultural and Life Sciences, The University of Tokyo, 1-1-1 Midori-cho, Nishitokyo, Tokyo 188-0002, Japan*
[d]*Institute of Botany, Slovak Academy of Sciences, Dúbravská cesta 14, SK-842 23 Bratislava, Slovak Republic*
[e]*Department of Plant Physiology, Faculty of Natural Sciences, Comenius University in Bratislava, Mlynská dolina B-2, SK-842 15 Bratislava, Slovak Republic*
**Corresponding author, e-mail: hat@alrc.tottori-u.ac.jp*

Received 28 July 2004; revised 22 November 2004

The effects of silicon application on the drought tolerance of sorghum (*Sorghum bicolor* (L.) Moench) were investigated for two cultivars differing in drought susceptibility. Silicon application ameliorated the decrease in dry weight under drought stress conditions, but had no effect on dry matter production under wet conditions. Under dry conditions, silicon-applied sorghum had a lower shoot to root (S/R) ratio, indicating the facilitation of root growth and the maintenance of the photosynthetic rate and stomatal conductance at a higher level compared with plants grown without silicon application. The diurnal determination of the transpiration rate indicated that the silicon-applied sorghum could extract a larger amount of water from drier soil and maintain a higher stomatal conductance. Very similar effects of silicon application were observed for both cultivars regardless of their drought susceptibility. These results suggest that silicon application may be useful to improve the drought tolerance of sorghum via the enhancement of water uptake ability.

Introduction

Sorghum (*Sorghum bicolor* (L.) Moench) is one of the most important crops of arid regions in Africa and Asia. Insecure water supply as a result of fluctuating precipitation and/or limited irrigation often causes a decrease in sorghum yield. Thus, it is important to enhance the drought tolerance of this economically important crop.

The application of certain mineral elements to various crops can influence their drought tolerance or traits involved in drought tolerance. For example, Purcell and King (1996) found that nitrogen supply to soybean enhanced its drought tolerance through an improvement in nodule activity. Phosphorus influences osmotic adjustment in leaf tissues in sorghum and bean (Alkaraki et al. 1996) and root characteristics in white clover (Singh and Sale 2000). Potassium contributes to the maintenance of osmotic adjustment in pearl millet (Ashraf et al. 2001) and to root growth in hibiscus (Egilla et al. 2001). Calcium increases antioxidant activity under drought stress conditions in liquorice (Li et al. 2003). The modification of fertilizer composition is therefore considered to be a useful method to improve crop productivity under drought conditions. However, few effects on drought tolerance have been reported for elements other than the major nutrients.

Certain seed plant species, mainly from the families Gramineae and Cyperaceae, accumulate large amounts of silicon. They are sometimes referred to as silicon accumulators. Silicon application to these plants ensures better growth, especially during environmental stress. Silicon application has been reported to alleviate the decrease in dry matter accumulation or photosynthetic

Abbreviations – ANOVA, analysis of variance.; DAS, days after sowing.; LAR, leaf area ratio.; NAR, net assimilation rate.; RGR, relative growth rate.; S/R ratio, shoot to root ratio.; WUE, water use efficiency.

rate caused by high salt concentration in various species of cereals (Matoh et al. 1986, Ahmad et al. 1992, Liang et al. 1996), high temperature (Okamoto 1969) and the toxicity of some heavy metals (Jarvis and Jones 1987, Hammond et al. 1995, Gu et al. 1998). A recent review on this subject is given in Ma (2004).

Silicon application may also be effective in enhancing the drought tolerance of plants. Under water stress conditions, such as soil drying and high water demand from the atmosphere, silicon-applied cereal crops have been reported to be able to retain a higher leaf water potential than crops grown without silicon application (Yoshida 1965, Matoh et al. 1991, Agarie et al. 1998). The formation of a silica – cuticle double layer on leaf epidermal tissue has been considered to be responsible (Yoshida 1965, Matoh et al. 1991). The active reaction of stomata to atmospheric humidity in rice (Agarie et al. 1998) and the decrease in the specific leaf area in wheat (Gong et al. 2003) have also been suggested to be involved in the inhibition of leaf water deficit. However, these data are insufficient to clarify completely the mechanism of improvement in drought tolerance caused by silicon application. As past studies have focused attention mainly on the prevention of excess water loss, as mentioned above, the effects of silicon application on water uptake ability, which cannot be ignored in a discussion of drought tolerance, remain unknown.

Endodermal tissue, which plays an important role in water transport across the root (Steudle and Peterson 1998), is known to accumulate large amounts of silicon in mature drought-tolerant sorghum cultivars (Lux et al. 2002). A similar observation has previously been observed in rice (Lux et al. 1999). These data, together with the high speed of silicon uptake and deposition by sorghum root (Lux et al. 2003), and the effects of losing root cell wall in sorghum (Hattori et al. 2003), suggest the possibility that silicon plays an important role in water transport and/or root growth of sorghum under drought conditions.

In terms of the effect of silicon on sorghum, information regarding drought tolerance and water uptake ability is lacking. In the present study, we focused on the effects of silicon application on the growth and water relations of sorghum under water-limited conditions to verify whether silicon may be useful to enhance the drought tolerance of this species. To achieve this purpose, the effects of silicon were assessed for two cultivars differing in drought tolerance. The silicon-induced physiological reactions of sorghum were analysed from the viewpoint of water relations, water use efficiency (WUE) and photosynthesis.

Materials and methods

Plant materials, growth conditions and silicon treatments

Two sorghum cultivars differing in drought tolerance were used as plant materials in the present study. Seeds of the two sorghum cultivars were provided by the Soil & Water Research Center, Agricultural Research Corporation, Sudan. Gadambalia is a local cultivar in Sudan and is drought tolerant. Tabat is a drought-sensitive cultivar released for the irrigated regions. The morphological and physiological adaptations of both cultivars on exposure to drought stress have been reported previously (Salih et al. 1999, Tsuji et al. 2001, 2003).

Pot experiments were conducted in a glasshouse at the Arid Land Research Center, Tottori University, Tottori, Japan. Plastic pots filled with 15.0 kg sand dune Regosol (collected from Tottori sand dunes) were used for the experiment. The pots were covered with aluminium foil to prevent an increase in soil temperature caused by solar radiation. Each pot was fertilized with nitrogen, phosphorus and potassium at a rate of 1.0, 1.0 and 3.3 g per pot, respectively. As the source of potassium, potassium silicate was used in the silicon-applied treatment (+ Si) and potassium chloride in the silicon-deficient treatment (– Si). In the + Si treatment, 5.0 g of silicon was added to each pot. Trace element fertilizer containing 0.21 g g^{-1} of MgO, 0.0045 g g^{-1} of MnO and 0.0045 g g^{-1} of B_2O_3 was also supplied to each pot at a rate of 1.5 g per pot. The soil pH in all pots was adjusted to pH 7.6 with calcium hydroxide. Five seeds of sorghum were sown per pot and, thereafter, seedlings were thinned to a single plant on the 12th day after sowing (DAS). At 23 DAS, 100 ml of potassium silicate solution (100 mg l^{-1}) was applied to pots of the +Si treatment. Potassium chloride solution was applied to the pots of the –Si treatment to yield the same total potassium as in the +Si treatment. The pH in both solutions was adjusted to pH 5.5 with HCl prior to application. Plants were grown until 50 DAS.

Dry treatments

The sorghum seedlings contained in pots were adequately irrigated to yield a soil water content of 0.08 g g^{-1} until 24 DAS. Dry treatment was initiated at 25 DAS. During the period of dry treatment until 50 DAS, the water content of the pot soil was adjusted gravimetrically every day to 0.03 g g^{-1} for the dry treatment and 0.08 g g^{-1} for the wet treatment. Plastic sheets coated with aluminium film were placed on the soil surface to prevent evaporation from the pots.

Growth analysis, photosynthetic rate and WUE

The photosynthetic rate, transpiration rate, stomatal conductance and intercellular CO_2 concentration of the third-last fully expanded leaves were measured under clear and sunny weather using a portable photosynthesis system (LI-6400, LI-COR Inc., Lincoln, NE) at 39 and 40 DAS. The leaf water potential of the same leaves was measured by a pressure chamber (Model 1000, PMS Instrument Co., Corvallis, OR) during the daytime (10.00–14.00 h) at 46 DAS. The leaf blade, stem and root system were separately sampled at 50 DAS. The leaf area was measured with a leaf area meter (AAL-410, Hayashi Denko Inc., Tokyo, Japan) and the dry weight of each organ was measured after drying

samples in an oven at 80°C for 72 h. At least three plants from each treatment were used for statistical analysis.

Growth analysis was performed on the basis of dry weight and leaf area measured before and after the dry treatment. The relative growth rate (RGR), net assimilation rate (NAR) and leaf area ratio (LAR) were calculated according to the following formulae:

$$\mathrm{RGR} = \frac{\ln w_2 - \ln w_1}{t_2 - t_1}$$

$$\mathrm{NAR} = \frac{w_2 - w_1}{t_2 - t_1} \times \frac{\ln L_2 - \ln L_1}{L_2 - L_1}$$

$$\mathrm{LAR} = \frac{\ln w_2 - \ln w_1}{w_2 - w_1} \times \frac{L_2 - L_1}{\ln L_2 - \ln L_1}$$

where w_i and L_i are the total dry weight (g) and leaf area (m^2) on day t_i, respectively. The days t_1 and t_2 are the initial and last days of the dry treatment period, respectively.

Diurnal changes in the water content of the soil (average value of a whole pot) and the transpiration rate per unit leaf area were calculated from the transition of the pot weight and leaf area at 49 DAS. The water content was converted to water potential according to the water content–water potential curve of the soil (Inoue and Nomura 1983). WUE was also calculated according to the following formula:

$$\mathrm{WUE} = \frac{w_2 - w_1}{T}$$

where T is the total amount of water used for transpiration during the dry treatment period.

Measurement of silicon concentration

The silicon concentration in the soil taken from the pots in the + Si and – Si treatments was measured by the submerged soil incubation method according to Nonaka and Takahashi (1988). An air-dried 10 g soil sample was submerged in 60 ml of distilled water in a 100 ml polyethylene container and placed in an incubator at 40°C for 1 week. After 1 week, the silicon concentration of the supernatant was measured by the molybdenum blue method.

The silicon concentration of the third-last fully expanded leaves was measured according to Lux et al. (2002). Briefly, the dried powdered plant sample was ashed in a muffle oven at 500°C for 5 h. The plant ash was dissolved in diluted HCl (1 : 1; 10 ml) at 100°C. The process of dissolving in HCl and evaporation to dryness was repeated three times. Then, diluted HCl (1 : 1; 15 ml) was added and the sample was heated at 100°C, filtered, placed into a ceramic crucible and ashed again in the oven at 540°C for 5 h. After cooling, the weight of Si was determined gravimetrically.

Statistical analysis

Data were analysed statistically by analysis of variance (ANOVA), with subsequent comparison of means by the least significant difference (LSD) test.

Results

Silicon concentration in soil and leaves

The soluble silicon concentration in sand dune Regosol from the Tottori region used for the experiment was 21.1 mg kg^{-1} dry soil for the – Si treatment and 30.6 mg kg^{-1} for the + Si treatment. The silicon concentration in leaf blades was increased by silicon fertilizer application regardless of the soil water regime (Tables 1 and 2). There were no significant differences in the silicon concentrations between the cultivars.

Dry matter production

Silicon application did not influence the dry weight of the plants before the initiation of the dry treatment (data not shown). The effect of silicon application on plant size became visibly clear as the plants grew (Fig. 1). At 50 DAS, the dry weight of plants given the + Si/dry treatment was significantly higher than those given the – Si/dry treatment (Tables 1 and 2). In the – Si/dry treatment, the plant dry weight decreased by 77–80% compared with the – Si/wet treatment. In contrast, in the + Si/dry treatment, the plant dry weight decreased by only 53–54% compared with the + Si/wet treatment. The effect of silicon on the dry weight showed a similar tendency for both cultivars, but the increase in shoot dry weight was relatively higher in cv. Gadambalia than in cv. Tabat. In the wet treatment,

Table 1. Effects of silicon application on shoot dry weight (SDW), root dry weight (RDW), total dry weight (TDW), shoot to root (S/R) ratio and silicon concentration (%) in leaves of cv. Gadambalia. Data are the means of three replications. Different letters indicate significant differences by LSD ($P < 0.05$). *, †, NS, significant at the 0.1% and 5% level and not significant by analysis of variance (ANOVA), respectively.

Treatment	SDW (g)	RDW (g)	TDW (g)	S/R ratio	Si concentration (%)
+ Si, wet	43.9^{a}	25.0^{a}	69.0^{a}	1.76^{a}	1.85^{a}
– Si, wet	37.4^{a}	22.6^{a}	60.0^{a}	1.66^{a}	1.09^{b}
+ Si, dry	19.2^{b}	13.1^{b}	32.2^{b}	1.50^{a}	1.56^{ab}
– Si, dry	8.6^{c}	3.7^{c}	12.3^{c}	2.41^{b}	0.61^{c}
Dry	*	*	*	†	†
Silicon	†	†	†	NS	*
Dry × silicon	NS	NS	NS	†	NS
LSD (0.05)	9.3	6.7	15.7	0.58	0.47

Table 2. Effects of silicon application on shoot dry weight (SDW), root dry weight (RDW), total dry weight (TDW), shoot to root (S/R) ratio and silicon concentration (%) in leaves of cv. Tabat. Data are the means of three replications. Different letters indicate significant differences by LSD ($P < 0.05$). *, †, ‡, NS, significant at the 0.1%, 1% and 5% level and not significant by analysis of variance (ANOVA), respectively.

Treatment	SDW (g)	RDW (g)	TDW (g)	S/R ratio	Si concentration (%)
+ Si, wet	38.8^{a}	32.7^{a}	71.5^{a}	1.25^{ab}	2.03^{a}
– Si, wet	36.0^{a}	33.8^{a}	69.8^{a}	1.10^{ab}	1.09^{bc}
+ Si, dry	14.7^{b}	18.0^{b}	32.7^{b}	0.82^{a}	1.59^{ab}
– Si, dry	9.3^{b}	6.4^{c}	15.8^{c}	1.44^{b}	0.98^{c}
Dry	*	*	*	NS	NS
Silicon	NS	NS	‡	NS	†
Dry × silicon	NS	NS	NS	‡	NS
LSD (0.05)	5.9	11.3	12.1	0.46	0.57

the dry weight was not affected by silicon application. A significantly lower shoot to root (S/R) ratio was observed in + Si/dry plants compared with – Si/dry plants. The effect of silicon application on the S/R ratio was unclear in the wet treatment. These tendencies were similar in both cultivars.

In both cultivars, RGR was not affected by silicon application in the wet treatment (Table 3). Although RGR was reduced in the dry treatment in both cultivars, silicon application significantly alleviated the decrease in RGR (Table 3). LAR was higher in the – Si/dry treatment than in the + Si/dry treatment (Table 3).

Assimilation rate and stomatal conductance

The decrease in NAR due to drought stress was significantly ameliorated by silicon application (Table 3). However, silicon had no effect on NAR in wet conditions. The photosynthetic rate, transpiration rate and stomatal conductance of sorghum measured in the daytime (10.00 –14.00 h) were maintained at a significantly higher level in the + Si/dry treatment than in the – Si/dry treatment (Fig. 2). The parameters observed in the – Si/dry treatment were only 30–40% of those found in the –Si/wet treatment, whereas, in the +Si/dry treatment, the values were at least 75% of those in the +Si/wet treatment. The influence of silicon application on the intercellular CO_2 concentration (C_i) was undetectable regardless of the soil water status. These tendencies were quite similar for both cultivars (only data from Gadambalia are shown in Fig. 2).

Fig. 1. Effect of silicon application on the growth of sorghum under dry conditions. Sorghum plants (cv. Gadambalia) were grown in silicon-applied soil (left) and non-applied soil (right). Plants were 47 days old (22 days after the initiation of dry treatment).

WUE and water relations

The WUE in the dry treatment was significantly higher than that in the wet treatment in both cultivars ($P < 0.05$, tested by ANOVA). However, silicon application itself had no effect on WUE in both wet and dry treatments (Fig. 3). The diurnal transition of the soil water potential and transpiration rate per unit leaf area showed different trends in relation to silicon application in the dry treatment, but not in the wet treatment (Table 4, Fig. 4). The soil water potential in the + Si/dry treatment was slightly lower than that in the – Si/dry treatment during 09.00–11.00 h; thereafter, it markedly decreased at 13.00 h. Despite the lower soil water potential, sorghum plants in the + Si/dry treatment maintained the same or higher transpiration rate than those in the – Si/dry treatment. The leaf water potential in the daytime was not significantly different between the + Si/dry and – Si/dry plants (Fig. 5). In the wet treatments, the leaf water potentials were higher than those in the dry treatments, but no effect of silicon was detected. These characteristics of the leaf water potential and diurnal changes in transpiration rate were commonly observed in both cultivars (only data from Gadambalia are shown in Figs 4 and 5).

Discussion

Silicon is an abundant element in soil, but plant-available silicon is usually present at rather low concentrations in soil solution. If there is plenty of available silicon in the plant rhizosphere, sorghum absorbs more silicon than normal from the soil solution. Supplemental application of silicon increased the shoot silicon concentration and led to higher dry matter production under drought conditions in the present study (Tables 1 and 2, Fig. 1). The similar dry weight for + Si/wet and – Si/wet treatments also indicated that the chloride anion added with potassium to the – Si treatments in this study did not

Table 3. Effects of silicon application on the relative growth rate (RGR), net assimilation rate (NAR) and leaf area ratio (LAR) during the dry treatment in two sorghum cultivars differing in drought tolerance. Data are the means of three replications. Different letters indicate significant differences by LSD ($P < 0.05$). *, †, ‡, NS, significant at the 0.1%, 1% and 5% level and not significant by analysis of variance (ANOVA), respectively.

	Gadambalia			Tabat		
Treatment	RGR ($g\,g^{-1}\,day^{-1}$)	NAR ($g\,m^{-2}\,day^{-1}$)	LAR ($\times 10^{-4}\,m^2\,g^{-1}$)	RGR ($g\,g^{-1}\,day^{-1}$)	NAR ($g\,m^{-2}\,day^{-1}$)	LAR ($\times 10^{-4}\,m^2\,g^{-1}$)
+ Si, wet	0.157^{a}	28.3^{a}	55.9^{a}	0.160^{a}	29.4^{ab}	55.0^{a}
– Si, wet	0.149^{a}	25.1^{ab}	59.5^{a}	0.171^{a}	34.3^{a}	51.1^{a}
+ Si, dry	0.126^{b}	21.3^{b}	59.5^{a}	0.127^{b}	24.2^{b}	52.7^{a}
– Si, dry	0.083^{c}	10.9^{c}	76.5^{b}	0.106^{c}	15.0^{c}	70.6^{b}
Dry	*	*	†	*	†	‡
Silicon	*	†	†	NS	NS	‡
Dry × silicon	†	‡	‡	†	‡	‡
LSD (0.05)	0.020	4.61	7.94	0.014	9.2	10.6

have a negative effect on the dry matter production of sorghum (Tables 1 and 2).

Several reports have described the effect of several other elements on drought tolerance (e.g. Egilla et al. 2001, Li et al. 2003). In terms of the improvement in growth under dry conditions, these elements seem to achieve this through the enhancement of dry matter production itself, rather than through the enhancement of properties responsible for drought tolerance. All of these elements improved dry matter production in both wet and dry conditions (e.g. Rodriguez et al. 1996). Silicon is distinct from these elements, as silicon-induced acceleration of dry matter production in sorghum is observed only when the plants are subjected to drought (Tables 1 and 2). The specificity of the effect of silicon to dry conditions indicates that silicon affects certain traits restricting dry matter production under water-limited conditions. This is discussed below.

The results of growth analysis indicated that the enhancement of drought tolerance observed in the +Si/dry treatment was due to a higher dry matter production per unit dry weight (RGR), which was accounted for by the higher assimilation rate (NAR) or photosynthesis rate (Table 3, Fig. 2). Although the plants in the –Si/dry treatment had a higher LAR, indicating a larger leaf area per unit dry weight, it did not result in an increase in the total amount of dry matter production compared with the + Si/dry plants, which had higher NAR. The analysis of the characteristics related to WUE may also provide

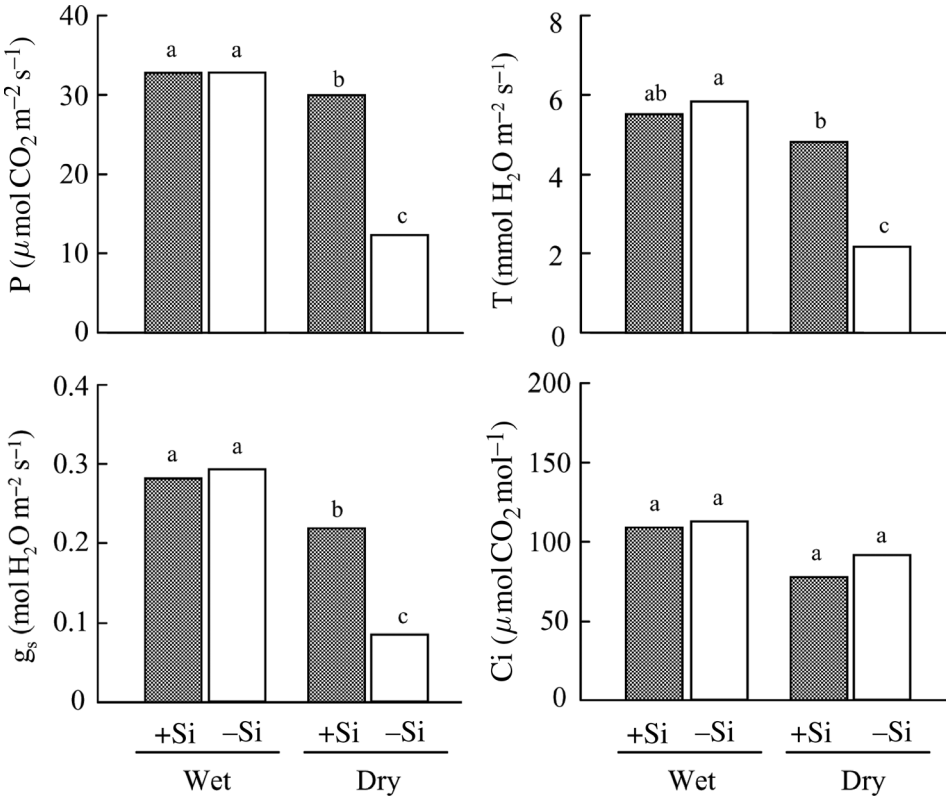

Fig. 2. Effects of silicon application and dry treatment on the photosynthetic rate (P), transpiration rate (T), stomatal conductance (g_s) and intercellular CO_2 concentration (C_i) in the third-last fully expanded leaf of cv. Gadambalia (drought-tolerant sorghum cultivar). Data are the means of three replications. Different letters in the figure indicate significant differences by LSD ($P < 0.05$).

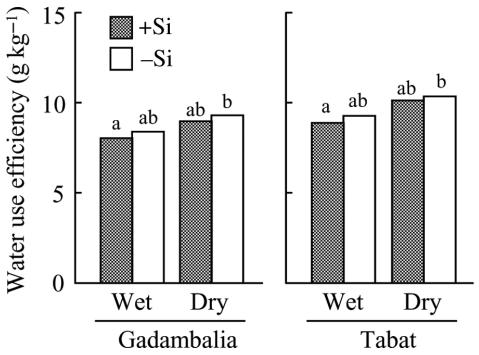

Fig. 3. Effects of silicon application and dry treatment on the water use efficiency of the two sorghum cultivars differing in drought tolerance. Data are the means of three replications. Different letters in the figure indicate significant differences by LSD ($P < 0.05$) for each cultivar.

an interpretation for the high drought tolerance of plants (Passioura 1977). The dry matter production of plants is determined by water consumption (transpiration) and WUE in addition to other factors. In the present study, although the WUE of sorghum increased with soil desiccation regardless of the cultivar, there were no significant changes in WUE with silicon application under either dry or wet conditions (Fig. 3). The higher dry matter production was achieved by an increase in transpiration rather than WUE. Thus, higher stomatal conductance, allowing a higher transpiration rate, was the main reason for the silicon-induced enhancement of photosynthesis under drought conditions. As stomatal conductance is mainly affected by leaf water status, we discuss the water relations of leaves below.

The transpiration rates in the + Si/dry treatment were considerably high around noon compared with those in the – Si/dry treatment (Figs 2 and 4, Table 4). The leaf water potential in the – Si/dry treatment decreased to almost − 2.0 MPa at midday (Fig. 5), which is the critical leaf water potential of sorghum leading to the closure of stomata (Tsuji, W. et al. 2004, unpublished data). In contrast, the leaf water potential in the + Si/dry treatment was above the critical potential. This indicated that, in the + Si/dry treatment, water uptake from the roots was more balanced with the high transpirational demand in the daytime and this prevented stomatal closure due to leaf water deficit, even when the soil was drying. One reason for the high water uptake may be the lower S/R ratio in the + Si/dry treatment (Tables 1 and 2), consequently allowing an increase in the root surface area per unit of leaf area. The lower S/R ratio in the + Si/dry treatment may compensate for the slower water flow from bulk soil to roots by expansion of the extractable root surface area (Sperry et al. 2002). In addition, hydraulic resistance in the water pathway through plants may play an important role in the increased water uptake, as certain nutrient elements can influence the hydraulic resistance of roots (Passioura 1988). Further physiological and ecological studies are needed to understand the drought-specific effects of silicon because the mechanism responsible for this phenomenon remains incompletely elucidated.

The observation that silicon increased the transpiration rate (Figs 2 and 4, Table 4) contradicted previous reports, which showed that silicon application in rice led to a decrease in transpiration via the formation of a cuticle – silica double layer, maintaining a high leaf water potential (Yoshida 1965, Matoh et al. 1991). Although there was a possibility that water loss from the cuticle might also have decreased with silicon application in sorghum plants, its effect on the total transpiration rate would have been quite small compared with that in rice. According to Matoh et al. (1991), the contribution of cuticular transpiration was about 25–39% of the total transpiration in rice, whereas it was only 3–9% in sorghum (Hattori, T. et al. 2004, unpublished data). The decrease in water loss from the cuticle would be masked by the increased transpiration from the stomata caused by silicon application.

The performances of the two cultivars were not significantly different with regard to the response to soil drying (Tables 1 and 2), except for the S/R ratio ($P < 0.01$, tested by ANOVA). Salih et al. (1999), Tsuji et al. (2001) and Tsuji et al. (2003) investigated the same two sorghum cultivars from a physiological and morphological viewpoint under drought conditions. They reported that cultivar differences

Table 4. Effects of silicon application and dry treatment on leaf area (LA), water uptake (WU) and transpiration rate per leaf area (T) during 09.00–13.00 h in two sorghum cultivars differing in drought tolerance. Data are the means of three replications. Different letters indicate significant differences by LSD ($P < 0.05$). *, †, ‡, NS, significant at the 0.1%, 1% and 5% level and not significant by analysis of variance (ANOVA), respectively.

	Gadambalia			Tabat		
Treatment	LA (m^2 plant^{-1})	WU (mol H_2O plant^{-1} h^{-1})	T (mmol H_2O m^{-2} s^{-1})	LA (m^2 plant^{-1})	WU (mol H_2O plant^{-1} h^{-1})	T (mmol H_2O m^{-2} s^{-1})
+ Si, wet	0.249^{a}	4.79^{a}	5.35^{a}	0.259^{a}	4.40^{a}	4.73^{a}
– Si, wet	0.242^{a}	4.40^{b}	5.07^{ab}	0.243^{a}	4.10^{b}	4.68^{a}
+ Si, dry	0.105^{b}	1.65^{c}	4.36^{b}	0.093^{b}	1.42^{c}	4.23^{a}
– Si, dry	0.066^{c}	0.64^{d}	2.70^{c}	0.072^{c}	0.75^{d}	2.90^{b}
Dry	*	*	*	*	*	*
Silicon	†	*	†	‡	*	†
Dry × silicon	‡	‡	‡	NS	NS	†
LSD (0.05)	0.018	0.34	0.75	0.020	0.28	0.50

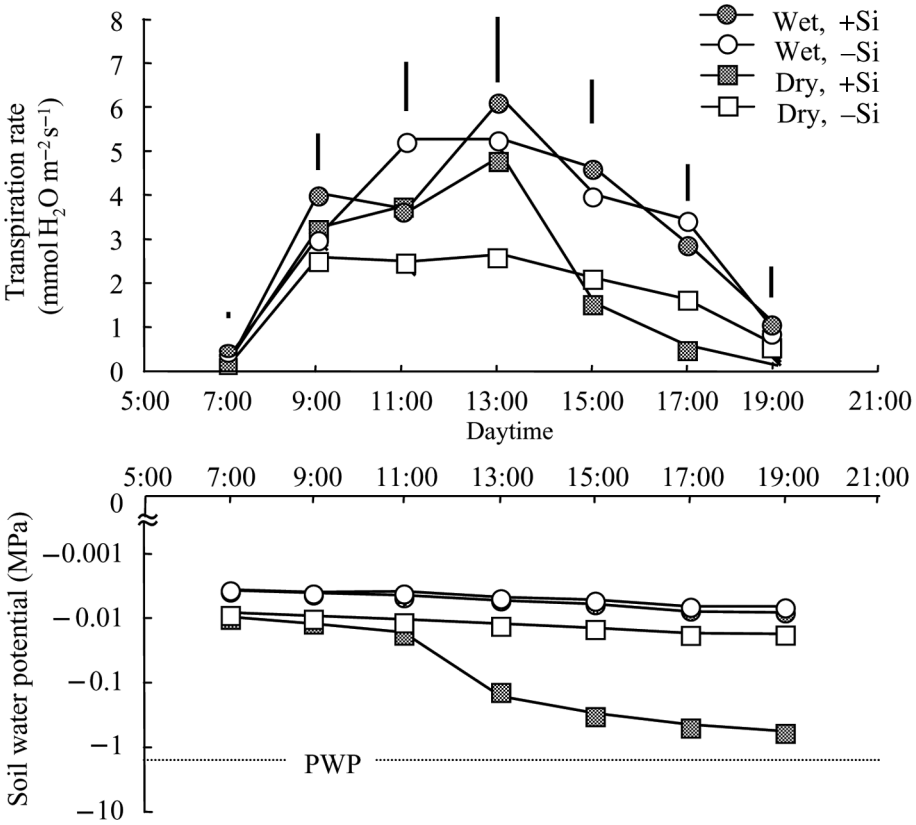

Fig. 4. Effects of silicon application and dry treatment on the diurnal change in transpiration rate per unit leaf area and the soil water potential in cv. Gadambalia (drought-tolerant sorghum cultivar). The soil water potential was calculated from the weight of the pots. The transpiration rate was derived from the decrease in pot weight and the total leaf area. Data are the means of three replications. Vertical bars represent the LSD (0.05) for each measurement. PWP, permanent wilting point.

in relation to drought tolerance resulted mainly from water uptake from the deep soil. In the present study, as the rooting zone was restricted by the limited pot volume, the availability of water was identical between the cultivars. This may have diminished the difference in dry matter production under drought conditions. With regard to silicon application, cultivar differences were ambiguous. Silicon application, however, apparently enhanced the dry matter production in both cultivars under drought conditions (Tables 1 and 2). This suggests that silicon application may be useful for the alleviation of drought stress in sorghum, irrespective of cultivar. Further research and field experiments are being performed at present to clarify the cultivar differences with respect to the effects of silicon.

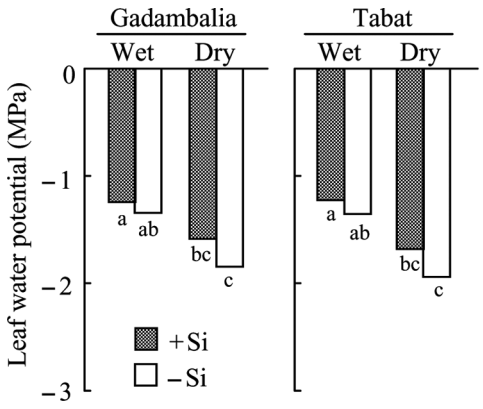

Fig. 5. Effects of silicon application and dry treatment on the leaf water potential. The leaf water potential was measured at 46 days after sowing (DAS) with the same leaves as used for photosynthetic measurement. Data are the means of three replications. Different letters in the figure indicate significant differences by LSD ($P < 0.05$) for each cultivar.

Acknowledgements – This work was supported by a grant for the 21st Century COE program from the Japan Society for the Promotion of Science and by a Research Fellowship from the Japan Society for the Promotion of Science for Young Scientists.

References

Agarie S, Uchida H, Agata W, Kubota F, Kaufman PB (1998) Effects of silicon on transpiration and leaf conductance in rice plants (*Oryza sativa* L.). Plant Prod Sci 1: 89–95

Ahmad R, Zaheer SH, Ismail S (1992) Role of silicon in salt tolerance of wheat (*Triticum aestivum* L.). Plant Sci 85: 43–50

Alkaraki GN, Clark RB, Sullivan CY (1996) Phosphorus nutrition and water stress effects on proline accumulation in sorghum and bean. J Plant Physiol 148: 745–751

Ashraf M, Ahmad A, McNeilly T (2001) Growth and photosynthetic characteristics in pearl millet under water stress and different potassium supply. Photosynthetica 39: 389–394

Egilla JN, Davies FT, Drew MC (2001) Effect of potassium on drought resistance of *Hibiscus rosa-sinensis* cv. Leprechaun: plant growth, leaf macro- and micronutrient content and root longevity. Plant Soil 229: 213–224

Gong HJ, Chen KM, Chen GC, Wang SM, Zhang CL (2003) Effects of silicon on growth of wheat under drought. J Plant Nutr 26: 1055–1063

Gu MH, Koyama H, Hara T (1998) Effects of silicon supply on amelioration of aluminum injury and chemical forms of aluminum in rice plants. Jpn J Soil Sci Plant Nutr 69: 498–505
Hammond KE, Evans DE, Hodson MJ (1995) Aluminium/silicon interactions in barley (*Hordeum vulgare* L.) seedlings. Plant Soil 173: 89–95
Hattori T, Inanaga S, Tanimoto E, Lux A, Luxová M, Sugimoto Y (2003) Silicon-induced changes in viscoelastic properties of sorghum root cell walls. Plant Cell Physiol 44: 743–749
Inoue M, Nomura Y (1983) Laboratory determination of dune sand water constants and soil water characteristic curves during the drying process. Sand Dune Res 30: 15–25
Jarvis SC, Jones LHP (1987) The absorption and transport of manganese by perennial ryegrass and white clover as affected by silicon. Plant Soil 99: 231–240
Li M, Wang GX, Lin JS (2003) Application of external calcium in improving the PEG-induced water stress tolerance in liquorice cells. Bot Bull Acad Sin 44: 275–284
Liang Y, Shen Q, Shen Z, Ma T (1996) Effects of silicon on salinity tolerance of two barley cultivars. J Plant Nutr 19: 173–183
Lux A, Luxová M, Abe J, Tanimoto E, Hattori T, Inanaga S (2003) The dynamics of silicon deposition in the sorghum root endodermis. New Phytol 158: 437–441
Lux A, Luxová M, Hattori T, Inanaga S, Sugimoto Y (2002) Silicification in sorghum (*Sorghum bicolor*) cultivars with different drought tolerance. Physiol Plant 115: 87–92
Lux A, Luxová M, Morita S, Abe J, Inanaga S (1999) Endodermal silicification in developing seminal roots of lowland and upland cultivars of rice (*Oryza sativa* L.). Can J Bot 77: 955–960
Ma JF (2004) Role of silicon in enhancing the resistance of plants to biotic and abiotic stresses. Soil Sci Plant Nutr 50: 11–18
Matoh T, Kairusmee P, Takahashi E (1986) Salt-induced damage to rice plants and alleviation effect of silicate. Soil Sci Plant Nutr 32: 295–304
Matoh T, Murata S, Takahashi E (1991) Effect of silicate application on photosynthesis of rice plants (in Japanese). Jpn J Soil Sci Plant Nutr 62: 248–251
Nonaka K, Takahashi K (1988) A method of measuring available silicates in paddy soils. Jpn Agric Res Q 22: 91–95
Okamoto Y (1969) Physiological studies on the effects of silicic acid upon rice plants XIII. Effects of silicic acid on the formation of organs and tissues of rice plants. Jpn J Crop Sci 38: 748–751
Passioura JB (1977) Grain yield, harvest index and water use of wheat. J Austr Inst Agric Sci 43: 117–120
Passioura JB (1988) Water transport in and to roots. Annu Rev Plant Physiol Plant Mol Biol 39: 245–265
Purcell LC, King CA (1996) Drought and nitrogen source effects on nitrogen nutrition, seed growth, and yield in soybean. J Plant Nutr 19: 969–993
Rodriguez D, Goudriaan J, Oyarzabal M, Pomar MC (1996) Phosphorus nutrition and water stress tolerance in wheat plants. J Plant Nutr 19: 29–39
Salih AA, Ali IA, Lux A, Luxová M, Cohen Y, Sugimoto Y, Inanaga S (1999) Rooting, water uptake, and xylem structure adaptation to drought of two sorghum cultivars. Crop Sci 39: 168–173
Singh DK, Sale PWG (2000) Growth and potential conductivity of white clover roots in dry soil with increasing phosphorus supply and defoliation frequency. Agron J 92: 868–874
Sperry JS, Stiller V, Hacke UG (2002) Soil water uptake and water transport through root systems. In: Waisel Y, Eshel A, Kafkafi U (eds) Plant Roots: the Hidden Half, 3rd edn. Marcel Dekker, New York, pp 663–681
Steudle E, Peterson CA (1998) How does water get through roots? J Exp Bot 49: 775–788
Tsuji W, Ali MEK, Inanaga S, Sugimoto Y (2003) Growth and gas exchange of three sorghum cultivars under drought stress. Biol Plant 46: 583–587
Tsuji W, Inanaga S, Sugimoto Y, Morita S, Ali MEK (2001) Morphological and physiological responses of root system to water stress in two sorghum cultivars. In: Proceedings of the 6th Symposium of the International Society of Root Research Extra Issue, Japanese Society for Root Research, Nagoya, Japan, pp 316–317
Yoshida S (1965) Chemical aspects of the role of silicon in physiology of the rice plant (in Japanese). Bull Nat Inst Agr Sci B15: 18–58

Edited by M.T. Tyree

Soil Science and Plant Nutrition (2006) **52**, 540–544 doi: 10.1111/j.1747-0765.2006.00057.x

ORIGINAL ARTICLE

Effects of the application of porous glass material treated with phosphate on the growth of tomato plants and the phyto-available phosphate in soil

Ryoji NAKAZAWA[1], Hisashi TOMEMORI[1], Atsuko HIRANO[2], Hidetoshi MOCHIZUKI[1], Ping AN[1] and Shinobu INANAGA[1]

[1]*Arid Land Research Center, Tottori University, Hamasaka 1390, Tottori 680-0001, and* [2]*Graduate School of Agriculture, Tottori University, Koyamacho-minami 4-101, Tottori 680-8553, Japan*

Abstract

We have previously reported the ability of porous glass material (PGM) to adsorb phosphate and that calcium contributed to this process. In the present investigation, the possible use of PGM to improve water quality (wastewater in particular) and the subsequent use of phosphate-adsorbed PGM as fertilizer were examined. We confirmed the phyto-availability of phosphate adsorbed onto PGM using tomato cultivation and an assay of truog-phosphate levels. Adsorption and release of phosphate in PGM was controlled by particle size. The findings suggest the possibility of using PGM of different particle sizes for efficient phosphate recycling in soil-water/plant systems.

Key words: phosphate, porous glass material, recycling, tomato, truog-phosphate.

INTRODUCTION

Eutrophication in a closed water system is caused by wastewater produced by households, industry and livestock. Phosphate in wastewater is a key substance that contributes to eutrophication. To solve this problem, prevention laws applied to closed water systems to maintain water quality have been legislated, and these laws have controlled the emission of phosphate. Nevertheless, the contamination of phosphate in closed water systems is still occurring (Kunimatsu 1995).

In contrast, phosphate is a key nutrient for the maintenance of crop productivity. Exhaustion of the origins of phosphate fertilizer (phosphate deposits) is, however, predicted to occur at some point in the twenty-first century (Koshino 1994).

To deal with the above problems, we have proposed the establishment of a recycling system of phosphate in the soil-water/plant system (Inanaga *et al.* 2005). In this system, phosphate-adsorption materials are added to the wastewater produced by households, industry and livestock effluents. Following this, the phosphate-adsorbed materials are collected and used as phosphate fertilizer.

In a previous paper, it was reported that porous glass material (PGM) adsorbed phosphate (Inanaga *et al.* 2005). Porous glass materials are recycled materials made from waste glasses and foaming agents (such as crushed shells and $CaCO_3$) (Hara *et al.* 1998). Porous glass materials are light-weight and have many pores. In addition, we found that the adsorption of phosphate is caused by the calcium in the foaming agents (Inanaga *et al.* 2005). From the above results and the finding that plants can use calcium-binding phosphate in soil (Takahashi 1998), it is expected that PGM can be used as the phosphate-adsorption materials in the above phosphate-recycling system. However, several investigators have reported that in phosphate-adsorption materials, phosphate adsorption is caused by the aluminum and iron in these materials (e.g. Yanagida and Jiang 1994; Tanada *et al.* 2003) and is, thus, not available for use by plants (Takahashi 1998). In this paper, we confirm the phyto-availability of phosphate-adsorbed PGM using cultivation examination and soil analysis.

MATERIALS AND METHODS

Preparation of porous glass material

Porous glass materials (Fig. 1) were provided by the Ehime Recycling Institute Company (Niihama, Ehime,

Correspondence: P. An, Arid Land Research Center, Tottori University, Hamasaka 1390, Tottori, 680-0001, Japan. Email: an.ping@alrc.tottori-u.ac.jp

Received 24 January 2006.
Accepted for publication 25 April 2006.

Figure 1 Porous glass materials without being crushed.

Japan). The manufacturing of PGM occurred, briefly, as follows. First, wood and metal impurities were removed from waste glasses and then the glasses were crushed to approximately 10 mm in diameter. Next, the crushed glasses were milled to pieces of approximately 500 μm in diameter. Crushed shells (oysters with the main component being $CaCO_3$) were also milled briefly and mixed with the milled glasses to 0.005 g g^{-1}, and then the mixture was burned at 900°C for 30 min. The PGM were crushed and sieved and PGM that were < 1, 1–2 or 2–4 mm in diameter (not enough material > 4 mm was collected) were used in the following experiments.

Phosphate-adsorption experiments

One gram of PGM (< 1, 1–2 and 2–4 mm diameter) was soaked in 5 mL of 1–100 mg L^{-1} phosphate (PO_4-P) solution (as KH_2PO_4) for 24 h and then the upper solution was obtained and filtered using 0.2 μm membrane filters (Millipore IC-Millex-LG, Tokyo, Japan). The phosphate concentrations in the filtrates were measured using the molybdenum-blue method (Aso *et al.* 1985).

Cultivation experiments

First, phosphate-adsorbed PGM was prepared. One gram of PGM (2–4 mm diameter) was soaked in 5 mL of 100 mg L^{-1} phosphate solution for 24 h, and then the upper solution was obtained and filtered using 0.2 μm membrane filters. The phosphate concentrations in the filtrates were measured using the molybdenum-blue method. This procedure was repeated six times to complete the phosphate-adsorption reaction. The remaining PGM was rinsed in 1.5 L kg^{-1} of 0.8 L L^{-1} ethanol and then the ethanol was removed and dried up. At this time, the retention of phosphate onto PGM was 646 (mg P kg^{-1} PGM). As a control, distilled-water-treated PGM was prepared using the above procedure but with the addition of distilled water rather than phosphate solution. The phosphate-adsorbed PGM and the distilled-water-treated PGM were used in the following cultivation experiments.

For the cultivation experiments, Tottori sand dune sand was used as the medium. The soil texture of the soil was S (sandy). The sandy soil consisted of 0.96 g g^{-1} of sand and 0.04 g g^{-1} of silt and clay. The truog-phosphate level was below the quantification limit, so the soil was classed as being deficient in phosphate. Porous glass material was added to air-dried sandy soil to 0.20 g g^{-1} and distilled water was also added to pF = 1.5. The mixtures were placed into 230-mL pots. Treatments were as follows: (1) no phosphate fertilizer + distilled-water-treated PGM (–P+G), (2) no phosphate fertilizer + phosphate-adsorbed PGM (–P+GP), (3) phosphate fertilizer + distilled-water-treated PGM (+P+G), (4) phosphate fertilizer + phosphate-adsorbed PGM (+P+GP), (5) phosphate fertilizer alone (+P). For each group, there were 15 replicates. The application of 'phosphate fertilizer' in (3), (4) and (5) was conducted by irrigation of 40 mL of 2.25-fold strength Hoagland solution into pots at 0, 15 and 30 days after the sowing of tomato (*Lycopersium esculentum* L. Fukuju-2) seeds. At this time, the total phosphate (100 mg P_2O_5 per pot) in Hoagland solution was applied to the sowing seeds. 'No phosphate fertilizer' in the –P+G and –P+GP treatments was conducted by application of Hoagland solution containing no phosphate. Tomato plants were grown in a plastic greenhouse for 44 days and then harvested. Following this, the plant materials were dried at 80°C for 72 h and the dry weights of shoots and roots were measured.

To estimate the effects of the application of phosphate-adsorbed PGM on the phyto-available phosphate in soil, we determined the truog-phosphate levels (Nanjo 1997) and the pH(H_2O) (Kamewada 1997) in the soil of each treatment as outlined above.

In the present study, we focus on two aspects of the fertilizer effects of PGM. One aspect is whether or not plants can use the phosphate that is adsorbed onto PGM. To determine this, we compared the results of treatments –P+G and –P+GP. The second aspect is that, after plants make use of phosphate provided from phosphate-adsorbed PGM, phosphate-free PGM remains. Does the phosphate-free PGM negatively affect soil phosphate fertility? To examine this, we compared treatments +P+G, +P+GP and +P.

We selected tomato as the plant material. PGMs release silicate as well as adsorb phosphate (Murakami 2003), and silicate is considered to be beneficial for certain plant species (Takahashi 1999). For example, silicate improves photosynthesis and provides tolerance to disease, environmental stress and insects; it also

Table 1 Phosphate adsorption of porous glass materials of different particle sizes

Particle sizes of porous glass materials	Initial phosphate concentrations (mg L^{-1})	Phosphate concentrations after 24 h (mg L^{-1})	Adsorption ratio (%)	Phosphate contents in porous glass materials (mg kg^{-1})
< 1 mm	1	0.90 ± 0.01	10.5 ± 0.80	0.52 ± 0.04
	10	7.26 ± 0.00	27.4 ± 0.32	13.7 ± 0.16
	100	70.4 ± 0.00	29.6 ± 0.13	148 ± 0.67
1–2 mm	1	0.76 ± 0.02	23.9 ± 1.92	1.19 ± 0.10
	10	6.86 ± 0.01	31.4 ± 0.55	15.7 ± 0.27
	100	64.9 ± 0.01	35.1 ± 1.11	176 ± 5.53
2–4 mm	1	0.67 ± 0.01	33.2 ± 1.37	1.66 ± 1.37
	10	5.81 ± 0.04	41.9 ± 3.76	18.3 ± 2.30
	100	47.3 ± 0.04	52.7 ± 4.17	237 ± 20.9

Data are mean ± standard error (n = 3).

increases crop yield in plants such as rice and cucumber. Therefore, to make it easier to analyze the fertilizer effects of PGM, we selected tomato plants because these plants do not appear to be affected by silicate application (Takahashi 1999). In addition, tomato plants are sensitive to a low concentration of phosphate (Tadano 1999), so it is easy to prepare phosphate-deficient tomato plants.

RESULTS AND DISCUSSION

To preliminarily determine the amount of PGM to be applied to the soil, the effects of PGM on soil physical properties (saturated hydraulic conductivity and water-holding capacity; soil water characteristic curves) were determined. The results showed that 0.2 g g^{-1} PGM did not affect these soil properties (data not shown). Therefore, the amount of PGM applied to the soil in the following experiments was 0.2 g g^{-1}. In addition, because the truog-phosphate level in soil treated with 0.2 g g^{-1} of +GP alone was not significantly different to that in the +P treatment, we expected to be able to determine the side effects of PGM as well as the provision of phosphate from the comparison between those two treatments.

In another preliminary experiment, we compared the phosphate adsorption of PGM of different particle sizes (< 1, 1–2 and 2–4 mm diameter). The highest adsorption was in the 2–4-mm particles at each phosphate concentration, followed by the 1–2-mm and < 1-mm particles (Table 1). These results show that larger-sized PGMs have a higher phosphate adsorption. In general, smaller-sized absorbents have a larger surface area and higher adsorption capacity. In contrast, PGMs have numerous pores of ~1 mm in diameter, as shown in Fig. 1, but these pores were destroyed in the smaller-sized material. The findings show that the phosphate adsorption of PGM is affected by physical factors, such as the number of pores, as well as chemical factors,

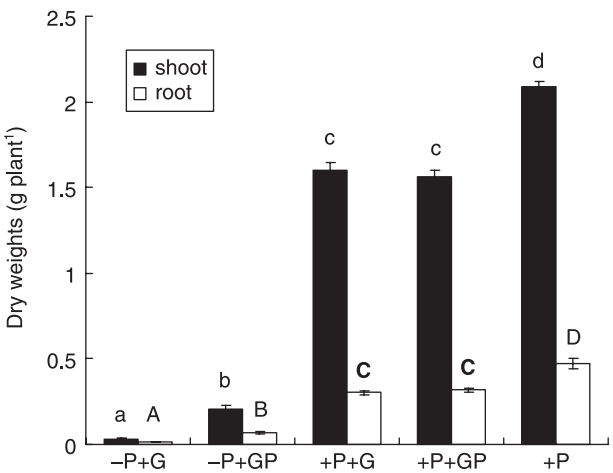

Figure 2 Effects of the application of porous glass materials on the growth of tomato plants. Results are mean ± standard error (n = 15). Letters (a–d, A–D) indicate significant differences between shoots and roots, respectively (P < 0.05).

such as the Ca contents of the material as previously reported (Inanaga *et al.* 2005). As the application of larger-sized (2–4 mm) PGM in polluted water systems may be more efficient in improving water quality, we used 2–4-mm particles of PGM.

The results of the cultivation experiments are shown in Fig. 2. Comparisons of –P+G and –P+GP showed that the total growth (shoot + root) observed in the –P+GP treatment (0.277 g per plant) was approximately 5.7-fold higher than that observed in the –P+G treatment (0.049 g per plant). This result indicates that phosphate is provided by phosphate-adsorbed PGM, which alleviates phosphate deficiency. In addition, plants in the –P+G treatment were the smallest of all plants from all treatments, and the typical symptom of phosphate deficiency (discoloration of leaves to red or purple) was observed (Fig. 3) (Takahashi 1998). From these results, it is confirmed that plants in the –P+G

Figure 3 Tomato plants grown under conditions of phosphate deficiency, with phosphate-adsorbed (left) or distilled-water-treated (right) porous glass materials.

treatment suffered from phosphate deficiency. Next, we compared the +P+G and +P+GP treatments and showed that there was no significant difference (Fig. 2). This result indicates that phosphate-free PGM does not negatively affect soil phosphate fertility.

In contrast, when we compared +P+G, +P+GP and +P, the growth of +P+G and +P+GP was slightly lower than that of +P (Fig. 2). We assume that there are two reasons for this phenomenon. One is that phosphate from the Hoagland solution is adsorbed by PGM, and the other is that PGM release a substance that is toxic to tomato plants. However, from the finding that there is no significant difference between treatments +P+G and +P+GP, the first reason is rejected, and the second reason is believed to be more likely. In a previous paper (Inanaga *et al.* 2005), we reported the alkalization of a solution by soaking PGM within the solution. The mechanism for this is proposed as follows (Maruta 1975): $CaCO_3$ is added as a foaming agent and is converted to CaO, and CO_2 gas is generated by burning. Foams are generated by CO_2. CaO reacts with H_2O and synthesizes $Ca(OH)_2$. This substance may cause the alkalization. Sandy soil has a neutral pH, so it may be greatly affected by PGM; however, the alkalinity of the materials may be useful for improving acidic soils. In the present study, the negative effects of PGM on plant growth are slight, so it is difficult to analyze the detailed mechanism that is responsible. This should be analyzed in future studies.

The results of truog-phosphate levels in the treatments with phosphate and/or PGM are shown in Table 2. The truog-phosphate level in –P+GP was higher than that in –P+G, and was not significantly different to that of +P. The highest growth rate was seen in +P, and +P was treated as the model for standard chemical fertilization. These results indicate that phosphate-adsorbed PGMs have the same potential as chemical phosphate fertilizer to act as fertilizers. However, there is no correlation between plant growth and truog-phosphate levels. This may be because of the release of inhibitors to plant growth from PGM causing alkalinity, as mentioned above. To clarify this point, the pH(H_2O) in treatments with phosphate and/or PGMs was measured. The pH(H_2O) was raised by the application of PGMs (Table 2). These results indicate that the alkalinity of PGMs may affect plant growth. If so, it may be appropriate to apply the PGM to acidic water systems and to acidic soils. In addition, comparisons between +P+G and +P showed that truog-phosphate levels increased as a result of the application of PGM that had not been treated with phosphate. This indicates that the alkalinity of PGMs may increase the solubility of phosphate fertilizer and insoluble phosphate (such as Al-P and Fe-P) in the soil.

Table 2 Effects of phosphate-treated porous glass materials on phyto-available phosphate and pH(H_2O) in sandy soil

Treatments	Truog-phosphate† (mg P_2O_5 100 g $soil^{-1}$)	pH(H_2O)†
–P+G	0.96 ± 0.37	7.7 ± 0.1
–P+GP	20.3 ± 2.29	7.2 ± 0.1
+P+G	24.8 ± 1.01	7.8 ± 0.1
+P+GP	37.4 ± 1.60	7.3 ± 0.0
+P	18.5 ± 0.09	6.5 ± 0.0

†Truog-P and pH(H_2O) in sandy soil alone were 0.60 ± 0.09 mg P_2O_5 100 g $soil^{-1}$ and 6.1 ± 0.0, respectively. Data are mean ± standard error (n = 3). ±P, presence or absence of phosphate fertilizer application; +G, application of porous glass materials treated without phosphate; +GP, application of porous glass materials treated with phosphate.

Smaller-sized PGM adsorbs lower amounts of phosphate (Table 1). This result indicates that phosphate adsorbed on larger-sized PGM may be released by crushing to smaller-sized PGM. To confirm this, phosphate-adsorbed PGM (2–4 mm diameter) was crushed to ~1 mm in diameter and truog-phosphate levels in the sandy soil that was applied to the crushed materials were measured. The resulting truog-phosphate level was 36.8 ± 2.1 mg P_2O_5 per 100 g of soil (pH[H_2O] = 8.5), which was higher than that in soil that was applied to phosphate-adsorbed PGM (2–4 mm diameter) alone (Table 2). From these results, the efficiency of the recycling system of phosphate, from the point of view of the mass balance of phosphate, may be improved by the use of larger-sized PGM in the improvement of water quality followed by the use of smaller-sized PGM as phosphate fertilizer.

Next, we discuss the practical use of wastewater treatment using PGMs. Techniques for the removal of phosphate from water systems, including coagulating sedimentation (e.g. Kitao 1978), activated sludge processing (e.g. Inamori and Sudo 1982), crystallization (e.g. Sunahara 1988) and removal with adsorbents (e.g. Tanada *et al.* 2003; Yanagida and Jiang 1994) have been reported. In the present study, we review these protocols from the viewpoints of suitability to different types of wastewater. Among these protocols, it is considered that activated sludge processing is appropriate for the treatment of wastewater containing large amounts of organic contaminants rather than removal using adsorbents (including PGMs) and crystallization. Crystallization is appropriate for the treatment of a great deal of wastewater containing high levels of phosphate, such as industrial wastewater, because of the high initial cost, compared with removal using adsorbents. Based on these findings, for example, removal using adsorbents (including PGMs) may be appropriate as an additive treatment after the primary treatment of wastewater by, for example, activated sludge processing. Additionally, because the previously reported adsorbents consist of aluminum and iron (e.g. Tanada *et al*. 2003; Yanagida and Jiang 1994), very little of the phosphate adsorbed by these materials is phyto-available; however, the phosphate adsorbed by PGMs is phyto-available and can be used as fertilizer. Very little of the phosphate-containing sediment obtained in coagulating sedimentation is phyto-available because of a similar reason. Thus, PGM is advantageous compared with the other adsorbents and coagulating sedimentation.

In the present study, we applied large amounts of PGMs (20% w/w) to soil. In future, for the practical use of PGMs in the field, the amount of PGM application should be reduced to improve the phosphate-adsorption capacity. For example, we have previously suggested that PGMs that have a high phosphate-adsorption ability can be manufactured by using large amounts of $CaCO_3$ as the foaming agent (Inanaga *et al.* 2005) and enlarging the particle size, as shown in the present study, also increases the phosphate-adsorption capacity. In addition, the use of PGMs in nursery bed for raising seedlings may be also useful.

In conclusion, it is confirmed that phosphate adsorbed onto PGM is available to plants. The findings of the present study suggest that at least some phosphate fertilizer can be provided by PGM and that using PGM of different particle sizes may aid the efficient recycling of phosphate in soil-water/plant systems.

ACKNOWLEDGMENTS

We thank the Ehime Recycling Institute Company for provision of porous glass materials. This research was supported by the 21st Center Of Excellence (COE) program "Arid Land Science Program" and a Tottori Prefecture Grant Aid for Environment Science.

REFERENCES

Aso S, Goto I, Takagi T, Takenaga H, Yosiba M 1985: Molybdenum-blue method. *In* Textbook for Inorganic Chemistry Experiment, Ed. S. Aso, pp. 175–177. Department of Agricultural Chemistry, Tokyo University of Agriculture, Tokyo.

Hara Y, Onizuka K, Yoshitake S, Aso N, Yoko M 1998: Example of greening of slope faces by using foamed glass materials. 33rd Summary of Japanese Geotechnical Society (JGS), 2253–2524.

Inamori Y, Sudo T 1982: Trend of biological removal of phosphate. *J. Water Waste*, **24**, 1095–1110.

Inanaga S, Nakazawa R, Tomemori H *et al.* 2005: Mechanism of phosphate-adsorption onto porous glass materials. *Man. Environ.*, **31**, 11–16.

Kamewada K 1997: pH (glass electrode method). *In* Analysis of Soil Environment, Eds T Kaneno, pp. 195–197. Hakuyusha, Tokyo.

Kitao T 1978: Evaluation and problem of protocols for removal of nitrogen and phosphorous. *Kogai-to-Taisaku*, **14**, 822–831.

Koshino M 1994: Phosphate fertilizer. *In* Encyclopedia of Soil, Plant Nutrition, and Environment, Eds T Matsusaka and A Awahara, pp. 256–257, Hakuyusha, Tokyo.

Kunimatsu T 1995: Water resource and water quality. *In* Agriculture and Environment, Eds K Kyuma and O Soda, pp. 73–147. Huminkyoukai, Tokyo.

Murakami M 2003: Basic research on improvement of soil and water by using porous glass materials (Master thesis). Graduate School of Agriculture, Tottori University, Tottori, Japan.

Maruta S 1975: Alkali-earth metals. *In* Summary of Inorganic Chemistry, pp. 48–52. Sankyoshuppan, Tokyo.

Nanjo M 1997: Phyto-available phosphate. *In* Analysis of Soil Environment, Eds T Kaneno, pp. 267–269, Hakuyusha, Tokyo.

Sunahara K 1988: Removal of phosphorous by crystallization. *Suisituozakukennkyu*, **11**, 617–621.

Tadano T 1999: Tolerance to phosphate-deficiency. *In* Plant Nutrition and Fertilizer Science, Ed. M Chino, pp. 133–138. Asakurashoten, Tokyo.

Takahashi E 1999: Silicate. *In* Plant Nutrition and Fertilizer Science, Ed. M Chino, pp. 95–98, Asakurashoten, Tokyo.

Takahashi K 1998: Phyto-available phosphate. *In* Encyclopedia for Soil Science and Plant Nutrition, Eds S Fujiwara, T Anzai, Y Ogawa and T Kato, p. 101, Nobunkyo, Tokyo.

Takahashi K 1998: Phosphate-deficiency. *In* Encyclopedia for Soil Science and Plant Nutrition, Eds S Fujiwara, T Anzai, Y Ogawa and T Kato, p. 135, Nobunkyo, Tokyo.

Tanada S, Kobayama M, Kawasaki N *et al.* 2003: Removal of phosphate by aluminium oxide hydroxide. *J. Colloid. Interface Sci.*, **257**, 135–140.

Yanagida T, Jiang Y 1994: Effects of heating temperature and additives on phosphate sorption coefficient of heated materials from the volcanic ash soils. *Jpn. J. Soil Sci. Plant Nutr.*, **65**, 171–174.

Planta (2004) 219: 450–458
DOI 10.1007/s00425-004-1245-2

ORIGINAL ARTICLE

Yanhua Qi · Yasuo Yamauchi · Jianqun Ling
Naoyoshi Kawano · Debao Li · Kiyoshi Tanaka

Cloning of a putative monogalactosyldiacylglycerol synthase gene from rice (*Oryza sativa* L.) plants and its expression in response to submergence and other stresses

Received: 28 January 2004 / Accepted: 24 February 2004 / Published online: 16 April 2004

Abstract Suppression subtractive hybridization was used to construct a subtractive cDNA library from plants of non-submerged and 7-day-submerged rice (*Oryza sativa* L., FR13A, a submergence-tolerant cultivar). One clone of the subtractive cDNA library, S23, was expressed abundantly during submergence. The full length of S23 was amplified using 5′- and 3′-rapid amplification of cDNA ends, and found to consist of 1,671 bp with an open reading frame of 1,077 bp (181–1257) encoding 358 amino acids. Its deduced amino acid sequence showed a high homology with monogalactosyldiacylglycerol synthase (UDPgalactose: 1,2-diacylglycerol 3-β-D-galactosyl transferase; EC 2.4.1.46, MGDG synthase) from *Arabidopsis thaliana*; therefore, we named the gene *OsMGD*. Time-course studies showed that the expression of *OsMGD* in the rice cultivars FR13A and IR42 (submergence-susceptive cultivar) during submergence was gradually increased and that expression in FR13A was higher than in IR42. The expression of *OsMGD* in FR13A was influenced by benzyladenine and illumination. The accumulation of *OsMGD* mRNA in both FR13A and IR42 was also increased by ethephon, gibberellin, drought and salt treatment, but cold stress had no effect on the expression of the gene. These results suggest that the expression of *OsMGD* mRNA requires benzyladenine or illumination, and that the process is also mediated by ethephon and gibberellin. Salt and drought stress have an effect similar to that of submergence. Furthermore, the enhanced expression of *OsMGD* may relate to photosynthesis, and play an important role during submergence.

Keywords Monogalactosyldiacylglycerol synthase · *Oryza* · OsMGD · Stress · Submergence · Suppression subtractive hybridization

Abbreviations BA: N^6-Benzyladenine · GA: Gibberellin · MGD: Monogalactosyldiacylglycerol synthase · RACE: Rapid amplification of cDNA ends

Introduction

Submergence tolerance of rice is an important trait for agricultural production. Two important factors, the limitation of gas diffusion under water and reduced irradiance, which impair photosynthesis and efficient utilization of carbohydrates, influence rice plant survival during submergence (Ram et al. 2002). Thus, survival during submergence may largely depend on an accumulation of a high concentration of carbohydrate prior to submergence and a capacity for maintaining energy production through rapid alcoholic fermentation under oxygen shortage. Under submergence conditions, glycolysis and alcoholic fermentation pathways become more active for energy production in plants (Arumugam Pillai et al. 2002). Increased alcoholic fermentation is thus a way to alleviate the adverse effect of anoxia on reduced production of energy for growth and maintenance processes during submergence. Genes related to anaerobic metabolism (such as those for glyceraldehyde-3-phosphate dehydrogenase, enolase, alcohol dehydrogenase, pyruvate decarboxylase and aldehyde dehydrogenase) are strongly induced under submergence (Umeda and Uchimiya 1994; Sachs et al. 1996; Nakazono et al. 2000).

The potential capacity for internode elongation is important for plant response under submergence (van der Knaap et al. 1998). To avoid drowning, deepwater rice has evolved the capacity to elongate very rapidly

Y. Qi · Y. Yamauchi · N. Kawano · K. Tanaka (✉)
Laboratory of Plant Biotechnology, Faculty of Agriculture, Tottori University, Koyama, 680-8553 Tottori, Japan
E-mail: jotanaka@muses.tottori-u.ac.jp
Tel.: +81-857-315638

J. Ling
Department of Applied Biological Resource Sciences, School of Agriculture, Ibaraki University, Ami-machi, Inashiki-gun, 300-0393 Ibaraki, Japan

D. Li
Institute of Biotechnology, Zhejiang University, Huajiachi Campus, 310029 Hangzhou, People's Republic of China

when it becomes submerged (van der Knaap et al. 1997). Internode elongation is partially induced by oxygen stress (Raskin and Kende 1984a). It was also found that internode elongation during submergence is controlled by the ratio of gibberellin to abscisic acid (Hoffman-Benning and Kende 1992), and that gibberellin activity could be enhanced by ethylene (Raskin and Kende 1984b). Submergence and gibberellin or ethylene treatment produce some similar effects on plants: they promoted rapid internode elongation and induced accumulation of expansin mRNA before the rate of growth started to increase (Cho and Kende 1997). During submergence, an ortholog of replication protein A1 (RPA1) and a putative type-1a plasma membrane receptor were also induced by gibberellin (van der Knaap et al. 1997, 1998). Submergence or ethylene treatment enhanced expression of the genes for 1-aminocyclopropane-1-carboxylate synthase (ACS) and oxidase (ACO) (Zarembinski and Theologis 1997; Mekhedov and Kende 1996). A novel ethylene-regulated gene, *OsUsp1*, which encoded a plant protein related to a prokaryotic universal stress protein family, was also expressed during submergence (Sauter et al. 2002).

Although numerous studies of submergence tolerance have been carried out, the molecular aspect is not yet clearly understood (Chang et al. 2000; Van Der Straeten et al. 2001; Arumugam Pillai et al. 2002). To further understand the mechanism of submergence tolerance, we studied some genes related to submergence tolerance. The present paper reports a new gene (*OsMGD*) in rice isolated by suppression subtractive hybridization (SSH) and the pattern of *OsMGD* expression in response to submergence, phytohormone, salt, drought, cold, dark and illumination treatments.

Materials and methods

Plant growth

Seeds of the rice (*Oryza sativa* L.) cultivars FR13A (submergence tolerant) and IR42 (submergence susceptive), obtained from the International Rice Research Institute (IRRI), were soaked in water at 30°C for 3 days, for germination. The germinated seeds were transplanted into a pot containing vermiculite. The seedlings were irrigated at 1-week intervals using HYPONEX nutrient solution diluted 1,000-fold with water. Three-week-old seedlings were submerged completely, about 20 cm under the water surface, for 1–7 days in a tank in a greenhouse. The water temperature was 25–30°C. Seedlings of the same age were either irrigated every day for 7 days with water containing 10^{-2} M ethephon, 10^{-5} M gibberellic acid (GA_3) (Raskin and Kende 1984a, 1984b), or a high concentration of salt (0.25 M NaCl), or they were subjected to drought (not irrigated) for 7 days. Cold treatment was performed at 4°C for 1 day. The seedlings were also grown under normal conditions as a control for Northern blot analysis. Two-week-old seedlings of FR13A were subjected to the following treatments for 0, 6, 18, 30, 42, and 54 h: darkness (the growing plants were placed in a black box), darkness plus N^6-benzyladenine (BA; 100 μM), light (white fluorescent lamps: 23–50 μmol photons m^{-2} s^{-1}) and light plus BA (Yamaryo at al. 2003). Leaves of the rice plants grown under the different conditions were harvested, frozen in liquid nitrogen and stored at −80°C until use.

RNA isolation

Total RNA was extracted by the SDS–phenol method (Bachem et al. 1996). Poly(A)$^+$ RNA was purified from total RNA using the Oligotex-dT 30 super kit (Roche).

Suppression subtractive hybridization

PCR-based suppression subtractive hybridization (SSH) was performed according to Diatchenko et al. (1996). SSH was carried out using a PCR-Select cDNA™ Subtraction Kit (Clontech) following the manufacturer's instructions. Aliquots (1.5 μg) of mRNA from non-submerged and submerged (for 7 days) rice plants were prepared as driver and tester RNA samples, respectively. After SSH, the products of PCR were sub-cloned into the pCR 2.1-TOPO vector (TOPO TA Cloning kits; Invitrogen). Positive colonies were picked out randomly for plasmid extraction, and digested with *Eco*RI. Northern blot hybridization was carried out to confirm the positive clone for submergence induction, and the plasmid was isolated using the Miniprep Kit (PE Applied Biosystems).

Northern blot analysis

Total RNA (30 μg) was run in 1.5% formaldehyde–agarose gels as described by Sambrook and Russell (2001), and blotted onto Hybond$^+$ membranes (Amersham–Pharmacia). The digoxigenin (DIG)-labeled PCR product was used as a probe for Northern hybridization following the manufacturer's instructions (PCR DIG Probe Synthesis kit; Roche). The membranes were washed twice with a solution containing 2×SSC (sodium chloride–sodium citrate buffer) and 0.1% SDS for 10 min at room temperature and twice with a solution containing 0.1×SSC and 0.1% SDS for 20 min at 65°C. The DIG Luminescence Detection Kit (Roche) was used for signal detection.

Isolation of full-length cDNA

5′- and 3′-rapid amplification of cDNA ends (RACE; Chenchik et al. 1998) were carried out to obtain the 5′- and 3′-terminals of the *OsMGD* gene using a SMART RACE cDNA Amplification kit (Clontech) following the manufacturer's instructions. An mRNA

sample (1 μg) from a 7-day-submerged rice plant (FR13A) was converted into first-strand cDNAs. We designed one gene-specific primer GSPR1 (5′-ACAATTTGCAGCCCATC GCTGGT-3′) and one nested gene-specific primer NGSPR1 (5′-CCCTCTGAACAAAGGACGACAGG-3′) in antisense orientation for the 5′-RACE. The gene-specific primer GSP2 (5′-CTGTCGTCCTTTGTTCAGAGGG-3′) and the nested specific primer NGSP2 (5′-ACCAGCGATGGGCTGCAAATTGT-3′) in sense orientation were used for 3′-RACE. The universal primer sequence and the nested universal primer (NUSP) for 5′-RACE and 3′-RACE refer to the user manual of the kit. The up-regulated clone S23 of length 672 bp (Fig. 1a, from 906 to 1577) was separated from the subtractive cDNA library. After sequencing S23, a fragment containing 1,577 bp (Fig. 1a, 1–1577) was amplified out using the primer pair GSPR1 and USP. Nested PCR primers, NGSPR1 and NUSP, were used for the reaction, since the PCR products were shown more clearly than GSPR1 and USP in a 1.5% agarose gel (data not shown). A 139-bp fragment of the 3′-terminus (Fig. 1a, 1533–1671) was amplified using GSP2 and USP. A nested PCR using NGSP2 and NUSP for 3′-RACE further confirmed the 3′-terminal sequence. GSP3 (5′-CTTTTTTTTTTTTTTTTTTTTTTGCTGCTG-3′) and GSPR4 (5′-GAATGGATATGTTACAAGTCGAGAG-3′) were applied to obtain the full-length cDNA. All PCR reactions were performed with the Advantage 2 PCR Enzyme system (Clontech) in a Takara PCR Thermal Cycler using the following protocol: 94°C for 5 s, 68°C for 10 s and 72°C for 3 min for 35 cycles. Nested PCR reactions were performed by the same protocol for 20 cycles. The PCR product was sub-cloned into pCR 2.1-TOPO vectors and sequenced.

cDNA sequence analysis

Sequencing was performed using the BigDye Terminator Cycle Sequencing Ready Reaction Kit, v 2.0 in an ABI PRISM System 3100 (Applied Biosystems), and following the cycle sequencing protocol for 25 cycles: 96°C for 10 s, 50°C for 5 s and 60°C for 4 min. The M13 forward primer (CTGGCCGTCGTTTTAC) and M13 reverse primer (CAGGAAACAGCTATGAC) were respectively used in these reactions. The Genetyx-SV-RC version6 (Software Development Co., Tokyo, Japan) and DDBJ Homology

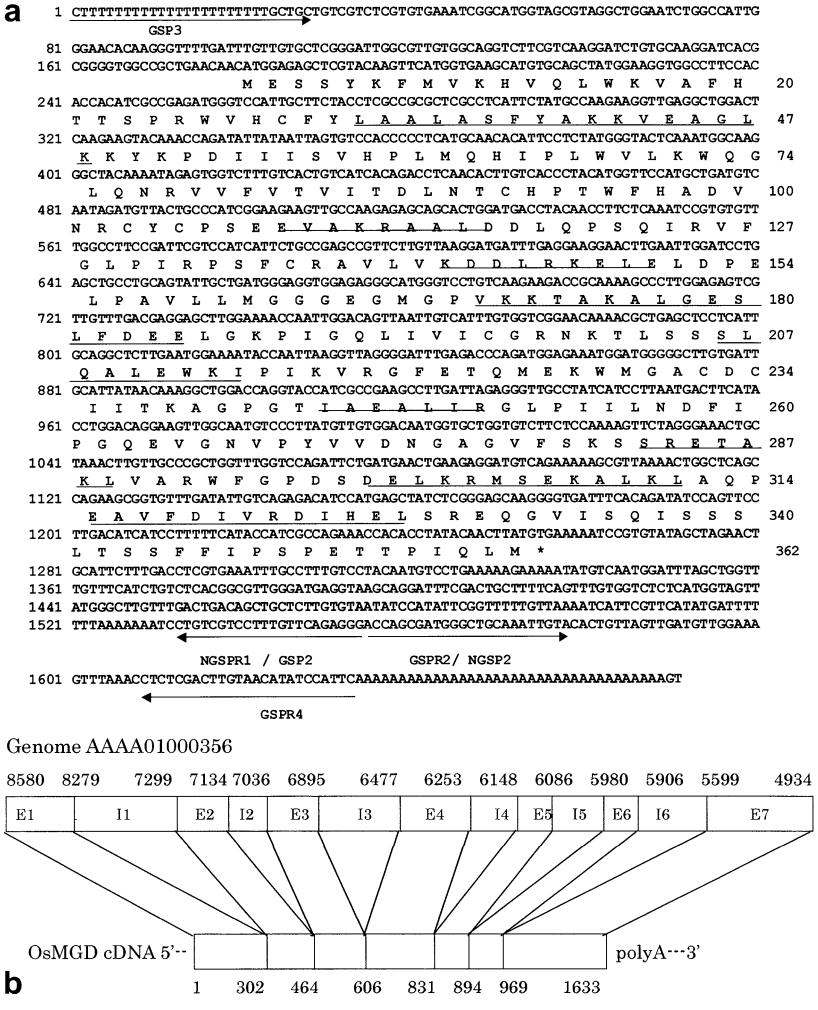

Fig. 1 a Nucleotide and deduced amino acid sequences of the rice (*Oryza sativa*) *OsMGD* cDNA (numbered on the *left* and *right* of the sequence, respectively). The positions of RACE primers are labeled (*arrows*). GSP2 and NGSP2 are used in 3′-RACE. GSPR1 and NGSPR1 are used in 5′-RACE; the latter two primers are the reverse complementary sequences of NGSP2 and GSP2. GSP3 and GSPR4 are used to amplify the full length of *OsMGD* cDNA. The positions of nine α-helices are indicated by *straight lines* under the amino acid sequence, and were determined using the secondary sequence prediction program available at the following internet address: http://npsa-pbil.ibcp.fr/cgi-bin. The sequence of *OsMGD* cDNA was registered in GenBank under accession number AB112060. **b** Comparison of *OsMGD* and genome fragment AAAA01000356. (From NCBI, http://www.ncbi.nlm.nih.gov/BLAST/Geno-me/PlantBlast.html. Plant choices: *Oryza sativa* ssp. *indica* WGS contigs.) *E1–7*, exons 1–7; *I1–6*, introns 1–6. The numbers on the genome and *OsMGD* indicate the sites of the exons and introns

Search systems were used for sequence analysis. Comparison between the gene and *Oryza sativa* genome was carried out using NCBI (http://www. ncbi. nlm.nih.gov/BLAST/Genome/PlantBlast.html; plant choices: *Oryza sativa* ssp. *indica* WGS contigs).

Results

cDNA clone of the *OsMGD* gene

The *OsMGD* cDNA contained 1,671 bp, with start codon at 181 bp and stop codon at 1,257 bp, coding 358 amino acids. The theoretical isoelectric point (pI) of the putative amino acid sequence is 8.33 and molecular weight (MW) is 39.9 kDa. The flank of the start codon ATG is AACATGG (Fig. 1a, 177–183), according to the "Kozak" rule. The putative amino acid sequence of the *OsMGD* gene may contain nine α-helices, according to secondary sequence prediction (Fig. 1a). In addition, the 1–23 site of the 5′-untranslated region in the *OsMGD* sequence (CTTTTTTTTTTTTTTTTTTTTTT) is very interesting. It looks like an antisense strand. Further study is necessary to understand if this sequence has any biological function. Based on the *OsMGD* cDNA sequence and a search of the genomic database for *Oryza sativa* (Indica cultivar), it was found that the *OsMGD* gene is well located in the 8580–4934 region of rice genome fragment AAAA01000356. Following the GT-AG rule, it was confirmed that there are seven exons and six introns in the *OsMGD* gene: the exon regions are in 8580–8279, 7299–7134, 7036–6895, 6477–6253, 6148–6086, 5980–5906, 5599–4934 and the intron regions are in 8278–7298, 7133–7035, 6894–6476, 6252–6147, 6085–5979, 5905–5598 of genome fragment AAAA01000356 (Fig. 1b).

Comparison of the deduced amino acid sequence of OsMGD with MGDG synthases from other plants

The deduced amino acid sequences of OsMGD and MGDG synthases from *Cucumis sativus*, *Spinacia oleracea* and *Arabidopsis thaliana* are aligned in Fig. 2. Seventy regions are completely identical in the four species. The putative amino acid sequence of OsMGD showed high homology to csMGD A (58.6%), soMGD A (58.4%), atMGD A (59.5%), and atMGD B (74.0%). In *Arabidopsis thaliana*, at least two classes of MGDG synthase homologues can be distinguished according to the length of the N-terminal portion of the hypothetical precursors (Miege et al. 1999). Experimental evidence indicated that type A exhibits a transit sequence of about 100 amino acids, with a cleavage site. On the other hand, the N-terminal sequence of type B is shorter (about 40 amino acids) than that of type A and does not exhibit any predictable cleavage site, as determined by the ChloroP program (Shimojima et al. 1997; Emanuelsson et al. 1999). The putative amino acid sequence of OsMGD has a strong transmembrane helix, from amino acids 18 to 40 in the N-terminus (by http://www.ch.embnet.org/cgi-bin/ TMPRED_form _parser). The most likely cleavage site is between positions 45 (A) and 46 (G) of the putative amino acid sequence (by http://www.cbs.dtu.dk/services/singnalP). The putative amino acid sequence of OsMGD is shorter by about 107–167 amino acid residues than the MGDG synthases of *Cucumis sativus*, *Spinacia oleracea* and *Arabidopsis thaliana*. However, the 5′-untranslated region (5′-UTR; 179 bp) of the *OsMGD* cDNA contains an upstream in-frame stop, TAG, at position 55–57 bp, that underlines the function of the subsequent ATG in starting the translation and eliminates the probability that the cDNA is not full length. So OsMGD seems not to belong to the type-A or type-B MGDG synthases mentioned above. It is therefore suggested that OsMGD might be a new type of MGDG synthase.

Time-course of expression of the *OsMGD* gene in cultivars FR13A and IR42 during submergence

The northern blot analysis of *OsMGD* during submergence (0–7 days) is shown in Fig. 3. The expression of *OsMGD* in FR13A and IR42 gradually increased with time of submergence. The expression of *OsMGD* mRNA in submerged (7th day) FR13A and IR42 seedlings was about 3-fold and 1.7-fold higher, respectively, than in non-submerged rice. Although the level of *OsMGD* mRNA was higher in FR13A than in IR42 at the 7th day of submergence, it had already reached a peak at the 4th day of submergence in IR42 and declined thereafter.

Expression of the *OsMGD* gene in the rice cultivar FR13A in response to dark, dark/BA, light, and light/BA treatments

The expression of *OsMGD* was greatly reduced in 2-week-old FR13A rice plants that were kept in the dark and irrigated with water for up to 54 h (Fig. 4a). However, when plants were irrigated with 100 μM BA solution in the dark, the *OsMGD* expression increased remarkably (Fig. 4b). The level of *OsMGD* expression remained fairly constant throughout the time course when plants were kept in the light and irrigated with water (Fig. 4c) but increased when irrigated with BA in the light (Fig. 4d).

Expression of the *OsMGD* gene in response to phytohormone treatments and various stresses

Expression of *OsMGD* in rice plants (FR13A and IR42) was also influenced by phytohormone treatments and various stresses (Fig. 5). Accumulation of mRNA was greatly increased by submergence, ethephon, GA treatment (GA_3), and drought or salt stresses. Moreover, expression in FR13A was higher than in IR42 under

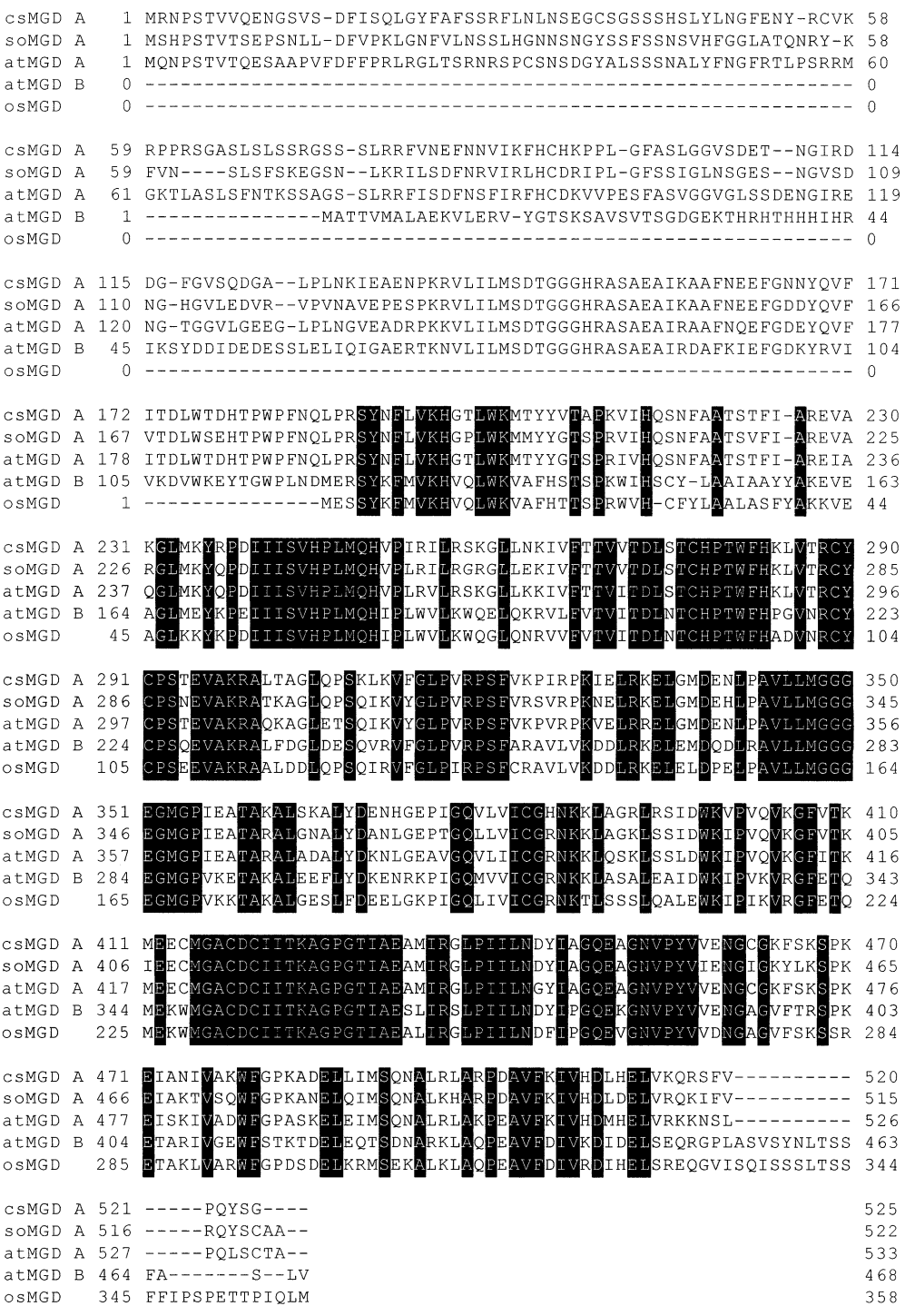

Fig. 2 Alignment of the deduced amino acid sequences of OsMGD and MGDG synthases from various plants. *csMGD A*, *Cucumis sativus* MGD A (GenBank U62622); *soMGD A*, *Spinacia oleracea* MGD A (GenBank AJ249607); *atMGD A*, *Arabidopsis thaliana* MGD A (At number, At4g31780); *atMGD B*, *A. thaliana* MGD B (At number, At5g20410); *OsMGD*, *Oryza sativa* MGD (GenBank AB112060). The *black shading* indicates identical amino acids

these conditions. The *OsMGD* gene did not accumulate in cold-treated rice plants.

Discussion

We constructed a subtractive cDNA library from non-submerged and submerged (7 days) rice plants. Using the cDNA library, a new submergence-related gene, *OsMGD*, was isolated and identified. The *OsMGD* gene encoded a putative polypeptide of 358 amino acids (Fig. 1). The putative polypeptide is highly homologous to the monogalactosyldiacylglycerol synthase (UDP galactose: 1,2-diacylglycerol 3-β-D-galactosyl transferase; EC 2.4.1.46, MGDG synthase) enzymes of *Cucumis sativus*, *Spinacia oleracea* and *Arabidopsis thaliana*, and we suggest that OsMGD might have a similar function. The lipid MGDG is a major structural component of photosynthetic membranes in chloroplasts. Its formation is catalyzed by MGD synthase (Jarvis et al. 2000).

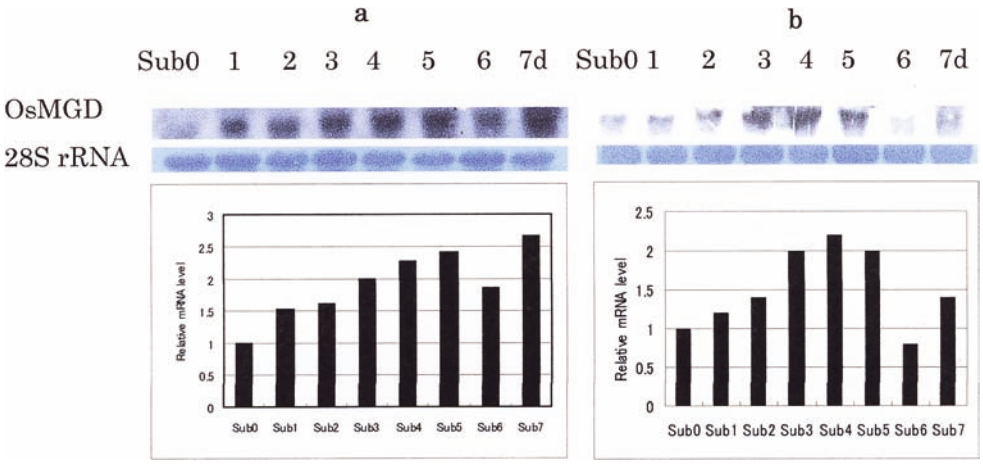

Fig. 3a,b Northern blot analysis of *OsMGD* gene expression in rice cultivars FR13A (**a**; submergence tolerant) and IR42 (**b**; submergence susceptive) during submergence from 0 to 7 days. *Sub0–Sub7* From non-submerged to submerged for 7 days. Thirty micrograms of total RNA from samples submerged for different times was loaded on each lane and probed with clone S23 using the PCR DIG Probe Synthesis kit. 28S rRNAs on Hybond^{+} membrane were stained with methylene blue. Relative levels of mRNA were analyzed by Scion image and Excel software

MGDG synthase transfers a galactose from UDP-galactose to 1,2-diacylglycerol in the chloroplast envelope (Joyard and Douce 1987). MGDG is not only a major constituent of the chloroplast membrane but also has an important role in photosynthesis (Murphy 1982; Murata et al. 1990). The small galactose of the head group and large unsaturated fatty acid chains of MGDG give it a cone-like molecular shape and a consequent predisposition to form non-lamellar, hexagonal-phase aggregates. The molecular shape of MGDG may be important for the structural organization of thylakoid membranes. Evidence also suggests that MGDG is more directly involved in certain photosynthetic reactions (Tremolieres et al. 1994). In addition, photosynthesis has

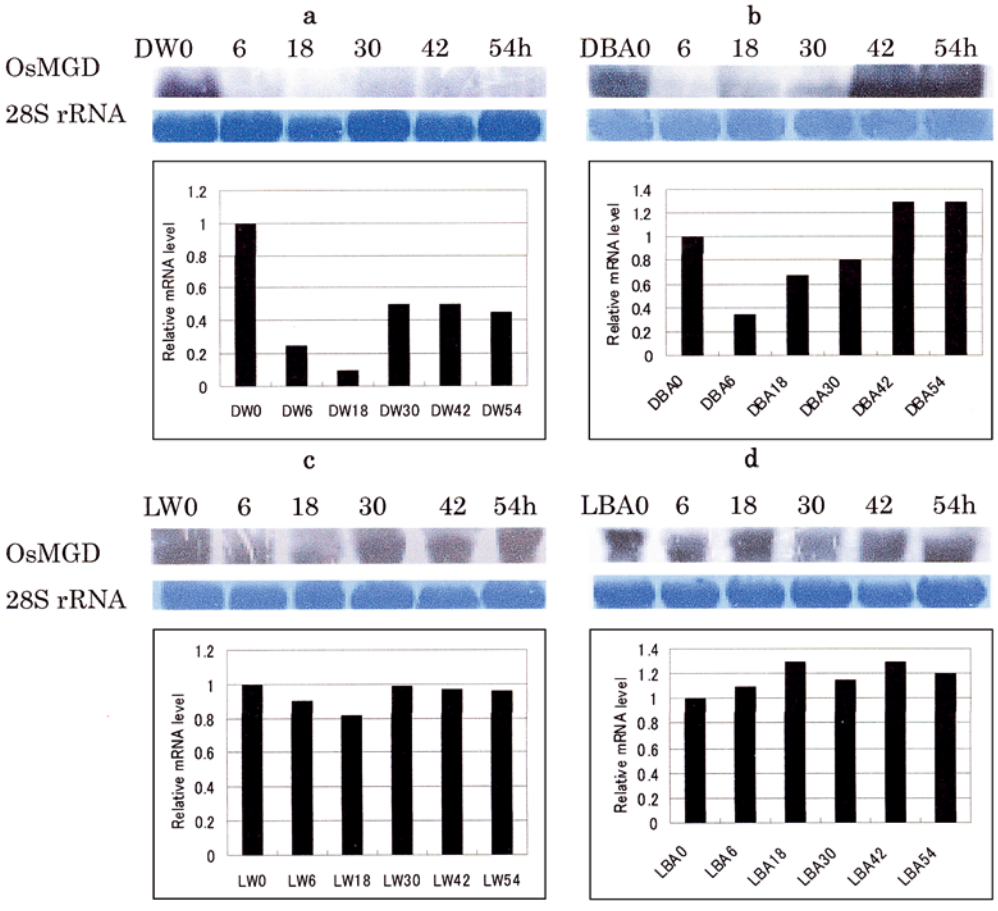

Fig. 4a–d Northern blot analysis of *OsMGD* gene expression in the rice cultivar FR13A in response to dark, dark/BA, light, and light/BA treatments. **a,b** Seedlings were placed in the dark for 0, 6, 18, 30, 42 and 54 h, and soaked with water (**a**) or BA (100 μM) solution (**b**). **c,d** Seedlings were illuminated with white fluorescent lamps: 23–50 μmol m^{-2} s^{-1} for 0, 6, 18, 30, 42 and 54 h, and soaked with water (**c**) or BA (100 μM) solution (**d**). *DW* Dark/water, *DBA* dark/BA, *LW* light/water, *LBA* light/BA. The northern blotting procedure was same as in Fig. 3

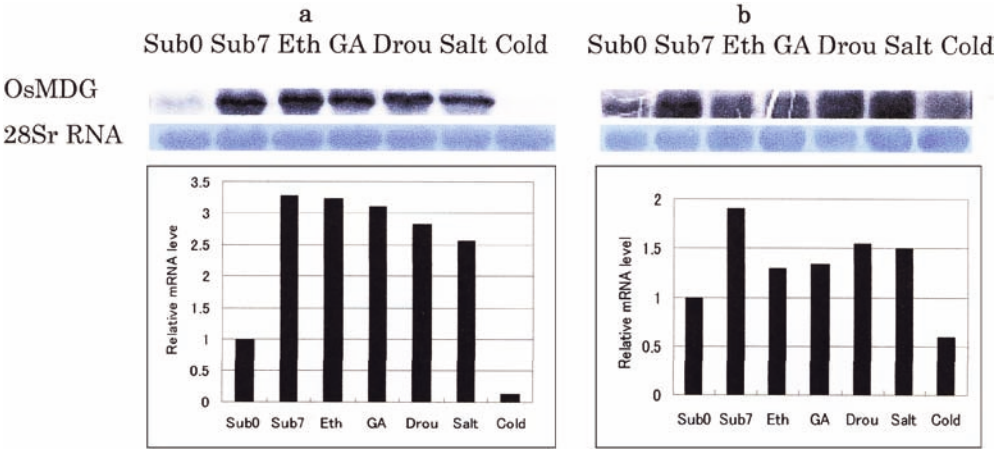

Fig. 5a,b Northern blot analysis of *OsMGD* expression in rice cultivars FR13A (**a**; submergence tolerant) and IR42 (**b**; submergence susceptive) subjected to phytohormone treatments and various stresses. *Sub0* No-submergence, *Sub7* submergence for 7 days, *Eth* 10^{-2} M ethephon, *GA* 10^{-5} M gibberellic acid, *Salt* 0.25 M NaCl, *Drou* drought (not irrigated) for 7 days, *Cold* exposed to 4°C for 1 day. The northern blotting procedure was same as in Fig. 3

a great effect on tolerance to submergence (Ram et al. 2002). Though the photosynthetic rate of the rice seedlings was reduced during submergence, the photosynthetic rate of FR13A remained higher than that of the submergence-sensitive cultivar IR42 (Kawano et al. 2002a, 2002b; Ella at al. 2003). The expression of the *OsMGD* gene in FR13A was higher than in IR42 during submergence (Fig. 3), indicating that *OsMGD* may be important for maintaining photosynthetic activity.

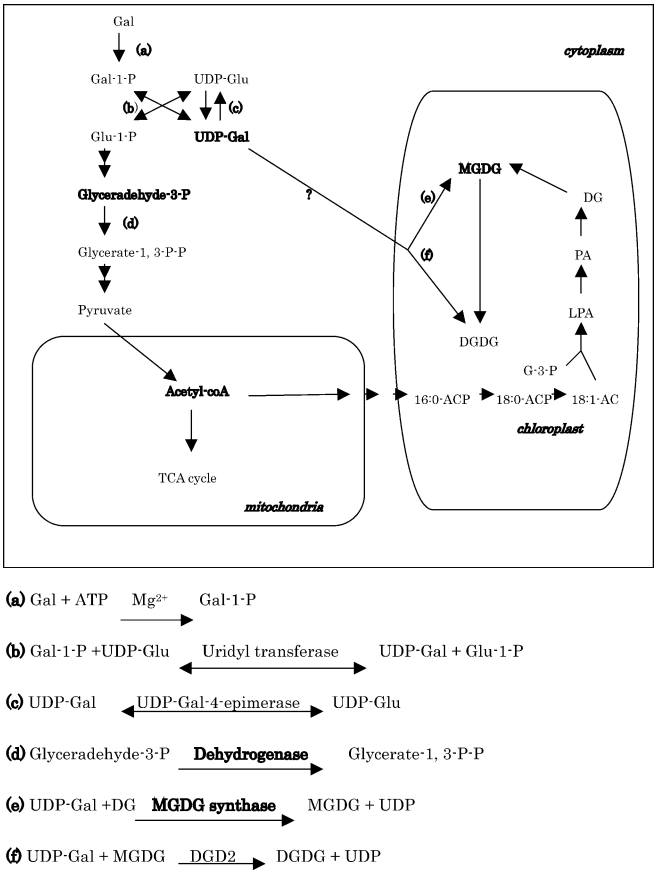

Fig. 6 A proposed model of the relationship between glycolysis and MGDG synthesis (refer to Shen and Wang 1991; Kelly and Dormann 2002; Ichihara 2001). *Gal* Galactose, *Gal-1-P* galactose-1-phosphate, *Glu-1-P* glucosel-1-phosphate, *UDP* uridine diphosphate, *TCA cycle* tricarboxylic acid cycle, *ACP* acyl carrier protein, *G-3-P* glycerol-3-phosphate, *LPA* lysophosphatidic acid, *PA* phosphatidic acid, *DG* 1,2-diacyl-*sn*-glycerol, *DGD2* an *Arabidopsis* gene encoding a UDP-galactose-dependent digalactosyldiacylglycerol synthase, *16:0* length of carbon chain: number of double bonds

The transcripts of *OsMGD* were influenced by BA and illumination treatments (Fig. 4). In the presence of exogenous BA, *OsMGD* expression was raised even in the dark (Fig. 4b), a response identical to that of the MGD gene of cucumber (Yamaryo at al. 2003). This might explain why the *OsMGD* transcripts were increased during submergence: though the light level under water is weaker than in air, the endogenous cytokinin may be stimulated during submergence, which would result in the increased expression of *OsMGD*.

It has been found that many submergence-related genes are regulated by phytohormones (see Introduction). Our data show that the expression of *OsMGD* is also induced by ethylene and gibberellin (Fig. 5). An increase in the rate of ethylene production was observed when deepwater rice was submerged (Raskin and Kende 1984a). The striking effects of total submergence on rice plants, elongation and chlorosis, were reproduced by applying ethylene under pressure (0.35 Pa) to non-submerged rice plants (Jackson et al. 1987). The elongation of internodes in rice is regulated by cooperative action between GA and ethylene (Raskin and Kende 1984b), so the expression of *OsMGD* may be mediated by GA and ethylene.

It was indicated that *OsMGD* was induced not only by submergence but also by drought and salt stress (Fig. 5). Both drought and salt stresses lead to dehydration in cells and there are many common mechanisms of response to these stresses (Hayashi et al. 2001). There have been some reports that salt tolerance might well be associated with membrane lipids. A salt-induced decrease in chloroplast lipids has been found (Harwood 1984). Moreover, severe reduction in galactolipid synthesis after salt stress has been observed in both olive (Zarrouk et al. 1995) and oilseed rape (Najine et al. 1995). Under drought stress, MGDG synthase activity

in rape (*Brassica napus*) was reduced (Benhassaine-Kesri et al. 2002). These results seem to contradict our data that *OsMGD* mRNA is increased by drought and salt treatment. The decrease in MGDG may trigger the expression of *OsMGD* in preparation for translation to MGDG synthase. Since the MGDG synthase gene belongs to a multigene family, the relationship between transcription and translation seems to be complicated. It is possible that the *OsMGD* gene is related to resistibility to submergence, salt and drought stresses.

Significant changes in several aspects of plant membrane lipids have been noted in response to low temperatures. In the eukaryote tomato, MGDG biosynthesis was inhibited at low temperature (Yu and Willemot 1996). This corresponds to our result that the *OsMGD* gene was not expressed at 4°C in rice plants.

Furthermore, the *OsMGD* gene also seems to be associated with glycolysis (see Fig. 6). Figure 6 shows a proposed model to elucidate the relationship between glycolysis and MGDG synthesis. UDP-galactose (UDP-Gal) is a substrate for MGDG and digalactosyldiacylglycerol (DGDG) synthesis (steps e, f). Moreover, UDP-Gal is an intermediate product for the entry of Gal into glycolysis (steps a–c). A key step of glycolysis is from glyceradehyde-3-phosphate to glycerate-1,3-bisphosphate, catalysed by glyceradehyde-3-phosphate dehydrogenase (step d). The expression of the OsGAPDH gene coding glyceradehyde-3-phosphate dehydrogenase is dramatically increased by submergence and anaerobiosis (Umeda and Uchimiya 1994; Sachs et al. 1996; Arumugam Pillai et al. 2002). Moreover, acetyl-CoA may be supplied as a substrate for the tricarboxylic acid cycle and lipid biosynthesis (Mellema et al. 2002). According to the above-mentioned relationship and the fact that the expression of *OsMGD* increased during plant submergence (Fig. 5), we suggest that MGDG synthesis and glycolysis might be associated and that *OsMGD* may play an important role during submergence.

A submergence-related gene, *OsMGD*, and its increase during submergence of rice plants are reported here for the first time, and this finding will supply a new train of thought in the study of submergence tolerance. More work is in progress to understand *OsMGD* gene function, and submergence-related genes could be discovered in succession by utilizing this subtractive cDNA library.

References

Arumugam Pillai M, Lihuang Z, Akiyama T (2002) Molecular cloning, characterization, expression and chromosomal location of OsGAPDH, a submergence responsive gene in rice (*Oryza sativa* L.). Theor Appl Genet 105:34–42

Bachem CW, Van der Hoeven RS, De Bruijin SM, Vreugdenhil D, Zabeau M, Visser RG (1996) Visualization of differential gene expression using a novel method of RNA fingerprinting based on AFLP: analysis of gene expression during potato tuber development. Plant J 9:745–753

Benhassaine-Kesri G, Aid F, Demandre C, Kader JC, Mazliak P (2002) Drought stress affects chloroplast lipid metabolism in rape (*Brassica napus*) leaves. Physiol Plant 115:221–227

Chang T, Kuo M-C, Khoo K-H, Inoue S, Inoue Y (2000) Developmentally regulated expression of a peptide: N-glycanase during germination of rice seeds (*Oryza sativa*) and its purification and characterization. J Biol Chem 275:129–134

Chenchik A, Zhu Y, Diatchenko L, Li R, Hill J, Siebert P (1998) Generation and use of high-quality cDNA from small amounts of total RNA by SMART PCR. In: Siebert P, Larrick J (eds) RT–PCR methods for gene cloning and analysis. Biotechniques Books, MA, pp 305–319

Cho HT, Kende H (1997) Expression of expansin genes is correlated with growth in deepwater rice. Plant Cell 9:1661–1671

Diatchenko L, Lau YFC, Campbell AP, Chenchik A, Moqadam F, Huang B, Lukyanov S, Lukyanov K, Gurskaya N, Sverdlov ED, Siebert PD (1996) Suppression subtractive hybridization: a method for generating differentially regulated or tissue-specific cDNA probes and libraries. Proc Natl Acad Sci USA 93:6025–6030

Ella E, Kawano K, Ito O (2003) Importance of active oxygen-scavenging system in the recovery of rice seedlings after submergence. Plant Sci 165:85–93

Emanuelsson O, Nielsen H, Von Heijne G (1999) ChloroP: a neural network-based method for predicting chloroplast transit peptides and their cleavage sites. Protein Sci 8:978–984

Harwood JL (1984) Effects of the environment on the acyl lipids of algae and higher plants. In: Siegenthaler P-A, Eichenberger W (eds) Structure, function and metabolism of plant lipids. Elsevier, Amsterdam, pp 543–550

Hayashi H, Sakamoto A, Murata N (2001) Gene engineering of salt tolerance in higher plants. In: Shinozaki K, Yamamoto M, Okamoto T, Yiwabuti M (eds) Molecular mechanisms of response and adaptation to environmental stimuli. Kyori, Japan, p 2221

Hoffman-Benning S, Kende H (1992) On the role of abscisic acid and gibberellin in the regulation of growth in rice. Plant Physiol 99:1156–1161

Ichihara K (2001) Low-temperature stress and biosynthesis of plant lipids. In: Shinozaki K, Yamamoto M, Okamoto T, Yiwabuti M (eds) Molecular mechanisms of response and adaptation to environmental stimuli. Kyori, Japan, pp 2158–2164

Jackson MB, Waters I, Setter T, Greenway H (1987) injury to rice plants caused by complete submergence: a contribution by ethylene. J Exp Bot 38:1826–1838

Jarvis P, Dormann P, Peto CA, Lutes J, Benning C, Chory J (2000) Galactolipid deficiency and abnormal chloroplast development in the *Arabidopsis* MGD synthase 1 mutant. Proc Natl Acad Sci USA 97:8175–8179

Joyard J, Douce R (1987) Lipids: structure and function. In: Stumpf PK (ed) Biochemistry of plants. Academic Press, New York, pp 215–274

Kawano N, Ella E, Ito O, Yamauchi Y, Tanaka K (2002a) Metabolic changes in rice seedlings with different submergence tolerance after desubmergence. Environ Exp Bot 47:195–203

Kawano N, Ella E, Ito O, Yamauchi Y, Tanaka K (2002b) Comparison of adaptability to flash flood between rice cultivars differing in flash flood tolerance. Soil Sci Plant Nutr 48:659–665

Kelly AA, Dormann P (2002) DGD2, an arabidopsis gene encoding a UDP-galactose-dependent digalactosyldiacylglycerol synthase is expressed during growth under phosphate-limiting conditions. J Biol Chem 277:1166–1173

Mekhedov SI, Kende H (1996) Submergence enhances expression of a gene encoding amino cyclopropane-1-carboxylate oxidase in deepwater rice. Plant Cell Physiol 37:531–537

Miege C, Marechal E, Shimojima M, Awai K, Block MA, Ohta H, Takamiya K, Douce R, Joyard J (1999) Biochemical and topological properties of type A MGDG synthase, a spinach chloroplast envelope enzyme catalyzing the synthesis of both prokaryotic and eukaryotic MGDG. Eur J Biochem 265:990–1001

Mellema S, Eichenberger W, Rawyler A, Suter M, Tadege M, Kuhlemeier C (2002) The ethanolic fermentation pathway supports respiration and lipid biosynthesis in tobacco pollen. Plant J 30:329–336

Murata N, Higashi S, Fujimura Y (1990) Glycerolipids in various preparations of photosystem II from spinach chloroplasts. Biochim Biophys Acta Bioenerg 1019:261–268

Murphy DJ (1982) The importance of non-planar bilayer regions in photosynthetic membranes and their stabilisation by galactolipids. FEBS Lett 150:19–26

Najine F, Marzouk B, Cherif A (1995) Sodium chloride effect on the evolution of fatty acid composition in developing rape. In: Kader J-C, Mazliak P (eds) Plant lipid metabolism. Kluwer, Dordrecht, pp 435–437

Nakazono M, Tsuji H, Li Y, Saisho D, Arimura S, Tsutsumi N, Hirai A (2000) Expression of a gene encoding mitochondrial aldehyde dehydrogenase in rice increases under submerged conditions. Plant Physiol 124:587–98

Ram PC, Singh BB, Singh AK, Ram P, Singh PN, Singh HP, Boamfa I, Harren F, Santosa E, Jackson MB, Setter TL, Reuss J, Wade LJ, Pal SV, Singh RK (2002) Submergence tolerance in rainfed lowland rice: physiological basis and prospects for cultivar improvement through marker- aided breeding. Field Crops Res 76:131–152

Raskin I, Kende H (1984a) Regulation of growth in stem sections of deep-water rice. Planta 160:66–72

Raskin I, Kende H (1984b) Role of gibberellin in the growth response of submerged deep water rice. Plant Physiol 76:947–950

Sachs MM, Subbiah CC, Saab IN (1996) Anaerobic gene expression and flooding tolerance in maize. J Exp Bot 47:1–15

Sambrook J, Russell DW (eds) (2001) Molecular cloning: A laboratory manual, 3rd edn. Cold Spring Harbor Laboratory Press, New York, p 7.31–7.34

Sauter M, Rzewuski G, Marwedel T, Lorbiecke R (2002) The novel ethylene-regulated gene *OsUsp1* from rice encodes a member of a plant protein family related to prokaryotic universal stress proteins. J Exp Bot 53:2325–2331

Shen T, Wang JY (1991) Glycolysis. In: Shen T, Wang JY (eds) Biochemistry. Higher education, Beijing, pp 79–91

Shimojima M, Ohta H, Iwamatsu A, Masuda T, Shioi Y, Takamiya KI (1997) Cloning of the gene of monogalactosyldiacylglycerol synthase and its evolutionary origin. Proc Natl Acad Sci 94:333–337

Tremolieres A, Dainese P, Bassi R (1994) Heterogenous lipid distribution among chlorophyll-binding proteins of photosystem II in maize mesophyll chloroplasts. Eur J Biochem 221:721–730

Umeda M, Uchimiya H (1994) Differential transcript levels of genes associated with glycolysis and alcohol fermentation in rice plants (*Oryza sativa* L) under submergence stress. Plant Physiol 106:1015–1022

Van der Knaap E, Jagoueix S, Kende H (1997) Expression of an ortholog of replication protein A1 (RPA1) is induced by gibberellin in deepwater rice. Proc Natl Acad Sci 18:9979–9983

Van der Knaap E, Jagoueix S, Kende H (1998) Transcript level for a gene encoding a Pputative type 1a plasma membrane receptor is induced by gibberellin in deepwater rice. Plant Cell Physiol 119:1127–1132

Van Der Straeten D, Zhou Z, Prinsen L, Van Onckelen HA, Van Montagu MC (2001) A comparative molecular-physiological study of submergence response in low land and deep water rice. Plant Physiol 125:955–968

Yamaryo Y, Kanai D, Awai K, Shimojima M, Masuda T, Shimada H, Takamiya K, Ohta H (2003) Light and cytokinin play a cooperative role in MGDG synthesis in greening cucumber cotyledons. Plant Cell Physiol 44:844–855

Yu H, Willemot C (1996) Inhibition of eukaryotic galactolipid biosynthesis in mature-green tomato fruits at chilling temperature. Plant Sci 113:33–41

Zarembinski TI, Theologis A (1997) Expression characteristics of OS-ACS1 and OS-ACS2, two members of the 1-aminocyclopropane-1-carboxylate synthase gene family in rice (*Oryza sativa* L. cv. Habiganj Aman II) during partial submergence. Plant Mol Biol 33:71–77

Zarrouk M, Seqqat-Dakhma W, Cherif A (1995) Salt stress effect on plant lipid metabolism in olive leaves. In: Kader J-C, Mazliak P (eds) Plant lipid metabolism. Kluwer, Dordrecht, pp 429–431

Plant Prod. Sci. 8(5) : 553 — 562 (2005)

Development and Distribution of Root System in Two Grain Sorghum Cultivars Originated from Sudan under Drought Stress

Wataru Tsuji[1], Shinobu Inanaga[1], Hideki Araki[2], Shigenori Morita[3], Ping An[1] and Kaori Sonobe[1]

([1]Arid Land Research Center, Tottori University, 1390, Hamasaka, Tottori, 680-0001, Japan;
[2]Faculty of Agriculture, Yamaguchi University, 1677-1, Yoshida, Yamaguchi, 753-8515, Japan;
[3]Graduate School of Agricultural and Life Sciences, The University of Tokyo, 1-1-1, Midori-cho, Nishitokyo, Tokyo, 188-0002, Japan)

Abstract : The difference in rooting pattern between two grain sorghum cultivars differing in drought tolerance was investigated under drought stress. The cultivars, Gadambalia (drought-tolerant) and Tabat (drought-susceptible), were grown in bottomless wooden or acrylic root boxes to examine root parameters. Gadambalia consistently exhibited higher dry matter production and leaf water potential than Tabat under drought stress in both root boxes. In the experiment with wooden root boxes, under a drought condition, Gadambalia extracted more water from deep soil layers (1.1-1.5 m), which was estimated from the reduction in soil water content, than Tabat. This was because Gadambalia had a significantly higher root length density in these soil layers. The high root length density was due to enhanced lateral root development in Gadambalia. In the other experiment with acrylic root boxes, though total root length in the upper soil layer (0-0.5 m) was declined by limited irrigation in both cultivars, the reduction in Gadambalia was moderate compared with that in Tabat owing to the maintenance of fine root growth. Unlike Tabat, Gadambalia had an ability to produce the nodal roots from higher internodes even under drought, which resulted in the high nodal root length of Gadambalia. The growth angle of nodal roots was significantly correlated with root diameter, and the nodal roots from the higher internodes had large diameters and penetrated into the soil more vertically. These results indicate that the responses of roots (i.e. branching and/or growth of lateral root, and nodal root emergence from higher internodes) to soil dryness could be associated with the drought tolerance of Gadambalia.

Key words : Branching of root, Drought stress, Drought tolerance, Growth angle of nodal root, Plagiogravitropism, Root diameter, Root length density, *Sorghum bicolor* (L.) Moench.

Water deficiency is a serious limitation to crop production in large areas of the world. Sorghum [*Sorghum bicolor* (L.) Moench] is one of the most important crops in arid and semi-arid regions where precipitation is low and highly variable. For sorghum production in these areas, the cultivars are expected to be tolerant to less rainfall and/or limited irrigation. We previously studied dry matter production and shoot water relations in response to water shortage in sorghum cultivars from Sudan (Tsuji et al., 2003) to understand eco-physiological strategies for drought adaptation of the African sorghum. Under soil drying conditions, a local cultivar with drought tolerance (Gadambalia) could maintain higher leaf water potential and photosynthetic rate than a drought-susceptible cultivar (Tabat) improved for irrigated cropping. These differences were likely influenced by the ability to extract water under soil drying condition, i.e., the contribution of root development especially in the deep soil profile. However, little is known about the contribution of root system to drought tolerance in sorghum cultivars.

Root distribution of monocotyledonous plants is the result of growth of different types of roots (Klepper, 1991). Depth and expansion of a root system are primarily determined by the trajectory of the axile roots consisting of seminal and nodal roots. Furthermore, rooting depth of the axile roots is determined by the growth direction and the length of the roots (Araki et al., 2000). In a field experiment, Nakamoto et al. (1991) observed that cultivars of maize and foxtail millet, whose nodal roots orientated downward, exhibited high root length density in deep soil layers. A positive correlation was reported between "Root Depth Index" and growth angle of wheat seminal roots (Oyanagi et al., 1993a), which

Received 19 April 2005. Accepted 11 June 2005. Corresponding author: W. Tsuji (tsun@alrc.tottori-u.ac.jp, fax +81-857-29-6199). This research was supported in part by a grant for the 21st Century COE program from the Japan Society for the Promotion of Science, Japan.

Abbreviations : BI, branching index; RLD, root length density; SDW, shoot dry weight; SRL, specific root length; TRL, total root length; VWC, volumetric water content; θ, growth angle of nodal roots; θ_m, mean growth angle of nodal roots; Ψ_L, leaf water potential.

are the deepest axile roots in the wheat root system (Morita et al., 1993; Araki and Iijima, 2001). Growth direction of axile roots in cereals is determined by plagiogravitropism (Oyanagi et al., 1993b). The intensity of the plagiogravitropism in axile roots is affected by genotypes (Nakamoto, 1991; Oyanagi et al., 1993a; Araki and Iijima, 2001), environmental factors such as soil temperature (Tardieu and Pellerin, 1991) and soil moisture (Nakamoto, 1993; Oyanagi et al., 1995), and internode positions from which axile roots emerged (Nakamoto et al., 1991; Araki et al., 2000). The growth direction of axile roots, which is determined by genotype-dependent plagiogravitropism and influenced by environmental factors, can be said to determine the shape of the root system.

Root distribution in soil is also determined by the extent of branching and elongation of lateral roots. Lateral roots compose a great proportion of root length in cereal crops (Yamauchi et al., 1987a). In water-limited environments, growth of the lateral roots is important for crops to acquire more water from a dry soil. Water extraction from given depths was closely related to root length density (Fukai and Cooper, 1995). The growth of the lateral roots is highly influenced by soil moisture (Kono et al., 1987; Pardales and Kono, 1990). Bañoc et al. (2000a) indicated that branching ability of the root would be involved in the genetic differences in adaptation to fluctuating soil moisture (dry-submerged cycle) in rice cultivars.

The objective of this study was to investigate the developmental patterns of the root systems of two sorghum cultivars differing in drought tolerance under drought stress. We compared the root distribution profiles in the soil and their modification by soil drying. As the factors determining the developmental pattern of roots, growth angle, length, initiation of nodal roots, and the extent of branching of lateral roots were also examined, and how the developmental responses of roots to soil dryness contribute to drought tolerance of the sorghum cultivars was discussed.

Materials and Methods

Plant materials and experiment site

Two grain-sorghum cultivars, Gadambalia (drought tolerant) and Tabat (drought susceptible), were used in the present study. Seeds of both cultivars were provided by the Agricultural Research Corporation (ARC), Sudan. Gadambalia is a local drought-resistant cultivar, and Tabat is an improved cultivar released for irrigated cultivation (Salih et al., 1999; Tsuji et al., 2003). Root distribution in the soil profile and rooting pattern of the axile and lateral roots were separately examined in a plastic greenhouse, under two contrasting soil water regimes (wet and dry), at the Arid Land Research Center, Tottori University, Japan. The study plot (110 m^2) was covered with a transparent plastic vinyl sheet that permitted transmission of more than 95% of incident solar radiation. The soil at the experimental site was sandy with about 98% sand to a depth of about 5.0 m. The two sorghum cultivars and two water regimes were arranged in a completely randomized design with three replications in the following two experiments.

Experiment 1. Soil water content and root distribution in the soil profile

The two sorghum cultivars were grown in bottomless wooden root boxes (0.3 m wide, 0.9 m long, 1.8 m high) made of veneer plywood boards (12 mm thick). The root boxes were filled with air-dried sandy soil at a bulk density of 1.5 Mg m^{-3}. A compound fertilizer containing major elements (N: P_2O_5: K_2O = 0.13: 0.13: 0.16 g g^{-1}) was applied to the root boxes at the rate of 15 g per root box as top dressing. A compound trace element fertilizer mainly containing MgO: MnO: B_2O_3: = 0.14: 0.003: 0.003 g g^{-1} and calcium hydroxide were also applied to each root box at rates of 10 g and 25 g, respectively, to supplement the fertility and to adjust the pH (7.6) of the acidic sandy soil. The root boxes were buried in soil by 1.7 m deep to fix them and prevent any increase in soil temperature caused by solar radiation. An observation pit was dug along the sidewall (0.3 m wide, 1.8 m high) of the root box. Ten seeds of sorghum per root box were sown in the central part of the root boxes, and seedlings were thinned to two plants per root box four wk after sowing. Irrigation water was adequately applied until the start of the soil water treatments. Fifty-two days after sowing, the last irrigation of root boxes to 0.35 m^3 m^{-3}, which is more than moisture holding capacity after 24 h was made. Thereafter, daily irrigation was applied only to the wet treatment, while irrigation in the dry treatment was completely withheld until the end of the experiment at 145 d after sowing.

At the flowering stage, 55 d after the start of water treatments, water potentials of flag leaves were measured with a pressure chamber (Model 1000, PMS Instrument Co.) between 1100 and 1400. At early maturity stage, four holes (28 mm diameter) were made at depths of 0.3, 0.7, 1.1 and 1.5 m on the sidewall, facing the observation pit beside the root box, to measure soil water content using a profile probe (Type PR1/4, Delta-T Devices). After access tubes were horizontally inserted into each hole, output values were measured at four positions in the tube. The average output values (V) were converted to volumetric water content (VWC) according to a calibration formula, VWC =1.4053V-0.1486 (r = 0.995). After measurement of VWC, larger holes (0.15 m diameter) were perforated at the same position for collecting roots. A metallic cylinder (0.15 m in diameter, 0.38 m length) was inserted into the soil to sample a soil core with roots. After collection of the soil core, a soil column of 20 mm adjacent to the

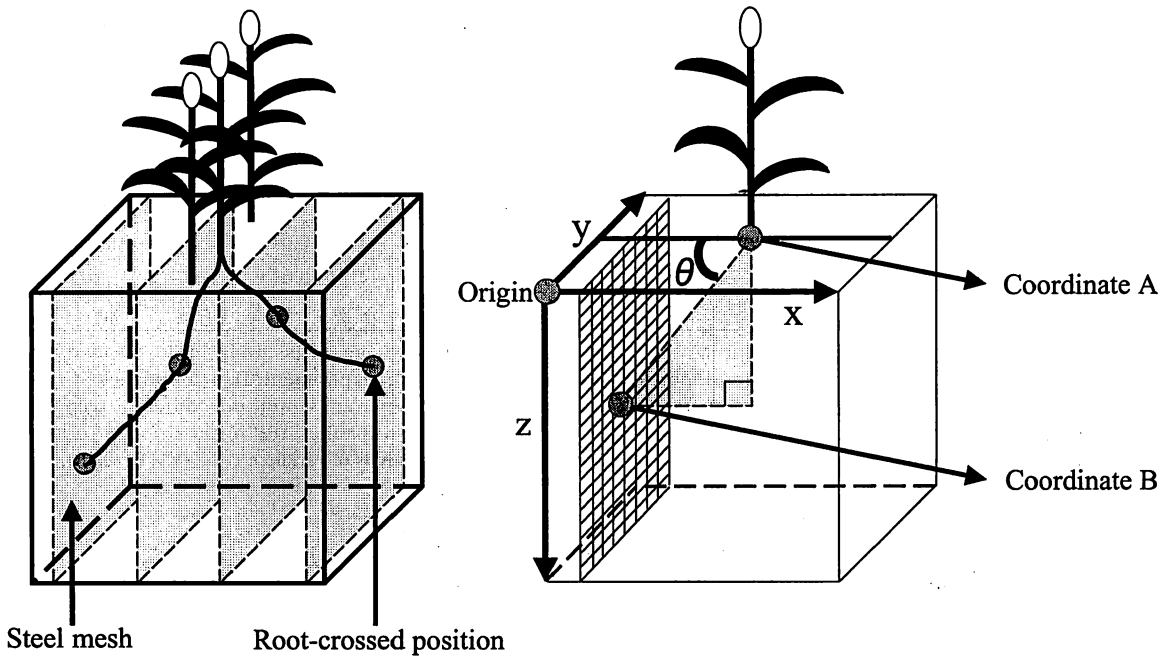

Fig. 1. Measurement of growth angle of nodal roots (θ). Root-crossing positions on each inner and outer steel meshes were recorded in the root box (Left). Model (Right) used for calculating θ according to a formula (see Materials and Methods) when one corner of the root box was determined as the origin O (0, 0, 0), and then coordinates A (plant base), and B (a root-crossing position on the meshes) were shown by (a_x, a_y, a_z) and (b_x, b_y, b_z), respectively.

wall of the root box was cut to remove roots bristling along the wall. The soil samples were carefully washed with showering tap water on a fine meshed sieve (less than 0.5 mm), and the collected roots were preserved in FAA solution (Formaldehyde: Acetic acid: 70% ethanol = 1: 1: 18). The root lengths were measured with a root length scanner (Root Length Scanner, Commonwealth Aircraft Co. Ltd.) to calculate the root length density (RLD). After measurement, the roots were dried in an oven at 80°C for 3 d, and weighed. Specific root length (a ratio of root length to root dry weight, SRL) was calculated from the root length and dry weight. SRL is an indicator of root morphology which shows the thickness of roots and/or extent of branching (Eissenstat, 1992). Dry weights of excised shoots were also weighed after dried in the oven at 80°C.

Experiment 2. Rooting pattern of nodal and lateral roots

The sorghum plants were grown in bottomless acrylic root boxes (0.5 m wide, 0.5 m long, 0.5 m high), which were placed on the sandy soil. The root boxes were covered with aluminum foil to prevent the rise in soil temperature caused by solar radiation. Four steel-wire meshes (4×4 mm) fixed by steel frames were vertically inserted at intervals of 0.15 m to observe the growth angle of nodal roots (Fig. 1). The steel meshes separated the rooting zone into three large compartments. Three plants at intervals of 0.1 m were grown between the inner two steel meshes (Fig. 1). The soil and fertilizers applied were the same as those in Experiment 1 with wooden root boxes. We applied 1.0 L of water to each root box from the top every day. The plants were subjected to two different irrigation treatments from 25 d after sowing. The wet treatment received 1.0 L water every day, while the dry treatment 0.5 L water every two days.

At the late vegetative stage on 25 d after the start of water treatments, water potentials of the highest fully expanded leaves were measured with a pressure chamber (Model 1000, PMS Instrument Co.) between 1000 and 1400. At the flowering stage, 52 d after the start of water treatments, the acrylic boards were removed to observe elongation direction and initiation of the nodal roots. At this time, Tabat in the dry treatment was still in the vegetative stage. The whole root system was carefully washed with running tap water. The position of the plant base (coordinate A) and the crossing position of the nodal roots on the steel meshes (coordinate B) were recorded with three-dimensional coordinates (Fig. 1). One corner of the root box was determined as the origin O (0, 0, 0), and then coordinate A and B were shown by (a_x, a_y, a_z) and (b_x, b_y, b_z), respectively. Growth angle of each nodal root (θ) was calculated by the following formula:

$$\theta = \tan^{-1}[|a_z-b_z|/\{(a_x-b_x)^2+(a_y-b_y)^2\}^{1/2}] \quad (0° \leqq \theta \leqq 90°)$$

Table 1. Shoot dry weight (SDW) and leaf water potential (Ψ_L) of two sorghum cultivars under wet and dry treatments in wooden and acrylic root-box experiments.

Cultivar	Treatment	SDW (g)		Ψ_L (MPa)	
		Wooden root-box	Acrylic root-box	Wooden root-box	Wooden root-box
Gadambalia	Wet	51.83±7.33	19.69±2.64^b	−1.09±0.03^a	−1.64±0.04^a
	Dry	49.87±2.76	12.39±1.35^c	−1.16±0.01^a	−2.15±0.09^b
Tabat	Wet	63.08±6.42	26.99±1.56^a	−1.09±0.04^a	−1.45±0.07^a
	Dry	44.78±3.78	4.47±1.23^d	−1.34±0.01^b	−2.91±0.08^c
$LSD_{0.05}$			5.82	0.08	0.23

The SDW and leaf water potential were measured at late ripening and flowering stage, respectively, in the wooden root-box, and at flowering and late vegetative stage, respectively, in the acrylic root-box experiment. Data are means of three replications ± standard errors. Values within a column followed by the different letter are significantly different according to LSD test at the 0.05 probability level. The letters and LSD value are not shown for the SDW in the wooden root-box experiment since interaction between cultivars and treatments was not found by analysis of variance (ANOVA, P=0.16).

where, θ represents the angle between soil surface and the line joining with the base of plant and the root-crossing points on the mesh, so the greater θ indicates that the nodal roots elongated vertically. Mean growth angle of nodal roots (θ_m) was calculated for each replicated plant.

After the determination of θ, internodes from which nodal roots emerged were traced. The number of nodal roots in each internode was also counted. The diameter of nodal roots at 5 mm from the base was simultaneously measured with a digital vernier caliper. The data above were limited to those from the nodal roots, i.e., no data were obtained for the seminal roots. In the root systems preserved in FAA solution, nodal and lateral roots were classified and their lengths were measured with a scale and a root length scanner (Root Length Scanner, Commonwealth Aircraft Co. Ltd.), respectively. Branching index (BI; Morita and Collins, 1990) was calculated as:

BI = Lateral root length/Nodal root length

BI indicates branching ability of parental roots and/or growth of lateral roots. After drying the roots in the oven at 80°C to obtain the dry weight, SRL was calculated. Dry weights of excised shoots were also weighed after drying in the oven at 80°C.

Results

1. Leaf water potential and shoot dry weight

Water potential of the leaves (Ψ_L) was lowered by limited water application more severely in the plants grown in the acrylic root boxes than in those grown in the wooden root boxes (Table 1). In the wooden root-box experiment, Ψ_L was hardly affected by the limited irrigation in Gadambalia, but significantly dropped to -1.34 MPa in Tabat. In the plants grown in the acrylic root boxes, the Ψ_L of Tabat dropped to below −2.9 MPa by drought, but that of Gadambalia only to −2.2 MPa.

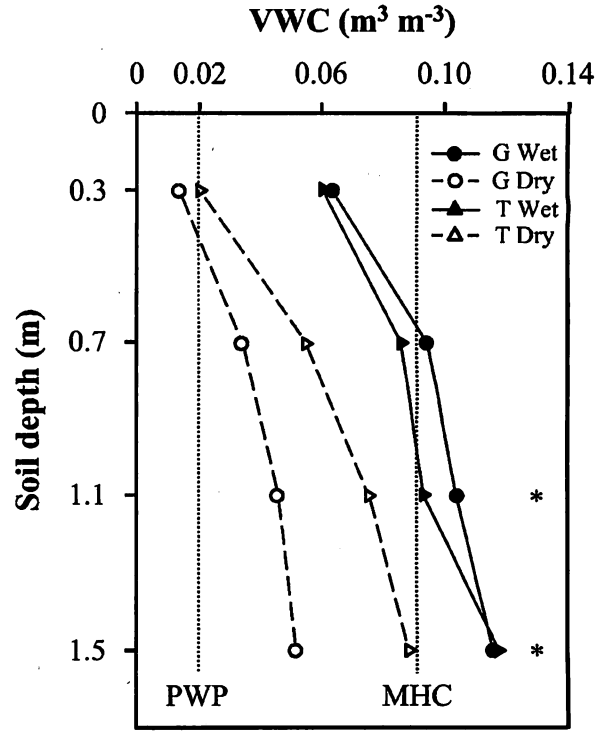

Fig. 2. Change in volumetric water content of soil (VWC) across soil depths in two sorghum cultivars, Gadambalia (G) and Tabat (T) under wet and dry treatments. Dotted lines indicate permanent wilting point (PWP) and moisture holding capacity after 24 h (MHC) of the sandy soil filled in root boxes. The * symbol indicates soil depths at which differences between cultivars under drought condition were significant at the 0.05 probability level.

A similar trend was observed in dry matter production (Table 1). In wet conditions, shoot dry weight (SDW) of Tabat was consistently higher than that of Gadambalia in both the wooden and acrylic root-box experiments. However, the SDW of Tabat in

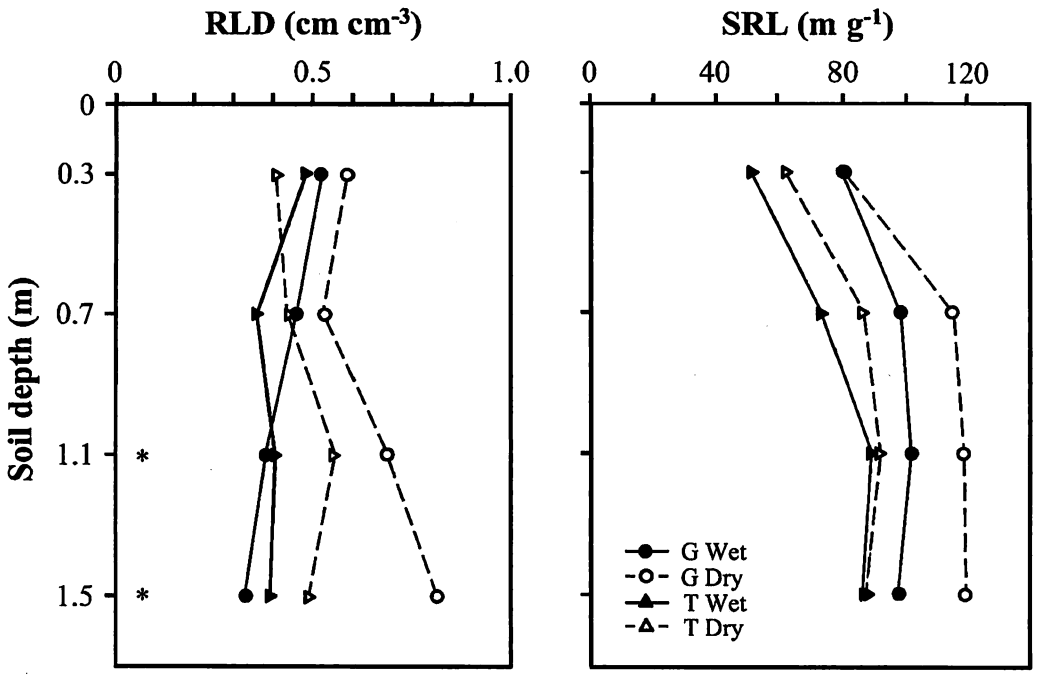

Fig. 3. Change in root length density (RLD) and specific root length (SRL) across soil depths in two sorghum cultivars, Gadambalia (G) and Tabat (T) under wet and dry treatments. The * symbol indicates soil depths at which differences between treatments in Gadambalia were significant at the 0.05 probability level.

Table 2. Total, nodal and lateral root length, branching index (BI) and specific root length (SRL) of whole root system of two sorghum cultivars under the wet and dry treatments.

Cultivar	Treatment	Total root length (m)	Nodal root length (m)	Lateral root length (m)	BI ($m\ m^{-1}$)	SRL ($m\ g^{-1}$)
Gadambalia	Wet	626.3±191.8	21.2±1.6	605.1±190.2	27.6±6.5	47.5± 6.2
	Dry	349.9± 28.7	13.0±2.7	336.9± 30.7	28.5±6.6	45.9± 1.1
Tabat	Wet	867.2±126.0	20.9±1.0	846.4±126.9	41.3±8.2	53.5±10.7
	Dry	205.2± 70.9	9.3±0.8	195.9± 70.7	20.9±7.9	36.5± 5.1

Data are means of three replications ± standard errors.

the dry treatment was significantly low compared with that in the wet treatment. In Gadambalia, the SDW in the dry treatment was hardly affected by the drought in the wooden root-box experiment, and was slightly lower than that in the wet treatment in the acrylic root-box experiment.

2. Water uptake and root distribution in the soil profile

In the wet treatment, the soils in the wooden root boxes with the two cultivars planted on them showed similar volumetric water content (VWC) at each soil depth (Fig. 2). Soil below 0.7 m in the dry treatment was significantly drier in the boxes with Gadambalia than those with Tabat. In the wet treatment, both cultivars exhibited a similar root length density (RLD) across soil depths (Fig. 3). However, the response to drought was markedly different between the cultivars. In the dry treatment, Tabat had a slightly higher RLD than in the wet treatment, though this increase was not significant at the 5% level. Although the RLD of Gadambalia in the wet treatment decreased with increasing depth, that in the dry treatment increased with increasing depth, especially in the deeper (1.1-1.5 m) soil layers ($P<0.05$). The specific root length (SRL) of Tabat was not affected by drought stress, but that of Gadambalia tended to increase in the dry treatment at 0.7-1.5 m depths, indicating that fine roots in these layers increased in response to the drought stress (Fig. 3).

3. Root length and branching

Detailed analysis on the length of the nodal and lateral roots was carried out for the roots in the

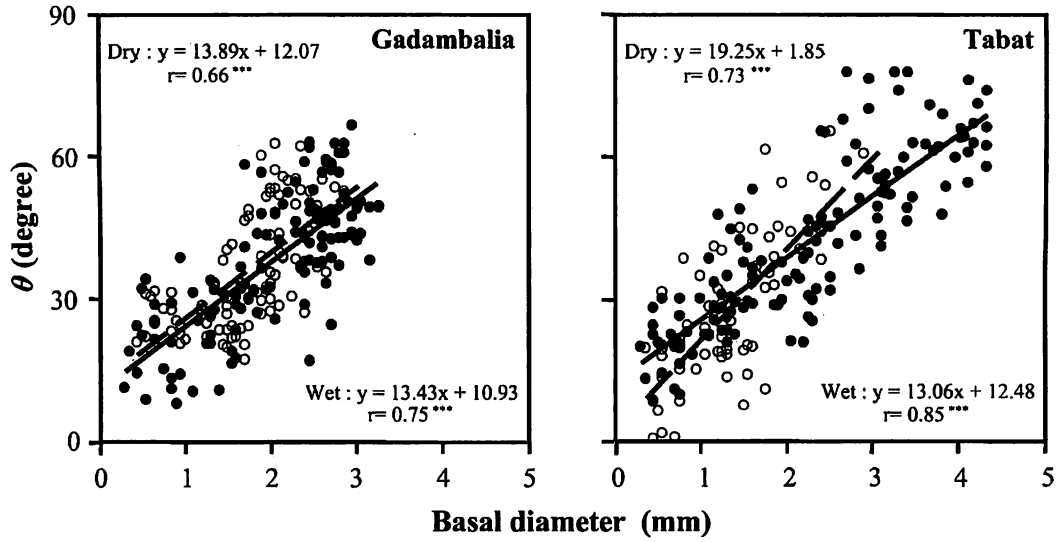

Fig. 4. Relationships between growth angle (θ) and basal diameter (5 mm from thebase) of nodal roots of two sorghum cultivars under wet (closed circle) and dry (open circle) treatments. Regression lines are solid and broken for wet and dry treatments, respectively. The *** symbol indicates the relationship were significant at the 0.001 probability level.

experiment with the acrylic root boxes. In the wet condition, Tabat developed the longest roots and showed the highest branching index (BI) and SRL (Table 2), indicating a higher branching ability than Gadambalia in non-stressed conditions. However, these parameters in Tabat were the lowest in the drought stress treatment. Although the total root length was reduced by drought in both cultivars, the reduction in Gadambalia was only 44.1%, while it was 76.3% in Tabat. Response of nodal and lateral roots to the drought stress also differed with the genotype. By dry treatment, the lengths of nodal and lateral roots were decreased by 38.7 and 44.3%, respectively, in Gadambalia, and 55.5 and 76.9%, respectively, in Tabat. The BI and SRL of Gadambalia were lower than those of Tabat in the wet treatment. These parameters were not affected by the drought stress in Gadambalia, but decreased by the drought stress in Tabat.

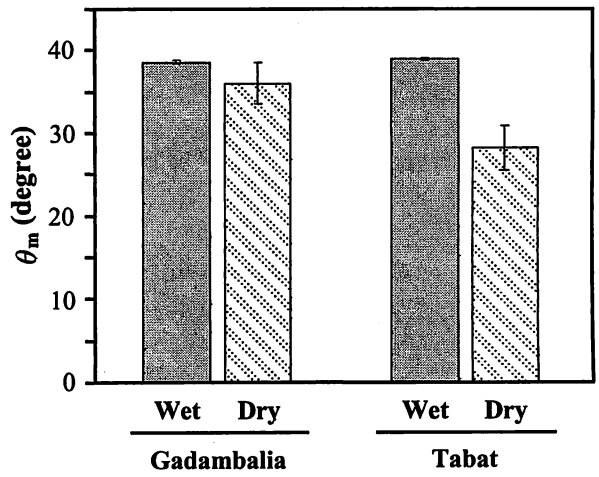

Fig. 5. Mean of the growth angle of nodal roots (θ_m) of two sorghum cultivars under wet and dry treatments. θ_m is represented by mean degree of deflection from the soil surface. Data are means of three replications ± standard errors.

4. Growth angle and initiation of nodal roots

The growth angles of nodal roots (θ) determined at the inner and outer meshes were highly correlated with each other ($r = 0.895$ at $P<0.001$). Therefore, only the angles determined at the inner meshes are presented in this paper.

In the whole root system, there were close relationships between θ and basal diameter of the nodal roots in both cultivars and treatments (Fig. 4). In the wet treatment, there was no genotypic difference in the mean growth angle of nodal roots (θ_m) and the slope of the regression line, i.e., increment of θ per unit root diameter (Figs. 4, 5). A relatively high θ was observed in Tabat grown in the wet soil since the plants had roots with large diameters. The slope of the regression lines of θ against the basal root diameter was not affected by the drought treatment in Gadambalia (Fig. 4). In Tabat, the slope was slightly increased by the drought treatment, but θ_m was significantly reduced due to the emergence of fewer nodal roots with large diameters (Figs. 4, 5).

Table 3 shows the θ of the roots emerged from each

Table 3. Growth angle of nodal roots (θ) at each internode in two sorghum cultivars under wet and dry treatments.

Cultivar	Treatment	θ (degree)							
		Internode							
		1st	2nd	3rd	4th	5th	6th	7th	8th
Gadambalia	Wet	20.6±2.9	25.2±2.7	34.4±3.5	40.7±0.7	44.0±1.9	52.0±2.3	55.6±2.7	–
	Dry	26.1±2.9	30.4±4.7	29.0±1.2	34.8±3.2	47.0±1.4	50.5±0.7	55.3±0.0	–
Tabat	Wet	25.4±2.6	24.3±2.9	29.6±0.3	36.0±1.1	46.5±5.0	58.6±7.0	64.6±0.1	67.7±0.0
	Dry	13.0±0.4	22.5±0.5	28.7±2.4	41.6±4.3	49.6±4.7	–	–	–

The θ is represented by degree of deflection from the soil surface, that is, the bigger the growth angle, the deeper the nodal roots elongate vertically. Dashes mean no emergence of nodal roots. Data are means of three replications ± standard errors.

Table 4. Number of nodal roots in total and at each internode of two sorghum cultivars under wet and dry treatments.

Cultivar	Treatment	Number of nodal roots								
		Internode								
		1st	2nd	3rd	4th	5th	6th	7th	8th	Total
Gadambalia	Wet	3.3±0.4	3.1±0.1	3.1±0.4	3.1±0.1	3.8±0.1	4.0±0.2	2.0±0.7	–	22.7±1.2
	Dry	3.0±0.2	2.4±0.7	3.1±0.2	3.4±0.3	3.8±0.3	3.7±0.4	1.9±1.0	–	21.3±0.2
Tabat	Wet	2.1±0.3	2.8±0.5	3.6±0.4	3.1±0.1	3.6±0.3	3.4±0.4	1.7±1.1	0.6±0.5	20.8±0.6
	Dry	2.8±0.5	2.9±0.4	3.3±0.4	3.3±0.2	1.0±0.5	–	–	–	13.3±0.9

Dashes mean no emergence of nodal roots. Data are means of three replications ± standard errors.

internode. The θ consistently increased as the rooting internodes were acropetally advanced irrespective of cultivars and treatments. The diameter of the nodal roots at higher internodes was also larger. The θ of roots emerged from the same internode was not different so much between Gadambalia and Tabat irrespective of treatments. Gadambalia produced roots at the 6th and 7th internodes even in the dry treatment as in the wet treatment (Table 4). In contrast, emergence of the roots from the higher internodes (6-8th) was inhibited by dry treatment in Tabat. This explains why the θ_m of Tabat in the dry treatment was reduced by drought stress.

Discussion

Tabat is a cultivar adapted to irrigation, which exhibited higher performance in dry matter production than Gadambalia on a well-irrigated soil (Table 1, Tsuji et al., 2003). In the dry condition, however, a reverse was the case. In Tabat, the SDW and Ψ_L were significantly reduced by drought stress even in the wooden root-box experiment, in which plants were exposed to moderate drought stress. In Gadambalia, the drought stress hardly influenced the SDW and Ψ_L in the wooden root-box experiment, but affected them in the acrylic root-box experiment. In addition, depletion of soil water in the root boxes with Gadambalia planted on it was greater than that in the root boxes with Tabat under the water-limited condition (Fig. 2). These results indicated that Gadambalia extracted more water, especially from deep soil, under drought stress. Salih et al. (1999) reported that Gadambalia had higher efficiency in extracting soil water from 0-0.9 m depth than Tabat although Gadambalia had a lower RLD. The present study indicated that Gadambalia extracted more water than Tabat from deeper soil layers (Fig. 2). Gadambalia grown in a root box had an extended RLD in 1.1-1.5 m depth in response to drought, but Tabat did not (Fig. 3). The increased SRL of Gadambalia in the soil deeper than 0.7 m indicated a vigorous development of fine roots under the dry condition (Fig. 3). The increased RLD (Fig. 3) would adaptively enhance water uptake from deeper soil layers, and allow better water relations in the shoot. This character might contribute to the drought tolerance of Gadambalia. Grain sorghum genotypes with drought tolerance from Australia also had a higher RLD in deep soil layers below 1.0 m than susceptible genotypes under drought stress conditions (Wright and Smith, 1983; Ludlow et al., 1990; Santamaria et al., 1990). These reports, together with ours, indicate that adaptive responses of the root development to soil dryness would be an important trait for drought tolerance in grain sorghum.

Lateral roots occupy a great proportion in the total length of the root system (Yamauchi et al., 1987b), and are responsible for a large portion of water extracted by the whole root system (Varney et al., 1993). The responses of roots to drought stress differed between

the sorghum cultivars used in this study even in the shallow soil layer. The smaller decrease in Total root length(TRL) under the drought condition in Gadambalia could be attributed to retention of a high BI and SRL on the nodal roots (Table 2). On the contrary, the significant reduction of TRL in the drought-stressed Tabat was attributed to the lower BI and SRL indicating that growth and initiation of the lateral roots were suppressed by drought stress. A drought-tolerant cultivar of upland rice also exhibited an extensive increase in the number of high-order lateral roots produced by first-order lateral roots under fluctuating soil moisture (Bañoc et al., 2000a). Morita et al. (1997) reported that moderate soil drying inhibited the elongation of primary seminal roots in wheat, but accelerated the compensatory branching of lateral roots. These changes in root growth appeared to be adaptive for water acquisition after rewatering (Morita et al., 1997). The crops including sorghum may be required to obtain the ability to generate and elongate the lateral roots under lowered soil water potential to keep BI higher to achieve drought tolerance. Otherwise, water extraction would be depressed by lack of roots resulting in a poor water status in the shoot and low productivity.

The decrease of nodal root length also accounted for the decrease of TRL in the dry treatment (Table 2). The reduction of the nodal root length was moderate in Gadambalia compared with that in Tabat. The inhibition of nodal roots elongation under drought stress has also been observed in sorghum (Pardales and Kono, 1990), sweet potato (Pardales et al., 2000) and rice (Bañoc et al., 2000b). The greater decrease of nodal root length in Tabat would be partly due to the reduction of the number of nodal roots (Table 4). Interestingly, the emergence of nodal roots from higher internodes was suppressed by drought stress in Tabat (Table 4), but was hardly affected in Gadambalia. Initiation and/or differentiation of primordia are sometimes delayed or suppressed by environmental stresses (Nemoto et al., 1995). So far, knowledge on nodal root emergence under soil drying is limited. Although a number of studies have been made on physiological processes involved in the differentiation of lateral roots, for example, the function of growth regulators like hormonal substrate, turgor maintenance by osmotic adjustment, and a role of carbon allocation (e.g. Wightman et al., 1980; Westgate and Boyer, 1985; Bañoc et al., 2000a), it is still unknown what determines differentiation of nodal roots in water-limited conditions.

In cereals such as maize, foxtail millet and wheat, growth angle of nodal and seminal roots characterized the root distribution profiles (Nakamoto et al., 1991; Oyanagi et al., 1993a, 1993b; Araki and Iijima, 2001). In the cultivars used in this study, there was a close positive correlation between θ and basal diameter of nodal roots irrespective of cultivars and treatments (Fig. 4). Similar correlations were also observed in other cereals such as lowland and upland rice, maize, and foxtail millet (Yamazaki et al., 1981; Yamazaki and Kaeriyama, 1982; Nakamoto et al., 1991; Araki et al., 2002). In sorghum cultivars, the growth angles of nodal roots are likely to be established by common morpho-physical processes proposed by Abe and Morita (1994) that the growth direction of axile roots may be primarily limited by their diameter. The nodal roots emerging from higher internodes had large diameters and elongated downward irrespective of cultivars and watering treatments (Table 3). Even in the dry treatment, the nodal roots emerged from the 6-7th internodes with the highest θ in Gadambalia, but not in Tabat. Stable emergence of the nodal roots at higher internodes in Gadambalia accounted for the higher θ_m under drought stress (Fig. 5) and would be partly responsible for the high RLD in deep soil layers. The hydrotropism induced by a water gradient in the medium influenced the growth angle of nodal roots in maize (Leopold and LaFavre, 1989; Nakamoto, 1993) and wheat (Oyanagi et al., 1992). However, this tropism might have little effect on the growth direction of nodal roots in sorghum since the θ of each nodal root was similar between the watering treatments in either cultivar (Table 3).

Water acquisition from deeper soil layers might be determined not only by the root length or root surface area but also by the physiological function of the roots, e.g. hydraulic conductivity (Sperry et al., 2002). Salih et al. (1999) reported that Gadambalia took up more water from deep soil layers despite its lower RLD than Tabat. Furthermore, Gadambalia, unlike Tabat, was not affected by drought stress in cross sectional area and capacity of late metaxylem vessels, which implied high hydraulic conductive potential of the nodal roots of Gadambalia. Functional aspects of roots may also be involved in the high ability to extract water from deep soil layers, and hence, the drought tolerance of Gadambalia. Further research to clarify the function of roots in water extraction by the sorghum cultivars is in progress.

Conclusion

The two sorghum cultivars with contrasting drought tolerance differed in the responses of their root systems to soil drying. The drought tolerance of Gadambalia is derived from deep rooting attribute and an ability to produce thick nodal roots elongating downward from higher internodes, as well as enhanced lateral root branching in deep soil layers under drought condition. In general, thick nodal roots persist longer and produce more and larger branch roots, thereby increasing root length density (Nguyen et al., 1997). Therefore, information on such nodal root emergence would facilitate breeding programs

and management practices for improving drought tolerance in sorghum.

Acknowledgements

The authors are grateful to Dr. Anthony Egrinya ENEJI and Dr. John GORHAM, visiting professors, Arid Land Research Center, Tottori University, Japan, for their invaluable comments and critical reading of the manuscript.

References

Abe, J. and Morita, S. 1994. Growth direction of nodal roots on rice: its variation and contribution to root system formation. Plant Soil 165 : 333-337.

Araki, H., Hirayama, M., Hirasawa, H. and Iijima, M. 2000. Which roots penetrate the deepest in rice and maize root systems? Plant Prod. Sci. 3 : 281-288.

Araki, H. and Iijima, M. 2001. Deep rooting in winter wheat: rooting nodes of deep roots in two cultivars with deep and shallow root systems. Plant Prod. Sci. 4 : 215-219.

Araki, H., Morita, S., Tatsumi, J. and Iijima, M. 2002. Physiol-morphological analysis on axile root growth in upland rice. Plant Prod. Sci. 5 : 286-293.

Bañoc, D. M., Yamauchi, A., Kamoshita, A., Wade, L. J. and Pardales, J. R. Jr. 2000a. Genotypic variations in response of lateral root development to fluctuating soil moisture in rice. Plant Prod. Sci. 3 : 335-343.

Bañoc, D. M., Yamauchi, A., Kamoshita, A., Wade, L. J. and Pardales, J. R. Jr. 2000b. Dry matter production and root system development of rice cultivars under fluctuating soil moisture. Plant Prod. Sci. 3 : 197-207.

Eissenstat, D. M. 1992. Costs and benefits of constructing roots of small diameter. J. Plant Nutr. 15 : 763-782.

Fukai, S. and Cooper, M. 1995. Development of drought-resistant cultivars using physio-morphological traits in rice. Field Crops Res. 40 : 67-86.

Klepper, B. 1991. Crop root system response to irrigation. Irrig. Sci. 12 : 105-108.

Kono, Y., Tomida, K., Tatsumi, J., Nonoyama, T., Yamauchi, A. and Kitano, J. 1987. Effects of soil moisture conditions on the development of root system of soybean plants (*Glycine max* Merr.). Jpn. J. Crop Sci. 56 : 597-607.

Leopold, A. C. and LaFavre, A. K. 1989. Interractions between red light, abscisic acid, and calcium in gravitropism. Plant Physiol. 89 : 875-87.

Ludlow, M. M., Santamaria, J. M. and Fukai, S. 1990. Contribution of osmotic adjustment to grain yield in *Sorghum bicolor* (L.) Moench under water-limited conditions. II . Water stress after anthesis. Aust. J. Agric. Res. 41 : 67-78.

Morita, S. and Collins, H. P. 1990. A method to describe root branching. Jpn. J. Crop Sci. 59 : 580-581.

Morita, S., Okuda, H. and Abe, J. 1993. Spatial distribution and structure of wheat root system. In Korean Society of Crop Science ed., Low-Input Sustainable Crop Production Systems in Asia. Korean Society of Crop Science, Seoul. 399-404.

Morita, S., Okuda, H. and Abe, J. 1997. Root system morphology of wheat grown under different soil moisture and transpiration rates after rehydration. J. Agric. Meteorol. 52 : 819-822.

Nakamoto, T., Shimoda, K. and Matsuzaki, A. 1991. Elongation angle of nodal roots and its possible relation to spatial root distribution in maize and foxtail millet. Jpn. J. Crop Sci. 60 : 543-549.

Nakamoto, T. 1993. Effect of soil water content on the gravitropic behavior of nodal roots in maize. Plant Soil 152 : 261-267.

Nemoto, K., Morita, S. and Baba, T. 1995. Shoot and root development in rice related to the phyllochron. Crop Sci. 35 : 24-29.

Nguyen, H. T., Babu, R. C. and Blum, A. 1997. Breeding for drought resistance in rice: Physiology and molecular genetics considerations. Crop Sci. 37 : 1426-1434.

Oyanagi, A., Sato, A. and Wada, M. 1992. Effect of water potential of culture medium on geotropic response of primary seminal root in Japanese wheat cultivars. Jpn. J. Crop Sci. 61 : 119-123.

Oyanagi, A., Nakamoto, T. and Wada, M. 1993a. Relationship between root angle of seedlings and vertical distribution of roots in the field in wheat cultivars. Jpn. J. Crop Sci. 62 : 565-570.

Oyanagi, A., Nakamoto, T. and Morita, S. 1993b. The gravitropic response of roots and the sharping of the root system in cereal plants. Environ. Exp. Bot. 33 : 141-158.

Oyanagi, A., Takahashi, H. and Suge, H. 1995. Interactions between hydrotropism and gravitropism in the primary seminal roots of *Triticum aestivum* L. Ann. Bot. 75 : 229-235.

Pardales, J. R. Jr. and Kono, Y. 1990. Development of sorghum root system under increasing drought stress. Jpn. J. Crop Sci. 59 : 752-761.

Pardales, J. R. Jr., Bañoc, D. M., Yamauchi, A., Iijima, M. and Esquibel, C. 2000. The effect of soil moisture fluctuation on root development during the establishment phase of sweetpotato. Plant Prod. Sci. 3 : 134-139.

Salih, A. A., Ali, I. A., Lux, A., Luxova, M., Cohen, Y., Sugimoto, Y. and Inanaga, S. 1999. Rooting, water uptake, and xylem structure adaptation to drought of two sorghum cultivars. Crop Sci. 39 : 168-173.

Santamaria, J. M., Ludlow, M. M. and Fukai, S. 1990. Contribution of osmotic adjustment to grain yield in *Sorghum bicolor* (L.) Moench under water-limited conditions. I . Water stress before anthesis. Aust. J. Agric. Res. 41 : 51-65.

Sperry, J. S., Stiller, V. and Hacke, U. G. 2002. Soil water uptake and water transport through root system. In Y. Waisel, A. Eshel and U. Kafkafi eds., Plant Roots: The Hidden Half, Third Edition. Marcel Deker Inc, New York. 663-681.

Tardieu, F. and Pellerin, S. 1991. Influence of soil temperature during root appearance on the trajectory of nodal roots of field grown maize. Plant Soil 131 : 207-214.

Tsuji, W., Ali, M. E. K., Inanaga, S. and Sugimoto, Y. 2003. Growth and gas change of three sorghum cultivars under drought stress. Biol. Plant. 46 : 583-587.

Varney, G. T., MuCully, M. E. and Canny, M. J. 1993. Sites of entry of water into the symplast of maize roots. New Phytol. 125 : 733-741.

Westgate, M. E. and Boyer, J. S. 1985. Osmotic adjustment and the inhibition of leaf, root, stem and silk growth at low water potentials in maize. Planta 164 : 540-549.

Wightman, F., Schneider, E. A. and Thimann, K. V. 1980. Hormonal factors controlling the initiation and development

of lateral roots. II . Effects of exogenous growth factors on lateral root formation in pea roots. Physiol. Plant. 49 : 304-314.

Wright, G. C. and Smith, R. C. G. 1983. Differences between two grain sorghum genotypes in adaptation to drought stress. II . Root water uptake and water use. Aust. J. Agric. Res. 34 : 627-636.

Yamauchi, A., Kono, Y. and Tatsumi, J. 1987a. Comparison of root system structures of 13 species of cereals. Jpn. J. Crop Sci. 56 : 618-631.

Yamauchi, A., Kono, Y. and Tatsumi, J. 1987b. Quantitative analysis on root system structures of upland rice and maize. Jpn. J. Crop Sci. 56 : 608-617.

Yamazaki, K., Morita, S. and Kawata, S. 1981. Correlations between the growth angles of crown roots and their diameters in rice plants. Jpn. J. Crop Sci. 50 : 452-456*.

Yamazaki, K. and Kaeriyama, N. 1982. The morphological characters and the growing directions of primary roots of corn plants. Jpn. J. Crop Sci. 51 : 584-590*.

*In Japanese with English summary

Soil Sci. Plant Nutr., **48** (1), 23–29, 2002

$^{22}Na^+$ and $^{36}Cl^-$ Mobility in Salinized Excised Leaves of Several Crop Plants

Satoshi Yamada, Atsushi Takeoka, and Masuo Yamanouchi

Faculty of Agriculture, Tottori University, Tottori, 680–8553 Japan

Received May 1, 2001; accepted in revised form October 16, 2001

Excised leaves of several crop plants were cultured in a nutrient solution containing $^{22}Na^+$ (816 Bq mL^{-1}) or $^{36}Cl^-$ (802 Bq mL^{-1}), and the mobility of $^{22}Na^+$ and $^{36}Cl^-$ between and within organs was investigated. Though $^{22}Na^+$ and $^{36}Cl^-$ seemed to be taken up depending on the transpiration in all the examined crops, the distribution pattern of $^{22}Na^+$ and $^{36}Cl^-$ and the concomitance between them varied among the crops as follows: 1) Though $^{22}Na^+$ and $^{36}Cl^-$ were taken up concomitantly in rice and maize, $^{22}Na^+$ and $^{36}Cl^-$ were well distributed all over the leaf in rice and reached the lower half of the leaf blade but moved only over a short distance from the midrib and the brims of the leaf blade in maize. 2) In soybean, $^{22}Na^+$ and $^{36}Cl^-$ were well distributed all over the leaf, and the possibility of the preferential intrusion of $^{36}Cl^-$ to the leaf was indicated. 3) In adzuki bean, $^{22}Na^+$ and $^{36}Cl^-$ were intensely distributed first to the petiole, then to the leaf veins, and finally to the mesophyll. The concomitance between $^{22}Na^+$ and $^{36}Cl^-$ could not be determined. 4) In pumpkin, $^{22}Na^+$ and $^{36}Cl^-$ were retained in the petiole for transfer to the leaf blade, and $^{36}Cl^-$ was taken up preferentially. These results suggested that in the excised leaves, the mobility of Na^+ and Cl^- was affected not only by the transpiration but also by the transport of Na^+ and Cl^- from the xylem to surrounding tissues and / or by the structure of leaf tissues.

***Key Words*: $^{36}Cl^-$ distribution, excised leaf, leaf structure, $^{22}Na^+$ distribution, transpiration.**

Since salinized agricultural lands, crop productivity is usually reduced by the restriction of water absorption and /or the disturbance in nutrient absorption, it is important to investigate the mechanisms of nutrient absorption under salinized conditions for the improvement of the productivity. Many studies on the characteristics of mineral absorption under salinized conditions have been centered on whole plant experiments which are important to analyze the responses of crops to salinized conditions in terms of productivity (Francois and Maas 1994). However, investigations on mineral absorption of whole plant do not enable to reveal the autonomous mobility of the ions in each individual organ, since the mobility of ions is assumed to be regulated by adjacent or separate organs.

In a previous paper, the distribution pattern of $^{22}Na^+$ in the petiole or leaf sheath with the leaf blade (hereafter referred to as PLB) and the detached petiole or leaf sheath without the leaf blade (hereafter referred to as DP) was investigated in several crops (López et al. 1999), where the distribution pattern of $^{22}Na^+$ and the relationship between the amount of transpiration and the amount of $^{22}Na^+$ absorbed in these excised leaves varied among the crops. Therefore, it was suggested that only passive processes such as mass flow could not account for Na^+ transport, and that Na^+ retention, Na^+ exclusion, or Na^+ transfer from the xylem flow to the xylem parenchyma cells might occur. However in the previous study, it was impossible to investigate in detail the mobility of $^{22}Na^+$ within organs such as that between the leaf vein and mesophyll, since the level of $^{22}Na^+$ in the segments of petioles or leaf sheaths and leaf blades was determined by using a γ-counter.

PLB and DP systems enable to investigate the mobility of elements absorbed from the xylem flow between and within organs by neglecting the effects of stems and roots, since the proximal ends of the petioles or leaf sheaths were soaked in the nutrient solution.

The objective of this study was to investigate the $^{22}Na^+$ and $^{36}Cl^-$ mobility between and within organs in PLB and DP subjected to NaCl treatment. Five main glycophytes were examined and the salt-tolerant and sensitive varieties were also examined for 3 out of the 5 crops. PLB and DP were cultured in a nutrient solution containing $^{22}NaCl$ or $Na^{36}Cl$, the amount of transpiration was measured and the distribution of $^{22}Na^+$ and $^{36}Cl^-$ in

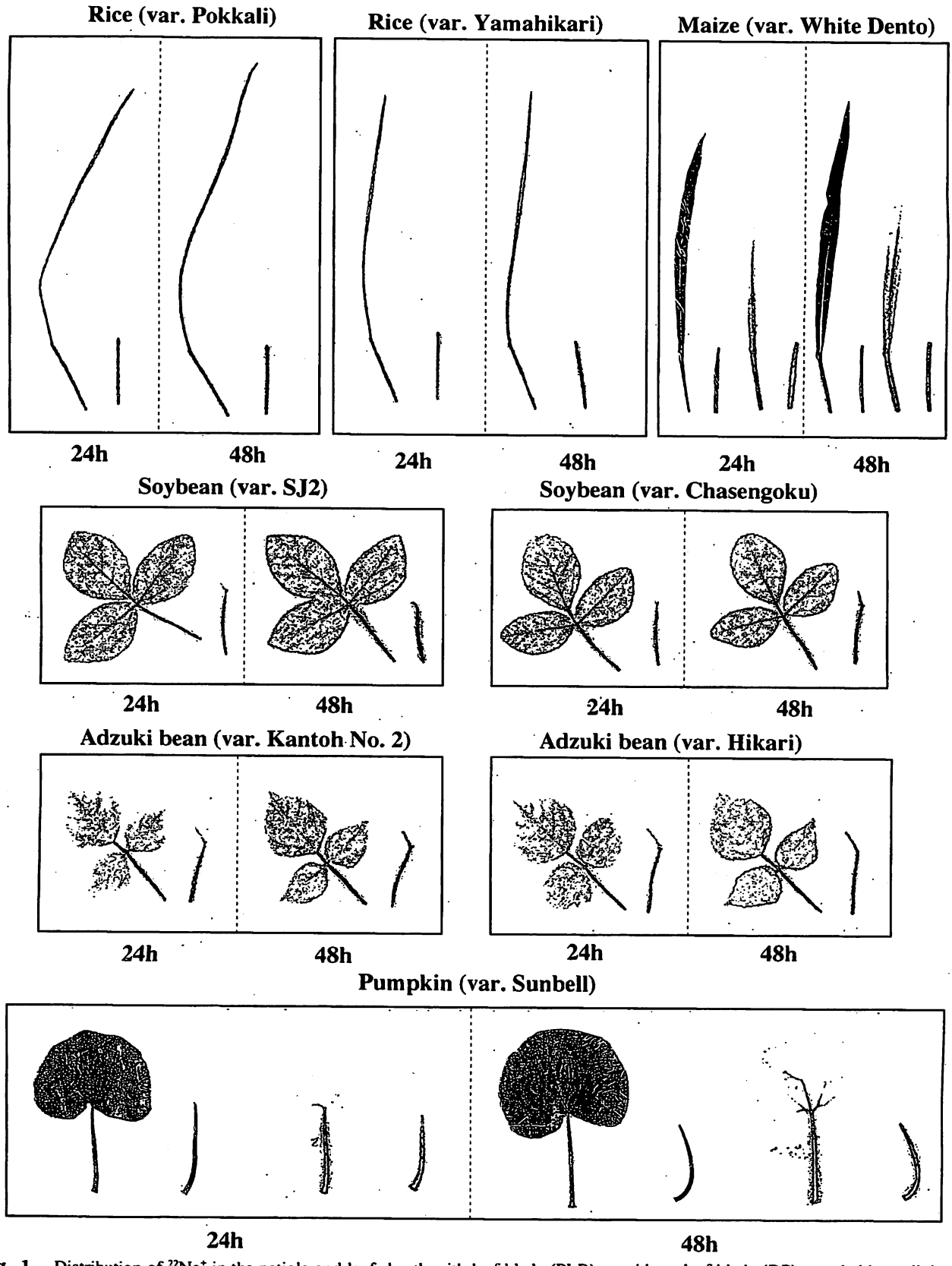

Fig. 1. Distribution of $^{22}Na^{+}$ in the petiole and leaf sheath with leaf blade (PLB) or without leaf blade (DP) revealed by radioluminography using an imaging analyzer. Images of PLB and DP are shown on the left and right sides of each window, respectively. For maize and pumpkin, the photographs of fresh specimens of PLB and DP are shown on the left side of each image.

these plant parts was visualized by radioluminography.

MATERIALS AND METHODS

Plant materials. The plant materials used were rice (*Oryza sativa* L. salt-tolerant variety: Pokkali and salt-sensitive variety: Yamahikari), maize (*Zea mays* L. var. White Dento), soybean (*Glycine max* Merr. salt-tolerant variety: SJ2 and salt-sensitive variety: Chasengoku), adzuki bean (*Phaseolus angularis* L. salt-tolerant variety: Kantoh No.2 and salt-sensitive variety: Hikari), and pumpkin (*Cucurbita pepo* L. var. Sunbell).

Plant culture and $^{22}Na^+$ and $^{36}Cl^-$ uptake. The method were previously described (Yamada et al. 2000) except for the use of a nutrient solution containing 40 mM NaCl labeled with $^{22}NaCl$ (816 Bq mL^{-1}) or $Na^{36}Cl$ (802 Bq mL^{-1}) for $^{22}Na^+$ and $^{36}Cl^-$ uptake, respectively.

Determination of the amount of transpiration and visualization of $^{22}Na^+$ and $^{36}Cl^-$. After plant culture, PLB and DP prepared as described previously (López et al. 1999) were transferred to 20 mL vials containing 2–3 mL of salinized nutrient solution. At 24 or 48 h after transfer to the vials, the amount of transpiration was calculated by the following equation.

$$\text{Amount of transpiration (mL)} = A - B$$

A: weight loss of the vial with the nutrient solution for the culture of PLB or DP for 24 or 48 h (g). B: weight loss of the vial with the nutrient solution without PLB or DP for 24 or 48 h (g). Methods of visualization of $^{22}Na^+$ and $^{36}Cl^-$ was described previously (Yamada et al. 2000).

The room temperature for $^{22}Na^+$ and $^{36}Cl^-$ uptake and for the determination of the amount of transpiration was adjusted to 25°C and the light intensity was 500–600 $\mu E\ s^{-1}\ m^{-2}$.

RESULTS

$^{22}Na^+$ distribution

In the PLB of both varieties of rice, $^{22}Na^+$ was well distributed all over the leaf sheaths and leaf blades after 24 h and the distribution became denser in both organs after 48 h (Fig. 1). In the DP of these two varieties of rice, the $^{22}Na^+$ density increased gradually distally, though $^{22}Na^+$ was also well distributed all over the leaf sheaths and the distribution became denser with time.

In the PLB of maize, $^{22}Na^+$ reached the middle part of the leaf blade to be distributed along the midrib after 24 h and the $^{22}Na^+$ intrusion continued upward along the midrib and the brims of the leaf blade after 48 h, while in DP, $^{22}Na^+$ was distributed all over the leaf sheath and the distribution became denser with time.

In the PLB and DP of both varieties of soybean, $^{22}Na^+$ was well distributed all over the petioles and leaf blades after 24 h, and the distribution became slightly denser in all these two organs in var. SJ2 while the density of

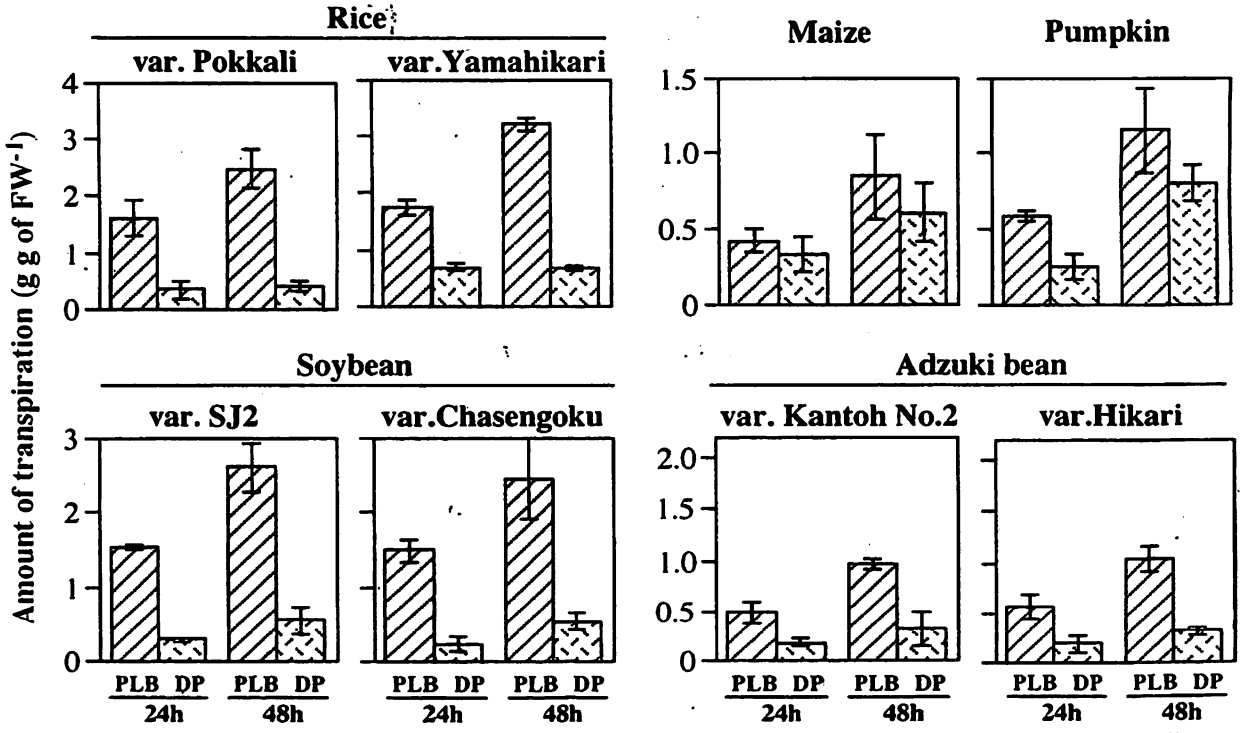

Fig. 2. Amounts of transpiration at 24 and 48 h after $^{22}Na^+$ absorption. Bars in figure indicate SD value (n = 3).

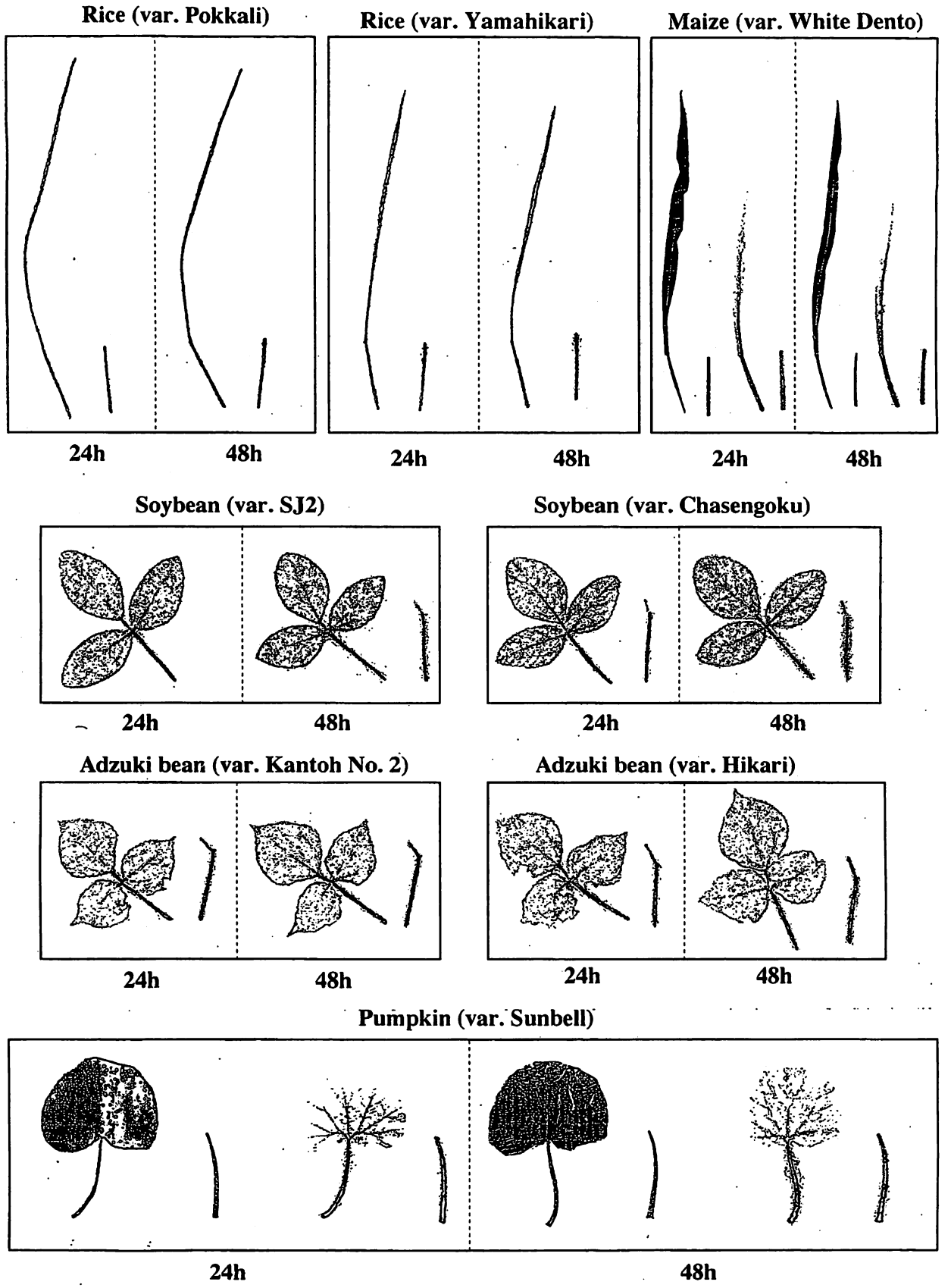

Fig. 3. Distribution of $^{36}Cl^-$ in PLB or DP revealed by radioluminography using an imaging analyzer. The other parts in the legend are the same as those in Fig. 1.

$^{22}Na^+$ did not change in var. Chasengoku after 48 h.

In the PLB and DP of both varieties of adzuki bean, $^{22}Na^+$ was intensely distributed to the petioles and leaf veins to some extent after 24 h, and densely distributed also to the mesophyll after 48 h. After 48 h, the distribution of $^{22}Na^+$ was slightly denser in var. Kantoh No. 2 than in var. Hikari.

In the PLB of pumpkin, $^{22}Na^+$ was distributed almost only all over the petiole after 24 h, and a slight distribution of $^{22}Na^+$ to the leaf veins was detected after 48 h, while in DP, $^{22}Na^+$ was sparsely distributed distally after 24 h and the distribution became denser with time.

Amount of transpiration for $^{22}Na^+$ absorption

In the two varieties of rice, the amount of transpiration increased with time in PLB but was constant in DP, and was slightly larger in var. Yamahikari than in var. Pokkali after 24 and 48 h (Fig. 2).

In maize and pumpkin, though the amount of transpiration in PLB and DP increased with time, the difference in the amount of transpiration between PLB and DP was the smallest in these crops.

In the PLB and DP of soybean and adzuki bean, the amount of transpiration increased with time and the increments were almost similar between the two varieties of each species.

$^{36}Cl^-$ distribution

In the PLB and DP of the two gramineous crops, the $^{36}Cl^-$ distribution pattern was vary similar to that of $^{22}Na^+$ (Fig. 3).

In the PLB and DP of both varieties of soybean, $^{36}Cl^-$ was well distributed all over the petioles and leaf blades after 24 h, and the distribution became slightly denser in var. SJ2 while the density of $^{36}Cl^-$ did not change in var. Chasengoku after 48 h, though the difference in the $^{36}Cl^-$ density between the leaf veins and mesophyll was less pronounced in var SJ2 than in var. Chasengoku.

In the PLB and DP of both varieties of adzuki bean, $^{36}Cl^-$ was distributed all over the petioles and leaf blades after 24 h, and the distribution became slightly denser in var. Kantoh No. 2 while the $^{36}Cl^-$ density did not change in var. Hikari after 48 h. The difference in the $^{36}Cl^-$ density between the leaf veins and the mesophyll was similar in the two varieties of adzuki bean.

In the PLB of pumpkin, $^{36}Cl^-$ was intensely distributed all over the petiole and to some extent to the leaf veins and mesophyll after 24 h, and the distribution became slightly denser in the leaf veins and mesophyll after 48 h, while in DP, $^{36}Cl^-$ was distributed all over the petiole after 24 h and the distribution became slightly denser with time.

Amount of transpiration for $^{36}Cl^-$ absorption

The amounts of transpiration in the $^{36}Cl^-$ absorption experiment were almost the same as those for the $^{22}Na^+$ absorption experiment, except that the amount of transpiration was smaller in both varieties of soybean and

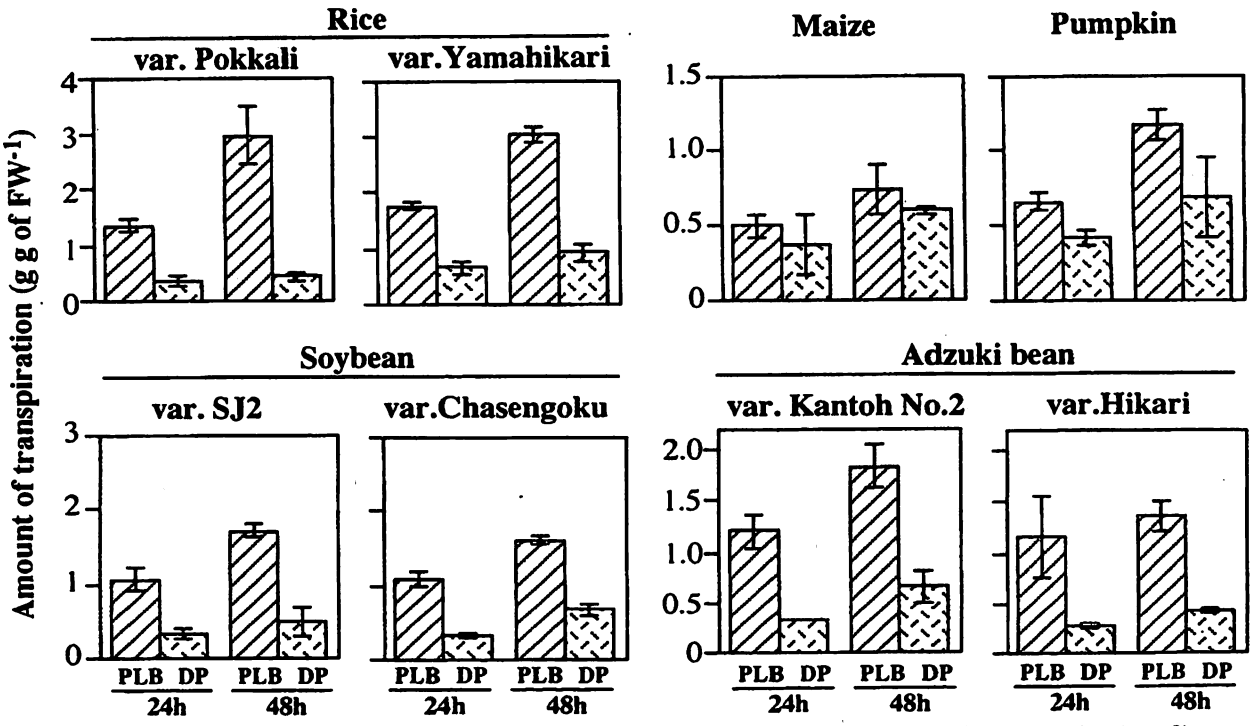

Fig. 4. Amounts of transpiration at 24 and 48 h after $^{36}Cl^-$ absorption. Bars in figure indicate SD value (n = 3).

was larger in both varieties of adzuki bean than those in the $^{22}Na^+$ absorption experiment (Fig. 4).

DISCUSSION

In this study, $^{22}Na^+$ and $^{36}Cl^-$ mobility between and within organs in the excised leaves treated with NaCl was investigated and the distribution of $^{22}Na^+$ and $^{36}Cl^-$ was visualized by radioluminography using an imaging analyzer (Imaging Analyzer BAS 2000, Fuji Film, Tokyo, Japan). In this method, the monochrome density expresses the radiant energy of $^{22}Na^+$ and $^{36}Cl^-$ captured in the imaging plate, and the radiant energy of these two radioisotopes is different. Therefore, the amounts of $^{22}Na^+$ and $^{36}Cl^-$ could be compared based on the density of each isotope as indicated in Figs. 1 and 3, respectively. Since the density of $^{22}Na^+$ and $^{36}Cl^-$ was assumed to roughly depend on the amount of transpiration, the amount of $^{22}Na^+$ and $^{36}Cl^-$ absorbed was assumed to depend on the amount of transpiration. Though the amount of net $^{22}Na^+$ and $^{36}Cl^-$ absorbed could not be compared, the mobility rate of $^{22}Na^+$ and $^{36}Cl^-$ could be estimated by the difference in the isotope density from 24 to 48 h after $^{22}Na^+$ and $^{36}Cl^-$ absorption.

The results of the $^{22}Na^+$ and $^{36}Cl^-$ distribution (Figs. 1 and 3) indicate that the distribution patterns of Na^+ and Cl^- varied among the crops; Na^+ and Cl^- were distributed all over the leaf in rice and soybean, upward along the midrib and the brims of the leaf blade in maize, intensely distributed to the petioles, to some extent to the leaf veins and subsequently to the mesophyll in adzuki bean, and the transport was restricted to the leaf blade in pumpkin. A considerable factor responsible for the variation in the distribution pattern was the transport system of these ions from the xylem to the surrounding parenchyma tissues. In a previous paper, it was reported that $^{22}Na^+$ was retained in the lower part of the petioles of PLB and DP and that the transport was restricted to the leaf blades in pumpkin (López et al. 1999). And it was also reported that Na^+ was excluded from the leaves of beans (Kramer et al. 1977) and corn (Yeo et al. 1977) by the reabsorption of Na^+ from the xylem sap to the surrounding tissues in the proximal region of the roots. The rate of transport of Na^+ and Cl^- from the xylem sap to the surrounding tissues might vary among the examined crops. The other considerable factor was the structure of the leaves. In this study, $^{22}Na^+$ and $^{36}Cl^-$ distribution became gradually and distally denser in rice and maize, which might be due to the similarity in the distribution of bundle sheaths. In adzuki bean, $^{22}Na^+$ and $^{36}Cl^-$ were intensely distributed to the petiole first, subsequently to the leaf veins, and finally to the mesophyll, and this phased distribution pattern might be closely related to the leaf structure and was clearly observed in pumpkin and indistinctly in soybean.

As described above, although the distribution pattern of Na^+ and Cl^- varied among the crops, the concomitance between Na^+ and Cl^- also seemed to vary among the crops. In rice and maize, $^{22}Na^+$ and $^{36}Cl^-$ were taken up concomitantly (Figs. 1 and 3). In soybean, the density of both $^{22}Na^+$ and $^{36}Cl^-$ seemed to be almost saturated after 24 h, though the amount of transpiration for the $^{36}Cl^-$ absorption experiment was remarkably smaller than that for the $^{22}Na^+$ absorption experiment (Figs. 2 and 4). Therefore, it is possible that Cl^- might have been taken up preferentially to PLB. In adzuki bean, since the distribution of $^{22}Na^+$ tended to become denser with time while the $^{36}Cl^-$ density was assumed to be already almost saturated after 24 h (Figs. 1 and 3), $^{36}Cl^-$ was apparently taken up preferentially to the leaf blade. However, since the amount of transpiration for the $^{36}Cl^-$ absorption experiment was roughly double of that for the $^{22}Na^+$ absorption experiment (Figs. 2 and 4), the preferential intrusion of $^{36}Cl^-$ could not be confirmed. In these two leguminous crops, the concomitance between $^{22}Na^+$ and $^{36}Cl^-$ should be examined under the same amount of transpiration. The difference in the amount of transpiration between the two experiments in soybean and adzuki bean was attributed to the subtle differences in the experimental conditions such as the humidity and solar radiation intensity from the window of the laboratory. The density of $^{36}Cl^-$ was almost constant in soybean and adzuki bean with an increase in the amount of transpiration with time, which indicated that Cl^- exclusion from the leaf blade occurred in the PLB of soybean and adzuki bean. In pumpkin, since the difference in the $^{36}Cl^-$ density between the leaf blade and petiole was much smaller than that of the $^{22}Na^+$ density (Figs. 1 and 3), it was considered that Cl^- intrusion occurred preferentially into the petiole and leaf blade. The studies in which the Na^+ / Cl^- ratio of several highly salinized crops was examined, revealed that the Na^+ / Cl^- ratio in leaves was 0.97 ± 0.14 in rice, 0.22 ± 0.12 in soybean and 0.64 ± 0.20 in adzuki bean (Yamanouchi et al. 1990a). Yamanouchi et al. (1990b) stated that in pumpkin, the total amount of Na^+ absorbed was remarkably small compared with that of Cl^-, Na^+ markedly accumulated in the stem and the transport was restricted to the leaf blade, resulting in high concentrations of K^+, Ca^{2+}, and Mg^{2+} without concomitance between Na^+ and Cl^-. Namely in a whole plant, Na^+ and Cl^- were taken up concomitantly in rice and Cl^- was taken up preferentially in soybean, adzuki bean, and pumpkin. It is interesting to note that the concomitance between Na^+ and Cl^- in whole plant occurred in the excised leaves of rice and pumpkin in this study.

In the current study, the excised leaves of the salt-tol-

erant and sensitive varieties were examined for rice, soybean, and adzuki bean. In the salt-tolerant varieties of rice such as Pokkali, the restriction of Na^+ accumulation in shoots was due to the Na^+-holding capacity and Na^+-excluding capacity of the roots (Yamanouchi 1989). The salt-tolerant varieties of soybean such as SJ2 showed lower concentrations of Na^+ and Cl^- in the leaf blade or stem than the sensitive varieties such as Chasengoku (Yamanouchi et al. 1989a), and the salt-tolerant varieties of adzuki bean such as Kantoh No. 2 showed a lower concentration of Na^+ in the leaf blades which depended on the Na^+-excluding capacity and / or the rate of Na^+ translocation to leaves (Yamanouchi et al. 1989b). Hence, salinity tolerance can be partly attributed to the mechanisms of Na^+ and Cl^- partition in the whole plant. In the PLB and DP systems in this study, Na^+ and Cl^- mobility in leaves could be investigated by neglecting the effects of stems and roots and it was revealed that the Na^+ and Cl^- mobility in the excised leaves was not different between the examined varieties of rice, and was almost the same between the examined varieties of soybean and adzuki bean. In conclusion, it can be stated that the leaves themselves only hardly display the salt-excluding mechanism and can not account for the salinity tolerance for rice, soybean, and adzuki bean.

REFERENCES

Francois LE and Maas EV 1994: Crop response and management on salt-affected soils. *In* Handbook of Plant and Crop Stress, Ed. M Pessarakli, p. 149–182, Marcel Dekker, Inc., New York / Basel / Hong Kong

Kramer D, Läuchli A, and Yeo AR 1977: Transfer cells in roots of *Phaseolus coccineux*: Ultrastructure and possible function in exclusion of sodium from the shoot. *Ann. Bot.*, **41**, 1031–1040

López R, Yamada S, and Yamanouchi M 1999: Comparison of sodium uptake by and transport in detached plant parts among several crops. *Soil Sci. Plant Nutr.*, **45**, 659–668

Yamada S, Takeoka A, and Yamanouchi M 2000: ^{32}P mobility in detached leaf of several crop plants. *Soil Sci. Plant Nutr.*, **46**, 969–974

Yamanouchi M 1989: The mechanisms of salinity tolerance in rice plants. Relationships between the varietal difference of salinity tolerance and characteristics of absorption and translocation of sodium ion (2). *Jpn. J. Soil Sci. Plant Nutr.*, **60**, 210–219 (in Japanese with English summary)

Yamanouchi M, Fujiyama H, Kimura Y, and Nagai T 1990a: The effects of sodium chloride on the absorption and the translocation of several ions in sugar beets, rice plants, soy beans, azuki beans, and kidney beans. The effects of sodium chloride on the absorption and the translocation of several ions in plants (2). *Jpn. J. Soil Sci. Plant Nutr.*, **61**, 173–176 (in Japanese with English summary)

Yamanouchi M, Fujiyama H, Koyama Y, and Nagai T 1989a: The mechanisms of salinity tolerance for soybean (*Glycine max* L.). Relationships between the varietal difference of salinity tolerance and the characteristics of absorption and translocation of sodium ion (6). *Jpn. J. Soil Sci. Plant Nutr.*, **60**, 437–442 (in Japanese with English summary)

Yamanouchi M, Fujiyama H, Matsumoto N, and Nagai T 1990b: The effects of sodium chloride on the absorption and the translocation of several ions in Cucurbitacea plants. The effects of sodium chloride on the absorption and the translocation of several ions in plants (1). *Jpn. J. Soil Sci. Plant Nutr.*, **61**, 1–7 (in Japanese with English summary)

Yamanouchi M, Susaki S, Wakusima T, and Fujiyama H 1989b: The mechanisms of salinity tolerance for azuki bean (*Phaseolus angularis* L.). Relationships between the varietal difference of salinity tolerance and characteristics of absorption and translocation of sodium ion (3). *Jpn. J. Soil Sci. Plant Nutr.*, **60**, 325–334 (in Japanese with English summary)

Yeo AR, Kramer D, Läuchli A, and Gullasch J 1977: Ion distribution in salt stressed mature *Zea mays* roots in relation to ultrastructure and retention of sodium. *J. Exp. Bot.*, **28**, 17–29

AERODYNAMIC FORCES ON AN AIRFOIL IN PITCHING AND/OR IN A PERIODICALLY VARYING WIND

Yutaka Hara, In-Seung Kang, Tomohiro Moriya, and Tsutomu Hayashi
Tottori University, 4-101 Koyama-cho, Tottori 680-8552, Japan
E-mail:hara@damp.tottori-u.ac.jp

Abstract: Direct measurement system of aerodynamic forces acting on a two-dimensional wing has been developed by using two force sensors. This equipment was employed to measure the aerodynamic characteristics of NACA 64_2A-015 wing section (symmetrical airfoil) and FX 63-137 wing section (asymmetrical airfoil) in a pitching motion and/or in a periodically varying wind. In the pitching motion, lift-to-drag ratio of the symmetrical airfoil shows larger hysteresis than the asymmetrical airfoil. Lift-to-drag ratio of both airfoils in a pitching motion and simultaneously in a periodically varying wind tends to increase more than the value of static measurement at small angle of attack.

1. Introduction

Our group has been studying and developing the straight-blade type vertical-axis wind turbines (VAWT). VAWT is mainly driven by the lift of the blades and the operation has no dependency on the wind direction. Recently, development of a practical VAWT useful for the place where wind direction is unstable is hoped. In the design or performance prediction of a VAWT, the aerodynamic force data of the blade airfoil are required for a large angle of attack (from -180 deg to +180 deg). Since the relative wind velocity and the angle of attack for a blade of a VAWT change periodically during the rotation, some problems, such as dynamic stall and vibrations, will occur.

In this research, direct measurement system of the aerodynamic forces acting on a two-dimensional wing has been developed by using two force sensors for the purpose of measuring the aerodynamic data quickly and correctly even in the range of large angle of attack. The aerodynamic characteristics of two-dimensional wings under the conditions of a pitching motion and/or a periodically varying wind were measured using this equipment and the results were investigated especially about the behavior of lift-to-drag ratio. The performed experimental conditions differ from those of practical wind turbines. The aim of this study is to make clear the effects of the periodically varying wind and the pitching motion on the aerodynamic characteristics of a two-dimensional wing. Our recent paper described the results on symmetrical airfoils [1]. The present paper focuses on the comparison between the characteristics of a symmetrical airfoil and those of an asymmetrical airfoil.

2. Experimental setup and method

The schematic diagram of the experimental setup is illustrated in Fig. 1. The measuring object is a wing model (movable blade) with the wingspan of 1m and the chord length of 0.25m. The airfoils used for this wing are: the symmetrical type NACA 64_2A-015 and the asymmetrical type FX 63-137. The outlines of the two airfoils are shown in Fig. 2. The wing models are made of fiberglass reinforced plastic (GFRP). To both ends of this movable blade, the stainless steel rods are attached at 25 percent of chord length from the leading edge, and two six-axis force sensors (NITTA Corp.) are attached on each end of the rods. Fixed blades with the wingspan of 100mm and 150mm, which have the same cross section as the movable blade, are placed close to both ends of the movable blade by connecting each other using two long connecting rods keeping out of touch with

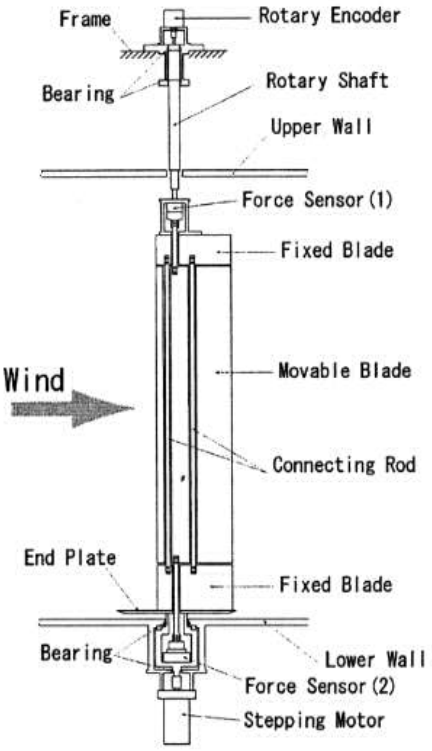

Figure 1. Experimental setup

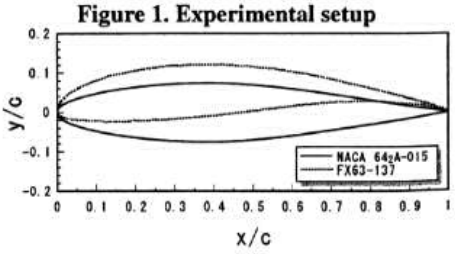

Figure2. Airfoils used in this study

the movable blade. An end plate with a diameter of 400mm is attached at the end of the bottom of fixed blade. The fixed blades and the end plate are structurally combined with the foundation parts of the force sensors. The whole unit, which includes the movable blade, two

fixed blades, the end plate and two force sensors, is installed at the center of the test section (1.5m x 1.5m x 3m) in the Wind Tunnel of Tottori University, Japan. The wind tunnel can generate periodically varying wind by changing the pitching angle of the fan. The whole unit rotates around the axis connecting two force sensors by controlling a stepping motor placed under the floor of the test section. The rotational angle, i.e. angle of attack (alpha), is measured by a rotary encoder.

3. Measurement Results

3.1 Static measurement of aerodynamic forces

Figures 3 and 4 are examples of quasi-static measurements of the aerodynamic force coefficients (i.e. CL: lift coefficient, CD: drag coefficient, CM: pitching moment coefficient of 1/4 chord length). The measurements have been performed at every 1 deg of the angle of attack. At each angle of attack, 100 data sets were acquired with the time interval of about 10 milli-second and the averaged values were recorded. One measurement through the range of 360 deg, i.e. clockwise measurement from -180 deg to +180 deg or counterclockwise measurement from +180 deg to -180 deg, took about 10 minutes.

The data shown in Fig.3 are the average of 5-time measurements in the clockwise direction about the airfoil of NACA 64_2A-015 under the conditions of wind velocity of 6.5 m/s (Re = 110000). Within the range of angle of attack of -30 deg to 30 deg, the data presented in Fig. 3 agree well with the experimental data obtained by Seki [2]. Judging from the local maximum of CL, the stall of the NACA 64_2A-015 airfoil under the condition of Re=110000 seems to take place at the angle of attack of about 12 deg.

Figure 4 is the aerodynamic characteristics of FX 63-137 under the condition of 6.1 m/s (Re=101000). Both the clockwise measurements and counterclockwise measurements are presented in this figure because the

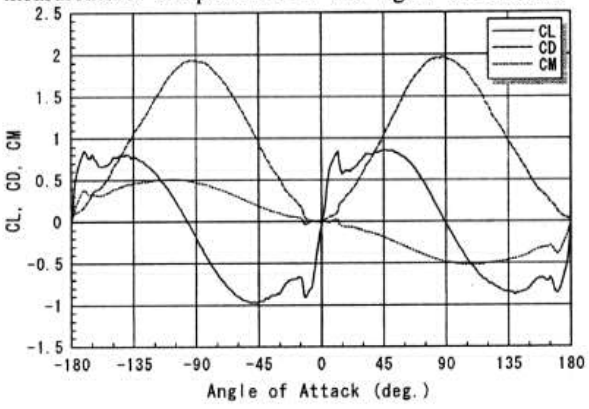

Figure3. Aerodynamic characteristics of NACA 64_2A-015 (Re=110000)

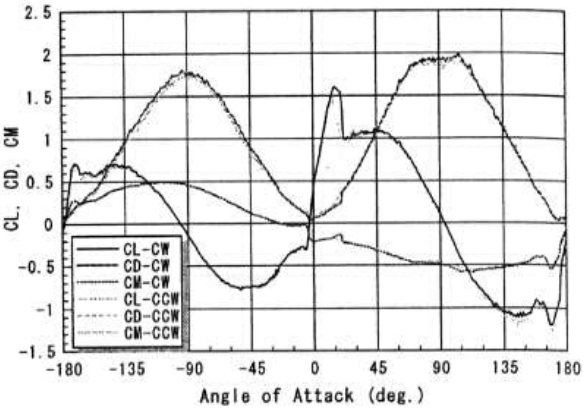

Figure 4. Aerodynamic characteristics of FX 63-137 (Re=101000)

hysteresis was observed around the stall angle. Note that obvious hysteresis has not been observed in the cases of quasi-static measurements of NACA 64_2A-015. Lift coefficient of FX 63-137 takes the local maximum at 15.5 deg in the clockwise measurement (process of the increase in angle of attack) and at 14.0 deg in the counterclockwise measurement (process of the decrease) in Fig.4.

3.2 Aerodynamic characteristics in pitching motion

Aerodynamic characteristics of the two airfoils in the pitching motion between 4 deg and 20 deg have been measured at a constant wind speed of about 9 m/s. The cycle of the pitching motion was set at 6 s (low speed), 4.5 s (medium speed), and 3 s (high speed). The variation in lift-to-drag ratio of the NACA 64_2A-015 airfoil is shown in Fig. 5, and that of the FX 63-137 airfoil in Fig. 6. The graphs shown in those figures are the ensemble averages of 50 times of the measurement data for each process of the increase in angle of attack and the decrease. The dotted lines presented in Fig. 5 and Fig. 6 are the lift-to-drag ratio measured in the static state. Although the symmetrical airfoil does not show clear

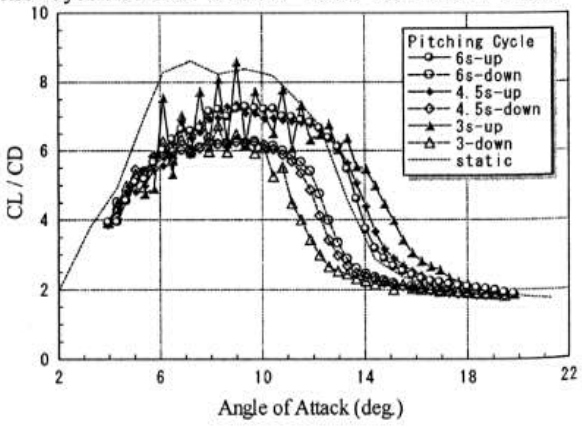

Figure 5. Lift-to-drag ratio of NACA 64_2A-015 airfoil in the pitching motion

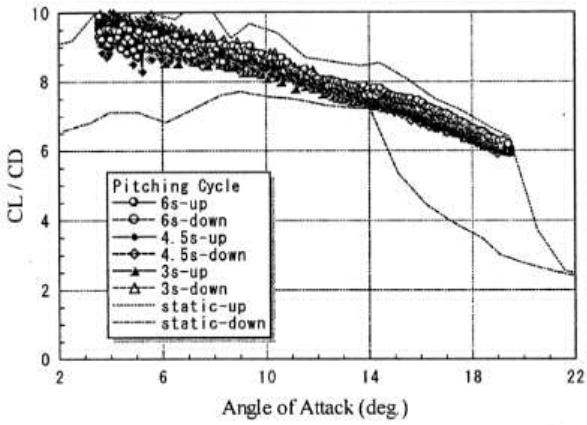

Figure 6. Lift-to-drag ratio of FX 63-137 airfoil in the pitching motion

hysteresis in the static measurement, obvious hysteresis of lift-to-drag ratio is observed in Fig. 5 and the hysteresis becomes large as the cycle of the pitching motion becomes short. On the other hand, the lift-to-drag ratio of the asymmetrical airfoil does not show the hysteresis in pitching motion, as shown in Fig. 6. The lift-to-drag ratio has less dependency on the speed of the pitching motion. The data of the lift-to-drag ratio in the pitching motion are between the quasi-static data in the process of increasing angle of attack and the quasi-static data in the process of decreasing angle of attack.

3.3 Aerodynamic characteristics in the pitching motion and the periodically varying wind

Figure 7 illustrates the behaviors in one cycle of lift-to-drag ratio of NACA 64_2A-015 and FX 63-137 when they are in the pitching motion and in the periodically varying wind of the range between 6 m/s and 12 m/s with the same cycle of 3.1 s. The phase difference between the angle of attack and the wind speed is 180 deg in Fig. 7.

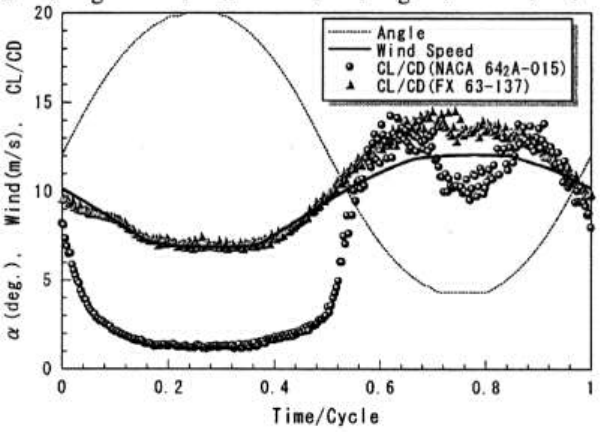

Figure 7. Lift-to-drag ratio of NACA 64_2A-015 and FX 63-137 in the periodically varying wind and the pitching motion (Cycle = 3.1sec, phase difference = 180 deg.)

Measurements were performed under the conditions of the phase differences of 0 deg, 90 deg, 180 deg, and 270 deg, respectively, in the cases of two different cycles (6.1 s and 3.1 s). The data of the lift-to-drag ratio are the ensemble averages of fifty cycles. The horizontal axis of the Fig. 7 is the time divided by the cycle of the periodically varying wind. In the portion where the angle of attack takes the smallest value, the lift-to-drag ratio of NACA 64_2A-015 tends to make a small dip and that of FX 63-137 has tendency to fluctuate. These phenomena were observed similarly in the cases of the other phase differences. The behavior of the lift-to-drag ratio changes more or less according to the cycle and the phase difference.

Figures 8 and 9 show the behaviors of the lift-to-drag ratio of NACA 64_2A-015 in the cases of the cycle of 6.1 s and 3.1 s, respectively. However, the horizontal axes of these figures are the angle of attack. Only two cases of the phase differences (0 deg and 180 deg) are presented in each figure in order to make it explicit illustration. The solid lines in Fig. 8 and Fig. 9 are the lift-to-drag ratio in the pitching motion in a constant wind speed of about 9 m/s. Figures 10 and 11 show the lift-to-drag ratio of FX 63-137 corresponding to Fig. 8 and Fig. 9. These figures (Fig. 8 - Fig. 11) make it clear that the behavior of the lift-to-drag ratio depends on the phase difference between the pitching motion and the periodically varying wind. Although there are a few exceptions, the lift-to-drag ratio when both pitching motion and periodically varying wind are performed simultaneously becomes larger at the small angle of attack (i.e. before static stall angle) than the value in pitching motion or in the static measurement. Lift-to-drag ratios in the cases of phase differences of 90 deg and 270 deg gave the higher values than the largest curve shown in Fig. 10 or Fig. 11, although the data are not presented in those figures. The increase in lift-to-drag ratio at the small angle of attack is large when the cycle is short. The variations in relative velocity and angle of attack which a blade of VAWT undergoes during the rotation are different from the variations given in the present

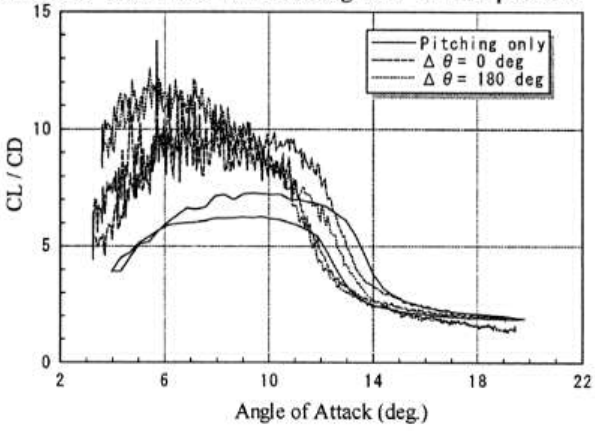

Figure8. Effects of the periodically varying wind on lift-to-drag ratio of NACA 64_2A-015 airfoil in the pitching motion with the cycle of 6.1 s

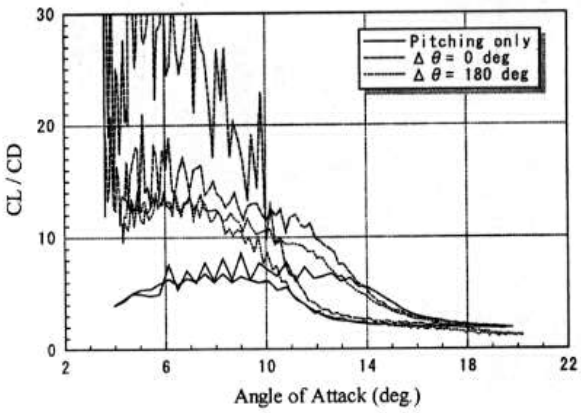

Figure 9. Effects of the periodically varying wind on lift-to-drag ratio of NACA 64_2A-015 airfoil in the pitching motion with the cycle of 3.1 s

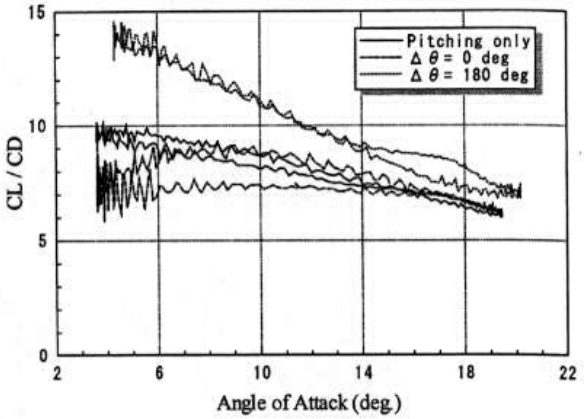

Figure11. Effects of the periodically varying wind on lift-to-drag ratio of FX 63-137 airfoil in the pitching motion with the cycle of 3.1 s

experiments. However, since the performance of VAWT depends directly on the lift-to-drag ratio of the blade; the above results suggest that the variation of the relative velocity could give additional effects on the performance of VAWT.

4. Conclusions

As for asymmetrical FX 63-137 airfoil, although the hysteresis was observed in quasi-static measurement of the aerodynamic forces, large hysteresis of the lift-to-drag ratio was not observed during a pitching motion at a constant wind speed. We observed that, when the pitching motion of the asymmetrical airfoil was carried out in the periodically varying wind, the tendency for the lift-to-drag ratio is to increase more than the value of static measurement at the small angle of attack. This phenomenon is similar to the cases of symmetrical NACA 64_2A-015 airfoil and the increase in lift-to-drag ratio is large when the cycle is short.

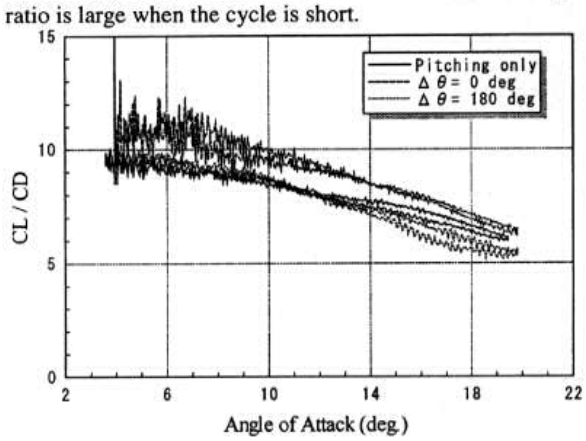

Figure 10. Effects of the periodically varying wind on lift-to-drag ratio of FX 63-137 airfoil in the pitching motion with the cycle of 6.1 s

Acknowledgement

This study was carried out as a part of the 21st century COE program "Arid-Land Science Program." The authors express the gratitude.

References

[1] Hara, Y., Kang, I., Moriya, T., Ariyasu, K., & Hayashi, T., *Proceedings of the Sixth KSME-JSME Thermal and Fluids Engineering Conference, Jeju, KOREA*, CD-ROM, JE.08, 2005.

[2] Seki, K., *Transactions of Japanese Society of Mechanical Engineering B*, (in Japanese), **57**, 1297, 1991.

Wind Tunnel Tests on a Different Phase Three-Stage Savonius Rotor*

Tsutomu HAYASHI**, Yan LI*** and Yutaka HARA****

In order to decrease the torque variation of a Savonius rotor and improve the starting characteristics, a new type of Savonius rotor, which has three stages with 120-degree bucket phase shift between the adjacent stages, has been designed and made. Wind tunnel tests make it clear that both the static and dynamic torque variations in one revolution of this three-stage rotor have been greatly smoothed in comparison with an ordinary one-stage rotor, which means the improvement of the starting characteristics. The torque characteristics of the rotors with guide vanes were also measured. The guide vanes increased the torque coefficient on the average in the low tip speed ratio but decreased the torque coefficient in high tip speed ratio. Although the present three-stage rotor needs improvement of the aspect ratio of each stage, the three-stage rotor with no guide vane had better torque characteristics than the one-stage rotor with guide vanes for tip speed ratio larger than 0.8.

Key Words: Wind Tunnel Test, Savonius Rotor, Wind Turbine, Different Phase, Torque Measurement

1. Introduction

The Savonius rotor conceived by the Finnish Engineer S.J. Savonius[1] in 1931 is a kind of drag type vertical-axis wind turbine. A basic configuration of this rotor has a "S-shaped" cross-section constructed by two semicircular buckets with a small overlap between them. And the principle of operation is based on the difference of drag between the convex and the concave parts of the buckets.

The Savonius rotor did not become popular for the purpose of electric power generation because of the low power efficiency in comparison with the lift type wind turbines. However, with the advantages of simple design and low construction cost, it is mainly used for water pumping and wind power on a small scale. By utilizing the large starting torque, the Savonius rotor may find another use as a starter for the other type of wind turbines that have worse starting characteristic, such as Darrieus rotor, Gyro mill, etc.

However, the torque characteristics of the Savonius rotor have two problems: the first one is the fairly large torque variation, which causes rotor's vibration and consequently decreases the rotor's durability. The second problem is that there are some angular positions where the static torque is negative or very small. This fact is an obstacle for the Savonius rotor when it is used as a starter. Therefore, many researchers have focused on improving the starting characteristics of Savonius rotor. Shedahl conducted some wind tunnel tests on a three-bucket rotor[2]. Khan stacked an ordinary Savonius rotor on another rotor with 90-degree phase shift[3]. For both the three-bucket rotor and the two-stage rotor, the negative starting torque range was decreased and the torque variation became slightly smaller than the ordinary rotor. However, those torque variations were still large for the purpose of a starter device. A Savonius rotor with twisted blades[4] had been proposed and it has good starting characteristics, but the cost becomes high due to the blade shape complexity. Some researchers focused on using auxiliary devices to improve the starting characteristic of the Savonius rotor: Sivasegaram used an asymmetrical box with a funnel-shaped wind inlet[5]; Alexander used a flat shield and a circular shield[6]; Several static guide vanes and a flow deflecting plate were tried by Ogawa[7],[8].

In this study, a new type of Savonius rotor is pro-

* Received 2nd August, 2004 (No. 04-4183)

** Department of Applied Mathematics and Physics, Faculty of Engineering, Tottori University, 4–101 Koyama-cho Minami, Tottori 680–8552, Japan.
E-mail: hayashi@damp.tottori-u.ac.jp

*** Graduate school of Engineering, Tottori University.
E-mail: lee@svr01.damp.tottori-u.ac.jp

**** Department of Applied Mathematics and Physics, Faculty of Engineering, Tottori University.
E-mail: hara@damp.tottori-u.ac.jp

posed and it has been tested with the wind tunnel. The new type rotor has three stages with 120-degree bucket phase shift between the adjacent stages. Stacking ordinary two-bucket type rotors with different phases is expected to give the torque averaging and the cost reduction. According to the authors' knowledge, there are no reports on measurements about the torque variation in one revolution of such a different phase three-stage Savonius rotor, which is called "three-stage rotor" simply hereafter. A number of wind tunnel tests were carried out with both the three-stage rotor and an ordinary one-stage rotor, and the results were compared. The tests included the fluctuation measurements of the static and dynamic torques in one revolution, and the average torque measurements at different rotational speeds. The torque characteristics of the rotors with guide vanes were also measured, because it has been known that the starting characteristic of Savonius rotor can be improved by installing guide vanes around the rotor[7]. Additionally, the guide vanes can be helpful as parts of frame having the safeguard function. The guide vane used in this study is very short in comparison with the rotor diameter. The arrangement of the guide vanes against wind was changed in order to investigate the effect of wind direction and number of guide vanes.

2. Nomenclature

d : Bucket diameter [m]
D : Rotor diameter [m]
H : Rotor height [m]
h : Height of each stage of the three-stage rotor [m]
S : Rotor overlap [m]
B : Width of guide vane
A_S : Rotor swept area [m^2]; $A_S = D \cdot H$
A_T : Wind tunnel outlet area [m^2]
β : Blockage ratio; $\beta = \dfrac{A_S}{A_T}$
OL : Rotor overlap ratio; $OL = \dfrac{S}{D}$
AR : Aspect ratio of the rotor; $AR = \dfrac{H}{d}$
AR_b : Aspect ratio of each stage of the three-stage rotor; $AR_b = \dfrac{h}{d}$
U : Wind velocity [m/s]
ρ : Density of air [kg/m^3]
ν : Kinematic viscosity [m^2/s]
Re : Reynolds number; $Re = \dfrac{UD}{\nu}$
n : Rotor revolution [rpm]
ω : Rotor angular speed [rad/s]
α : Bucket rotation angle [degree]
λ : Tip speed ratio; $\lambda = \dfrac{\omega D}{2U}$
T : Torque [N·m]
T_S : Static torque [N·m]
P : Power [W]

C_t : Torque coefficient; $Ct = \dfrac{T}{\frac{1}{4}\rho A_S D U^2}$

C_{ts} : Static torque coefficient; $Cts = \dfrac{T_S}{\frac{1}{4}\rho A_S D U^2}$

C_p : Power coefficient; $Cp = \dfrac{P}{\frac{1}{2}\rho A_S U^3}$

3. Experimental Detail

3.1 Test rotors

Figure 1 and Table 1 show the geometry and main sizes of the three-stage rotor and a one-stage rotor with guide vanes. The tests were carried out in an open-circuit type wind tunnel with an outlet section of 1.5×1.5 m^2, which generates wind speed up to 25 m/s. The previous studies[2),(6)] showed that large blockage ratio affected the rotor performance. The rotors used in this study have relatively small swept area of $A_S = 0.076$ m^2, which give the wind tunnel blockage ratio of 3.5%. According to Ushiyama, a rotor with large aspect ratio gets better power efficiency[9]. However, considering the importance of small blockage ratio and convenience of measurement, aspect ratio $AR = 1.25$ was selected for both types of the test rotors. Therefore, the aspect ratio for each stage of the

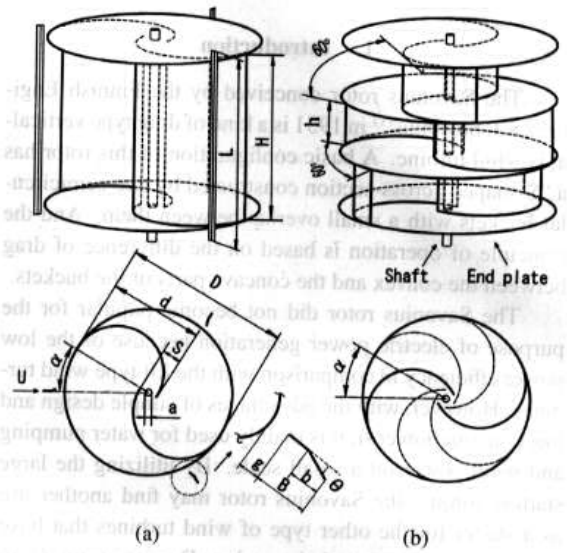

Fig. 1 Geometry of the test rotors and guide vanes: (a) the one-stage rotor with three guide vanes, (b) the three-stage rotor with no guide vane

Table 1 Main sizes of the test rotors and a guide vane

Rotor		Guide vane	
D	0.33m	B	0.025m
d	0.184m	b	0.015m
H	0.23m	L	0.29m
h	0.074m	g	0.01m
a	0.015m	θ	15°

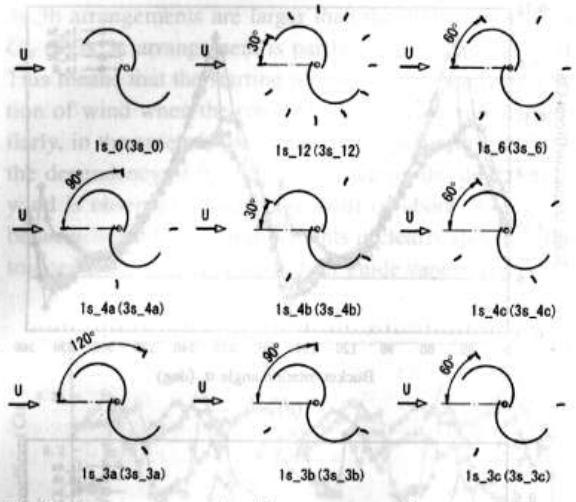

Fig. 2 Arrangements of guide vanes around the one-stage rotor and their symbols. The symbols in the parentheses correspond to the three-stage rotor's arrangements.

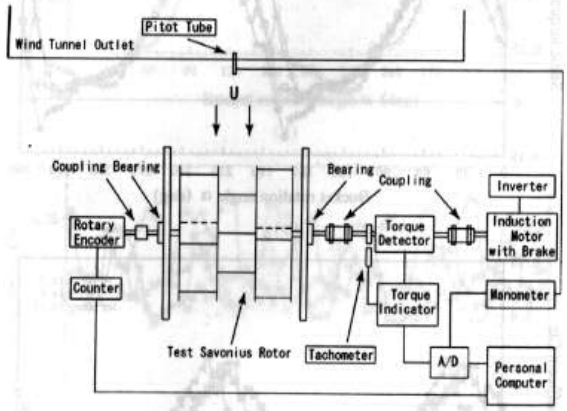

Fig. 3 Schematic diagram of the experimental system

three-stage rotor is $AR_b = 0.4$. The overlap ratio of the test rotors was decided as $OL = 0.2$ according to the other researchers' studies, in which the proper overlap ratios were found between 0.15 and 0.25[2),(9)]. The guide vanes have the length of 0.29 m and the width of 0.025 m, and they are bent near the center of the width as shown in Fig. 1 (a). The number of guide vanes tested in this study is 3, 4, 6, and 12. In the case of three and four guide vanes, three different arrangements of guide vanes were tested. The guide vane arrangements and the symbols are shown in Fig. 2. For example, the symbol of "1s_3b" represents the arrangement "b" having three guide vanes of the one-stage rotor and the symbol of "3s_4a" represents the arrangement "a" having four guide vanes of the three-stage rotor.

3.2 Experimental methodology

Figure 3 shows the schematic diagram of the experimental system. A test rotor was placed at the same height as the center of the wind tunnel outlet and 2 m (6D) downstream from the outlet. The rotor torque was measured by a digital torque detector (ONO SOKKI, SS-005), which was located between the rotor and an induction motor equipped with a brake (MITSUBISHI ELECTRIC, ZKB-2.5HBN). The sampling time of the data acquisition is 1 ms. The revolution of the induction motor was controlled by an inverter, and was measured by a digital tachometer. A rotary encoder (ONO SOKKI, RP-432Z) was used to measure the rotation angle of the rotor shaft. The wind speed was measured by a Pitot tube. The photos of two test rotors are shown in Fig. 4.

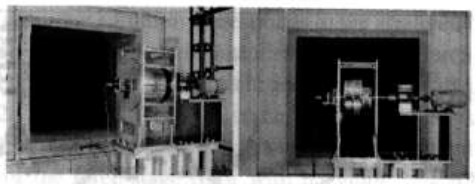

(a) (b)

Fig. 4 Photos of the test rotors: (a) the one-stage rotor with guide vanes, (b) the three-stage rotor with no guide vane

When the static characteristics were measured, the rotor shaft was fixed by the brake of induction motor. The static torque was measured at the interval of about 5 degrees of bucket rotation angle and was averaged for ten seconds under a steady wind speed. Wind speeds for the static measurements of the rotors with no guide vane were 6, 9 and 12 m/s, which correspond to the Reynolds numbers of 1.4×10^5, 2.1×10^5, and 2.8×10^5, respectively. The measurements for the rotors with guide vanes were conducted only under the condition of 12 m/s.

In the dynamic torque measurements, a rotor was operated with a constant revolution speed under a steady wind speed (U = 6,9,12,15 and 18 m/s). The dynamic torque was measured for ten seconds and was averaged. The whole dynamic torque characteristics were obtained by changing the conditions of rotational speed and wind speed. The dynamic torque variation in one revolution was obtained by the measurement of torque and rotation angle using the sampling time of 0.5 ms and the data was ensemble-averaged for about 100 revolutions.

4. Results and Discussions

4.1 Static torque characteristics

Figure 5 shows the averaged static torque variations in one revolution of each type of the rotors with no guide vane under different wind speeds. It is found that the wind speed, that is, the Reynolds number Re, has little effect on the static torque coefficients C_{ts} for both types of the rotors. Therefore, the other measurements were carried out only under the condition of wind speed of 12 m/s. The coefficient C_{ts} of the one-stage rotor has a cycle of 180 degrees and the variation of C_{ts} is very large. Note that the value of C_{ts} becomes negative in the ranges of the angle $\alpha = 140°–170°$ and 320°–350°. The maximum

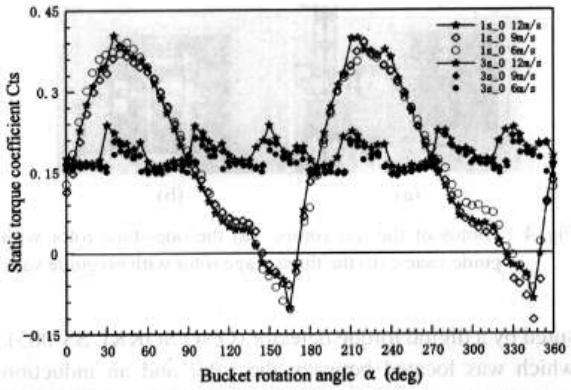

Fig. 5 Static torque coefficients of the rotors with no guide vane under the conditions of $U = 6, 9, 12$ m/s

values of the C_{ts} appear near the rotational angles of 40° and 210°. It also should be noted that there are two small bumps in the C_{ts} variations at the angles around 135° and 315°. The bumps are attributed to the overlap[7]. On the other hand, the coefficient C_{ts} of the three-stage rotor has a cycle of 60 degrees, which corresponds to the number of the buckets. The peak-to-peak value of the static torque coefficient becomes small to the extent of about 1/6 of that of the one-stage rotor. In the other words, the static torque of the three-stage rotor is averaged and kept almost constant. Additionally, a bump is observed in each cycle of the C_{ts} in addition to a main peak of torque. The bump may be attributed to the overlap of each stage of the three-stage rotor by the similarity to the one-stage rotor.

Figure 6 (a)–(c) show the C_{ts} of the one-stage rotor with guide vanes at a wind speed of 12 m/s. The result of the one-stage rotor with no guide vane (1s_0) is also shown in each plot as the reference. In the case of three guide vanes, as shown in Fig. 6 (a), the torque characteristics of 1s_3a and 1s_3c arrangements are similar. Those C_{ts} becomes larger than that of the case of 1s_0, especially in the ranges of $\alpha = 30°$–$60°$ and $\alpha = 210°$–$240°$. In addition to that, the ranges ($\alpha = 150°$–$165°$ and $\alpha = 330°$–$345°$) in which the C_{ts} takes negative value become smaller than the ranges of 1s_0 ($\alpha = 140°$–$170°$ and $\alpha = 320°$–$350°$). On the other hand, the C_{ts} of 1s_3b arrangement has the maximum torque coefficient of the same level as 1s_0 but does not take negative value at any rotational angle. Consequently, the range of fluctuation in torque of 1s_3b becomes smaller than that of 1s_0. Figure 6 (b) shows the C_{ts} of 1s_4a, 4b, and 4c arrangements. The C_{ts} of all arrangements with four guide vanes does not take negative value at any rotational angle. The maximum values of C_{ts} in all arrangements are larger than 1s_0. Therefore, the starting characteristic of the rotor with four guide vanes is better than the rotor with three guide vanes. The static torque variations in the cases of six and twelve guide vanes are shown in Fig. 6 (c). It is clear that the range of fluctuation in torque becomes smaller with increase of the number of

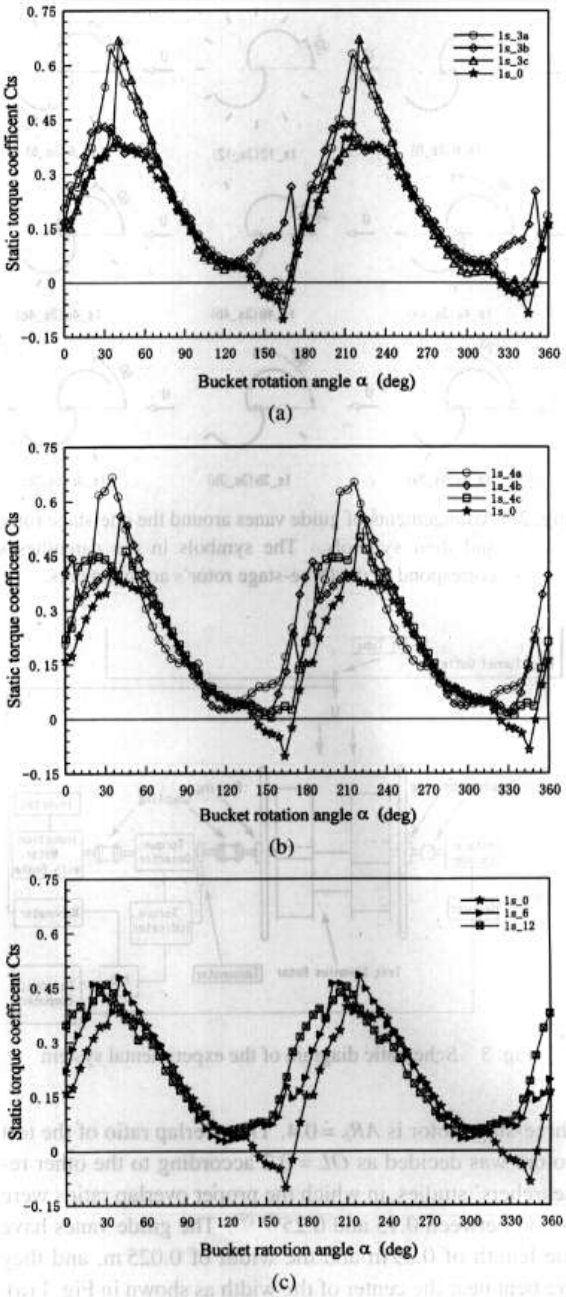

Fig. 6 Static torque coefficients of the one-stage rotor (U = 12 m/s): (a) with 3 guide vanes, (b) with 4 guide vanes, (c) with 6 and 12 guide vanes

guide vanes.

Figure 7 (a), (b) and Fig. 8 (a)–(c) show the static torque coefficients C_{ts} of the three-stage rotors with the same guide vane arrangements as the one-stage rotor under the condition of 12 m/s. In the case of three guide vanes shown in Fig. 7 (a), the cycle of 60 degrees in static torque variation, together with a little of periodicity of 180 degrees, is recognized to the same extent as the case of no guide vane (3s_0). However, the C_{ts} of 3s_3a and

3s_3b arrangements are larger than the 3s_0 case and the C_{ts} of 3s_3c arrangement is partly smaller than the 3s_0. This means that the starting torque depends on the direction of wind when the rotor has three guide vanes. Similarly, in the case of four guide vanes shown in Fig. 7 (b), the dependency of the starting torque on the direction of wind is observed. And phase shift of about 30 degrees between the different arrangements is clearly shown in the torque variation of the case of four guide vanes. The phase shift of torque variation corresponds to the arrangement of guide vanes, which were installed with the difference of 30-degree between the different arrangements as shown in Fig. 2. In Fig. 8 (a)–(c), the static torque coefficients of 6 and 12 guide vane cases are shown as compared with the case of the three-stage rotor with no guide vane. From these figures, it is obvious that installing a lot of guide vanes around the three-stage rotor makes the range of fluctuation of static torque smaller and increases the averaged

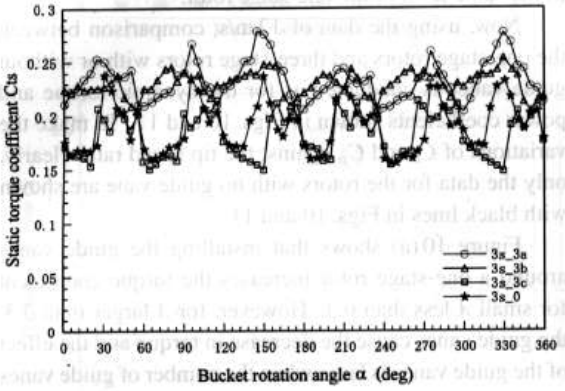

(a)

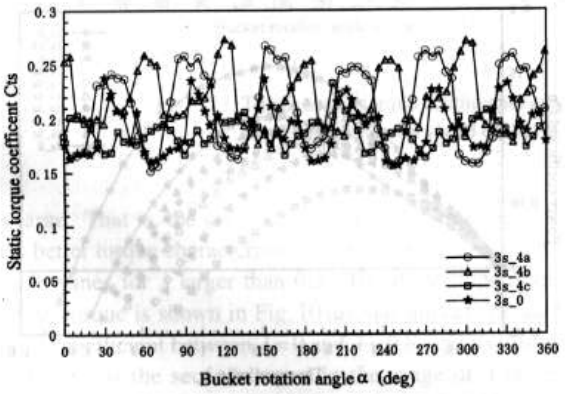

(b)

Fig. 7 Static torque coefficients of the three-stage rotor (U = 12 m/s): (a) with 3 guide vanes, (b) with 4 guide vanes

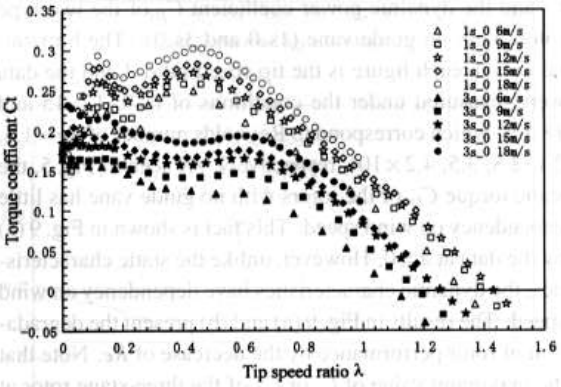

(a)

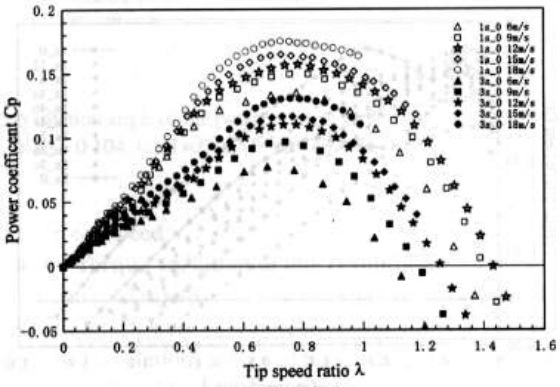

(b)

Fig. 9 The characteristics of the test rotors with no guide vane under the condition of U = 6, 9, 12, 15 and 18 m/s: (a) torque coefficient, (b) power coefficient

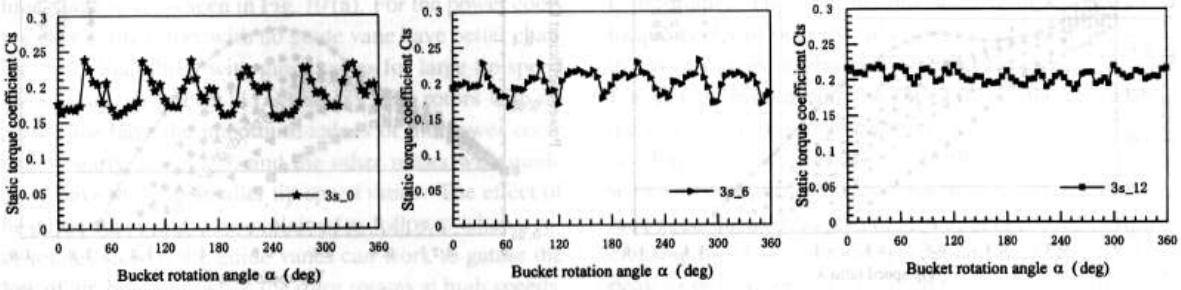

(a) (b) (c)

Fig. 8 Static torque coefficients of the three-stage rotor (U = 12 m/s): (a) with no guide vanes, (b) with 6 guide vanes, (c) with 12 guide vanes

value of torque coefficient. In other words, more guide vanes make the starting characteristics of the three-stage rotor better. By the way, in the case of 3s_12 arrangement, the existence of twelve torque peaks is recognized during one revolution, as seen in Fig. 8 (c). However, it is not clear to what these peaks are attributed. The cause may be the twelve guide vanes or the effect of overlap or the signal noise produced from the torque detector.

4.2 Dynamic torque and power coefficients

Figure 9 (a) and (b) are the dynamic torque coefficient C_t and the dynamic power coefficient C_p of the two type rotors with no guide vane (1s_0 and 3s_0). The horizontal axis in each figure is the tip speed ratio λ and the data were measured under the conditions of 6, 9, 12, 15 and 18 m/s, which correspond to Reynolds number of $Re = 1.4$, 2.1, 2.8, 3.5, 4.2×10^5, respectively. As seen in Fig. 5, the static torque C_{ts} of the rotors with no guide vane has little dependency on wind speed. This fact is shown in Fig. 9 (a) by the data at $\lambda = 0$. However, unlike the static characteristics, the dynamic characteristics have dependency on wind speed. The results in Fig. 9 (a) and (b) present the degradation of rotor performance by the decrease of Re. Note that the maximum value of C_t or C_p of the three-stage rotor at each wind speed is about 75% of that of the one-stage rotor. The much inferiority of the three-stage rotor is caused by small aspect ratio of each stage as described before. In other words, the distance between end plates of each stage becomes too close, which makes the performance of the three-stage rotor worse. As shown in the other studies, the difference of power coefficients between the rotors with three-time difference of aspect ratio is about 20–30%[9]. If the aspect ratio of each stage of the three-stage rotor is enlarged, the performance can be expected to increase up to the same level of the one-stage rotor.

Now, using the data of 12 m/s, comparison between the one-stage rotors and three-stage rotors with or without guide vanes is conducted as for the dynamic torque and power coefficients shown in Figs. 10 and 11. To make the variations of C_t and C_p against the tip speed ratio clearly, only the data for the rotors with no guide vane are shown with black lines in Figs. 10 and 11.

Figure 10 (a) shows that installing the guide vanes around a one-stage rotor increases the torque coefficient for small λ less than 0.3. However, for λ larger than 0.3, the guide vanes cause the decrease in torque and the effect of the guide vanes is large when the number of guide vanes

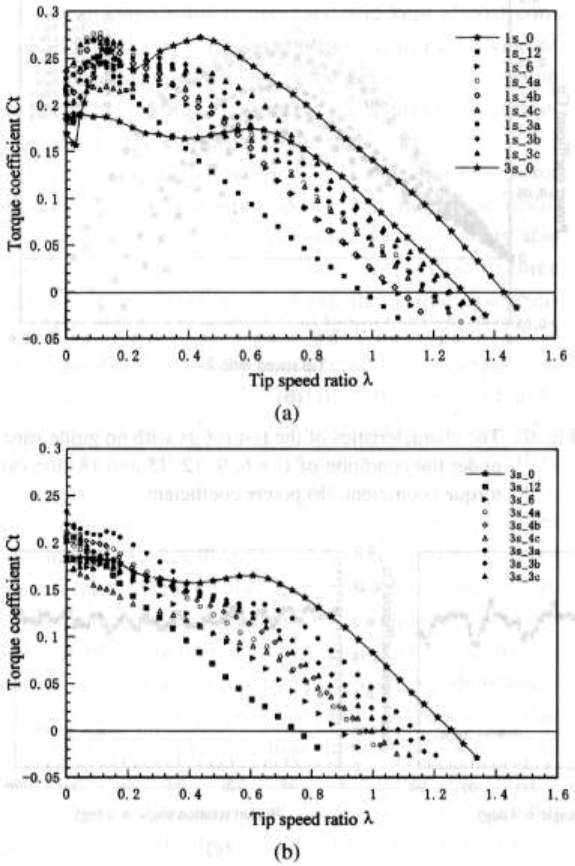

Fig. 10 Torque coefficients of the test rotors with guide vanes ($U = 12$ m/s): (a) the one-stage rotors, (b) the three-stage rotors

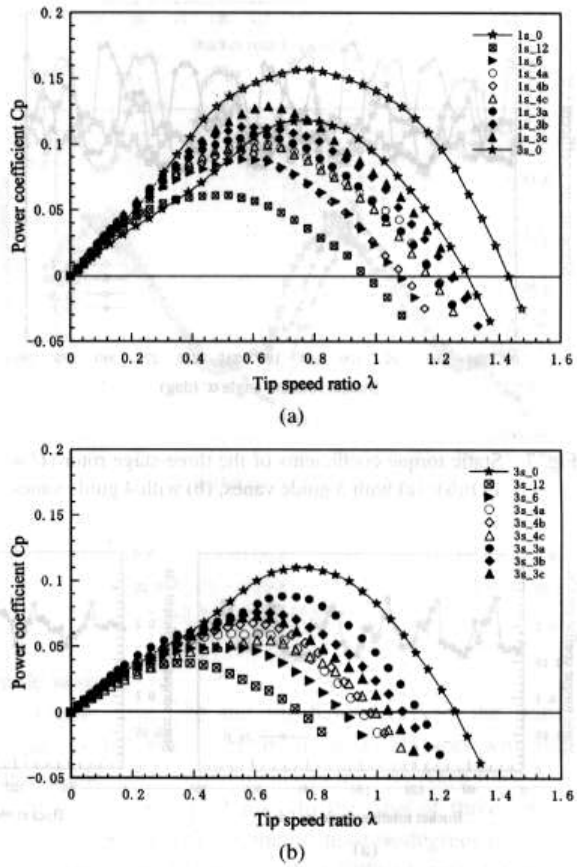

Fig. 11 Power coefficients of the test rotors with guide vanes ($U = 12$ m/s): (a) the one-stage rotors, (b) the three-stages rotors

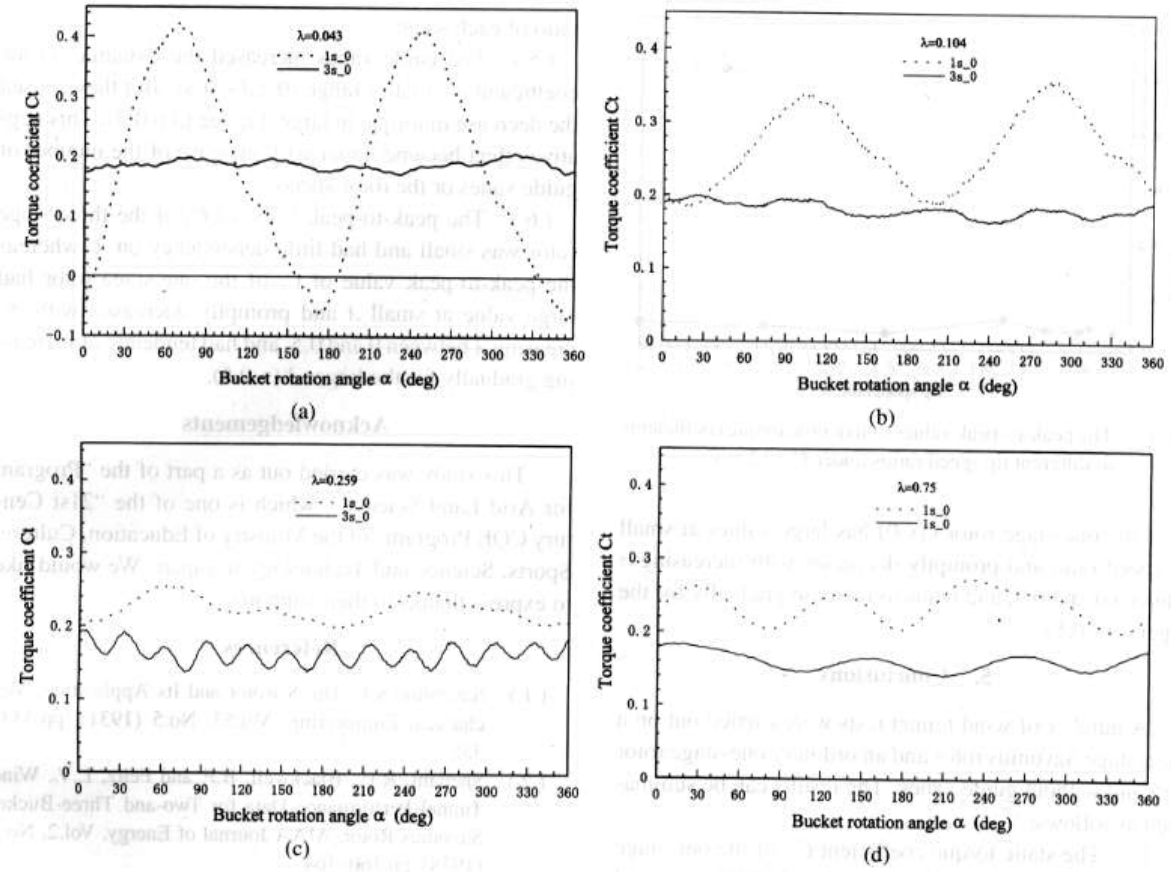

Fig. 12 The dynamic torque coefficient against bucket rotation angle of the two test rotors under $U = 12$ m/s at the tip speed of (a) $\lambda = 0.043$, (b) $\lambda = 0.104$, (c) $\lambda = 0.025\,9$, (d) $\lambda = 0.75$

is large. That is, the one -stage rotor with no guide vane has better torque characteristics than the other rotors with guide vanes for λ larger than 0.3. The three-stage rotor, whose torque is shown in Fig. 10 (a), has almost constant torque coefficient between $\lambda = 0$ and $\lambda = 0.8$, and its torque coefficient is the second largest in the range of λ larger than 0.8. The torque coefficient of the three-stage rotor with no guide vane is again shown in Fig. 10 (b) together with the cases of the three-stage rotor with guide vanes. This figure shows the same effect of the guide vane for the three-stage rotor as seen in Fig. 10 (a). For the power coefficients C_p, the rotors with no guide vane have better characteristics than those with guide vanes for large tip speed ratios as shown in Fig. 11 (a) and (b). The rotors with no guide vane have the maximum values of the power coefficient nearly at $\lambda = 0.8$, and the other rotors with guide vanes have those at smaller tip speed ratios. The effect of the guide vanes might be explained as follows: when a rotor rotates slowly, the guide vanes can work to gather the flow of air, however, when the rotor rotates at high speeds, the guide vanes, especially those installed downwind, become obstacles against the flow of air. This negative effect becomes larger with increase of the number of guide vanes or the rotor speed.

4.3 Torque variation in one revolution

Figure 12 (a)–(d) show the dynamic torque coefficients C_t which were ensemble-averaged with the data for about 100 revolutions at typical tip speed ratios ($\lambda = 0.043$, 0.104, 0.259 and 0.75). The wind speed for the experiments is 12 m/s and the origin of the bucket rotation angle α is upwind direction. The behavior of dynamic torque for $\lambda = 0.043$ is almost the same as the static torque behavior shown in Fig. 5, although the amplitude of the variation of C_t is smaller. The C_t of the one-stage rotor has two main torque peaks in one revolution and it has negative value in two α ranges, in the case of small tip speed ratio (see Fig. 12 (a)), even during the rotation. On the other hand, the C_t of the three-stage rotor has six torque peaks in one revolution, which corresponds to the number of buckets with different phases, in the case of small tip speed ratio. However, the number of the torque peaks varies with increasing the tip speed ratio, as seen in Fig. 12 (b)–(d). The peak-to-peak value of C_t for each rotor with no guide vane is shown as a function of λ in Fig. 13. The peak-to-peak value of C_t of the three-stage rotor (3s_0) is small and has little dependency on λ, whereas the peak-to-peak value of

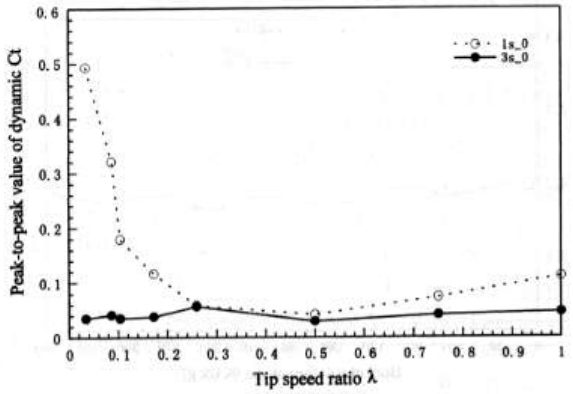

Fig. 13 The peak-to-peak values of dynamic torque coefficients at different tip speed ratios under $U = 12$ m/s

C_t of the one-stage rotor (1s_0) has large values at small tip speed ratio and promptly decreases with increasing λ between 0 and 0.5, and tends to increase gradually for the larger λ (>0.5).

5. Conclusions

A number of wind tunnel tests were carried out on a three-stage Savonius rotor and an ordinary one-stage rotor with and without guide vanes. The results can be summarized as follows:

(1) The static torque coefficient C_{ts} of the one-stage rotor with no guide vane had a cycle of 180 degrees and its variation was very large. In the ranges of the rotational angle $\alpha = 140°–170°$ and $320°–350°$, the C_{ts} took negative value. Two small bumps attributed to the overlap were observed in the C_{ts} variation at the angles around 135° and 315°.

(2) The static torque coefficient C_{ts} of the three-stage rotor with no guide vane had a cycle of 60 degrees, which corresponded to the number of the buckets. The variation of the C_{ts} became very small to the extent of about 1/6 of the one-stage rotor. The bumps attributed to the overlap were observed in each cycle of the static torque coefficient of the three-stage rotor.

(3) The guide vanes increased the static torque coefficient on the average and decreased its fluctuation when increasing the number of them. Different arrangement of the guide vanes gave the different variation of the static torque coefficient, which means the dependency of the starting torque on the direction of wind.

(4) Unlike the static characteristics, the dynamic characteristics had dependency on wind speed. At each wind speed, the maximum values of C_t and C_p of the three-stage rotor were much smaller than those of the one-stage rotor. However, this inferiority of the three-stage rotor could be expected to dissolve by enlarging the aspect ratio of each stage.

(5) The guide vanes increased the dynamic torque coefficient in small λ range ($0 < \lambda < 0.3$). But they caused the decrease in torque in large λ range ($\lambda > 0.3$). This negative effect became larger with increase of the number of guide vanes or the rotor speed.

(6) The peak-to-peak value of C_t of the three-stage rotor was small and had little dependency on λ, whereas the peak-to-peak value of C_t of the one-stage rotor had large value at small λ and promptly decreased with increasing λ between 0 and 0.5, and had tendency of increasing gradually for the larger λ (>0.5).

Acknowledgements

This study was carried out as a part of the "Program for Arid Land Science", which is one of the "21st Century COE Program" of the Ministry of Education, Culture, Sports, Science and Technology in Japan. We would like to express thanks to their supports.

References

(1) Savonius, S.J., The S-Rotor and Its Application, Mechanical Engineering, Vol.53, No.5 (1931), pp.333–338.

(2) Shedahl, R.E., Blackwell, B.F. and Feltz, L.V., Wind Tunnel Performance Data for Two-and Three-Bucket Savonius Rotor, AIAA Journal of Energy, Vol.2, No.3 (1978), pp.160–164.

(3) Khan, M.H., Model and Prototype Performance Characteristics of Savonius Rotor Windmill, Wind Engineering, Vol.2, No.2 (1978), pp.75–85.

(4) Grinspan, A.S., Suresh Kumar, P., Saha, U.K. and Mahanta, P., Performance of Savonious wind Turbine Rotor with Twisted Bamboo Blades, Proceedings of 19th Canadian Congress of Applied Mechanics, Calgary, Alberta, Canada, Vol.2 (2003), pp.412–413.

(5) Sivasegaram, S., Design Parameters Affecting the Performance of Resistance-Type Vertical-Shaft Wind Rotors-An Experimental Investigation, Wind Engineering, Vol.1, No.3 (1977), pp.207–217.

(6) Alexander, A.J. and Holownia, B.P., Wind Tunnel Tests on a Savonius Rotor, Journal of Industrial Aerodynamics, Vol.3 (1978), pp.343–351.

(7) Ogawa, T., Tahara, K. and Suzuki, N., Wind Tunnel Performance Data of the Savonius Rotor with Circular Guide Vanes, Bulletin of JSME, (in Japanese) Vol.29, No.253 (1986), pp.2109–2114.

(8) Ogawa, T. and Yoshida, H., The Effects of a Deflecting Plate and Rotor End Plates on Performances of Savonius-Type Wind Turbine, Bulletin of JSME, (in Japanese) Vol.29, No.253 (1986), pp.2115–2121.

(9) Ushiyama, I., Nagai, H. and Shinoda, J., Experimentally Determining the Optimum Design Configuration for Savonius Rotors, Trans. Jpn. Soc. Mech. Eng., (in Japanese), Vol.52, No.480, B (1986), pp.2973–2982.

A Study on a Water Maker System using Peltier Devices

Tsutomu Hayashi[1], Wei Liu[2], Kengo Nojima[3], Yutaka Hara[1] & Kotaro Tagawa[4]

[1]Department of Applied Mathematics and Physics, Tottori University, Japan
[2]Post Doctoral 21 Century COE, Tottori University, Japan, liu@svr01.damp.tottori-u.ac.jp
[3]Industrial Research Institute of Tottori Prefecture, Japan
[4]Faculty of Regional Sciences, Tottori University, Japan

Keywords: Water maker system, Peltier devices, Arid regions, Coefficient of performance

Abstract: *This research aims to develop a water maker system, which condenses water vapor in the atmosphere, for irrigation water and drinking water in the arid regions. In this study, the water maker system using the Peltier device as a freezer function only by direct-current source was made. The experiment was conducted in the following environmental conditions: 20 ℃ (40, 60, 80% RH) and 30 ℃ (40, 50, 60% RH), which could be controlled in the laboratory. In each environment, the effect of the surface area of a heat exchanger and change of air flow rate on the water production rate was investigated. In this study, the characteristics of the water maker system were clarified.*

1. Introduction

It is necessary to obtain a stable reserve of drinking water, medical water, and irrigation water for human life in arid regions. The problem is serious in the area where rain falls little; therefore it is important to develop the permanent water maker system in place of existing groundwater. Since humidity changes with the difference in temperature between day and night, fog is generated at night in some arid regions along the seashore. It is then possible to obtain the permanent and economical water maker system if water vapor in the atmosphere is condensed efficiently.

It is important to produce refrigeration with the coefficient of performance (COP) for water maker system [1], and the compressor (COP=2-5) with large cooling capability is used for a common dehumidifier. However it is not environmentally friendly since the chlorofluocarbon is used. Moreover, social maintenance is inadequate, and periodic maintenance and quick repair are difficult in arid regions.

In this research, the water maker system with the easy structure using the Peltier device was made. It aims to develop the water maker system suitable for the arid regions. A Peltier device is a small and lightweight device, which can make a difference of temperature only via passing direct-current source. Although COP (COP=0.3-0.6) is small, not using chlorofluorocarbon and not having a movable part, it is suitable for the arid regions.

This study investigated the following: the effect of change of the surface area of a heat exchanger and the air flow on water production rate under the different temperature and humidity environment in order to clarify main characteristics of the water maker system using Peltier device.

2. Experimental details

Figure 1 shows the experimental setup. The water maker system consists of a heat exchanger (Copper), eight Peltier devices, two sets of cooling and fan units fin (ALPHA, FH10040A), and a ventilation fan (FAN-362). The size of the Peltier device used in the study is 40mm × 40mm × 4.2mm as shown in Figure 2 [2]. Three heat exchangers, 80mm, 120mm and 160mm in width b [mm], were tested in the experiment. The surface area for 160mm heat exchanger was too big to cool the air sufficiently, thus 80mm and 120mm heat exchangers were used in this study. Experiments were performed in a chamber, in which the temperature and humidity were kept at constant conditions as follows: 20 ℃ with 40, 60, 80% RH, and 30 ℃ with 40, 50, 60% RH. In this experiment, electric power was supplied to the system by a stabilized DC source. The input voltage applied to the Peltier device was set at 10V. The air flow rate was controlled by the voltage (0V, 4 -14V/piece: interval 2V) change of a ventilation fan. We measured the air temperature in three locations using thermocouple: inlet, middle, and outlet of the heat exchanger. The effect of heat exchanger size, air flow rate, and environment condition on water production rate were studied.

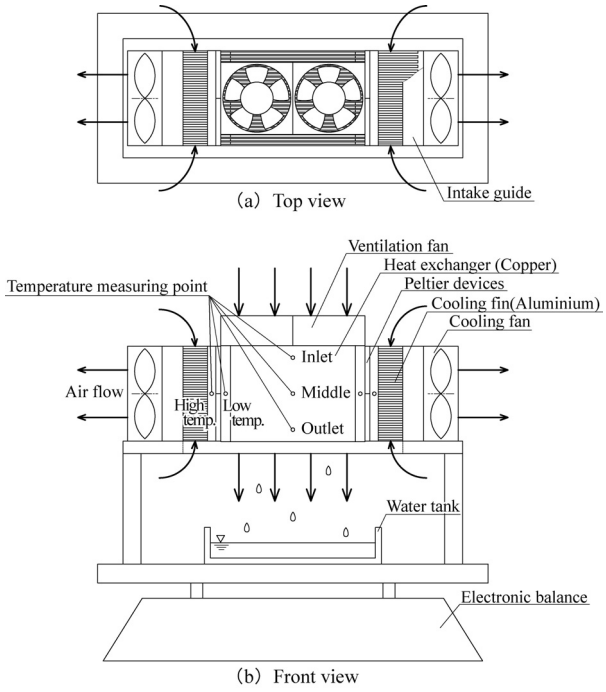

Figure 1. Schematic diagram of experimental setup

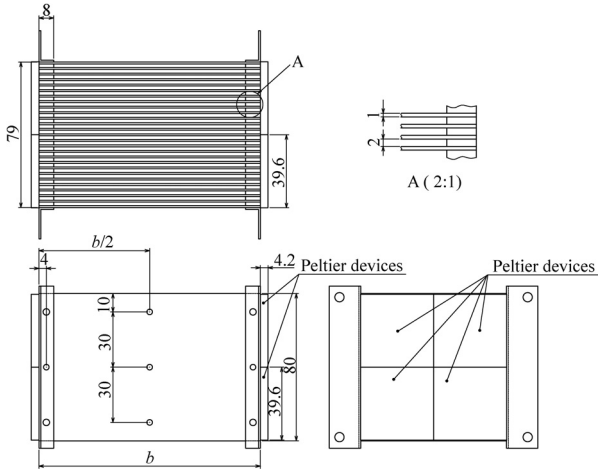

Figure 2. Dimensions of heat exchanger and Peltier devices

3. The calculation method for water production rate

Water production rate by cooling can be calculated from the performance of the refrigeration. Before describing the calculation method, the various amounts of states of moist air are explained [3], [4]. Saturation vapor pressure P_a [Pa] is given by the following approximation formulas, when temperature T [ºC] is known.

$$P_a = 6.11 \times 10^{\frac{aT}{(T+b)}} \quad (1)$$

On the water surface: a=7.5, b=237.3 (-30 to 100ºC)
On the ice surface: a=9.5, b=265.3 (-50 to 0ºC)
Vapor pressure P_w is shown as

$$P_w = P_a \times (\frac{\varphi}{100}) \quad (2)$$

φ[%] is relative humidity. Absolute humidity ω [kg/kg'] is the mass of water vapor present in 1kg dry air. It is expressed as follows:

$$\omega = 0.622 \times \frac{P_w}{P - P_w} \quad (3)$$

Here, P [Pa] is atmospheric pressure.

Enthalpy is total heat of the moisture air, and is the sum of sensible heat and latent heat. Enthalpy H [J/kg] is given by the following formula.

$$H = 1.005 \times T + \omega \times (2500 + 1.861 \times T) \quad (4)$$

The amount of cooled air is decided by the performance of refrigeration. Heat during the cooling process can be calculated multiplying by the difference of enthalpy before and after air cooling. Amount of heat required cooling air Q [W] is obtained by the following formula.

$$Q = M \times (H_1 - H_2) \quad (5)$$

where, M [kg/s] is the mass rate of air flow. H_1 and H_2 are enthalpy of before and after air cooling.

If amount of absorbing heat of the Peltier device Q_p is known, assuming Q=Q_p, theoretical water production per 1 second M_w [kg/s] can be obtained by the following formula:

$$M_w = M \times (\omega_1 - \omega_2) \quad (6)$$

4. Results and discuss

In this research, two ventilation cases: natural convection and forced convection were studied. In the natural convection case, the ventilation fans were removed from the system. In the forced convection case, air wind speed in outlet was controlled between 0m/s and 1.6m/s to investigate the effect of the air flow.

4.1. Natural convection

Figure 3 shows water production rate and the cooled air temperature in the natural convection case. The cooled air temperature was measured in outlet of heat exchanger as shown in Figure 1, and the average experimental value for the last 30 minutes in the second half was used when the experiment conditions was in a stationary state. When not ventilating in each environment condition, the water production rate with the large surface area of the heat exchanger width b=120mm had exceeded that with b= 80mm.

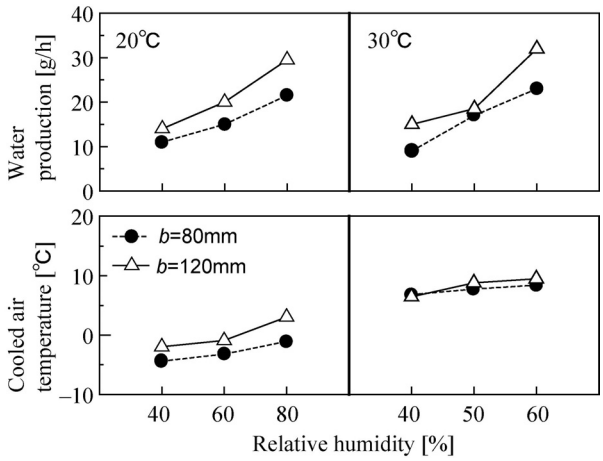

Figure 3. Water production rate and the cooled temperature in the natural convection case

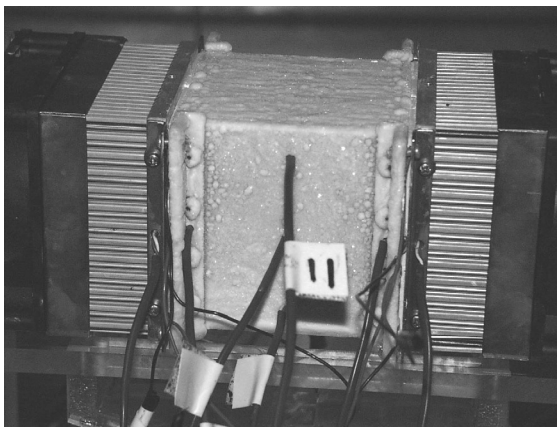

Figure 4. Photograph of the heat exchanger with the frost

Moreover, in the 20 ºC environment condition, the cooled air temperature was less than the freezing point on all the conditions except *b*= 120mm, 80% RH, and the frost adhered to the heat exchanger as shown in Figure 4.

4.2. Forced convection

Figure 5 shows the maximum water production rate in each environment and the air flow rate at that time, and the cooled air temperature. The overall trend showed no significant difference when *b*= 80mm and *b*= 120mm, as the experiment of values in these cases came to be dependant upon the cooling capability of the Peltier device. This is because the Peltier device with small absorbing heat cannot enlarge the air flow rate, the influence of the air flow rate does not appear between *b*= 80mm and *b*= 120mm (except 20 ºC, 80% RH). Water production rate was the maximum when cooled air temperature was between 2.5 to 4.8 ºC (an average of 3.5 ºC) below the dew point as shown in Figure 5. It is necessary only to control the air flow rate when air temperature is set in this range in actual use. The maximum of water production rate in the experiment was 65.5g/h in environment condition of 20 ºC and 80% RH (*b*= 120mm).

Figure 6 shows that water production rate and the cooled air temperature vary with air flow rate in the environment condition of 20 ºC and 80% RH. In the experiment, although ventilation was performed, since some air wind speed was too low to measure, and it is regarded as 0m^3/s in Figure 6.

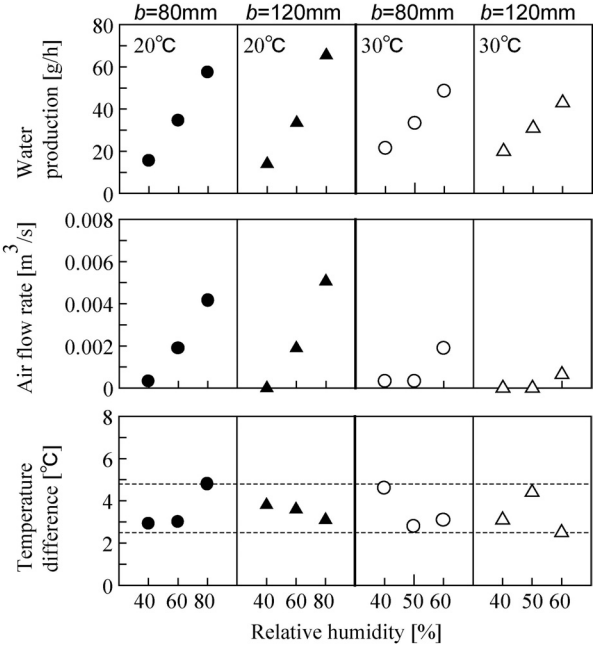

Figure 5. Water production rate, air flow rate and the cooled temperature in the forced convection case

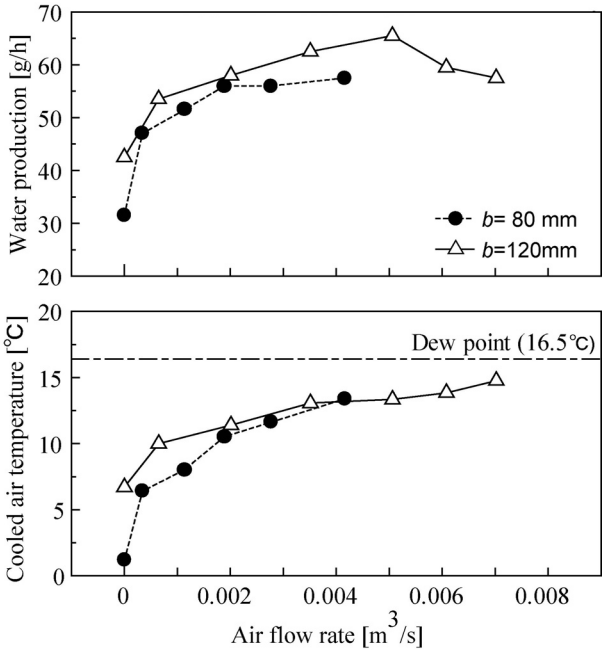

Figure 6. Water production rate and the cooled air temperature vary with air flow rate

The water production rate increased with increasing air flow rate. However, the water production rate started to decrease when the cooled air temperature neared the dew point with increasing air flow rate. The difference of the water production rate had arisen between *b*= 80mm and *b*= 120mm as the air flow became high. Since wind speed at *b*= 80mm increased about 1.5 times than that at *b*= 120mm in the case of the same air flow rate as shown in Figure 7, therefore the influence of wind speed appeared when the air flow rate was more than 0.003m^3/s.

Figure 8 shows comparison of the experimental and calculated value for water production rate and the air flow rate in each environmental condition.

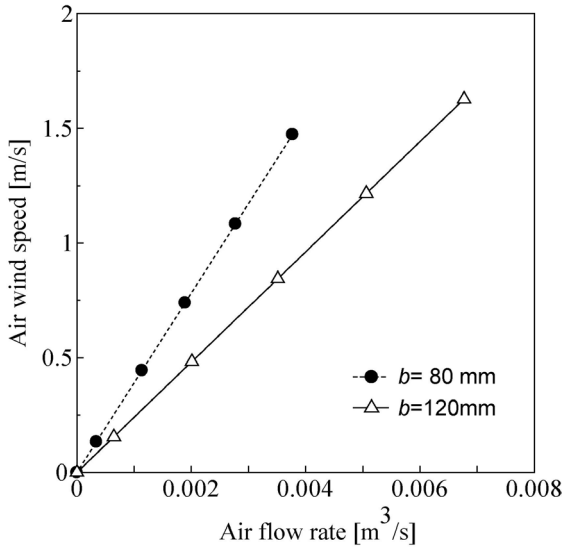

Figure 7. Comparison of the wind speed between *b*=80mm and *b*=120mm

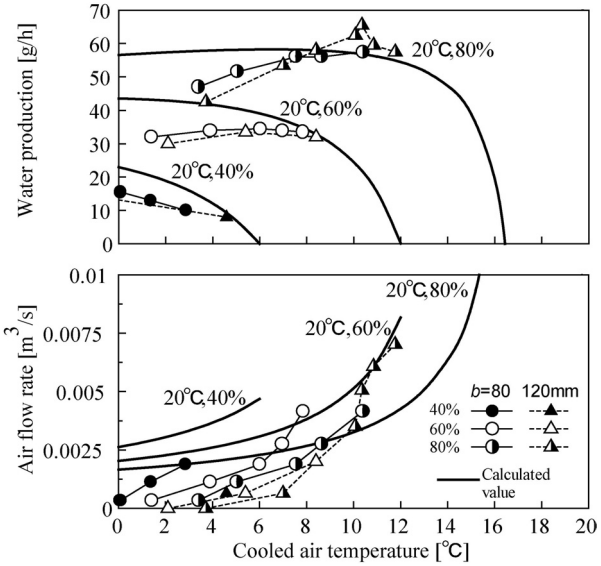

Figure 8. Comparison of the experimental and calculated value for water production rate and the air flow rate

The measured value for the temperature inclined high, since the cooled air temperature measured in the heat exchanger central part, and the cooled air temperature rose by condensation heat. Actually in the experiment, even if the cooled air temperature had exceeded the dew point, condensation occurred, and condensation stopped at about 3 ºC more than the dew point. To compare with a calculation value, the measured cooled air temperature value subtracted 3 ºC from the experimental value as shown in Figure 8. The calculation value shown as a solid line computed from a formula (6), when assuming absorbing heat 80W which multiplied electric power 160W to a Peltier device by COP=0.5 of the Peltier device. When an experiment value was compared with a calculation value, it was observed that the maximum water production rate in the experiment approached calculation value with high relative humidity, producing high water efficiency.

5. Conclusions

A trial production for the water maker system using the Peltier devices was conducted; its performance was investigated. The following results were elucidated.

(1) Equipment efficiency is dependent on absorbing heat of the Peltier device, no appreciable difference exists in the maximum water production rate and the air flow rate between *b*=80mm and *b*=120mm.

(2) Water production rate becomes the maximum, when the cooled air temperature is in the range 2.5 to 4.8 ºC (an average of 3.5 ºC) below the dew point.

(3) For the water maker system, producing water efficiency becomes large with high relative humidity.

6. References

[1] Jesse S. Doolittle, 1960, Thermodynamics for engineers, International textbook company, Pennsylvania.

[2] Tsutomu Hayashi et al. 2004, A Study on a Water Maker System using Peltier Devices, The Japan Society of Mechanical Engineers Branch conference, Japan, No.045-2 (I), pp.109-110.

[3] Virgil M. Faires, 1962, Thermodynamics, Maruzen Company Limited, Tokyo.

[4] Yunus A. Cengel & Michale A. Boles, 1994, Themodynamics: An Engineering Approach, McGraw-Hill, Inc.

Acknowledgement

This study was carried out under the Cooperative Research Program of Arid Land Research Center, Tottori University. As a part of the 21st century COE program, the gratitude was expressed by all authors.

Return

A Study on Water Making System Using Renewable Energy in Tottori Sand Dune (Analysis of the System Efficiency by Simulation)

Tsutomu Hayashi[*1], Kenji Tanaka[*1], Yutaka Hara[*1], Wei Liu[*2], Kengo Nojima[*3] & Kotaro Tagawa[*4]

[*1] Department of Applied Mathematics and Physics, Tottori University, Japan
[*2] Post Doctoral, 21 century COE program, Tottori University, Japan
[*3] Industrial Research Institute of Tottori Prefecture, Japan
[*4] Faculty of Regional Sciences, Tottori University, Japan

Abstract Objective of this study is development of a water making system that can produce good quality water useful in arid region for drinking, medical treatment and irrigation, using electric power generated by renewable energy (especially, wind energy). A simple and tough water maker was composed of eight Peltier devices, copper heat exchanger and fans. The best driving environment and the operating condition of the system were examined by indoor experiments. Our research group is planning to conduct the outdoor experiments with the water making system at Tottori Sand Dune. A meteorological observation system has already been installed at the site and has been collecting the meteorological data. In this research, water production rate was simulated based on the indoor experiments data and the observed meteorological data. In the simulation, the operation of water maker was assumed to be controlled by both the dew point and the battery level. The water production rates were calculated at the different settings of dew point and wind turbine performance. The system obtained the highest efficiency at the controlled dew point of 10°C when using the meteorological data of November, 2004.

Keywords: Water Making System, Water Maker, Peltier Device, Renewable Energy

1. INTRODUCTIONS

In arid region, obtaining a stable reserve of water is one of the most important problems for people living there. In this research, a system which can easily produce clean water from water vapor in the atmosphere has been studied and developed. Most of the arid regions are blessed with renewable energy such as wind energy or solar energy. Therefore, wind power and/or solar power is appropriate for the energy source of the water making system and the development of a sustainable system is expected. At the arid regions along the west coast of a continent, where rainfall is small but humidity is high, night fogs often occur due to the large temperature difference between daytime and night. Especially in such arid regions, the water making system might operate efficiently by condensing water vapor at night.

In our research group, a simple and tough water maker with Peltier devices has been proposed, and the characteristic of the water maker was clarified by indoor experiments. Now, the authors are planning to conduct outdoor experiments with the water making system consisted of the water maker and a meteorological observation system at Tottori Sand Dune. The meteorological observation system has already been installed at the site and has been collecting the meteorological data. Also, the amount of water production has been calculated by using the indoor experiment data and the observed meteorological data, based on assumption that electric power to the system is supplied only wind turbine. In this research, the influence of the electric power generated by the wind turbine on the water production rates was examined. Moreover, the optimal operating conditions for the control of the system were clarified.

2. THEORY OF THE WATER MAKING BY COOLING

Water vapor in the atmosphere can be condensed by cooling the moisture air below the dew point. Amount of heat required to cool air can be calculated multiplies by mass flow rate and the difference of enthalpy before and after cooling air. Therefore, amount of heat required to cool the air in one-second q [kJ/s] is given by the following formula,

$$q = m_a \times (h_1 - h_2) \tag{1}$$

where, m_a [kg/s] is mass flow rate of air, h_1 [kJ/kg], h_2 [kJ/kg] are enthalpy before and after cooling air. Amount of heat removed from air is decided by performance of the refrigeration. If amount of absorbing heat of Peltier device q_p[kJ/s] is known, assuming $q = q_p$, the amount of air cooled is decided. In other words, air flow rate is given by the following formula.

$$m_a = q_p / (h_1 - h_2) \tag{2}$$

Since the amount of air cooled was decided, water production

rate per one-second m_w [kg/s] is obtained by the following formula,

$$m_w = m_a(x_1 - x_2) \quad (3)$$

where, x_1 [kg'/kg], x_2 [kg'/kg] are absolute humidity before and after cooling air.

3. WATER MAKER AND METEOROLOGICAL OBSERVATION SYSTEM

3.1 Water maker

Figure 1 shows the schematic diagram of the water maker using the Peltier device in the research. On both sides of the heat exchanger, four Peltier devices (two series, 4 parallel, 8 piece in total), and cooling fin and fan were set up. The heat exchangers with two types of width (b=80,120mm) were used in experiment. The ventilation fan was set up directly in the upper of the heat exchangers, one fan was used in the case of b=80mm, and two fans were used in the case of b=120mm. Also, when the experiments were performed with no ventilating, the fans were removed. The indoor experiments were carried out in a constant temperature and relative humidity chamber, in which the temperature and relative humidity were set six environments of 20°C with 40, 60, 80%RH, and 30°C with 40, 50, 60% RH. The influences of the heat exchanger width and air flow rate on water production rate during one hour under each condition were investigated [2]. Fig. 2 shows the comparison between the experimental values and the calculated values of the water production rate and the air flow rate in the environment of 20°C with 40, 60 and 80%RH. The experimental values of the maximum water production rate approached the calculated values as high relative humidity increases, and the efficiency of the water production increased as shown in Fig. 2.

3.2 Meteorological observation system

The schematic diagram of the meteorological observation system is shown in Fig. 3, and the measurement items are shown in Table 1. The system was set up in Arid Land Research Center of the Tottori University. The system was consisted of anemovane, humidity/temperature meter and photovoltaic module were installed, and the hyetometer was set up beside the system. The height of the observation pole was 4.5m and the anemovane was set at the top of the pole. The electric power for the system was supplied by the battery charged with the solar pane. And the obtained data was saved in the memory of the logger box.

Table 1. Measurement items

Measurement items	Sampling
Wind speed	Every one second
Wind direction	Every one second
Temperature	Average for ten minutes
Humidity	Average for ten minutes
Amount of insolation	Average for ten minutes
Amount of rainfall	Integrate for ten minutes

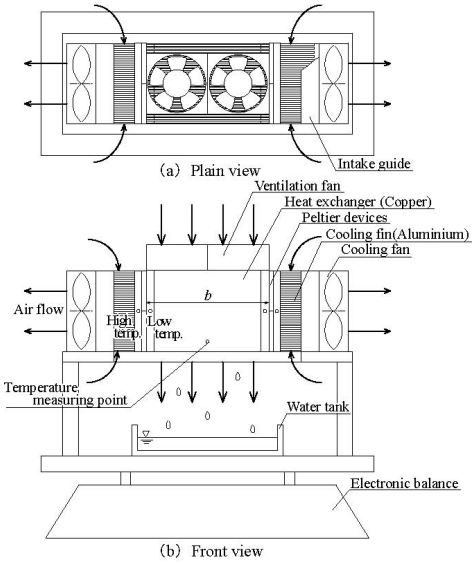

Fig.1 Schematic diagram of water maker

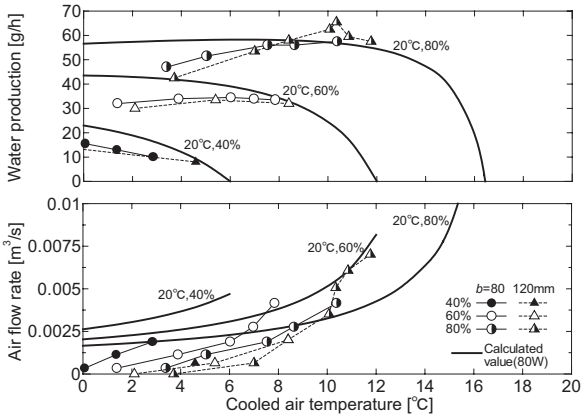

Fig.2 Experimental and calculated values of water production and air flow rate

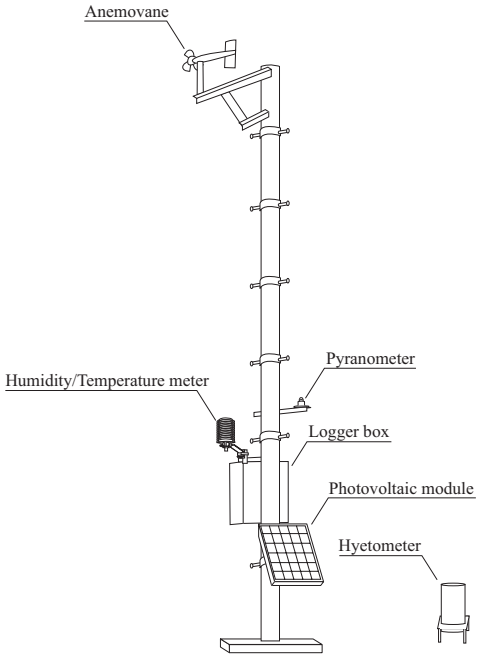

Fig.3 Schematic diagram of meteorological observation system

4. CONDITIONS FOR THE CALCULATION

It is assumed that the electric power for the water maker is supplied by only wind turbine and the operation of water maker is controlled by both the dew point and the battery level. The control by the dew point is performed when the dew point is more than datum value, and the control by the battery is performed when battery level is more than 10%. The case of three types of wind turbines (rated power 220W, 340W and 460W) were assumed as shown in Fig. 4. Also, the battery with the capacity 200Ah was assumed. The water production rate was calculated by using the indoor experiments data and the observed meteorological data at Tottori Sand Dune (November, 2004). In the calculation, the air was cooled to 3°C below the dew point based on the results of indoor experiments and the controlled dew point was varied 3°C to 12°C in each wind turbine. Moreover, the calculation was carried out in the case of adding the operating conditions for the relative humidity, controlling when relative humidity is more than datum value (70%RH, 80%RH and 90%RH).

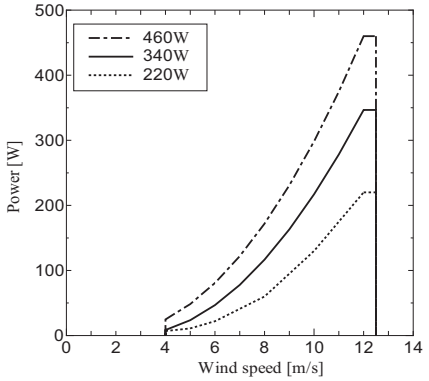

Fig.4 Power curve of wind turbines

5. RESULTS AND DISCUSSION

The results of calculation when controlled dew point is varied in each wind turbine are shown in Fig. 5. The water production rate is calculated using the data of November, 2004. The water production rate rises as the size of the wind turbine becomes large. And the fluctuation band of water production rate becomes large as the size of the wind turbine becomes large. That is, the operation by the dew point is important when electricity generated becomes large contrasts to the electric consumption of the equipment.

The results of calculation are shown in Fig. 6 in the case of using of the wind turbine with rated power 340W and adding the control of the relative humidity. And, Fig.7 shows the energy efficiency with the condition as shown in Fig.6. Energy efficiency is given by dividing the water production rate by the input electricity to equipment,

$$E_e = M_w / W_{in} \qquad (4)$$

where E_e [kg/kW] is energy efficiency of the system, M_W [kg] is monthly water production, and W_{in} [kW] is input electricity to equipment.

In the case of 80%RH, Fig. 6 shows that water production rate is increasing compared with no relative humidity control. In the case of relative humidity control 90%RH, however, it is less than case of no relative humidity control. Therefore, although water production rate can expect to increase when relative humidity adds to controlled condition, it decreases if relative humidity is set too high. From Fig. 7, energy efficiency was improved in each relative humidity control condition when controlled dew point became high. And energy efficiency also improves when relative humidity adds to controlled condition.

From Figs. 6 and 7, the energy efficiency is high when controlled dew point is high, but water production rate decreases when it become too high. In this research, it is assumed that prototype water maker is used. However, when extended water maker is used in practice, the energy efficiency became more important as it is possible that the number of sheets of Peltier device increases.

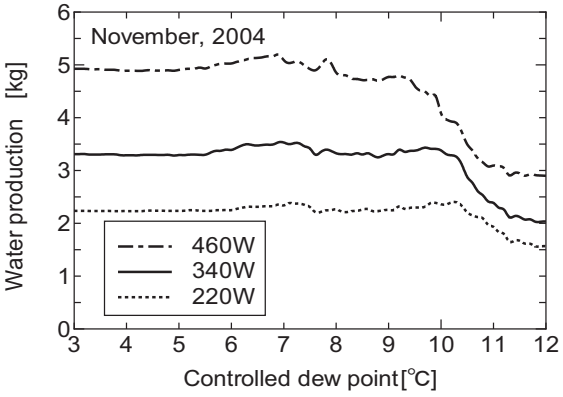

Fig.5 Water production by difference of wind turbine

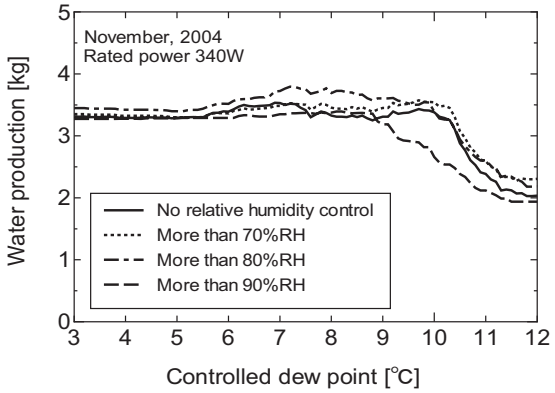

Fig.6 Water production by relative humidity control

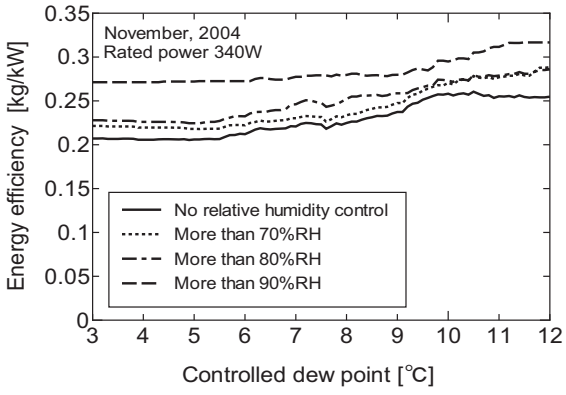

Fig.7 Energy efficiency

Therefore, the efficiency of water making system is evaluated from water production rate and energy efficiency.

The system efficiency E_S [kg^2/kW] is defined as multiply water production rate by energy efficiency.

$$E_s = M_w \times E_e \qquad (5)$$

The evaluated values of the system efficiency in each control condition are shown in Fig. 8. In each relative humidity control, the evaluated values of the system efficiency were obtained the highest value in about 10°C when relative humidity control was other than 90%RH. Furthermore, the maximum value of the system efficiency was obtained maximum when controlled relative humidity was 80%RH and the controlled dew point was 10°C. In the case of this controlled condition, monthly water production was 3.5 kg, and energy efficiency was 0.27 kg/kW.

The result of a calculation at that case for one month is shown in Fig. 9. The water production range shown in figure is water production rate in the case of assuming to operate without dependence on the battery level. In this case, monthly water production is 8.5 kg. Thus it produces 40% of 8.5 kg in the case of electric power supplied by only wind turbine (rated power 340W). Although there are many water production ranges in the first half of November, it is recognized that water making system cannot be operated because of the shortage of the electricity generated. In the latter half of November, battery level (electricity generated) is enough, but there are few production possibility boundaries. So, it is recognized that the system cannot operate.

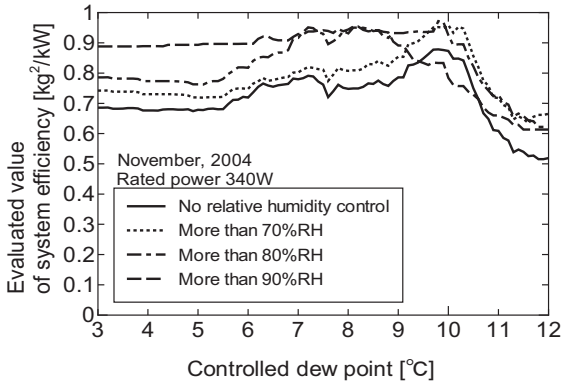

Fig.8 Evaluated value of system efficiency

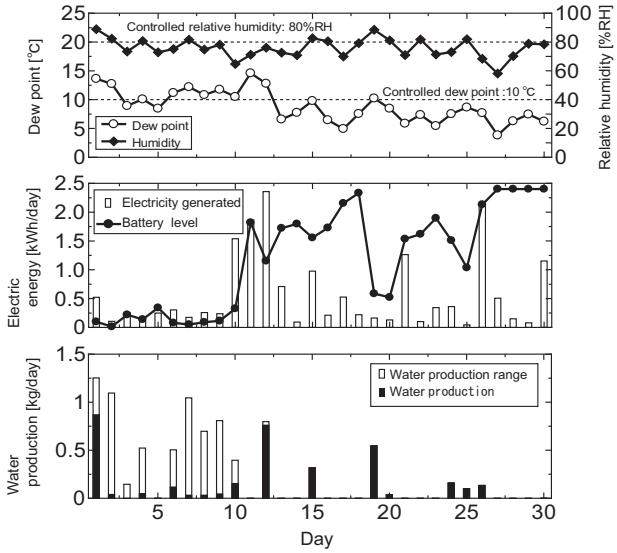

Fig.9 Calculated value in Tottori Sand Dune

6. CONCLUSIONS

As a result of calculation based on the indoor experiments data and the observed meteorological data for the water maker using the Peltier device, the following results were elucidated.

(1) Water production rate increases when electricity generated by a wind turbine becomes large, and the dependence on the control conditions of water production rate becomes high.

(2) By adding relative humidity control, improvement of energy efficiency can be expected and the increase of water production rate can also be expected.

(3) The highest efficiency of the system is obtained at the controlled dew point of 10°C and controlled relative humidity of 80%RH in the case of the meteorological data at Tottori Sand Dune in November, 2004.

ACKNOWLEDGEMENT

This study was carried out under the Cooperative Research Program of Arid Land Research Center, Tottori University. As apart of the 21st century COE program, the gratitude was expressed by all authors.

REFERENCES

[1] Ichimatsu Tanishita, Engineering Thermodynamics, Syoukabou company, pp.221-227 (1995).

[2] Tsutomu Hayashi et al, A Study on a Water Maker System Using Peltier Devices, The Japan Society of Mechanical Engineers Branch Conference, Japan, No.045-2(I), pp.109-110 (2004).

Return

Characteristics of a Straight-Bladed Vertical Axis Wind Turbine in Periodically Varying Wind

In-Seung KANG[1], Kenichi ARIYASU[1], Yutaka HARA[1],
Tsutomu HAYASHI[1] and Ion PARASCHIVOIU[1,2]

[1] Department of Applied Mathematics and Physics, Tottori University,
4-101 Koyama-cho, Tottori 680-8552, Japan
[2] Department of Mechanical Engineering, Ecole Polytechnique Montreal,
P.O. Box 6079, Station Centre-ville, Montreal, Quebec, Canada H3C 3A7

Abstract An experimental study of the torque characteristics for a straight-bladed vertical axis wind turbine (VAWT) in periodically varying wind speed is presented. The amplitude of the periodically varying wind speed was fixed at 2m/s with the average wind speed of 8m/s and the cycles of 2.9 s, 4.5 s, and 5.9 s were chosen. The VAWT with NACA 0012 blade sections (chord length = 0.075m) having the rotor radius of 0.3 m and the rotor height of 0.469 m was rotated by a induction motor. We studied several experimental models by changing the number of blades (2 to 5 blades) in order to investigate the influence of rotor solidity on the wind turbine performance. The averaged torque curve in the case of the periodically varying wind is almost the same as the torque in the case of the constant wind speed. However, in the case of five-blade rotor, the torque in the periodically varying wind became larger than that in the constant wind near the tip-speed-ratio region where the maximum torque was obtained. The torque and rotational speed follow the change of the wind speed. This trend is better if the rotor solidity becomes larger.

Keywords: Wind Turbine, VAWT, Solidity, Periodically Varying Wind, Torque Characteristics

1. INTRODUCTION

Recently, straight-bladed vertical axis wind turbines (VAWT), whose torque characteristics are independent of wind direction variation, have been attracting people's attention due to the possibility to be suitable for the changeable wind conditions. One of our goals of study is development of a practical VAWT having high efficiency even in bad wind conditions like changeable wind direction. We already conducted experiments[1] in order to investigate the solidity dependence of our trial models of VAWT by using a wind tunnel. However, wind used in such wind tunnel test is constant speed in general, and experiments to investigate the response of a wind turbine to the wind speed variation have hardly been reported so far. Our group carried out the measurements of aerodynamic forces acting on a two-dimensional blade in a periodically varying wind to investigate the behaviors of the aerodynamic force coefficients in the wind speed variation[2].

In this study, the torque characteristics of the straight-bladed vertical axis wind turbine are measured in both the periodically varying wind (PVW) and the constant velocity wind (CVW) in order to compare the rotor behaviors in the different wind conditions. The number of blades of the rotors and the cycle of the PVW are changed as the parameters in a series of experiments to investigate the dependence of VAWT on them.

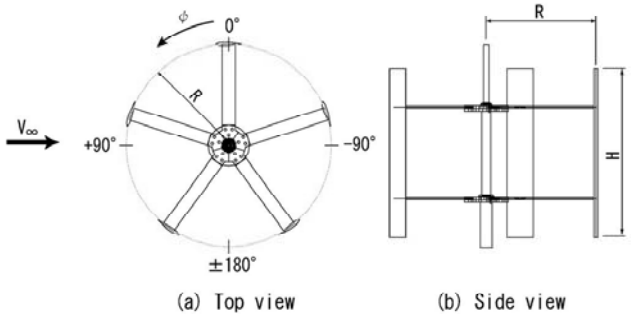

Fig. 1 Diagram of the rotor of VAWT with 5 blades

Table 1 Specification of the VAWT

Number of Blade : B	2～5
Rotor Radius : R	0.300m
Rotor Height : H	0.4688m
Blade Chord Length : c	0.075m
Projected Area : A=2RH	0.281 ㎡
Material	Carbon
Blade Airfoil	NACA 0012

2. EXPERIMENTAL SETUP AND METHOD

Figure 1 shows a diagram of the rotor of VAWT with five blades. The cross-sectional form of the blade is symmetrical NACA 0012 airfoil. The number of blades can be changed from two to five. The specification of the rotor is shown in Table 1, and the photographs of the rotors with different numbers of blades are shown in Fig. 2.

The diagram of our experimental system is shown in Fig. 3. The wind tunnel used in the experiment is the Eiffel type, and its outlet is a 1.5 m × 1.5 m square. The center of the wind turbine rotor is located at 1.5m downstream from the center of the wind tunnel outlet. The rotor axis is held by two ball bearings, and is combined through couplings with both the torque detector and the induction motor which is controlled by an inverter. Rotational number of the rotor was fixed in every about 30 rpm in the range from 30 rpm to 510 rpm. The obtained torque data were corrected by adding the braking torque measured when the axis from which all blades were removed was rotated at the same rotational number.

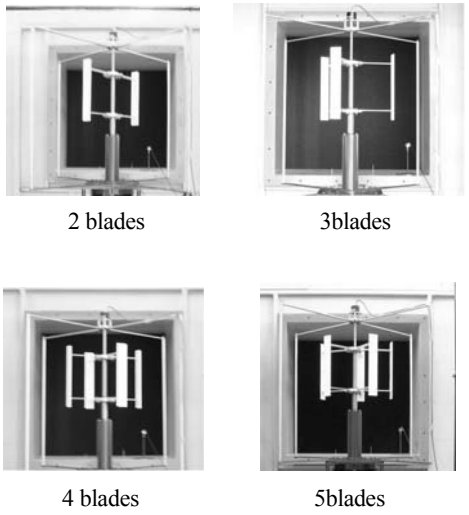

Fig. 2 Photos of the rotors with different number of blades

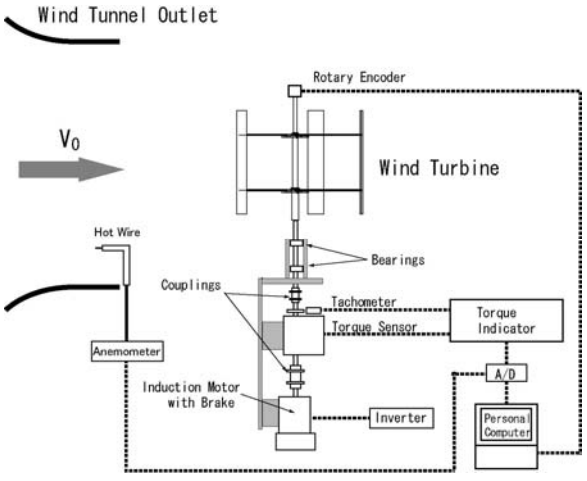

Fig. 3 Experimental setup

The periodically varying wind was generated by variation of the pitch angle of the axial blower in the wind tunnel. The average wind speed of the PVW is 9 m/s and the amplitude is about 2 m/s. The cycle (Tw) of the PVW was set to 5.9 s, 4.5 s, and 2.9 s. Wind speed was measured at the wind tunnel outlet using a hot-wire anemometer.

3. EXPERIMENTAL RESULTS AND DISCUSSIONS

The time-averaged power coefficients (Cp) measured in the constant velocity wind (CVW) and the periodically varying wind (PVW) are shown in Fig. 4 and Fig. 5, in which only the results in the cases of 2-blade and 5-blade rotors are given. The wind speed of the CVW is 9m/s; the cycle of PVW in Fig. 4 is Tw = 5.9 s and that in Fig. 5 is Tw = 2.9 s. As shown in Fig. 4 and Fig. 5, roughly speaking, the time-averaged Cp measured in the PVW and the Cp in the CVW are almost the same. This tendency is the same in the cases of 3-blade and 4-blade rotors, too. However, if seen in detail, the Cp in the PVW is somewhat larger than that in the CVW at the tip speed ratio of λ = 0.8-1.5 in the case of 2-blade rotor and at λ = 1.5-1.7 in the case of 5-blade rotor.

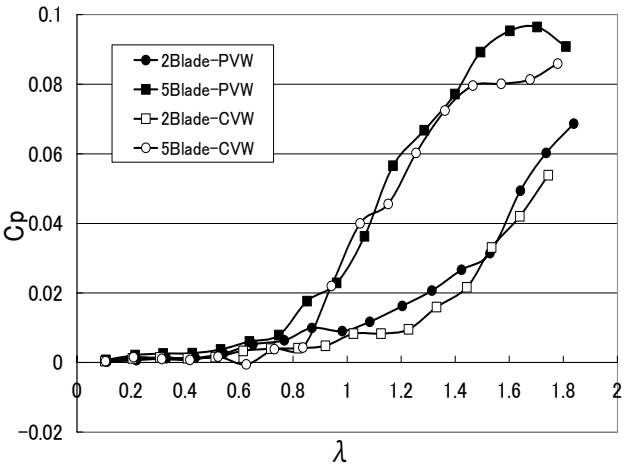

Fig. 4 Power characteristics (Tw = 5.9 s)

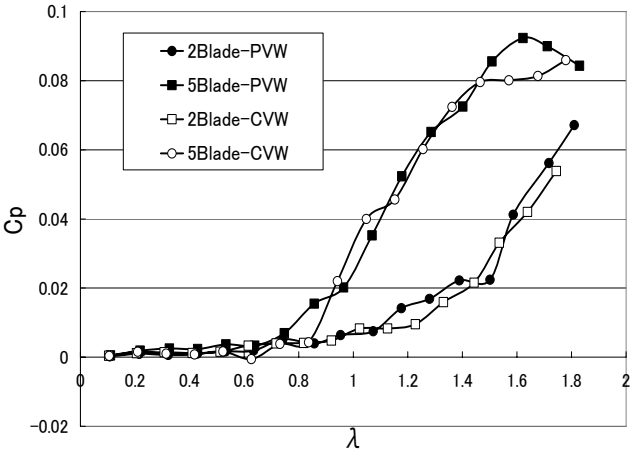

Fig. 5 Power characteristics (Tw = 2.9 s)

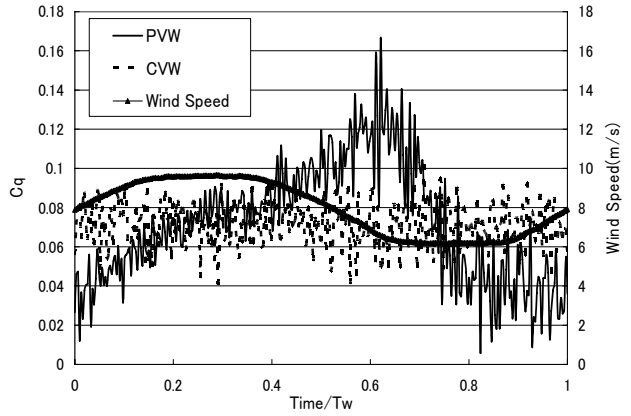

Fig. 6 Comparison of torque variations in PVW and CVW (5 blades, Tw = 2.9 s, λ = 1.5)

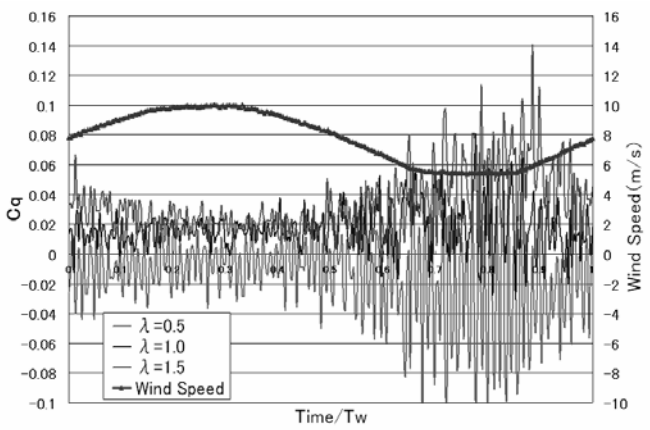

Fig. 7 Dependence of torque characteristics on tip speed ratio (2 blades, Tw = 2.9 s)

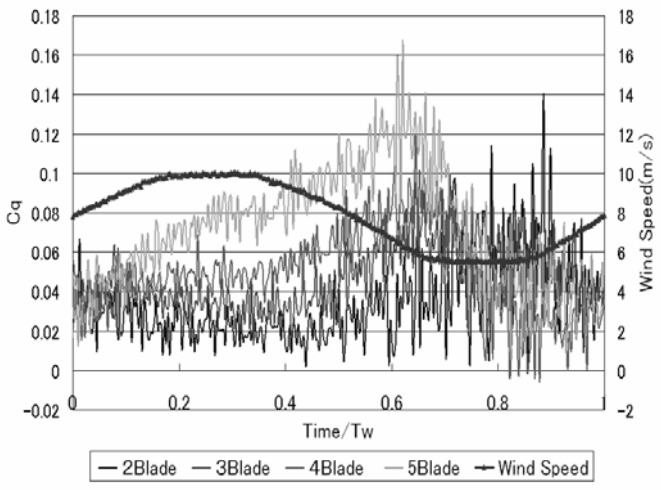

Fig. 8 Dependence of torque characteristics on the number of blades (Tw = 2.9 s, λ = 1.5)

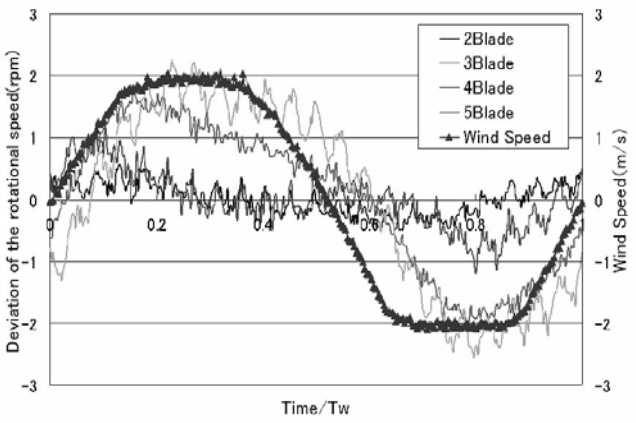

Fig. 9 Deviation of the rotational speed in each case of different number of blades (Tw = 2.9 s, λ = 1.5)

Figure 6 shows the comparison of torque variations of 5-blade rotor in the CVW and the PVW when the cycle of PVW is 2.9 s and λ = 1.5. In this figure, the ensemble-averaged wind speed is also shown together with the ensemble-averaged torque coefficients (Cq). The data used for the ensemble average in the case of Tw = 2.9 s includes nine cycles. The abscissa of the graph in Fig. 6 is non-dimensional time on the basis of the cycle of PVW. The torque coefficient (Cq) in the PVW fluctuates larger than the Cq in the CVW. The averaged value (0.075) of Cq in the PVW is larger than that (0.070) in the CVW. This tendency is observed in the case of Tw = 5.9 s as well. This corresponds to the superiority of Cp around λ = 1.6 in the PVW in the case of 5-blade rotor in Fig. 5.

The ensemble-averaged torque variations under the conditions of 2-blade rotor and Tw = 2.9 s are shown in Fig. 7, in which the data for λ = 0.5 and 1.5 are compared. In the case of 2-blade rotor, when the wind speed is small, the Cq fluctuates larger at any value of λ. That is, the torque coefficient of a VAWT is influenced by wind speed variation. This tendency is observed in the case of Tw = 5.9 s, too.

Figure 8 shows the torque behaviors of the rotors with different numbers of blades in the periodically varying wind of Tw = 2.9 s. The tip speed ratio in Fig. 8 is λ = 1.5. Clear dependence of the torque variations on the number of blade is observed. The Cq of the 2-blade rotor, as seen in Fig. 7, increases in the domain of low wind speed. On the other hand, the Cq of 5-blade rotor gradually increases in the domain of high wind speed and decreases in the low wind speed domain rapidly. This difference is observed in PVW of Tw = 5.9 s, too. Obviously, the averaged value (0.067) of Cq of 5-blade rotor is larger than that (0.035) of 2-blade rotor.

Deviation of the rotational speed which has been measured simultaneously with the torque of Fig. 8 is shown in Fig. 9. This figure shows that the follow-up nature of the VAWT to the wind speed variation becomes higher as the number of blades increases.

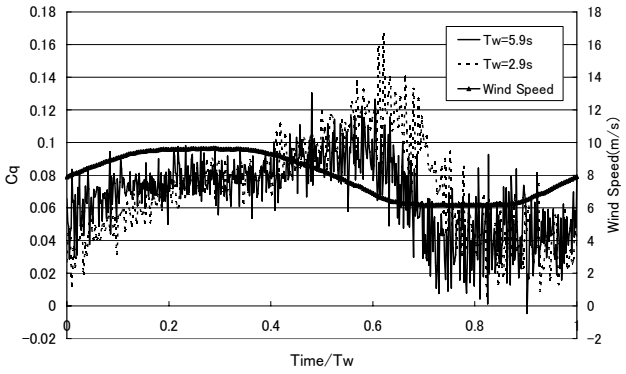

Fig. 10 Dependence of torque characteristics on the cycle of PVW (5 blades, λ = 1.5)

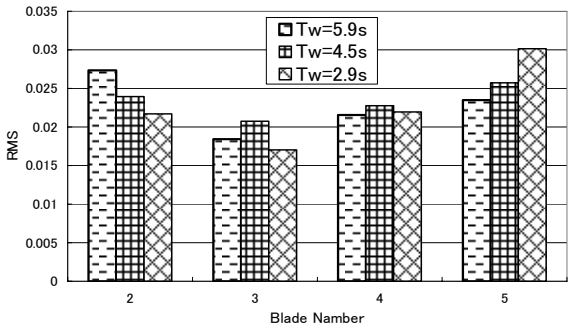

Fig. 11 Root mean square of the torque coefficient in each case under the condition of λ=1.5

The torque coefficients in the cases of Tw = 5.9 s and 2.9 s are compared in Fig. 10 under the conditions of 5 blades and λ = 1.5. The Cq in the case of Tw = 2.9 is larger than the Cq in the case of Tw = 5.9 s in the domain of non-dimensional time from 0.6 to 0.75. On the other hand, in the domain from 0 to 0.2, the Cq in the case of Tw = 2.9 s is smaller than that in the case of Tw = 5.9 s. That is, when the variation of wind speed becomes faster, even if the amplitude of the periodic varying wind holds the same level, the torque variation acting on the wind turbine might become larger.

Root mean square of the torque coefficient in each case under the condition of λ=1.5 is shown in Fig. 11. As seen in Fig. 10, the torque fluctuation of 5-blade rotor gets larger as the cycle of PVW becomes short. However, the case of 2-blade rotor shows the contrary tendency. In addition, obvious tendency can not be found in the case of 3 blades and 4 blades.

5. CONCLUSIONS

The torque characteristics of straight-bladed Vertical Axis Wind Turbines (VAWT) were measured in both the periodically varying wind (PVW) and the constant velocity wind (CVW) in order to compare the rotor behaviors in the different wind conditions. The averaged Cp in PVW is almost the same as that in CVW. However, in the 5-blade case, the Cp in PVW became larger than the Cp in CVW at the rotational conditions near λ = 1.6. The follow-up nature of the VAWT to the wind speed variation becomes higher as the number of blades increases. Torque fluctuation of the 5-blade rotor gets larger as the cycle of PVW becomes short, although the 2-blade rotor shows the contrary tendency.

ACKNOWLEDGEMENT

This study was carried out as a part of the 21st century COE program "Program for Arid Land Science". The authors express the gratitude.

REFERENCES

[1] Hayashi, T., Hara, Y., Moriya, T., Tagawa, K. and Nozima, K., The Study on the Solidity Dependency of the Straight-Bladed Vertical Axis Wind Turbine, Proceedings of the 42nd general meeting and lecture meeting of Chugoku-Shikoku branch of JSME, No.045-1, 307-308 (2004).

[2] Hara, Y., Kang, I., Moriya, T., Ariyasu, K. and Hayashi, T., Development of a Measuring System with Two Force Sensors of Aerodynamic Forces Acting on a Two-Dimensional Wing, The Sixth KSME-JSME Thermal and Fluids Engineering Conference (CD-ROM), JE-08, (2005).

Return

Short Report

Urinary protein 1/Clara cell 16 concentrations and lung functions in male subjects with pneumoconiosis

Kazuhiko Kotani[1], Isao Kawabata[2], Haosheng Mu[1], Youichi Kurozawa[1] and Yoshihisa Itoh[2]

Addresses
[1]Division of Health Administration and Promotion, Faculty of Medicine, Tottori University, 86 Nishi-cho, Yonago 683-8503; [2]Department of Laboratory Medicine, Asahikawa Medical College, Asahikawa, Japan

Correspondence
Dr Kazuhiko Kotani
Email: kakotani@grape.med.tottori-u.ac.jp

Abstract

Background Protein 1 (P1)/Clara cell 16 kDa protein (CC16, previously named CC10), a potentially immunosuppressive protein secreted by non-ciliated cells of the tracheobronchial epithelium, has been found to be a new useful lung-specific biomarker in several pathological lung conditions. Particularly, urinary P1 (uP1) may reflect the altered lung functions in pneumoconiosis.

Methods We investigated the relationship between uP1 values and lung functions in 31 non-smoking pneumoconiotic males (mean age 73 years) with a history of dust exposure work in shipbuilding. The protein was measured using an originally prepared enzyme-linked immunosorbent assay system. The forced expiratory volume in 1 s % ($FEV_{1.0}$%) and % vital capacity (%VC) were tested with a spirometer.

Results The mean values of uP1 were 4.62 ± 4.82 (mean $\pm$ standard deviation) ng/mol creatinine. A univariable correlation test showed a significant positive correlation between uP1 and %VC ($r = 0.356$, $P = 0.049$). Also, a multiple regression analysis, when adjusted for age, disease duration, $FEV_{1.0}$% and %VC, showed a significant correlation of uP1 with %VC ($\beta = 0.467$, $P = 0.030$).

Conclusion The results suggest that a decreased uP1, corroborated by a decreased %VC, may be the result of damage to secretory cells. Measurement of uP1 may become a possible index of fibrotic changes in pneumoconiosis.

Ann Clin Biochem 2007; **44**: 560–562

Introduction

Pneumoconiosis, chronic inflammation in the lung with subsequent fibrosis and possible development of malignancy, is an occupational disease caused by the long-term inhalation of dust particles. The applicability of classical imaging, spirometric methods, and biomarkers in serum or bronchoalveolar fluid (BALF) is, however, limited to assessing lung risk in each dust-affected worker.[1] New sensitive and specific markers have been sought to overcome this.

Protein 1 (P1), also called Clara cell protein (CC16, previously named CC10) or CC secretion protein (CCSP), is a low molecular weight protein of 16 kDa, synthesized by non-ciliated bronchiolar Clara cells and secreted in large amounts into the lumen of the lung tract. P1 is an immunosuppressant and downregulates the activation of the Th1 cell immune system, thus protecting from tissue injuries.[1–4] Serum and BALF P1 have been shown to change in several pathological lung conditions such as silica- and asbestos-exposed fibrosis or injury by fire smoke and ozone.[1–3] Because of its low molecular weight, P1 easily leaks from the lung epithelial lining fluid into the systemic circulation and is thus filtered through the kidney into urine. Antigen and antibody measurements in urine have drawn attention as a non-invasive marker. Few studies have been reported on the clinical significance of the relationship between urinary P1 (uP1) and lung conditions.[5]

The current incidence of pneumoconiosis in Japan has decreased compared with the previous incidence. Shipyard welders unrelated to silica- and asbestos-exposed populations may be increasingly at risk of pneumoconiosis.[6] We thus investigated uP1 in terms of its clinical relevance to lung functions in pneumoconiotic

Table 1 *Correlations of urinary protein 1 with pneumoconiosis-related factors*

	r (*P* value)	*β* (*P* value)
Age (years)	0.120 (0.521)	0.256 (0.282)
Duration after diagnosis (years)	−0.035 (0.854)	−0.336 (0.182)
$FEV_{1.0}$%	0.055 (0.767)	−0.093 (0.642)
%VC	0.356 (0.049*)	0.467 (0.030*)

$FEV_{1.0}$, forced expiratory volume in one second; VC, vital capacity; *r*, Pearson rank correlation; *β*, multiple regression coefficient; *Statistical significance

men with a history of dust exposure work in shipbuilding.

Subjects and methods

A total of 31 Japanese men with pneumoconiosis, aged 61–85 (72.8 ± 6.8, mean ± standard deviation [SD]) years, were enrolled in this study. Eligible subjects were non-smokers including an ex-smoker who had abstained from smoking for more than 10 years. They had neither a history nor clinical features of kidney and prostate diseases. Their overnight fasted values of serum creatinine (Cre) were normal (<0.1 mmol/L). Their lung X-rays showed Categories I–III (no severe classes) of the diagnostic criteria based on the 1982 Japanese Classification of Radiographs of Pneumoconiosis by the Ministry of Labour that agrees with the 1980 classification by International Labour Organization.[6] The mean duration after the definite diagnosis of pneumoconiosis was 13.4 years. P1 levels in the first morning urine were measured using an enzyme-linked immunosorbent assay (originally developed using recombinant P1 and its monoclonal antibodies:[7] coefficient of variation [CV] in the intra- and inter-assay was 4.3% and 3.8%, respectively[8]), and were corrected by urinary Cre by an enzymatic method (Kainos, Tokyo, Japan) using a Hitachi autoanalyzer (Hitachi-705, Hitachi, Japan: CV in the intra- and inter-assay was 2.0% and 3.0%, respectively; data assessed in our laboratory). For lung function tests with a spirometer (CHESTAC-33, Tokyo, Japan), the forced expiratory volume in 1 s % ($FEV_{1.0}$%) and % vital capacity (%VC) were measured for the same individuals. The study was approved by the Tottori University Ethics Committee and each subject gave informed consent. The relation between uP1 levels and pneumoconiosis-related factors such as age, disease duration, and $FEV_{1.0}$% and %VC values were examined by the Pearson's rank correlation test and multiple regression analysis. $P < 0.05$ was considered significant.

Results

The mean values (±SD) of uP1 were 4.62 ± 4.82 ng/mol Cre, while those of $FEV_{1.0}$% and %VC were 69.4 ± 11.3% and 86.7 ± 22.1%, respectively. In a univariable correlation test, %VC among lung function tests showed a significant positive correlation with uP1 levels (Table 1). Moreover, a multivariable correlation test showed that %VC significantly and positively correlated with uP1. No correlations among age and the disease duration and uP1 were found.

Discussion

Regarding the practical use of uP1, it is important to show its accurate reflection of prerenal pathophysiologic changes in the lung irrespective of many influencing factors from its production to excretion in urine. The novel finding of the present study is that it correlated with %VC in pneumoconiotic men with a history of work in shipbuilding. The serum decrease of P1 has been ascribed to damage to secretory cells in the bronchiolar tree, resulting in a reduction in P1 synthesis and P1-transferable pool size in fibrotic processes.[1–4] In turn, the decreased uP1 with reduced %VC appears to be explanted similarly. Provided the renal function is normal and urine specimens are properly collected in a routine manner, a decreased uP1 probably indicates susceptibility to alveolar inflammation as an unfavourable prognostic factor.

Our study had some limitations: a small sample size, the cross-sectional design, the restriction of subjects based on the disease severity and smoking, and no traceable dust exposure data such as duration and dose.

The current use of urine analyses as indicators for prerenal events has become expanded. As one of these markers, the measurement of uP1 may become a non-invasive useful index to speculate on fibrotic changes, and it may also be an additive chemical lung function test. We can at least apply this method to pneumoconiotic subjects.

References

1 Petrek M, Hermans C, Kolek V, Fialova J, Bernard A. Clara cell protein (CC16) in serum and bronchoalveolar lavage fluid of subjects exposed to asbestos. *Biomarkers* 2002; 7: 58–67

2 Itoh Y, Ishii S, Okutani R, Asano Y, Kawai T. Protein 1: its purification and application in clinical medicine. *J Clin Lab Anal* 1993; **7**: 394–400
3 Bernard AM, Gonzalez-Lorenzo JM, Siles E, Trujillano G, Lauwerys R. Early decrease of serum Clara cell protein in silica-exposed workers. *Eur Respir J* 1994; **7**: 1932–7
4 Morimoto Y, Nagatomo H, Hirohashi M, *et al.* Expression of Clara cell secretory protein in the lungs of rats exposed to crystalline silica *in vivo*. *J Occup Health* 2005; **47**: 504–9
5 Itoh Y. Urine protein 1 (Clara cell 10 kDa protein) (in Japanese). *Nippon Rinsho* 2004; **62**(Suppl. 11): 113–5
6 Takigawa T, Kishimoto T, Nabe M, *et al.* The current state of workers' pneumoconiosis in relationship to dusty working environments in Okayama Prefecture, Japan. *Acta Med Okayama* 2002; **56**: 303–8
7 Shijubo N, Itoh Y, Yamaguchi T, Abe S. Development of an enzyme-linked immunosorbent assay for Clara cell 10-kDa protein: in pursuit of clinical significance of sera in patients with asthma and sarcoidosis. *Ann NY Acad Sci* 2000; **923**: 268–79
8 Ishii S, Itoh Y, Okutani R, Asano Y, Kawai T. Development of an enzyme-linked immunosorbent assay for protein 1. *Contrib Nephrol* 1993; **101**: 71–7

Accepted for publication 5 June 2007

(CAS-JSPS Core University Program Japan-China Joint Open Seminar on Combating Desertification and Development in Inland China of Year 2007, Yangling, Shaanxi Province, P. R. China)

Factors Associated with Health Related Quality of Life in Inhabitants of the Loess Plateau Region

MU, Haosheng[1], KUROZAWA Y.[1], KOTANI, K.[1], LIU Guobin[2], LIU,Pulin.[2], NISHIO Shunichiro[3], ITO T.[3], TSUNEKAWA Atsushi[3]

([1] Division of Health Administration and Promotion, Faculty of Medicine, Tottori University, Japan, [2] Institute of Soil and Water Conservation, Chinese Academy of Sciences and Ministry of Water Resources, China, [3] Arid Land Research Center, Tottori University, Japan)

Abstract: Desertification and drought already present a serious threat to the well-being and health level of the local populations in arid, semi-arid and dry sub-humid areas. However, in the Loess Plateau of semi-arid area, there are very few studies that have examined health level, especially on the aspect of the health-related quality of life (HRQoL). HRQoL is considered as a subset concept of Quality of Life (QoL). QoL has been defined as 'a person's subjective sense of well-being, derived from current experience of life as a whole'. In general, HRQoL is accepted as a multi-dimensional concept that encompasses the components of physical, psychological, social, spiritual, and role functioning, as well as general well-being. The aim of this study was to assess HRQoL of inhabitants in the Loess Plateau region, and to explore relationships of social factors, lifestyle and health conditions with their HRQoL.

In Yan'an City, Shaanxi Province, we selected four suburban farm village communities, which are typical villages from a socioeconomic or agricultural system viewpoint. A survey of HRQoL and the potential risk factors was carried out by questionnaire during August and September 2005. The subjects were the heads of households (or their deputies) of the communities. Trained staff interviewed the subjects in accordance with the questionnaire.

HRQoL was assessed on the basis of a 36-item short form health survey (SF-36). The original SF-36 questionnaire included eight dimensions: body pain, general health (GH) perception, general mental health (MH), physical functioning, social functioning, emotional role, physical role, and vitality (VT). In this study, however, with the aim of keeping the questionnaire simple, only the three dimensions of GH, VT and MH from the SF-36 were investigated. The potential risk factors influencing HRQoL were used social factors (education, economic income, medical insurance and access to hospital), lifestyles (regular physical exercise, cigarette smoking and alcohol intake) and health conditions (chronic diseases and respiratory symptoms).

The scoring of each dimension (GH, VT, MH) was performed according to the SF-36 scoring rules. For each dimension, categorical responses were converted into numerical scores ranging from 0 to 100; the higher the score, the better the HRQoL. Student's t test and analysis of variance were used to explore characteristics of study subjects and the HRQoL scores including GH, VT and MH. Correlation coefficient analysis between each factor and HRQoL

including GH, VT and MH. Correlation coefficient analysis between each factor and HRQoL (GH, VT, MH) was conducted. Then, multiple regression analysis was applied to explore factors influencing HRQoL.

There were a total of 248 valid responses from 252 subjects who completed the questionnaire, and the response rate was 98.4%. Among 248 subjects, 163 (65.7%) were men, and 85 (34.3%) were women. The scores for women were lower than those for men, and the difference in VT and MH was statistically significant. Mean age of the study subjects was 44.15±11.71 years. HRQoL scores decreased with increasing age, but the differences were not statistically significant except for GH. The average annual income per person was 2998.4±2270.7 (CNY) in men and 2303.0±1090.2 (CNY) in women. 89.5% of men and 86.7% of women had medical insurance. Average time to the nearest hospital was approximately 20 min, with a maximum of 90 min. 19.8% of men and 87.7% of women had never smoked or were former smokers. 60.9% of men and 97.5% of women had moderate or no intake of alcohol. 12.3% of men and 15.9% of women suffered from chronic diseases. 19.3% of men and 39.5% of women had respiratory symptoms in the past 6 months.

Multiple regression analysis was performed on the main variables which were significantly correlated with HRQoL. These variables were gender, age, income, access to hospital, medical insurance, physical exercise, smoking, chronic diseases and respiratory symptoms. The standardized partial regression coefficients of chronic diseases with GH and VT were statistically significant. The standardized partial regression coefficients between respiratory symptoms and VT and MH were significant. The standardized partial regression coefficients between access to hospital and GH and VT, and medical insurance and MH were statistically significant. There was also a statistically significant correlation between age and GH, and between income and MH.

The HRQoL scores for women were lower than those for men. The main factors related to HRQoL were health conditions including chronic diseases and respiratory symptoms, the regional medical conditions including access to hospital and medical insurance and economic income in the Loess Plateau region.

Corresponding Author: Mu Haosheng,
Division of Health Administration and Promotion, Faculty of Medicine,
Tottori University
86 Nishi-cho, Yonago 683-8503, Japan
Tel: ++81-859-38-6113
Fax: ++81-859-38-6110
E-mail: muhaosheng@hotmail.com

Return

INTERNATIONAL PERSPECTIVES

Although most of the information presented in the Journal refers to situations within the United States, environmental health and protection know no boundaries. The Journal periodically runs International Perspectives to ensure that issues relevant to our international constituency, representing over 60 countries worldwide, are addressed. Our goal is to raise diverse issues of interest to all our readers, irrespective of origin.

Health-Related Quality of Life and Recognition of Desertification Among Inhabitants of the Loess Plateau Region of China: Findings for City and Village Communities

Haosheng Mu, M.D.
Youichi Kurozawa, M.D., Ph.D.
Kazuhiko Kotani, M.D., Ph.D.
Guobin Liu, Ph.D.
Pulin Liu, Ph.D.
Atsushi Tsunekawa, Ph.D.
Shunichiro Nishino
Takehiko Y. Ito, Ph.D.

Abstract

This article elucidates the health-related quality of life (HRQOL) the recognition of desertification among people living in the semi-arid Loess Plateau of China. HRQOL was assessed with a three-dimensional survey of general health perception, vitality, and general mental health based on a 36-item short-form health survey (SF-36). Scores for general health perception were approximately the same in the city and the village communities. Vitality and mental health scores were significantly lower for women in the village communities than for other groups. In the village communities, HRQOL was significantly and positively correlated with income. The inhabitants of the village communities were more satisfied with their life situation than those in the city, in spite of the economic gap between them. Levels of recognition of desertification were lower in the village communities than in the city.

Introduction

In arid, semi-arid, and dry sub-humid areas, desertification and drought already present a serious threat to the well-being and health of the local populations. Desertification and drought influence malnutrition and famine, dehydration diseases, other infectious diseases, respiratory diseases, and burning injuries (United Nations Convention to Combat Desertification, n.d.). Studies in Saudi Arabia and the city of Lanzhou in China have shown the serious harm that inhalable particulates can cause to human health (Huang, Wang, & Wang, 2001; Li, Zen, Shao, & Shi, 2002; Nouh, 1989). In the semi-arid Loess Plateau of China, desertification presents a serious threat. Anti-desertification policies, such as the "Grain for Green" project, have been implemented by the government. Desertification also has a bearing on quality of life. The level of recognition of desertification varies among the inhabitants living there. Currently, very few studies have examined this issue (Mu, Kurozawa, Wang, & Kotani, 2006). Our study targeted the health-related quality of life (HRQOL) and recognition of desertification among people living in city and village communities of the semi-arid Loess Plateau of China.

Methods

In Yan'an City, Shanxi Province, we selected A, B, and C as three city communities in the city area and D, E, F, and G as four suburban farm village communities in Baota District and Ansai County belonging to Yan'an City (Figure 1). These villages are typical from socioeconomic and agricultural-system viewpoints. A survey of HRQOL, recognition of desertification, and economic status was carried out by questionnaire during August and September 2005. The participants were the heads of households or their deputies (if the heads of households could not reply) in the selected communities. In the city communities, the staff distributed self-administered questionnaires to the participants and collected them later. In the village communities, trained staffs interviewed the participants in accordance with the questionnaire because of some difficulties participants had in understanding the questionnaire exactly.

HRQOL was assessed on the basis of a 36-item short-form health survey. The original questionnaire included eight dimensions: bodily pain, general health perception,

FIGURE 1

Map of the Study Area

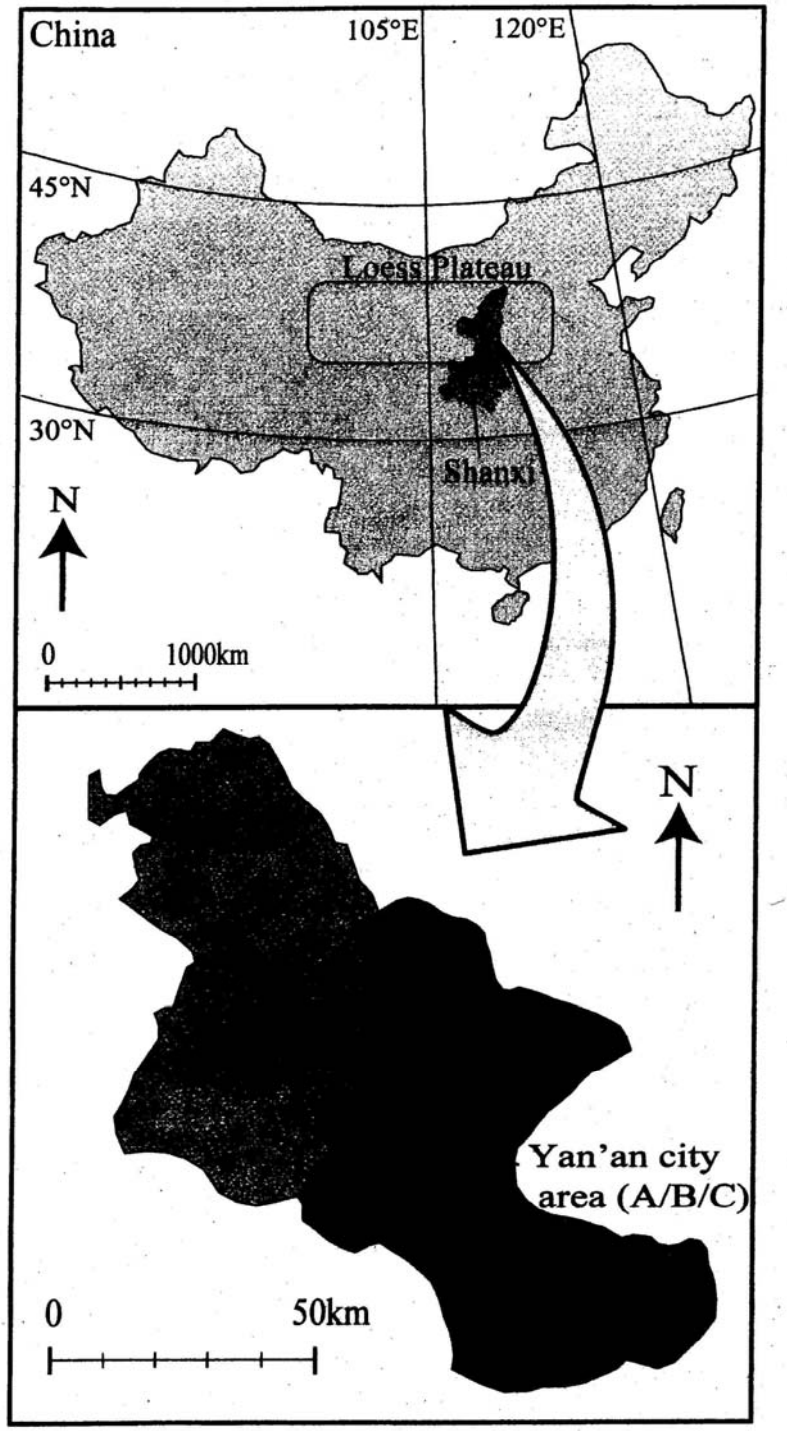

A, B, and C indicate three city communities; and D, E, F, and G indicate four suburban farm village communities.

general mental health, physical functioning, social functioning, role-emotional, role-physical, and vitality (Ware, Snow, Kosinski, & Gandek, 1993). Only the three dimensions—general health perception (GH), vitality (VT), and general mental health (MH)—were investigated so that the questionnaire could be kept simple. The scoring of each dimension was performed according to the scoring protocol (Fukuhara & Suzukamo, 2004). Responses for all items were coded by category, numeric scores of the items belonging to the same dimension were added up, and the raw score of the dimension was calculated. For each dimension, the raw scores were converted into numerical scores ranging from 0 to 100. The higher the scores were, the better the outcomes.

The questions related to life satisfaction were worded as follows: "Are you satisfied with your 1) income, 2) housing conditions, 3) groceries for meals, 4) fuels for cooking and heating, and 5) human relationships with friends and neighbors?" The response options were "definitely yes," "mostly yes," "don't know," "mostly not," and "definitely not." They were scored on a scale from 5 (definitely yes) to 1 (definitely no). The total scores for life satisfaction, therefore, ranged from 25 to 5. The question about recognition of desertification was worded as follows: "Do you consider the problem of Chinese desertification to be serious?" The response choices were "not serious," "not so serious," and "serious or very serious."

In addition, for each household taking part in the questionnaire, information on the total household income in 2004 was requested. The annual income per person was calculated as the total household income divided by the number of family members.

The groups were compared by analysis of variance. A Chi-square test was used to assess differences between proportions. Partial correlation coefficients were used for the estimation of correlations, and the test of significant difference depended on an analysis of variance. A p-value of $<.05$ was accepted as statistically significant.

Results

Table 1 gives the characteristics of the study populations. There were a total of 195 responses from participants in the city communities and 248 responses from participants in the village communities. A total of 443 participants were interviewed, with response rates estimated to be 86 percent and 100 percent in

the city and village communities, respectively. Two-thirds of the participants were men. The mean ages of the city and village community groups were 44.8 and 44.2 years, respectively. In addition, educational achievement differed significantly between the two groups.

Table 2 gives the average annual income per person for the seven communities. The average annual incomes of the city communities (A, B, C) ranged from 6,336 to 8,649 Chinese yuans (CNY) (1 CNY = $0.124), while those of the village communities (D, E, F, G) ranged from 1,720 to 3,907 CNY. Thus, the average annual incomes of the city communities were three times those of the village communities.

Table 3 gives the HRQOL results, including general health perception, vitality, mental health, life satisfaction, and recognition of desertification, by gender and age, for the city and village communities. The scores for general health perception were approximately the same in the city and village communities, with the scores tending to decrease with age. The scores for vitality were significantly lower in the village communities than in the city communities. Vitality and mental health scores were significantly lower among the women in the village communities than in the other groups. The scores for life satisfaction were significantly higher in the village communities than in the city communities. The percentage of people in the village communities who answered "serious or very serious" to the question about the problem of Chinese desertification was significantly lower than in the city communities.

Table 4 gives the correlations of HRQOL, life satisfaction, and recognition of desertification with the characteristics of the study subjects. The scores for general health perception, vitality, and general mental health were significantly correlated with income in the village communities. In the city communities, only the vitality scores were correlated with income. Figure 2 shows the relationship between the average HRQOL scores (GH, VT, MH) and the average annual income per person in the seven communities. The average score for HRQOL was correlated with average annual income in the village communities.

TABLE 1

Characteristics of Study Population

Characteristic	City		Village	
	n	Percentage	*n*	Percentage
Gender				
Male	126	64.6	164	66.1
Female	69	35.4	84	33.9
Age (years)				
20–39	84	43.5	89	36.0
40–59	75	38.9	133	53.8
60–80	34	17.6	25	10.1
Mean ± SD	44.76 ± 13.81		44.15 ± 11.71	
Education (years)				
0–8	48	24.9	243	97.9
9+	145	75.1	5	2.1
Mean ± SD	4.81 ± 1.57		1.92 ± 0.92	

SD = standard deviation.

TABLE 2

Population and Average Annual Income per Person in City and Village Groups, 2004

Location	Group	Population		Income (CNY) (Mean ± SD)
		n	Percentage	
City				
	A	50	11.3	7,210 ± 3,161
	B	97	21.9	8,649 ± 3,796
	C	48	10.8	6,336 ± 5,034
	Total	195	44.0	7,735 ± 4,088
Village				
	D	59	13.3	3,092 ± 2,266
	E	59	13.3	1,720 ± 1,180
	F	65	14.7	2,256 ± 1,386
	G	65	14.7	3,907 ± 2,119
	Total	248	56.0	2,760 ± 1,973

Discussion

A large number of methods for evaluating health-related quality of life have been developed during the past three decades. The 36-item short-form health survey questionnaire was designed for use in clinical practice and research, health policy evaluation, and general population surveys (Ware et al., 1993). Furthermore, the 36-item short-form health survey is one of the most frequently used generic measurements of HRQOL (Ohsawa, Ishiba, Oshida, Yamanouchi, & Sato, 2003), and it has been widely used for medical research and health evaluation in China (Liu et al., 2001; Liu, Guo, Au, & Sun, 2006; Shu et al., 2004; Zhang, He, et al., 2001). Generally speaking, the reliability and validity of the questionnaire have been found to be acceptable. In our study, the HRQOL of the inhabitants of the semi-arid Loess Plateau of China was assessed with a three-dimensional survey of general health perception, vitality, and general mental health. General health perception was approximately the same in the city and village communities. Vitality and mental health scores were significantly lower for women in the village communities than for other groups. The vitality score assesses energy and fatigue. A low score for vitality means that a person feels tired and worn out all the time. The mental health score assesses

TABLE 3

Health-Related Quality-of-Life Scores by Gender and Age Group in City and Village Communities

Parameter	Age Group	City		Village		*p*-Value[a]
		Men	Women	Men	Women	
General health perception (mean ± SD, possible score = 0–100)	20–39	64.02 ± 18.49	60.15 ± 16.87	64.88 ± 15.82	60.30 ± 16.12	
	40–59	59.27 ± 17.19	53.13 ± 16.19	57.73 ± 16.71	53.31 ± 14.21	
	60–80	46.00 ± 17.58	48.43 ± 25.12	48.53 ± 18.73	33.67 ± 16.69	
	Total	58.87 ± 18.85	56.23 ± 17.86	58.76 ± 17.30	55.24 ± 6.59	.373
Vitality (mean ± SD, possible score = 0–100)	20–39	65.76 ± 12.62	61.13 ± 12.67	59.38 ± 15.95	58.59 ± 12.55	
	40–59	60.90 ± 15.06	62.50 ± 14.16	59.47 ± 11.09	51.56 ± 13.80	
	60–80	60.23 ± 11.50	57.14 ± 19.24	57.89 ± 13.15	44.79 ± 17.42	
	Total	62.82 ± 13.59	61.21 ± 13.89	59.26 ± 12.87	54.44 ± 13.93	<.001
Mental health (mean ± SD, possible score = 0–100)	20–39	64.13 ± 12.84	63.59 ± 12.59	60.42 ± 14.69	58.25 ± 0.41	
	40–59	58.62 ± 13.94	64.38 ± 13.05	59.42 ± 10.62	53.75 ± 10.91	
	60–80	57.95 ± 17.23	61.43 ± 16.26	60.26 ± 10.47	53.33 ± 9.83	
	Total	60.82 ± 14.35	63.65 ± 12.99	59.81 ± 11.89	55.90 ± 10.65	.002
Life satisfaction (mean ± SD, possible score = 5–25)	20–39	14.42 ± 3.68	13.30 ± 4.86	15.58 ± 3.51	15.93 ± 3.41	
	40–59	14.13 ± 4.95	15.83 ± 3.85	16.89 ± 2.31	14.86 ± 2.84	
	60–80	15.18 ± 3.85	16.00 ± 3.61	16.74 ± 2.77	15.00 ± 3.69	
	Total	14.45 ± 4.22	14.55 ± 4.51	16.48 ± 2.81	15.34 ± 3.21	<.001
Recognition of desertification (%)	20–39	67.3	74.2	43.5	37.5	
	40–59	68.2	95.8	55.2	38.9	
	60–80	81.8	71.4	36.8	16.7	
	Total	70.4	82.3	49.7	36.6	<.001

[a] Tests of significant difference were performed for men and women in the city and village communities.

TABLE 4

Correlations of Health-Related Quality of Life with the Characteristics of the Study Participants

Parameter	Correlation for City Participants				Correlation for Village Participants			
	Gender	Age	Education	Income	Gender	Age	Education	Income
General health perception	–0.159*	–0.216**	0.180*	–0.083	–0.130*	–0.313†	0.005	0.140*
Vitality	–0.078	–0.169*	0.009	0.258**	–0.113	–0.049	0.108	0.168**
Mental health	0.063	–0.183*	–0.096	0.116	–0.110	–0.022	0.067	0.161*
Life satisfaction	0.035	0.114	–0.031	0.196*	–0.137*	0.077	–0.063	0.201**
Recognition of desertification	0.123	0.149	0.166*	0.044	–0.079	0.040	0.074	0.076

* $p \leq .05$.
** $p \leq .01$.
† $p \leq .001$.

psychological distress and well-being. A low score for mental health means that a person feels nervous and depressed all the time. Xu and co-authors and Mo speculate that the low scores may be related to the social status of women in the village communities (Mo, 2005; Xu et al., 2005). Wang and Yang have concluded that the social status of women and their position in the family are lower because of the lower educational level in the village communities (Wang & Yang, 2005).

In this study, HRQOL in the village communities was found to be significantly correlated with economic income. Studies of HRQOL were performed in Sichuan province (Li, Liu, Li, & Ren, 2001) and Baotou city (Zhang, Lu, et al., 2001). They reported that the key steps in promoting HRQOL include the improvement of people's income (Li et al.; Zhang, Lu, et al.). We suggest that the increase in income as a consequence of anti-desertification policies and other socioeconomic factors has improved the HRQOL levels of inhabitants in the village communities of the semi-arid Loess Plateau of China.

The inhabitants of the village communities were more satisfied with their life situation than those of the city, in spite of the economic gap between them. Thus, life satisfaction was not determined by income. Chen has reported

that, although elderly urban people have a higher standard of living than their rural counterparts, they do not feel better than the latter group (Chen, 2003). This finding relates to differences in educational level and life expectancy (Meng & Xiang, 1996).

On the other hand, levels of understanding of desertification were lower in the village communities than in the city communities. There are a great many differences between city and village people with respect to their perceptions of the importance of environmental protection. Education on environmental protection and health (e.g., the harm of air pollution from a sandstorm to human health) usually is carried out in the city. In addition, because education levels are higher in the cities than in the village communities, people in the cities more easily understand the knowledge and behaviors required for environmental protection. For this reason, people living in city communities are ahead of those in village communities in their appreciation of environmental protection issues (Cui & Gao, 1999). We think that a lack of education among people in the village communities cannot be ignored, and that environmental education may be needed in order to improve levels of understanding in the village communities.

The study reported here had some limitations: Data were collected in personal interviews in the villages, while a questionnaire was used in the cities. This methodological difference may have introduced a bias into the results. Also, the study was limited to participants and communities in the Yan'an regions. It is therefore difficult to extrapolate the findings of the study to the general population of the semi-arid Loess Plateau of China. Further studies in other regions of the Loess Plateau of China are needed.

Conclusions

We investigated HRQOL and recognition of desertification among people in the semi-arid Loess Plateau of China. HRQOL was assessed with a three-dimensional survey of general health perception, vitality, and general mental health based on a 36-item short-form health survey (SF-36). The HRQOL was significantly lower for women in the village communities than for other groups. In the village communities, HRQOL was significantly correlated to economic income. Levels of recognition of desertification were lower in the village communities than in the city. These results suggest that it is necessary to increase incomes and improve the social status of women in order to promote HRQOL in inhabitants of the Loess Plateau region.

FIGURE 2

Relationship Between Average HRQOL Scores (GH, VT, MH) and Average Annual Income per Person for Seven Communities

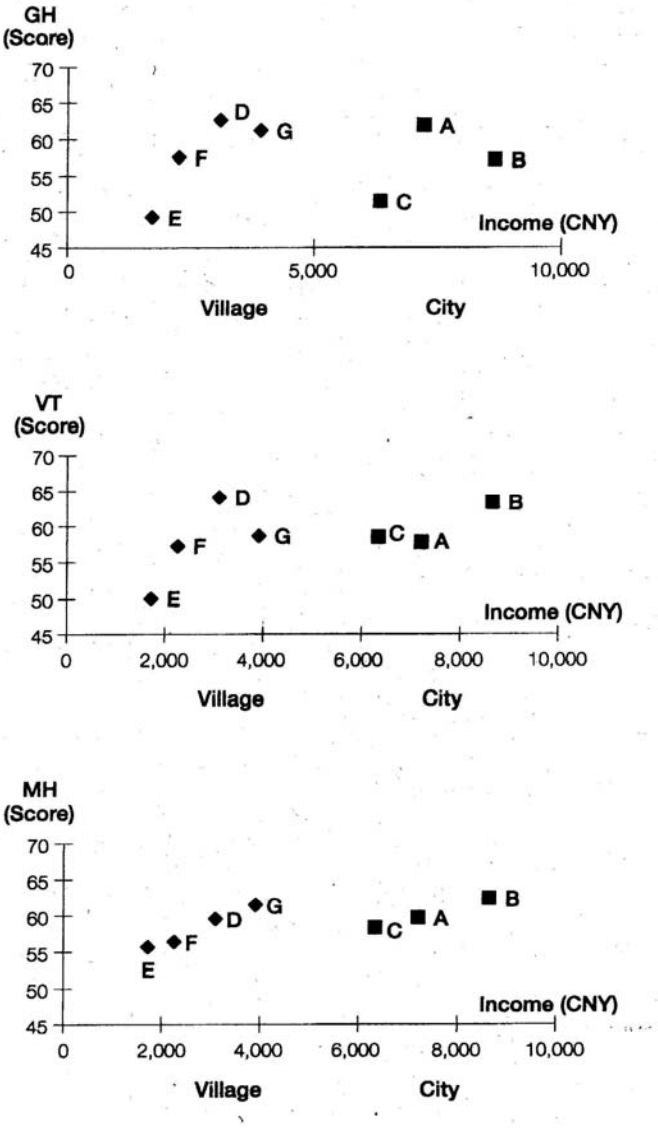

GH = general health perception; VT = vitality; MH = general mental health. A, B, and C indicate three city communities; D, E, F, and G indicate four village communities.

Acknowledgments: The study reported here was supported by the 21st Century COE Program of the Japanese Ministry of Education, Culture, Sports, Science and Technology.

Corresponding author: Haosheng Mu, Division of Health Administration and Promotion, Faculty of Medicine, Tottori University, 86 Nishi-cho, Yonago, Japan 683-8503. E-mail: muhaosheng@hotmail.com.

REFERENCES

Chen, C.X. (2003). Life and contentment: A comparison between the elderly in suburb village and urban area of Beijing [In Chinese with English abstract]. *Market and Demographic Analysis, 9,* 66-70.

Cui, Y.Q., & Gao, M.F. (1999). Differences and analysis of environmental sense between urban and rural of Xiangfan City [In Chinese with English abstract]. *Journal of Xiangfan University, 20,* 64-67.

Fukuhara, S., & Suzukamo, Y. (2004). *Manual of SF-36v2, Japanese version.* (pp. 3-84). Kyoto: Institute for Health Outcomes & Process Evaluation Research.

Huang, Y.X., Wang, X.W., & Wang, B.J. (2001). The relationship between respiratory system disease and the sandstorm weather in Lanzhou [In Chinese with English abstract]. *Gansu Meteorology, 19,* 41-44.

Li, H., Zeng, F.G., Shao, L.Y., & Shi, Z.B. (2002). Current status of study on the human health effects of inhalable particulates [In Chinese with English abstract]. *Journal of Environment and Health, 19,* 85-87.

Li, N.X., Liu, C.J., Li, J., & Ren, X.H. (2001). Factors that influence the quality of life Sichuan population [In Chinese with English abstract]. *Journal of West China University of Medical Sciences, 32,* 247-249.

Liu, C.J., Li, N.X., Ren, X.H., Li, J., Zhang, J., & Sun, D. (2001). Feasibility of using short form 36 in Chinese population [In Chinese with English abstract]. *Journal of West China University of Medical Sciences, 32,* 39-42.

Liu, H.B., Guo, H.Q., QU, B., Sun, G. (2006). Evaluation the amended SF-36 health survey in an elderly population [In Chinese with English abstract]. *Chinese Journal of Health Statistics, 23,* 27-30.

Meng, C., Xiang, MJ. (1996). Comparative study of elderly life satisfaction differences between the urban and rural area [In Chinese with English abstract]. *Chinese Journal of Gerontology, 16,* 106-108.

Mo, W.B. (2005). Thinking on rural women suffered from family violence in China [In Chinese with English abstract]. *Journal of China Women's University, 17,* 26-29.

Mu, H.S., Kurozawa, Y.I., Wang, F., & Kotani, K.H. (2006). A study on the quality of life among the elderly population in the Loess Plateau region of China [In Chinese with English abstract]. *Chinese Journal of Health Education, 22,* 38-41.

Nouh, M.S. (1989). Is the desert lung syndrome (nonoccupational dust pneumoconiosis) a variant of pulmonary alveolar microlithiasis? Report of 4 cases with review of the literature. *Respiration, 55,* 122-126.

Ohsawa, I., Ishiba, T., Oshida, Y., Yamanouchi, K., & Sato, Y. (2003). Subjective health values of individuals with diabetes in Japan: Comparison of utility values with the SF-36 scores. *Diabetes Research and Clinical Practice, 62,* 9-16.

Shu, Q., Lin, J., Liu, H.X., & Li, X.F. (2004). Quality of life of 151 patients with systemic lupus erythematosus [In Chinese with English abstract]. *Chinese Journal of Rheumatology, 8,* 420-423.

United Nations Convention to Combat Desertification. (n.d., updated December 14, 2000). *The health impacts of desertification and drought.* Retrieved June 30, 2006, from http://www.unccd.int/knowledge/menu.pup.

Wang, C.Y., & Yang, K. (2005). Current women's education situation and causal factors in rural areas in Hubei [In Chinese with English abstract]. *Women's Academy at Shandong, 67,* 62-64.

Ware, J.E., Snow, K.K., Kosinski, M., & Gandek, B. (1993). *SF-36 health survey manual and interpretation guide.* Boston: The Health Institute, New England Medical Center.

Xu, X., Zhu, F.C., O'Campo, P., Koenig, M.A., Mock, V., & Campbell, J. (2005). Prevalence of and risk factors for intimate partner violence in China. *American Journal of Public Health, 95,* 78-85.

Zhang, H., Lu, ZQ., Wang, S.H., Cheng, Z.Y., Zhang, C.F., & Qi, L. (2001). Exploring the quality of life among the 601 elderly in the pastoral area in Baotou city [In Chinese with English abstract]. *Journal of Baotou Medical College, 17,* 262-264.

Zhang, J., He, T.W., Luo, D.R., Liu, C.J., Chen, F.J., & Yuan, H.J. (2001). Validating the SF-36 on stroke patients [In Chinese with English abstract]. *Chinese Journal of Behavioral Medical Science, 10,* 416-418.